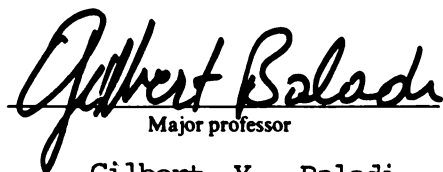




This is to certify that the
dissertation entitled
THE EFFECTS OF GRAIN CHARACTERISTICS
ON THE SHEAR STRENGTH OF
COHESIONLESS SOILS

presented by
THOMAS T.H. WU

has been accepted towards fulfillment
of the requirements for
DOCTORAL degree in CIVIL ENGR.


Major professor

Gilbert Y. Baladi

Date 6.10.85



RETURNING MATERIALS:
Place in book drop to
remove this checkout from
your record. FINES will
be charged if book is
returned after the date
stamped below.

--	--	--

**THE EFFECTS OF GRAIN CHARACTERISTICS ON
THE SHEAR STRENGTH OF COHESIONLESS SOILS**

By

**THOMAS T. H. WU
JUNE 10, 1985**

A DISSERTATION

**Submitted to
Michigan State University
in partial fulfillment of the requirements
of the degree of**

DOCTOR OF PHILOSOPHY

Department of Civil Engineering

1985

ABSTRACT

THE EFFECTS OF GRAIN CHARACTERISTICS ON THE SHEAR STRENGTH OF COHESIONLESS SOILS

By

**THOMAS T. H. WU
JUNE 10, 1985**

The large particle size involved in the construction of earth and rockfill dams makes the problem of predicting the effects of the grain characteristic on their shear behavior. Present procedures use a sequence of correction factors whereby the strength of prototype materials is correlated to that of reconstructed laboratory specimens using smaller particle sizes. The effects of particle angularity and grain shape however, are neglected. A solution to this problem was obtained by introducing a modeling criterion whereby the prototype materials can be modeled using reconstructed conventional laboratory soil specimens; and by verifying the following hypothesis.

**"LARGE PARTICLE SOILS OPERATED UPON BY A STATIC LOAD
INPUT PRODUCES A DEFORMATION OUTPUT RESPONSE.
RELATING THE TWO IS A SOIL-CHARACTERISTICS-DEPENDENT
FUNCTION THAT CONTAINS WITHIN IT THE PROPERTIES OF**

THE SOILS. THIS FUNCTION IS OBTAINED, IN A MATHEMATICAL SENSE, USING STATISTICAL MODELS WITHOUT THE NEED TO SIMULATE RESPECTIVE SOIL PERFORMANCE OR TO DETERMINE VALUES FOR PRESELECTED DESCRIPTORS. THE FUNCTION CAN BE EMPLOYED TO PREDICT THE SHEAR STRENGTH OF COHESIONLESS MATERIALS WHEN SUBJECTED TO AN IMPOSED LOAD."

Two distinctly different series of parallel gradation curves were selected for the study. The laboratory soil specimens were made to possess different maximum grain size, and particle angularity and shape. Triaxial compression tests were conducted using a wide range of specimen and test variables. The test results were then utilized to:

- a) Evaluate the effects of grain size, grain shape, sample gradation, moisture content, and confining pressure upon the shear behavior of the materials; and
- b) Develop a strength prediction model whereby the shear strength of the prototype material can be calculated using that of laboratory reconstructed conventional size soil specimens.

The modeling criterion and the strength model presented in this study closely predict the compressive static triaxial drained strength of the prototype materials.

TO MY BELOVED PARENTS

ACKNOWLEDGEMENTS

The writer wishes to express his sincere appreciation to his academic advisor, Dr. Gilbert Y. Baladi, Associate Professor of Civil and Environmental Engineering, for his encouragement, guidance, and aid throughout the writer's doctoral studies. Thanks also to the other members of the doctoral committee: Dr. D. F. Sibley, Associate Professor of Geological Science; Dr. R. W. Lyles, Assistant Professor of Civil and Environmental Engineering; Dr. R. K. Wen, Professor of Civil and Environmental Engineering; and Dr. G. L. Cloud, Professor of Metallurgy, Mechanics, and Material Science. The writer also wishes to express his appreciation to Miss Amina Mechkor for her valuable contributions in the experimental work.

Many thanks are also extended to the writer's officemate Dr. Bill Sproule for his helpful suggestions and thoughtfulness during the course of this study; and to Mrs. Siham Baladi for her love and care during the writer's stay at Michigan State University.

Thanks are also extended to the Division of Engineering Research and the Department of Civil and environmental Engineering at Michigan State University for the financial

assistance.

Last, but not least, special appreciation, admiration, and love are given to the writer's family for their continuous encouragement, love, and mental as well as financial supports throughout all the years.

TABLE OF CONTENTS

	Page
LIST OF TABLES	viii
LIST OF FIGURES	xii
LIST OF SYMBOLS	xxvii
 CHAPTER	
1 INTRODUCTION	1
2 REVIEW OF LITERATURE	4
2.1 General	4
2.2 Shear Strength of Cohesionless Soils	5
2.2.1 Effect of Grain Size and Gravel Content	5
2.2.2 Effect of Grain Size Distribution	15
Example 1	19
Example 2	21
Example 3	21
Example 4	22
2.2.3 Effect of Grain Shape	22
2.2.4 Effect of Relative Density or Void Ratio	24
2.2.5 Effect of Specimen Size	25
2.2.6 Effect of Moisture Content	28
2.2.7 Effect of Confining Pressure	31
2.3 Maximum and Minimum Density	32
2.4 Angle of Repose	38
2.5 Summary.....	38
3 TEST MATERIALS, SAMPLE MIXING, AND TEST PROCEDURES	40
3.1 General	40
3.2 Test Materials	40
3.2.1 Parallel Gradation Curves	42
3.2.2 Sample Blending	48
3.2.3 Grain Shape	54
3.2.3.1 Particle's Sphericity	55
3.2.3.2 Particle's Angularity	70
3.3 Sample Mixing Procedure	75
3.4 Test Procedures	76
3.4.1 Angle of Repose	76
3.4.2 Maximum and Minimum Density Tests	79

CHAPTER		Page
	3.4.2.1 Maximum Density Test	79
	Note 1	81
	Note 2	82
	3.4.2.2 Minimum Density Test	82
	3.4.3 Static Triaxial Test	83
	3.4.4 Volume Change Due to Confining Pressure	92
	Note	94
4	TESTS RESULTS, ANALYSIS AND DISCUSSION	95
4.1	General	95
4.2	Maximum and Minimum Dry Densities	98
	4.2.1 Effect of Grain Size	101
	4.2.2 Effect of Sample Gradation	116
	4.2.3 Effect of Grain Shape	123
4.3	Angle of Repose	132
	4.3.1 Effect of Grain Size	133
	4.3.2 Effect of Sample Gradation	136
	4.3.3 Effect of Grain Shape	139
4.4	Volume Change	146
4.5	Triaxial Test Results	161
	One Percent Strain Level	162
	Six Percent Strain Level	162
	Peak Stress Level	163
	Ultimate Stress Level	163
4.6	Ultimate Strength and Critical Void Ratio	188
	4.6.1 Effect of Grain Size	192
	4.6.2 Effect of Sample Gradation	202
	4.6.3 Effect of Grain Shape	202
4.7	Strength Model	206
	Example 1	208
	Example 2	210
4.8	Peak Strength	213
	4.8.1 Effect of Grain Size	214
	Gravel Content	230
	Fine Content	233
	4.8.2 Effect of Sample Gradation	237
	4.8.3 Effect of Grain Shape	242
4.9	Strength at the Six Percent Strain Level	249
	4.9.1 Effect of Grain Size	254
	4.9.2 Effect of Sample Gradation	257b
	4.9.3 Effect of Grain Shape	262

CHAPTER	Page
4.10 Strength at the One Percent Strain Level	264
4.10.1 Effect of Grain Size	268
4.10.2 Effect of Sample Gradation	273
4.10.3 Effect of Grain Shape	278
4.11 Confining Pressure	282
4.12 Moisture Content	295
5 SUMMARY, CONCLUSIONS AND RECOMMENDATIONS	308
5.1 General	308
5.2 Effect of Grain Size	309
5.3 Effect of Sample Gradation	310
5.4 Effect of Grain Shape	310
5.5 Effect of Confining Pressure	311
5.6 Effect of Moisture Content	311
5.7 Future Research Needs	312
REFERENCES	314
APPENDICES	
APPENDIX A	322
APPENDIX B	336
APPENDIX C	343
APPENDIX D	346
APPENDIX E	349

LIST OF TABLES

TABLE	Page
2.1 TYPICAL VALUES OF FRICTION ANGLES FOR GRANULAR SOILS (38).....	8
2.2 SUMMARY OF THE EFFECT OF GRAIN SIZE ON THE SHEAR STRENGTH OF COHESIONLESS MATERIALS.....	16
2.3 REPRESENTATIVE VALUE OF THE TOTAL ANGLE OF INTERNAL FRICTION FOR SAND AND SILT (78).....	18
3.1 PERCENT GRAVEL AND SAND, COEFFICIENT OF UNIFORMITY, COEFFICIENT OF CURVATURE, AND CLASSIFICATION OF THE NATURAL TEST MATERIAL	43
3.2 GRAIN SIZES OF THE CRUSHED AND PULVERIZED MATERIAL.....	44
3.3 CALCULATED PERCENT RETAINED BY WEIGHT ON EACH SIEVE FRACTION TO GENERATE FIVE PARALLEL GRADATION CURVES OF SERIES A, AND THE ZERO PERCENT FINE CURVE	49
3.4 CALCULATED PERCENT RETAINED BY WEIGHT ON EACH SIEVE FRACTION TO GENERATE SIX PARALLEL GRADATION CURVES OF SERIES B, AND THE ZERO PERCENT FINE CURVE	50
3.5 PERCENT GRAVEL, SAND, AND FINE CONTENT BY WEIGHT, ATTERBERG LIMITS, UNIFORMITY COEFFICIENT, COEFFICIENT OF CURVATURE, AND THE UNIFIED SOIL CLASSIFICATION SYSTEM OF ALL SAMPLES OF SET A.....	52
3.6 PERCENT GRAVEL, SAND, AND FINE CONTENT BY WEIGHT, ATTERBERG LIMITS, UNIFORMITY COEFFICIENT, COEFFICIENT OF CURVATURE, AND THE UNIFIED SOIL CLASSIFICATION SYSTEM OF ALL SAMPLES OF SET B.....	53
3.7 MEASURED $(Y/Z)_{i,j}$ RATIO FOR THE TWENTY FIVE RANDOMLY SELECTED PARTICLES (I) PER SIEVE (J) OF THE CRUSHED AND PULVERIZED MATERIAL, AND THE CALCULATED AVERAGE $(Y/Z)_{i,\Delta v}$	63

Table	Page
3.8 MEASURED $(Y/Z)_{i,j}$ RATIO FOR THE TWENTY FIVE RANDOMLY SELECTED PARTICLES (I) PER SIEVE (J) OF THE NATURAL MATERIAL, AND THE CALCULATED AVERAGE $(Y/Z)_{i,av}$	64
3.9 PARTICLE SPHERICITY $(PS)_{i,j}$ FOR THE TWENTY FIVE RANDOMLY SELECTED PARTICLES (I) PER SIEVE (J) AND THE AVERAGE SPHERICITY $(PS)_{j,av}$ OF THE CRUSHED AND PULVERIZED MATERIAL.....	66
3.10 PARTICLE SPHERICITY $(PS)_{i,j}$ FOR THE TWENTY FIVE RANDOMLY SELECTED PARTICLES (I) PER SIEVE (J) AND THE AVERAGE SPHERICITY $(PS)_{j,av}$ OF THE NATURAL MATERIAL.....	67
3.11 SAMPLE SPHERICITY (SS) AND ANGULARITY (SA) OF SERIES A OF THE CRUSHED AND PULVERIZED MATERIAL.....	68
3.12 SAMPLE SPHERICITY (SS) AND ANGULARITY (SA) OF SERIES B OF THE CRUSHED AND PULVERIZED MATERIAL.....	69
3.13 SAMPLE SPHERICITY (SS) AND ANGULARITY (SA) OF SERIES A AND B OF THE NATURAL AND 50/50 MATERIALS.....	71
3.14 PARTICLE ANGULARITY $(PA)_{i,j}$ FOR THE TWENTY FIVE RANDOMLY SELECTED PARTICLES (I) PER SIEVE (J) AND THE AVERAGE ANGULARITY $(PA)_{j,av}$ OF THE CRUSHED AND PULVERIZED MATERIAL.....	73
3.15 PARTICLE ANGULARITY $(PA)_{i,j}$ FOR THE TWENTY FIVE RANDOMLY SELECTED PARTICLES (I) PER SIEVE (J) AND THE AVERAGE ANGULARITY $(PA)_{j,av}$ OF THE NATURAL MATERIAL.....	74
4.1 PERCENT FINE CONTENT; MAXIMUM PARTICLE SIZE; MAXIMUM AND MINIMUM DENSITIES; MAXIMUM, MINIMUM, AND CRITICAL VOID RATIOS; ULTIMATE ANGLE OF INTERNAL FRICTION; AND ANGLE OF REPOSE OF THE SAMPLES.....	165
4.2 SUMMARY OF TRIAXIAL TEST RESULTS OF SERIES A SAMPLES.....	168

Table	Page
4.3 SUMMARY OF TRIAXIAL TEST RESULTS OF SERIES B SAMPLES.....	173
4.4 SUMMARY OF TRIAXIAL TEST RESULTS OF THE ONE HUNDRED PERCENT FINE CONTENT SAMPLE.....	178
4.5 SUMMARY OF TRIAXIAL TEST RESULTS OF THE NATURAL AND COMBINED MATERIALS.....	179
4.6 SUMMARY OF TRIAXIAL TEST RESULTS UTILIZING A CONFINING PRESSURE OF 5 PSI AND WET SOILS OF SERIES A SAMPLES.....	183
A.1 MEASURED X, Y AND Z DIMENSIONS OF PARTICLE NUMBER (I) RETAINED ON SIEVE NUMBER (J) OF THE CRUSHED AND PULVERIZED MATERIAL.....	322
A.2 MEASURED X, Y, AND CALCULATED Z DIMENSIONS OF PARTICLE NUMBER (I) RETAINED ON SIEVE NUMBER (J) OF THE CRUSHED AND PULVERIZED MATERIAL.....	326
A.3 MEASURED X, Y AND Z DIMENSIONS OF PARTICLE NUMBER (I) RETAINED ON SIEVE NUMBER (J) OF THE NATURAL MATERIAL.....	329
A.4 MEASURED X, Y, AND CALCULATED Z DIMENSIONS OF PARTICLE NUMBER (I) RETAINED ON SIEVE NUMBER (J) OF THE NATURAL MATERIAL.....	333
B.1 REQUIRED SOIL DENSITY AND WEIGHT OF THE TRIAXIAL TEST SPECIMENS OF SERIES A SAMPLES FOR A RANGE OF RELATIVE DENSITY.....	336
B.2 REQUIRED SOIL DENSITY AND WEIGHT OF THE TRIAXIAL TEST SPECIMENS OF SERIES B SAMPLES FOR A RANGE OF RELATIVE DENSITY.....	337
B.3 THE REQUIRED WEIGHT OF THE SOIL RETAINED ON EACH SIEVE FRACTION FOR A RANGE OF RELATIVE DENSITY, SERIES A SAMPLES.....	338
B.4 THE REQUIRED WEIGHT OF THE SOIL RETAINED ON EACH SIEVE FRACTION FOR A RANGE OF RELATIVE DENSITY, SERIES A SAMPLES.....	340
C.1 MAXIMUM AND MINIMUM DENSITIES AND VOID RATIOS OF SERIES A SAMPLES, C/P MATERIAL.....	343

C.2	MAXIMUM AND MINIMUM DENSITIES AND VOID RATIOS OF SERIES B SAMPLES, C/P MATERIAL.....	344
C.3	MAXIMUM AND MINIMUM DENSITIES AND VOID RATIOS OF SERIES A AND B SAMPLES, NATURAL AND 50/50 MATERIALS.....	345
D.1	ANGLE OF REPOSE OF SERIES A SAMPLES, C/P MATERIAL.....	346
D.2	ANGLE OF REPOSE OF SERIES B SAMPLES, C/P MATERIAL.....	347
D.3	ANGLE OF REPOSE OF SERIES A AND B SAMPLES, NATURAL AND 50/50 MATERIALS.....	348

LIST OF FIGURES

FIGURE	Page
2.1 SHEAR STRESS VERSUS NORMAL STRESS FOR MATERIAL WITH DIFFERENT GRAVEL CONTENT (35).....	10
2.2 SCALPING, SACLPING AND REPLACEMENT, AND PARALLEL GRAIN SIZE DISTRIBUTION CURVES.....	12
2.3 PARALLEL GRAIN SIZE DISTRIBUTION CURVES FOR OROVILLE AND PYRAMID DAMS AND CRUSHED BASALT MATERIALS (61).....	13
2.4 MAXIMUM PARTICLE SIZE VERSUS PEAK ANGLE OF INTERNAL FRICTION FOR OROVILLE AND PYRAMID DAMS AND CRUSHED BASALT MATERIALS (61).....	14
2.5 GRAIN SIZE DISTRIBUTION CURVES.....	20
2.6 EMPIRICAL RELATIONSHIP BETWEEN MAXIMUM AND MINIMUM DRY DENSITIES AND COEFFICIENT OF UNIFORMITY (43).....	35
2.7 RELATIONSHIP BETWEEN MAXIMUM AND MINIMUM VOID RATIOS AND COEFFICIENT OF UNIFORMITY (85).....	36
3.1 GRAIN SIZE DISTRIBUTION CURVE OF THE NATURAL TEST MATERIAL.....	41
3.2 PARALLEL GRADATION CURVES, SERIES A.....	46
3.3 PARALLEL GRADATION CURVES, SERIES B.....	47
3.4 SCHEMATIC REPRESENTATION OF THE X, Y, Z DIMENSIONS OF A SOIL PARTICLE.....	57
3.5 MEDIAN VALUES OF Y/Z AND X/Y RATIOS VERSUS EQUIVALENT GRAIN SIZE DIAMETER OF THE CRUSHED AND PULVERIZED MATERIAL.....	59
3.6 MEDIAN VALUES OF Y/Z AND X/Y RATIOS VERSUS EQUIVALENT GRAIN SIZE DIAMETER OF THE NATURAL MATERIAL.....	60
3.7 A SCHEMATIC REPRESENTATION OF PARTICLE ANGULARITY AND ITS QUANTIFYING SCALE.....	72

FIGURE		Page
3.8	SCHEMATIC DIAGRAM OF THE SPLIT MOLD OF THE TRIAXIAL APPARATUS.....	84
3.9	SCHEMATIC DIAGRAM OF THE TRIAXIAL CELL ASSEMBLY.....	86
3.10	LVDT SET-UP.....	87
3.11	LOAD CELL SET-UP.....	88
4.1	RELATIONSHIP BETWEEN THE PERCENT FINE CONTENT AND THE MAXIMUM GRAIN SIZE OF SERIES A AND B SAMPLES.....	99
4.2	MAXIMUM AND MINIMUM DRY DENSITIES VERSUS PERCENT FINE CONTENT OF THE SOIL OF SERIES A SAMPLES.....	102
4.3	MAXIMUM AND MINIMUM DRY DENSITIES VERSUS PERCENT FINE CONTENT OF THE SOIL OF SERIES B SAMPLES.....	103
4.4	SCHEMATIC REPRESENTATION OF THE EFFECT OF PARTICLE BREAKDOWN ON ITS TOTAL SURFACE AREA AND VOLUME.....	104
4.5	CALCULATED VERSUS MEASURED MAXIMUM AND MINIMUM DRY DENSITIES OF SERIES A AND B SAMPLES.....	108
4.6	MAXIMUM AND MINIMUM DRY DENSITIES VERSUS THE MAXIMUM GRAIN SIZE OF SERIES A SAMPLES.....	109
4.7	MAXIMUM AND MINIMUM DRY DENSITIES VERSUS THE MAXIMUM GRAIN SIZE OF SERIES B SAMPLES.....	110
4.8	MINIMUM AND MAXIMUM VOID RATIOS VERSUS PERCENT FINE CONTENT OF SERIES A SAMPLES.....	112
4.9	MINIMUM AND MAXIMUM VOID RATIOS VERSUS PERCENT FINE CONTENT OF SERIES B SAMPLES.....	113
4.10	CALCULATED VERSUS ACTUAL MINIMUM AND MAXIMUM VOID RATIOS OF SERIES A AND B SAMPLES.....	115
4.11	MAXIMUM AND MINIMUM DRY DENSITIES VERSUS PERCENT FINE CONTENT OF SERIES A AND B SAMPLES.....	117

FIGURE	Page
4.12 MAXIMUM AND MINIMUM DRY DENSITIES VERSUS THE MAXIMUM GRAIN SIZE OF SERIES A AND B SAMPLES.....	118
4.13 DIFFERENCES IN MAXIMUM AND MINIMUM DRY DENSITIES BETWEEN SERIES A AND B SAMPLES VERSUS PERCENT FINE CONTENT OF THE SAMPLES.....	120
4.14 MAXIMUM AND MINIMUM DRY DENSITIES VERSUS COEFFICIENT OF UNIFORMITY OF SERIES A AND B SAMPLES (43).....	122
4.15 MAXIMUM DRY DENSITY VERSUS PERCENT FINE CONTENT OF SERIES A AND B SAMPLES THAT CONSISTED OF THE C/P, NATURAL, AND 50/50 MATERIALS.....	125
4.16 MINIMUM DRY DENSITY VERSUS PERCENT FINE CONTENT OF SERIES A AND B SAMPLES THAT CONSISTED OF THE C/P, NATURAL, AND 50/50 MATERIALS.....	126
4.17 MAXIMUM AND MINIMUM DRY DENSITIES VERSUS SAMPLE ANGULARITY OF SERIES A AND B SAMPLES.....	127
4.18 MAXIMUM AND MINIMUM DRY DENSITIES VERSUS SAMPLE ANGULARITY OF SERIES A AND B SAMPLES (37).....	130
4.19 MAXIMUM AND MINIMUM DRY DENSITY VERSUS PERCENT COMBINATION OF THE C/P AND NATURAL MATERIALS.....	131
4.20 ANGLE OF REPOSE VERSUS PERCENT FINE CONTENT OF SERIES A AND B SAMPLES.....	134
4.21 CALCULATED VERSUS MEASURED ANGLE OF REPOSE OF SERIES A AND B SAMPLES.....	137
4.22 DIFFERENCES IN THE ANGLE OF REPOSE BETWEEN SERIES A AND B SAMPLES VERSUS PERCENT FINE CONTENT.....	138
4.23 ANGLE OF REPOSE VERSUS THE MAXIMUM GRAIN SIZE OF SERIES A AND B SAMPLES.....	140
4.24 ANGLE OF REPOSE VERSUS PERCENT FINE CONTENT OF SERIES A AND B SAMPLES THAT CONSISTED OF THE C/P NATURAL, AND 50/50 MATERIALS.....	142

FIGURE	Page
4.25 ANGLE OF REPOSE VERSUS THE MAXIMUM GRAIN SIZE OF SERIES A AND B SAMPLES THAT CONSISTED OF THE C/P, NATURAL, AND 50/50 MATERIALS.....	143
4.26 ANGLE OF REPOSE VERSUS SAMPLE ANGULARITY OF SAMPLES NUMBER 1 OF SERIES A AND 4 OF SERIES B....	144
4.27 ANGLE OF REPOSE VERSUS PERCENT COMBINATION OF THE C/P AND NATURAL MATERIALS.....	145
4.28 PERCENT VOLUME CHANGE FOR A CONFINING PRESSURE OF 5 PSI VERSUS INITIAL RELATIVE DENSITY OF SERIES A SAMPLES.....	148
4.29 PERCENT VOLUME CHANGE FOR A CONFINING PRESSURE OF 25 PSI VERSUS INITIAL RELATIVE DENSITY OF SERIES A SAMPLES.....	149
4.30 PERCENT VOLUME CHANGE FOR A CONFINING PRESSURE OF 50 PSI VERSUS INITIAL RELATIVE DENSITY OF SERIES A SAMPLES.....	150
4.31 RELATIVE DENSITY CHANGE FOR A CONFINING PRESSURE OF 5 PSI VERSUS PERCENT FINE CONTENT OF SSRIES A SAMPLES.....	151
4.32 RELATIVE DENSITY CHANGE FOR A CONFINING PRESSURE OF 25 PSI VERSUS PERCENT FINE CONTENT OF SSRIES A SAMPLES.....	152
4.33 RELATIVE DENSITY CHANGE FOR A CONFINING PRESSURE OF 50 PSI VERSUS PERCENT FINE CONTENT OF SSRIES A SAMPLES.....	153
4.34 VALUES OF THE PARAMETERS S, B , AND I OF EQUATION 4.13 VERSUS INITIAL RELATIVE DENSITY OF SERIES A SAMPLES FOR A CONFINING PRESSURE OF 5 PSI.....	155
4.35 VALUES OF THE PARAMETERS S, B , AND I OF EQUATION 4.13 VERSUS INITIAL RELATIVE DENSITY OF SERIES A SAMPLES FOR A CONFINING PRESSURE OF 25 PSI.....	156
4.36 VALUES OF THE PARAMETERS S, B , AND I OF EQUATION 4.13 VERSUS INITIAL RELATIVE DENSITY OF SERIES A SAMPLES FOR A CONFINING PRESSURE OF 50 PSI.....	157

FIGURE	Page
4.37 NORMALIZED STRENGTH DIFFERENCE VERSUS VOID RATIO OF SERIES A SAMPLES FOR A CONFINING PRESSURE OF 5 PSI.....	190
4.38 NORMALIZED STRENGTH DIFFERENCE VERSUS VOID RATIO OF SERIES B SAMPLES FOR A CONFINING PRESSURE OF 5 PSI.....	191
4.39 MAXIMUM, MINIMUM, AND CRITICAL VOID RATIOS VERSUS PERCENT FINE CONTENT OF SERIES A SAMPLES.....	193
4.40 MAXIMUM, MINIMUM, AND CRITICAL VOID RATIOS VERSUS PERCENT FINE CONTENT OF SERIES B SAMPLES.....	194
4.41 CALCULATED VERSUS ACTUAL CRITICAL VOID RATIO OF SERIES A AND B SAMPLES.....	196
4.42 ULTIMATE ANGLE OF INTERNAL FRICTION VERSUS PERCENT FINE CONTENT OF SERIES A AND B SAMPLES FOR A CONFINING PRESSURE OF 5 PSI.....	197
4.43 ULTIMATE ANGLE OF INTERNAL FRICTION VERSUS MAXIMUM GRAIN SIZE OF SERIES A AND B SAMPLES FOR A CONFINING PRESSURE OF 5 PSI.....	198
4.44 CALCULATED VERSUS MEASURED ULTIMATE ANGLE OF INTERNAL FRICTION OF SERIES A AND B SAMPLES.....	201
4.45 ULTIMATE ANGLE OF INTERNAL FRICTION VERSUS PERCENT FINE CONTENT OF SERIES A AND B SAMPLES THAT CONSISTED OF THE C/P, NATURAL, AND 50/50 MATERIALS FOR A CONFINING PRESSURE OF 5 PSI.....	203
4.46 ULTIMATE ANGLE OF INTERNAL FRICTION VERSUS SAMPLE ANGULARITY OF SERIES A AND B SAMPLES FOR A CONFINING PRESSURE OF 5 PSI.....	204
4.47 TYPICAL STRESS-STRAIN AND STRESS-VOID RATIO CURVES FOR LOOSE AND DENSE SOIL SPECIMENS (36)....	207
4.48 PEAK ANGLE OF INTERNAL FRICTION VERSUS RELATIVE DENSITY OF SERIES A SAMPLES FOR A CONFINING PRESSURE OF 5 PSI.....	209

FIGURE	Page
4.49 PEAK ANGLE OF INTERNAL FRICTION VERSUS VOID RATIO OF SERIES A SAMPLES FOR A CONFINING PRESSURE OF 5 PSI.....	211
4.50 NORMALIZED STRENGTH DIFFERENCE VERSUS RELATIVE DENSITY OF SERIES A SAMPLES FOR A CONFINING PRESSURE OF 5 PSI.....	216
4.51 NORMALIZED STRENGTH DIFFERENCE VERSUS PERCENT DILATATION OF SERIES A SAMPLES FOR A CONFINING PRESSURE OF 5 PSI.....	217
4.52 NORMALIZED STRENGTH DIFFERENCE VERSUS PERCENT DILATATION OF SERIES B SAMPLES FOR A CONFINING PRESSURE OF 5 PSI.....	218
4.53 VALUES OF THE SLOPE OF THE NORMALIZED STRENGTH DIFFERENCE LINES VERSUS PERCENT FINE CONTENT OF SERIES A AND B SAMPLES.....	222
4.54 CALCULATED VERSUS MEASURED PEAK ANGLE OF INTERNAL FRICTION FOR SERIES A SAMPLES.....	224
4.55 CALCULATED VERSUS MEASURED PEAK ANGLE OF INTERNAL FRICTION FOR SERIES B SAMPLES.....	225
4.56 PEAK ANGLE OF INTERNAL FRICTION VERSUS PERCENT FINE CONTENT OF SERIES A SAMPLES FOR A CONFINING PRESSURE OF 5 PSI, AND FIVE VALUES OF THE PERCENT DILATATION.....	227
4.57 PEAK ANGLE OF INTERNAL FRICTION VERSUS PERCENT FINE CONTENT OF SERIES B SAMPLES FOR A CONFINING PRESSURE OF 5 PSI, AND FIVE VALUES OF THE PERCENT DILATATION.....	228
4.58 PERCENT COMBINATION OF GRAVEL AND SAND VERSUS PERCENT FINE CONTENT FOR SERIES A SAMPLES.....	231
4.59 PERCENT COMBINATION OF GRAVEL AND SAND VERSUS PERCENT FINE CONTENT FOR SERIES B SAMPLES.....	232

FIGURE	Page
4.60 ANGLE OF INTERLOCKING FRICTION VERSUS PERCENT FINE CONTENT OF SERIES A SAMPLES FOR A CONFINING PRESSURE OF 5 PSI, AND THREE VALUES OF THE PERCENT DILATATION.....	235
4.61 ANGLE OF INTERLOCKING FRICTION VERSUS PERCENT FINE CONTENT OF SERIES B SAMPLES FOR A CONFINING PRESSURE OF 5 PSI, AND THREE VALUES OF THE PERCENT DILATATION.....	236
4.62 ANGLE OF INTERLOCKING FRICTION VERSUS PERCENT FINE CONTENT OF SERIES A AND B SAMPLES FOR A CONFINING PRESSURE OF 5 PSI, AND THREE VALUES OF THE PERCENT DILATATION.....	238
4.63 ANGLE OF INTERLOCKING FRICTION VERSUS MAXIMUM GRAIN SIZE OF SERIES A AND B SAMPLES FOR A CONFINING PRESSURE OF 5 PSI, AND THREE VALUES OF THE PERCENT DILATATION.....	240
4.64 NORMALIZED STRENGTH DIFFERENCE VERSUS PERCENT DILATATION OF SERIES A AND B SAMPLES THAT CONSISTED OF THE NATURAL AND 50/50 MATERIALS FOR A CONFINING PRESSURE OF 5 PSI.....	243
4.65 CALCULATED VERSUS MEASURED PEAK ANGLE OF INTERNAL FRICTION OF SERIES A AND B SAMPLES THAT CONSISTED OF THE NATURAL AND 50/50 MATERIALS.....	245
4.66 PEAK ANGLE OF INTERNAL FRICTION VERSUS SAMPLE ANGULARITY OF SAMPLE 1 OF SERIES A FOR A CONFINING PRESSURE OF 5 PSI, AND FIVE VALUES OF THE PERCENT DILATATION.....	246
4.67 PEAK ANGLE OF INTERNAL FRICTION VERSUS SAMPLE ANGULARITY OF SERIES A AND B SAMPLES FOR A CONFINING PRESSURE OF 5 PSI, AND TWO VALUES OF THE PERCENT DILATATION.....	248
4.68 NORMALIZED STRENGTH AT 6% STRAIN LEVEL VERSUS PERCENT DILATATION OF SERIES A SAMPLES FOR A CONFINING PRESSURE OF 5 PSI.....	251
4.69 NORMALIZED STRENGTH AT 6% STRAIN LEVEL VERSUS PERCENT DILATATION OF SERIES B SAMPLES FOR A CONFINING PRESSURE OF 5 PSI.....	252

FIGURE	Page
4.80 VALUES OF THE INTERCEPT OF THE NORMALIZED STRENGTH LINES AT 1% STRAIN LEVEL VERSUS PERCENT FINE CONTENT OF SERIES A AND B SAMPLES....	270
4.81 CALCULATED VERSUS MEASURED ANGLE OF INTERNAL FRICTION AT 1% STRAIN LEVE FOR SERIES A AND B SAMPLES.....	272
4.82 ANGLE OF INTERNAL FRICTION AT 1% STRAIN LEVEL VERSUS PERCENT FINE CONTENT OF SERIES A SAMPLES FOR A CONFINING PRESSURE OF 5 PSI, AND THREE VALUES OF THE PERCENT DILATATION.....	274
4.83 ANGLE OF INTERNAL FRICTION AT 1% STRAIN LEVEL VERSUS PERCENT FINE CONTENT OF SERIES B SAMPLES FOR A CONFINING PRESSURE OF 5 PSI, AND THREE VALUES OF THE PERCENT DILATATION.....	275
4.84 ANGLE OF INTERNAL FRICTION AT 1% STRAIN LEVEL VERSUS MAXIMUM GRAIN SIZE OF SERIES A AND B SAMPLES FOR A CONFINING PRESSURE OF 5 PSI, AND THREE VALUES OF THE PERCENT DILATATION.....	276
4.85 ANGLE OF INTERNAL FRICTION AT 1% STRAIN LEVEL VERSUS PERCENT FINE CONTENT OF SERIES A AND B SAMPLES FOR A CONFINING PRESSURE OF 5 PSI, AND THREE VALUES OF THE PERCENT DILATATION.....	277
4.86 ANGLE OF INTERNAL FRICTION AT 1% STRAIN LEVEL VERSUS SAMPLE ANGULARITY OF SERIES A AND B SAMPLES FOR A CONFINING PRESSURE OF 5 PSI, AND THREE VALUES OF THE PERCENT DILATATION.....	279
4.87 NORMALIZED STRESS DIFFERENCE VERSUS AXIAL STRAIN OF SAMPLES WITH THE SAME PERCENT DILATATION THAT CONSISTED OF THE C/P AND NATURAL MATERIALS.....	280
4.88 AXIAL STRAIN AT PEAK STRENGTH VERSUS PERCENT DILATATION OF THE SAMPLE 1 OF SERIES A THAT CONSISTED OF C/P AND NATURAL MATERIALS FOR A CONFINING PRESSURE OF 5 PSI.....	281
4.89 ULTIMATE ANGLE OF INTERNAL FRICTION VERSUS PERCENT FINE CONTENT OF SERIES A SAMPLES FOR THREE VALUES OF THE CONFINING PRESSURE.....	284

FIGURE	Page
4.90 ULTIMATE ANGLE OF INTERNAL FRICTION OF SERIES A SAMPLES VERSUS CONFINING PRESSURE.....	285
4.91 ANGLE OF INTERLOCKING FRICTION VERSUS CONFINING PRESSURE FOR SAMPLE 1 OF SERIES A, AND THREE VALUES OF THE PERCENT DILATATION.....	287
4.92 ANGLE OF INTERLOCKING FRICTION VERSUS CONFINING PRESSURE FOR SAMPLE 3 OF SERIES A, AND THREE VALUES OF THE PERCENT DILATATION.....	288
4.93 ANGLE OF INTERLOCKING FRICTION VERSUS CONFINING PRESSURE FOR SAMPLE 5 OF SERIES A, AND THREE VALUES OF THE PERCENT DILATATION.....	289
4.94 PEAK ANGLE OF INTERNAL FRICTION VERSUS CONFINING PRESSURE FOR SAMPLE 1 OF SERIES A, AND THREE VALUES OF THE PERCENT DILATATION.....	291
4.95 PEAK ANGLE OF INTERNAL FRICTION VERSUS CONFINING PRESSURE FOR SAMPLE 3 OF SERIES A, AND THREE VALUES OF THE PERCENT DILATATION.....	292
4.96 PEAK ANGLE OF INTERNAL FRICTION VERSUS CONFINING PRESSURE FOR SAMPLE 5 OF SERIES A, AND THREE VALUES OF THE PERCENT DILATATION.....	293
4.97 AXIAL STRAIN AT PEAK STRENGTH VERSUS PERCENT DILATATION OF SERIES A SAMPLES FOR THREE VALUES OF THE CONFINING PRESSURE.....	294
4.98 PEAK ANGLE OF INTERNAL FRICTION VERSUS PERCENT DILATATION OF SAMPLE 1 OF SERIES A THAT CONSISTED OF DRY AND WET MATERIALS FOR A CONFINING PRESSURE OF 5 PSI.....	298
4.99 PEAK ANGLE OF INTERNAL FRICTION VERSUS PERCENT DILATATION OF SAMPLE 2 OF SERIES A THAT CONSISTED OF DRY AND WET MATERIALS FOR A CONFINING PRESSURE OF 5 PSI.....	299
4.100 PEAK ANGLE OF INTERNAL FRICTION VERSUS PERCENT DILATATION OF SAMPLE 3 OF SERIES A THAT CONSISTED OF DRY AND WET MATERIALS FOR A CONFINING PRESSURE OF 5 PSI.....	300

FIGURE	Page
4.101 PEAK ANGLE OF INTERNAL FRICTION VERSUS PERCENT DILATATION OF SAMPLE 4 OF SERIES A THAT CONSISTED OF DRY AND WET MATERIALS FOR A CONFINING PRESSURE OF 5 PSI.....	301
4.102 PEAK ANGLE OF INTERNAL FRICTION VERSUS PERCENT DILATATION OF SAMPLE 5 OF SERIES A THAT CONSISTED OF DRY AND WET MATERIALS FOR A CONFINING PRESSURE OF 5 PSI.....	302
4.103 DIFFERENCE IN THE ANGLES OF INTERNAL FRICTION BETWEEN THE WET AND DRY MATERIALS OF SERIES A SAMPLES FOR A CONFINING PRESSURE OF 5 PSI AND ZERO PERCENT DILATATION.....	304
4.104 PEAK ANGLE OF INTERNAL FRICTION VERSUS PERCENT FINE CONTENT OF SERIES A SAMPLES FOR TWO VALUES OF THE MOISTURE CONTENT, A CONFINING PRESSURE OF 5 PSI, AND ZERO PERCENT DILATATION.....	305
E.1 NORMALIZED PRINCIPAL STRESS DIFFERENCE VERSUS AXIAL STRAIN FOR A CONFINING PRESSURE OF 5 PSI, AND DIFFERENT RELATIVE DENSITY (D_r) OF SAMPLE 1 OF SERIES A OF THE C/P MATERIAL.....	349
E.2 NORMALIZED PRINCIPAL STRESS DIFFERENCE VERSUS AXIAL STRAIN FOR A CONFINING PRESSURE OF 5 PSI, AND DIFFERENT RELATIVE DENSITY (D_r) OF SAMPLE 2 OF SERIES A OF THE C/P MATERIAL.....	350
E.3 NORMALIZED PRINCIPAL STRESS DIFFERENCE VERSUS AXIAL STRAIN FOR A CONFINING PRESSURE OF 5 PSI, AND DIFFERENT RELATIVE DENSITY (D_r) OF SAMPLE 3 OF SERIES A OF THE C/P MATERIAL.....	351
E.4 NORMALIZED PRINCIPAL STRESS DIFFERENCE VERSUS AXIAL STRAIN FOR A CONFINING PRESSURE OF 5 PSI, AND DIFFERENT RELATIVE DENSITY (D_r) OF SAMPLE 4 OF SERIES A OF THE C/P MATERIAL.....	352
E.5 NORMALIZED PRINCIPAL STRESS DIFFERENCE VERSUS AXIAL STRAIN FOR A CONFINING PRESSURE OF 5 PSI, AND DIFFERENT RELATIVE DENSITY (D_r) OF SAMPLE 5 OF SERIES A OF THE C/P MATERIAL.....	353

FIGURE	Page
E.6	NORMALIZED PRINCIPAL STRESS DIFFERENCE VERSUS AXIAL STRAIN FOR A CONFINING PRESSURE OF 5 PSI, AND DIFFERENT RELATIVE DENSITY (D_r) OF SAMPLE 1 OF SERIES B OF THE C/P MATERIAL..... 354
E.7	NORMALIZED PRINCIPAL STRESS DIFFERENCE VERSUS AXIAL STRAIN FOR A CONFINING PRESSURE OF 5 PSI, AND DIFFERENT RELATIVE DENSITY (D_r) OF SAMPLE 3 OF SERIES B OF THE C/P MATERIAL..... 355
E.8	NORMALIZED PRINCIPAL STRESS DIFFERENCE VERSUS AXIAL STRAIN FOR A CONFINING PRESSURE OF 5 PSI, AND DIFFERENT RELATIVE DENSITY (D_r) OF SAMPLE 4 OF SERIES B OF THE C/P MATERIAL..... 356
E.9	NORMALIZED PRINCIPAL STRESS DIFFERENCE VERSUS AXIAL STRAIN FOR A CONFINING PRESSURE OF 5 PSI, AND DIFFERENT RELATIVE DENSITY (D_r) OF SAMPLE 5 OF SERIES B OF THE C/P MATERIAL..... 357
E.10	NORMALIZED PRINCIPAL STRESS DIFFERENCE VERSUS AXIAL STRAIN FOR A CONFINING PRESSURE OF 5 PSI, AND DIFFERENT RELATIVE DENSITY (D_r) OF SAMPLE 6 OF SERIES B OF THE C/P MATERIAL..... 358
E.11	NORMALIZED PRINCIPAL STRESS DIFFERENCE VERSUS AXIAL STRAIN FOR A CONFINING PRESSURE OF 5 PSI, AND DIFFERENT RELATIVE DENSITY (D_r) OF SAMPLE 100 (ONE HUNDRED PERCENT FINE CONTENT) OF SERIES A OR B OF THE C/P MATERIAL..... 359
E.12	NORMALIZED PRINCIPAL STRESS DIFFERENCE VERSUS AXIAL STRAIN FOR A CONFINING PRESSURE OF 5 PSI, AND DIFFERENT RELATIVE DENSITY (D_r) OF SAMPLE 1 OF SERIES A OF THE NATURAL MATERIAL..... 360
E.13	NORMALIZED PRINCIPAL STRESS DIFFERENCE VERSUS AXIAL STRAIN FOR A CONFINING PRESSURE OF 5 PSI, AND DIFFERENT RELATIVE DENSITY (D_r) OF SAMPLE 3 OF SERIES A OF THE NATURAL MATERIAL..... 361
E.14	NORMALIZED PRINCIPAL STRESS DIFFERENCE VERSUS AXIAL STRAIN FOR A CONFINING PRESSURE OF 5 PSI, AND DIFFERENT RELATIVE DENSITY (D_r) OF SAMPLE 4 OF SERIES B OF THE NATURAL MATERIAL..... 362

FIGURE

Page

E.15	NORMALIZED PRINCIPAL STRESS DIFFERENCE VERSUS AXIAL STRAIN FOR A CONFINING PRESSURE OF 5 PSI, AND DIFFERENT RELATIVE DENSITY (D_r) OF SAMPLE 1 OF SERIES A OF THE 50/50 MATERIAL.....	363
E.16	NORMALIZED PRINCIPAL STRESS DIFFERENCE VERSUS AXIAL STRAIN FOR A CONFINING PRESSURE OF 25 PSI, AND DIFFERENT RELATIVE DENSITY (D_r) OF SAMPLE 1 OF SERIES A OF THE C/P MATERIAL.....	364
E.17	NORMALIZED PRINCIPAL STRESS DIFFERENCE VERSUS AXIAL STRAIN FOR A CONFINING PRESSURE OF 25 PSI, AND DIFFERENT RELATIVE DENSITY (D_r) OF SAMPLE 2 OF SERIES A OF THE C/P MATERIAL.....	365
E.18	NORMALIZED PRINCIPAL STRESS DIFFERENCE VERSUS AXIAL STRAIN FOR A CONFINING PRESSURE OF 25 PSI, AND DIFFERENT RELATIVE DENSITY (D_r) OF SAMPLE 3 OF SERIES A OF THE C/P MATERIAL.....	366
E.19	NORMALIZED PRINCIPAL STRESS DIFFERENCE VERSUS AXIAL STRAIN FOR A CONFINING PRESSURE OF 25 PSI, AND DIFFERENT RELATIVE DENSITY (D_r) OF SAMPLE 4 OF SERIES A OF THE C/P MATERIAL.....	367
E.20	NORMALIZED PRINCIPAL STRESS DIFFERENCE VERSUS AXIAL STRAIN FOR A CONFINING PRESSURE OF 25 PSI, AND DIFFERENT RELATIVE DENSITY (D_r) OF SAMPLE 5 OF SERIES A OF THE C/P MATERIAL.....	368
E.21	NORMALIZED PRINCIPAL STRESS DIFFERENCE VERSUS AXIAL STRAIN FOR A CONFINING PRESSURE OF 25 PSI, AND DIFFERENT RELATIVE DENSITY (D_r) OF SAMPLE 4 OF SERIES B OF THE C/P MATERIAL.....	369
E.22	NORMALIZED PRINCIPAL STRESS DIFFERENCE VERSUS AXIAL STRAIN FOR A CONFINING PRESSURE OF 50 PSI, AND DIFFERENT RELATIVE DENSITY (D_r) OF SAMPLE 1 OF SERIES A OF THE C/P MATERIAL.....	370
E.23	NORMALIZED PRINCIPAL STRESS DIFFERENCE VERSUS AXIAL STRAIN FOR A CONFINING PRESSURE OF 50 PSI, AND DIFFERENT RELATIVE DENSITY (D_r) OF SAMPLE 2 OF SERIES A OF THE C/P MATERIAL.....	371

FIGURE	Page
E.24 NORMALIZED PRINCIPAL STRESS DIFFERENCE VERSUS AXIAL STRAIN FOR A CONFINING PRESSURE OF 50 PSI, AND DIFFERENT RELATIVE DENSITY (Dr) OF SAMPLE 3 OF SERIES A OF THE C/P MATERIAL.....	372
E.25 NORMALIZED PRINCIPAL STRESS DIFFERENCE VERSUS AXIAL STRAIN FOR A CONFINING PRESSURE OF 50 PSI, AND DIFFERENT RELATIVE DENSITY (Dr) OF SAMPLE 4 OF SERIES A OF THE C/P MATERIAL.....	373
E.26 NORMALIZED PRINCIPAL STRESS DIFFERENCE VERSUS AXIAL STRAIN FOR A CONFINING PRESSURE OF 50 PSI, AND DIFFERENT RELATIVE DENSITY (Dr) OF SAMPLE 5 OF SERIES A OF THE C/P MATERIAL.....	374
E.27 NORMALIZED PRINCIPAL STRESS DIFFERENCE VERSUS AXIAL STRAIN FOR A CONFINING PRESSURE OF 50 PSI, AND DIFFERENT RELATIVE DENSITY (Dr) OF SAMPLE 4 OF SERIES B OF THE C/P MATERIAL.....	375
E.28 NORMALIZED PRINCIPAL STRESS DIFFERENCE VERSUS AXIAL STRAIN FOR A CONFINING PRESSURE OF 5 PSI, AN AVERAGE WATER CONTENT OF 4.92%, AND DIFFERENT RELATIVE DENSITY (Dr) OF SAMPLE 1 OF SERIES A OF THE C/P MATERIAL.....	376
E.29 NORMALIZED PRINCIPAL STRESS DIFFERENCE VERSUS AXIAL STRAIN FOR A CONFINING PRESSURE OF 5 PSI, AN AVERAGE WATER CONTENT OF 5.32%, AND DIFFERENT RELATIVE DENSITY (Dr) OF SAMPLE 2 OF SERIES A OF THE C/P MATERIAL.....	377
E.30 NORMALIZED PRINCIPAL STRESS DIFFERENCE VERSUS AXIAL STRAIN FOR A CONFINING PRESSURE OF 5 PSI, AN AVERAGE WATER CONTENT OF 4.98%, AND DIFFERENT RELATIVE DENSITY (Dr) OF SAMPLE 3 OF SERIES A OF THE C/P MATERIAL.....	378
E.31 NORMALIZED PRINCIPAL STRESS DIFFERENCE VERSUS AXIAL STRAIN FOR A CONFINING PRESSURE OF 5 PSI, AN AVERAGE WATER CONTENT OF 4.94%, AND DIFFERENT RELATIVE DENSITY (Dr) OF SAMPLE 4 OF SERIES A OF THE C/P MATERIAL.....	379

FIGURE

Page

E.32	NORMALIZED PRINCIPAL STRESS DIFFERENCE VERSUS AXIAL STRAIN FOR A CONFINING PRESSURE OF 5 PSI, AN AVERAGE WATER CONTENT OF 5.11%, AND DIFFERENT RELATIVE DENSITY (D_r) OF SAMPLE 5 OF SERIES A OF THE C/P MATERIAL.....	380
E.33	NORMALIZED PRINCIPAL STRESS DIFFERENCE VERSUS AXIAL STRAIN FOR A CONFINING PRESSURE OF 5 PSI, AN AVERAGE WATER CONTENT OF 9.15%, AND DIFFERENT RELATIVE DENSITY (D_r) OF SAMPLE 1 OF SERIES A OF THE C/P MATERIAL.....	381
E.34	NORMALIZED PRINCIPAL STRESS DIFFERENCE VERSUS AXIAL STRAIN FOR A CONFINING PRESSURE OF 5 PSI, AN AVERAGE WATER CONTENT OF 9.60%, AND DIFFERENT RELATIVE DENSITY (D_r) OF SAMPLE 2 OF SERIES A OF THE C/P MATERIAL.....	382
E.35	NORMALIZED PRINCIPAL STRESS DIFFERENCE VERSUS AXIAL STRAIN FOR A CONFINING PRESSURE OF 5 PSI, AN AVERAGE WATER CONTENT OF 9.69%, AND DIFFERENT RELATIVE DENSITY (D_r) OF SAMPLE 3 OF SERIES A OF THE C/P MATERIAL.....	383
E.36	NORMALIZED PRINCIPAL STRESS DIFFERENCE VERSUS AXIAL STRAIN FOR A CONFINING PRESSURE OF 5 PSI, AN AVERAGE WATER CONTENT OF 9.75%, AND DIFFERENT RELATIVE DENSITY (D_r) OF SAMPLE 4 OF SERIES A OF THE C/P MATERIAL.....	384
E.37	NORMALIZED PRINCIPAL STRESS DIFFERENCE VERSUS AXIAL STRAIN FOR A CONFINING PRESSURE OF 5 PSI, AN AVERAGE WATER CONTENT OF 9.96%, AND DIFFERENT RELATIVE DENSITY (D_r) OF SAMPLE 5 OF SERIES A OF THE C/P MATERIAL.....	385

LIST OF SYMBOLS

B, I, S = parameters of the volume change equations.

C_c = coefficient of curvature.

C_u = coefficient of uniformity.

D = Capillary tube diameter.

D_c = diameter of the circle whose area is equivalent to the area covered by the soil particle in question when laid on its longest side.

D_i = diameter of the circle inscribed into the area covered by the soil particle in question when laid on its longest side.

D_{MAX} = maximum particle size.

D_r = final or simply the relative density of a soil specimen.

D_{r1} = initial relative density of a soil specimen

D_r = the change in the relative density of a soil specimen due to the application of the confining pressure.

e = void ratio.

e_{MAX} = maximum void ratio.

e_{MIN} = minimum void ratio.

e_{cr} = critical void ratio.

EXP = exponential function.

G_s = specific gravity of the soil.

H_c = height of capillary rise.
 LOG = logarithm to base 10.
 n = porosity.
 NSD = normalized strength difference ratio.
 PA = particle angularity.
 PD = percent dilatation.
 PF = percent fine content of the soil.
 PR = percent retained by weight.
 PS = particle sphericity.
 SA = sample angularity.
 SP = slope of the best fit lines.
 SS = sample angularity.
 T = water surface tension.
 V = volume of the mold.
 V_{sp} = volume of a sphere.
 W = total weight of a soil sample.
 W_c = weight of container.
 W_M = weight of the standard compaction mold with the
 base pedestal.
 W_{NET} = weight of dry soil.
 W_{sc} = weight of dry soil and container.
 W_T = total weight of the standard compaction mold mold,
 base pedestal and soil.
 ϵ = vertical strain.
 $\epsilon_{1\%}$ = the one percent strain level.
 $\epsilon_{6\%}$ = the six percent strain level.

γ = dry density (unit weight) of the soil.
 γ_{MAX} = maximum dry density.
 γ_{MIN} = minimum dry density.
 γ_w = unit weight of water.
 ϕ = total angle of internal friction.
 ϕ_I = angle of interlocking friction.
 ϕ_P = peak angle of internal friction.
 ϕ_R = angle of repose.
 ϕ_S = angle of sliding friction.
 ϕ_U = ultimate angle of internal friction.
 $\phi_{1\%}$ = angle of friction at the one percent strain level.
 $\phi_{6\%}$ = angle of friction at the six percent strain level.
 σ_1 = major principal stress.
 σ_3 = minor principal stress.
 τ_R = normal radial stress.
 $\tau_{R,z}$ = shear stress.
 σ_θ = normal circumferential stress.

CHAPTER 1

INTRODUCTION

The increasing demand for better means and reliability for prediction of the stress-strain relationship of large particle soils, coupled with the ever present need to provide more realistic assessment of the influence of the grain characteristics on the shear behavior of cohesionless materials, make it very important that the Geotechnical profession be provided with a reliable modeling technique whereby the effects of grain size, sample gradation, and grain shape can be accurately evaluated. The presence of large size particles causes difficulties in determining the strength parameters of the materials utilizing conventional laboratory equipment. The relevant properties of the prototype materials (that contain large size particles) could be evaluated by using laboratory reconstructed specimens with smaller particle sizes.

The maximum particle size that can be tested in the laboratory is generally equivalent to one six of the diameter of the soil specimen. For the conventional triaxial specimen diameter of 2.8 inches (71 mm) the maximum grain size which can be tested is equal to or less than 0.5 inch (12.7 mm). Thus, the selection of a suitable grain size distribution for the laboratory soil is crucial to the

investigation. Several procedures are commonly used to overcome this problem. These include scalping the large particles; scalping and replacement of the large particles; or crushing the large particles to reconstruct laboratory specimens utilizing particle size distribution curves parallel to that of the prototype materials. The procedure to be employed will depend on the given prototype materials. Nevertheless, each procedure has some disadvantages. The parallel grain size distribution procedure is utilized in this study.

In addition, the density, particle angularity, grain shape, and moisture content of the soil specimens to be tested in the laboratory should be equivalent to those of the prototype materials. A literature review concerning the effects of specimen and test variables on the shear strength of cohesionless soils is presented in Chapter 2. In this study, soil specimens were reconstructed to possess several different densities, and three grain shapes (angularities). A detailed description of all soil specimens is presented in Chapter 3.

One hundred and seventy eight triaxial compression tests were conducted utilizing dry and moist soil specimens, three levels of confining pressure, two series of parallel gradation curves, three different grain shapes (angularities), and several soil specimen densities. The effects of these variables on the triaxial shear strength of

the soils are presented and discussed in Chapter 4. Due to the large volume of the test results, they were condensed, tabulated and/or plotted in the Appendices. The test results that are relevant to the discussion are presented in the appropriate Chapter.

Finally, the angle of repose, and the maximum and minimum densities of the soil specimens were also evaluated and discussed in Chapter 4. Chapter 5 summarizes the findings, conclusions and recommendations of this study.

CHAPTER 2

REVIEW OF LITERATURE

2.1 GENERAL

In the early stage of development of material testing, evaluation of soil strength consisted of special or limited observations of the shear surface behind a retaining structure (8, 16, 75)*. Later, a soil shear test was introduced by Collin (14), and a triaxial test by Adams and Nicholson (4). In the early 1930's, engineers were witnessing rapid evolvement of the triaxial test in the United States, Germany and the Netherlands (12, 40, 65). Along with these developments, theories of shear strength of soils as a continuous media were also evolved. Generally, these theories describe the shear strength of soils by means of fundamental strength parameters that are directly applicable to design problems (64). The strength parameters are a function of several factors such as intermolecular and grain boundary forces, thixotropy, volume change characteristics, and soil textures. These factors are important for fundamental understanding of the shear behavior of soils.

* Figures in brackets indicate reference number.

Moreover, there exists a considerable number of physical variables influencing the shear behavior of soils. Some of these variables are apparatus and test method dependent; others are specimen and soil dependent. In the following sections, past and present investigations of the effects of some of the specimen and test variables on the shear strength of cohesionless materials and their state of compaction are reviewed. These variables are:

- a) grain size (percent fine or percent gravel content);
- b) grain size distribution (sample gradation);
- c) grain shape (particle angularity);
- d) relative density or void ratio;
- e) specimen size;
- f) moisture content; and
- g) confining pressure.

2.2 SHEAR STRENGTH OF COHESIONLESS SOILS

In this section, the effects of test and specimen variables on the shear strength of cohesionless soils are reviewed. For convenience, this Section is divided into seven subsections for each of the above listed variables.

2.2.1 EFFECT OF GRAIN SIZE AND GRAVEL CONTENT

The shear strength of cohesionless soils is a primary function of their frictional property which intimately depends on the physical motion between particles (83). This

motion includes: a) particles sliding and rolling relative to each other, and b) particles plucking and displacement from their interlocking seats. Thus, the total frictional property of granular soils which is described by their total angle of internal friction (ϕ) can be separated into two independent components:

- a) Sliding or ultimate friction (ϕ_s or ϕ_u) which is governed by microscopic interlocking of particles due to their surface roughness at contact points.
- b) Interlocking friction (ϕ_i) which consists of physical restraints to relative particle translation affected by adjacent particles.

The interlocking friction is affected by the sample dilatancy which is a function of the state of compaction of the soil. That is, the denser the soil sample, the higher the degree of interlocking and consequently the higher is the interlocking friction (ϕ_i).

The shear stress required to overcome particles interlocking and to bring the soils to a free-sliding position is greatly affected by the soil grain size (38). This conclusion however, is not consistent throughout the literature. Indeed, conflicting findings and opinions concerning the effects of grain size and/or percent gravel content upon the shear strength of cohesionless soils can be found. These are summarized below.

- a) The shear strength of cohesionless soils increases as

the particle size increases (21, 22, 35, 38, and 59).

b) The shear strength of cohesionless soils decreases as the particle size increases (45, 46, 57, 61, 62, and 70).

c) The shear strength of cohesionless soils is not affected by the grain size (9, 78, 80, and 87).

In his book, Hough (38) stated that the shear strength of cohesionless soils increases with increasing grain size. Table 2.1 (38) presents typical variations of: a) the ultimate angle of internal friction (ϕ_u); b) the total or peak angle of internal friction at peak strength (ϕ_p); and c) the angle of repose (ϕ_R) for a range of grain size from silt to gravel. From the table, It can be noticed that the silt size particles possess the lowest friction angle while the gravel size particles possess the highest. These observations however, should be considered cautiously because the effect of soil gradation on the friction angles was neglected.

Holtz and Gibbs (35) studied the effects of grain size on the shear strength of cohesionless materials by varying the percent gravel content of the test samples. Thirteen drained triaxial shear tests were conducted on soil samples with a range of gravel content from 0.0 to 65 percent. They concluded that for the same relative density, the drained shear strength of the soil samples increases as the percent gravel content increases from 0.0 to 50 percent as shown in

TABLE 2.1 TYPICAL VALUES OF FRICTION ANGLES FOR GRANULAR SOILS (38).

Classification	angle of Repose (deg.)	Angle of Internal Friction		
		At Ultimate Strength (deg.)	At Peak Sterngth	
			Med. Dense (deg.)	Dense (deg.)
GRAVEL & SAND	32 to 36	32 to 36	36 to 42	40 to 48
SAND (well graded)	30 to 34	30 to 34	34 to 40	38 to 46
SAND (uniform, fine to med.)	26 to 30	26 to 30	30 to 34	32 to 36
SILT (nonplastic)	26 to 30	26 to 30	28 to 32	30 to 34

Figure 2.1. In the Figure, test "T" with 50 percent gravel content yielded the highest shear strength, while test "M" with 0.0 percent gravel content yielded the lowest. For most tests, an increase in gravel content (grain size) resulted in an increase in the shear strength. Test "U" however, with a gravel content of 65 percent showed a decrease in the shear strength. Holtz and Gibbs attributed the decrease in the shear strength of this last test to the poor gradation of the soil due to a high gravel content. It should be noted herein that Holtz and Gibbs's samples possessed different gradation and coefficient of uniformity (Cu). Their conclusions were strictly based on percent gravel content and thus neglecting the effects of sample gradation and coefficient of uniformity on sample strength.

In a similar study, Donaghe et al. (21, 22) concluded that for the same relative density, the shear strength of cohesionless soils increases as the percent gravel content increases. Again, the effects of sample gradation were neglected.

During the foundation investigation of Encino dam in 1978, Wu (82) found that the alluvial soil in the dam's foundation contained approximately 60 percent gravel (particle larger than 0.2 inch (4.75 mm)). In his cyclic triaxial test program however, the gravel content of the specimens was limited to a maximum of 50 percent. This limitation was found necessary to maintain an adequate ratio

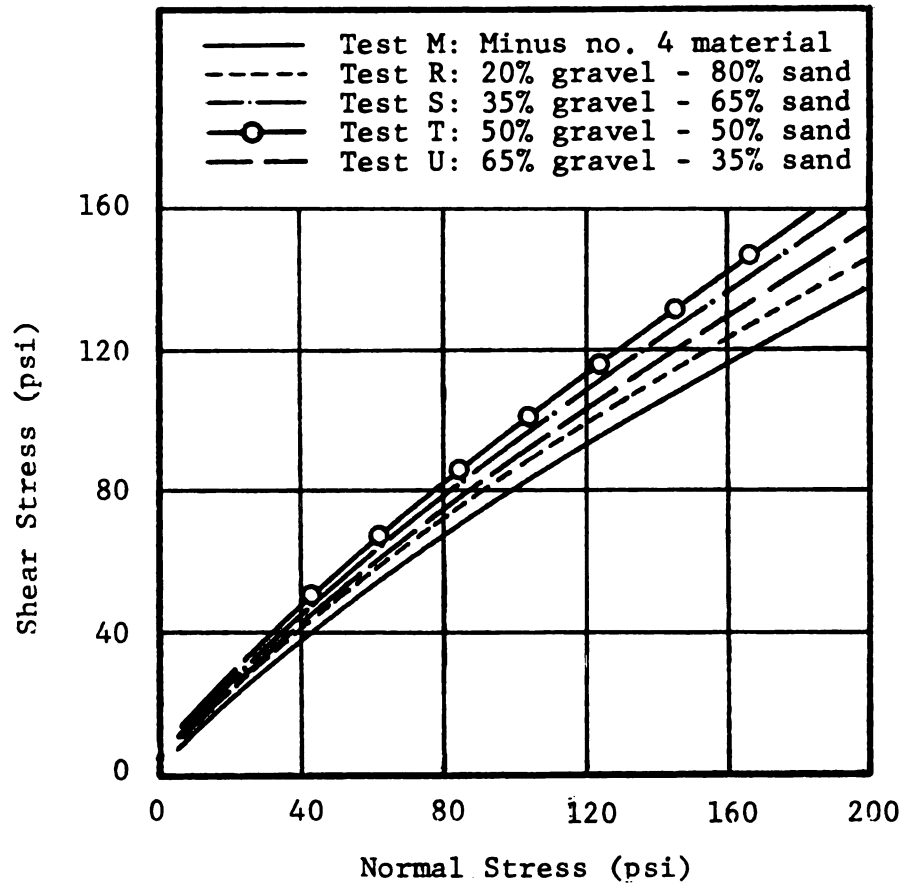


FIGURE 2.1 SHEAR STRESS VERSUS NORMAL STRESS FOR MATERIAL WITH DIFFERENT GRAVEL CONTENT (35).

of fine to gravel content. The materials making up the cyclic triaxial specimens were obtained using scalping and scalping/replacement techniques as shown in Figure 2.2. Wu concluded that increasing gravel content from zero to 30 percent tends to increase the cyclic triaxial strength. This trend however, was reversed when the gravel content increased above the 30 percent level. He attributed this to the scalping and scalping/replacement procedures.

Marachi (61) performed series of drained triaxial compression tests on rock fill materials that were blended to form parallel gradation curves as shown in Figure 2.3. The significance of the parallel gradation curves is that all samples possess the same gradation and coefficient of uniformity. Marachi concluded that, for a constant initial void ratio of the test specimens, the shear strength increases as the particle size decreases. His test results are shown in Figure 2.4. From the figure it can be seen that the smaller the particle size, the higher the shear strength of the materials. Similar conclusions were also made by Kirkpatrick (45) and Koerner (46).

Terzaghi and Peck (78) stated that "the grain size has no influence on the relative density and bearing capacity or shear strength of sand".

Vallerga et al. (80) evaluated the effects of particle shape and size on the strength of uniformly graded materials consisted of particle sizes of up to 0.2 inch (4.75mm) in

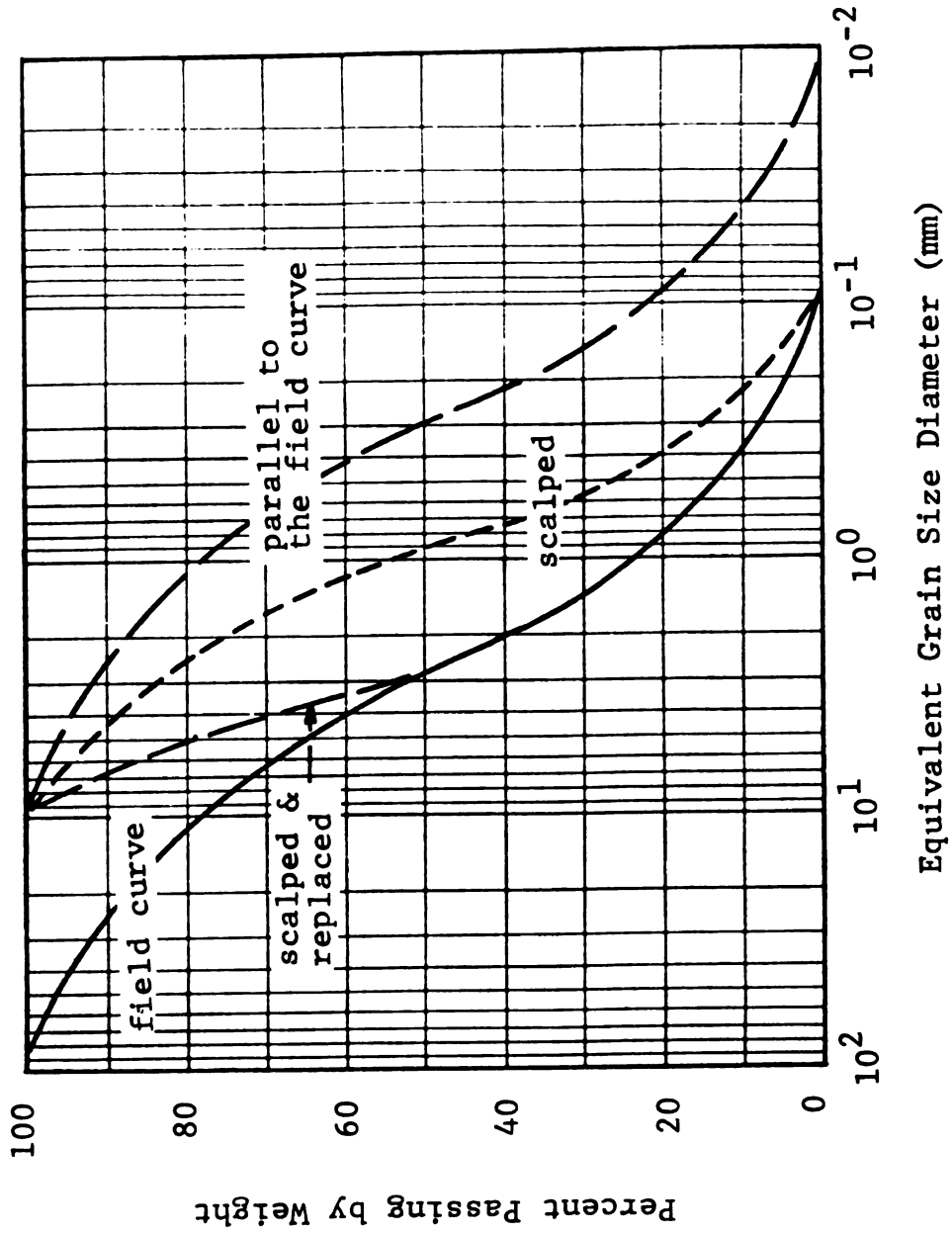


FIGURE 2.2 SCALPING, SCALPING AND REPLACEMENT, AND PARALLEL GRAIN SIZE DISTRIBUTION CURVES.

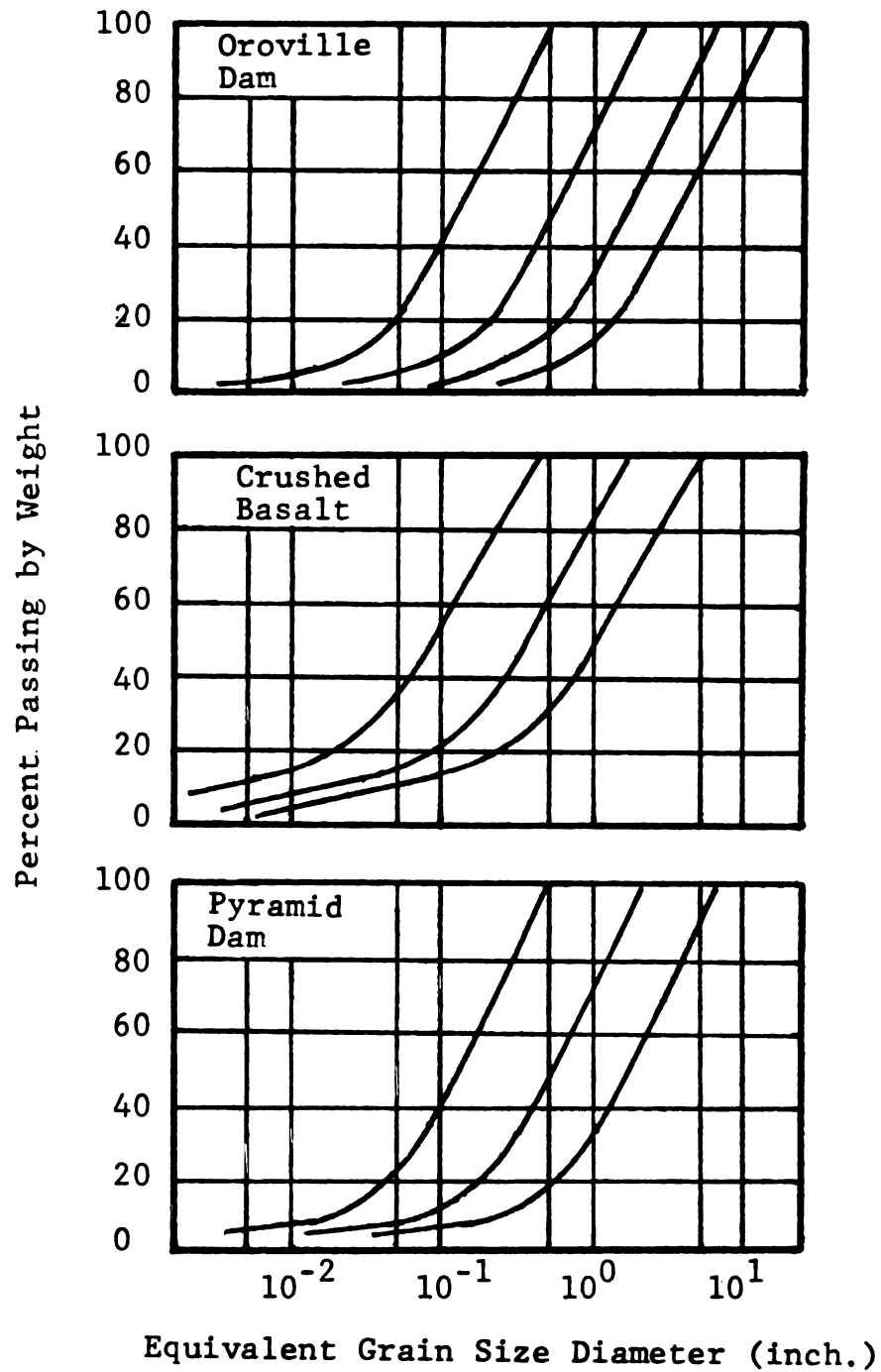


FIGURE 2.3 PARALLEL GRAIN SIZE DISTRIBUTION CURVES FOR OROVILLE AND PYRAMID DAMS AND CRUSHED BASALT MATERIALS (61).

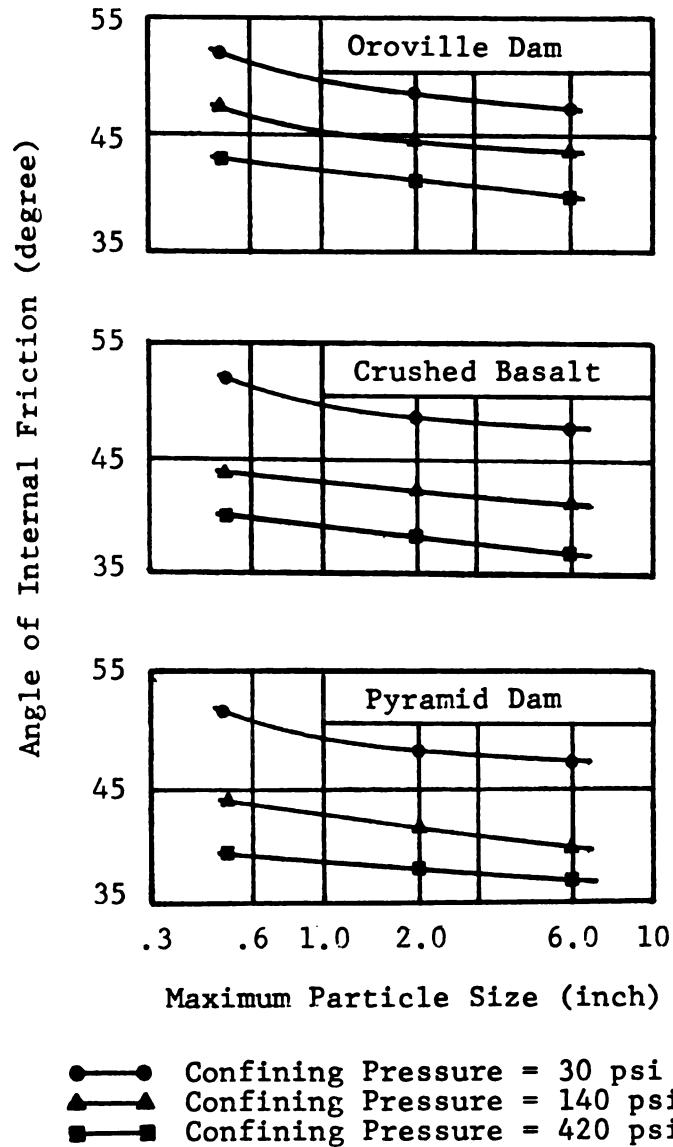


FIGURE 2.4 MAXIMUM PARTICLE SIZE VERSUS PEAK ANGLE OF INTERNAL FRICTION FOR OROVILLE AND PYRAMID DAMS AND CRUSHED BASALT MATERIALS (61).

diameter. They concluded that the particle size has no effect on the angle of internal friction. Also, Zelasko et al. (87) conducted triaxial compression tests to study the shear strength of uniform and well graded sands. They concluded that the effect of particle size on strength is small or virtually zero.

To this end, it is clear that researchers have reached different and conflicting conclusions and opinions concerning the effects of grain size on the shear strength of cohesionless soils. The differences however, do not necessarily represent the true behavior of the soils. They are mainly related to the basis on which the analyses of the shear strength were conducted. Some researchers analyzed the shear strength of the soil samples at a constant relative density, others used a constant void ratio. Still others did not separate variables that may affect the shear strength of the soils. Table 2.2 provides a summary of past studies concerning the effects of grain size and/or gravel content on the shear strength of granular soils and the basis on which the analyses were conducted.

2.2.2 EFFECT OF GRAIN SIZE DISTRIBUTION

First, it shall be noted herein that the terms grain size distribution, sample gradation, and coefficient of uniformity are used throughout this dissertation to express in a qualitative and/or quantitative terms, the general

TABLE 2.2 SUMMARY OF THE EFFECT OF GRAIN SIZE ON THE SHEAR STRENGTH OF COHESIONLESS MATERIALS.

Source	Maximum Particle Size (inch) (mm)	Type of Test	Conclusion	Conclusion Based On a constant value of	Uniformity of the test Material
Bishop (9)	1.25 (31.8)	D	1*	n	uniformly graded
Vallerga, et al (80)	0.20 (4.8)	T	1*	e	uniformly graded
Zelasko (87)	0.03 (0.9)	T	1*	e	varied
Kirkpatrick (45)	0.08 (2.0)	T	2*	n	uniformly graded
Koerner (46)	0.10 (2.5)	T	2*	e	uniformly graded
Leslie (57)	3.00 (76.2)	T	2*	e	very well graded
Marachi (61)	6.00 (152.4)	T	2*	e	well graded
Marshall (62)	8.00 (203.2)	T	2*	n	varied
Rowe (70)	0.04 (1.0)	S	2*	n	varied
Zeller et al (88)	3.94 (100.0)	T	2*	n	very well graded
Donaghe, et al (22)	3.00 (838.2)	T	3*	Dr	very well Graded
Holtz & Gibbs (35)	3.00 (76.2)	T	3*	Dr	varied
Lewis (59)	0.25 (6.4)	D	3*	Dr	uniformly graded

1* = The shear strength is not affected by particle size.

2* = The shear strength decreases as the particle size increases.

3* = The shear strength increases as the particle size increases.

D = Direct shear test.

T = Triaxial compression test.

S = Sliding test (or angle of repose test).

n = porosity.

e = void ratio.

Dr = Relative density.

shape of the grain size distribution curve of the soil.

As noted in Section 2.2, the total or peak angle of internal friction (ϕ) of cohesionless soils consists of two components, sliding or ultimate friction (ϕ_s or ϕ_u) and interlocking friction (ϕ_i). The first is mainly a function of the soil minerals and surface roughness (microscopic interlocking), while the latter is a function of the degree macroscopic interlocking which is a function of the degree of compaction of the soil. The higher the degree of compaction of the soil, the higher the soil density, the degree of interlocking, and the total angle of internal friction.

Terzaghi and Peck (78) stated that "Depending principally upon the relative density, the value of the total angle of friction may range between fairly wide limits; the grain size distribution and the shape of the grains also have an influence". Table 2.3 (78) lists representative values of the total angle of internal friction for sands and silts.

Koerner (46) studied the effects of sample gradation on the strength of cohesionless materials using three single mineral soils (quartz, feldspar, and calcite). In his study, the coefficient of uniformity (C_u) of the test materials was varied from 1.25 to 5.00. The quartz soils were tested under saturated and air dried conditions using both drained and undrained triaxial tests. The feldspar and

**TABLE 2.3 REPRESENTATIVE VALUE OF THE TOTAL ANGLE OF
INTERNAL FRICTION FOR SAND AND SILT (78).**

Type of material	peak Angle of friction (ϕ_p)	
	Loose	Dense
Sand, round grains, uniform	27.5	34.0
Sand, angular grains, well graded	33.0	45.0
Sandy gravels	35.0	50.0
Silty sand	27-33	30-34
Inorganic silt	27-30	30-35

calcite soils were saturated first, then tested under drained conditions. Koerner concluded that:

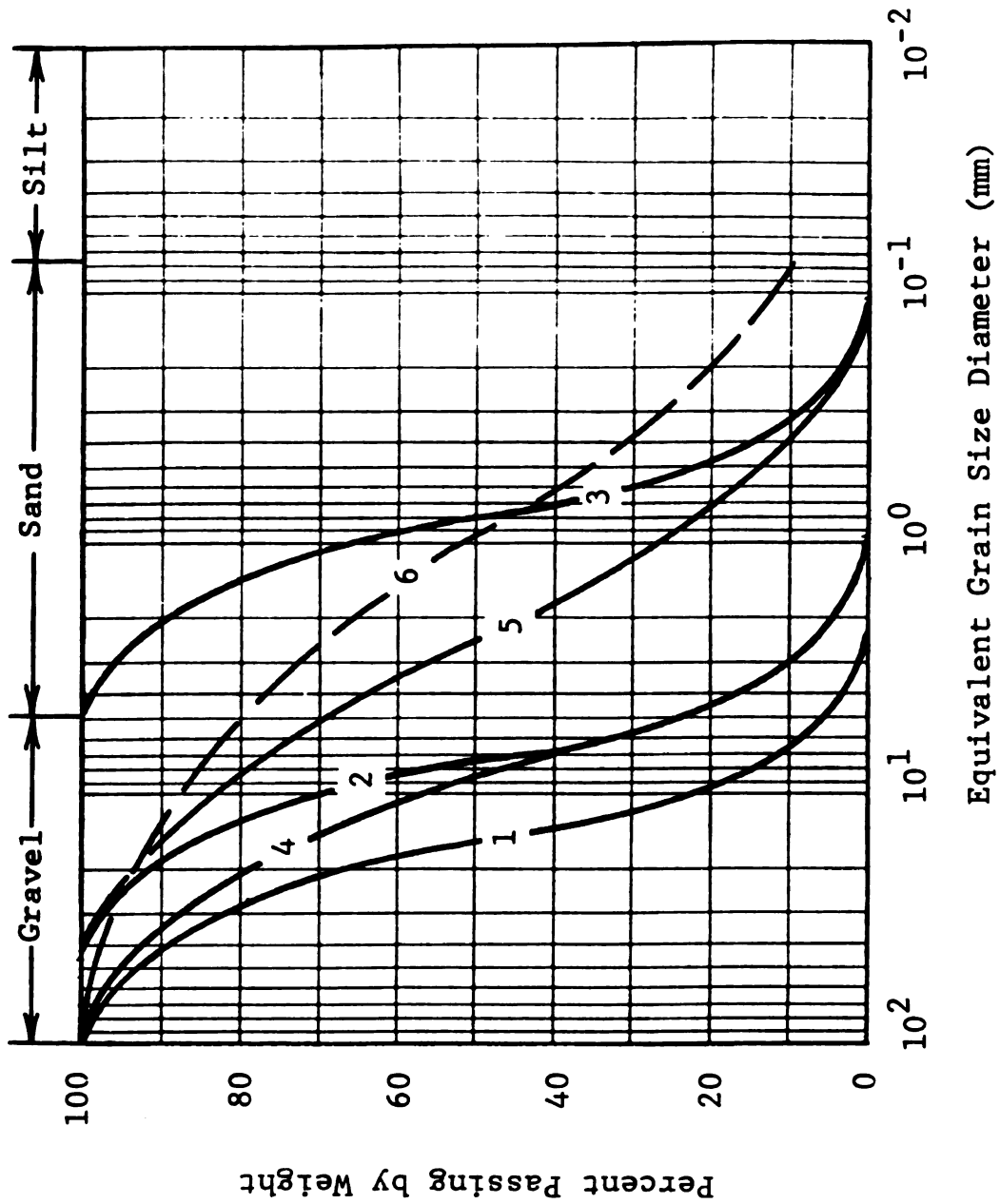
- a) the angle of internal friction for the feldspar and calcite samples increases with increasing value of the coefficient of uniformity (C_u); and
- b) the effect of C_u on the internal friction of the quartz sample is negligible.

Kirkpatrick (45) and Zelasko (87) performed similar study using sand materials. The coefficient of uniformity (C_u) of the samples however, was varied only from 1.2 to 1.5 in Kirkpatrick's study, and from 1.2 to 2.0 in Zelasko's. Due to the limited range of C_u , they were unable to make any clear conclusion regarding the effects of sample gradation on the shear strength of the soil samples.

The effects of grain size and percent gravel content on the shear strength of cohesionless soils were reviewed in Subsection 2.2.1 above, while the effect of sample gradation is reviewed in this Subsection. This should not necessarily mean that the three variables (grain size, percent gravel content, and sample gradation) are independent of each other. Indeed, the three variables are somehow interrelated. This point can be illustrated using several examples.

EXAMPLE 1:

Consider the five gradation curves shown in Figure 2.5.



Curves 1, 2 and 3 (as labeled in the figure) are parallel and possess the same type gradation and a constant coefficient of uniformity (C_u). The percent gravel content however, varies from 95 percent for curve 1 to zero percent for curve 3, and the maximum grain size of curve 1 is much larger than that of curve 3. Thus, for a constant coefficient of uniformity, the higher the gravel content, the larger is the maximum particle size.

EXAMPLE 2:

The percent gravel content of curves 2 and 4, in Figure 2.5, is the same, 77%. The coefficient of uniformity however, varies from 2.8 for curve 2 to 4.0 for curve 4. Also, the maximum grain size of curve 2 is lower than that of curve 4. Thus, for a constant percent gravel content, the higher the coefficient of uniformity, the larger is the maximum grain size.

EXAMPLE 3:

The maximum particle size of the soils of curves 2 and 5 of Figure 2.5 is constant and equal to 1.6 inch (40 mm). The percent gravel content of curve 2 is 77% and that of curve 5 is 30%. Also, the coefficient of uniformity of the soils of curve 2 is 2.8 and that of curve 5 is 8.75. Thus, for a constant maximum particle size, the higher

the percent gravel content, the lower is the coefficient of uniformity.

EXAMPLE 4:

Consider curve 6 in Figure 2.5 relative to curves 2, and 3. From the figure, it can be seen that the three variables (coefficient of uniformity, grain size, and percent gravel content) of the soils of curve 6 are independently altered relative to the other five curves.

Furthermore, extra care should be taken when studying the effects of sample gradation (coefficient of uniformity), grain size, and percent gravel content on the shear strength of cohesionless soils. An arbitrary change in the sample gradation may lead to changes in the other two variables. Consequently, the effect of one variable may unseat the effects of the others.

2.2.3 EFFECT OF GRAIN SHAPE

The shape of a soil particle is generally described using two terms: particle angularity and particle sphericity. The former is a qualitative term used to describe the soil particle as rounded, subrounded, subangular or angular; whereas the latter is a quantitative term that can be obtained by measuring and calculating the proximity of a particle to a circumscribing sphere. This

calculation however, has not yet been standardized. Koerner (46) defined sphericity as the ratio of projected particle area to the area of the smallest circumscribing sphere; whereas Kolbuszewski (48) suggested the following expression:

$$PS = D_c/D_i \quad (2.1)$$

where: PS = particle sphericity;

D_c = the diameter of the circle whose area is equivalent to the area covered by the particle in question when laid on its longest side; and

D_i = the diameter of the circle inscribed into the same area.

The grain shape of granular soils have significant effect on their engineering properties. Thus, any study of the stress-strain characteristics of this type of soils shall consider the effect of their grain shape.

Holubec and D'Appolonia (37) studied the effects of particle shape on the maximum and minimum void ratios, and on the shear strength of cohesionless soils. They observed that the particle shape has a minor influence on the minimum void ratio, but a major influence on the maximum void ratio. Also, their test results have indicated that the shear strength of cohesionless soils increases with increasing particle angularity. That is, rounded particles possess lower shear strength than angular ones. In a similar study, Zelasko (87), concluded that the higher the angularity of

the soil particles, the higher the shear strength of the soil.

Koerner (46), evaluated the effects of particles angularity and sphericity on the shear strength of the soils. He concluded that the higher the angularity, and the lower the sphericity of the soil particles, the higher the shear strength of the soils. The angle of interlocking friction (ϕ_i) however, is not affected by the particle shape.

In a different type of study, Dickin (19) examined the influence of grain shape on the limiting porosities of cohesionless materials. Maximum porosity of the soil samples were determined by depositing the soil in water as suggested by Kolbuszewski (47). Minimum porosity, on the other hand, was obtained by vibrating the sample under water. He concluded that both maximum and minimum porosities decrease as the particle sphericity increases.

2.2.4 EFFECT OF RELATIVE DENSITY OR VOID RATIO

The relative density (D_r) of a cohesionless soil can be expressed in terms of its maximum, minimum, and natural densities (equation 2.2), or in terms of its maximum, minimum and natural void ratios (equation 2.3).

$$D_r(\%) = \frac{\gamma_{MAX}(\gamma - \gamma_{MIN})}{\gamma(\gamma_{MAX} - \gamma_{MIN})} \quad (2.2)$$

OR

$$Dr(\%) = \frac{e_{MAX} - e}{e_{MAX} - e_{MIN}} \quad (2.3)$$

where: Dr = relative density;

γ_{MAX} = the maximum obtainable density of the soil structure;

γ_{MIN} = the minimum possible density of the soil structure;

γ = the density of the soil specimen in question;

e_{MAX} = maximum void ratio;

e_{MIN} = minimum void ratio; and

e = the natural void ratio or the void ratio of the soil specimen in question.

The total shearing resistance of cohesionless soils is a function of their state of compaction or packing. This is generally expressed by the relative density of the soil. Increasing the relative density of a soil sample will increase its total shearing resistance (9, 13, 15, 35, 37, 46, 73, 81, and 83). Moreover, Siddiqi (73) concluded that the angle of internal friction of cohesionless soils increases linearly with increasing relative density.

2.2.5 EFFECT OF SPECIMEN SIZE

The non-uniformity of the stress distributions within a triaxial test specimen is mainly due to the effects of the friction at the end plates (72). This problem has been

under consideration by several investigators since the turn of the 19th century. Different assumptions were made and analytical solutions were published. These ranged from the linear elastic solution by Filon (28) using glued ends assumption, Pickett (69) using a multiple Fourier technique, D'Appolonia and Newmark (18) using a framework analogy, Balla (6) using plane assumption, and Moore (66) using unconfined specimen, to non-linear constitutive equations by Perloff and Pombo (68).

Since the specimen sides are free from shearing stress, the values of the shear stress ($\tau_{r,z}$) at the top and bottom ends of the specimen must be equal to zero. However, except for Filon's study, all the solutions involve relatively high values of shearing stress ($\tau_{r,z}$) at both ends of the specimen, and inconsistent values of the normal radial and circumferential stresses (τ_r , and σ_θ).

Experimental studies of the effects of end restraints on the shear strength of soils during compressive tests can also be found in the literature. The experimental work done by Taylor (76), and summarized by Rutledge (71) led to the conclusion that reliable test results could be obtained (with soil specimens having regular ends) provided that the length to diameter ratio of the specimen was in the range of 1.5 to 3.0. Consequently, triaxial test apparatus were standardized using regular ends with a length to diameter ratio of 2.0 to 2.5.

Later Rowe (70) introduced a combination of rubber sheeting and silicone grease to develop frictionless ends for triaxial compression test specimens. Barden and McDermott (7) tested compacted clay soils using lubricated and non-lubricated platens. They concluded that the effective strength parameters are the same when the results are compared using specimens with a length to diameter ratio of 2.0. The same conclusion was also reached by Bishop and Henkel (10) regarding the maximum angle of shearing resistance of the sand they tested. Duncan and Dunlop (26) concluded that "unless it is necessary to measure volumetric strains in drained tests on sand, the advantages gained from the use of lubrication are not worth the trouble".

Another aspect of the influence of sample size on the shear strength of soils in triaxial compression tests deals with the ratio of the specimen diameter to the maximum particle size of the soils. In an effort to study the effects of specimen diameter relative to the maximum particle size of the test materials, Vallergera et al (80) analysed Holtz's (35) test results and conducted new triaxial compression tests on cohesionless soils using 2.8 inch (71 mm) diameter specimens with particle sizes ranging from 0.01 to 0.2 inch (0.15 to 4.75 mm). The results of their investigations showed that drained strengths of the small size test specimens with high gravel contents were significantly higher than the strengths of the larger test

specimens. This finding coincided with those obtained by Marachi (61), and Donaghe and Cohen (20). Marachi used three different specimen sizes of 36, 12 and 2.8 inch (914, 305, and 71 mm) in diameter. For all tests, the specimen diameter to maximum particle size ratio was held constant at 6.0. He concluded that the angle of internal friction for the 36 inch (914 mm) diameter specimens was about 1.0 to 1.5 degrees lower than that of the 12 inch (305 mm) specimens, and 3 to 4 degrees lower than the 2.8 inch (71 mm) specimens. Nevertheless, for triaxial compression tests, the consensus between researchers is that the effect of the ratio of specimen diameter to the maximum particle size, on the compressive strength of cohesionless soils can be neglected if it is set at a value of 6.0 or better.

2.2.6 EFFECT OF MOISTURE CONTENT

The presence of moisture in cohesionless soils play two roles:

- a) it acts as a lubricant between particles causing the shear resistance to decrease; and
- b) it causes negative or positive pore water pressure in the sample prior to or during shear.

Since most of the shearing strength in cohesionless soils is mainly attributed to particles interlocking, the value of the total angle of internal friction (ϕ) is not appreciably different whether the soil is wet or dry (78).

Lee, Seed and Dunlop (55) studied the effects of moisture content on the shear strength of cohesionless soils. They conducted fully drained triaxial compression tests using oven dry, air dry and 100 percent saturated sands. They found that the oven dried sand was considerably stronger than the 100 percent saturated sand. The value of the shear strength of the air dried sand was intermediate between the two extremes.

For an intermediate degree of saturation (between zero and unity), the influence of surface tension between the water and the soil particles comes into play. Surface tension causes sand particles to adhere to each other due to capillary action. This gives rise to a phenomenon called apparent cohesion, i.e., sand may acquire tensile strength as a result of interparticle adhesion due to capillary action, or negative pore water pressure (2). Moreover, the apparent cohesion contributes an explanation for the bulking behavior of sands. A mass of dry sand if moistened and then shovelled and dropped loosely into a heap is subjected to volume increase. The finer the grains, the greater is the increase in volume. This volume change is also water content dependent. At water content of 5 to 6%, maximum bulking occurs. No bulking should take place for 100 percent saturated soil (2).

Hanyama (33) studied the effects of water content on the shearing characteristics of granular soils. He performed

drained triaxial compression tests on material having a range of particle size from 5 to less than 0.074 mm (passing sieve #200). He concluded that:

- a) The axial strain at failure, the critical void ratio, and the dilatency (volume change) of the sample decreases with increasing water content.
- b) The deviator stress at failure (the difference between the major and minor principle stresses at failure) increases in the range of water content from 5 to 10 percent, and decreases at approximately a constant rate with increasing water content above 10 percent.
- c) The angle of shearing resistance and the apparent cohesion of the soil sample were independently affected by its moisture content. For all samples with a relative density of more than 70 percent and a water content of lower than 10 percent, the angle of shearing resistance was constant, whereas it decreased for other values of relative density and water content. Also, for a range of water contents from 10 to 20 percent, and for any relative density of the sample, a maximum apparent cohesion value was noted. The apparent cohesion of the sample however, decreased considerably with an increase in moisture content above the 20 percent level.
- d) The decrease in the shear strength with an increase

in water content is due to the reduction of the structural effect (grain interlocking and particles rearrangement).

2.2.7 EFFECT OF CONFINING PRESSURE

In general, granular soils consist of discrete particles and are not readily influenced by surface type forces (83). Rather, the behavior of such soils is governed by gravitational and mechanical forces.

For a particular soil grain and mineral, the resistance to sliding at each contact point is directly proportional to the normal force at that point. Hence, the overall resistance to sliding increases as the confining stress in a triaxial chamber increases. This proportionality, however, is not linear. At a relatively high contact pressure (confining pressure), soil particles are forced to become flatter and the microscopic interlocking decreases. Consequently the shear deformation and the angle of sliding friction (ϕ_s) decreases. This phenomenon was widely observed and reported throughout the literature (9, 13, 38, 50, 61). Further, this type of sliding action causes no significant volume change.

The effect of the confining pressure on the interlocking angle of friction (ϕ_i) depends upon the initial packing of the test specimen. For initially loose soils, confining pressure will tend to compress the specimen resulting in a

denser packing and hence higher degree of interlocking. As the confining pressure increases, particles interlocking increases up to a certain point after which the pressure at contact points becomes critically high resulting in a breakdown of sharp corners and consequently a decrease in the degree of interlocking. For initially dense specimens, on the other hand, the breakdown of the particles takes place at lower confining pressure than that for loose specimens. Thus the angle of interlocking friction (ϕ_1) for dense specimens decreases with increasing confining pressure. Koerner (46) tested poorly graded sand using confining pressures of 10, 20 and 30 psi. He observed that the failure envelopes possessed a gradual increase in the strength intercept (apparent cohesion) due to interlocking of the large particles.

The effect of confining pressure on the total angle of internal friction (ϕ) is well documented in the literature (13, 35, 46, 50, 87). In General, the total angle of internal friction decreases with increasing confining pressure. This generalization however, may not hold for low values of confining pressure (0 to 50 psi) and for loosely packed soils (21).

2.3 MAXIMUM AND MINIMUM DENSITY

Maximum and minimum density values are used extensively to compute the relative density of the soil in question (see

equation 2.2). The relative density, on the other hand, is being used for control of compaction of cohesionless soils in earth fill structures, and for estimating the in-situ angle of internal friction. Thus, a reliable determination of the relative density of a natural soil deposit should be made prior to the estimation of its engineering behavior. Further, it should be noted herein that relative density alone is not sufficient to characterize the engineering properties of the soil. It is possible for two sands, for example, to have identical relative densities but significantly different engineering behavior.

Maximum and minimum density values of cohesionless soils are a function of several soil variables such as grain size and shape, grain size distribution, specific gravity, and test method. The latter had been standardized by the American Society for Testing and Material (ASTM), and the American Association of State Highway and Transportation Official (AASHTO) (1, and 3). These tests however, are limited and cannot be used for all types of soils. Consequently, researchers have used several different test procedures to study the effects of the soil variables on the maximum and minimum densities. In addition They have developed several criteria to estimate maximum and minimum densities that are based on elaborate test methods (86). If however, reliable estimations of the maximum and minimum densities can be made from soil index properties, then the

determination of relative density values for cohesionless materials will be greatly facilitated.

Hutchinson and Townsend (39) studied the effect of grain size distribution of fine and medium sands on their maximum and minimum densities. Maximum density tests were conducted using a vibrational method; while Kolbuszewski's (47) and Wu's (81) test procedures were utilized for the minimum density tests. They concluded that maximum and minimum densities can be expressed in terms of the slope of the grain size distribution curve, and the modal grain size diameter.

Johnston (43) used the U.S. Army Corps of Engineers standard test procedures to determine maximum and minimum densities of cohesionless soils. He developed an empirical correlation between maximum and minimum dry densities and the coefficient of uniformity of the soil. This is shown in Figure 2.6. Also, Youd (85) studied the effect of the coefficient of uniformity (C_u) on maximum and minimum void ratios (minimum and maximum densities) of sands using the ASTM standard test procedure D2049-69. Figure 2.7 depicts his test results (the maximum and minimum void ratios) plotted against the coefficient of uniformity for different particle angularity. It can be seen from the figure that the higher the coefficient of uniformity the lower the maximum and minimum void ratios. Also, the higher the angularity the higher the void ratios.

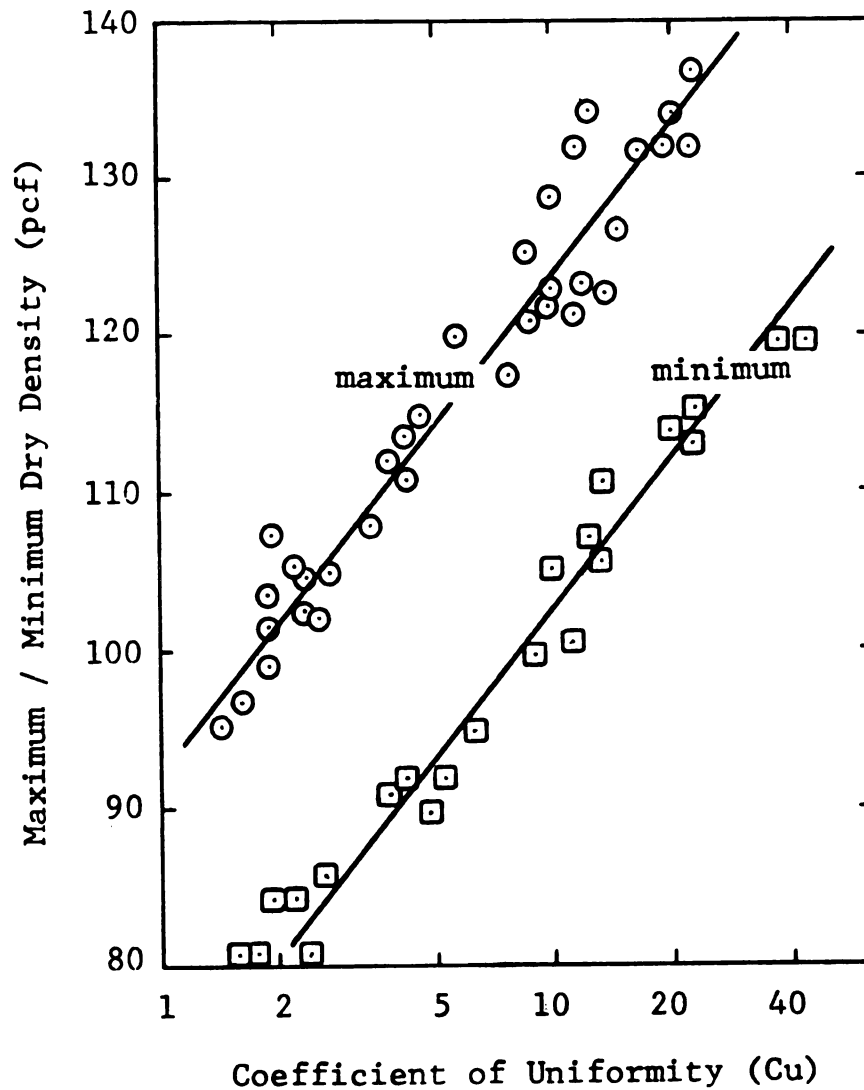


FIGURE 2.6 EMPIRICAL RELATIONSHIP BETWEEN MAXIMUM AND MINIMUM DRY DENSITIES AND COEFFICIENT OF UNIFORMITY (43).

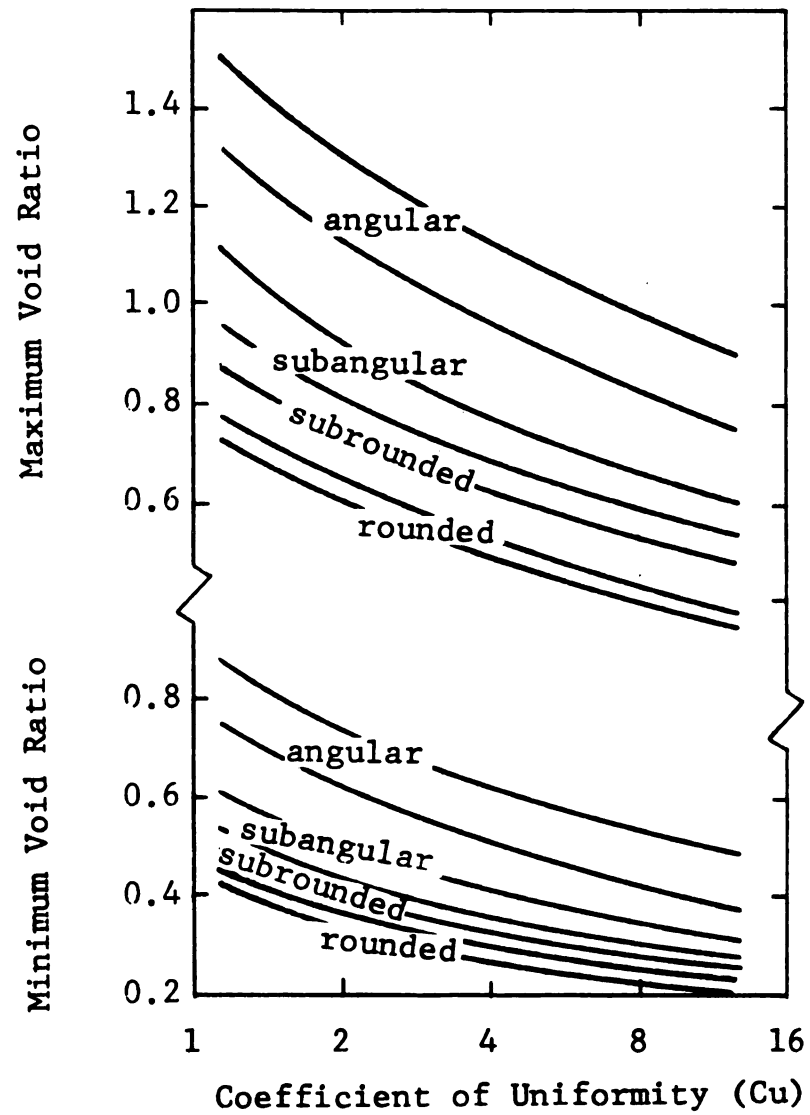


FIGURE 2.7 RELATIONSHIP BETWEEN MAXIMUM AND MINIMUM VOID RATIOS AND COEFFICIENT OF UNIFORMITY (85).

Korfiatis and Manikopoulos (49) correlated the maximum dry density of sands to their grain size distribution, percent fine content, and the volume of the fine material. Their correlations are based on theoretical formulations that were established using experimental results.

Edil et al (27) studied the effect of grain size and shape, and grain size distribution on the packing behavior of quartziferous sands. The packing behavior was evaluated with respect to the maximum and minimum void ratios. They concluded that the maximum and minimum void ratios and the void ratio spread (the difference between maximum and minimum void ratios) increases as the particle roundness decreases; and the better the sample gradation the lower the maximum and minimum void ratios and the void ratio spread. They also concluded that the particle size has a little to no influence on the packing behavior.

Finally, it should be noted that the relative density of a soil (also called the density index) is very sensitive to the values of the maximum and minimum densities of that soil. The reason being that the relative density is calculated (see equation 2.2) using the difference between the maximum and minimum densities. A variation in the value of the maximum or minimum density of one or two pounds per cubic foot may result in a difference of five to ten percent in the relative density value (34, 77, 79, and 85). Thus, extreme care should be taken during the tests as to obtain

reliable and reproduceble results.

2.4 ANGLE OF REPOSE

The angle of repose (ϕ_R) represents the angle of internal friction of a granular material at its loosest possible state (36, 38, and 50). Even though there is no relationship between the angle of repose and the angle of internal friction (ϕ) obtained from a triaxial compression test, the former can be used to represent the lowest possible boundary of the latter.

The angle of repose is measured by gently pouring a granular soil from a single point above a flat horizontal surface, the soil will form a conical pile. As more material is poured on the pile, the soil particles slip and slide down the slope to a stable position. The angle of this slope with respect to the horizontal plane is known as the angle of repose of the material.

As it may be expected, the angle of repose of a granular material is a function of the grain size and shape. Research in this area however, is very much limited to non-existence. Hough (38) presented a typical range of the angle of repose for different materials. His data are summarized in Table 2.1.

2.5 SUMMARY

The effects of grain characteristics, and sample and

test variables upon the shear strength of cohesionless soils were reviewed. It was found that:

- a) There are conflicting findings and opinions among researchers concerning the effects of grain size upon the shear strength of cohesionless soils. These are summarized in Table 2.2.
- b) Improving sample gradation may increase the shear strength of the soils.
- c) The shear strength increases as the particle angularity increases.
- d) The shear strength increases as the relative density of the test specimen increases.
- e) The effect of the maximum particle size (oversize particles) can be neglected if the ratio of specimen diameter to the maximum particle size of the soil is equal to or greater than six.
- f) The shear strength increases as the moisture content increases to a certain value after which it decreases.
- g) The shear strength decreases as the test confining pressure increases.

CHAPTER 3

TEST MATERIALS, SAMPLE MIXING AND TEST PROCEDURES

3.1 GENERAL

This chapter deals with the test material, sample mixing and preparations, sample installation in a triaxial cell, triaxial cell assembly, and the test procedures utilized in this research program. A basic knowledge of the components of the test system is hereby assumed. The conventional standard three inch-diameter triaxial test system is well documented and described throughout the literature.

3.2 TEST MATERIALS

The original material used in this investigation consists of a natural deposit of rounded to subrounded aggregates that were obtained from a local building supply shop. The aggregates consist of the following percent mixture by weight: granite 39%, sand stone 20%, meta-quartzite 11%, dolomite 11%, limestone 11%, and chert 8%.

Figure 3.1 depicts the grain size distribution curve of the natural (original) test material. The coefficient of uniformity (C_u), and the coefficient of curvature (C_c) are shown in the figure. The characteristics of the grain size distribution curve of the material and the breakdown of its

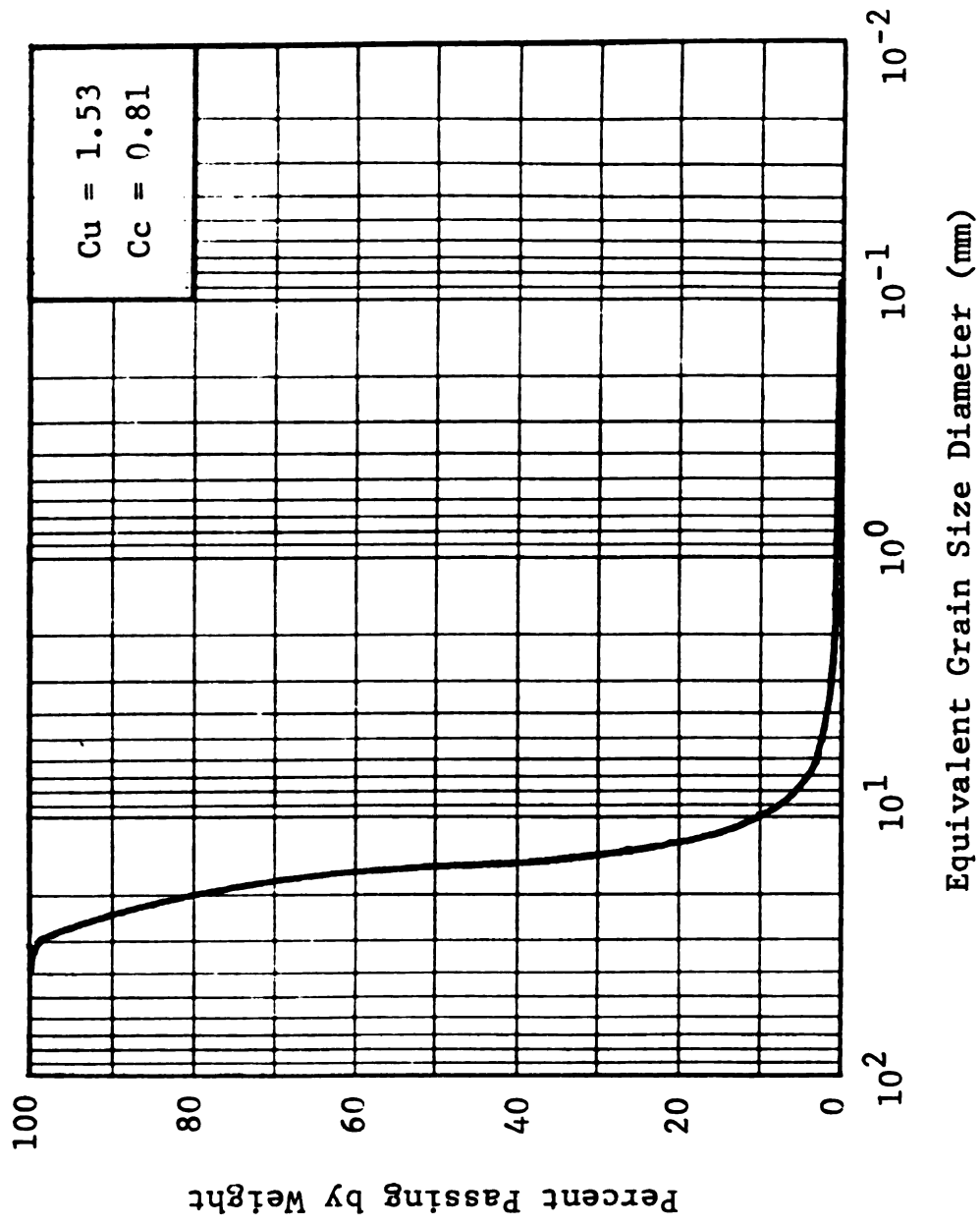


FIGURE 3.1 GRAIN SIZE DISTRIBUTION CURVE OF THE NATURAL TEST MATERIAL.

particle sizes are listed in Table 3.1. The material was classified as poorly graded gravel (GP) in accordance with the Unified Soil Classification System (USCS).

In order to generate different particle shapes (angularity), smaller particle sizes, and different grain size distribution curves than that shown in Figure 3.1, the natural material was crushed (using a Bico crusher, serial number 61561) and then pulverized (using a Bico pulverizer, serial number 61569). The crushed and pulverized materials were then sieved. The material retained on each sieve was then placed in a storage bag which was labeled according to the sieve size. Table 3.2 summarizes the grain sizes of the crushed and pulverized materials.

3.2.1 PARALLEL GRADATION CURVES

Recall that the objectives of this research study include the evaluation of the effects of grain size, sample gradation, and grain shape on the strength of cohesionless materials. In order to accomplish the second objective (the effects of sample gradation), two types of gradation curves were arbitrarily selected (curves A and B). The maximum particle size of the soil of curves A and B are 0.375 and 0.5 inches (9.53 and 12.7 mm) respectively. Their respective coefficients of uniformity are equal to 45.0 and 8.89. Thus, curve A can be described as very well-graded

TABLE 3.1 PERCENT GRAVEL AND SAND, COEFFICIENT OF UNIFORMITY, COEFFICIENT OF CURVATURE, AND CLASSIFICATION OF THE NATURAL TEST MATERIAL.

Soil Fraction or Component	Percent by Weight
* Coarse Grained Soil: - Gravel Coarse (75.000 to 19.000mm) 19.30 Fine (19.000 to 4.750mm) 77.20 - Sand Coarse (4.750 to 2.000mm) 2.00 Medium (2.000 to 0.425mm) 0.70 fine (0.425 to 0.075mm) 0.50	
* Fine Grained Soil: - Silt (less than 0.075mm) 0.30	
Coefficient of Uniformity (Cu) = 1.53 Coefficient of curvature (Cc) = 0.81 Classification According to USCS = <u>GP</u>	

1 inch = 25.4 mm.

TABLE 3.2 GRAIN SIZES OF THE CRUSHED AND PULVERIZED MATERIAL.

Sieve Size	Sieve Opening (mm)	Material size (mm)	Plastic bag Number
1/2"	12.700	-12.700	1/2
3/8"	9.500	-12.70, +9.500	3/8
4	4.750	-9.50, +4.750	4
8	2.360	-4.75, +2.360	8
16	1.180	-2.36, +1.180	16
30	0.600	-1.18, +0.600	30
50	0.300	-0.60, +0.300	50
100	0.150	-0.30, +0.150	100
200	0.075	-0.15, +0.075	200
pan	-	-0.075	Pan

1 inch = 25.4 mm.

while curve B as well graded.

To accomplish the first objective (the effects of grain size), two series of four and five additional curves were calculated that are respectively parallel to curves A and B. These two series of curves are designated series A and B. Figure 3.2 depicts series A curves, curve number (1) in the figure represents curve A while the curves numbered 2, 3, 4, and 5 are parallel to curve A or (1). Figure 3.3 shows series B curves. Again, curve number (1) in the figure represents curve B while curves number 2, 3, 4, 5, and 6 are parallel to curve B or (1). Finally, the parallel curves of series A and B were calculated using the following equation.

$$(PR)_{J,K} = (PR)_{J-1,K-1} \quad (3.1)$$

where: PR = percent retained on sieve J by weight;
 J = designate sieve number (J = 1 to 7); and
 K = curve number (K = 2 to 5 for series A and 2 to 6 for series B).

To summarize, Series A, consists of five parallel gradation curves that are labeled curve 1 through 5 in Figure 3.2. The coefficient of uniformity and the coefficient of curvature of all five curves are the same and equal to 45.0 and 1.58 respectively. Series B on the other hand, consists of six parallel gradation curves as shown in Figure 3.3. Again the coefficient of uniformity and the coefficient of curvature for all six curves are the same and

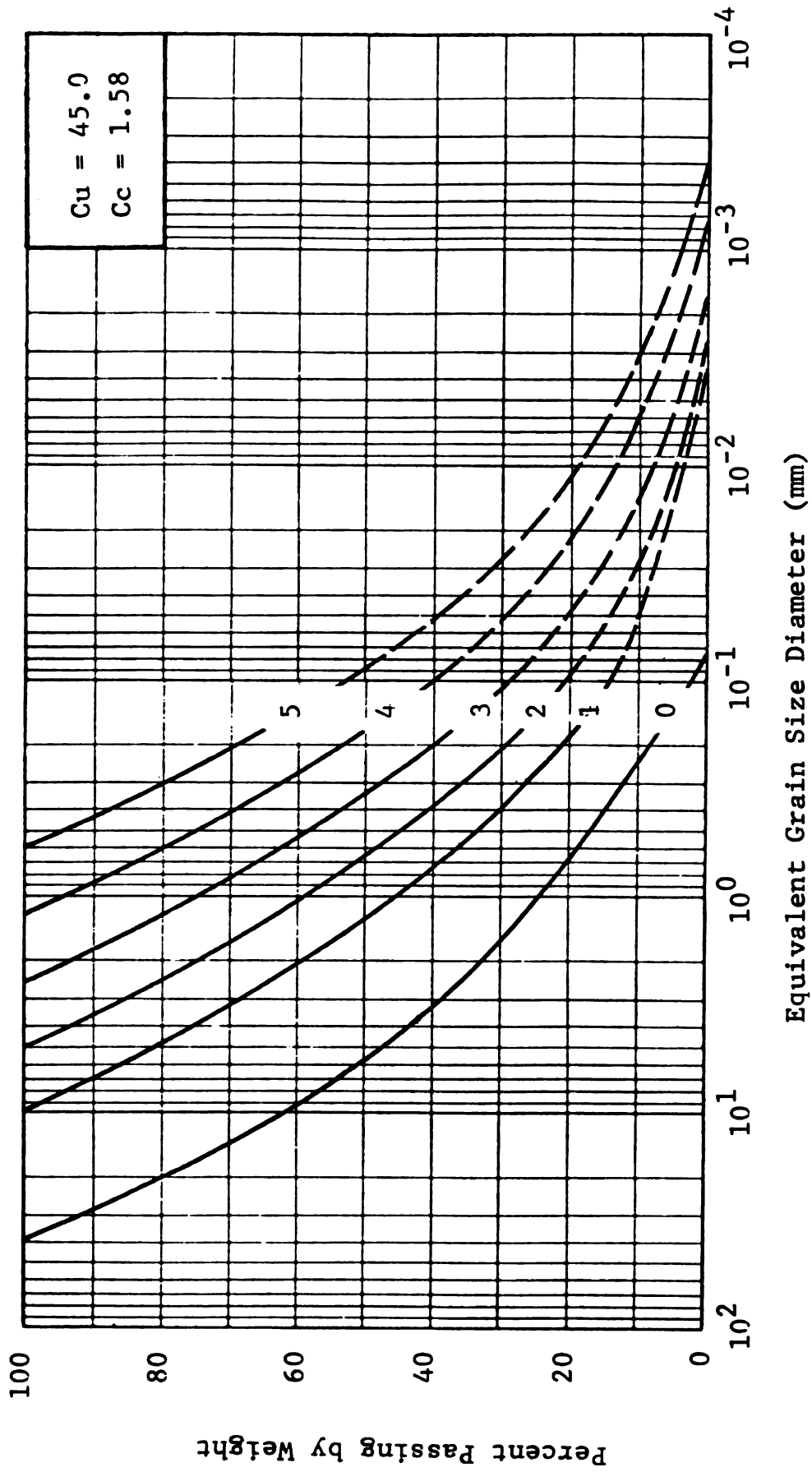


FIGURE 3.2 PARALLEL GRADATION CURVES, SERIES A.

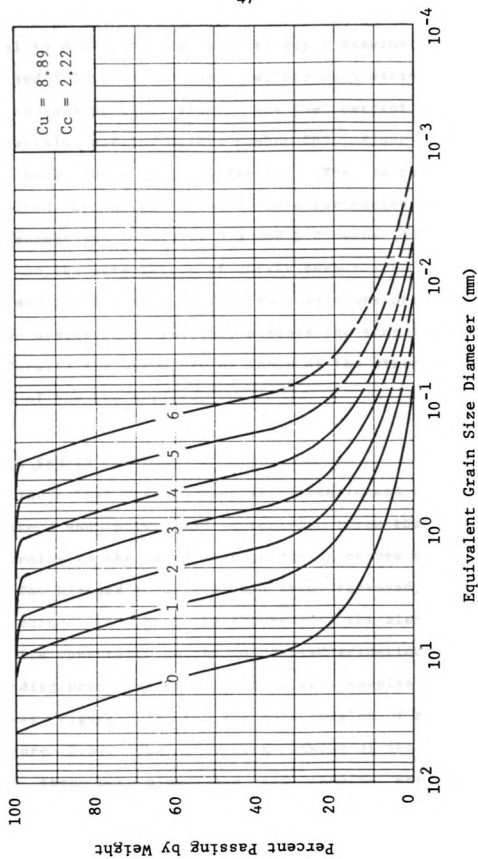


FIGURE 3.3 PARALLEL GRADATION CURVES, SERIES B.

equal to 8.89 and 2.22 respectively. Examination of Figures 3.2 and 3.3 indicates that, within each series, the maximum and average particle sizes, and the percent fine content (materials passing sieve number 200, finer than 0.074 mm) for each curve are different. The calculated percent retained by weight on each sieve for series A and B curves are summarized in Tables 3.3 and 3.4 respectively.

The characteristics of curves number zero (0) of Figures 3.2 and 3.3 are that no fine materials are present (passing sieve number 200); yet they possess the same coefficients of uniformity and curvature as those of the other curves within each of the two series.

3.2.2 SAMPLE BLENDING

The actual test samples were then formed by blending the crushed and pulverized materials (from the storage bags) according to the calculated gradation curves of series A and B. The blended materials were then resieved, weighed and recombined to check the accuracy of the blending procedure and its conformity to the calculated gradation curves. This blending procedure produced five soil samples of series A curves (Figure 2.3), and six soil samples of series B curves (Figure 3.3). The Atterberg limits of the fine materials were then determined and all samples were classified according to the USCS. Further, specific gravity tests were conducted on all samples. The Atterberg limits and specific

TABLE 3.3 CALCULATED PERCENT RETAINED BY WEIGHT ON EACH SIEVE FRACTION TO GENERATE FIVE PARALLEL GRADATION CURVES OF SERIES A, AND THE ZERO PERCENT FINE CURVE.

Sieve Number (J)	Sieve Size	Sieve Opening (mm)	% Retained by Weight, Sample No. (K)					
			0	1	2	3	4	5
-	1.50"	38.100	0	0	0	0	0	0
-	3/4"	19.050	19.20	0	0	0	0	0
-	3/8"	9.500	19.03	0	0	0	0	0
1	#4	4.750	14.08	19.20	0	0	0	0
2	#8	2.360	12.18	19.03	19.20	0	0	0
3	#16	1.180	9.42	14.08	19.03	19.20	0	0
4	#30	0.600	8.15	12.18	14.08	19.03	19.20	0
5	#50	0.300	5.93	9.42	12.18	14.08	19.03	19.20
6	#100	0.150	5.00	8.15	9.42	12.18	14.08	19.03
7	#200	0.075	7.00	5.93	8.15	9.42	12.18	14.08
Pan	-	-	0.00	12.00	17.93	26.08	35.50	47.68

1 inch = 25.4 mm.

TABLE 3.4 CALCULATED PERCENT RETAINED BY WEIGHT ON EACH SIEVE FRACTION TO GENERATE SIX PARALLEL GRADATION CURVES OF SERIES B, AND THE ZERO PERCENT FINE CURVE.

Sieve No. (J)	Sieve Size	Sieve Opening (mm)	% Retained by Weight, Sample Number (K)						
			0	1	2	3	4	5	6
-	1.5"	38.100	0	0	0	0	0	0	0
-	3/4"	19.050	29.59	0	0	0	0	0	0
-	3/8"	9.500	36.81	0.61	0	0	0	0	0
1	#4	4.750	13.81	28.98	0.61	0	0	0	0
2	#8	2.360	6.81	36.81	28.98	0.61	0	0	0
3	#16	1.180	4.15	13.81	36.81	28.98	0.61	0	0
4	#30	0.600	3.08	6.81	13.81	36.81	28.98	0.61	0
5	#50	0.300	2.07	4.15	6.81	13.81	36.81	28.98	0.61
6	#100	0.150	1.68	3.08	4.15	6.81	13.81	36.81	28.98
7	#200	0.075	2.00	2.07	3.08	4.15	6.81	13.81	36.81
	Pan	-	0.00	3.68	5.75	8.83	12.98	19.79	33.60

1 inch = 25.4 mm.

gravity test results, and the sample classification are summarized in Tables 3.5 and 3.6 for series A and B samples respectively. It can be noted from Tables 3.5 and 3.6 that all soil samples possess the same specific gravity. This was expected since the samples were made up from the same natural (original) materials.

Recall that all samples within any one series possess the same type of gradation, and that the maximum and average particle sizes and the percent fine by weight are different. The significance of this, in this study, is that the effects of sample gradation on the sample strength within any one series is eliminated. Thus, the effects of maximum particle size, or percent fine on sample strength can be had when the strength of all samples within a series are compared. On the other hand, the effects of gradation on sample strength, can be studied when the strength of any sample from one series is compared to that of the second series provided that both samples possess the same percent fine or maximum particle size.

Finally, samples 1 through 5 of series A, and 1 through 6 of series B were tested using a standard triaxial cell that can accomodate 3.00 inch (76.2mm) diameter specimen. Consequently, the maximum particle size of any soil specimen to be tested in such a set-up shall be restricted to one sixth of the specimen diameter. This shall eliminate or at least minimize the effects of the specimen size to maximum

TABLE 3.5 PERCENT GRAVEL, SAND, AND FINE CONTENT BY WEIGHT, ATTERBERG LIMITS, UNIFORMITY COEFFICIENT, COEFFICIENT OF CURVATURE, AND THE UNIFIED SOIL CLASSIFICATION SYSTEM OF ALL SAMPLES OF SET A.

Soil Fraction or Component	Sample Number (K)					
	0	1	2	3	4	5
* Coarse-Grained						
- Gravel						
Coarse	22.0	0.0	0.0	0.0	0.0	0.0
Fine	<u>30.0</u>	<u>19.2</u>	<u>0.0</u>	<u>0.0</u>	<u>0.0</u>	<u>0.0</u>
Total Gravel	52.0	19.2	0.0	0.0	0.0	0.0
- Sand						
Coarse	16.0	23.8	23.0	4.0	0.0	0.0
Medium	18.0	27.0	36.0	42.0	30.0	10.0
Fine	<u>14.0</u>	<u>18.0</u>	<u>23.1</u>	<u>27.9</u>	<u>34.5</u>	<u>52.3</u>
Total Sand	48.0	68.8	82.1	73.9	64.5	52.3
* Fine-Grained						
Silt	0.0	12.0	17.9	26.1	35.5	47.7
Uniformity Coefficient	45.0	45.0	45.0	45.0	45.0	45.0
Coefficient of Curvature	1.58	1.58	1.58	1.58	1.58	1.58
Atterberg Limits						
Liquid Limit	-	21.9	21.9	21.9	21.9	21.9
Plastic "	-	21.62	21.62	21.62	21.62	21.62
Plasticity Index	-	0.28	0.28	0.28	0.28	0.28
USCS Symbol	GW	SW-SM	SM	SM	SM	SM
Specific Gravity	2.74	2.74	2.74	2.74	2.74	2.74

TABLE 3.6 PERCENT GRAVEL, SAND, AND FINE CONTENT BY WEIGHT, ATTERBERG LIMITS, UNIFORMITY COEFFICIENT, COEFFICIENT OF CURVATURE, AND THE UNIFIED SOIL CLASSIFICATION SYSTEM OF ALL SAMPLES OF SET B.

[illegible]

particle size ratio on sample strength (see Chapter 2). Since the maximum particle size of series A and B samples (excluding samples number zero (0)) is equal to or less than 0.50 inch (12.7 mm), (see Tables 3.3 and 3.4) it resulted in a sample diameter to maximum particle size ratio of 6.0 or better.

3.2.3 GRAIN SHAPE

One of the objectives of this research study is to evaluate the effect of particle shape on the strength of cohesionless soils. As described in the previous section, soil samples of series A and B were prepared by using the crushed and pulverized material which, in general, consists of subangular to angular particles. The natural material, on the other hand, consists mainly of rounded to subrounded particles. In order to study the effect of the grain shape on the material strength, it was thought to blend the natural material to form samples that are in conformity with series A and B gradation curves. This would generate samples consist of rounded to subrounded particles and possess the same types of gradation as the subangular to angular samples. However, only a limited amount of the natural material having particle sizes smaller than sieve size number 8, 0.1 inch (2.4 mm) was available (see Figure 3.1). Consequently, only selected samples of series A and B were prepared and tested using the 100% natural, as well as

a combination by weight of 50% natural and 50% crushed and pulverized materials. Approximately, one ton of the natural material was sieved. Soil particles that passed through the 0.50 inch (12.7 mm) sieve were retained and stored in different plastic bags (see Table 3.2). A portion of this material (100% rounded to subrounded) was used to make up selected samples of series A and B. The other part was mixed with the crushed and pulverized materials to generate a combination by weight of 50% natural and 50% crushed and pulverized materials per each sieve fraction. This combination was also used to make up selected samples of series A and B.

To summarize, within each series, the soils were blended or combined to possess three different shapes :

- a) 100% subangular to angular (all samples);
- b) 100% rounded to subrounded (selected samples); and
- c) a combination of the above at 50% by weight for each sieve fraction (selected samples).

Grain shape herein is defined by sphericity and angularity of the particles. The particle shape of the natural, crushed and pulverized, and combined materials are described in detail in the following subsections.

3.2.3.1 PARTICLE SPHERICITY

Twenty five particles of the natural and crushed and pulverized material were randomly selected from each sieve

fraction (storage bag) and individually examined using a magnifying glass and a micrometer with an accuracy of 0.005 mm or an electron microscope (Olympus, Vanox). The electron microscope was used to measure only two dimensions of all particles passing sieve number 30 (finer than 0.6mm). Due to particle's surface roughness, the accuracy of the electron microscope was distorted when the height (the third dimension) of the particle was measured. The magnifying glass and the micrometer were used for all particles retained on sieve number 30 (coarser than 0.6 mm). All three dimensions of every particle were measured and designated as X, Y, or Z, where X represents the longest dimension while Z represents the shortest one as shown in Figure 3.4. The value of X (the particle's longest dimension) was also designated as the diameter of the smallest possible sphere that can contain the particle in question. The volume of the sphere (V_{SP}) was then approximated using equation (3.2).

$$V_{SP} = (4/3)\pi(X/2)^3 \approx X^3/2 \quad (3.2)$$

The sphericity (PS) of each particle was then calculated using the following equation:

$$PS = X^3 / [(X)(Y)(Z)] = X^2 / [(Y)(Z)] = (X/Y)^2 (Y/Z) \quad (3.3)$$

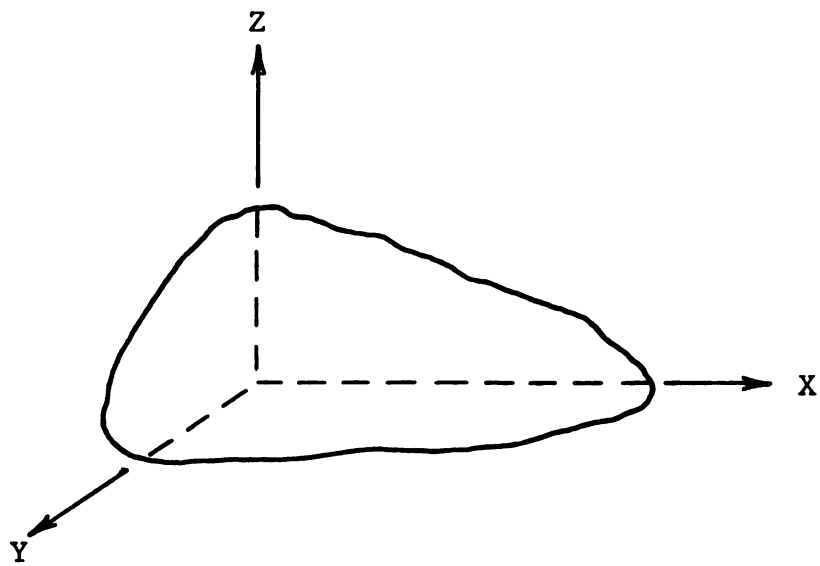


FIGURE 3.4 SCHEMATIC REPRESENTATION OF THE X, Y, Z DIMENSIONS OF A SOIL PARTICLE.

Beside quantifying the sphericity, the advantage of using equation (3.3) is that the terms (X/Y) and (Y/Z) can be also used to designate particle's elongation and flatness. For example:

$(X/Y) > 3.0$ describes an elongated particle,

$(Y/Z) > 3.0$ describes a flat particle.

As stated above, all particles passing sieve number 30 (finer than 0.6 mm) were examined using the electron microscope. The third dimension (Z) of these particles was not measured due to their surface roughness which distorted the focus of the microscope. Consequently, a statistical scheme was developed to estimate the third dimension of these particles.

Figures 3.5 and 3.6 show plots of the median values of all measured (X/Y) and (Y/Z) ratios versus particle grain size for the crushed and pulverized, and natural materials respectively. Each data point in the figures represents the median of 25 measurements. Examination of the figures indicates that the median values of the ratios (X/Y) and (Y/Z) are more or less constant and independent of the grain size in question. This observation was expected because of:

- a) the random nature of the crusher and pulverizer mechanisms (two disks counter rotating against each

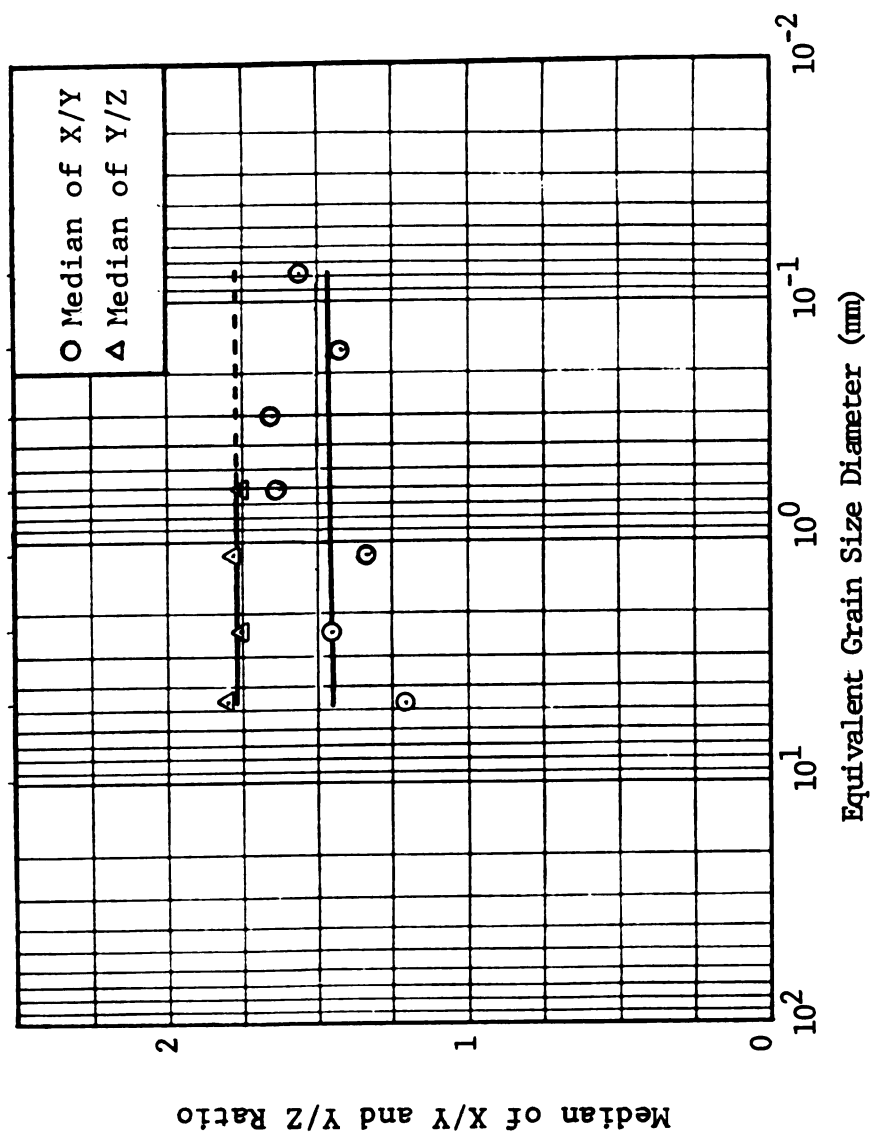


FIGURE 3.5 MEDIAN VALUES OF Y/Z AND X/Y RATIOS VERSUS EQUIVALENT GRAIN SIZE DIAMETER OF THE CRUSHED AND PULVERIZED MATERIAL.

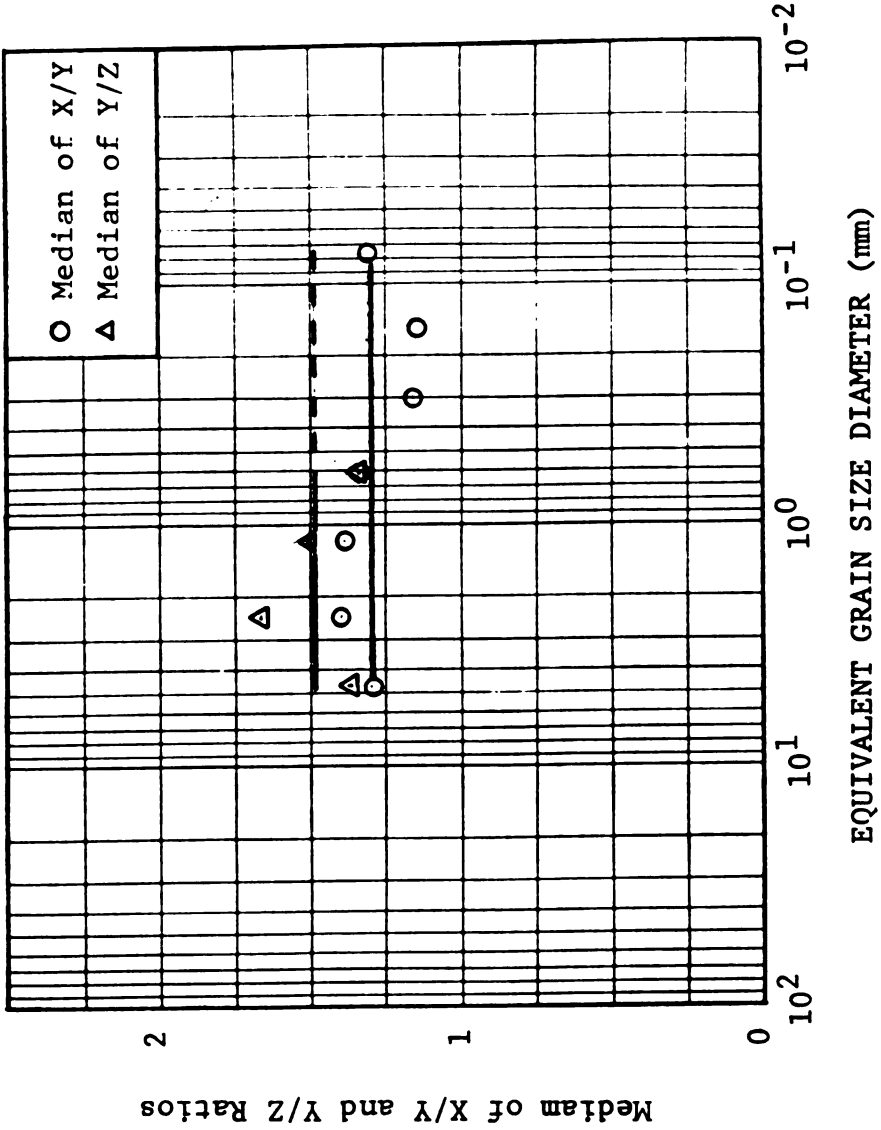


FIGURE 3.6 MEDIAN VALUES OF Y/Z AND X/Y RATIOS VERSUS EQUIVALENT GRAIN SIZE DIAMETER OF THE NATURAL MATERIAL.

other while the distance between them was varied randomly) which generated random particle breakage;

- b) the random natural weathering process to which the natural material was subjected to (the source of the natural material was the shore line of lake Michigan).

Therefore, it was assumed that the median value of (Y/Z) from the measured data (all particles coarser than 0.6 mm) can be extended to govern those particles finer than 0.6 mm. Such an assumption was found reasonable in lieu of all measured data and the median of (X/Y) . Consequently, it was decided to use the median value of (Y/Z) to calculate the (Z) dimension of all particles finer than 0.6 mm. Using this value however, in conjunction with the measured (Y) dimension of all particles finer than 0.6 mm to calculate their (Z) dimension was found unreasonable. The reason being is that the variation of (Y/Z) within each sieve was lost. Thus, another method was developed to retain the variation of said ratio while keeping the median of (Y/Z) compatible to that measured using particles from the other sieves. This method consists of the following steps:

- a) Assign all measured values of X , Y , and Z dimensions subscripts I, J where I indicates particle number ($I = 1$ to 25) and J indicates sieve number ($J = 1$ to 7). Sieve 1 being sieve number 4 and sieve 7 is sieve number 200.

- b) For all four sieves where $(Y)_{i,j}$, and $(Z)_{i,j}$ dimensions (of all 25 particles per sieve) were measured, calculate the ratio of $(Y/Z)_{i,j}$ and arrange them in 4 columns (one column per sieve) in a decending order. Thus, in column 1 (for sieve 1) $(Y/Z)_{1,1} > (Y/Z)_{2,1} > \dots > (Y/Z)_{25,1}$, and for column 2, $(Y/Z)_{1,2} > (Y/Z)_{2,2} > \dots > (Y/Z)_{25,2}$..etc.
- c) Calculate the average value $(Y/Z)_{i,av}$ for each row of the matrix $(Y/Z)_{i,j}$ using equation 3.4.

$$(Y/Z)_{i,av} = (1/4) \sum_{j=1}^4 (Y/Z)_{i,j} \quad (3.4)$$

- d) Use the calculated average ratio from equation (3.4), and the measured $(Y)_{i,j}$ dimension of all particles finer than 0.6 mm ($j = 5$ to 7) to calculate the $(Z)_{i,j}$ dimension using equation (3.5).

$$(Z)_{i,j} = (Y)_{i,j} / (Y/Z)_{i,av} \quad (3.5)$$

- e) Assign the calculated value of $(Z)_{i,j}$ to the i^{th} particle of the j^{th} sieve in question where Z was not measured.

As stated above, the advantage of this method is that the variation of the calculated dimension $(Z)_{i,j}$ is the same as the average variation of the measured ones. Tables (3.7) and (3.8) provide lists of the measured $(Y/Z)_{i,j}$ and

TABLE 3.7 MEASURED $(Y/Z)_{i,j}$ RATIO FOR THE TWENTY FIVE RANDOMLY SELECTED PARTICLES (I) PER SIEVE (J) OF THE CRUSHED AND PULVERIZED MATERIAL, AND THE CALCULATED AVERAGE $(Y/Z)_{i,av}$.

Particle Number I	Measured (Y/Z) _{I, J} of Particle I Retained on Sieve J				Calculated (Y/Z) _{I, AV}
	Sieve Size/Sive Number (J)				
	4/1	8/2	16/3	30/4	
1	1.00	1.10	0.97	1.00	1.02
2	1.02	1.11	1.03	1.00	1.04
3	1.11	1.15	1.07	1.21	1.14
4	1.13	1.19	1.15	1.23	1.18
5	1.19	1.21	1.18	1.38	1.24
6	1.19	1.23	1.32	1.41	1.29
7	1.24	1.30	1.36	1.42	1.33
8	1.27	1.38	1.36	1.42	1.36
9	1.41	1.50	1.55	1.56	1.51
10	1.43	1.53	1.64	1.57	1.54
11	1.43	1.58	1.65	1.60	1.57
12	1.58	1.71	1.78	1.69	1.69
13	1.81	1.75	1.82	1.75	1.78
14	1.82	1.88	1.85	1.77	1.83
15	1.87	2.24	1.85	1.83	1.95
16	1.93	2.40	1.96	2.00	2.07
17	1.94	2.43	2.00	2.00	2.09
18	2.22	2.44	2.43	2.20	2.32
19	2.38	2.75	2.57	2.29	2.50
20	2.59	2.79	2.65	2.44	2.62
21	2.76	3.19	2.69	2.90	2.89
22	2.77	3.20	2.70	3.13	2.95
23	2.80	3.33	3.00	3.60	3.18
24	2.82	4.50	3.20	4.00	3.63
25	3.85	4.86	4.30	4.40	4.15
Median	1.81	1.75	1.82	1.75	1.78

TABLE 3.8 MEASURED $(Y/Z)_{I,J}$ RATIO FOR THE TWENTY FIVE RANDOMLY SELECTED PARTICLES (I) PER SIEVE (J) OF THE NATURAL MATERIAL, AND THE CALCULATED AVERAGE $(Y/Z)_{I,AV}$.

Particle Number I	Measured (Y/Z) _{I, J} of Particle I Retained on Sieve J				Calculated (Y/Z) _{I, AV}
	Sieve Size/Sive Number (J)				
	4/1	8/2	16/3	30/4	
1	1.03	1.03	1.00	1.00	1.02
2	1.06	1.13	1.04	1.00	1.06
3	1.15	1.13	1.10	1.00	1.10
4	1.16	1.15	1.14	1.05	1.13
5	1.17	1.31	1.14	1.07	1.17
6	1.20	1.35	1.17	1.04	1.20
7	1.21	1.35	1.30	1.14	1.25
8	1.23	1.55	1.30	1.20	1.32
9	1.26	1.56	1.33	1.22	1.34
10	1.28	1.57	1.38	1.23	1.37
11	1.34	1.62	1.39	1.23	1.40
12	1.35	1.63	1.45	1.29	1.42
13	1.38	1.67	1.50	1.33	1.47
14	1.38	1.71	1.50	1.40	1.50
15	1.44	1.73	1.50	1.43	1.53
16	1.54	1.76	1.58	1.50	1.60
17	1.59	1.79	1.67	1.54	1.63
18	1.60	1.91	1.67	1.60	1.70
19	1.79	1.94	1.67	1.67	1.77
20	1.88	1.95	1.75	1.69	1.82
21	1.89	2.00	1.83	1.77	1.88
22	2.27	2.06	2.00	1.83	2.04
23	2.40	2.12	2.22	1.93	2.17
24	2.49	2.13	2.62	2.15	2.35
25	2.54	2.63	2.62	2.67	2.62
Median	1.38	1.67	1.50	1.33	1.47

calculated $(Y/Z)_{i,av}$ ratios for the crushed and pulverized, and natural materials respectively. Tables (A.1) and (A.2) of Appendix A provide lists of all measured and calculated $(X,Y,Z)_{i,j}$ for the crushed and pulverized, and natural materials respectively.

In addition, the sphericity $(PS)_{i,j}$ of all particles were calculated using equation (3.3). The average sphericity per sieve was then calculated. These values are listed in Tables (3.9) and (3.10) for the crushed and pulverized, and natural materials respectively.

The sphericity of the samples of series A and B were then calculated using the data from Tables 3.9 and 3.10 and equation 3.6.

$$(SS)_K = \frac{\sum_{J=1}^7 (PR/100)_J (PS)_{J,av}}{1.0 - (PF/100)_K} \quad (3.6)$$

where: $(SS)_K$ = sample sphericity;

PR = percent retained by weight;

PF = percent fine content by weight;

K = sample number (K = 1 to 5 for series A and 1 to 6 for series B);

J = sieve number (j = 1 to 7); and

$(PS)_{J,av}$ = average particle sphericity per sieve J.

Tables 3.11, and 3.12, summarize samples sphericity for the crushed and pulverized soil samples of series A and B

TABLE 3.9 PARTICLE SPHERICITY $(PS)_{I,J}$ FOR THE TWENTY FIVE RANDOMLY SELECTED PARTICLES (I) PER SIEVE (J) AND THE AVERAGE SPHERICITY $(PS)_{J,\Delta V}$ OF THE CRUSHED AND PULVERIZED MATERIAL.

Particle Number I	(PS) _{I,J} of Particle I Retained on Sieve J						
	Sieve Size/Sive Number (J)						
	4/1	8/2	16/3	30/4	50/5	100/6	200/7
1	4.77	1.81	5.16	2.84	2.16	5.74	2.31
2	1.71	5.14	4.68	10.56	7.03	2.32	3.38
3	3.02	3.46	2.80	2.82	1.22	4.24	1.44
4	2.75	7.59	3.88	4.20	3.89	2.73	1.88
5	3.27	6.33	2.34	7.61	3.23	11.84	2.01
6	2.74	8.08	1.87	2.83	6.05	4.99	1.84
7	4.01	3.35	9.45	4.86	4.24	5.80	7.23
8	2.31	2.73	4.89	16.81	4.25	3.58	4.87
9	2.62	3.60	4.02	6.06	3.37	5.68	5.30
10	3.26	4.80	6.82	2.59	4.80	1.90	1.84
11	3.51	2.24	6.18	6.08	6.97	1.93	5.85
12	2.96	7.77	3.13	6.94	3.74	6.49	9.23
13	2.18	4.67	2.86	2.29	2.52	4.54	2.78
14	2.22	5.76	2.50	4.25	4.17	5.16	4.44
15	4.12	2.40	2.32	4.13	2.46	1.99	2.61
16	5.50	6.39	6.33	4.08	5.08	6.01	8.61
17	2.30	2.57	4.25	4.21	2.49	3.50	14.46
18	2.74	3.84	3.25	9.34	4.13	5.30	3.51
19	1.66	9.24	4.84	11.36	10.89	1.93	1.85
20	1.75	1.16	6.78	2.19	12.93	5.83	3.94
21	2.75	4.55	2.08	3.85	8.01	2.43	5.67
22	1.42	3.28	3.38	5.35	10.46	3.93	3.70
23	1.73	3.61	1.93	7.11	5.66	1.99	14.55
24	3.69	2.66	2.00	20.06	11.04	12.06	20.07
25	2.90	4.63	8.37	3.77	14.23	3.83	3.17
Average	2.75	3.84	3.88	4.25	4.25	4.24	3.70

TABLE 3.10 PARTICLE SPHERICITY $(PS)_{I,J}$ FOR THE TWENTY FIVE RANDOMLY SELECTED PARTICLES (I) PER SIEVE (J) AND THE AVERAGE SPHERICITY $(PS)_{J,AV}$ OF THE NATURAL MATERIAL.

Particle Number I	(PS) _{I,J} of Particle I Retained on Sieve J						
	Sieve Size/Sive Number (J)						
	4/1	8/2	16/3	30/4	50/5	100/6	200/7
1	2.32	2.67	3.13	4.18	2.27	2.21	1.59
2	2.28	2.43	4.50	4.82	1.45	1.27	1.81
3	2.68	4.97	2.44	2.74	2.48	1.63	2.48
4	4.68	3.05	3.49	1.78	1.33	4.98	1.54
5	1.54	3.73	2.68	2.82	3.27	2.01	1.42
6	3.84	6.68	3.62	3.60	1.65	1.52	2.21
7	2.79	1.20	2.54	2.44	1.36	1.43	2.51
8	1.95	3.08	2.40	3.25	2.10	3.26	2.52
9	1.91	2.74	1.56	4.46	2.34	3.24	2.09
10	1.78	4.60	7.28	2.72	1.94	1.63	1.72
11	3.45	1.87	5.66	2.80	1.40	1.62	4.63
12	2.19	3.37	1.84	3.16	2.04	1.83	1.75
13	2.45	3.66	2.64	2.10	1.97	2.95	2.71
14	2.80	3.46	2.34	2.66	4.17	1.72	4.17
15	2.81	2.47	3.26	2.08	1.59	1.60	1.94
16	3.26	2.07	2.78	2.72	2.78	2.68	5.93
17	2.44	2.50	4.34	1.54	1.68	2.12	3.00
18	2.67	3.17	4.92	3.89	1.82	8.40	1.70
19	3.55	2.73	1.62	5.56	2.19	3.05	2.55
20	1.76	4.12	3.19	2.81	1.82	2.84	2.07
21	2.84	1.79	1.68	1.64	2.14	2.65	3.46
22	2.82	2.65	3.28	2.13	2.16	2.23	8.16
23	3.43	3.38	2.16	1.00	3.39	2.47	3.03
24	2.70	1.83	3.15	2.59	3.74	5.80	3.56
25	2.58	2.85	2.24	2.74	3.32	4.18	8.32
Average	2.70	3.03	3.15	2.89	2.26	2.77	3.07

**TABLE 3.11 SAMPLE SPHERICITY (SS) AND ANGULARITY (SA) OF
SERIES A OF THE CRUSHED AND PULVERIZED MATERIAL.**

Sieve Size (J)	Sample Number (I)									
	1		2		3		4		5	
	PS _J	PA _J	PS _J	PA _J	PS _J	PA _J	PS _J	PA _J	PS _J	PA _J
+3/8" -# 4	0.55	0.66	-	-	-	-	-	-	-	-
+# 4 -# 8	0.85	0.66	0.86	0.66	-	-	-	-	-	-
+# 8 -# 16	0.60	0.45	0.81	0.61	0.82	0.62	-	-	-	-
+# 16 -# 30	0.50	0.39	0.58	0.46	0.79	0.62	0.79	0.62	-	-
+# 30 -# 50	0.55	0.34	0.71	0.44	0.82	0.51	1.10	0.69	1.11	0.69
+# 50 -#100	0.38	0.28	0.44	0.33	0.56	0.42	0.65	0.49	0.88	0.66
+#100 -#200	0.32	0.19	0.44	0.26	0.51	0.30	0.67	0.39	0.77	0.45
Total	3.75	2.97	3.84	2.76	3.50	2.47	3.21	2.19	2.76	1.80
SS/SA	4.26	3.38	4.68	3.36	4.74	3.34	4.98	3.40	5.28	3.44

SS = sample sphericity. PS_J = particle sphericity of sieve J
SA = sample angularity. PA_J = particle angularity of sieve J

TABLE 3.12 SAMPLE SPHERICITY (SS) AND ANGULARITY (SA) OF SERIES B OF THE CRUSHED AND PULVERIZED MATERIAL.

Sieve Size (J)	Sample Number (I)											
	1		2		3		4		5		6	
	PS _J	PA _J	PS _J	PA _J	PS _J	PA _J	PS _J	PA _J	PS _J	PA _J	PS _J	PA _J
+3/8" -# 4	0.85	1.02	-	-	-	-	-	-	-	-	-	-
+# 4 -# 8	1.65	1.27	1.32	1.02	-	-	-	-	-	-	-	-
+# 8 -# 16	0.59	0.44	1.56	1.19	1.26	0.95	-	-	-	-	-	-
+# 16 -# 30	0.28	0.22	0.57	0.45	1.52	1.19	1.22	0.96	-	-	-	-
+# 30 -# 50	0.24	0.15	0.39	0.25	0.80	0.50	2.13	1.33	1.72	1.07	-	-
+# 50 -#100	0.14	0.11	0.19	0.14	0.32	0.24	0.64	0.48	1.70	1.27	1.37	1.02
+#100 -#200	0.11	0.07	0.17	0.10	0.23	0.13	0.37	0.22	0.75	0.44	2.01	1.17
Total	3.86	3.28	4.20	3.15	4.13	3.01	4.36	2.99	4.17	2.78	3.38	2.19
SS/SA	4.01	3.41	4.46	3.35	4.53	3.30	5.01	3.43	5.19	3.46	5.09	3.30

SS = sample sphericity. PS_J = particle sphericity of sieve J
 SA = sample angularity. PA_J = particle angularity of sieve J

respectively. The samples sphericity of the 100% natural and 50% combined materials of series A and B are listed in Table 3.13.

3.2.3.2 PARTICLE ANGULARITY

Particle angularity is a measure of the degree of curvature of the particle. In qualitative terms, particle's angularity can be described as rounded, subrounded, subangular, or angular. Particle's angularity, in this study is quantified using a scale from 1.0 to 4.0 as shown in Figure 3.7. A value of 1.0 describes a perfectly rounded particle, while a value of 4.0 describes an angular particle.

As noted above, 25 particles per sieve (per storage bag) were randomly selected and examined using a magnifying lense or an electron microscope. After measuring the dimensions of each particle, a schematic diagram of its general shape was made and its angularity was qualitatively described. Later a quantitative value was assigned based on Figure 3.7. Tables 3.14, and 3.15 provide lists of particle's angularity $(PA)_{i,j}$ as well as the average particle's angularity per sieve $(PA)_{i,\Delta v}$ for all crushed and pulverized, and natural materials respectively.

The angularity of series A and B samples were then calculated using the data in Tables 3.14 and 3.15 and the following equation.

TABLE 3.13 SAMPLE SPHERICITY (SS) AND ANGULARITY (SA) OF SERIES A AND B OF THE NATURAL AND 50/50 MATERIALS.

Sieve Size (J)	Sample Number (I)/Soil Series (Material)									
	1/A(N)		2/A(N)		3/A(N)		1/A(C)		4/B(N)	
	PS _J	PA _J	PS _J	PA _J	PS _J	PA _J	PS _J	PA _J	PS _J	PA _J
+3/8" -# 4	0.52	0.29	-	-	-	-	0.54	0.48	-	-
+# 4 -# 8	0.58	0.29	0.58	0.29	-	-	0.71	0.47	-	-
+# 8 -# 16	0.44	0.32	0.60	0.43	0.60	0.43	0.52	0.38	0.02	0.01
+# 16 -# 30	0.35	0.29	0.41	0.33	0.55	0.45	0.42	0.34	0.84	0.68
+# 30 -# 50	0.21	0.14	0.28	0.18	0.32	0.21	0.38	0.24	0.83	0.55
+# 50 -#100	0.23	0.14	0.26	0.16	0.34	0.20	0.30	0.21	0.38	0.23
+#100 -#200	0.18	0.09	0.25	0.12	0.27	0.14	0.25	0.14	0.21	0.10
Total	2.51	1.56	2.38	1.51	2.10	1.43	3.12	2.26	2.28	1.57
SS/SA	2.85	1.77	2.90	1.84	2.85	1.94	3.55	2.57	2.62	1.80

SS = sample sphericity. PS_J = particle sphericity of sieve J
 SA = sample angularity. PA_J = particle angularity of sieve J
 1A(N) = sample one, series A, natural material.
 1B(C) = sample one, series B, combined material (50/50).

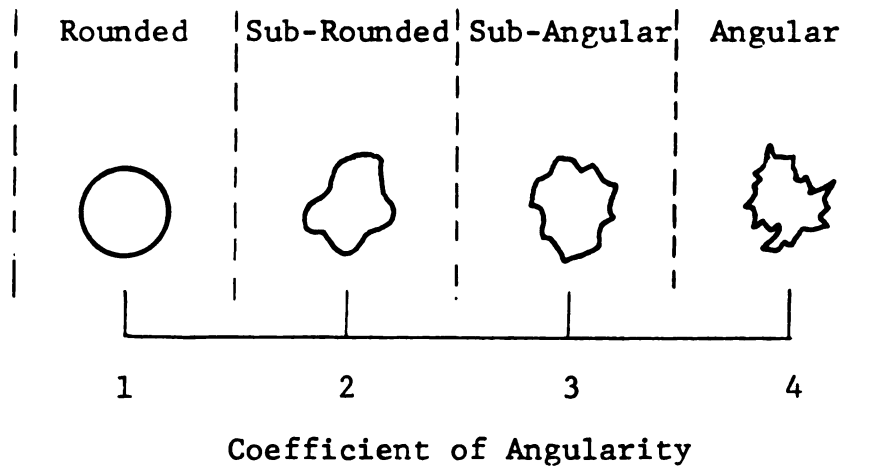


FIGURE 3.7 A SCHEMATIC REPRESENTATION OF PARTICLE ANGULARITY AND ITS QUANTIFYING SCALE.

TABLE 3.14 PARTICLE ANGULARITY $(PA)_{I,J}$ FOR THE TWENTY FIVE RANDOMLY SELECTED PARTICLES (I) PER SIEVE (J) AND THE AVERAGE ANGULARITY $(PA)_{J,AV}$ OF THE CRUSHED AND PULVERIZED MATERIAL.

Particle Number I	$(PA)_{I,J}$ of Particle I Retained on Sieve J						
	Sieve Size/Sieve Number (J)						
	4/1	8/2	16/3	30/4	50/5	100/6	200/7
1	4.00	3.50	2.50	3.00	3.50	3.50	4.00
2	3.50	3.50	3.00	2.50	3.50	4.00	3.50
3	3.50	3.00	3.50	2.50	3.50	3.50	3.50
4	2.00	4.00	3.00	3.00	3.50	3.50	3.50
5	2.00	3.00	4.00	2.50	3.50	3.50	3.00
6	3.50	4.00	3.00	2.50	3.50	3.50	3.50
7	4.00	4.00	4.00	3.00	3.50	3.50	3.00
8	3.50	4.00	3.00	3.00	4.00	3.50	3.50
9	3.00	2.50	3.50	3.00	4.00	3.50	3.00
10	4.00	3.50	3.50	2.50	4.00	3.50	3.00
11	3.00	3.00	3.50	3.50	3.50	3.50	3.50
12	3.50	3.50	3.50	3.50	3.50	3.50	3.00
13	4.00	3.50	2.50	2.50	3.50	3.50	3.00
14	3.50	3.50	2.50	3.00	4.00	3.50	3.50
15	3.00	4.00	3.00	3.00	3.50	3.50	3.00
16	3.50	2.50	3.50	3.00	4.00	3.50	3.00
17	3.50	3.00	3.50	2.50	3.00	3.00	3.00
18	3.00	3.00	3.50	3.00	3.00	3.50	3.50
19	4.00	3.50	4.00	3.00	3.50	3.50	3.50
20	3.40	4.00	3.00	3.50	4.00	3.50	3.00
21	4.00	4.00	3.00	3.50	3.50	3.50	3.00
22	3.50	4.00	3.00	3.00	4.00	3.00	3.00
23	3.50	4.00	2.50	3.50	4.00	3.00	3.00
24	4.00	3.00	3.00	4.00	3.00	3.50	3.00
25	4.00	3.00	3.50	2.50	3.50	3.50	3.00
Average	3.46	3.46	3.24	3.24	3.60	3.46	3.18

TABLE 3.15 PARTICLE ANGULARITY $(PA)_{I,J}$ FOR THE TWENTY FIVE RANDOMLY SELECTED PARTICLES (I) PER SIEVE (J) AND THE AVERAGE ANGULARITY $(PA)_{J,\Delta v}$ OF THE NATURAL MATERIAL.

Particle Number I	$(PA)_{I,J}$ of Particle I Retained on Sieve J						
	Sieve Size/Sieve Number (J)						
	4/1	8/2	16/3	30/4	50/5	100/6	200/7
1	1.50	1.50	2.00	2.50	1.50	1.50	1.50
2	1.50	1.50	3.00	2.50	1.50	1.50	1.50
3	1.50	1.50	2.00	2.00	1.50	1.50	1.50
4	1.50	1.50	2.00	2.50	1.50	3.00	1.50
5	1.50	1.50	2.00	3.50	1.50	2.50	1.50
6	1.50	1.50	2.00	2.00	1.50	1.50	1.50
7	1.50	1.50	2.00	3.00	1.50	1.50	1.50
8	1.50	1.50	2.00	3.00	1.50	2.00	2.00
9	1.50	1.50	2.00	2.00	1.50	2.00	2.50
10	1.50	1.50	2.00	2.00	1.50	1.50	1.50
11	1.50	1.50	3.00	2.00	1.50	1.50	2.00
12	1.50	1.50	2.50	2.00	1.50	1.50	2.00
13	1.50	1.50	3.00	2.00	1.50	2.50	1.50
14	1.50	1.50	2.00	2.50	1.50	1.50	1.50
15	1.50	1.50	3.00	2.00	1.50	1.50	1.50
16	1.50	1.50	2.00	2.00	1.50	2.00	1.50
17	1.50	1.50	2.50	2.00	1.50	1.50	1.50
18	1.50	1.50	3.00	3.00	1.50	2.00	2.00
19	1.50	1.50	2.00	3.00	1.50	2.00	2.00
20	1.50	1.50	2.00	3.00	1.50	2.00	2.00
21	1.50	1.50	2.00	3.00	1.50	1.50	1.50
22	1.50	1.50	2.00	2.00	1.50	1.50	1.50
23	1.50	1.50	2.00	1.50	1.50	1.50	1.50
24	1.50	1.50	2.00	2.50	1.50	2.00	1.50
25	1.50	1.50	2.00	2.00	1.50	1.50	1.50
Average	1.50	1.50	2.24	2.36	1.50	1.66	1.50

$$(SA)_K = \frac{\sum_{J=1}^7 (PR/100)_J (PA)_{J,AV}}{1.0 - (PF/100)_K} \quad (3.7)$$

where: SA = sample angularity;
 PR = percent retained on sieve J by weight;
 PF = percent fine content by weight (PF = 0.0 to 1.0);
 J = sieve number;
 K = sample number; and
 (PA)_{J,AV} = average particle angularity per sieve J

The angularity of all the samples of series A and B are summarized in Tables 3.11, 3.12, and 3.13.

3.3 SAMPLE MIXING PROCEDURE

Recall that the crushed and pulverized materials were sieved and separated into different storage bags, and two series of gradation curves were calculated. The test samples that corresponding to each gradation curve were then formed by blending the appropriate amount of materials from each plastic bag. The following sample mixing procedure was established and followed throughout this study.

- a) Estimate the total weight (W) of the soil sample to be tested. This weight will vary and it depends on the type of test and the relative density of the sample.

- b) Calculate the weight of the material $(W)_J$ required from each sieve fraction (each plastic bag) using the following equation:

$$(W)_J = (W)(PR)_J \quad (3.8)$$

where: (W) = total sample weight from step (a) above;

$(PR)_J$ = percent retained on sieve J (from Tables 3.3 or 3.4.

- c) Obtain the material from plastic bag J (corresponding to sieve J) and weigh it to nearest 0.1 gr from the calculated value of $(W)_J$.
- d) Repeat step (c) above for all sieves.
- e) Combine all weighted materials and mix thoroughly to form the soil sample with the desired density.

3.4 TEST PROCEDURES

Five different tests were conducted on all samples. These are: angle of repose, maximum and minimum density, static triaxial test, and volume change due to the application of the confining pressure. The test procedure for each of these tests is outlined in the following subsections.

3.4.1 ANGLE OF REPOSE

Several different test procedures were used to measure the angle of repose of all samples. the following method was

proven to be the most reliable and yielded consistent test results with the lowest value of the angle of repose. The test equipment consisted of:

- a) three-inch diameter Shelvy tube (the four connection holes were closed);
- b) two plastic caps;
- c) a protractor;
- d) a camera;
- e) a flat and horizontal surface; and
- f) a 4"x4" plate.

The test procedure consisted of the following steps:

- a) Mix 4.5 pounds (about 2000 gr) of the appropriate material (crushed and pulverized, natural, or a combination of 50/50 percent by weight) to form the sample to be tested using the sample mixing procedure as outlined in section 3.3 above.
- b) Place the bottom cap on the Shelvy tube and place the tube in the upright position on the horizontal and flat surface.
- c) pour the materials gently into the shelvy tube (to avoid particle segregation, incline the shelvy tube so that the materials will slide slowly against the tube's wall).
- d) Place the top cap on the Shelvy tube.
- e) Lay the tube down horizontally on the flat surface and loosen up the soil by gently rolling the tube on

the surface.

- f) Uncap the bottom end of the tube.
- g) Hold the 4"x4" plate flat against the bottom end of the tube.
- h) Let the tube stand in the upright position on the flat surface.
- i) Withdraw the plate from the bottom end of the tube.
- j) Uncap the top of the tube.
- k) Lift the tube slowly upward and let the soil fall to form a pile.
- l) When the tube is empty, place it on the side. Do not disturb the soil.
- m) Take a picture of the pile of soil with the camera centered parallel to the flat surface.
- n) Gently, slide the protractor into the pile and measure the slope of the pile relative to the horizontal surface.
- o) Repeat step (n) above at three to six different locations of the pile.
- p) If the measured angle of repose from all locations showed a variation of more than four degrees, then restart from step b above.
- q) Calculate the angle of repose as the average value of all measurements.
- r) Keep the developed picture for your record.

3.4.2 MAXIMUM AND MINIMUM DENSITY TESTS

Standard maximum density test procedures (ASTM, AASHTO,...etc.) were not followed in this study. This is due to the variables being analysed. The standard test procedure calls for compacting the samples if the percent fine content (-number 200 sieve) exceeds 15%. This resulted in particles breakdown and consequently altered the sample gradation and the particle sizes. Therefore, a modified version of the standard test procedures were developed for all samples whereby the sample gradation, particle size and percent fine would not change after the test. The standard minimum density test (ASTM D-4254) was also modified and used in this study.

3.4.2.1 MAXIMUM DENSITY TEST

The equipment consisted of:

- a) a standard 1/30 cubic foot compaction mold;
- b) a standard 15 pounds asphalt cement compaction hammer;
- c) a straight edge;
- d) a balance with sensitivity of 0.5 gr; and
- e) a vibrating table (modified from a Cenco-Meizer sieve shaker made by Central Scientific Company. The vibration frequency and amplitude were set to maximum).

A step by step test procedure is outlined below:

- a) Estimate the sample maximum density.
- b) Calculate the amount of materials required to fill up the compaction mold using the estimated maximum density.
- c) Mix the sample using the procedure outlined in section 3.3 above.
- d) Oven dry the materials over night under 230 F (110 C).
- e) weigh the compaction mold with the base plate attached, record this weight on a data sheet as (W_M).
- f) Attach the mold's collar.
- g) Place the mold on top of the vibrating table.
- h) Divide the soil to four equal parts.
- i) Place one quarter of the soil (one layer) in the compaction mold.
- j) Place the hammer in a vertical position on top of the soil; the hammer is being used as a surcharge.
- k) Vibrate the soil for a period of 2 minutes, during this period hold the hammer down and keep it in the vertical position.
- l) Turn the vibrator off while holding the hammer down against the soil. This is crucial to the test result because as you turn the vibrator off its frequency may cross-over the natural frequency of the system causing high amplitude.

- m) Repeat steps (j, k, and l) for the other three layers.
- n) For the last layer, the mold should slightly overflows with soil.
- o) Accurate estimation of the amount of the material to fill-up the mold is desired (see notes 1 and 2 below).
- p) Remove the hammer and place it on the side.
- q) Remove the mold from the vibrating table and disattach its collar.
- r) Trim-off the excess soils using the straight edge.
- s) Weigh the mold with soils and record the weight on the data sheet as (W_T).
- t) Calculate the maximum density using equation (3.9).

$$\gamma_{MAX} = (W_T - W_M)/V \quad (3.9)$$

where: γ_{MAX} = maximum density (pcf);

W_M = weight of the compaction mold;

W_T = total weight of mold plus soil; and

V = volume of the mold.

- u) Retain the material for minimum density test.

NOTE 1

If the required weight of the material to form the sample is significantly over-estimated then the extra material should not be used to overflow the mold. This may cause fine particles to settle in

between coarser ones which may result in higher percent fine than required.

NOTE 2

If the required weight of the material to form the sample is significantly underestimated then additional soils mixing is required, This may lead to non-uniform sample.

For these two cases, another estimation of the maximum dry density shall be made for the given test and the material shall be remixed accordingly. i.e. repeat the test.

3.4.2.2 MINIMUM DENSITY TEST

The equipment consisted of:

- a) a standard 1/30 cubic foot compaction mold;
- b) a spoon;
- c) a straight edge; and
- d) a balance sensitive to 0.5 gr.

The test procedure consisted of the following steps:

- a) Use the same material from the maximum density test.
- b) Weigh the compaction mold with the base plate attached, record this weight on a data sheet as (W_M).
- c) Place one spoonful of soil into the mold at a time, until the mold is full, care should be exercised not

to disturb the soils in the mold.

- d) Trim off excess materials using the straight edge.
- e) Remove the mold's collar.
- f) Weigh the mold with the soil and record this weight on the data sheet as (W_T).
- g) Calculate the minimum density using equation (3.10).

$$\gamma_{MIN} = (W_T - W_M) / V \quad (3.10)$$

where: γ_{MIN} = minimum density (pcf); and

V = the volume of the mold.

- h) Sieve the materials and place it back in the appropriate storage bag according to their grain sizes.

3.4.3 STATIC TRIAXIAL TEST

The apparatus consisted of:

- a) modified Wykeham Farrance (WF 10791) two parts 3 inch split mold sampler, see Figure 3.8.
- b) rubber membrane (Soil Test T612).
- c) General Electric vacuum pump with adjustable vacuum pressure (0.0 to 25 inch mercury), and a vacuum gauge.
- d) one pound hammer with 2 inch diameter base surface.
- e) four inch diameter membrane stretcher.
- f) Wykeham Ferrance loading frame (WF-10070), Triaxial cell (WF-10755-sp), 3 inch diameter base pedestal (WF-10783), top cap (WF-10760), O-ring (WF-10830),

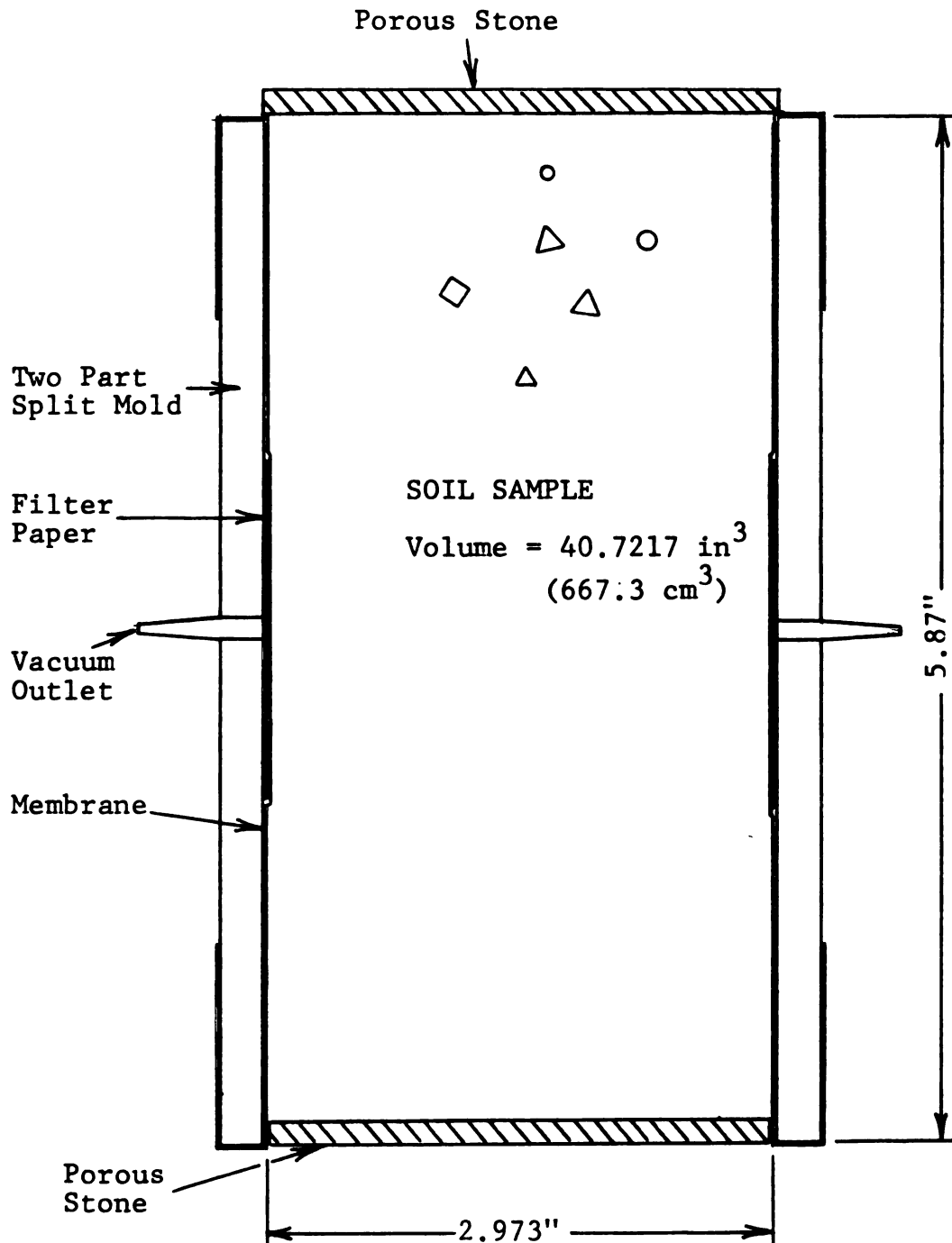


FIGURE 3.8 SCHEMATIC DIAGRAM OF THE SPLIT MOLD OF THE TRIAXIAL APPARATUS.

porous discs (WF-10840), and pressure gauge (WF-11660).

- g) Fairchild pressure regulator (model 10).
- h) Schaevitz linear variable differential transducer (LVDT) model (GCA-121-500), power supply (PCB-501), power oscillator (PCB-214), signal conditioner (PCB-441), voltage display (PCB-DTR-350), dual limit analog comparator (PCB-303C), flat load cell (FLU-5SP2-0211), and 3.5 digits display (PCB-DTR-350).
- i) MTS signal conditioner and power supply.
- j) Simpson 460 digital Voltmeter.

Figure 3.9 shows a schematic diagram of the triaxial cell assembly. Figures 3.10, and 3.11 depict the power supply and set-up of the LVDT and load cell respectively.

A step by step test procedure for the triaxial compression test utilized in this study is outlined below:

- a) Select the initial relative density of the specimen, calculate the specimen density (γ) using equation (3.11), and the specimen weight (W) using equation (3.12).

$$\gamma = (\gamma_{MAX})(\gamma_{MIN}) / ((1 - D_r)(\gamma_{MAX} - D_r \gamma_{MIN})) \quad (3.11)$$

$$W = (V)(\gamma) \quad (3.12)$$

where: γ_{MAX} = maximum dry density;

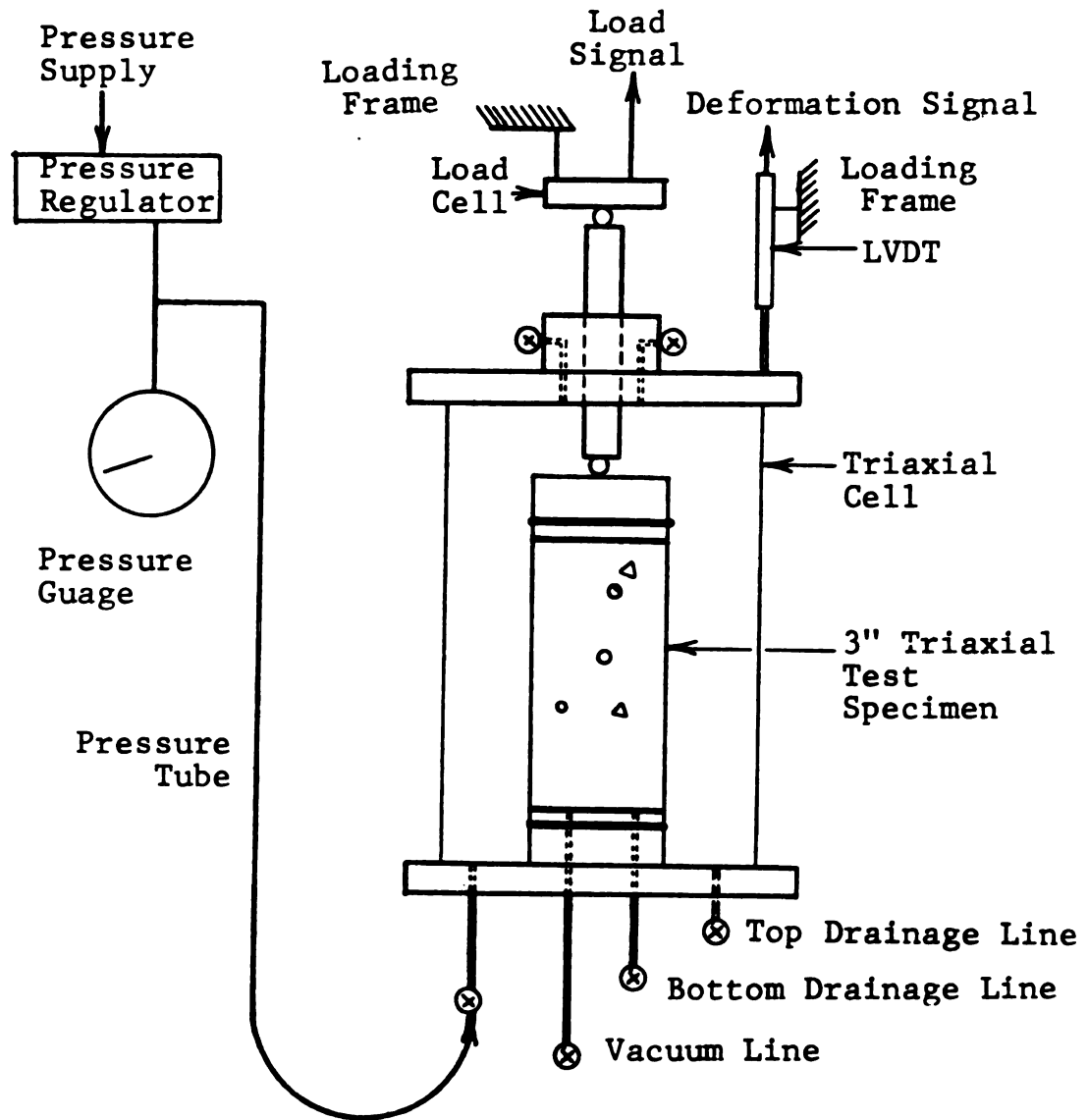


FIGURE 3.9 SCHEMATIC DIAGRAM OF THE TRIAXIAL CELL ASSEMBLY.

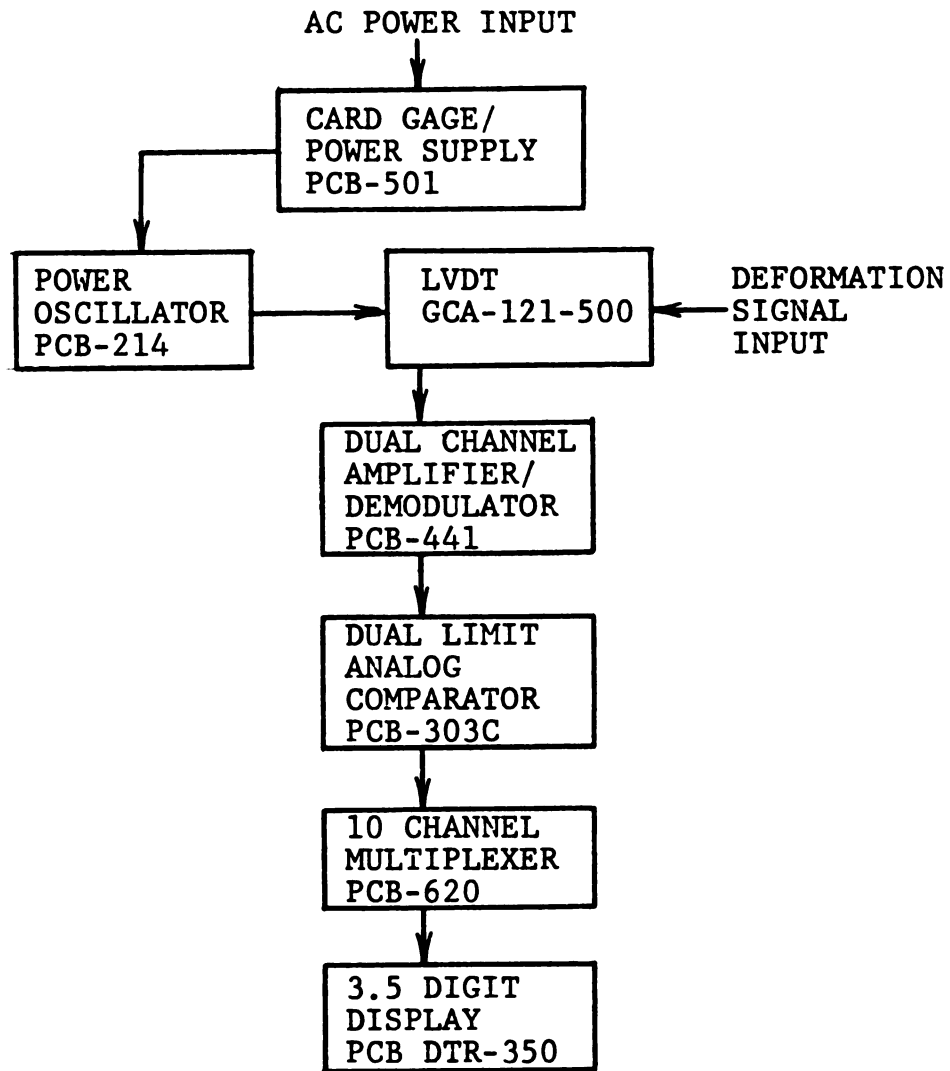


FIGURE 3.10 LVDT SET-UP.

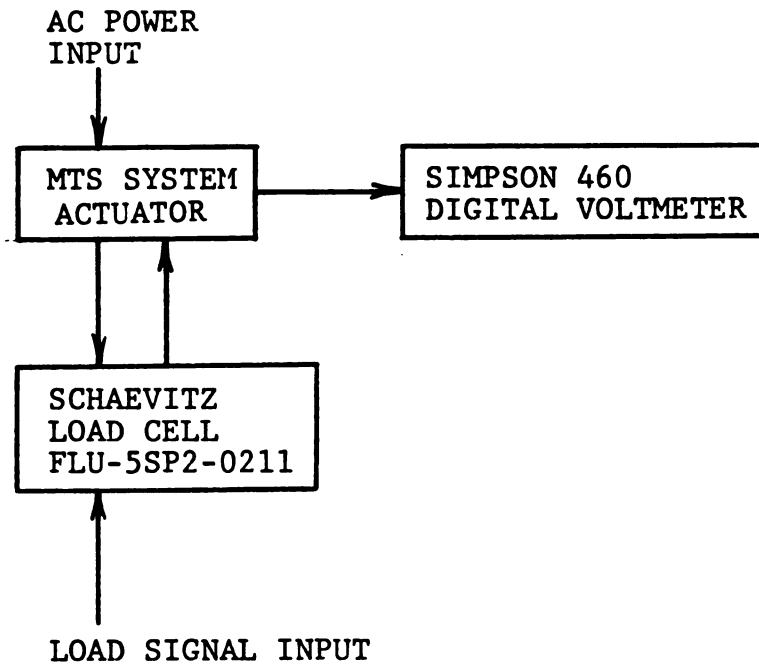


FIGURE 3.11 LOAD CELL SET-UP.

γ_{min} = minimum dry density;

γ = specimen density;

D_r = selected relative density; and

V = volume of the split mold.

For convenience, the soil density and the total specimen weight could be calculated for a range of relative density by using equations 3.11 and 3.12 and then tabulated for later use. In this study, Tables B.1 and B.2 of Appendix B were prepared for several specimens of series A and B samples and used throughout the testing program.

- b) Weigh and mix the soil according to the sample mixing procedure. For convenience, the weight of the fraction of the materials required from each storage bag (per sieve) could be calculated and tabulated for each relative density in question. For this study, the calculations are listed in Tables B.3 and B.4 of Appendix B for series A and B samples respectively.
- c) After mixing and for dry test only, place the soil into the oven and leave it to dry overnight under 110 C. Next day, weigh the dry soil with the container (W_{sc}).
- d) For wet test, calculate the amount of mixing water required, mix the water and soil thoroughly, store it in a plastic bag and let it set overnight for even

moisture distribution. Next day, weigh the moist soil with the plastic bag (W_{sc}).

- e) Turn on the power supply for the LVDT and the load cell, and the vacuum pump.
- f) Secure the two parts of the split mold together using clamps.
- g) Affix membrane to the split mold. Place two pieces of filter paper in between the membrane and the inside surface of the mold to cover the vacuum holes. This will avoid any possible membrane damage while applying vacuum to remove trapped air between the membrane and the mold.
- h) Connect the vacuum lines to the mold and remove the trapped air while smoothing the membrane.
- i) Place one porous disc at the bottom end of the split mold and cover it with a filter paper.
- j) Place the soil into the mold in four different layers; lightly tamp and vibrate each layer so that the final height of each soil layer in the mold is approximately equal to quarter of the height of the mold. In this step, care shall be taken to avoid particle segregation or non-uniform specimen density. To achieve the target relative density at the end of this step, all the dry materials shall be placed into the mold.
- k) Smooth the specimen surface by pressing down the soil

using the top cap. Place a filter paper on top of the soil, a porous disc on top of the paper, and then the top cap.

- l) Lightly tap the top cap using the one pound hammer to densify the top soil.
- m) weigh the container (W_c), and calculate the net weight of the soil in the mold ($W_{net} = W_{sc} - W_c$).
- n) Calculate and check the density of the specimen by dividing the net weight of the soil by the net volume of the split mold.
- o) Disconnect the vacuum lines from the split mold, and secure the membrane to the top cap using rubber bands.
- p) Place one O-ring and a few rubber bands around the base pedestal of the triaxial cell, and then place the split mold with the specimen on top of the pedestal.
- q) Secure the membrane around the base pedestal and top cap; connect the vacuum line to the bottom drainage line of the triaxial equipment; vacuum the specimen; and remove the clamps and the split mold. Note that the vacuum shall be equal to or less than the test confining pressure.
- r) Use the membrane stretcher to place another membrane around the specimen if double membrane is needed.
- s) Place and secure the triaxial chamber.

- t) Raise the loading platform of the triaxial system until the steel ball on top of the piston touches the bottom of the load cell or the loading gear.
- u) Close all valves except the vacuum's; adjust the cell pressure regulator to the desired confining pressure; open the confining pressure valve while disconnecting the vacuum line.
- v) Check specimen leakage now and throughout the test periodically.
- w) Check and record initial LVDT(s) and load cell readings.
- x) Turn the loading mechanism on and record the data.
- y) Throughout the test, check the confining pressure and specimen leakage.
- z) At the end of the test, disassemble the specimen; weigh the material and check the specimen density.
- zz) For wet test only, determine the final water content.

3.4.4 VOLUME CHANGE DUE TO CONFINING PRESSURE

Throughout this program, the specimen volume change during the triaxial tests was not measured due to lack of proper equipment. However, the specimen volume change due to the application of the confining pressure was measured, and the specimen initial density was adjusted accordingly. This volume change was found to be significant for all loose to medium dense specimens. The following procedure was used

to prepare the soil specimen and measure its volume change due to the application of the confining pressure (hydrostatic pressure).

- a) Prepare the specimen as outlined in Section 3.4.3 above using steps (a) through (p).
- b) Secure the membrane around the base pedestal and top cap using O-rings and rubber bands; connect the vacuum line to the sample in the triaxial cell (the vacuum should be equal or less than the test confining pressure).
- c) Make four initial measurements of the specimen's height using a micrometer.
- d) Remove the clamps and split mold.
- e) Use the membrane stretcher to place a second membrane around the specimen.
- f) Place and secure the triaxial chamber.
- g) Apply the confining pressure then wait several minutes; turn-off the confining pressure while reconnecting the vacuum to the specimen.
- h) Disassemble the cell without disturbing the specimen.
- i) Make four measurements of the specimen height using a micrometer.
- j) Make five measurements of the specimen diameter at five different locations equally spaced from the bottom pedestal.
- k) Calculate the new volume of the specimen.

- 1) The difference between the original volume and the calculated one is the volume change of the specimen due to the application of the confining pressure.

NOTE:

IF A SECOND MEMBRANE IS ADDED AFTER THE REMOVAL OF THE SPLIT MOLD, THEN ITS THICKNESS SHOULD BE SUBTRACTED FROM THE MEASURED DIAMETER OF THE SPECIMEN.

CHAPTER 4

TEST RESULTS, ANALYSIS AND DISCUSSION

4.1 GENERAL

Physical characteristics of cohesionless soils such as grain size, grain size distribution, and grain shape have a direct bearing on the engineering behavior of these soil masses. Study of the effects of such soil characteristics on its behavior and response under loading conditions can be very tedious and complicated especially if large-particled soils are involved. Unlike small-particled soils whose properties can be easily determined using standardized test procedures and available apparatus, determination of the properties of large-particled soils involve expensive, very specialized and, for most cases, unavailable equipment. In general, this research has been directed to study the effects of particle characteristics on the shear strength of cohesionless materials, and in particular, to analyse the strength of large-particled soils using that of smaller size particles.

The structure of this chapter consists of eleven major sections:

4.2 Maximum and minimum dry densities.

- 4.3 Angle of repose.
- 4.4 Volume change.
- 4.5 Triaxial test results.
- 4.6 Strength models.
- 4.7 Ultimate strength and critical void ratio.
- 4.8 Peak strength.
- 4.9 Strength at the six percent strain level.
- 4.10 Strength at the one percent strain level.
- 4.11 Confining pressure.
- 4.12 Moisture content.

Each section is divided to several subsections where the effect of one soil and/or test variable is discussed and the test results are presented.

To this end, it may be appropriate to review the test samples and to establish an abbreviation system that the reader may find helpful throughout this Chapter.

- a) Two series (A and B) of soil samples were prepared, the first (series A) consists of five samples while the latter consists of six. The only difference between the samples within any one series is the maximum particle size or the percent fine content (passing number 200 sieve). The difference between the two series, on the other hand, is the soil gradation. Moreover, all the samples of series A and B were prepared using the crushed and pulverized (C/P) material.

- b) Within each series, selected samples were prepared such that the only variable of the soils is the particle shape. The samples were made up of natural material, crushed and pulverized (C/P) material, and a combination of 50% natural and 50% crushed and pulverized materials (50/50). Thus, in this Chapter, the terms C/P abbreviates crushed and pulverized while 50/50 abbreviates a combination of 50% natural and 50% C/P by weight.
- c) In the triaxial test program, samples of series A and B were tested using different densities. Therefore, the term triaxial test specimen (or simply specimen) refers to one sample of series A or B that is formed at one density. For example, five triaxial test specimens of different densities may be prepared using sample 1 of series A. Further, due to the close proximity of the percent fine content of the samples of series B, only samples 1, 4, 5, and 6 were tested and analyzed.

The grain size distribution of the soil samples herein is described in terms of the coefficient of uniformity (Cu). Series A and B samples possess Cu of 45 and 8.89 respectively. Also, due to the nature of the grain size distribution curves within any one series (parallel gradation curve), the maximum grain size of the soil sample

is a function of its percent fine content and vice versa as shown in Figure 4.1. The functional relationship relating the two variables (percent fine content and maximum grain size), in this case, was obtained using the best fit curves and is expressed by equations 4.1 and 4.2 for series A and B samples respectively.

$$PF = -0.176 \{1.0 - 3.187 \text{ EXP}[-0.66(\text{LOG } D_{\text{MAX}})]\} \quad (4.1)$$

$$PF = -0.040 \{1.0 - 6.726 \text{ EXP}[-1.19(\text{LOG } D_{\text{MAX}})]\} \quad (4.2)$$

where: PF = percent fine content (PF = 0.0 to 1.0);

EXP = exponential function;

LOG = logarithm to base 10; and

D_{MAX} = maximum particle size.

Further, it was decided to study the effect of particle size on the shear strength of the material by mainly using the percent fine content of the soil. However, the maximum particle size of the soil sample was also utilized in this study to provide a better understanding of the effects of grain size and soil gradation on the sample behavior.

4.2 MAXIMUM AND MINIMUM DRY DENSITIES.

Maximum and minimum dry densities of cohesionless soils depend to a large extent on the grain characteristics (such as grain size, grain size distribution, and particle shape) the specific gravity of the soil, and to a lesser extent, on

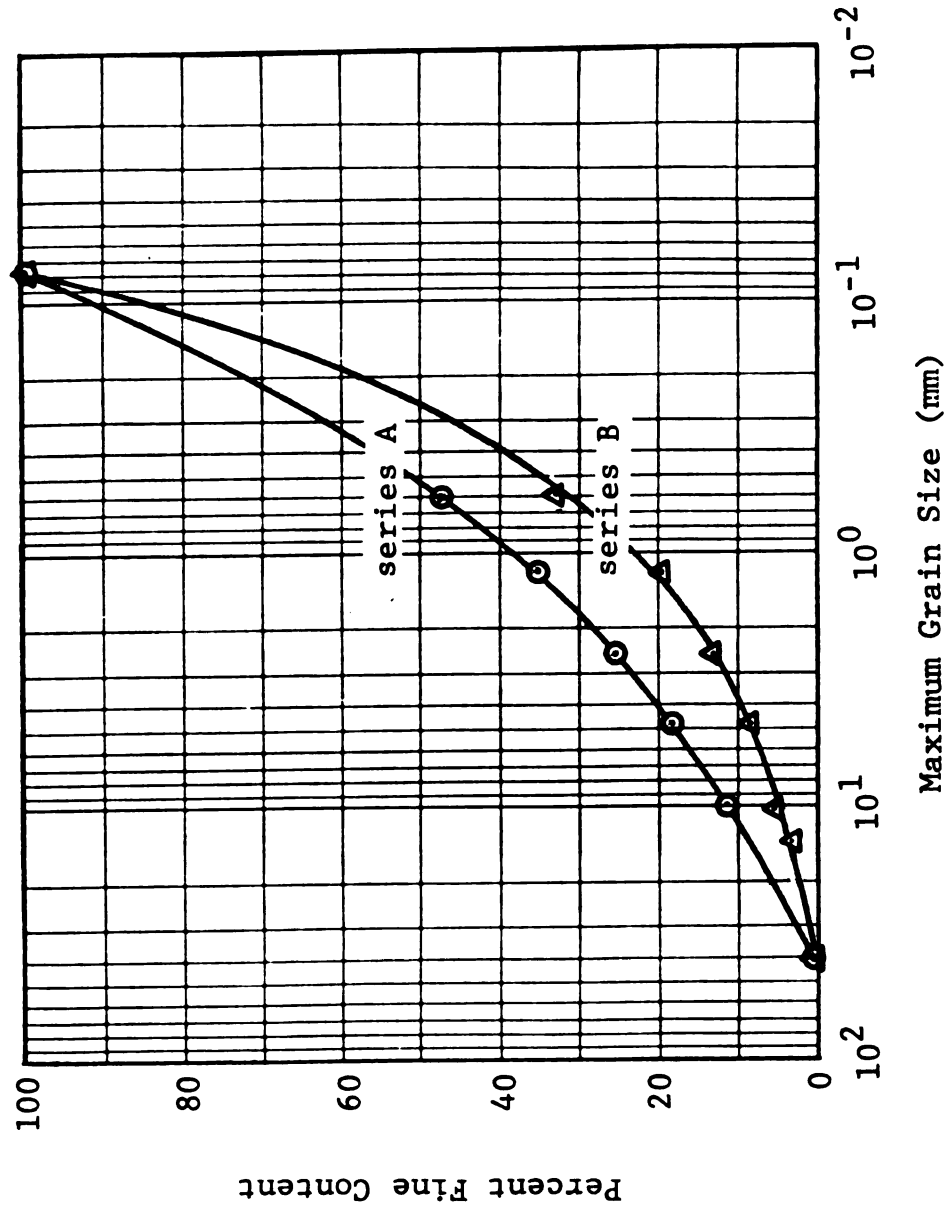


FIGURE 4.1 RELATIONSHIP BETWEEN THE PERCENT FINE CONTENT AND THE MAXIMUM GRAIN SIZE OF SERIES A AND B SAMPLES.

the test method and procedure. In this research study, a modified version of the standard ASTM maximum dry density test (D-2049) was utilized (see chapter 3) for all samples including those which possess percent fine content (passing number 200 sieve) of up to 100%. The reason being is that when compaction techniques were used, the soil experienced particle breakdown and consequent changes in the gradation and grain shape. The objective herein is to study the effects of the grain size, sample gradation, and grain shape upon the strength of the materials. The utilized vibratory test method produced no such particle breakdown. Moreover, the 0.033 ft³ (948 cm³) mold was used rather than the standardized 0.1 ft³ (2832 cm³) mold. Because of:

- a) the limited amount of the material retained on some sieves that was available; and
- b) the technique used gave values consistent with maximum densities obtained using the standard mold on two of the samples with the largest particle sizes utilized in this study.

Further, by using the same apparatus and test method and procedure for all soil samples, their effects on the test results were neutralized. Minimum densities of the soil samples were determined using the above noted ASTM standard test procedure except that (for the same reasons noted above) the smaller mold was used instead of the standard size one.

In the following subsections, the test results and the effects of the grain size, sample gradation (grain size distribution), and grain shape on the values of the maximum and minimum dry densities are presented and discussed.

4.2.1 EFFECT OF GRAIN SIZE

At least two maximum and minimum dry density tests were conducted on each sample of series A and B. In all tests the variations of maximum or minimum dry density values, for each sample, were within one percent of each other. Nevertheless, the absolute maximum and minimum values were selected. These values are presented in Tables C.1 and C.2 of Appendix C for series A and B samples respectively. It can be noted from the tables that, for all samples of series A and B, the maximum density value ranges from 134.4 to 102.6 pcf (2.15 to 1.64 g/cm³) while the minimum density value ranges from 111.0 to 68.3 pcf (1.78 to 1.09 g/cm³).

Figures 4.2 and 4.3 depict the maximum and minimum dry density values plotted as a function of the percent fine content of series A and B samples respectively. Examination of these figures indicates that the maximum and minimum dry densities decrease with increasing percent fine content. This finding was expected and it is consistent with that reported throughout the literature. An explanation of this could be illustrated by using Figure 4.4. The solid cube shown in the figure with one unit length, width and height,

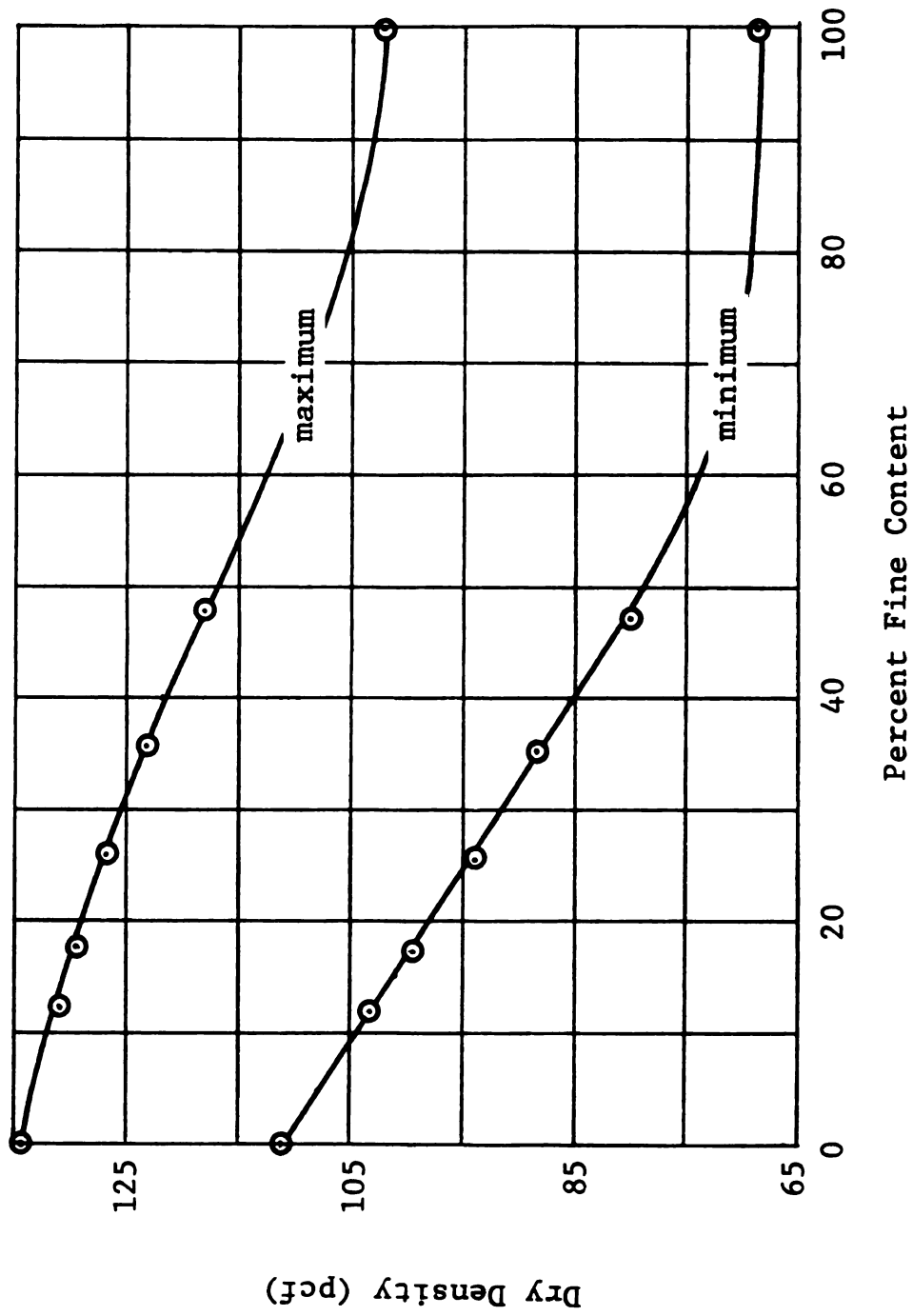


FIGURE 4.2 MAXIMUM AND MINIMUM DRY DENSITIES VERSUS PERCENT FINE CONTENT OF THE SOIL OF SERIES A SAMPLES.

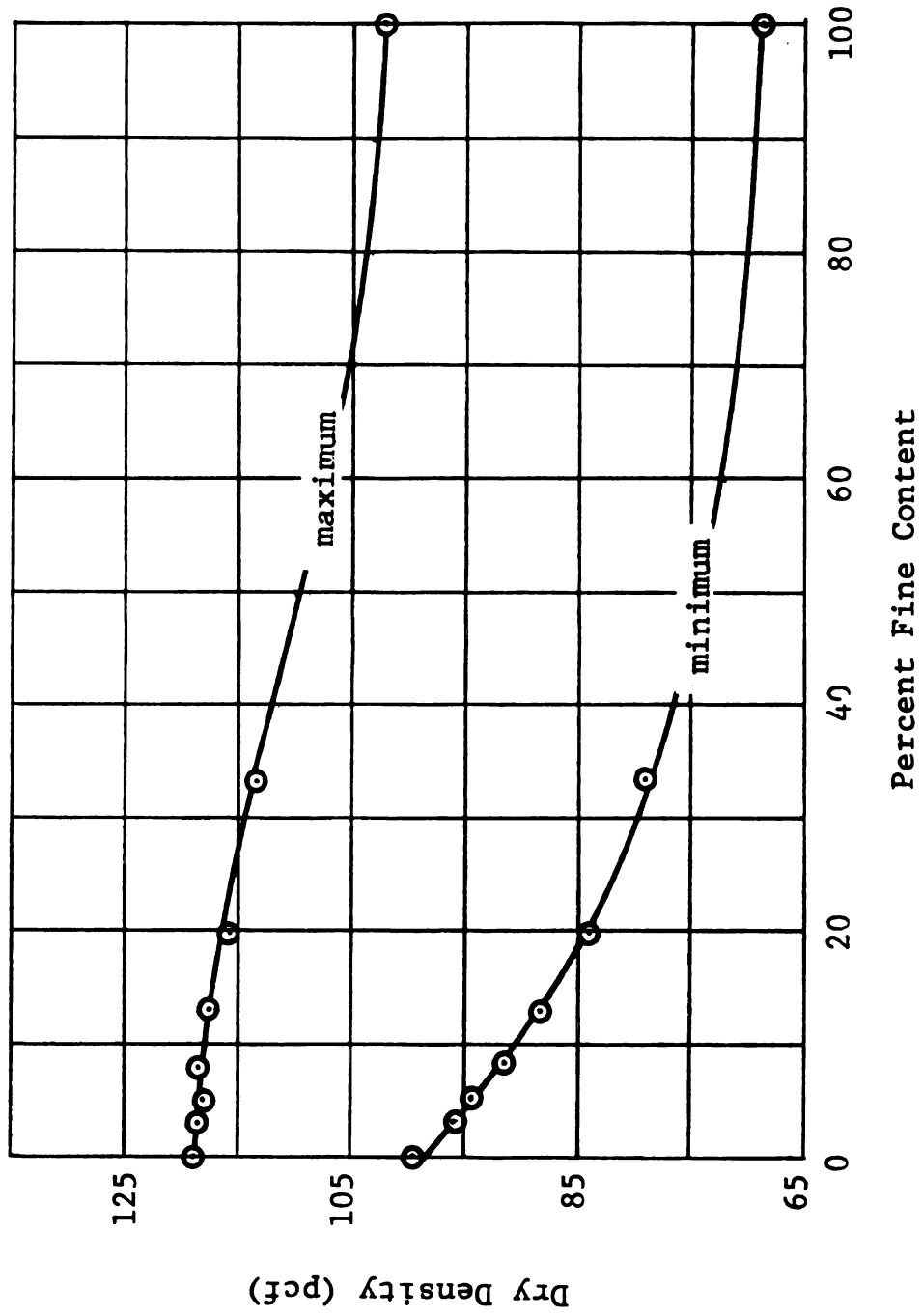
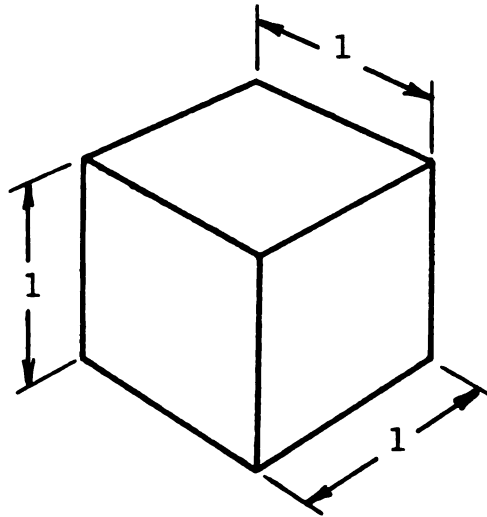
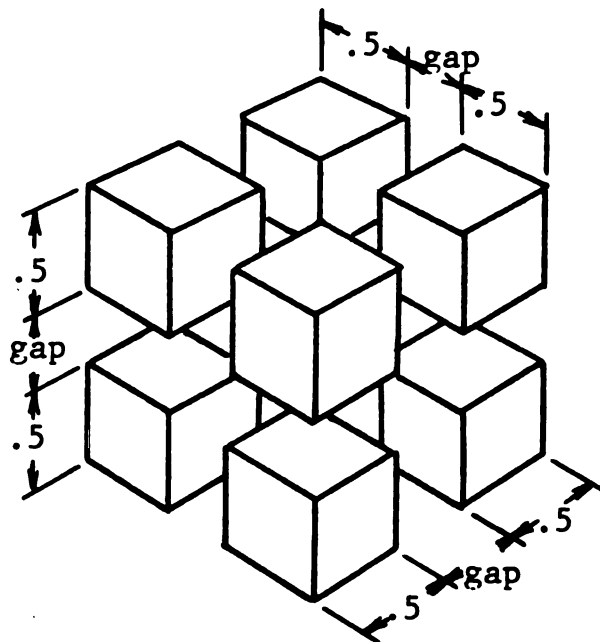


FIGURE 4.3 MAXIMUM AND MINIMUM DRY DENSITIES VERSUS PERCENT FINE CONTENT OF THE SOIL OF SERIES B SAMPLES.



a) Solid Cube with One Unit Length, Width and Height.



b) Eight Cubes of Half Unit Length, Width and Height.

FIGURE 4.4 SCHEMATIC REPRESENTATION OF THE EFFECT OF PARTICLE BREAKDOWN ON ITS TOTAL SURFACE AREA AND VOLUME.

represents an aggregate. The surface area of this aggregate is equal to six units area. The aggregate is then divided into eight smaller cubes of equal sizes. The total surface area of these eight cubes is equal to 12 unit area. Translating this occurrence into the crushing of the aggregates, in which they are broken into smaller fragments, the crushed materials will have higher total surface area when compared to the total surface area of the original aggregates. Further crushing and/or pulverization will lead to further increase in the total surface area. The volume of voids between aggregates is directly proportional to the surface area, i.e. it is equal to or greater than the surface area times the space gap between the aggregates. Therefore as the total surface area of the soil grain increases, the void space within the soil sample increases, and consequently, for constant volume and weight of the solid, the dry density decreases.

It should be noted herein that for a cubical array of uniform and sphere particles, the maximum and minimum void ratios are theoretically constant (0.9084 and 0.3514 respectively) and independent of the diameter of the particle. However, the smaller the diameter, the higher the number of contact points between particles and the higher the required compaction effort to achieve the maximum density. Thus, for a constant compaction effort, one may expect a change in the density as the diameter of the

particle changes. Further, sample gradation and the percent fine material available to fill-up the void spaces between larger particles influence the minimum and maximum void ratios as well as the limiting densities.

Upon examination of the test results presented in Figures 4.2 and 4.3, two general equations were selected to model the maximum and minimum dry densities of the samples in terms of their percent fine content. The parameters of the equations were then calibrated to minimize the absolute error between the actual data and those calculated by using the equations. The final models are presented below as equations 4.3 and 4.4 for series A samples.

$$\gamma_{MAX} = \frac{134.4 - 93.3 (PF)}{1 - 0.50(PF)} \text{EXP}[0.22(PF)^{6.0}] \quad (4.3)$$

$$\gamma_{MIN} = 111 - 64.0(PF)\{1 - 0.68 \text{EXP}[-.72(PF)^{-2.7}]\} \quad (4.4)$$

whereas for series B samples:

$$\gamma_{MAX} = \frac{119.2 - 84.2(PF)}{1 - 0.60(PF)} \text{EXP}[0.16(PF)^{4.0}] \quad (4.5)$$

$$\gamma_{MIN} = 98.0 - 73.0(PF)\{1 - 0.98 \text{EXP}[-.50(PF)^{-1.04}]\} \quad (4.6)$$

where: γ_{MAX} = maximum dry density;

γ_{MIN} = minimum dry density;

PF = percent fine content (PF = 0.0 to 1.0); and

EXP = exponential function.

The locus of the 45 degree line in Figure 4.5 represents the correspondence between the measured and calculated maximum and minimum densities (using equations 4.3 through 4.6). It is of importance to note that:

- a) The absolute maximum difference between the calculated and measured values is 0.88 pcf (0.014 gm/cm³).
- b) The calculated values of the maximum and minimum dry densities were within 0.74 percent of all measured data of series A and B samples.

It was stated in Section 4.1 above that the effect of grain size on the soil behavior will be studied using the percent fine content of the soil, and that the percent fine content and maximum grain size of soil samples having parallel gradation curves are two dependent variables. To verify this, the values of the maximum and minimum dry densities of series A and B samples are plotted against their maximum grain size in Figures 4.6 and 4.7 respectively. Examination of these figures indicates that the values of the maximum and minimum dry density of all samples decrease as the maximum grain size decreases. This finding is similar and compatible to that of the effect of percent fine content. Indeed, the functional relationship relating the maximum and minimum densities to the maximum grain size can be had by substituting equations 4.1 and 4.2 into equations 4.3 through 4.6.

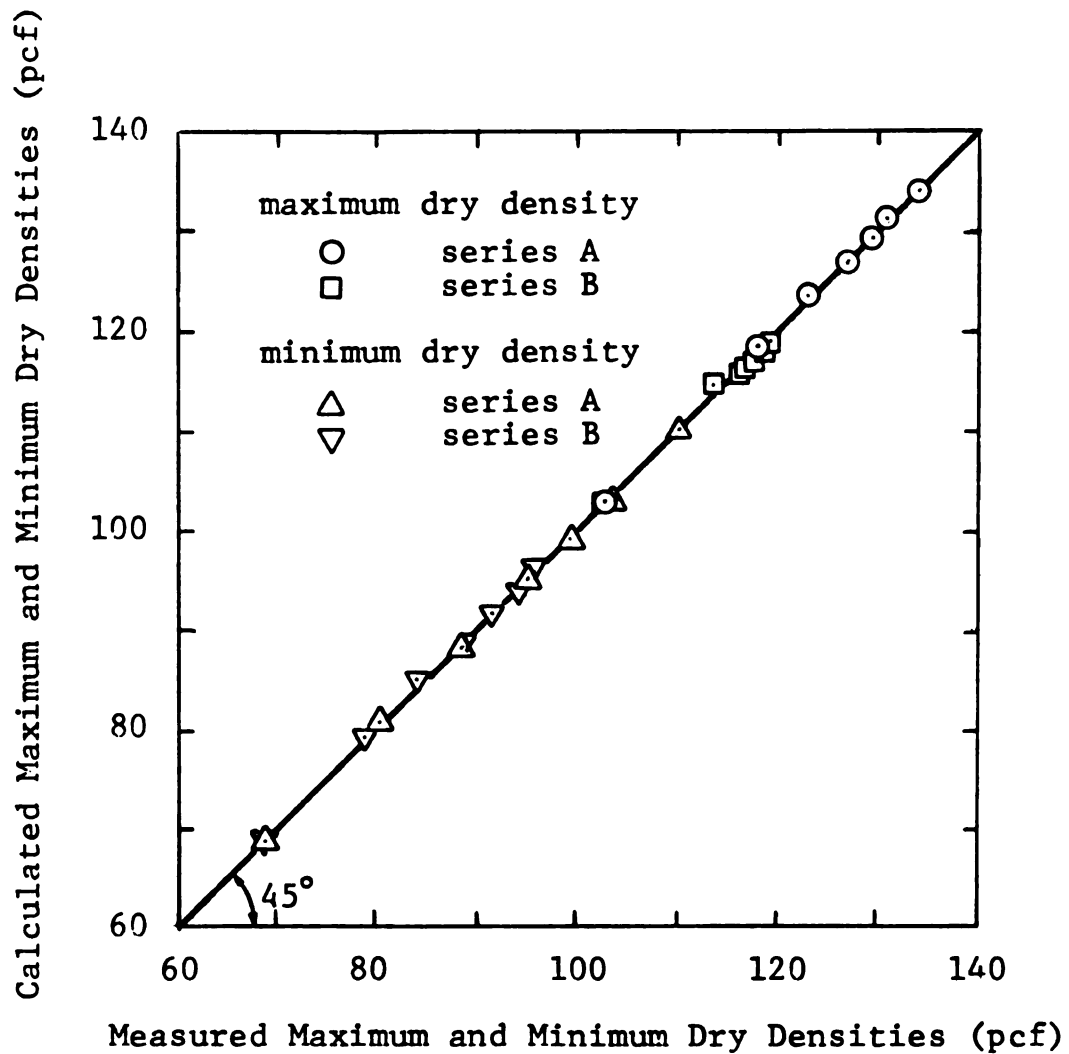


FIGURE 4.5 CALCULATED VERSUS MEASURED MAXIMUM AND MINIMUM DRY DENSITIES OF SERIES A AND B SAMPLES.

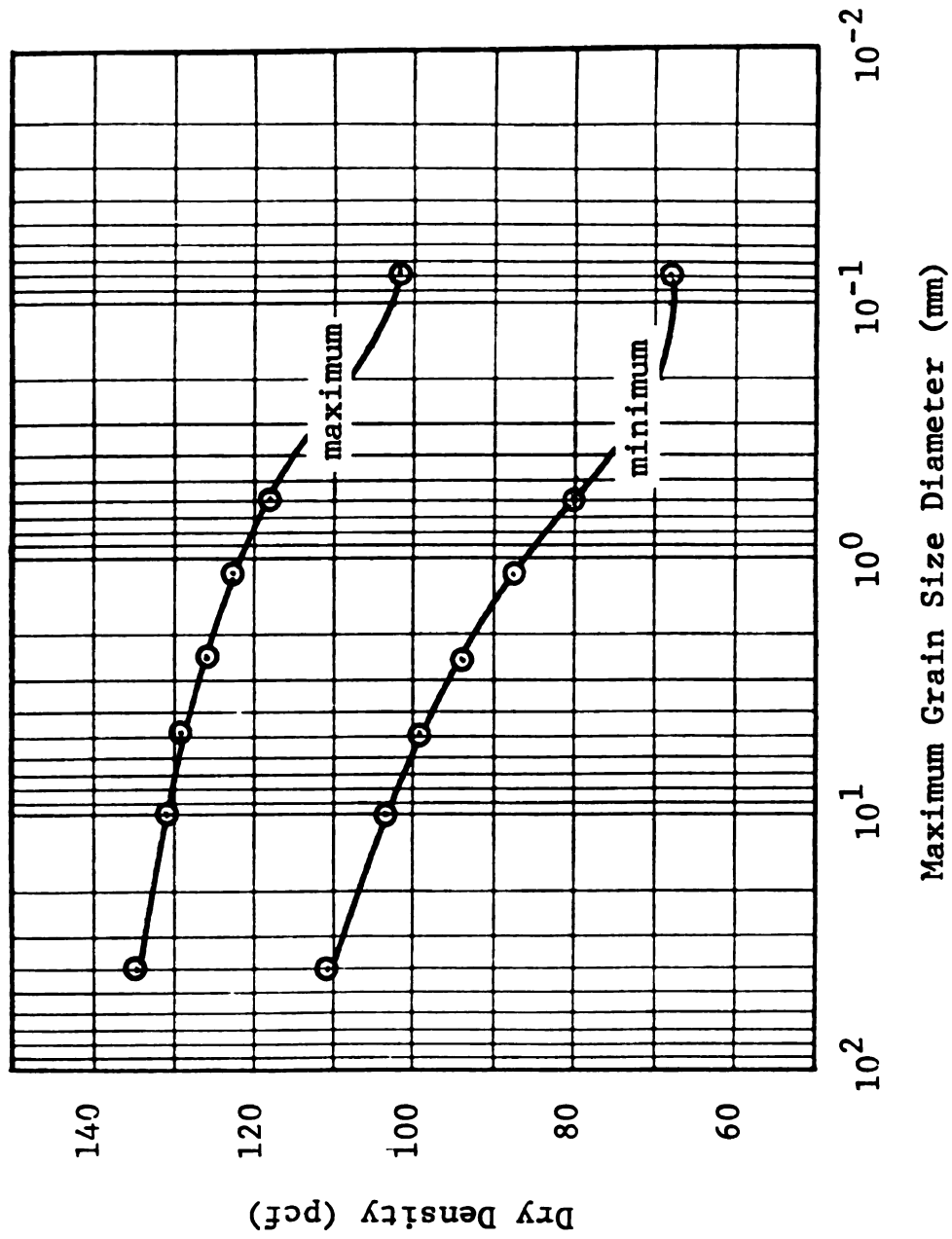


FIGURE 4.6 MAXIMUM AND MINIMUM DRY DENSITIES VERSUS THE MAXIMUM GRAIN SIZE OF SERIES A SAMPLES.

FIGURE 4.7 MAXIMUM AND MINIMUM DRY DENSITIES VERSUS THE MAXIMUM GRAIN SIZE OF SERIES B SAMPLES.

Knowing the maximum and minimum dry densities, and the specific gravity of the soils, the maximum and minimum void ratios can then be calculated using equations 4.7 and 4.8.

$$e_{MIN} = \frac{\gamma_w(G_s)}{\gamma_{MAX}} - 1 \quad (4.7)$$

$$e_{MAX} = \frac{\gamma_w(G_s)}{\gamma_{MIN}} - 1 \quad (4.8)$$

where e_{MIN} = minimum void ratio;

e_{MAX} = maximum void ratio;

γ_w = unit weight of water; and

G_s = specific gravity of the soil.

The values of the maximum and minimum void ratios were calculated using equations 4.7 and 4.8 and the measured values of the minimum and maximum dry densities. The calculated values are listed in Tables C.1 and C.2 in Appendix C. It can be noted that, for all samples of series A and B, the value of the maximum void ratio ranges from 0.5385 to 1.5008, and the value of the minimum void ratio ranges from 0.2707 to 0.6651. Figures 4.8 and 4.9 show plots of the calculated minimum and maximum void ratios versus percent fine content of series A and B samples respectively. The data were modeled using equations 4.9 and 4.10 for series A samples, and equations 4.11 and 4.12 for series B.

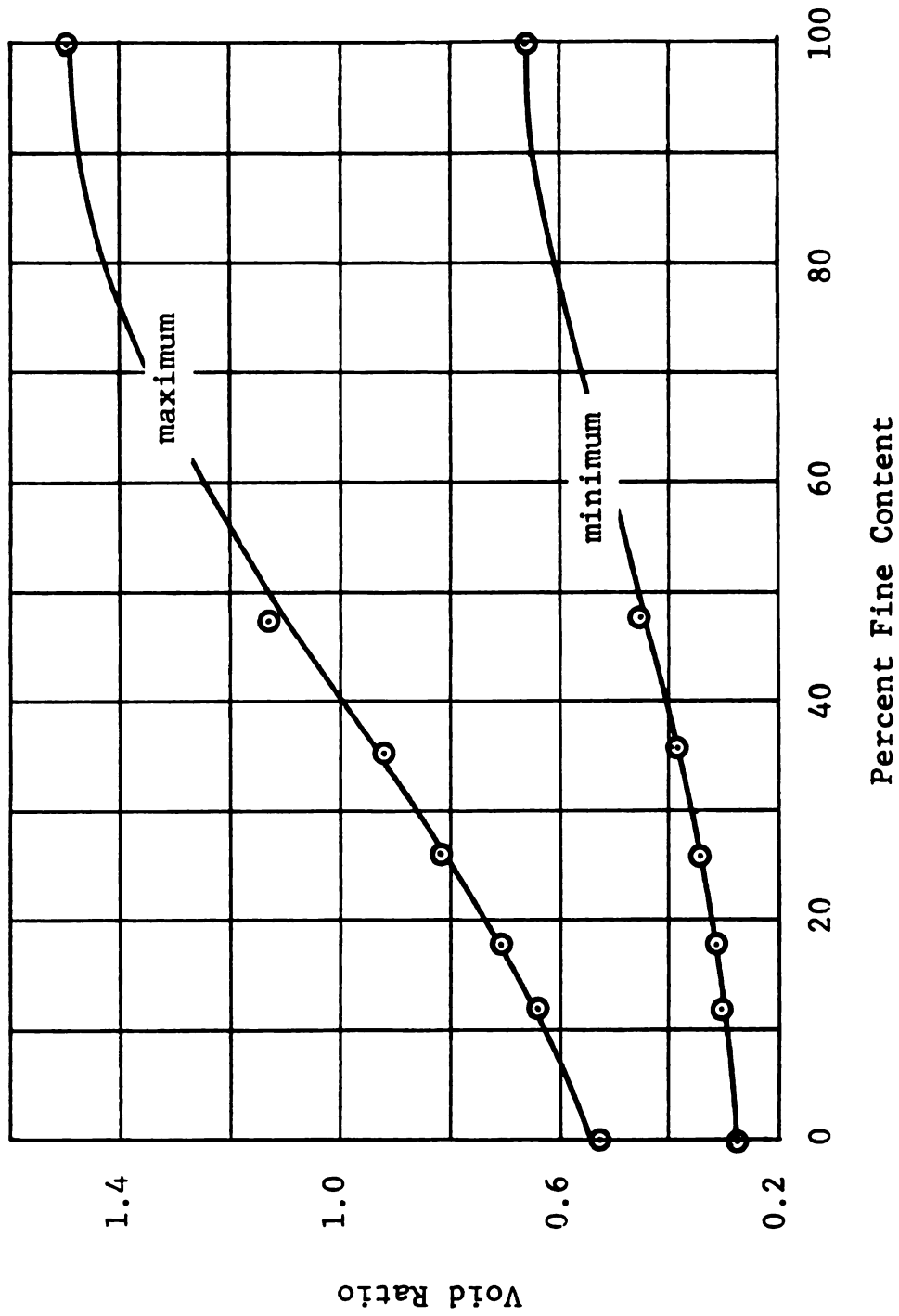


FIGURE 4.8 MINIMUM AND MAXIMUM VOID RATIOS VERSUS PERCENT FINE CONTENT OF SERIES A SAMPLES.

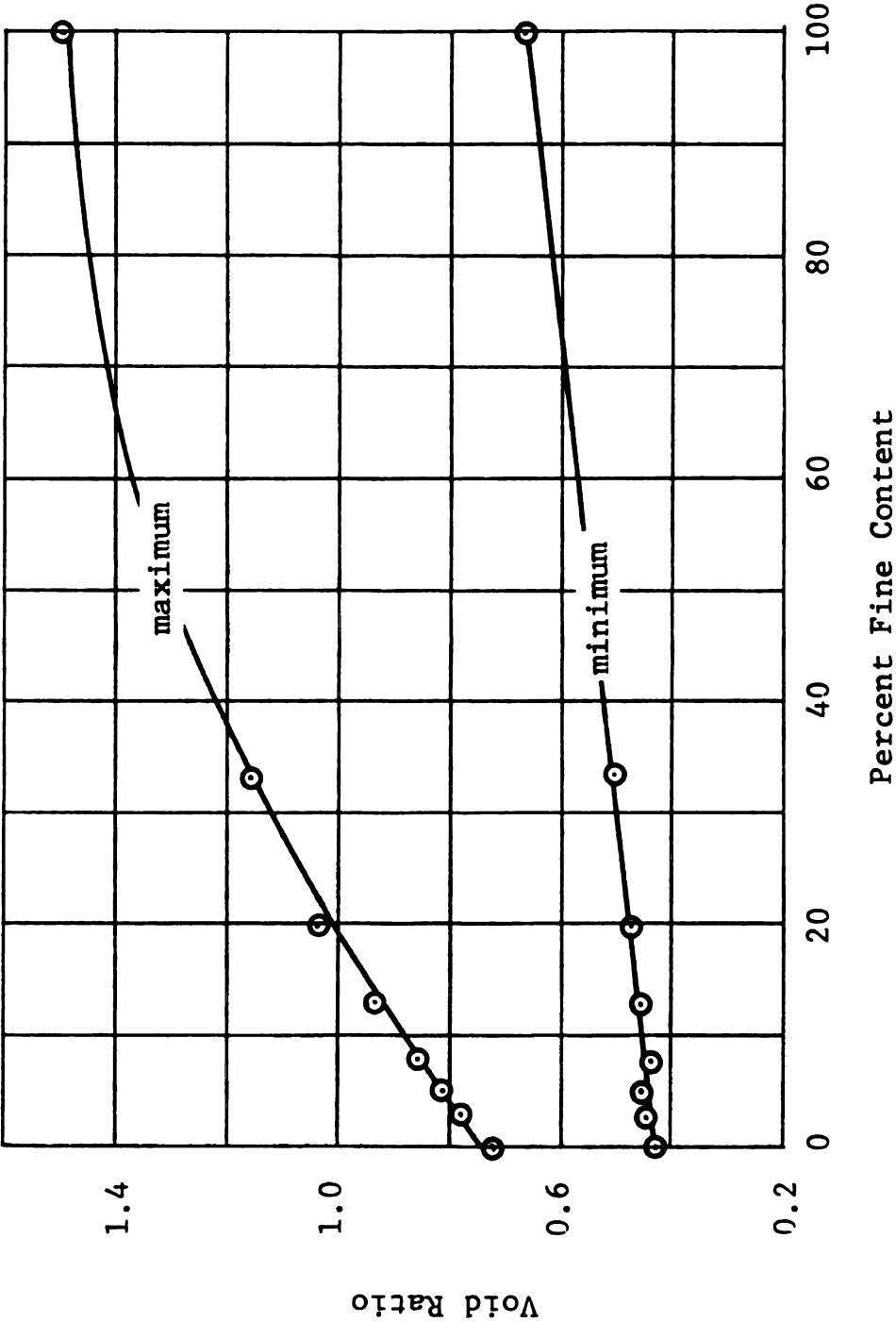


FIGURE 4.9 MINIMUM AND MAXIMUM VOID RATIOS VERSUS PERCENT FINE CONTENT OF SERIES B SAMPLES.

$$e_{MIN} = 0.27 \frac{1 + 0.22(PF)}{1 - 0.69(PF)} \text{EXP}[-0.48(PF)^{5.0}] \quad (4.9)$$

$$e_{MAX} = 0.54 \frac{1 + 0.97(PF)}{1 - 0.696(PF)} \text{EXP}[-0.84(PF)^{3.2}] \quad (4.10)$$

$$e_{MIN} = 0.42 \frac{1 + 0.58(PF)}{1 - 0.00(PF)} \text{EXP}[-0.00(PF)^{1.0}] \quad (4.11)$$

$$e_{MAX} = 0.72 \frac{1 + 2.26(PF)}{1 + 0.02(PF)} \text{EXP}[-0.43(PF)^{1.6}] \quad (4.12)$$

where all terms are as before.

The locus of the forty five degree line in Figure 4.10 represents the correspondence between the calculated maximum and minimum void ratios using equations 4.9 through 4.12 and those using equations 4.7 and 4.8. It should be noted that the absolute maximum difference between the two values is 0.0386 or 3.4 percent.

Further examination of Figures 4.2, 4.3, 4.8 and 4.9 indicates that, at low percent fine content, the slopes of the minimum dry density and maximum void ratio curves are much steeper than those of the maximum dry density and minimum void ratio curves. Also the slope of the curves decreases as the percent fine content increases. Thus, the percent fine content of the samples have higher effects on the minimum dry density and maximum void ratio than on the maximum dry density and minimum void ratio. Similar

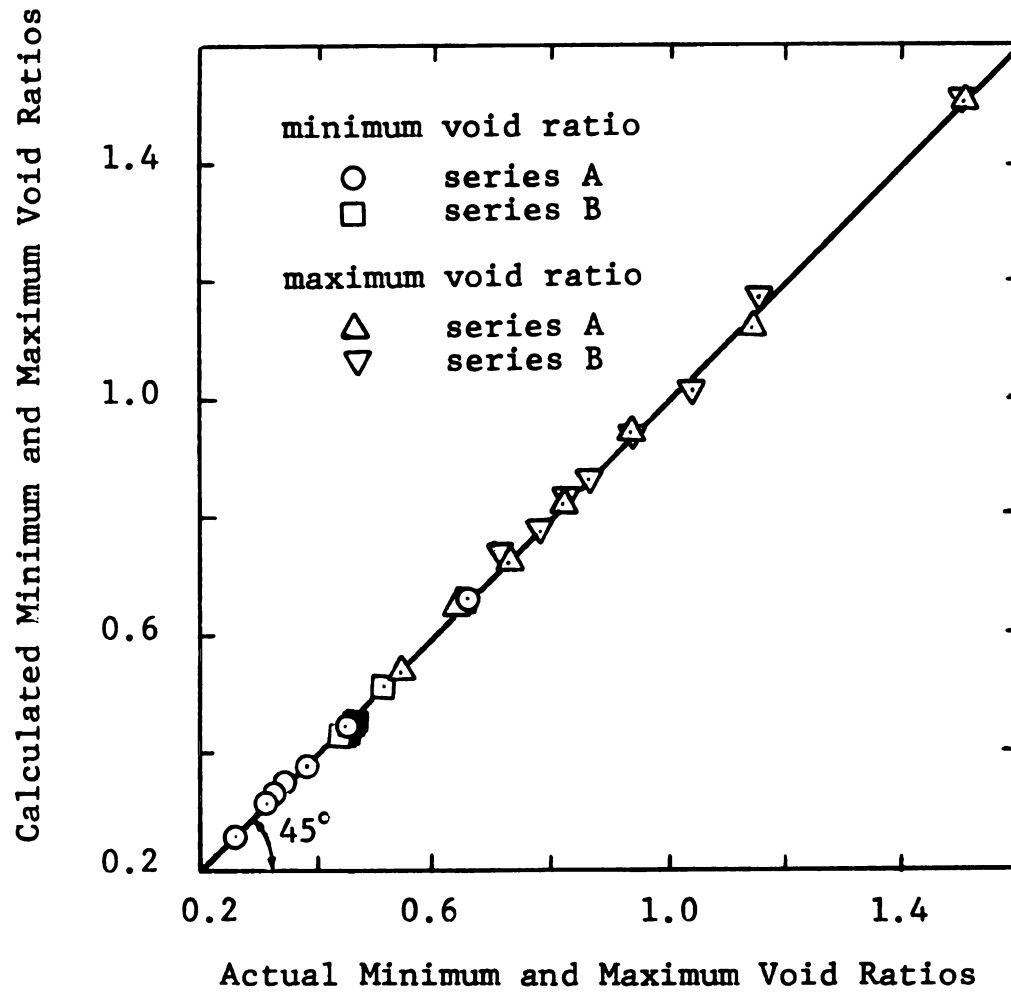


FIGURE 4.10 CALCULATED VERSUS ACTUAL MINIMUM AND MAXIMUM VOID RATIOS OF SERIES A AND B SAMPLES.

observations were also noted by several other investigators (38, 50, and 85). Youd (85) ,however, concluded that "Contrary to previous studies, it was found that particle size per se has no significant influence on the density limits".

4.2.2 EFFECT OF SAMPLE GRADATION

Recall that the soil of series A and B samples possess coefficients of uniformity of 45.0 and 8.89 respectively, and that the percent fine content and maximum grain size of the soil samples within each series vary. Thus, the effect of the independent variable "sample gradation" on maximum and minimum dry densities of the soil samples can be studied by utilizing the available test results of series A and B samples. Figures 4.11 and 4.12 depict the maximum and minimum dry densities of all soil samples of series A and B plotted against their percent fine content and maximum grain size respectively. Examination of the figures indicates that:

- a) For the same percent fine content or maximum particle size, the higher the coefficient of uniformity (C_u) the higher the values of the maximum and minimum dry density.
- b) For fine grained soils (one hundred percent passing sieve number 200), the maximum and minimum dry densities are independent of the sample gradation

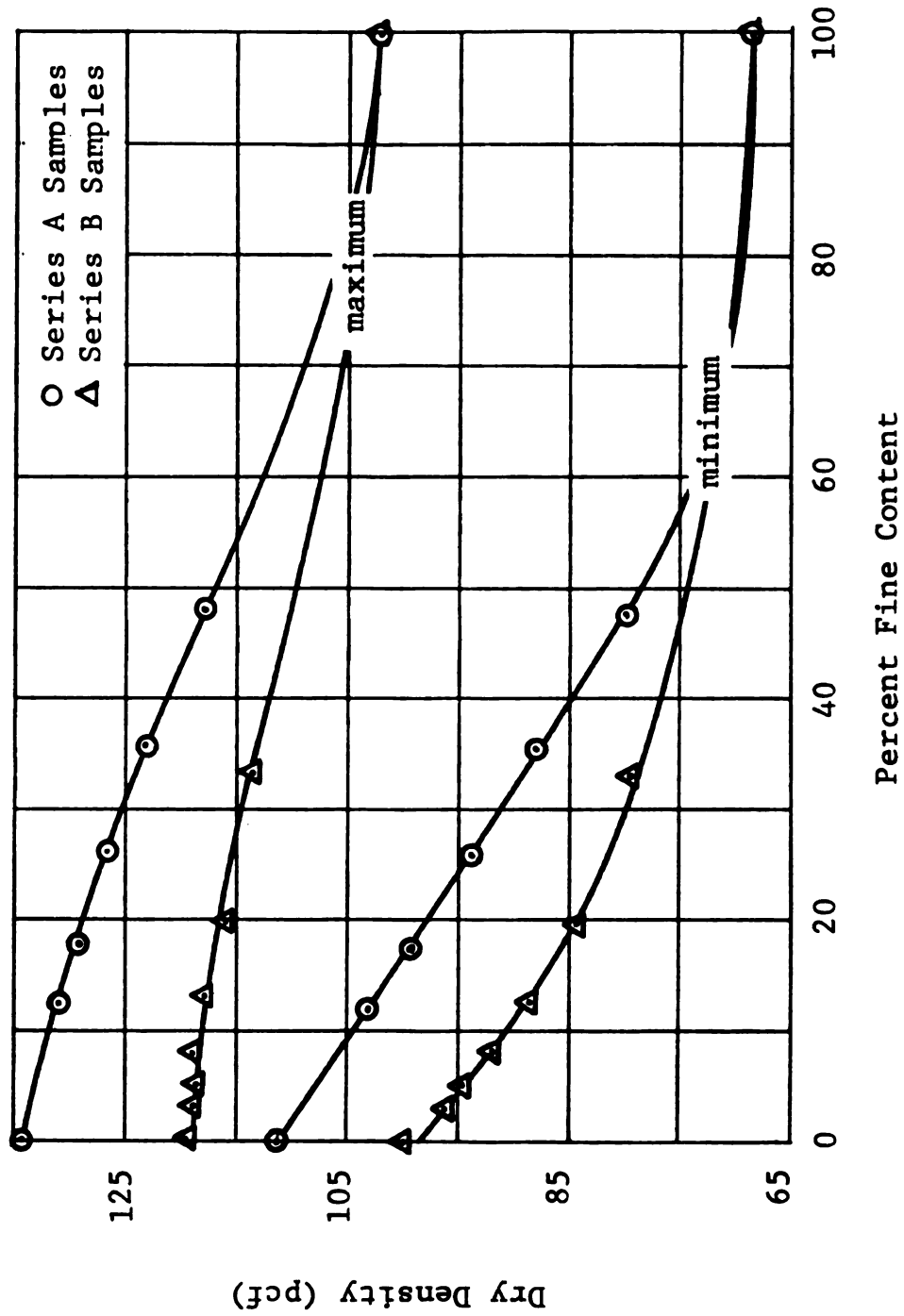


FIGURE 4.11 MAXIMUM AND MINIMUM DRY DENSITIES VERSUS PERCENT FINE CONTENT OF SERIES A AND B SAMPLES.

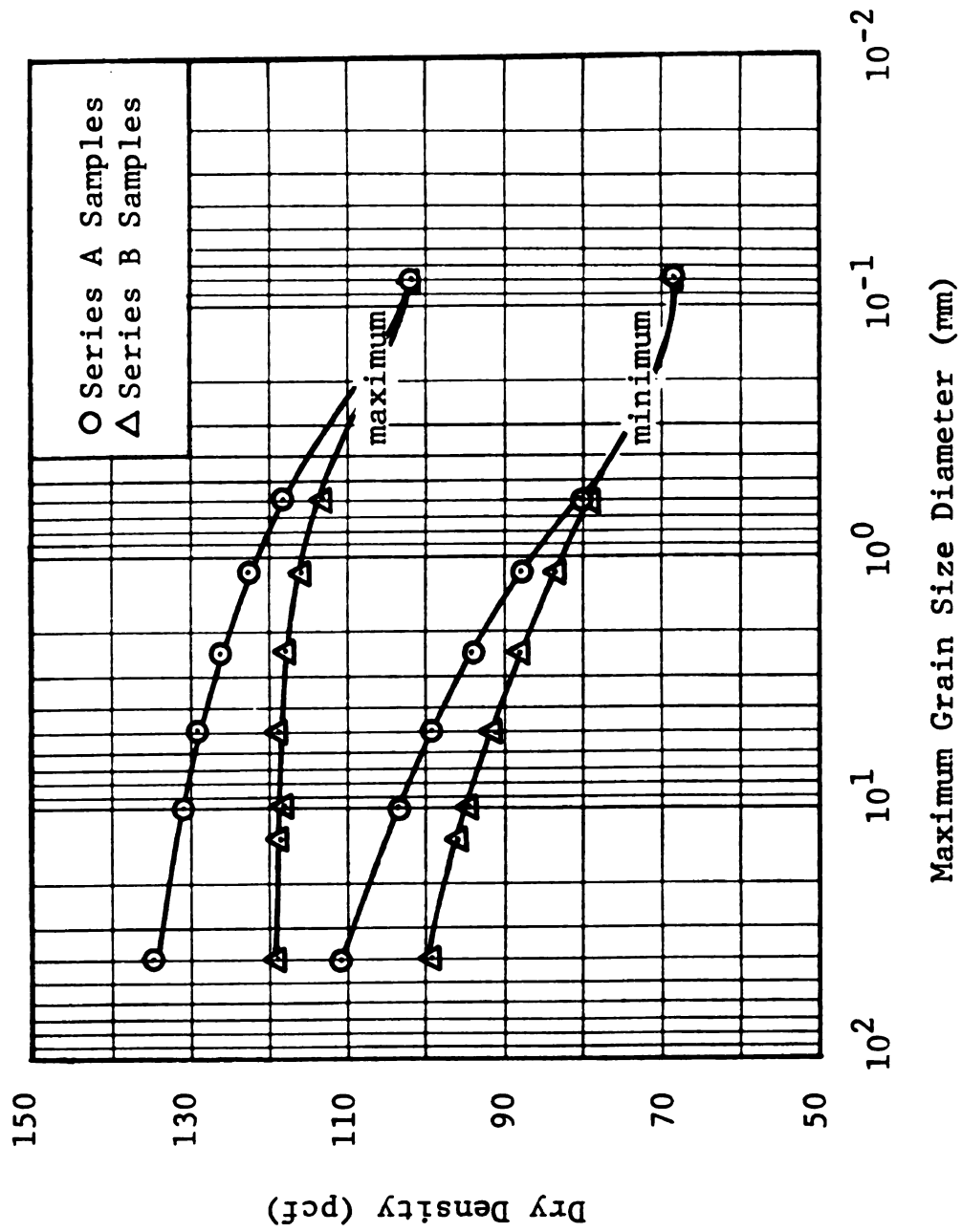


FIGURE 4.12 MAXIMUM AND MINIMUM DRY DENSITIES VERSUS MAXIMUM GRAIN SIZE OF SERIES A AND B SAMPLES.

(coefficient of uniformity).

- c) The lower the percent fine content and the higher the maximum grain size of the soil samples, the higher the influence of sample gradation on the maximum and minimum dry densities.
- d) The higher the C_u , the higher the effect of percent fine content of the samples on their maximum and minimum dry densities.

The last observation could be illustrated by plotting the differences between the maximum and minimum dry densities of series A and B samples against the percent fine content of the soil as shown in Figure 4.13. Examination of the figure indicates:

- a) That the difference between the values of the maximum dry density of series A and B samples decreases as the percent fine increases.
- b) That the difference between the values of the minimum dry density of series A and B samples increases slightly as the percent fine content increases from zero to about fifteen percent, and it decreases for higher percent fine content.

Thus, the effect of sample gradation on the minimum dry density is maximum at a percent fine content of the soil of about fifteen percent. An explanation of this observation could be as follow:

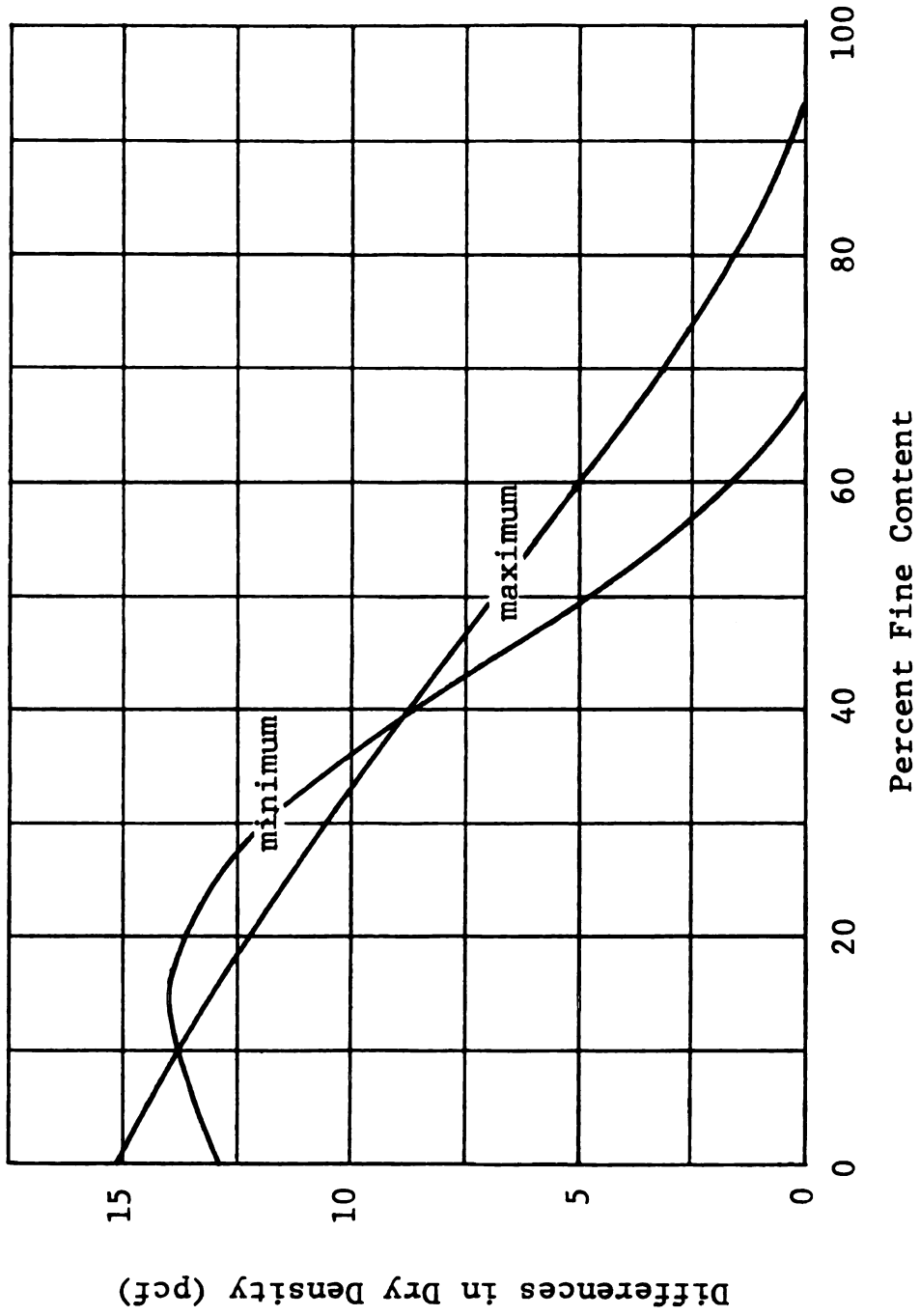


FIGURE 4.13 DIFFERENCE IN MAXIMUM AND MINIMUM DRY DENSITIES BETWEEN SERIES A AND B SAMPLES VERSUS PERCENT FINE CONTENT OF THE SAMPLES.

As the percent fine content of a soil increases, coarse particles lose contact between each other and they become suspended (floating) in the fine materials. Consequently, the fines dominate the sample behavior. Since the same fine material is used for series A and B samples, then the effect of sample gradation is expected to diminish as the percent fine content approaches one hundred.

Since only two types of gradation, two values of the coefficient of uniformity (C_u) are utilized in this study, the functional relationship relating maximum and minimum dry densities of the soil samples to their (C_u) could not be accurately modeled (because such relationship could be linear, hyperbolic, or exponential). Johnston (43) found a linear-logarithmic type relationship between C_u and the maximum and minimum dry densities for cohesionless soils with zero percent fine content. Therefore, the test results of this study are compared and discussed herein against Johnston's.

In Figure 4.14, the solid lines depict Johnston's relationship for maximum and minimum dry densities. The test results of this investigation for zero, twelve, thirty, fifty, and one hundred percent fine content of series A and B samples are also shown. Examination of the figure indicates that:

a) In general, the test results of this study (maximum

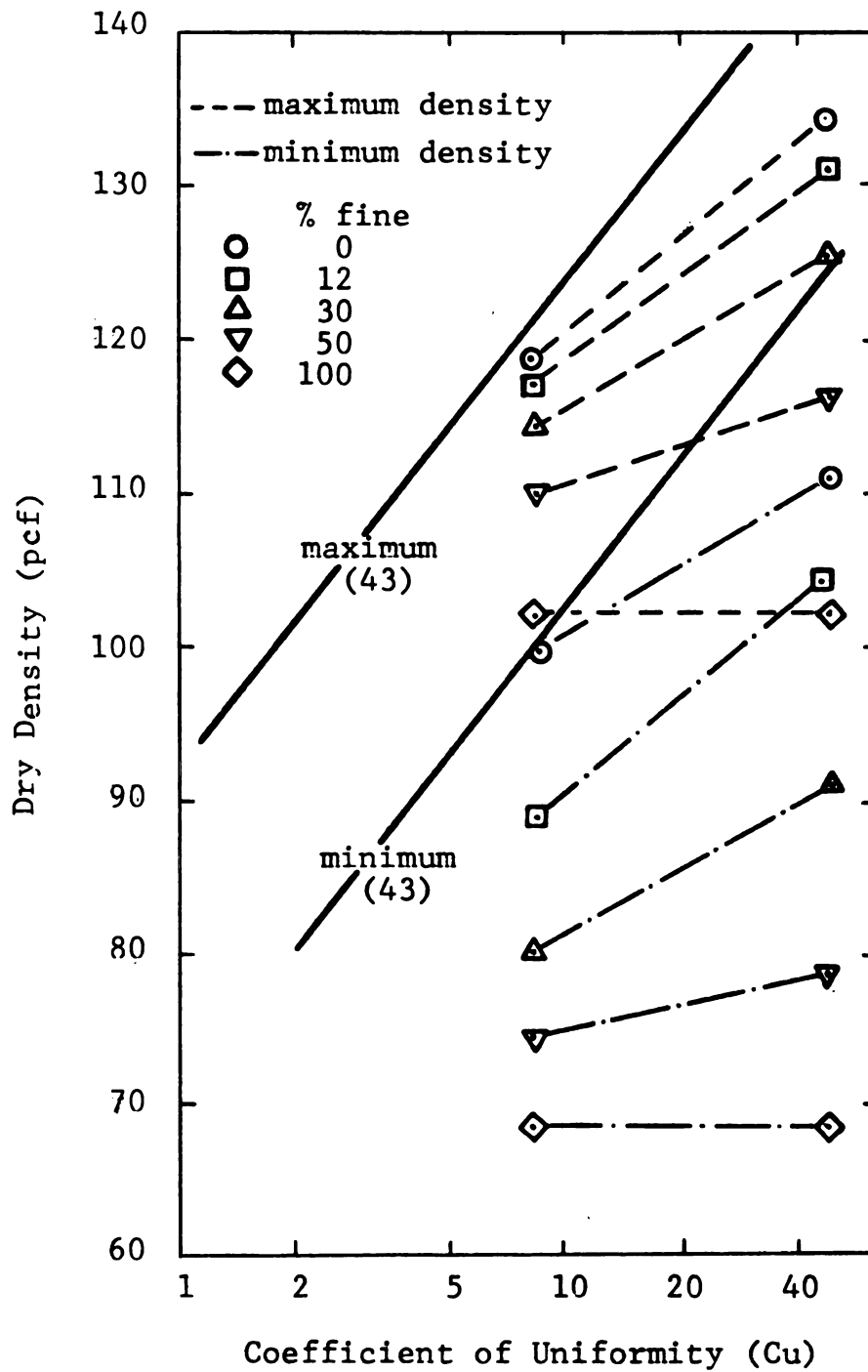


FIGURE 4.14 MAXIMUM AND MINIMUM DRY DENSITIES VERSUS COEFFICIENT OF UNIFORMITY OF SERIES A AND B SAMPLES, (43).

and minimum dry densities) are in conformity with Johnston's relationship.

- b) For the same percent fine content, the better the sample gradation (higher Cu), the higher the maximum and minimum dry densities.
- c) For the same percent fine content, the slope of the lines for maximum and minimum densities are approximately the same, and thus the Cu possesses the same effect on both maximum and minimum dry density of the samples.
- d) The higher the percent fine content of the samples the lower the slope of the lines and the lower is the effect of Cu on the limiting densities.
- e) For the one hundred percent fine content, the maximum and minimum dry densities are independent of the coefficient of uniformity.

Finally, the difference between the test results at zero percent fine content and those of Johnston's could be attributed to the difference in the grain shape and perhaps, to differences in the test method.

4.2.3 EFFECT OF GRAIN SHAPE

At least two maximum and minimum dry density tests were conducted on samples 1, 2 and 3 of series A, and 4 of series B using the natural material (rounded to subrounded), and

sample 1 of series A and 4 of series B using the combination of 50% crushed and pulverized and 50% natural material (50/50). Results of these tests are presented in Table C.3 of Appendix C. It should be noted that, for all duplicate tests, the variations of the maximum and minimum dry densities were within 1%.

Figure 4.15 shows plots of the maximum dry density versus percent fine content of the test samples. Similar plots for the minimum dry density are shown in Figure 4.16. Figure 4.17 depicts the maximum and minimum dry densities of the test samples plotted against the coefficient of sample angularity (SA). Examination of the figures indicates that:

- a) Regardless of the particle shape, the maximum and minimum dry densities decrease as the percent fine content of the samples decreases (Figures 4.15 and 4.16).
- b) The effect of sample angularity on the maximum and minimum dry densities of the samples decreases as the percent fine content increases (Figures 4.15 and 4.16).
- c) The higher the coefficient of sample angularity, the lower the maximum and minimum densities of the samples (Figure 4.17).

The first finding is consistent with that of, and it was explained in, Subsection 4.2.1 (Effect of Grain Size). An explanation of the second finding is presented herein.

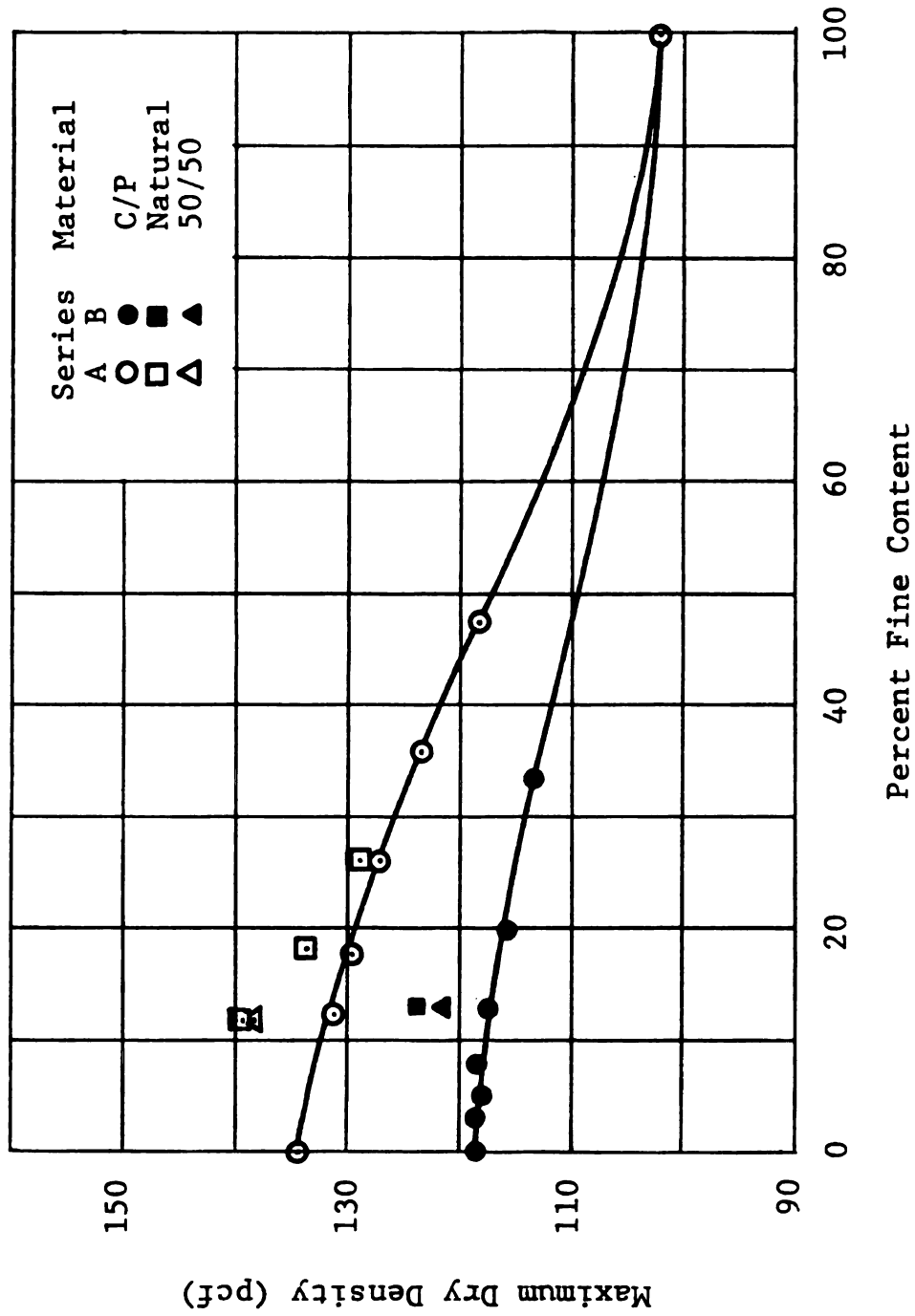


FIGURE 4.15 MAXIMUM DRY DENSITY VERSUS PERCENT FINE CONTENT OF SERIES A AND B SAMPLES THAT CONSISTED OF C/P, NATURAL, AND 50/50 MATERIALS.

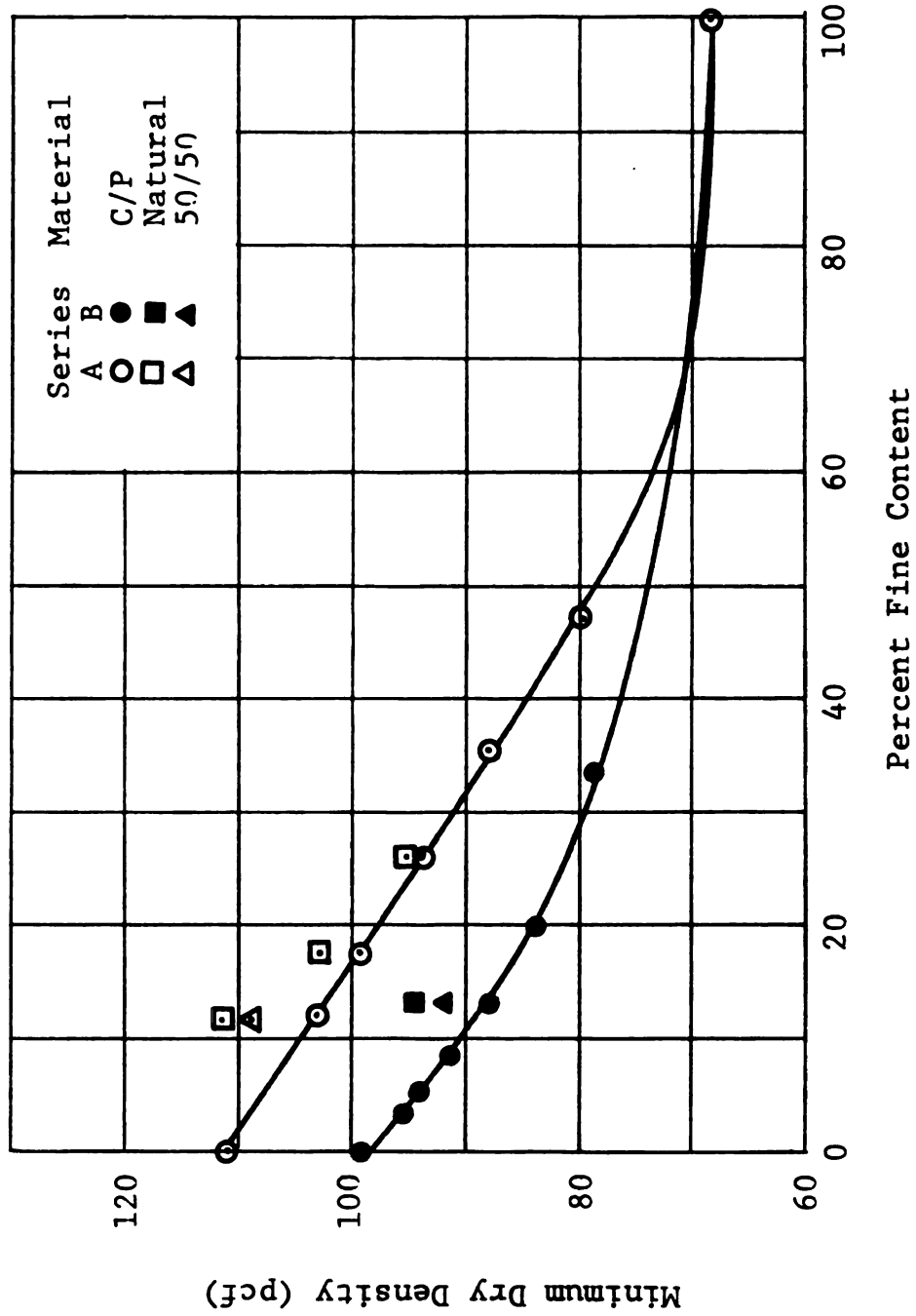


FIGURE 4.16 MINIMUM DRY DENSITY VERSUS PERCENT FINE CONTENT OF SERIES A AND B SAMPLES THAT CONSISTED OF C/P, NATURAL, AND 50/50 MATERIALS.

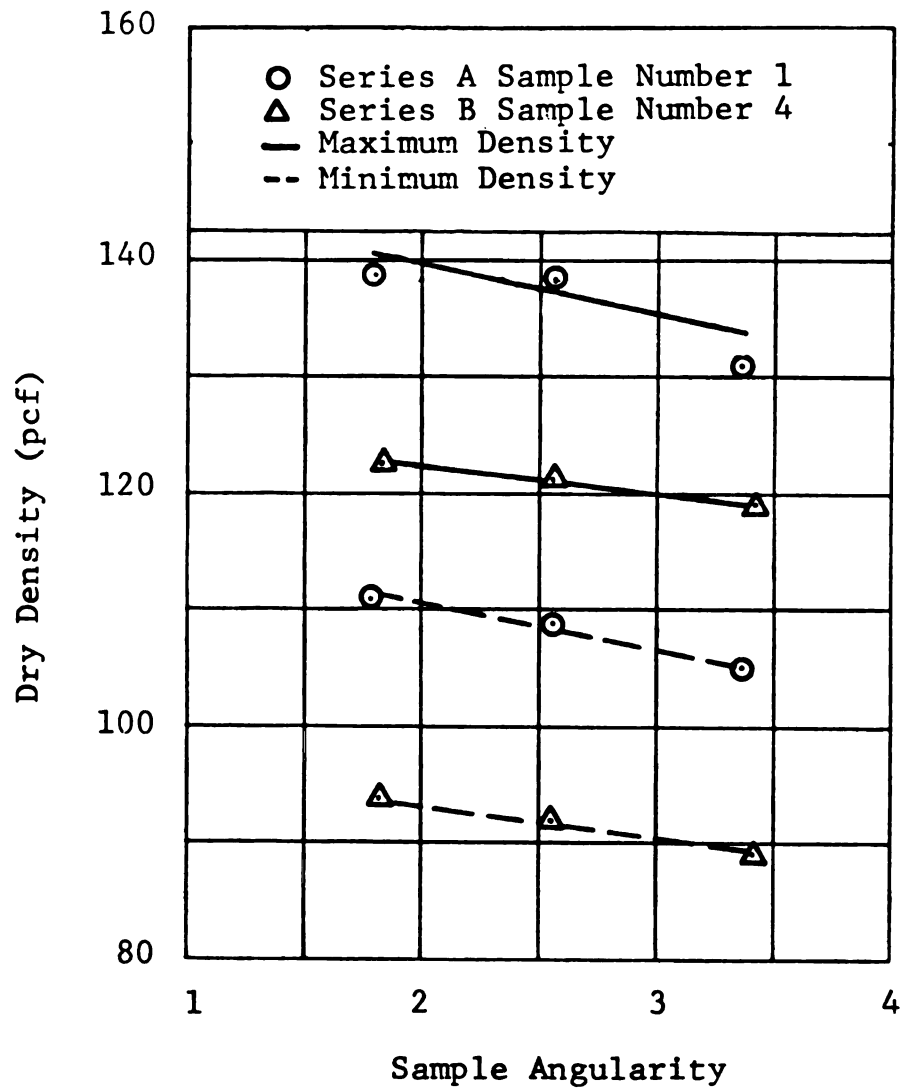


FIGURE 4.17 MAXIMUM AND MINIMUM DRY DENSITIES VERSUS SAMPLE ANGULARITY OF SERIES A AND B SAMPLES.

As the percent fine content of the soil samples increases, sand and/or gravel particles become isolated and suspended (floating) in the fine material. Consequently, the fine material dominates the sample and affect its response. Thus, the effect of the shape of the coarse particles decreases as more and more of these particles become isolated in the fine. In addition, the shape of the fine particles possesses no effect on the sample behavior. That is the maximum and minimum densities of soils consist of one hundred percent rounded or angular and flat fine particles (per se) are the same and independent of the particle shape. To verify this, two specimens of sample 3 of series A were prepared. The first was mixed using one hundred percent natural materials (rounded to subrounded). The second specimen was mixed using the same coarse material as that of the first specimen except that the natural fine material was replaced by the C/P fine materials. Maximum and minimum dry density tests were then conducted using these two samples and the test results were then compared. It was found that the differences in the maximum or minimum dry densities between the two samples were within the testing error (1%).

The third finding was expected and it is consistent with that found in the literature. Rounded particles in a soil matrix (due to their own weights) can freely move and slide on top of each other to a denser type of particle arrangement than that of angular particles. The grain shape

(angularity) of the latter will resist such movement and sliding due to particle interlocking. It is very well known, in the pavement industry, 'that asphalt or concrete mixes made up of rounded particles will possess higher density than those with crushed aggregates. Also, the former mixes are less stable than the latter. Moreover, Figure 4.18 depicts the test results of this study as well as those of Holubec and D'Appolonia's (37). Examination of the figure indicates that:

- a) For this study, the effect of sample angularity on the maximum and minimum dry densities of the soil is the same and consistent with that of the maximum dry density of Holubec and D'Appolonia.
- b) For Holubec and D'Appolonia study, the particle angularity have a higher influence on the minimum dry density than on the maximum.

The differences in the findings could be attributed to the different characteristics of the test materials. Holubec and D'appolonia's test materials possessed a coefficient of uniformity of 1.5 to 1.9 and zero percent fine content.

Finally, Figure 4.19 shows plots of the maximum and minimum dry densities as a function of the percent combination of the natural and C/P materials. It can be noted from the figure that the relationship between dry densities and the percent combination can be approximated by a linear function and that the higher the percent rounded

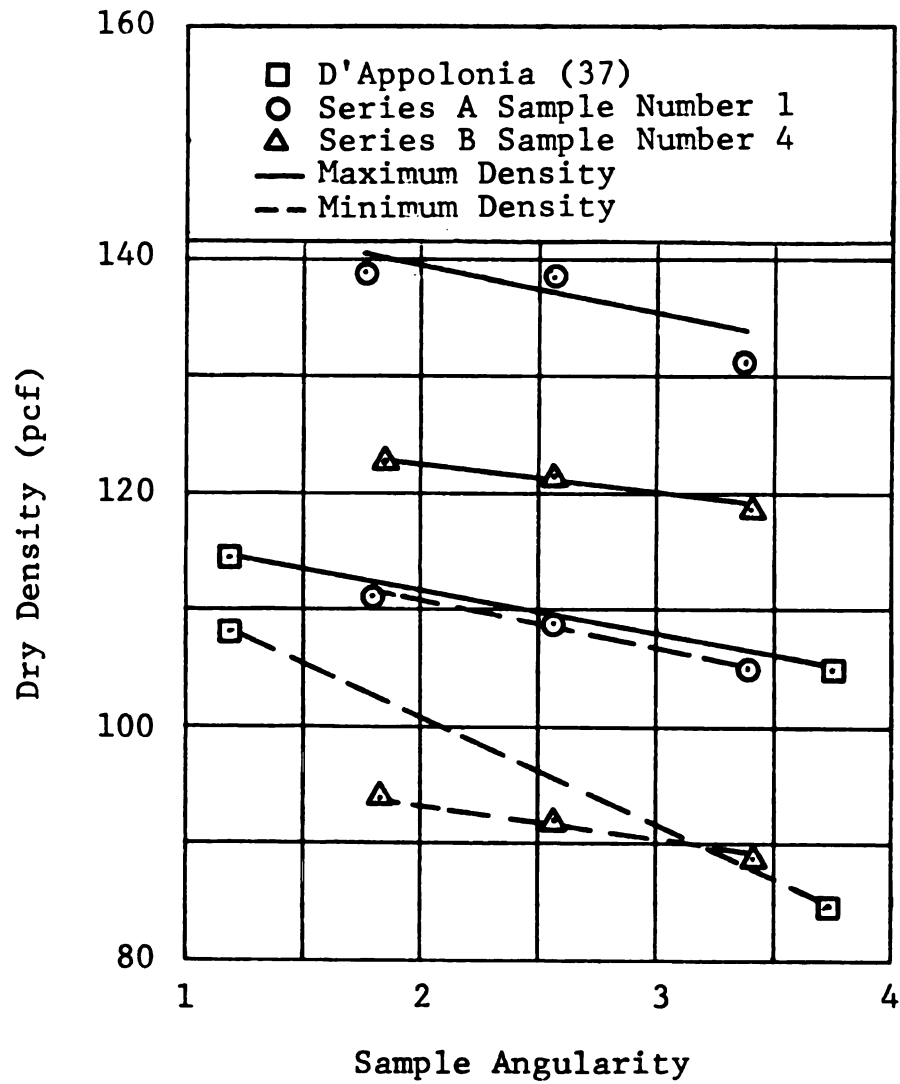


FIGURE 4.18 MAXIMUM AND MINIMUM DRY DENSITIES VERSUS SAMPLE ANGULARITY OF SERIES A AND B SAMPLES, (37).

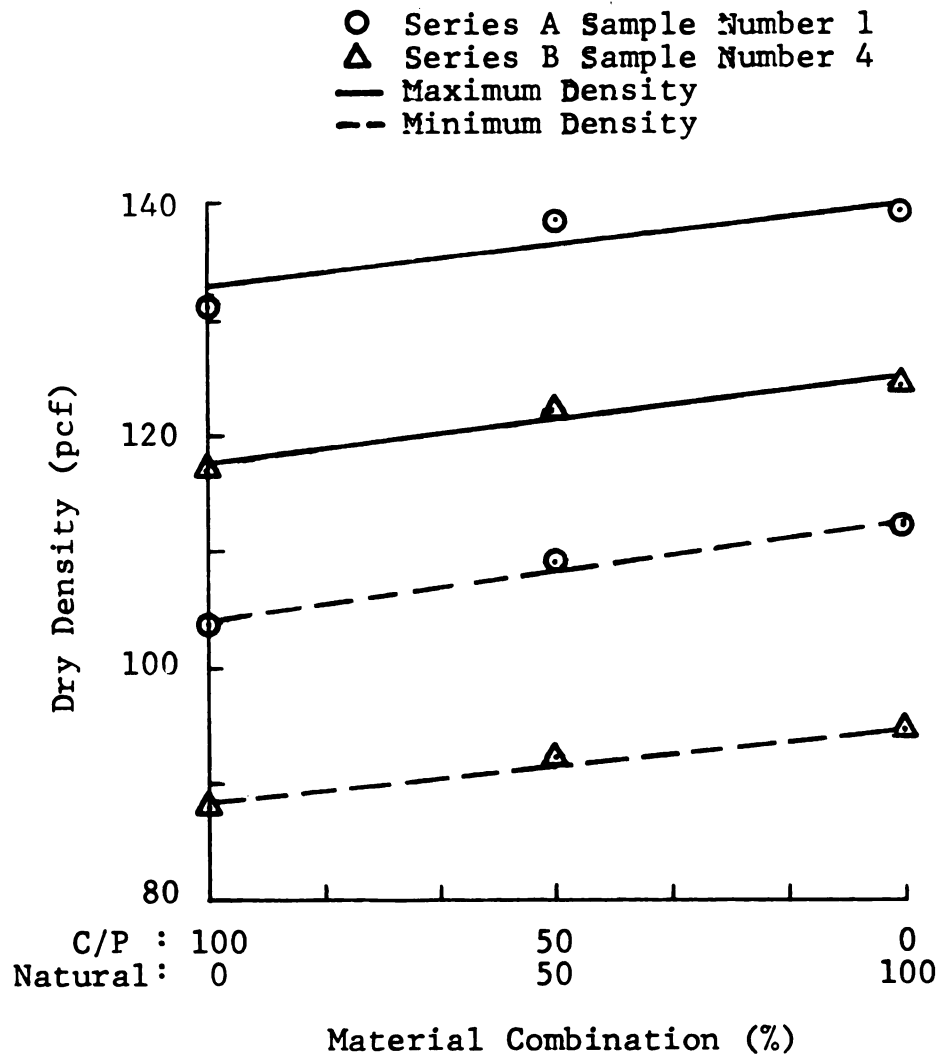


FIGURE 4.19 MAXIMUM AND MINIMUM DRY DENSITIES VERSUS PERCENT COMBINATION OF THE C/P AND NATURAL MATERIALS.

material the higher the densities.

4.3 ANGLE OF REPOSE

The angle of repose (ϕ_R) represents the angle of internal friction of a dry cohesionless soil at its loosest possible state and it depends to a large extent on the grain characteristics of the material.

In general, the angle of repose is measured by pouring a dry soil from a single point (such as a cone) located at 6 inch (15.2 cm) above a leveled and horizontal surface to form a conical pile. As more soil is deposited on the pile, particles would slip and slide down the slope to a more stable position. The angle of the slope with respect to the horizontal is a measure of the angle of repose of the soil. This method however, was found unsuitable in this study. Soil samples with high percent fine contents experienced arching effect and a honeycomb type structure which blocked the one inch (2.54 cm) cone opening and prohibited the soil particles from pouring freely. A larger cone opening was found impractical because the soil was dropping from the cone rather than pouring through it. Consequently, a new test procedure (pull-up method) was developed and utilized in this investigation for all the samples of series A and B (low and high percent fine contents). The test procedure is outlined in Chapter 3.

Angle of repose tests were conducted on samples of

series A and B. At least three measurements (at different locations) of the slope of the conical pile were taken for each sample, and the average value was then calculated. The measured and average values of the angle of repose are summarized in Tables D.1 and D.2 of Appendix D for the C/P material, and in Table D.3 for the natural and 50/50 materials. It can be noted that, for all samples, the value of the angle of repose ranges from a high of 37.75 to a low of 23.67 degrees.

In the following subsections, the effects of grain size, sample gradation, and grain shape on the angle of repose are discussed.

4.3.1 EFFECT OF GRAIN SIZE

Figure 4.20 shows a plot of the angle of repose versus the percent fine contents of series A and B samples that consisted of the C/P materials. Examination of the figure indicates that the value of the angle of repose of the soil samples decreases as the percent fine content increases. This finding was expected and compatible to that reported in the literature (38). An explanation of this is given next. First, recall that the angle of repose represents the angle of friction of the soil at their loosest possible state or maximum void ratio. Second, from Figures 4.8 and 4.9, it can be noted that the higher the percent fine content, the higher the maximum void ratio. Thus, the angle of repose

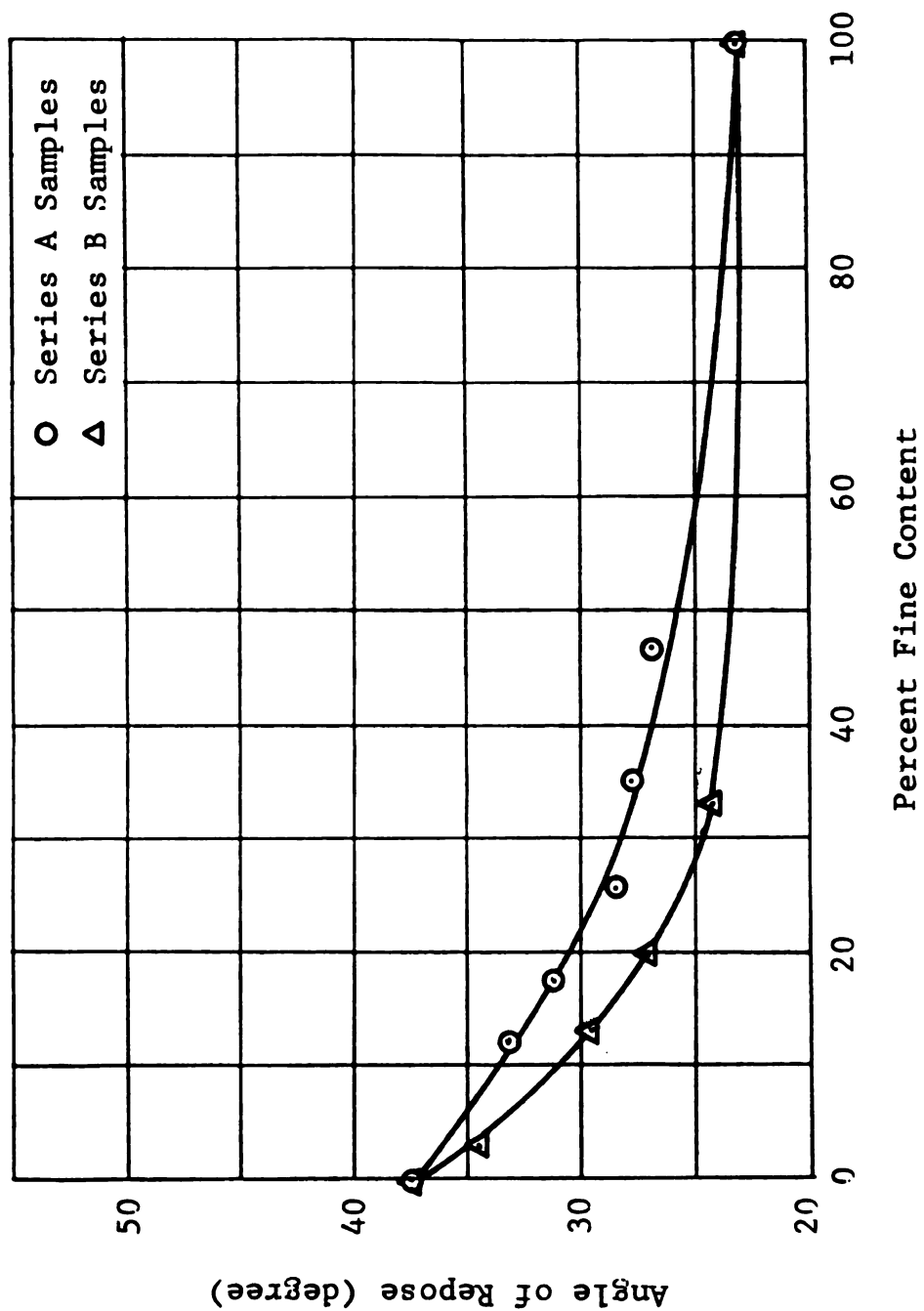


FIGURE 4.20 ANGLE OF REPOSE VERSUS PERCENT FINE CONTENT OF SERIES A AND B SAMPLES.

tests were conducted using soil samples with different void ratios. The higher the void space in the soil, the less the contact area of the solid, and the higher the contact pressure due to the weight of the soil. Consequently, the soil particles, under the higher contact pressure, will slide to a lower and more stable slope resulting in a lower value of the angle of repose. In addition, the potential of stacking up large particled soils on a vertical face, per se, is much greater than that of fined particled soils. This is mainly due to the high potential of creating horizontal or near horizontal surfaces during stacking upon which other particles will rest in a stable position.

The relationship relating the angle of repose to the percent fine content of the soil were then modeled using equations 4.13 and 4.14 for series A and B samples respectively.

$$\phi_R = 37.75 - 42.45 (PF) \{EXP[-1.1(PF)^{0.96}]\} \quad (4.13)$$

$$\phi_R = 37.75 - 115.0 (PF) \{EXP[-2.1(PF)^{0.82}]\} \quad (4.14)$$

where: ϕ_R = angle of repose;

PF = percent fine content (PF = 0.0 to 1.0); and

EXP = exponential function.

The correspondence between the measured data and those

calculated using equations 4.13 and 4.14 is shown in Figure 4.21. It should be noted that the maximum absolute difference between the calculated and measured data is 1.0 degree or 3.86 percent.

4.3.2 EFFECT OF SAMPLE GRADATION

Recall that the soil samples of series A and B possess coefficient of uniformity (Cu) of 45.0 and 8.89 respectively. Thus, the effect of samples gradation on the angle of repose can be studied by comparing the test results of the soil samples of the two series.

Examination of Figure 4.20 indicates that the higher the coefficient of uniformity, the higher the angle of repose. That is the more uniform the soil sample, the lower the angle of repose. This observation can be illustrated by subtracting equation 4.14 from equation 4.13 and plotting the differences between the two equations as a function of the percent fine content of the samples. Such a plot is shown in Figure 4.22. Examination of the figure indicates that for zero and 100 percent fine contents of the soil, the angle of repose is independent of the sample gradation. The effect of samples gradation however, is maximum for a fine content of about 22.5 percent. That is the sample gradation have its maximum effect on the angle of repose at an optimum fine content of the soil of 22.5 percent.

The above finding however, should be taken cautiously

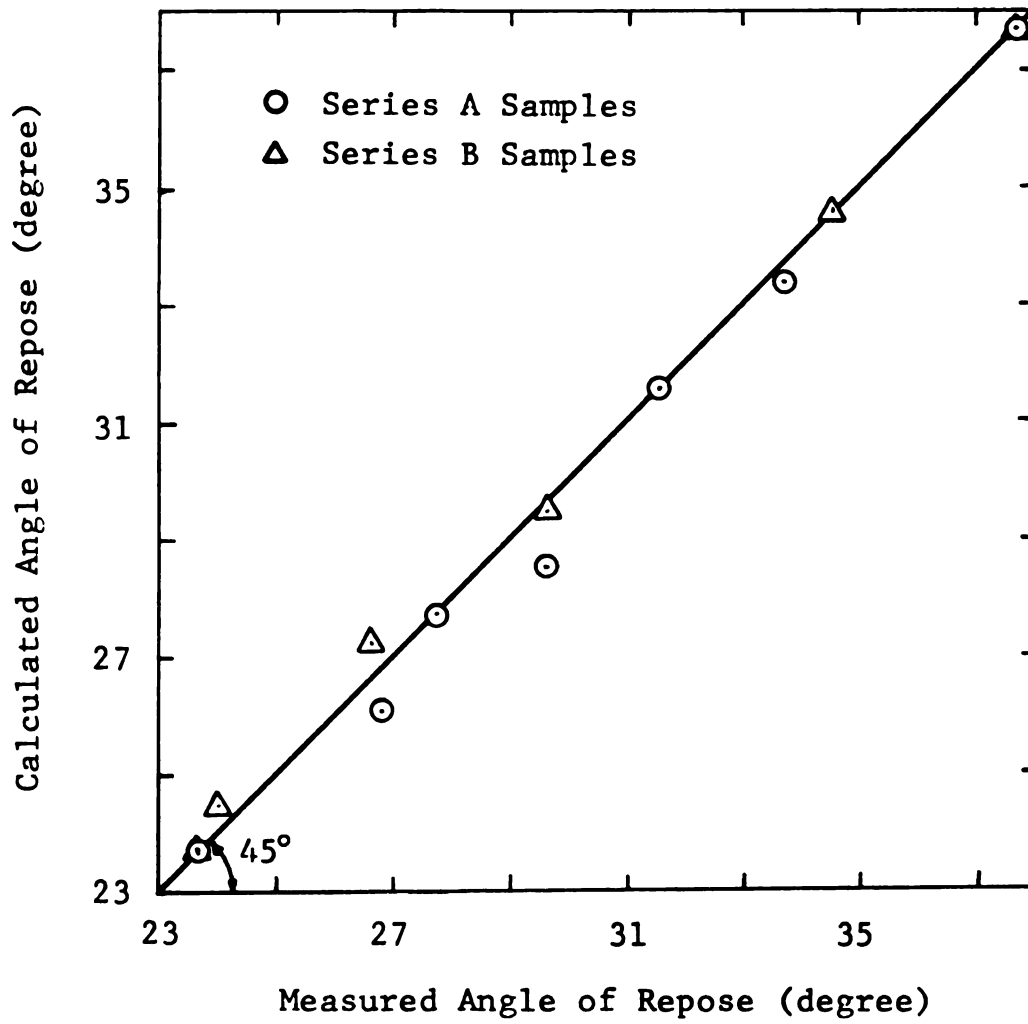


FIGURE 4.21 CALCULATED VERSUS MEASURED ANGLE OF REPOSE OF SERIES A AND B SAMPLES.

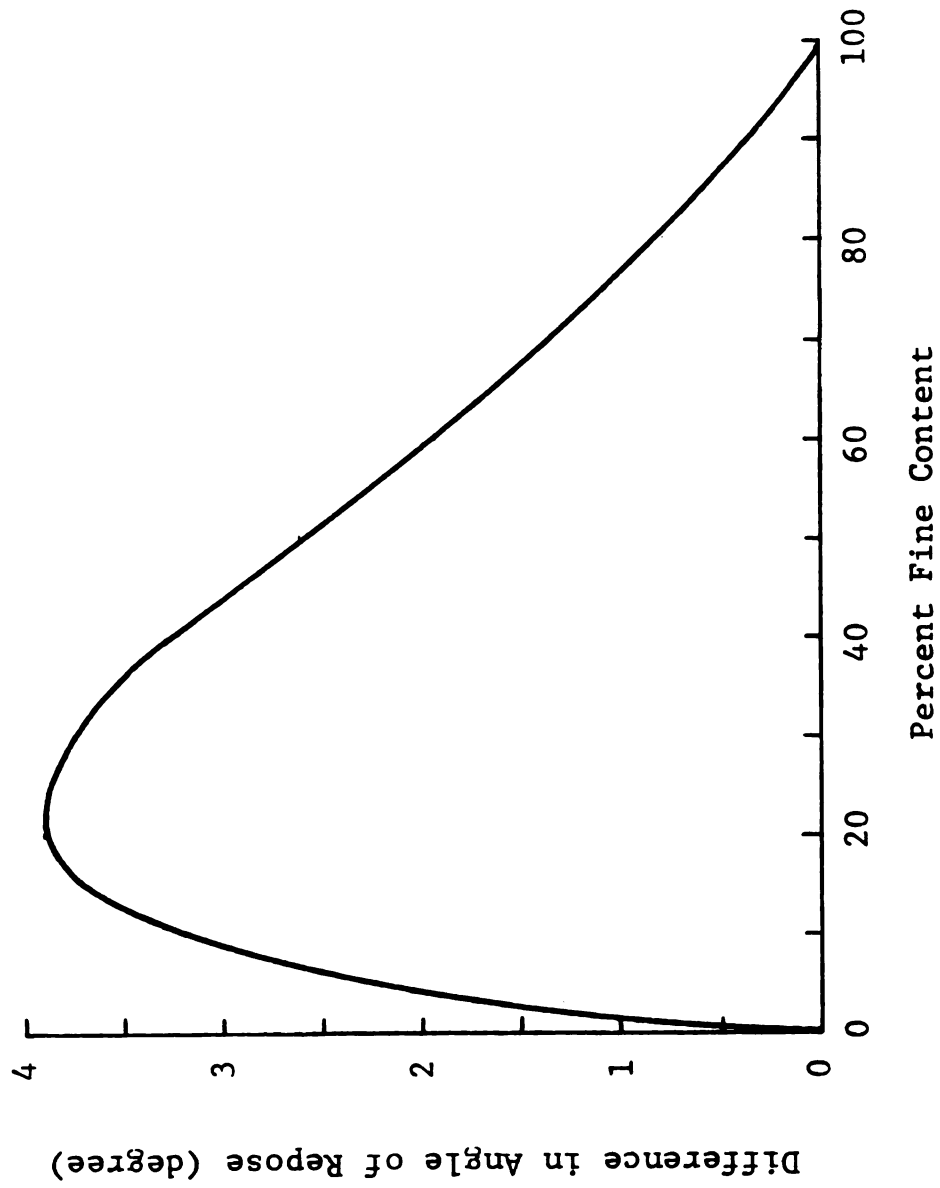


FIGURE 4.22 DIFFERENCES IN THE ANGLE OF REPOSE BETWEEN SERIES A AND B SAMPLES VERSUS PERCENT FINE CONTENT.

when studying the effect of gradation on the angle of repose using the percent fine content of the soil. Consider Figure 4.23 in which the values of the angle of repose are plotted against the maximum particle size of the soil samples of series A and B. Examination of the figure indicates that:

- a) The angle of repose decreases as the maximum particle size decreases. This is compatible to the effect of percent fine content of the samples.
- b) For the same maximum grain size of the soil, the angle of repose is independent of the sample gradation. This is in conflict to that reported above based on the percent fine content of the soil.

The finding in item b above suggests that the frictional property of a soil (the angle of repose) is dependent on the individual particle characteristics (grain size and shape) rather than the gradation of a collection of particles.

4.3.3 EFFECT OF GRAIN SHAPE

Recall that (see Chapter 3) the test materials were crushed and pulverized and then recombined to possess three different grain shapes. These are the C/P, natural and 50/50 materials. Selected samples of the natural and 50/50 materials were tested and their angle of repose were measured. These are samples 1, 2, and 3 of series A and 4 of series B using the natural material, and samples 1 of series A and 4 of series B using the 50/50 material.

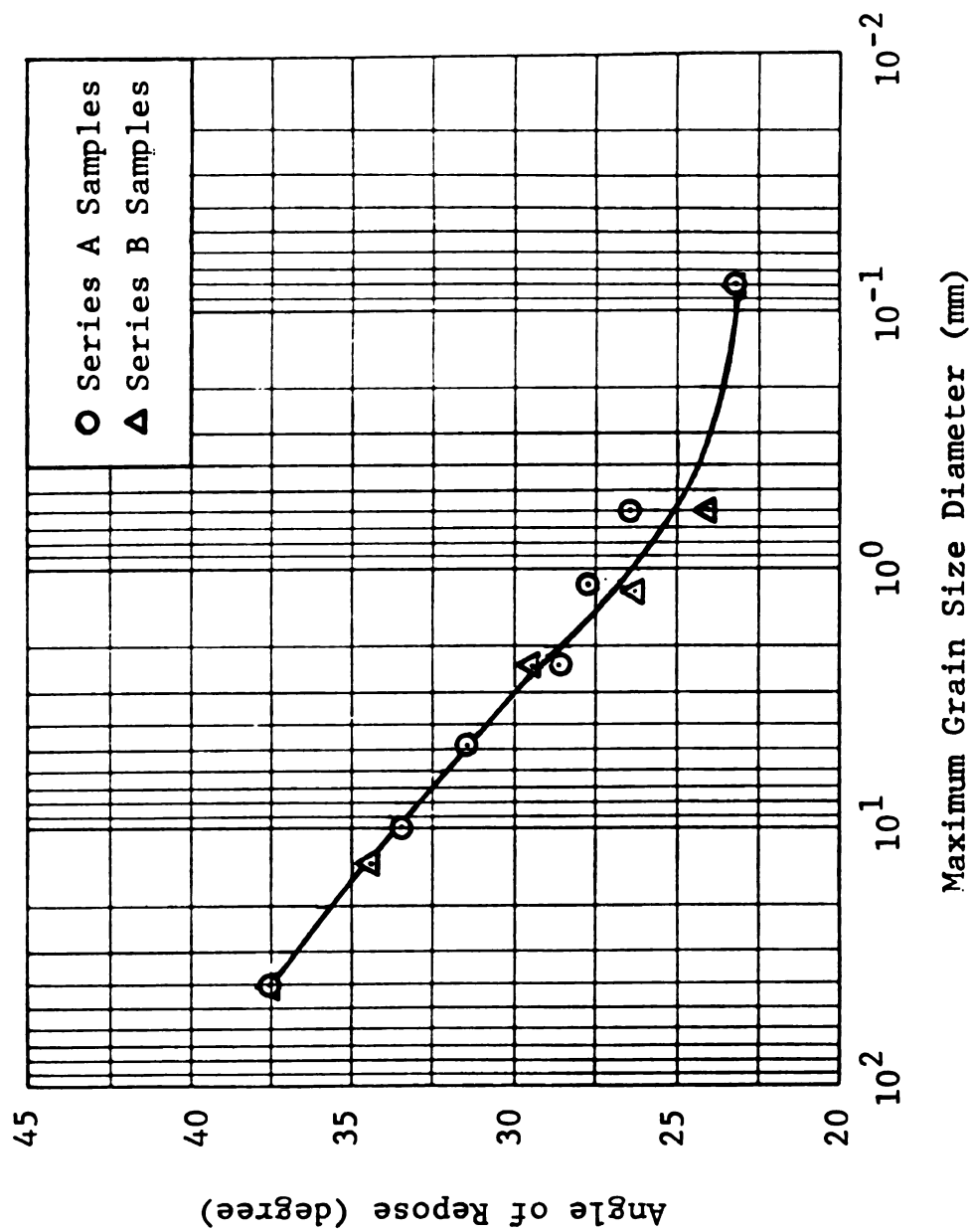


FIGURE 4.23 ANGLE OF REPOSE VERSUS THE MAXIMUM GRAIN SIZE OF SERIES A AND B SAMPLES.

Figures 4.24, and 4.25 depict the angle of repose of the soil of series A and B, and the selected samples plotted against the percent fine content and the maximum particle size of the soil. Figure 4.26 shows plots of the angle of repose of the selected samples as a function of the particle angularity of the samples. Finally, Figure 4.27 depicts the angle of repose plotted against the percent combination of the natural and C/P materials. Examination of the Figures indicates that:

- a) The effect of particle shape on the angle of repose decreases as the percent fine content increases, or the maximum particle size decreases (Figures 4.24 and 4.25).
- b) The higher the particle angularity the higher the angle of repose of the soil (Figure 4.26).
- c) The angle of repose of the soils decreases as the percent C/P materials of the soil sample decreases (Figure 4.27).

That is the C/P material (subangular to angular) possesses the highest angle of repose while the natural material possesses the lowest. Further, as the percent fine content increases, or the maximum particle size of the soil samples decreases the effect of grain shape on the angle of repose becomes negligible. This was expected and consistent with the findings of Subsections 4.3.1, and 4.3.2. Since the grains of the C/P material are more angular than those of

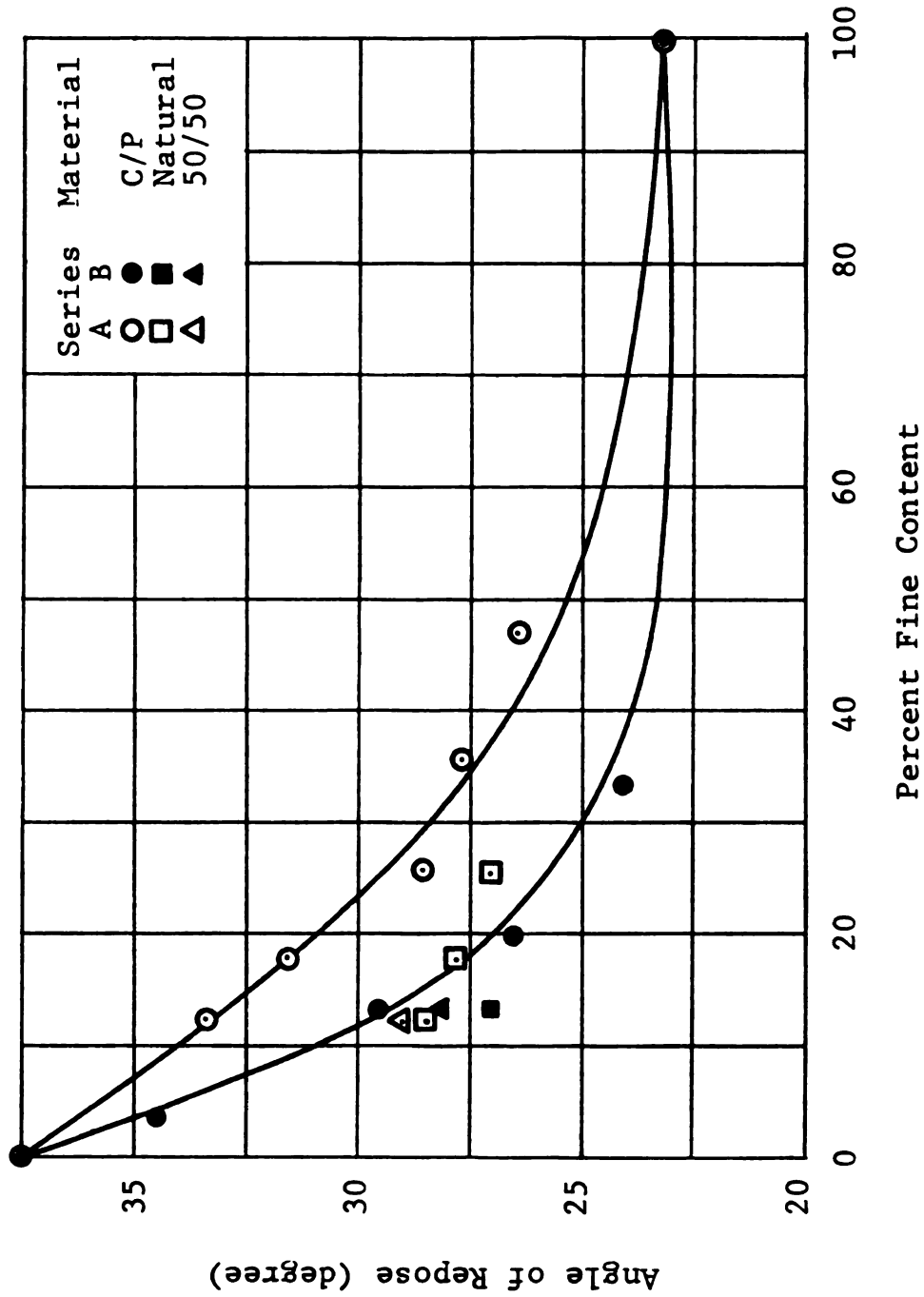


FIGURE 4.24 ANGLE OF REPOSE VERSUS PERCENT FINE CONTENT OF SERIES A AND B SAMPLES THAT CONSISTED OF THE C/P, NATURAL, AND 50/50 MATERIALS.

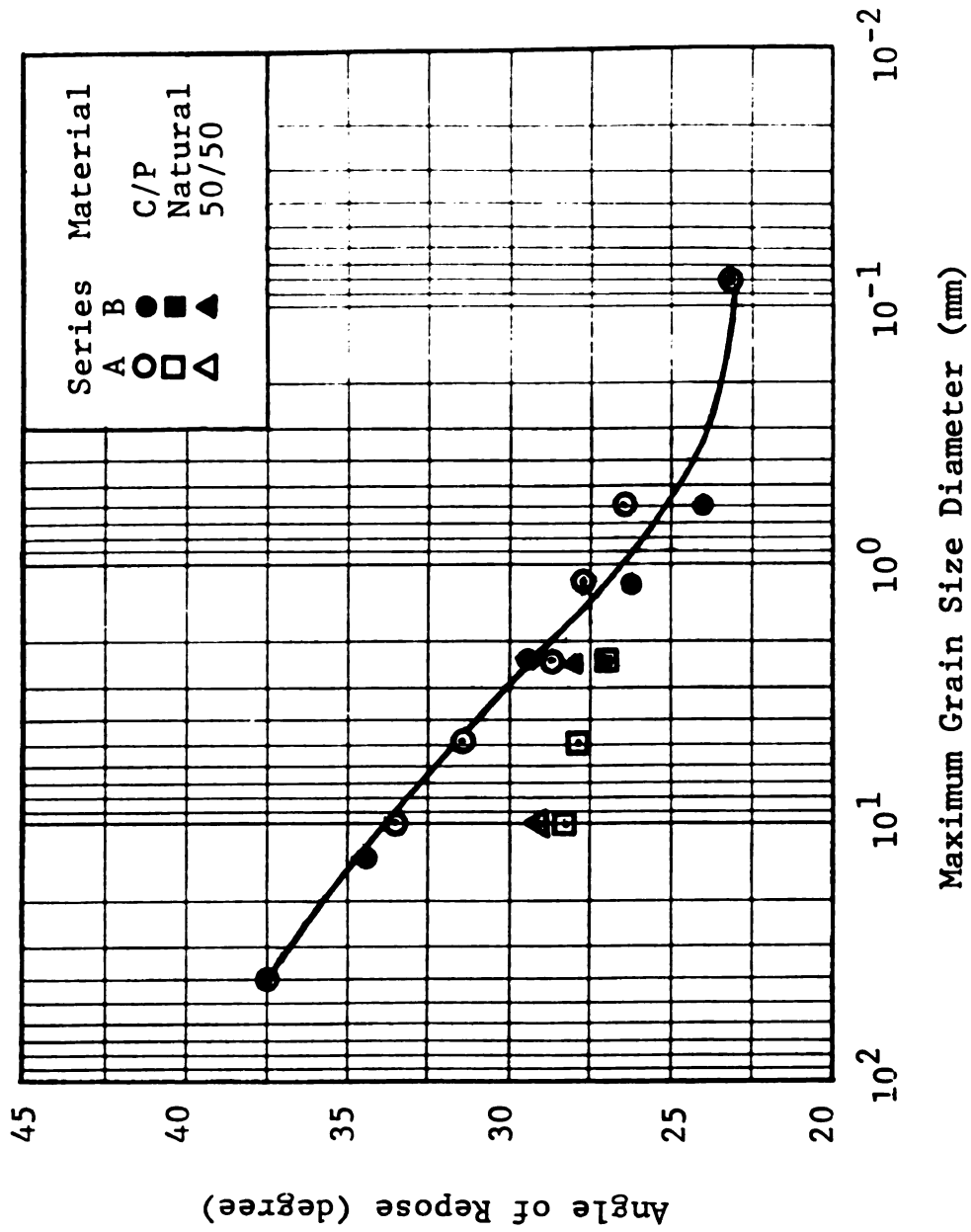


FIGURE 4.25 ANGLE OF REPOSE VERSUS THE MAXIMUM GRAIN SIZE OF SERIES A AND B SAMPLES THAT CONSISTED OF THE C/P, NATURAL, AND 50/50 MATERIALS.

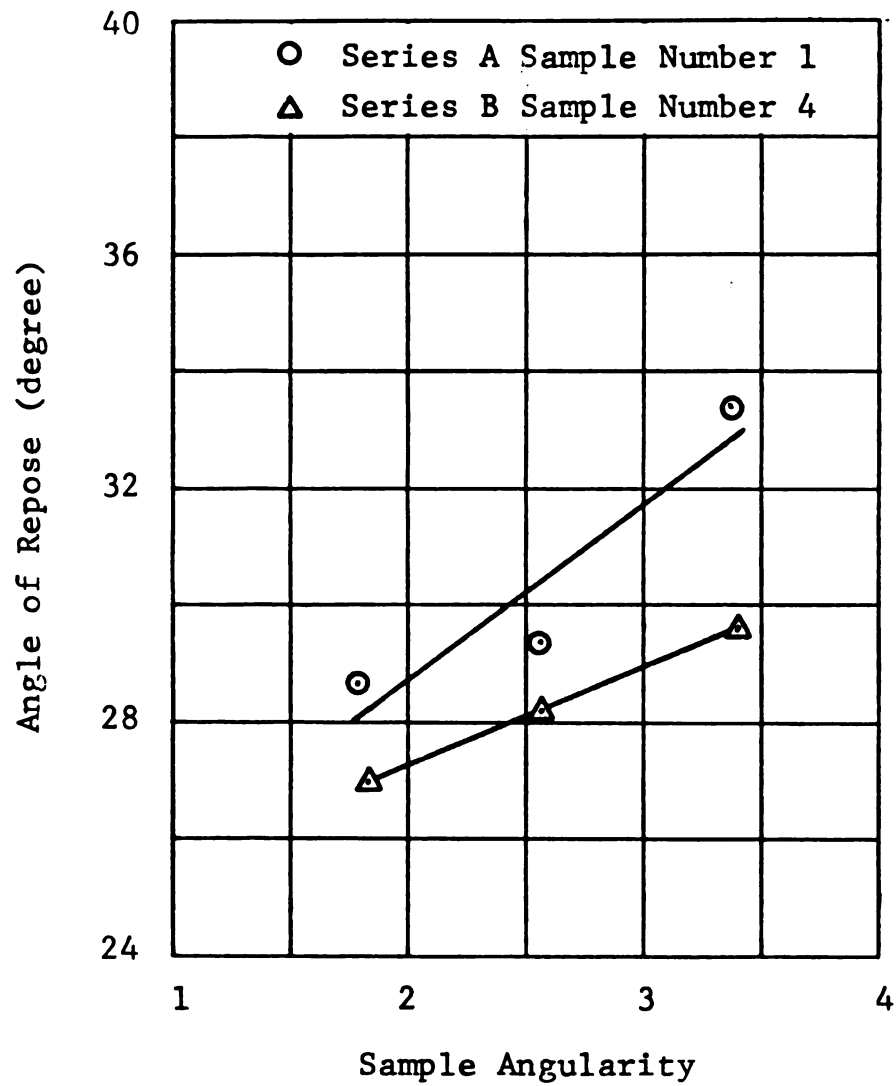


FIGURE 4.26 ANGLE OF REPOSE VERSUS SAMPLE ANGULARITY OF SAMPLES NUMBER 1 OF SERIES A AND NUMBER 4 OF SERIES B.

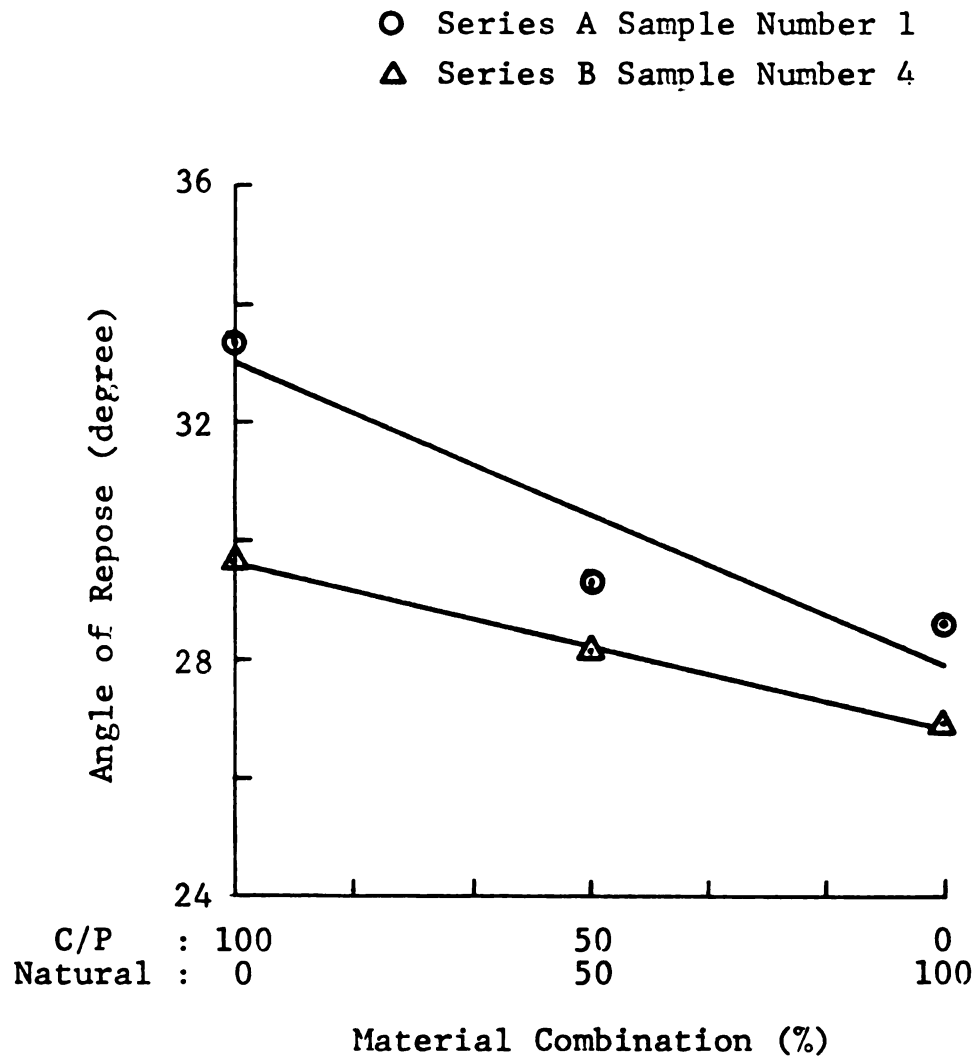


FIGURE 4.27 ANGLE OF REPOSE VERSUS PERCENT COMBINATION OF THE C/P AND NATURAL MATERIALS.

the natural material, their resistant to sliding and rolling on top of each other is also higher and consequently, they possess higher angle of repose.

4.4 VOLUME CHANGE

Throughout the triaxial test program, the sample volume change (sample dilatation and contraction) during shear was not measured due to the unavailability of proper equipment. It was noticed however, that loose to medium dense dry specimens experienced large volume change during the application of the confining pressure. Since the analysis of the triaxial test results are based upon the initial density of the soil sample, it was decided to measure the sample volume change due to the application of the confining (hydrostatic) pressure and to adjust the sample density accordingly. The test procedure utilized herein is explained in Chapter 3.

It should be noted that wet specimens experienced insignificant volume change (the volume change was almost zero) due to the application of the confining pressure of 5 psi. No wet tests were conducted under higher confining pressures.

In this Section and throughout the remaining parts of this dissertation, the term "initial density" will be used to indicate the specimen density prior to the application of the confining pressure. "Specimen density" or "soil density"

indicates the specimen or soil density after the application of the confining pressure.

Three different confining pressures of 5, 25, and 50 psi (34.5, 172.4, and 344.8 kN/m²) were utilized in this study. Soil specimens of series A and B samples were blended and prepared at relative densities of 0.4, 0.6, and 0.8 and tested under the various confining pressures. The volume change of the specimens due to the application of the confining pressure was then measured. Figures 4.28, 4.29, and 4.30 depict the percent volume change for various initial relative densities of series A samples and for confining pressures of 5, 25, and 50 psi (34.5, 172.4, and 344.8 kN/m²) respectively. The volume change data were then utilized to calculate the corresponding changes in relative density of the samples. Figures 4.31, 4.32, and 4.33 show plots of the change of the relative density versus the percent fine content of series A samples for three confining pressures. Each curve in the figures represents one initial relative density of the soil specimen. The curves were then modeled using the following equation:

$$\Delta Dr = I + S(PF)\{EXP[B(PF)]\} \quad (4.15)$$

where: I, S, and B are model parameters that are dependent on the confining pressure, sample initial density, and the coefficient of uniformity;

PF = percent fine content (PF = 0.0 to 1.0); and

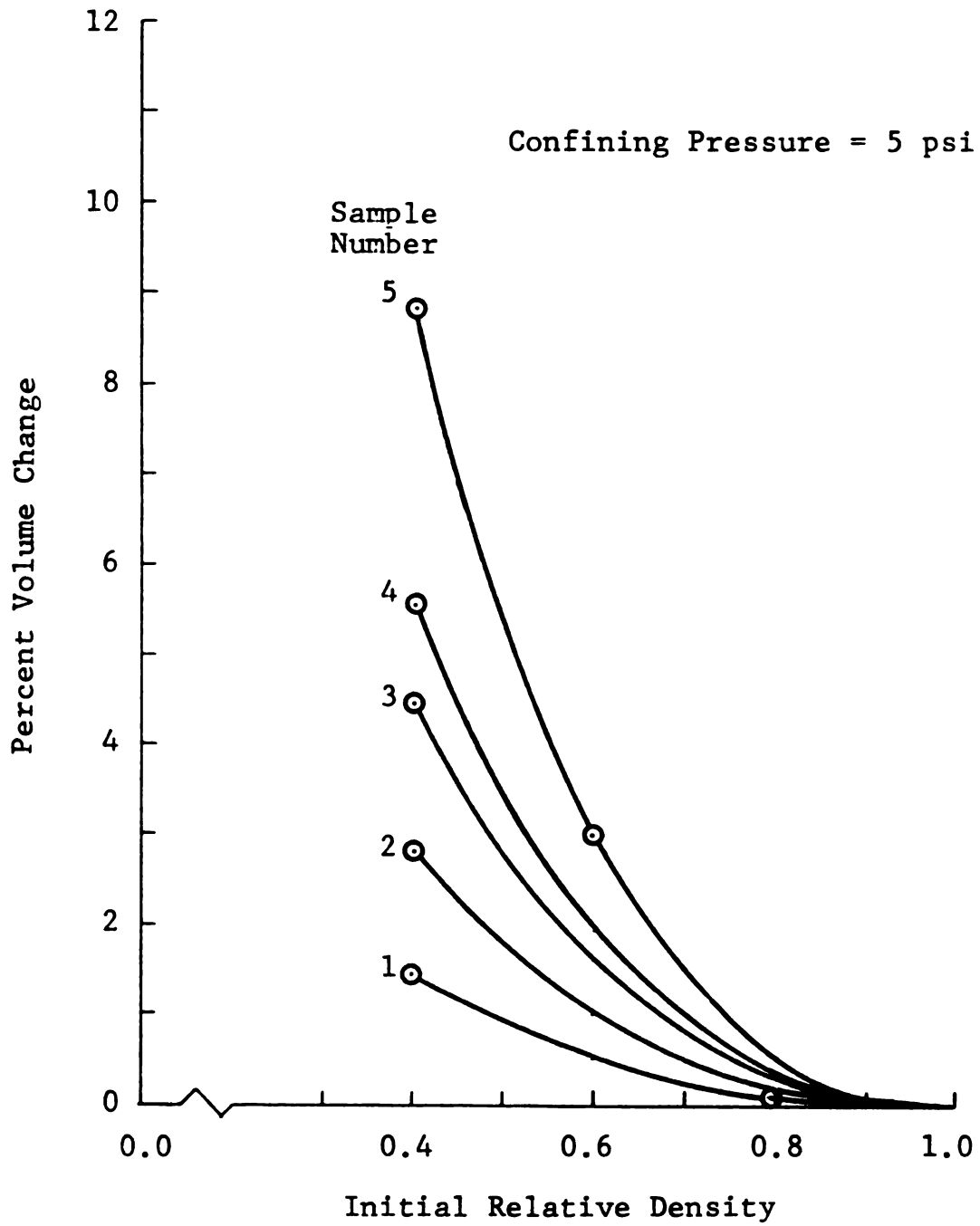


FIGURE 4.28 PERCENT VOLUME CHANGE FOR A CONFINING PRESSURE OF 5 PSI VERSUS INITIAL RELATIVE DENSITY OF SERIES A SAMPLES.

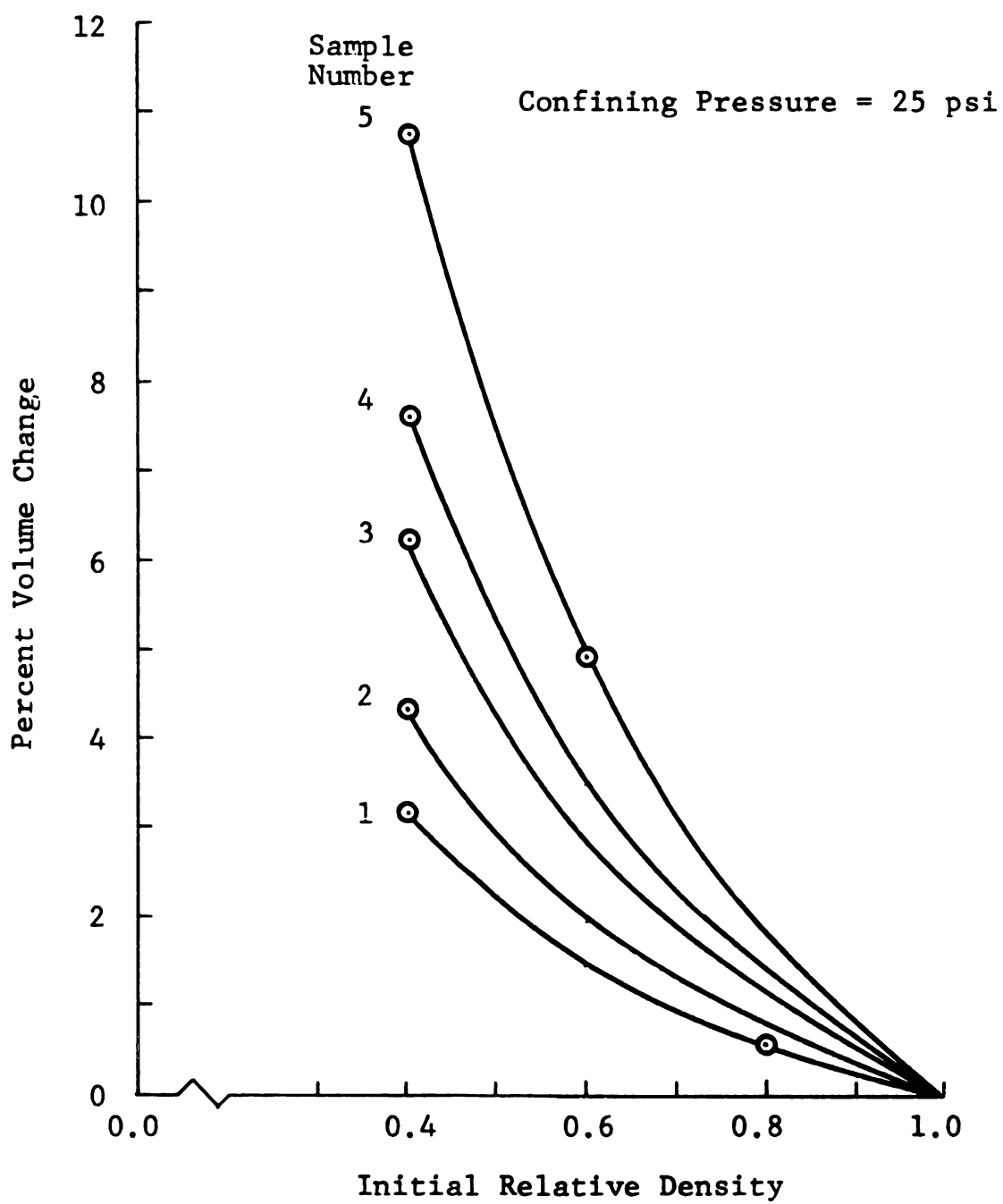


FIGURE 4.29 PERCENT VOLUME CHANGE FOR A CONFINING PRESSURE OF 25 PSI VERSUS INITIAL RELATIVE DENSITY OF SERIES A SAMPLES.

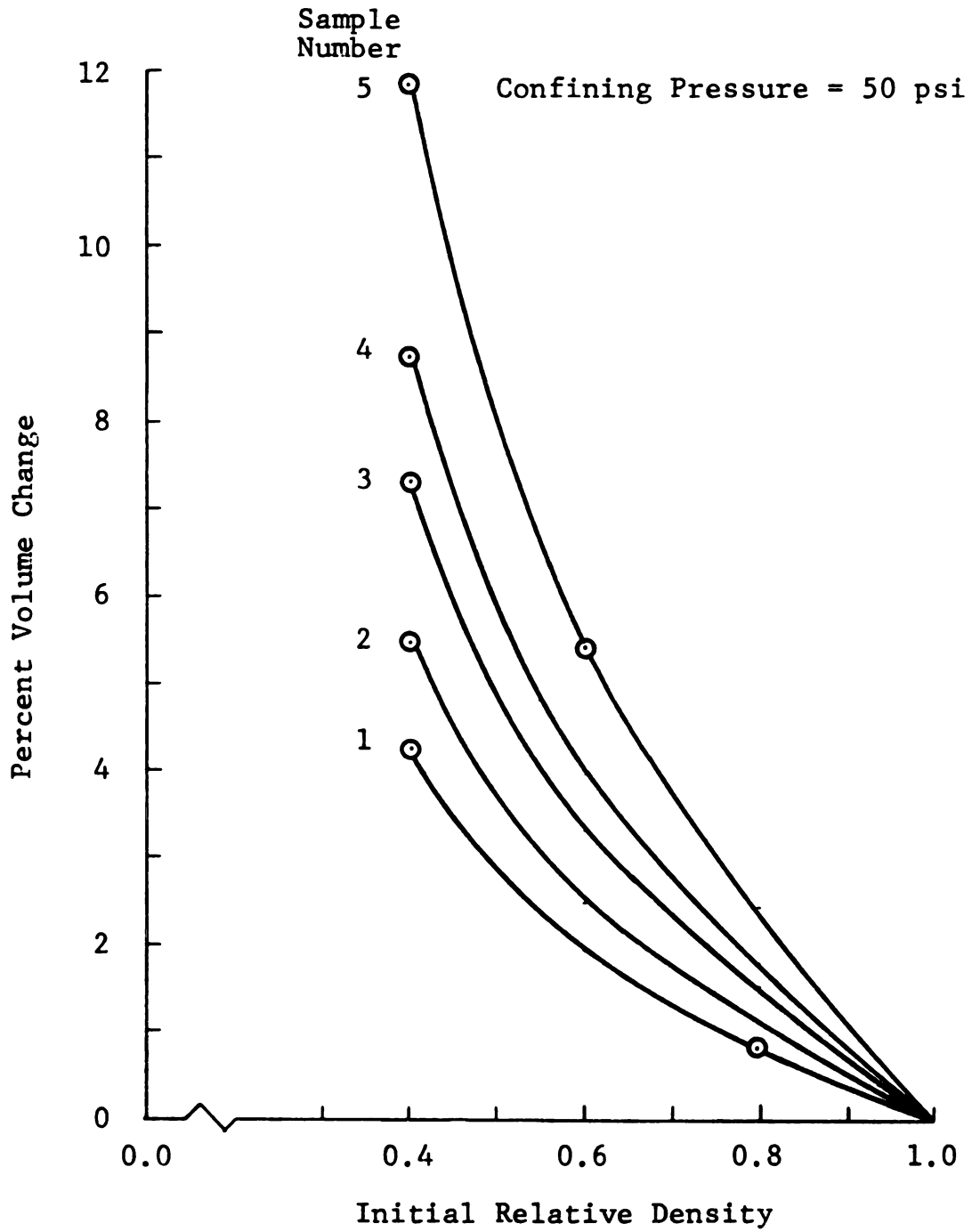


FIGURE 4.30 PERCENT VOLUME CHANGE FOR A CONFINING PRESSURE OF 50 PSI VERSUS INITIAL RELATIVE DENSITY OF SERIES A SAMPLES.

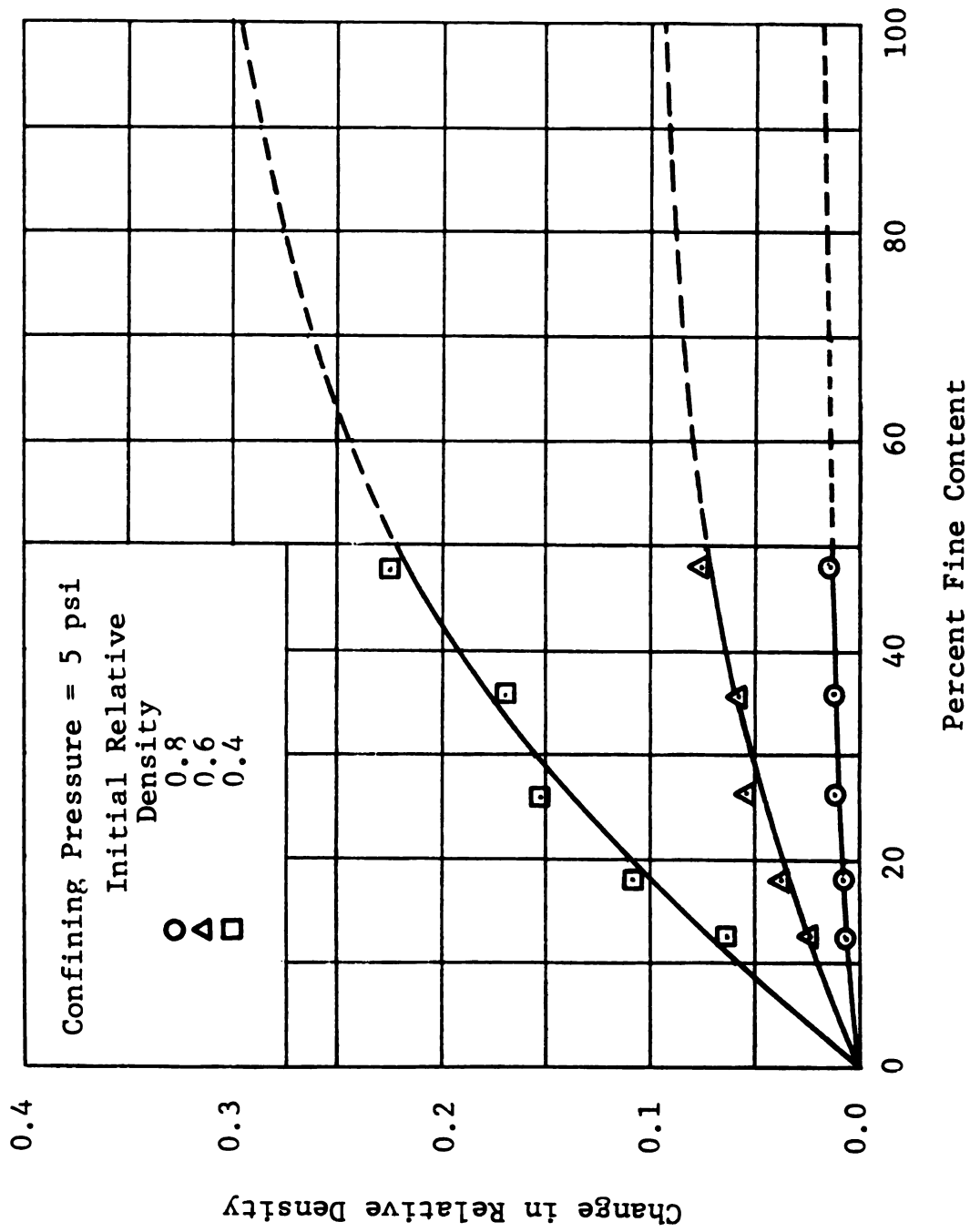


FIGURE 4.31 RELATIVE DENSITY CHANGE FOR A CONFINING PRESSURE OF 5 PSI VERSUS PERCENT FINE CONTENT OF SERIES A SAMPLES.

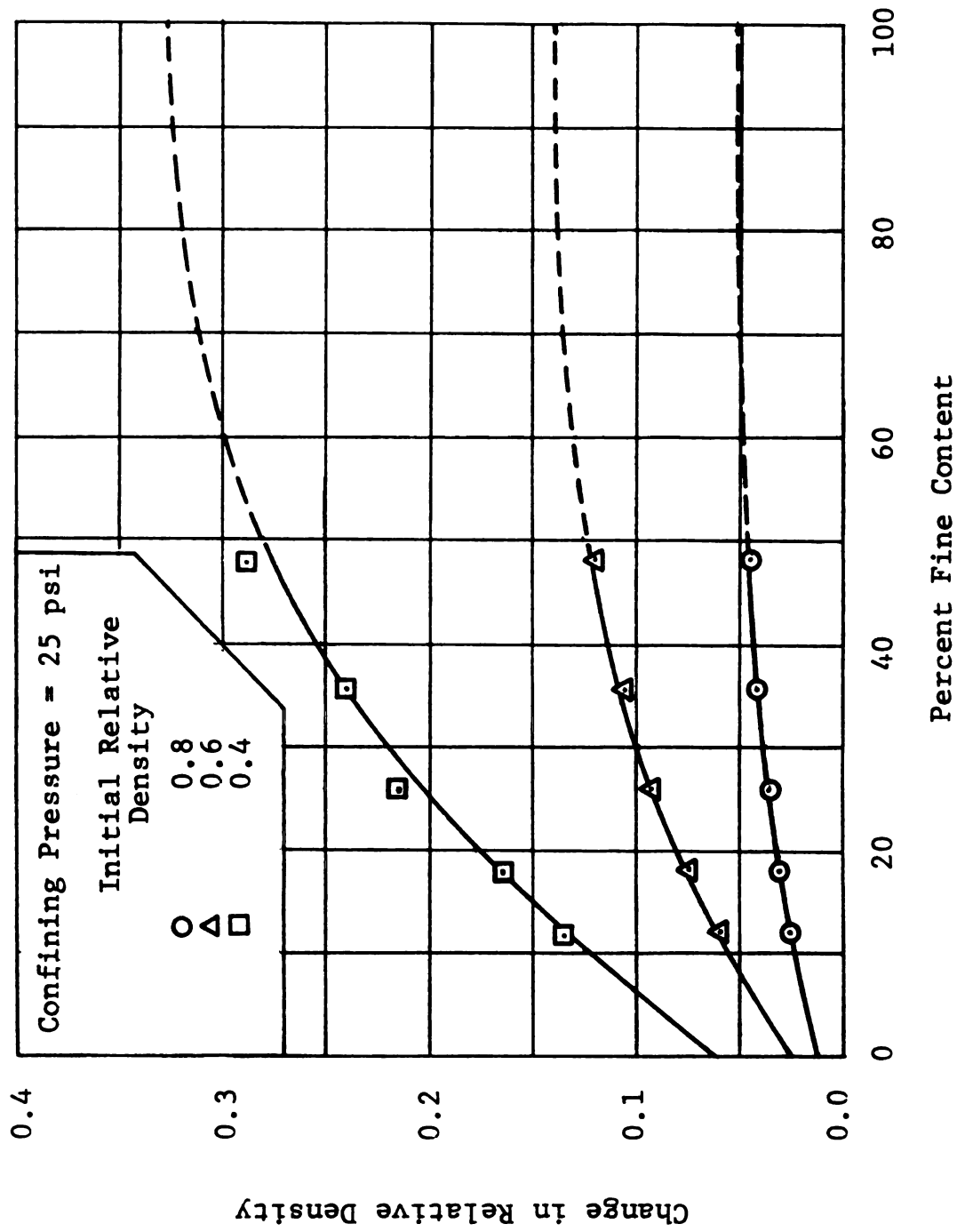


FIGURE 4.32 RELATIVE DENSITY CHANGE FOR A CONFINING PRESSURE OF 25 PSI VERSUS PERCENT FINE CONTENT OF SERIES A SAMPLES.

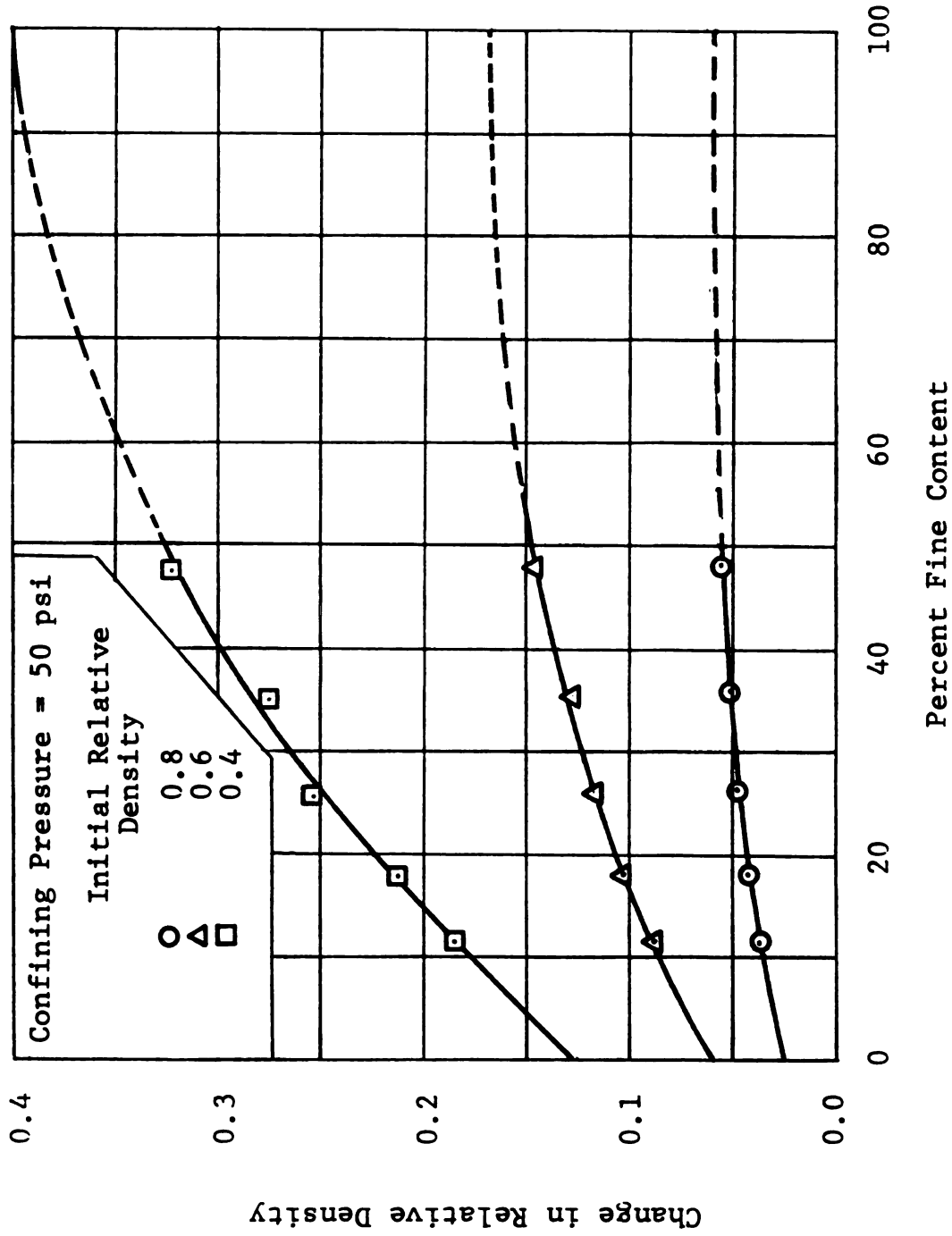


FIGURE 4.33 RELATIVE DENSITY CHANGE FOR A CONFINING PRESSURE OF 50 PSI VERSUS PERCENT FINE CONTENT OF SERIES A SAMPLES.

ΔDr = the change in the initial relative density due to the application of the confining pressure.

The model parameters were then calibrated by utilizing the test results. Figure 4.34, 4.35, and 4.36 show plots of the values of the parameters versus the initial density of series A samples for the indicated confining pressure. The functional relationships relating the values of the parameters to the initial relative density of series A samples were then developed and incorporated into equation 4.15.

Further, the test results of series B samples showed similar trend to that of series A samples. Consequently, similar plots were developed, and the same procedure and equation forms were utilized to develop and calibrate the parameters of the model for series B samples. The final equations for series A and B samples were then compared and the effect of the coefficient of uniformity on the change of the initial relative density of the samples was then studied. This resulted in three different equations (4.16, 4.17, and 4.18) for confining pressure of 5, 25, and 50 psi (34.5, 172.4, and 344.8 kN/m²) respectively.

$$\Delta Dr = \frac{4.53}{Cu^{0.28}} PF(1-Dr_I) \{ EXP[-3.9(Dr_I)^{2.73}] - 2.225(PF) + 1.3(PF)(Dr_I)^{-0.11} \} \quad (4.16)$$

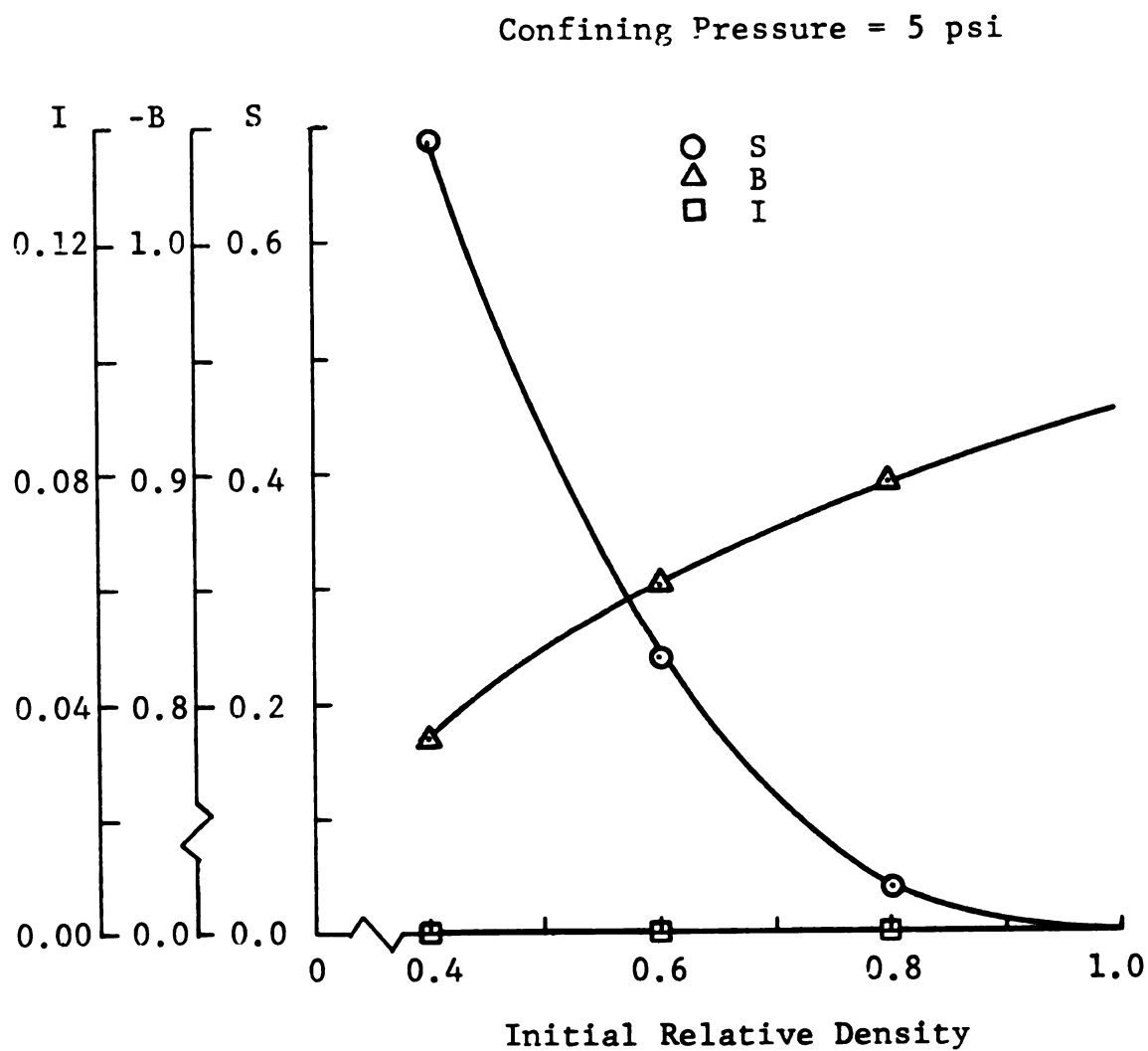


FIGURE 4.34 VALUES OF THE PARAMETERS S, B, AND I OF EQUATION 4.13 VERSUS INITIAL RELATIVE DENSITY OF SERIES A SAMPLES FOR A CONFINING PRESSURE OF 5 PSI.

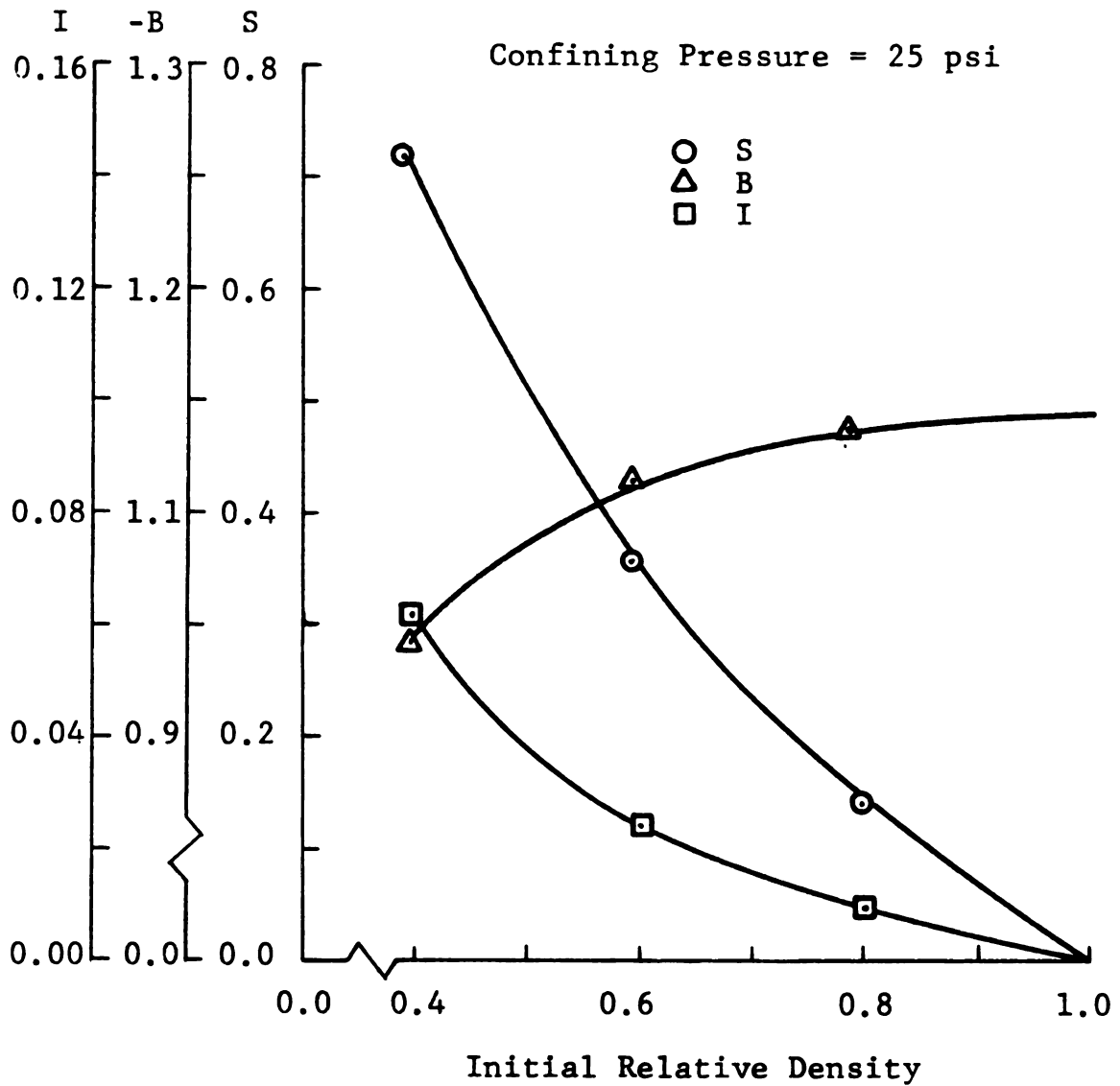


FIGURE 4.35 VALUES OF THE PARAMETERS S, B, AND I OF EQUATION 4.13 VERSUS INITIAL RELATIVE DENSITY OF SERIES A SAMPLES FOR A CONFINING PRESSURE OF 25 PSI.

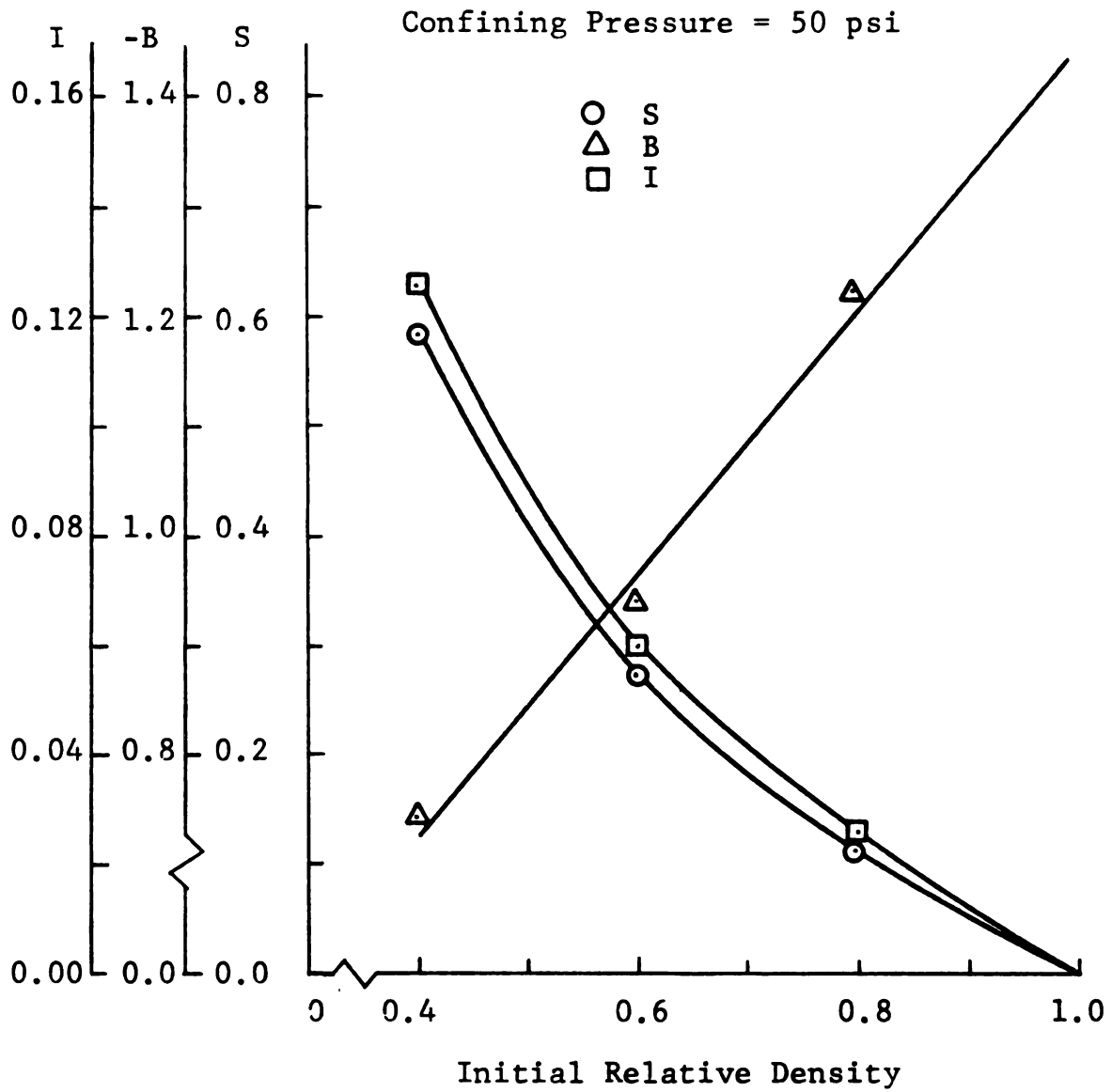


FIGURE 4.36 VALUES OF THE PARAMETERS S, B, AND I OF EQUATION 4.13 VERSUS INITIAL RELATIVE DENSITY OF SERIES A SAMPLES FOR A CONFINING PRESSURE OF 50 PSI.

$$\Delta Dr = \frac{7.75}{Cu^{0.28}} (1-Dr_i) \{ 0.01 \text{EXP}[0.386(Dr_i)^{-1.341}] + (PF) \text{EXP}[-1.66(Dr_i)^{0.79} - 1.197(PF) + 0.021(PF)(Dr_i)^{-2.55}] \} \quad (4.17)$$

$$\Delta Dr = \frac{7.08}{Cu^{0.28}} (1-Dr_i) \{ 0.0001 \text{EXP}[6.029(Dr_i)^{-0.123}] + 0.04(PF) \text{EXP}[-1.63(Dr_i)^{-0.373} - 0.227(PF) - 1.213(PF)(Dr_i)] \} \quad (4.18)$$

where: Dr_i = sample initial relative density;

Cu = coefficient of uniformity of the sample;

PF = percent fine content of the sample ($PF = 0.0$ to 1.0);

EXP = exponential function; and

ΔDr = relative density change due to the application of the confining pressure.

In addition, the change in the relative density of the selected samples of series A and B with the natural and 50/50 materials was studied utilizing only 5 psi (34.5 kN/m²) confining pressure. The reason being is that the triaxial test program of these samples were conducted using only one confining pressure of 5 psi. It was found that the change in the relative density (due to the application of the confining pressure) of the selected samples of series A and B with the natural and 50/50 materials is slightly less than those with the C/P materials. Consequently, the

change in their relative density could be calculated by using equation 4.16 with reduction factors. Equations 4.19 and 4.20 express the changes of the relative density of the selected samples of series A and B that consisted of the natural and 50/50 materials respectively.

$$\Delta Dr = 0.66(\text{equation 4.16}) \quad (4.19)$$

$$\Delta Dr = 0.89(\text{equation 4.16}) \quad (4.20)$$

The accuracy of equations 4.16 through 4.20 were examined using the measured data. It was found that the maximum absolute error between the calculated and measured values of the change in relative densities of all samples is 0.0132.

To summarize, it was found that (in the triaxial test) the soil samples experienced significant volume change during the application of the confining pressure. Consequently, tests were conducted and the sample volume change due to the application of the confining pressure was measured. The corresponding change in the sample relative density was then calculated and the sample density was adjusted accordingly. Based upon the test results, equations 4.16 through 4.20 were then developed whereby the change in relative density of any soil specimen could be calculated.

Examination of the test results, Figures 4.28 through 4.36, and equations 4.16 through 4.20 yielded the following

important observations concerning the change in the sample relative density during the application of the confining pressure.

- a) The higher the percent fine content of the soil, the higher the change in the sample initial relative density.
- b) The higher the coefficient of uniformity of the soil sample, the lower the change in the sample initial relative density.
- c) The higher the amount of the crushed and pulverized material in the soil sample, the higher the angularity, and the higher the change in the sample initial relative density.
- d) The higher the confining pressure, the higher the change in the sample initial relative density.

The first three observations could be explained using the samples initial density. Recall that (see Section 4.2) the higher the percent fine content, the lower the density of the samples, and the higher the percent voids; the better the sample gradation, the higher the density; and the higher the percent C/P material, the lower the density. Consequently, it should be expected that the lower the density, the higher the sample volume change under the applied pressure. The fourth observation is trivial, that is (for any material) the higher the applied pressure, the higher the compressibility.

4.5 TRIAXIAL TEST RESULTS

The main objective of this investigation is to study the effects of grain size, grain size distribution, grain shape, soil density, and moisture content upon the stress-strain characteristics of cohesionless materials. To accomplish this objective, An experimental design matrix was established and the triaxial test program was executed accordingly. A total of 138 drained triaxial compression tests were conducted on dry cohesionless soils utilizing the C/P, natural, and 50/50 materials, and three levels of confining pressure of 5, 25, and 50 psi (34.5, 172.4, and 344.8 kN/m²). In addition, forty drained triaxial compression tests were conducted utilizing one confining pressure of 5 psi (34.5 kN/m²), and samples 1 through 5 of series A that consisted of the moist C/P material. For each sample, several triaxial test specimens were prepared and tested utilizing different initial relative density. All tests were carried up to the six percent strain level. Few tests on each sample were carried up to twenty percent strain level or beyond to be able to measure the ultimate angle of internal friction (ultimate strength). It should be noted herein that the term sample refers to all samples of series A and B, while the terms triaxial specimen, soil specimen or simply specimen refers to any one sample of series A or B that is prepared at one particular relative density and using one of the three different materials (C/P,

natural, 50/50). Thus, several specimens could be made from any one sample of series A or B.

In order to study the stress-strain characteristics of the soils, four different points along the stress-strain curve were selected at different strain or stress levels. These are the one and six percent strain levels, and the peak and ultimate stress levels.

ONE PERCENT STRAIN LEVEL

The one percent strain level represents, in general, a point on the stress-strain curve below the peak strength of the sample. The significance of this point is that most geotechnical design problems such as bearing capacity, and slope stability utilizes an allowable stress at such strain level or smaller, or an angle of internal friction calculated in the vicinity of the one percent strain level by means of a factor of safety.

SIX PERCENT STRAIN LEVEL

The six percent strain level represents a point on the stress-strain curve that is either higher or lower than the strain at peak strength (strain at peak strength is confining pressure, moisture content, and soil density dependent). The importance of this point is that, loose soils will undergo large deformation (high strain) before a significant part of the angle of internal

friction is mobilized. Also (in general and for low confining pressure), the six percent strain level is located at an intermediate point between the strain at peak strength and that at ultimate.

PEAK STRESS LEVEL

The peak stress represents a point on the stress-strain curve where the angle of internal friction of a densely packed cohesionless soil is fully mobilized. This point, in general, is used on a daily basis in the design and analysis of several foundation problems such as ultimate bearing capacity and critical slope angle. The peak strength of cohesionless soils is a function of the sliding and interlocking frictions between the soil particles.

ULTIMATE STRESS LEVEL

The ultimate stress of soils represents that point on the stress-strain diagram where the soil will undergo a continuous deformation at a constant load. Also, this strength is related to the sliding friction between soil particles which is a function of the surface characteristics of the particles.

Figures E.1 through E.27 of Appendix E. show the stress-strain curves of all the dry test specimens of series

A and B samples. Table 4.1 summarizes data pertinent to the triaxial test program, and data analysis and discussion that are presented in later Sections. It should be noted that, for all tests, the axial strain was calculated as the ratio of the vertical deformation of the specimen to its original length. Also, the major principal stress was calculated using only area correction method based on the axial strain. No corrections were made for end plates or membrane compliance and/or penetration.

Tables 4.2 through 4.5 summarize the following triaxial test results for the dry samples of series A and B.

- a) The test confining pressure.
- b) The initial density of the soil specimen (the density before the application of the confining pressure);
- c) The initial and specimen relative densities.
- d) The specimen void ratio (the void ratio of the soil specimen after the application of the confining pressure).
- e) The angles of internal friction of the soil specimen at the one and six percent strain levels.
- f) The peak or ultimate angle of internal friction of the soil specimen.
- g) The axial strain at peak strength.

Table 4.6 summarizes the same type of data for the wet tests. Figures E.28 through E.37 of Appendix E show the stress-strain curves of the wet specimens.

TABLE 4.1 PERCENT FINE CONTENT; MAXIMUM PARTICLE SIZE; MAXIMUM AND MINIMUM DENSITIES; MAXIMUM, MINIMUM, AND CRITICAL VOID RATIOS; ULTIMATE ANGLE OF INTERNAL FRICTION; AND ANGLE OF REPOSE OF THE SAMPLES.

Series	A						
Material	Crushed and Pulverized						
Sample Number	0	1	2	3	4	5	100
Percent Fine Content	0.0	12.0	17.9	26.1	35.5	47.7	100.0
Max. Particle Size (inch)	1.5	0.38	0.19	0.09	0.05	0.02	0.003
Max. Density (pcf)	134.4	131.0	129.5	126.5	123.0	118.0	102.6
Min. Density (pcf)	111.0	103.5	99.5	94.0	88.5	80.0	68.3
Max. void Ratio	0.539	0.650	0.716	0.817	0.930	1.135	1.501
Min. Void Ratio	0.271	0.304	0.319	0.350	0.388	0.447	0.665
Critical Void Ratio							
at 5 psi	-	0.470	0.485	0.525	0.550	0.610	0.860
25 psi	-	0.464	-	0.515	-	0.600	-
50 psi	-	0.463	-	0.510	-	0.590	-
Ultimate Angle of Friction (ϕ_u)							
at 5 psi	-	35.69	35.38	34.42	33.41	33.62	31.59
25 psi	-	42.44	-	40.24	-	38.05	-
50 psi	-	40.27	-	38.43	-	37.33	-
Angle of Repose (ϕ_r)	37.75	33.67	31.61	28.50	27.75	26.76	23.67

TABLE 4.1 CONTINUED.

Series	B							
Material	Crushed and Pulverized							
Sample Number	0	1	2	3	4	5	6	100
Percent Fine Content	0.0	3.68	5.75	8.75	12.93	19.79	33.60	100.0
Max. Particle Size (inch)	1.50	0.50	0.38	0.19	0.09	0.05	0.02	0.003
Max. Density (pcf)	119.0	118.7	118.2	118.9	117.5	116.4	113.6	102.6
Min. Density (pcf)	99.0	95.9	94.4	91.8	88.5	83.9	79.1	68.3
Max. void Ratio	0.725	0.781	0.809	0.860	0.929	1.036	1.160	1.501
Min. Void Ratio	0.435	0.439	0.445	0.436	0.453	0.467	0.503	0.665
Critical Void Ratio at 5 psi	-	0.600	-	-	0.650	0.670	0.715	0.860
Ultimate Angle of Friction (ϕ_u) at 5 psi	-	37.43	-	-	34.09	33.20	32.30	31.59
Angle of Repose (ϕ_r)	37.75	34.50	-	-	29.63	26.60	24.00	23.67

TABLE 4.1 CONTINUED.

Series	A			B		
Material	Natural			50/50	Natural	50/50
Sample Number	1	2	3	1	4	4
Percent Fine Content	12.0	17.9	26.1	12.0	19.79	19.79
Max. Particle Size (inch)	0.38	0.19	0.09	0.38	0.09	0.09
Max. Density (pcf)	139.6	133.6	128.7	139.0	124.1	121.8
Min. Density (pcf)	111.9	102.8	94.7	109.1	94.56	92.2
Max. void Ratio	0.526	0.662	0.804	0.565	0.806	0.851
Min. Void Ratio	0.223	0.278	0.332	0.229	0.376	0.403
Critical Void Ratio at 5 psi	0.410	-	0.505	0.420	0.560	-
Ultimate Angle of Friction (ϕ_u) at 5 psi	33.00	-	31.60	34.06	31.90	-
Angle of Repose (ϕ_r)	28.75	27.88	27.00	29.25	27.00	28.00

TABLE 4.2 SUMMARY OF TRIAXIAL TEST RESULTS OF SERIES A SAMPLES.

Sample 1, Series A, Crushed and Pulverized Material									
σ_3	γ_i	Dr_i	Dr	e	$\phi_{1\%}$	$\phi_{6\%}$	ϕ_P	ϵ_P	PD
5	113.2	40.80	46.70	.4882	22.62	35.06	35.69	20.0	-10.94
5	117.3	56.00	58.40	.4477	25.38	35.74	37.34	6.0	13.40
5	118.6	60.70	62.70	.4328	29.67	38.51	38.70	5.0	22.36
5	124.1	79.10	79.40	.3750	40.01	44.90	47.53	3.5	57.09
5	128.0	91.20	91.30	.3337	43.62	45.75	50.19	2.7	81.91
5	130.3	97.90	97.90	.3109	48.32	46.40	55.88	2.5	95.61
25	113.0	39.90	53.70	.4638	17.35	39.27	42.44	12.0	0.12
25	113.1	40.00	54.00	.4629	19.47	38.93	*	*	0.69
25	115.4	49.20	58.40	.4476	20.78	40.71	43.60	11.5	10.22
25	116.1	51.71	60.07	.4420	18.08	41.17	43.93	11.5	13.72
25	116.8	54.40	61.80	.4369	22.02	42.06	44.05	10.1	17.52
25	118.4	60.10	66.00	.4214	22.62	42.84	*	*	26.56
25	120.1	65.70	69.90	.4080	23.54	43.51	44.29	9.0	34.91
25	124.4	80.10	82.30	.3649	27.35	47.55	47.55	6.0	61.78
25	127.6	89.86	90.90	.3352	32.34	50.41	50.54	5.6	80.30
25	127.6	90.00	91.00	.3348	32.04	48.04	48.04	5.5	80.55
50	112.9	39.70	58.60	.4470	16.14	37.98	*	*	10.04
50	118.4	58.70	68.70	.4120	18.08	40.80	*	*	31.94
50	119.2	62.60	70.40	.4061	19.47	41.81	43.67	10.0	35.70
50	124.4	80.00	83.40	.3611	23.20	44.72	*	*	63.93
50	127.6	90.00	91.60	.3327	29.16	48.60	48.64	6.0	81.74

σ_3 = Confining pressure (psi).

γ_i = Initial density (pcf).

Dr_i = Initial relative density.

Dr = Relative density (after confining pressure).

e = Void ratio (after confining pressure).

$\phi_{1\%}$ = Angle of friction at the 1% strain level (degree).

$\phi_{6\%}$ = Angle of friction at the 6% strain level (degree).

ϕ_P = Peak angle of internal friction (degree).

ϵ_P = Axial strain at peak strength.

PD = Percent dilatation.

* = No data.

TABLE 4.2 CONTINUED.

Sample 2, Series A, Crushed and Pulverized Material									
σ_3	γ_i	Dr_i	Dr	e	$\phi_{1\%}$	$\phi_{6\%}$	ϕ_P	ϵ_P	PD
5	109.7	40.00	50.90	.5139	20.14	33.17	35.38	20.0	-17.38
5	115.3	59.30	63.20	.4650	25.38	36.50	*	*	12.03
5	117.0	64.30	67.10	.4496	26.39	37.98	38.12	6.6	21.29
5	118.0	67.60	69.80	.4388	31.20	39.62	39.69	5.5	27.78
5	125.7	89.90	90.10	.3581	38.30	42.64	45.27	3.0	76.31
5	126.1	91.00	91.20	.3537	39.77	44.18	47.04	3.5	78.95
5	128.1	96.30	96.30	.3334	44.90	45.07	50.67	2.5	91.16
25	109.7	40.10	56.90	.4901	17.35	38.25	*	*	*
25	115.5	59.90	67.20	.4491	19.47	39.77	*	*	*
25	122.1	79.90	82.80	.3871	26.19	44.35	*	*	*
25	122.1	80.00	82.80	.3871	26.19	47.02	*	*	*
25	126.1	91.00	92.10	.3501	29.67	47.17	*	*	*
50	109.7	40.80	61.60	.4714	15.03	36.87	*	*	*
50	115.5	59.70	70.10	.4376	17.79	39.64	*	*	*
50	122.0	79.60	83.90	.3827	21.04	43.22	*	*	*
50	126.0	90.80	92.70	.3477	26.39	46.32	46.32	6.0	*

 σ_3 = Confining pressure (psi). γ_i = Initial density (pcf). Dr_i = Initial relative density. Dr = Relative density (after confining pressure). e = Void ratio (after confining pressure). $\phi_{1\%}$ = Angle of friction at the 1% strain level (degree). $\phi_{6\%}$ = Angle of friction at the 6% strain level (degree). ϕ_P = Peak angle of internal friction (degree). ϵ_P = Axial strain at peak strength.

PD = Percent dilatation.

* = No Data.

TABLE 4.2 CONTINUED.

Sample 3, Series A, Crushed and Pulverized Material									
σ_3	γ_i	Dr_i	Dr	e	$\phi_{1\%}$	$\phi_{6\%}$	ϕ_p	ϵ_p	PD
5	104.6	39.40	55.70	.5568	16.75	30.81	34.42	20.0	-18.17
5	110.8	59.00	64.60	.5152	18.08	32.71	*	*	5.60
5	114.5	69.60	71.90	.4812	26.88	37.11	37.11	6.7	25.03
5	118.3	80.00	80.80	.4396	33.34	39.02	39.27	4.5	48.80
5	122.0	89.60	90.20	.3957	37.93	41.46	44.62	3.3	73.89
5	126.3	99.60	99.60	.3519	46.24	42.44	51.33	2.2	98.91
25	104.8	40.10	61.80	.5283	16.79	35.69	40.24	20.0	-8.06
25	111.0	59.60	68.90	.4952	17.35	39.62	41.88	9.6	12.00
25	111.1	60.00	69.40	.4928	17.35	38.77	*	*	13.45
25	114.5	69.60	75.80	.4631	20.78	42.23	43.73	9.6	31.45
25	118.4	80.10	83.70	.4261	23.99	43.04	*	*	53.88
25	122.3	90.00	91.50	.3897	28.27	45.92	*	*	75.94
25	124.2	94.67	95.40	.3715	31.97	50.83	51.03	5.6	86.97
50	104.7	39.70	65.50	.5110	13.52	35.69	*	*	-0.63
50	111.2	60.10	71.70	.4821	15.83	37.43	*	*	17.44
50	114.4	69.40	77.20	.4564	17.19	40.23	42.80	9.9	33.50
50	118.4	80.20	84.50	.4224	18.79	40.34	*	*	54.75
50	122.2	89.80	92.00	.3873	25.38	44.80	*	*	76.69
50	124.1	94.50	95.60	.3706	26.39	47.47	47.47	6.4	87.13

 σ_3 = Confining pressure (psi). γ_i = Initial density (pcf). Dr_i = Initial relative density. Dr = Relative density (after confining pressure). e = Void ratio (after confining pressure). $\phi_{1\%}$ = Angle of friction at the 1% strain level (degree). $\phi_{6\%}$ = Angle of friction at the 6% strain level (degree). ϕ_p = Peak angle of internal friction (degree). ϵ_p = Axial strain at peak strength.

PD = Percent dilatation.

* = No data.

TABLE 4.2 CONTINUED.

Sample 4, Series A, Crushed and Pulverized Material									
σ_3	γ_1	Dr_1	Dr	e	$\phi_{1\%}$	$\phi_{6\%}$	ϕ_P	ϵ_P	PD
5	98.4	39.20	53.70	.6390	17.94	30.94	33.41	20.0	-55.07
5	99.7	40.00	57.00	.6212	16.60	30.66	33.41	20.0	-44.06
5	106.3	60.00	65.40	.5757	17.94	30.60	33.41	20.0	-15.90
5	111.4	73.30	76.70	.5148	27.35	35.06	35.69	4.8	21.78
5	114.0	80.00	80.70	.4929	29.92	37.43	37.63	4.5	35.33
5	122.9	100.0	100.0	.3884	46.08	43.43	52.40	2.4	100.00
25	99.7	40.20	59.10	.6098	13.69	34.42	*	*	*
25	106.4	59.90	70.20	.5497	16.60	36.87	*	*	*
25	114.1	80.10	84.00	.4750	21.78	40.93	*	*	*
25	118.4	90.00	91.80	.4328	26.88	44.25	*	*	*
50	99.6	39.80	67.70	.5632	14.70	34.42	*	*	*
50	106.3	59.60	72.70	.5362	16.45	36.87	*	*	*
50	114.1	80.00	84.90	.4701	18.92	39.02	*	*	*
50	118.4	89.90	92.20	.4306	23.43	42.23	*	*	*

σ_3 = Confining pressure (psi).

γ_1 = Initial density (pcf).

Dr_1 = Initial relative density.

Dr = Relative density (after confining pressure).

e = Void ratio (after confining pressure).

$\phi_{1\%}$ = Angle of friction at the 1% strain level (degree).

$\phi_{6\%}$ = Angle of friction at the 6% strain level (degree).

ϕ_P = Peak angle of internal friction (degree).

ϵ_P = Axial strain at peak strength.

PD = Percent dilatation.

* = No data.

TABLE 4.2 CONTINUED.

Sample 5, Series A, Crushed and Pulverized Material									
σ_3	γ_i	Dr_i	Dr	e	$\phi_{1\%}$	$\phi_{6\%}$	ϕ_p	ϵ_p	PD
5	91.5	38.90	61.60	.7113	17.20	28.27	33.62	20.0	-62.26
5	91.8	40.00	62.50	.7051	16.14	27.35	33.62	20.0	-58.45
5	99.3	60.20	68.30	.6652	17.79	28.70	33.62	20.0	-33.93
5	107.5	79.40	80.60	.5807	28.27	34.74	35.08	4.0	18.01
5	107.5	79.50	80.70	.5797	26.39	35.25	37.33	3.7	18.62
5	114.0	92.60	92.70	.4975	40.93	39.02	47.27	2.5	69.15
5	115.5	95.50	95.50	.4817	44.90	*	48.72	2.2	78.90
5	116.9	98.00	98.00	.4609	45.25	39.52	49.89	2.1	91.60
25	92.1	40.70	69.40	.6576	12.46	30.81	*	*	-37.72
25	99.1	59.85	72.05	.6394	13.34	35.38	38.90	10.7	-25.80
25	99.2	60.10	72.40	.6370	14.70	34.42	*	*	-24.23
25	107.7	79.80	84.50	.5538	20.53	37.98	*	*	30.26
25	112.6	89.80	92.00	.5023	27.07	43.94	*	*	63.98
25	115.3	94.98	95.93	.4753	33.75	46.40	49.21	4.9	81.66
50	91.8	39.90	72.10	.6391	11.72	31.20	*	*	-34.41
50	99.1	59.87	74.35	.6236	13.34	34.74	39.53	12.0	-23.55
50	99.2	60.20	74.80	.6205	15.03	34.29	*	*	-21.37
50	107.8	80.00	85.60	.5463	16.60	36.70	*	*	30.62
50	112.6	90.00	92.60	.4982	21.41	40.29	*	*	64.33
50	115.1	94.67	95.91	.4754	29.16	47.52	47.63	6.9	80.31

 σ_3 = Confining pressure (psi). γ_i = Initial density (pcf). Dr_i = Initial relative density. Dr = Relative density (after confining pressure). e = Void ratio (after confining pressure). $\phi_{1\%}$ = Angle of friction at the 1% strain level (degree). $\phi_{6\%}$ = Angle of friction at the 6% strain level (degree). ϕ_p = Peak angle of internal friction (degree). ϵ_p = Axial strain at peak strength.

PD = Percent dilatation.

* = No data.

TABLE 4.3 SUMMARY OF TRIAXIAL TEST RESULTS OF SERIES B SAMPLES.

Sample 1, Series B, Crushed and Pulverized Material									
σ_3	γ_i	Dr_i	Dr	e	$\phi_{1\%}$	$\phi_{6\%}$	ϕ_P	ϵ_P	PD
5	108.1	58.70	60.20	.5750	32.15	39.52	39.54	6.2	15.49
5	113.1	79.10	79.30	.5095	37.15	43.04	43.43	5.0	56.07
5	113.2	79.60	79.80	.5077	36.43	42.84	43.00	5.0	57.19
5	116.3	91.40	91.40	.4681	40.24	45.92	47.39	4.3	81.72
5	116.5	92.00	92.00	.4660	42.23	45.92	47.77	4.0	83.02

σ_3 = Confining pressure (psi).

γ_i = Initial density (pcf).

Dr_i = Initial relative density.

Dr = Relative density (after confining pressure).

e = Void ratio (after confining pressure).

$\phi_{1\%}$ = Angle of friction at the 1% strain level (degree).

$\phi_{6\%}$ = Angle of friction at the 6% strain level (degree).

ϕ_P = Peak angle of internal friction (degree).

ϵ_P = Axial strain at peak strength.

PD = Percent dilatation.

TABLE 4.3 CONTINUED.

Sample 3, Series B, Crushed and Pulverized Material									
σ_3	γ_i	Dr_i	Dr	e	$\phi_{1\%}$	$\phi_{6\%}$	ϕ_P	ϵ_P	PD
5	107.6	64.40	66.60	.5776	30.00	42.44	42.44	6.0	26.93
5	114.7	87.50	87.70	.4884	40.01	43.62	44.90	3.0	73.02

σ_3 = Confining pressure (psi).
 γ_i = Initial density (pcf).
 Dr_i = Initial relative density.
 Dr = Relative density (after confining pressure).
 e = Void ratio (after confining pressure).
 $\phi_{1\%}$ = Angle of friction at the 1% strain level (degree).
 $\phi_{6\%}$ = Angle of friction at the 6% strain level (degree).
 ϕ_P = Peak angle of internal friction (degree).
 ϵ_P = Axial strain at peak strength.
PD = Percent dilatation.

TABLE 4.3 CONTINUED.

Sample 4, Series B, Crushed and Pulverized Material									
σ_3	γ_i	Dr_i	Dr	e	$\phi_{1\%}$	$\phi_{6\%}$	ϕ_P	ϵ_P	PD
5	104.8	62.80	66.40	.6132	25.89	37.90	37.95	7.1	18.70
5	107.0	70.00	72.00	.5848	29.58	*	39.39	5.0	33.13
5	109.1	76.50	77.50	.5602	29.58	39.93	39.93	6.3	45.63
5	109.8	78.40	79.20	.5520	30.41	40.09	40.09	5.4	49.80
5	110.5	80.50	81.10	.5430	34.74	40.71	42.07	4.4	54.37
5	115.8	95.40	95.40	.4750	40.01	49.12	50.06	4.6	88.92
5	116.1	96.40	96.40	.4703	41.81	47.46	49.91	4.4	91.36
5	117.1	98.80	98.80	.4587	41.38	49.12	53.70	4.0	97.21
25	109.1	76.50	81.10	.5434	21.41	41.47	43.66	11.3	*
25	110.4	80.30	83.90	.5296	29.16	44.44	44.76	8.7	*
25	117.1	98.90	99.00	.4569	28.27	44.81	45.44	7.0	*
50	109.1	76.60	83.50	.5315	18.79	39.52	42.18	12.0	*
50	110.5	80.70	86.20	.5189	26.68	43.24	44.23	9.5	*
50	117.1	98.90	99.20	.4572	22.02	44.18	46.10	9.0	*

σ_3 = Confining pressure (psi).

γ_i = Initial density (pcf).

Dr_i = Initial relative density.

Dr = Relative density (after confining pressure).

e = Void ratio (after confining pressure).

$\phi_{1\%}$ = Angle of friction at the 1% strain level (degree).

$\phi_{6\%}$ = Angle of friction at the 6% strain level (degree).

ϕ_P = Peak angle of internal friction (degree).

ϵ_P = Axial strain at peak strength.

PD = Percent dilatation.

* = No data.

TABLE 4.3 CONTINUED.

Sample 5, Series B, Crushed and Pulverized Material									
σ_3	γ_i	Dr_i	Dr	e	$\phi_{1\%}$	$\phi_{6\%}$	ϕ_P	ϵ_P	PD
5	102.5	65.00	69.30	.6416	23.76	35.67	35.62	7.1	14.01
5	104.3	70.00	72.80	.6217	27.35	35.99	36.28	5.8	23.83
5	113.0	92.30	92.40	.5103	43.62	39.02	49.24	3.4	78.79
5	113.4	93.20	93.30	.5052	44.18	39.76	48.77	3.0	81.30
5	113.8	94.20	94.30	.4998	41.81	40.93	47.58	3.2	83.93

σ_3 = Confining pressure (psi).

γ_i = Initial density (pcf).

Dr_i = Initial relative density.

Dr = Relative density (after confining pressure).

e = Void ratio (after confining pressure).

$\phi_{1\%}$ = Angle of friction at the 1% strain level (degree).

$\phi_{6\%}$ = Angle of friction at the 6% strain level (degree).

ϕ_P = Peak angle of internal friction (degree).

ϵ_P = Axial strain at peak strength.

PD = Percent dilatation.

TABLE 4.3 CONTINUED.

Sample 6, Series B, Crushed and Pulverized Material									
σ_3	γ_i	Dr_i	Dr	e	$\phi_{1\%}$	$\phi_{6\%}$	ϕ_P	ϵ_P	PD
5	98.5	65.00	71.50	.6904	22.02	34.42	34.72	5.5	11.61
5	100.5	69.90	74.20	.6727	27.82	*	35.89	4.5	19.97
5	108.3	88.80	89.20	.5739	39.02	*	44.40	3.0	66.62
5	109.5	91.50	91.70	.5568	41.60	*	47.24	3.0	74.69

σ_3 = Confining pressure (psi).
 γ_i = Initial density (pcf).
 Dr_i = Initial relative density.
 Dr = Relative density (after confining pressure).
 e = Void ratio (after confining pressure).
 $\phi_{1\%}$ = Angle of friction at the 1% strain level (degree).
 $\phi_{6\%}$ = Angle of friction at the 6% strain level (degree).
 ϕ_P = Peak angle of internal friction (degree).
 ϵ_P = Axial strain at peak strength.
PD = Percent dilatation.
* = No data.

TABLE 4.4 SUMMARY OF TRIAXIAL TEST RESULTS OF THE ONE HUNDRED PERCENT FINE CONTENT SAMPLE.

Sample 100, Series A or B, Crushed and Pulverized Material									
σ_3	γ_i	Dr_i	Dr	e	$\phi_{1\%}$	$\phi_{6\%}$	ϕ_p	ϵ_p	PD
5	93.8	81.40	82.70	.8100	23.76	34.55	34.69	4.9	25.65
5	100.2	95.20	95.30	.7044	36.29	36.87	41.16	3.2	79.84
5	102.4	99.80	99.80	.6672	38.51	36.87	43.71	2.9	98.92

σ_3 = Confining pressure (psi).

γ_i = Initial density (pcf).

Dr_i = Initial relative density.

Dr = Relative density (after confining pressure).

e = Void ratio (after confining pressure).

$\phi_{1\%}$ = Angle of friction at the 1% strain level (degree).

$\phi_{6\%}$ = Angle of friction at the 6% strain level (degree).

ϕ_p = Peak angle of internal friction (degree).

ϵ_p = Axial strain at peak strength.

PD = Percent dilatation.

TABLE 4.5 SUMMARY OF TRIAXIAL TEST RESULTS OF THE NATURAL AND COMBINED MATERIALS.

Sample 1, Series A, Natural Material									
σ_3	γ_i	Dr_i	Dr	e	$\phi_{1\%}$	$\phi_{6\%}$	ϕ_P	ϵ_P	PD
5	120.9	40.10	44.50	.4003	24.85	33.41	33.43	6.1	10.28
5	131.3	79.80	80.10	.2997	37.71	37.15	41.08	2.2	59.58
5	137.8	94.60	94.60	.2395	49.25	36.87	50.06	1.4	91.27

σ_3 = Confining pressure (psi).

γ_i = Initial density (pcf).

Dr_i = Initial relative density.

Dr = Relative density (after confining pressure).

e = Void ratio (after confining pressure).

$\phi_{1\%}$ = Angle of friction at the 1% strain level (degree).

$\phi_{6\%}$ = Angle of friction at the 6% strain level (degree).

ϕ_P = Peak angle of internal friction (degree).

ϵ_P = Axial strain at peak strength.

PD = Percent dilatation.

TABLE 4.5 CONTINUED.

Sample 3, Series A, Natural Material									
σ_3	γ_i	Dr_i	Dr	e	$\phi_{1\%}$	$\phi_{6\%}$	ϕ_P	ϵ_P	PD
5	105.4	39.00	48.00	0.577	15.83	29.58	31.60	-	-41.95
5	112.3	60.10	63.10	0.507	22.02	31.59	32.04	11.5	-0.87
5	119.6	79.80	80.30	0.425	33.06	34.42	38.70	3.0	46.23
5	124.3	91.20	91.30	0.374	43.61	37.15	47.17	2.0	76.07
5	124.5	91.70	91.80	0.371	43.81	36.34	45.88	1.7	77.60

σ_3 = Confining pressure (psi).

γ_i = Initial density (pcf).

Dr_i = Initial relative density.

Dr = Relative density (after confining pressure).

e = Void ratio (after confining pressure).

$\phi_{1\%}$ = Angle of friction at the 1% strain level (degree).

$\phi_{6\%}$ = Angle of friction at the 6% strain level (degree).

ϕ_P = Peak angle of internal friction (degree).

ϵ_P = Axial strain at peak strength.

PD = Percent dilatation.

TABLE 4.5 CONTINUED.

Sample 4, Series B, Natural Material									
σ_3	γ_1	Dr_1	Dr	e	$\phi_{1\%}$	$\phi_{6\%}$	ϕ_P	ϵ_P	PD
5	110.3	60.00	63.30	0.534	25.89	34.15	34.34	4.8	14.33
5	116.6	79.30	79.90	0.462	34.42	36.58	41.15	3.2	52.99
5	120.4	90.20	90.30	0.418	38.25	38.25	44.28	3.4	77.36

σ_3 = Confining pressure (psi).

γ_1 = Initial density (pcf).

Dr_1 = Initial relative density.

Dr = Relative density (after confining pressure).

e = Void ratio (after confining pressure).

$\phi_{1\%}$ = Angle of friction at the 1% strain level (degree).

$\phi_{6\%}$ = Angle of friction at the 6% strain level (degree).

ϕ_P = Peak angle of internal friction (degree).

ϵ_P = Axial strain at peak strength.

PD = Percent dilatation.

TABLE 4.5 CONTINUED.

Sample 1, Series A, 50/50 Material									
σ_3	γ_i	Dr_i	Dr	e	$\phi_{1\%}$	$\phi_{6\%}$	ϕ_p	ϵ_p	PD
5	101.8	48.60	53.10	0.387	26.88	36.58	36.79	6.6	17.33
5	124.2	56.60	59.50	0.366	30.41	36.98	37.76	3.9	28.53
5	132.1	81.00	82.10	0.289	43.48	39.24	45.92	2.1	68.43
5	137.1	95.00	95.00	0.246	51.50	42.02	54.75	1.9	91.20

σ_3 = Confining pressure (psi).

γ_i = Initial density (pcf).

Dr_i = Initial relative density.

Dr = Relative density (after confining pressure).

e = Void ratio (after confining pressure).

$\phi_{1\%}$ = Angle of friction at the 1% strain level (degree).

$\phi_{6\%}$ = Angle of friction at the 6% strain level (degree).

ϕ_p = Peak angle of internal friction (degree).

ϵ_p = Axial strain at peak strength.

PD = Percent dilatation.

TABLE 4.6 SUMMARY OF TRIAXIAL TEST RESULTS UTILIZING A CONFINING PRESSURE OF 5 PSI AND WET SOILS OF SERIES A SAMPLES.

Sample 1, Series A, Crushed and Pulverized Material								
w(%)	γ	Dr	e	$\phi_{1\%}$	$\phi_{6\%}$	ϕ_P	ϵ_P	PD
3.74	111.3	33.34	.5345	42.23	41.38	42.4	0.9	-38.76
4.88	117.0	55.11	.4591	47.57	47.75	49.85	1.7	6.55
5.14	119.8	64.85	.4254	50.25	49.12	51.21	2.5	26.80
5.92	123.5	77.21	.3826	59.11	52.14	59.47	1.2	52.52
9.44	109.6	26.31	.5589	28.27	32.33	32.33	6.0	-53.42
9.28	116.9	54.42	.4615	40.48	44.37	45.81	2.5	5.11
9.32	120.1	66.50	.4224	43.43	44.00	48.42	2.5	28.59
8.56	123.2	76.27	.3858	42.84	46.55	49.14	2.7	50.58

w(%) = Water content in percent.

γ = Density (pcf).

Dr = Relative density (after confining pressure).

e = Void ratio (after confining pressure).

$\phi_{1\%}$ = Angle of friction at the 1% strain level (degree).

$\phi_{6\%}$ = Angle of friction at the 6% strain level (degree).

ϕ_P = Peak angle of internal friction (degree).

ϵ_P = Axial strain at peak strength.

PD = Percent dilatation.

TABLE 4.6 CONTINUED.

Sample 2, Series A, Crushed and Pulverized Material								
w(%)	γ	Dr	e	$\phi_{1\%}$	$\phi_{6\%}$	ϕ_p	ϵ_p	PD
5.22	108.0	34.01	.5811	43.04	42.44	43.55	2.5	-57.80
4.97	109.6	39.92	.5576	46.55	43.04	47.17	1.5	-43.66
5.02	115.5	59.73	.4788	52.10	46.24	52.10	1.0	3.70
6.05	119.7	72.69	.4273	54.40	48.86	54.70	1.3	34.70
9.62	109.7	39.99	.5573	35.06	37.40	37.40	6.0	-43.49
9.64	115.0	58.08	.4854	44.00	42.64	46.07	2.2	-0.24
9.61	118.1	67.89	.4464	46.86	44.55	49.65	2.0	23.21
9.51	121.6	78.57	.4039	45.75	45.75	48.53	2.2	48.74

w(%) = Water content in percent.

γ = Density (pcf).

Dr = Relative density (after confining pressure).

e = Void ratio (after confining pressure).

$\phi_{1\%}$ = Angle of friction at the 1% strain level (degree).

$\phi_{6\%}$ = Angle of friction at the 6% strain level (degree).

ϕ_p = Peak angle of internal friction (degree).

ϵ_p = Axial strain at peak strength.

PD = Percent dilatation.

TABLE 4.6 CONTINUED.

Sample 3, Series A, Crushed and Pulverized Material								
w(%)	γ	Dr	e	$\phi_{1\%}$	$\phi_{6\%}$	ϕ_P	ϵ_P	PD
4.94	103.4	35.32	.6519	38.51	40.24	40.43	5.0	-72.53
4.96	106.9	46.81	.5983	42.11	42.64	43.40	3.1	-41.87
5.16	110.8	58.90	.5419	49.88	40.01	51.17	1.5	-9.63
4.87	118.2	79.77	.4444	58.29	48.86	58.96	1.5	46.03
9.60	104.9	40.31	.6286	40.93	38.77	41.43	1.2	-59.21
9.78	110.1	56.87	.5515	44.00	40.24	44.86	1.6	-15.16
9.66	114.6	69.91	.4905	48.86	42.02	49.34	1.4	19.74
9.72	118.2	79.72	.4448	51.50	41.60	52.92	1.7	45.82

w(%) = Water content in percent.

γ = Density (pcf).

Dr = Relative density (after confining pressure).

e = Void ratio (after confining pressure).

$\phi_{1\%}$ = Angle of friction at the 1% strain level (degree).

$\phi_{6\%}$ = Angle of friction at the 6% strain level (degree).

ϕ_P = Peak angle of internal friction (degree).

ϵ_P = Axial strain at peak strength.

PD = Percent dilatation.

TABLE 4.6 CONTINUED.

Sample 4, Series A, Crushed and Pulverized Material								
w(%)	γ	Dr	e	$\phi_{1\%}$	$\phi_{6\%}$	ϕ_P	ϵ_P	PD
4.92	98.3	35.64	.7368	36.29	39.52	39.52	6.0	-115.59
5.10	101.6	46.03	.6805	43.51	40.01	43.51	1.2	-80.75
4.97	105.5	57.51	.6184	48.59	42.02	49.02	1.5	-42.34
4.75	110.2	70.31	.5491	53.13	47.61	53.92	1.4	0.56
9.71	99.5	39.45	.7162	38.25	35.99	38.58	1.4	-102.83
9.84	105.2	56.60	.6233	45.58	41.38	45.60	1.1	-45.39
9.73	110.0	69.79	.5519	49.38	41.81	49.91	1.4	-1.21
9.73	113.8	79.36	.5001	54.48	45.58	55.37	1.4	30.85

w(%) = Water content in percent.

γ = Density (pcf).

Dr = Relative density (after confining pressure).

e = Void ratio (after confining pressure).

$\phi_{1\%}$ = Angle of friction at the 1% strain level (degree).

$\phi_{6\%}$ = Angle of friction at the 6% strain level (degree).

ϕ_P = Peak angle of internal friction (degree).

ϵ_P = Axial strain at peak strength.

PD = Percent dilatation.

TABLE 4.6 CONTINUED.

Sample 5, Series A, Crushed and Pulverized Material								
w(%)	γ	Dr	e	$\phi_{1\%}$	$\phi_{6\%}$	ϕ_P	ϵ_P	PD
5.03	89.7	33.55	.9041	31.97	36.58	36.60	6.0	-65.74
5.79	93.3	44.24	.8306	37.98	38.51	39.31	2.7	-49.32
4.81	98.6	58.48	.7322	44.90	40.48	45.21	1.3	-27.32
4.81	105.1	74.25	.6241	52.24	45.25	53.12	1.5	-3.15
10.09	91.5	39.03	.8664	30.00	32.75	32.75	6.0	-57.32
9.88	97.1	54.74	.7584	42.44	38.51	42.97	1.5	-33.18
10.12	102.0	66.98	.6743	46.40	42.23	47.57	1.7	-14.37
9.73	107.3	78.92	.5922	51.06	45.25	52.30	1.6	3.99

w(%) = Water content in percent.

γ = Density (pcf).

Dr = Relative density (after confining pressure).

e = Void ratio (after confining pressure).

$\phi_{1\%}$ = Angle of friction at the 1% strain level (degree).

$\phi_{6\%}$ = Angle of friction at the 6% strain level (degree).

ϕ_P = Peak angle of internal friction (degree).

ϵ_P = Axial strain at peak strength.

PD = Percent dilatation.

In the following Section, the ultimate strength and the critical void ratio of series A and B samples are discussed.

4.6 ULTIMATE STRENGTH AND CRITICAL VOID RATIO

As noted above, most drained triaxial compression tests were terminated at an axial strain level of six percent. In order to be able to measure the ultimate strength (ultimate angle of internal friction) of the soil, few tests were carried up to twenty percent strain level or greater utilizing dense and loose specimens. Since the ultimate strength is independent of the specimen density, tests conducted on all specimens of the same soil sample are expected to yield an equal ultimate shear strength. It was observed however that the ultimate shear strength of dense soil specimens was slightly higher (about 0.5 to 2.0 degrees) than that of loose specimens. The reason of this could be attributed to the residual degree of interlocking between the soil particles after volume dilatation. Table 4.1 summarizes the ultimate angle of internal friction and the critical void ratio of all test specimens.

The critical void ratio of each sample of series A and B was estimated by using the triaxial test data obtained from all the soil specimens of that sample. First, the ultimate strength (ϕ_u) of each sample and the peak strength (peak angle of internal friction, (ϕ_p) of each specimen were measured. The strength difference ($\phi_p - \phi_u$) was then

normalized relative to the ultimate strength by using equation (4.21).

$$NSD = (\phi_P - \phi_U) / (\phi_U) \quad (4.21)$$

where: NSD = normalized strength difference;

ϕ_P = the peak angle of internal friction of the soil specimen; and

ϕ_U = the ultimate angle of internal friction of the soil sample of series A and B.

Figures 4.37 and 4.38 depict the normalized strength difference plotted against the void ratio of the soil specimen (the void ratio after the application of the confining pressure). The solid curves in the figures were drawn to best fit the data. It can be noted from the figures that for each sample of series A and B, the lower the void ratio the higher the normalized strength difference (NSD). This is so because the lower the void ratio of the soil specimen the denser the soil and the higher is the peak strength (peak angle of internal friction). It should be noted herein that the data in the figures represent those of dense specimens. The test data of the loose specimens would overlap the void ratio axis and consequently they were not plotted. That is for all loose specimen the NSD is zero because the peak and ultimate angles of internal friction are equal. Furthermore, the points along the curves represent test data from dense soil specimens while the

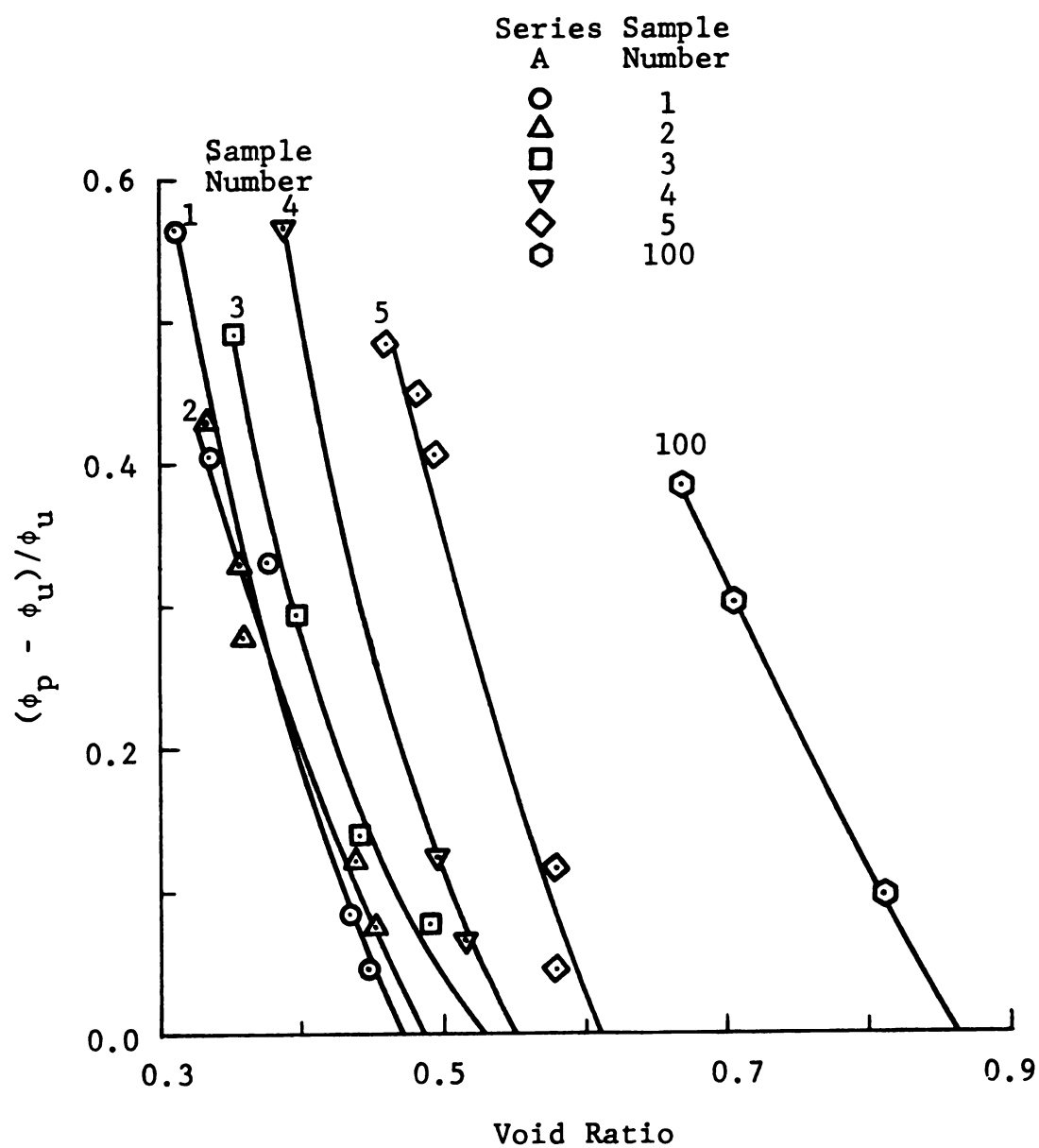


FIGURE 4.37 NORMALIZED STRENGTH DIFFERENCE VERSUS VOID RATIO OF SERIES A SAMPLES FOR A CONFINING PRESSURE OF 5 PSI.

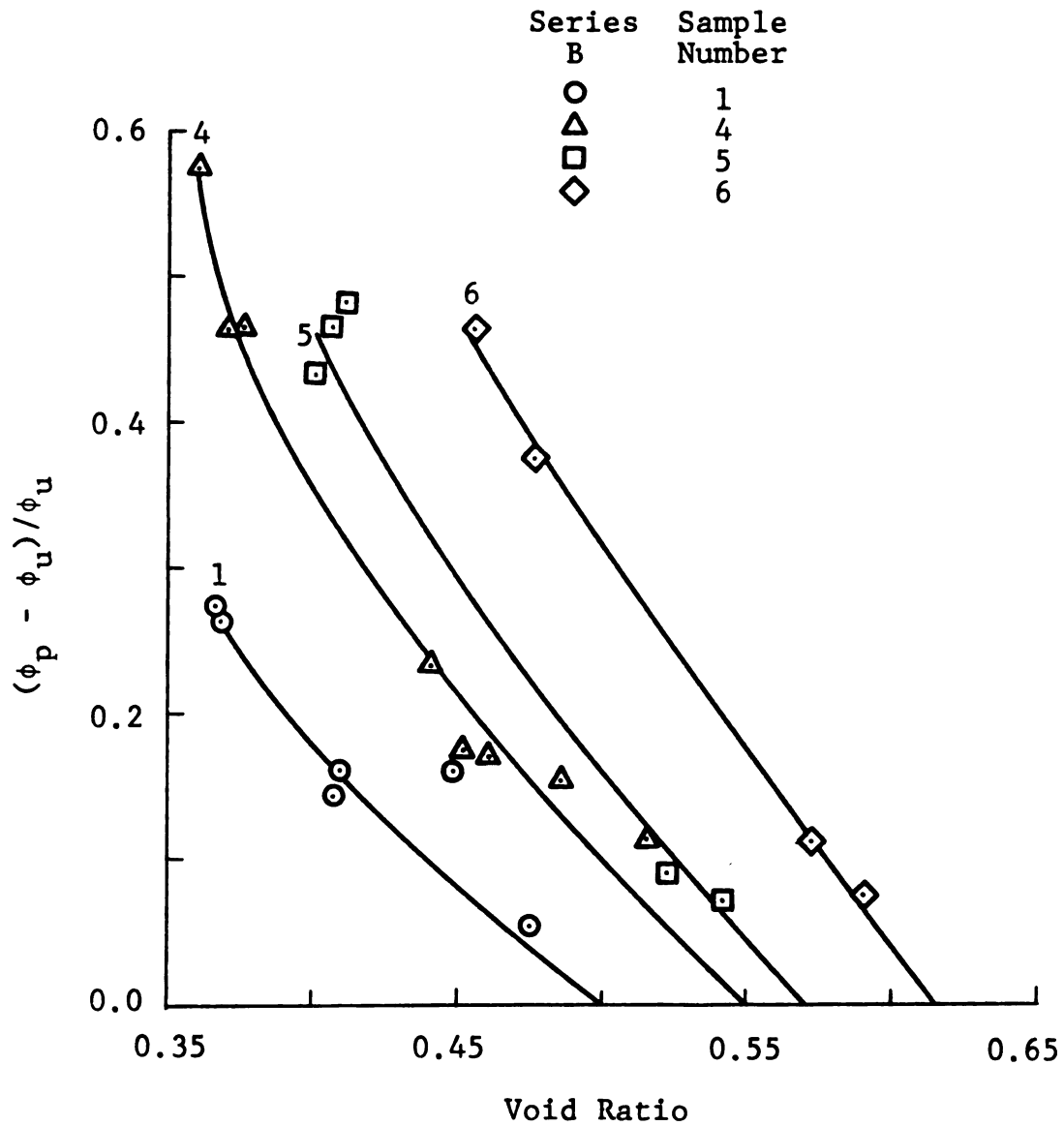


FIGURE 4.38 NORMALIZED STRENGTH DIFFERENCE VERSUS VOID RATIO OF SERIES B SAMPLES FOR A CONFINING PRESSURE OF 5 PSI.

locus of the void ratio axis immediately to the right of the intersection point of each curve represent data from loose soil specimens. Nevertheless, the intersection of the best fit curve of each sample of series A and B with the void ratio axis represents the first occurrence where the NSD is zero. Thus, the value of the void ratio at the intersection point of each curve corresponds to the critical void ratio of the sample represented by that curve. The same procedure was also utilized to estimate the critical void ratio of all samples of the natural and 50/50 materials. Table 4.1 summarizes the critical void ratio and the ultimate angle of internal friction of all samples.

The effect of grain size, sample gradation, and grain shape on the ultimate strength (ultimate angle of internal friction) and the critical void ratio of series A and B samples are discussed in the following Subsections.

4.6.1 EFFECT OF GRAIN SIZE

Figures 4.39 and 4.40 depict the critical, and the maximum and minimum void ratios plotted against the percent fine contents of series A and B samples respectively. It can be seen from the figures that the void ratio increases as the percent fine content of the sample increases. Also, the difference between the critical and minimum void ratio is approximately constant for all samples. The effect of grain size on the maximum and minimum void ratios of the

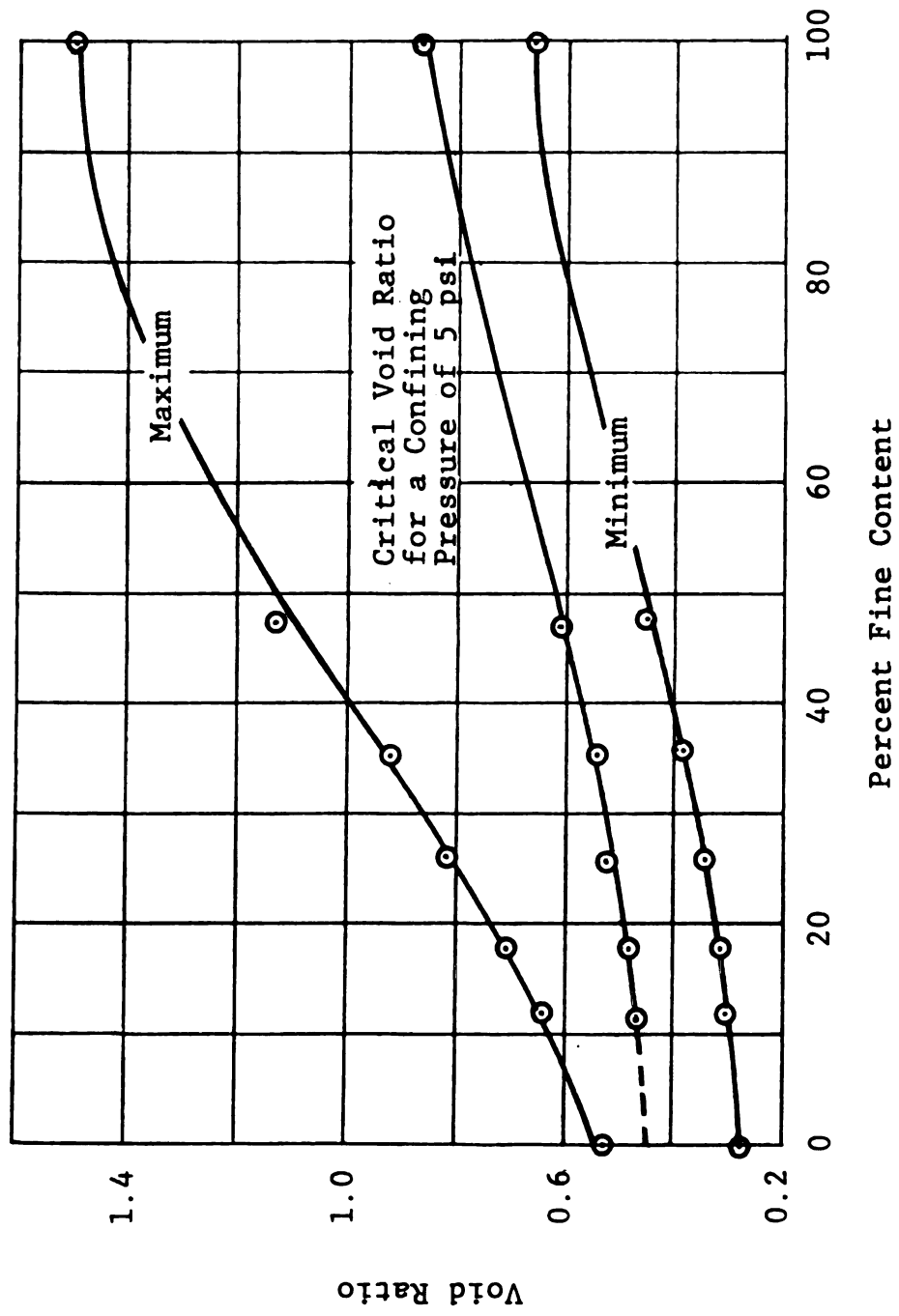


FIGURE 4.39 MAXIMUM, MINIMUM AND CRITICAL VOID RATIOS VERSUS PERCENT FINE CONTENT OF SERIES A SAMPLES.

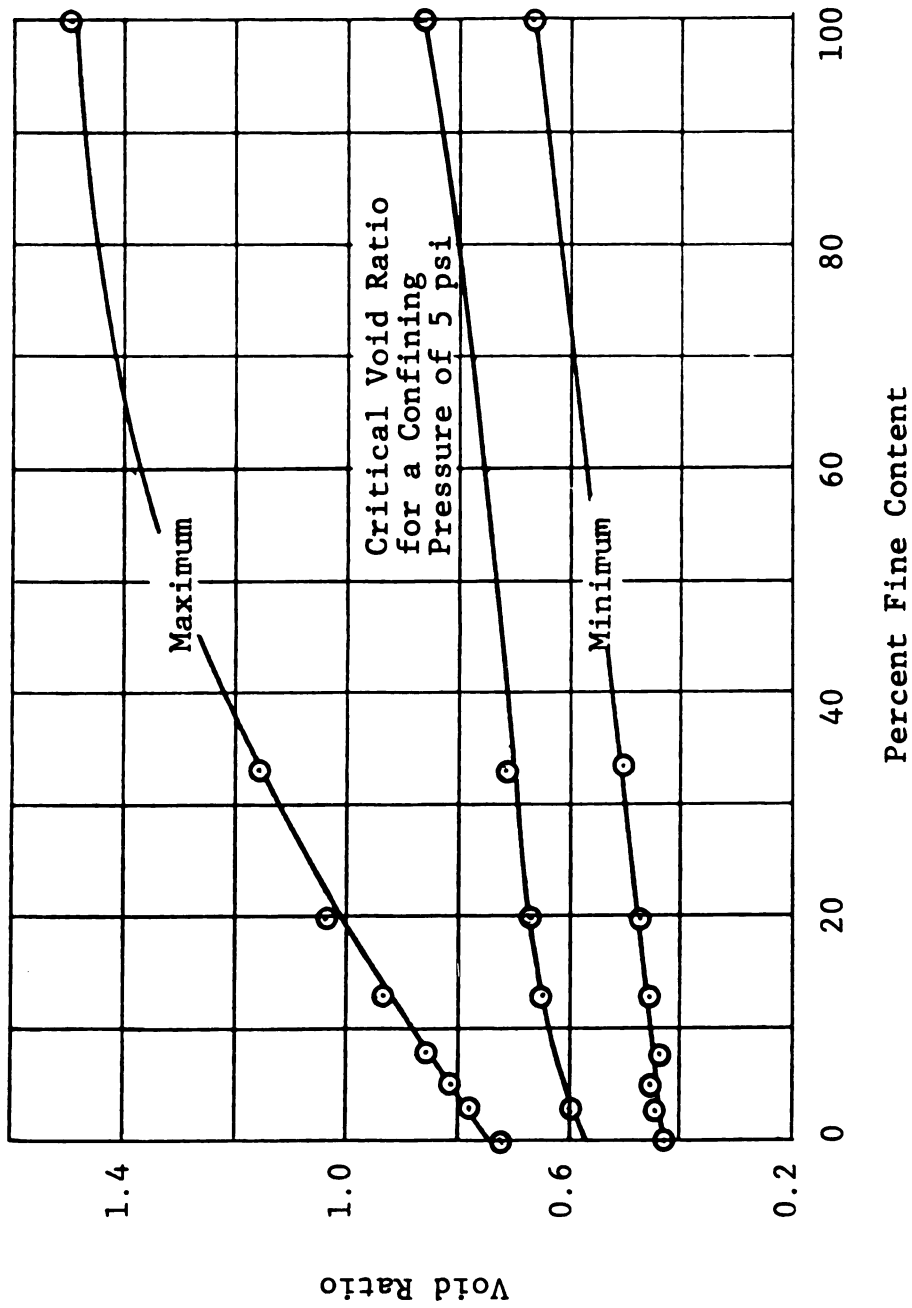


FIGURE 4.40 MAXIMUM, MINIMUM AND CRITICAL VOID RATIOS VERSUS PERCENT FINE CONTENT OF SERIES B SAMPLES.

samples was discussed in Section 4.2. The relationships between the critical void ratio and the percent fine content of the samples were modeled herein using equations 4.22 and 4.23 for series A and B samples respectively.

$$e_{CR} = 0.44 \frac{1.0 - 0.32(PF)}{1.0 - 0.84(PF)} \text{EXP}[-0.77(PF)^{5.0}] \quad (4.22)$$

$$e_{CR} = 0.57 \frac{1.0 + 6.34(PF)}{1.0 + 4.66(PF)} \text{EXP}[0.15(PF)^{2.5}] \quad (4.23)$$

where: e_{CR} = critical void ratio;

PF = percent fine content of the soil sample (PF = 0.0 to 1.0); and

EXP = exponential function.

The correspondence between the actual critical void ratio data and those calculated using equations 4.22 and 4.23 is shown in Figure 4.41. It should be noted that the maximum absolute percent difference between the calculated and actual data is 2.38%.

Figures 4.42 and 4.43 show plots of the ultimate angle of internal friction versus the percent fine content and the maximum grain size of series A and B samples. Examination of the figures indicates that the higher the percent fine content and the lower the maximum grain size of the soil, the lower the ultimate angle of internal friction. In general, the ultimate angle of internal friction is a

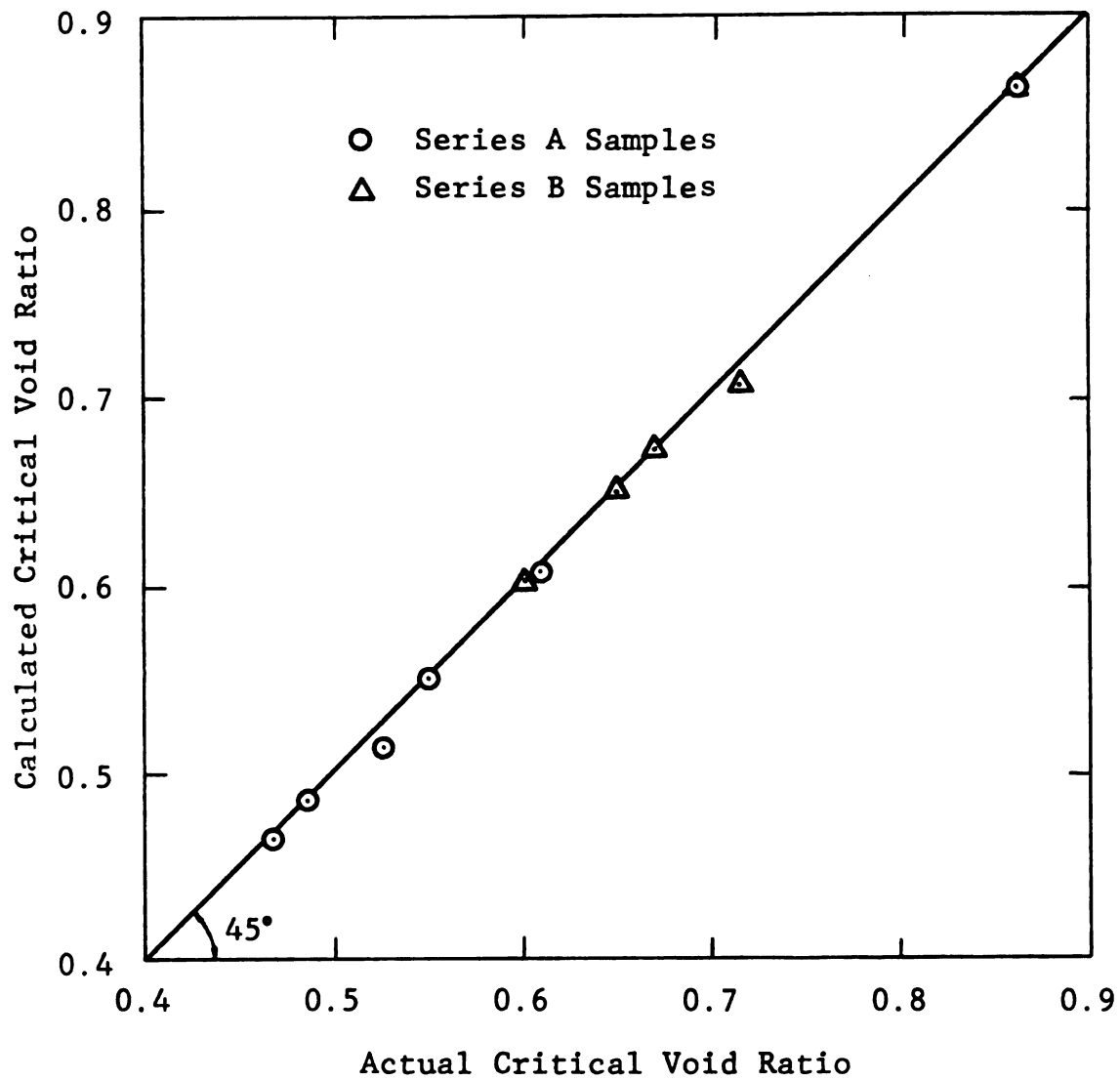


FIGURE 4.41 CALCULATED VERSUS ACTUAL CRITICAL VOID RATIO OF SERIES A AND B SAMPLES

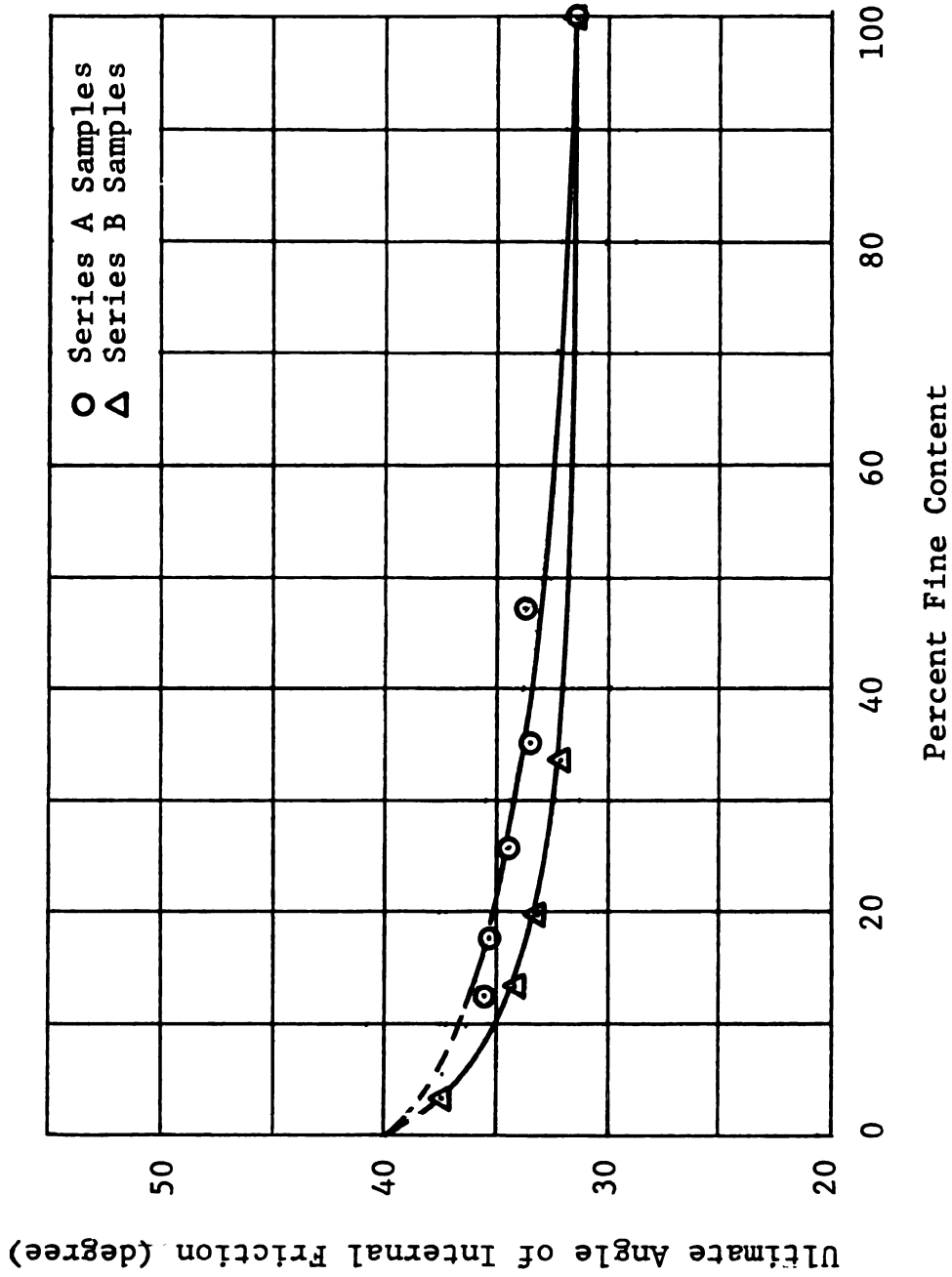


FIGURE 4.42 ULTIMATE ANGLE OF INTERNAL FRICTION VERSUS PERCENT FINE CONTENT OF SERIES A AND B SAMPLES FOR A CONFINING PRESSURE OF 5 PSI.

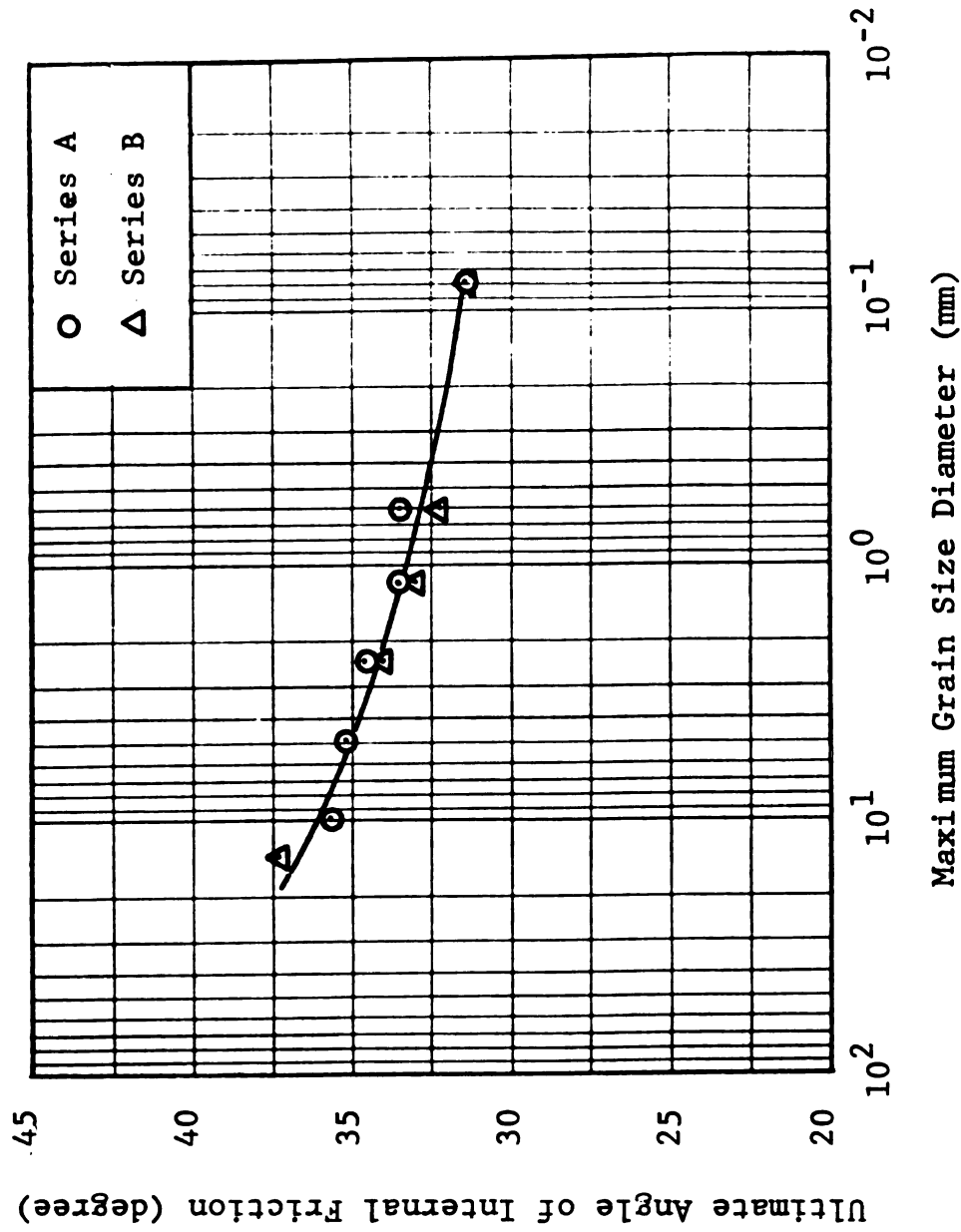


FIGURE 4.43 ULTIMATE ANGLE OF INTERNAL FRICTION VERSUS MAXIMUM GRAIN SIZE OF SERIES A AND B SAMPLES FOR A CONFINING PRESSURE OF 5 PSI.

measure of the particle resistance to sliding due to friction. Thus, the microscopic surface roughness of the particles, which is a function of the soil minerals, has a major influence on the ultimate angle of internal friction. Since the same types of soil minerals were used in all of series A and B samples, then it is reasonable to assume that they possess the same ultimate angle of internal friction. The test data, however, shows that the ultimate angle of internal friction decreases as the percent fine content increases or maximum particle size decreases. The reason for this is two fold:

- a) The lower the percent fine content and the higher the maximum particle size of the sample the higher the surface irregularities of the sample. That is along the shear plane (failure plane) in the sample, the coarser the particles the higher the surface irregularity. Consequently, individual particle would have to override or to trample the adjacent particle before it can slide from its position. This action results in a higher resistance to sliding. As the percent fine increases, surface irregularities will be filled up with the fine particles providing a smoother riding surface and consequently less resistance to sliding.
- b) As the percent fine content of the samples increases their critical void ratio increases. Thus, the

wt

rep

cal

fri

dis

0.4

ultimate angle of internal friction is being compared, for different samples, at different critical void ratio.

A general type of equation was then selected to model the data of Figure 4.42. The parameters of the equation were then calibrated by using the test results. This resulted in equations 4.24 and 4.25 for series A and B samples respectively.

$$\phi_u = 40.0 \{1.0 - 45.25(PF) \text{EXP}[-5.37(PF)^{0.14}]\} \quad (4.24)$$

$$\phi_u = 40.0 \{1.0 - 5.87 (PF) \text{EXP}[-3.33(PF)^{0.33}]\} \quad (4.25)$$

where: ϕ_u = ultimate angle of internal friction in degree;
 PF = percent fine content of the soil sample (PF = 0.0 to 1.0); and
 EXP = exponential function.

The locus of the forty five degree line of Figure 4.44 represent the correspondence between the measured and calculated values of the ultimate angle of internal friction. It should be noted that the absolute maximum difference between the measured and calculated values is 0.44 degree or 1.31 percent.

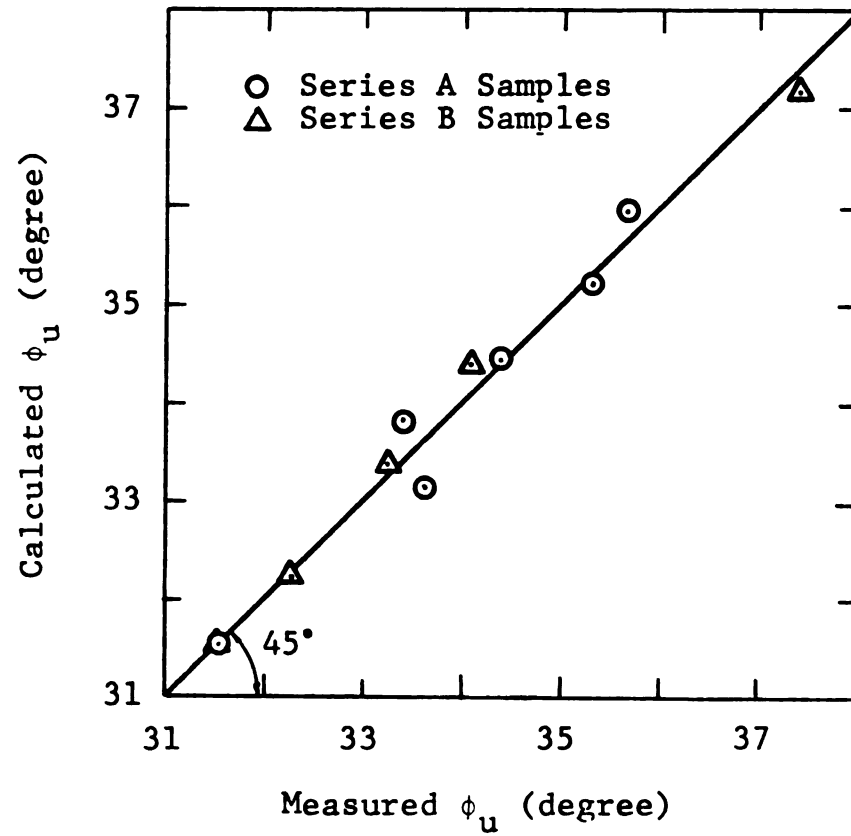


FIGURE 4.44 CALCULATED VERSUS MEASURED ULTIMATE ANGLE OF INTERNAL FRICTION OF SERIES A AND B SAMPLES.

4.6.2 EFFECT OF SAMPLE GRADATION

The effect of sample gradation on the ultimate angle of internal friction can be studied by comparing the test results of series A samples against those of series B. Examination of Figures 4.42 and 4.43 indicates that the effect of sample gradation on the ultimate angle of internal friction is negligible. It should be noted that the maximum difference between the values of the ultimate angle of internal friction of series A and B samples is 1.7 degree when compared at the same percent fine content. The difference is much less than one degree when the data are compared at the same maximum grain size of the sample. Further, if equations 4.1 and 4.2 are to be substituted into equations 4.24 and 4.25 then the resulting equations would be similar and, for the same maximum grain size, they would yield approximately the same results.

4.6.3 EFFECT OF GRAIN SHAPE

Figure 4.45 displays plots of the ultimate angle of internal friction of series A and B samples that consisted of the C/P, natural, and 50/50 materials versus the percent fine content of the samples. Figure 4.46 depicts the ultimate angle of internal friction plotted against the coefficient of sample angularity. Examination of the figures indicates that the higher the coefficient of

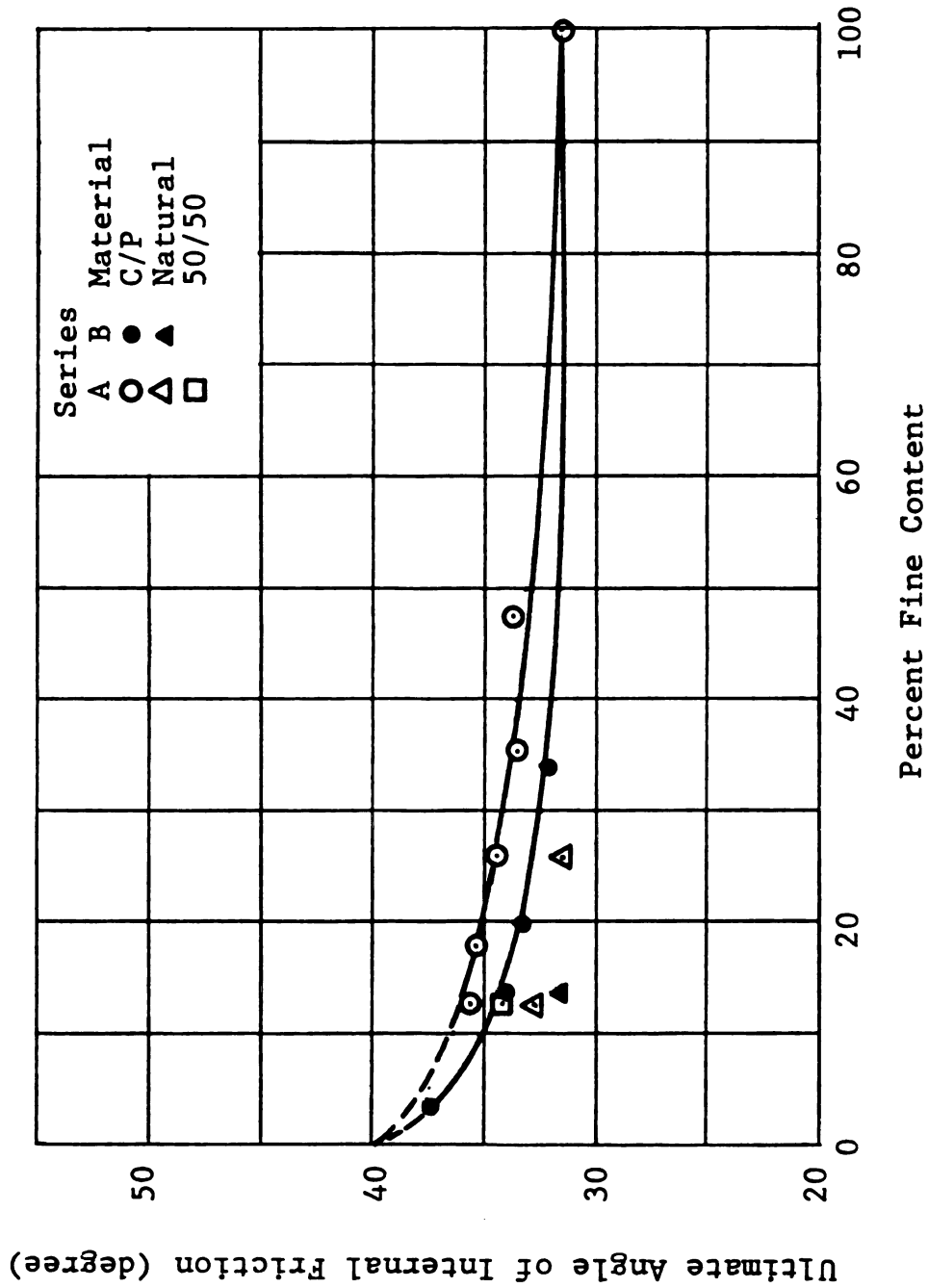


FIGURE 4.45 ULTIMATE ANGLE OF INTERNAL FRICTION VERSUS PERCENT FINE CONTENT OF SERIES A AND B SAMPLES THAT CONSISTED OF THE C/P, NATURAL, AND 50/50 MATERIALS FOR A CONFINING PRESSURE OF 5 PSI.

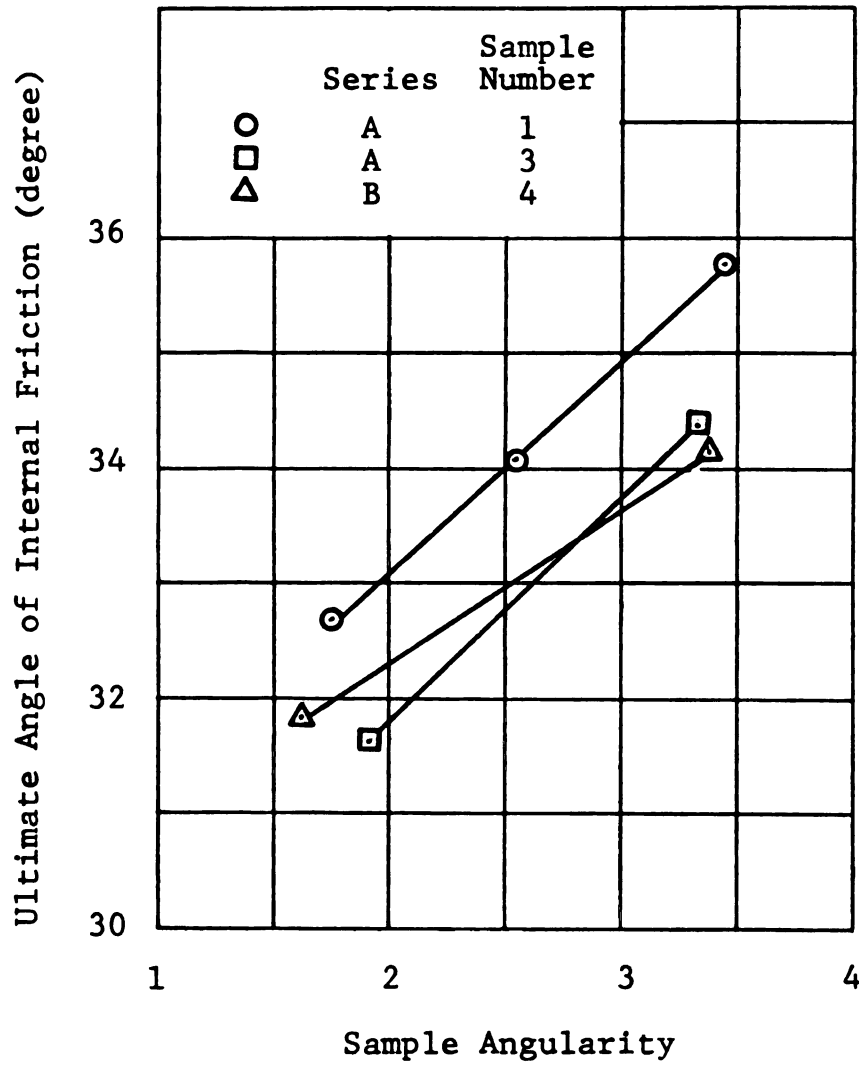


FIGURE 4.46 ULTIMATE ANGLE OF INTERNAL FRICTION VERSUS SAMPLE ANGULARITY OF SERIES A AND B SAMPLES FOR A CONFINING PRESSURE OF 5 PSI.

an

an

C/

Th

re

Fi

re

an

ty

eq

se

ϕ_u

ϕ_u

wh

in

wo

wo

angularity of the soil samples, the higher the ultimate angle of internal friction. That is the higher the percent C/P material of the soil, the higher the ultimate friction. This was expected and it is consistent with the data reported in the literature. Also, it can be seen from Figure 4.46 that, in the range of the test data, the relationship between the ultimate angle of internal friction and the particle angularity can be expressed by a linear type function. Substituting the linear function into equations 4.24 and 4.25 yielded the following equations for series A and B samples respectively.

$$\phi_u = \{35.81 + 1.15(SA)\} \{1.0 - 45.25(PF) \text{EXP}[-5.37(PF)^{0.14}]\} \quad (4.26)$$

$$\phi_u = \{35.81 + 1.15(SA)\} \{1.0 - 5.87 (PF) \text{EXP}[-3.33(PF)^{0.33}]\} \quad (4.27)$$

where: ϕ_u = the ultimate angle of internal friction in degree;

SA = sample angularity; and

PF = percent fine content of the soil sample (PF = 0.0 to 1.0).

Again, if equations 4.1 and 4.2 are to be substituted into equations 4.26 and 4.27 then the resulting equations would be similar and, for the same maximum grain size, they would yield approximately the same results.

4.7 STRENGTH MODEL

The characteristics of the stress-strain diagram of a cohesionless soil vary and depend upon the density and moisture content of the soil specimen, and the confining pressure. Figure 4.47a shows typical stress-strain curves of loose and dense soil specimens (36). It can be seen that dense soil possesses a peak strength (maximum principal stress difference) after which the stress drops to a constant value (ultimate strength) while the soil undergoes a continuous deformation (strain). On the other hand, the principal stress difference for loose soil increases with increasing strain until a constant stress level (ultimate strength) is reached. Figure 4.47b depicts the principal stress difference versus the void ratio of the same soil specimens. It can be seen from the figure that the dense specimen experiences an increase in the void ratio while the loose one undergoes a decrease as the stress increases. At ultimate strength however, both samples would have approximately the same void ratio. This is called the critical void ratio and it is defined as the void ratio at which cohesionless soils experience no volume change during shear. Any soil specimen with an initial void ratio of less than its critical void ratio is called a dense specimen and it will undergo a volume dilatation (volume increase) during shear. If the void ratio of the soil specimen is higher

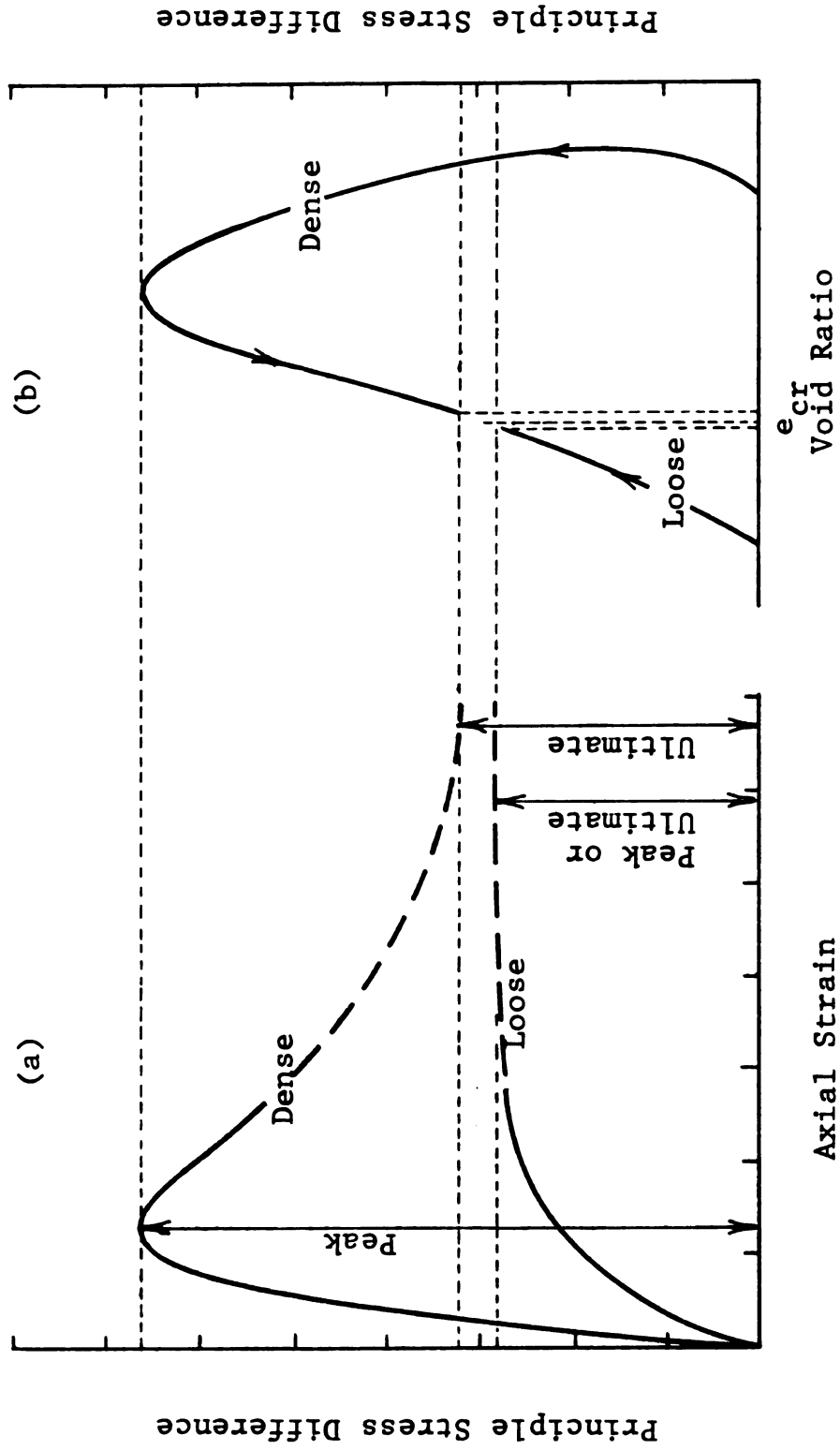


FIGURE 4.47 TYPICAL STRESS-STRAIN AND STRESS-VOID RATIO CURVES FOR LOOSE AND DENSE SOIL SPECIMENS (36).

than its critical void ratio, then the soil specimen is loose and it will stand a volume decrease during shear. Further, the value of the critical void ratio is dependent upon the soil in question and the test confining pressure(67).

Traditionally, strength of soil specimens are compared, studied and/or analysed using the void ratio or the relative density of the soils. This method was proven to be useful when analysing the strength variation of one type of soil (loose or dense) due to variations in the soil density and/or void ratio. If different types of soils are involved however, the method may be inaccurate and may lead to conflicting conclusions. This point could be illustrated using the following examples:

EXAMPLE 1.

In this study, series A samples possess the same type of gradation but different percent fine contents and maximum particle size. Several dry dense and loose soil specimens of each sample were tested using drained triaxial compression tests. Figure 4.48 shows plots of the peak angle of internal friction versus the relative density of the soil specimens. The ultimate angles of internal friction, and the critical relative densities (correspond to the critical void ratios) of all samples are also shown in the figure. It can be noted from the

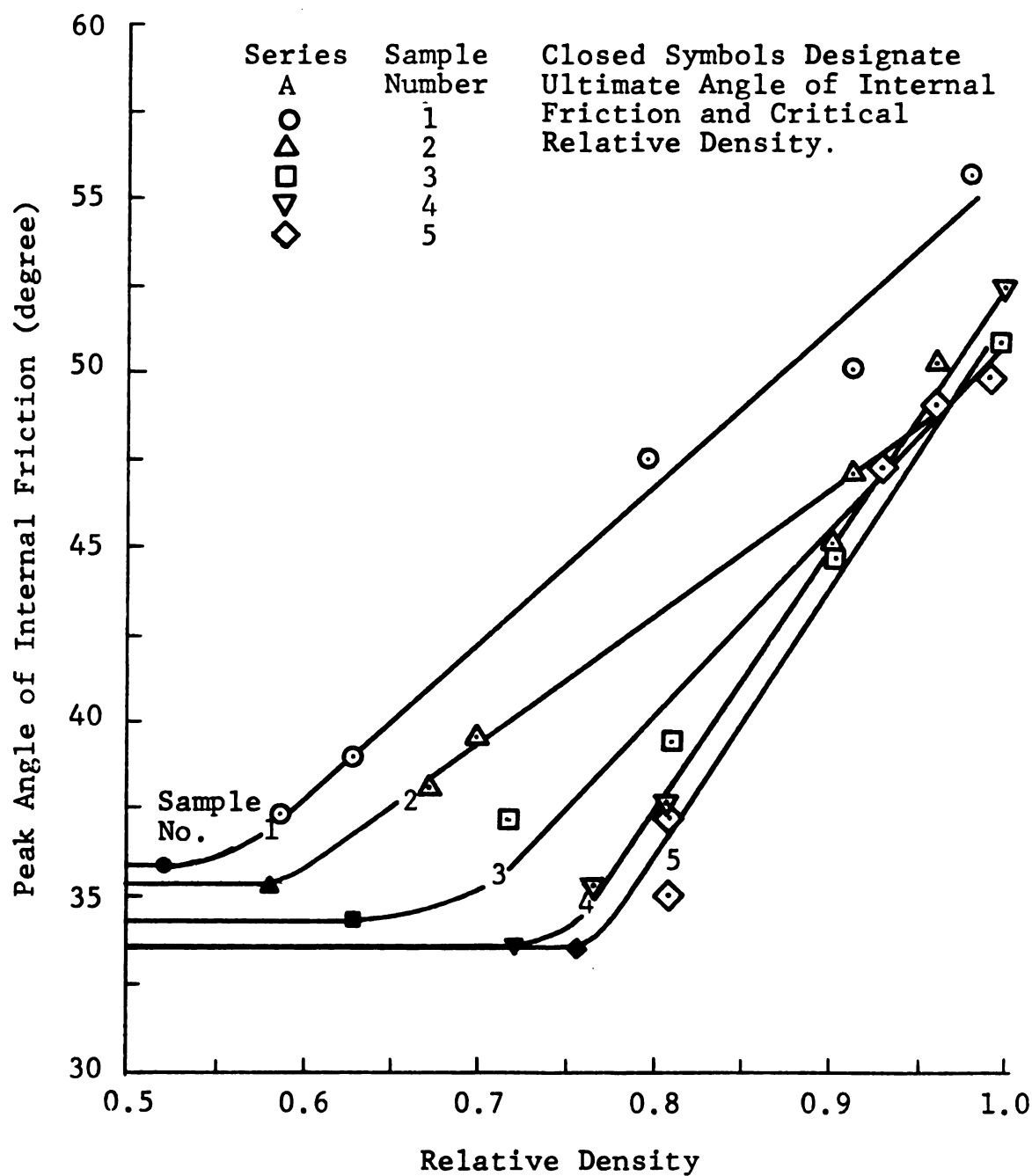


FIGURE 4.48 PEAK ANGLE OF INTERNAL FRICTION VERSUS RELATIVE DENSITY OF SERIES A SAMPLES FOR A CONFINING PRESSURE OF 5 PSI.

figure that for all soil specimens of any one sample (one soil type), the higher the relative density the higher the angle of internal friction. If the peak angles of internal friction of all samples (different types of soils) are to be compared against each other using a constant relative density value (for example 0.7), then samples 4 and 5 are on the loose side of the curves, sample 3 is in the vicinity of the critical void ratio, and samples 1 and 2 are on the dense side. Thus, the samples possess different behavior during shear and consequently, their strength cannot be compared. Nevertheless, if such comparison is to be made then the following conclusion can be drawn:

"FOR THE SAME RELATIVE DENSITY, THE HIGHER THE MAXIMUM GRAIN SIZE (OR THE LOWER THE PERCENT FINE CONTENT) OF THE SOIL THE HIGHER THE STRENGTH".

Similar conclusion was also reached by several other researchers (see Section 2.2.1).

EXAMPLE 2.

Figure 4.49 depicts the same data of example 1 plotted against the void ratio of the soil specimens. It can be seen from the figure that for all specimens of one sample (same soil type), the lower the void ratio the higher the angle of internal friction. Also, if the data from all samples are to be compared at the same

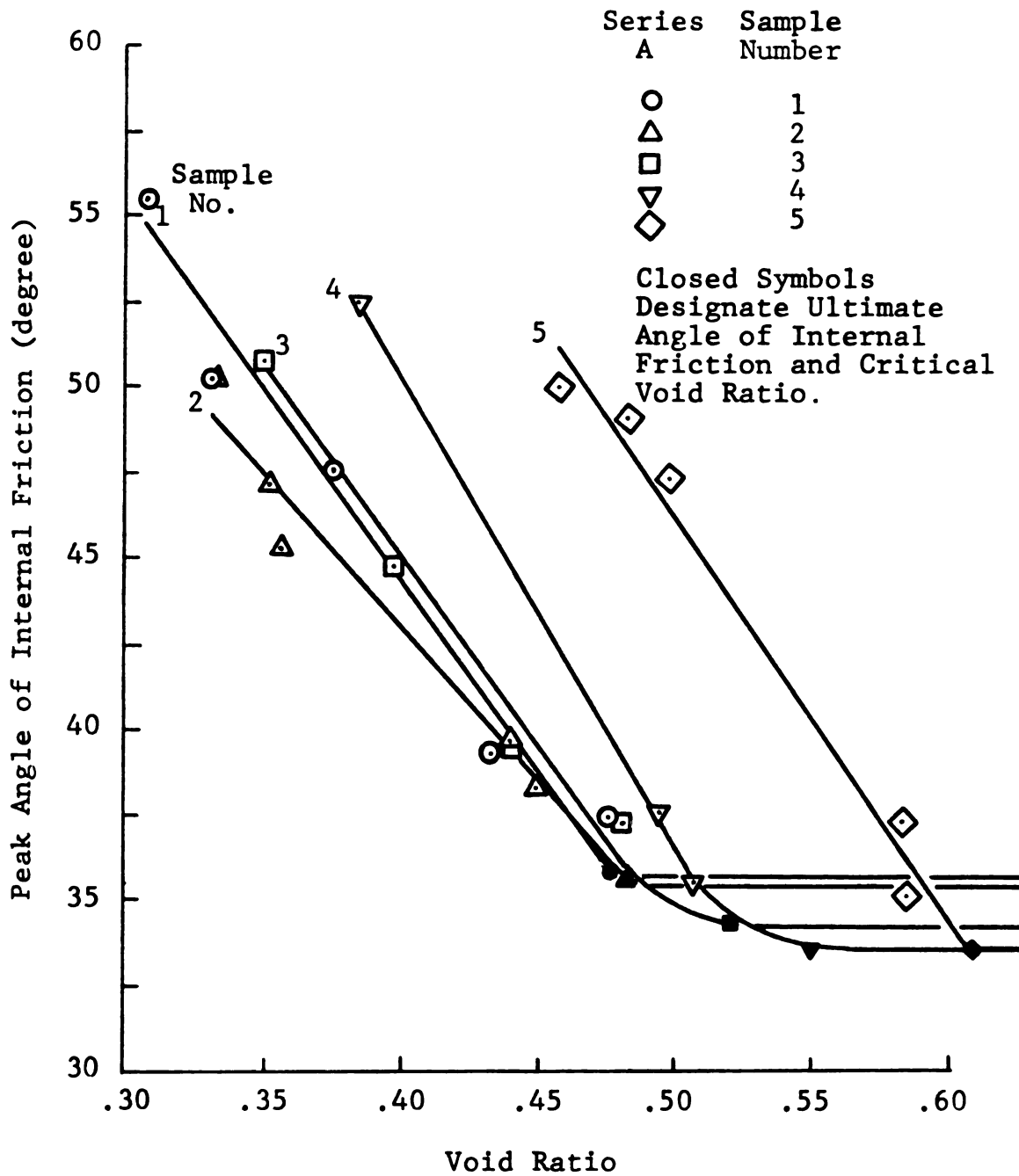


FIGURE 4.49 PEAK ANGLE OF INTERNAL FRICTION VERSUS VOID RATIO OF SERIES A SAMPLES FOR A CONFINING PRESSURE OF 5 PSI.

the

that

poss

two

view

deve

the

this

A and

the

equat

where

void ratio then the following conclusion can be made:

"FOR THE SAME VOID RATIO, THE HIGHER THE MAXIMUM GRAIN SIZE (OR THE LOWER THE PERCENT FINE CONTENT) OF THE SOIL THE LOWER THE STRENGTH".

Again, similar conclusion was reached by several other researchers (see Section 2.2.1).

It is clear that the conclusion of example 1 is exactly the opposite of that of example 2. The reason for this is that at the same relative density, different types of soils possess different void ratios and vice versa. Also, these two examples illustrate, to some extent, the conflicting views in the literature (see Section 2.2.1), and the need to develop a new technique and/or analysis procedure whereby the strength of different types of soils can be studied.

To this end, a new model was developed and utilized in this study to analyse the strength of all samples of series A and B. The model is based upon the dilatant behavior of the soil and it can be expressed using the following equation:

$$PD = (e_{CR} - e)/(e_{CR} - e_{MIN}) \quad (4.28)$$

where: PD = percent dilatation of the soil specimen
(percent volume change);

e_{CR} = the critical void ratio of the soil (the void ratio at which the soil will experience no volume change);

per

trial

soil

4.8

1

the p

e = the void ratio of the soil; and

e_{min} = the minimum void ratio of the soil (it corresponds to the maximum dry density).

Irrespective of the soil's type, the advantages of the percent dilatation model include:

- a) For zero percent dilatation, all cohesionless soils will experience no volume change during shear i.e., the void ratio of the soil will be the critical one.
- b) For a positive value of the percent dilatation, all cohesionless soils will possess a void ratio less than the critical and will experience similar behavior (volume increase) during shear.
- c) For a negative percent dilatation, all cohesionless soils will possess a void ratio higher than the critical void ratio, will undergo a volume increase during shear, and will have a peak angle of internal friction equal to the ultimate angle of internal friction.

The percent dilatation model and its relevance to the analysis and discussion of the strength of cohesionless soils are presented in the following Sections.

4.8 PEAK STRENGTH

The peak strength of a cohesionless soil corresponds to the peak stress (or maximum principal stress difference) on

th
ex
(c
fo

wh

spe
cha
moi
of
str
pre
of
Sec

4.8.

ratio
the
inac
such
lite

the stress-strain curve. In general, the peak strength is expressed in terms of the peak angle of internal friction (ϕ_p) or simply the angle of shearing resistance using the following equation:

$$\phi_p = \sin^{-1}[(\sigma_1 - \sigma_3)/(\sigma_1 + \sigma_3)] \quad (4.29)$$

where: ϕ_p = peak angle of internal friction;

σ_1 = major principal stress at failure; and

σ_3 = minor principal stress at failure.

The peak strength or (ϕ_p) of a cohesionless soil specimen depends to a large extent on the soil grain characteristics, specimen density, confining pressure, and moisture content. In the following Subsections, the effects of grain size, sample gradation, and grain shape on the peak strength of dry cohesionless soils tested under a confining pressure of 5 psi (34.5 kN/m²) are discussed. The effects of confining pressure and moisture content are discussed in Sections 4.11 and 4.12.

4.8.1 EFFECT OF GRAIN SIZE

It was noted in Section 4.7 above that using the void ratio or the relative density of the soil specimen to study the strength of different types of soils may lead to inaccurate conclusions. Table 2.2 provides a summary of such conflicting conclusions that are reported in the literature. Similar findings could also be made by using

th

di

of

dra

lin

rat

inc

per

the

str

fun

can

den

max

low

net

soi

was

as s

dila

samp

of

4.50

the test data. Figure 4.37 depicts the normalized stress difference (NSD) versus the void ratio of the soil specimens of series A samples. The solid curves in the figure were drawn to best fit the test data. The intersections of these lines with the void ratio axis indicate the critical void ratio of the sample in question. Examination of the figure indicates that, for a constant void ratio, the higher the percent fine content (the lower the maximum grain size) of the soil, the higher the NSD and consequently the higher the strength. The same NSD data are plotted in Figure 4.50 as a function of the relative density of the soil specimen. It can be seen from the figure that, for a constant relative density, the higher the percent fine content (the lower the maximum grain size) of the soil, the lower the NSD and the lower the strength. Thus, the need to develop a new methodology whereby the test data of different types of soils could be analysed was recognized in this study. This was accomplished by using the percent dilatation model (PD) as stated in Section 4.7 above.

Figures 4.51 and 4.52 depict the NSD versus the percent dilatation (PD) of the test specimens of series A and B samples respectively. It should be noted that the NSD data of Figure 4.51 are the same as those of Figures 4.37 and 4.50. The characteristics of Figures 4.51 and 4.52 are:

- a) If the void ratio of the soil specimens is lower than the critical void ratio (i.e., dense to relatively

1

0.
0.
0.
 $(\phi_p - \phi_u)/\phi_u$
0.
0.
0.
0.
0.
0.

FIGURE

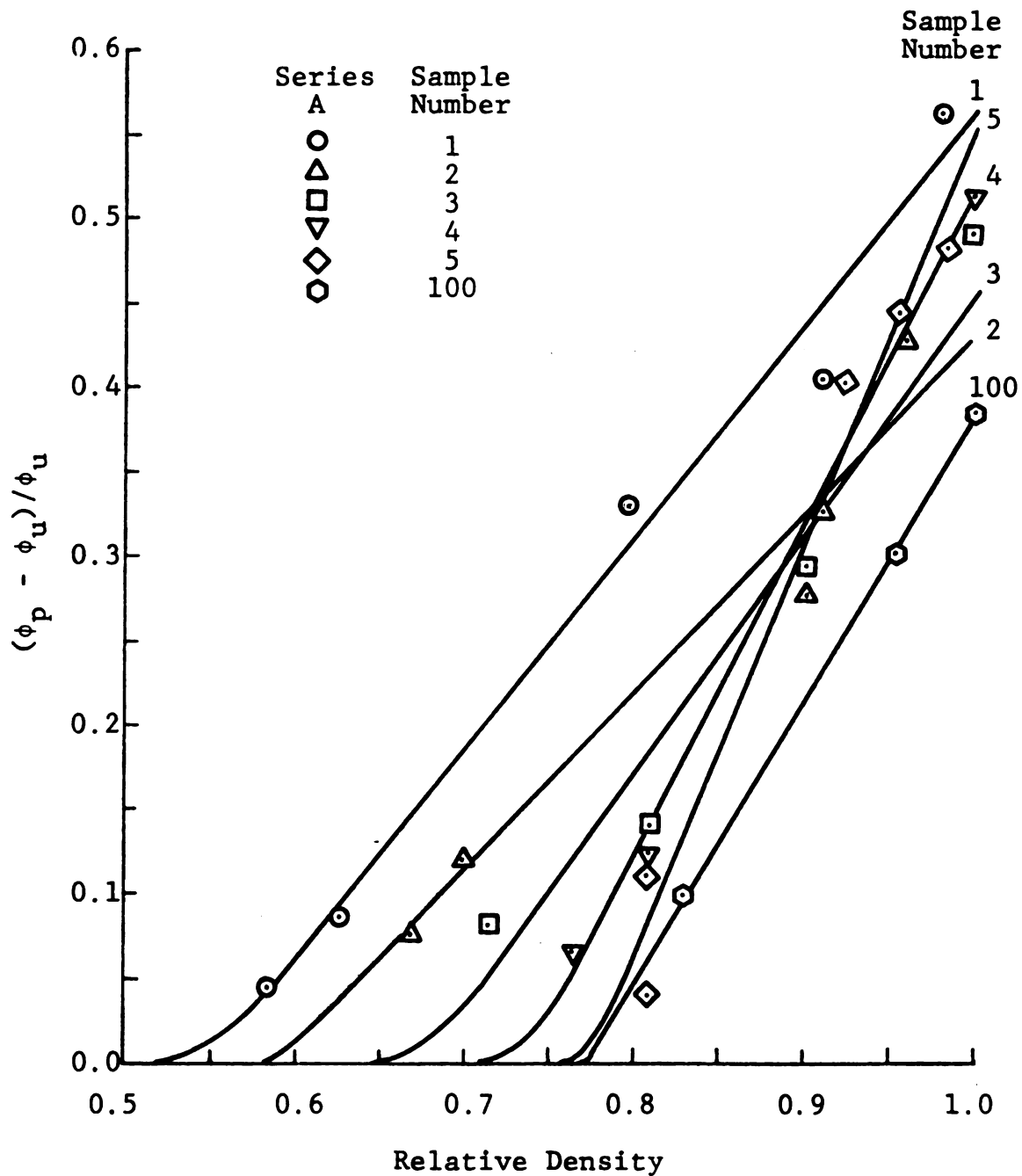


FIGURE 4.50 NORMALIZED STRENGTH DIFFERENCE VERSUS RELATIVE DENSITY OF SERIES A SAMPLES FOR A CONFINING PRESSURE OF 5 PSI.

1

0

0

$$(\psi_p - \psi_u) / \psi_u$$

0

0.

0.

FIGURE

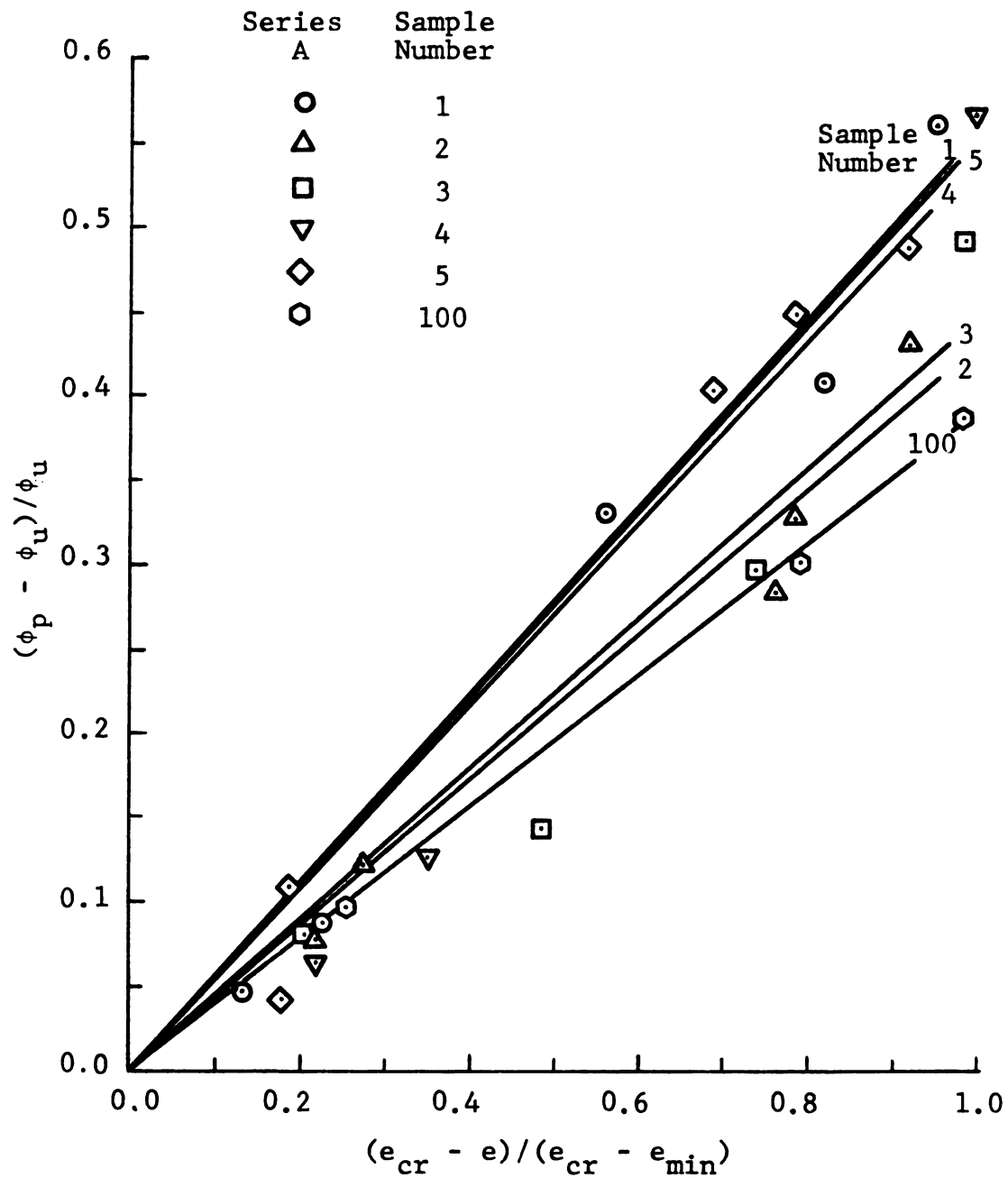


FIGURE 4.51 NORMALIZED STRENGTH DIFFERENCE VERSUS PERCENT DILATATION OF SERIES A SAMPLES FOR A CONFINING PRESSURE OF 5 PSI.

1

$\phi_p - \phi_u$ / ϕ_u

0

0

0

1.5

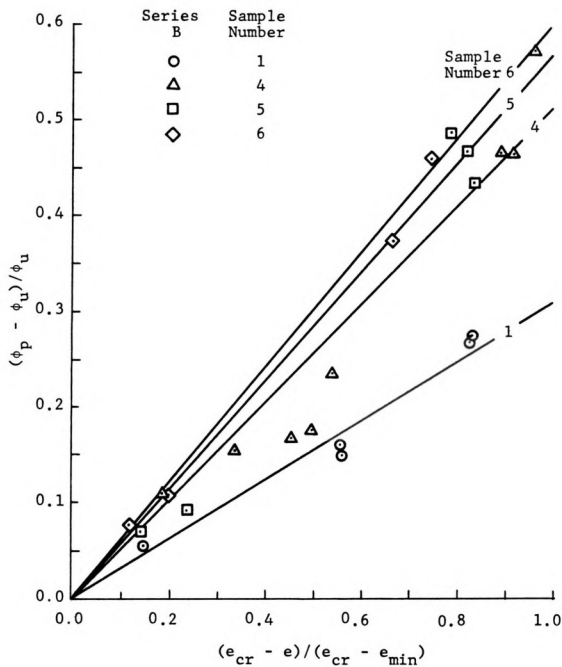


FIGURE 4.52 NORMALIZED STRENGTH DIFFERENCE VERSUS PERCENT DILATATION OF SERIES B SAMPLES FOR A CONFINING PRESSURE OF 5 PSI.

test

diff

regi

soil

will

thos

exper

with

under

2

utili

obtai

herei

figur

never

data

dense specimens) then the test data will be located in the first quarter of the axes system (as shown in the figures).

- b) If the soil specimens are loose (i.e., the void ratio is higher than the critical) then the test data will be located along the negative part of the PD axis.
- c) If the void ratio of the soil specimens is equal to the critical void ratio then the data points will be located at the origin.

The benefit of the percent dilatation model is that the test data, as shown in the figures, are separated into different regions whereby the soil specimens in any one region possess similar behavior during shear. For example: soil specimens with data points located in the first quarter will undergo a volume dilatation (expansion) during shear; those with data points at the origin of the axes will experience no volume change during shear; and soil specimens with data points along the negative part of the PD axis will undergo volume decrease during shear.

The test data of Figures 4.51 and 4.52 were then utilized and equations of the best fit lines were then obtained using least square analysis. It should be noted herein that the best fit lines (the solid lines in the figures) were made to pass through the origin by adding several data points with zero coordinates to every set of data representing any one sample of series A or B. The

str

fol

wh

ser

straight lines in the figures were modeled using the following general equation:

$$NSD = (\phi_P - \phi_U) / (\phi_U) = SP \frac{(e_{CR} - e)}{(e_{CR} - e_{MIN})} \quad (4.30)$$

where: NSD = normalized stress ratio;

ϕ_P = peak angle of internal friction in degree;

ϕ_U = ultimate angle of internal friction in degree;

e_{CR} = critical void ratio;

e_{MIN} = minimum void ratio;

e = the void ratio of the soil specimen; and

SP = slope of the best fit line.

Examination of Figures 4.51 (series A samples) and 4.52 (series B samples) indicates that:

- a) The higher the percent dilatation of the soil, the higher the NSD and the higher the strength of the soil. This was expected because the higher the PD the denser the soil and the higher the degree of particle interlocking.
- b) There is no consistent (decreasing or increasing) order of the magnitude of the slopes of the best fit lines of series A and B samples. Since the only difference between the samples within one series is the percent fine content (maximum particle size) of the sample then the slope of the lines is a function of the grain size of the samples.

of

4.1

fin

the

as

two

abo

the

dec

abo

fro

the

mod

san

SP

SP

the

To study the effect of grain size on the peak strength of the samples, the slopes of the best fit lines of Figures 4.51 and 4.52 are plotted in Figure 4.53 against the percent fine content of the soils. It can be seen from the figure that the values of the slope (for series A samples) decrease as the percent fine content increases from zero to about twenty; increase as the percent fine content increases from about twenty to about forty five; and they decrease thereafter. For series B samples, the values of the slope decrease as the percent fine content increases from zero to about four; increase as the percent fine content increases from about four to about thirty eight; and they decrease thereafter. Nevertheless, the curves of Figure 4.53 were modeled using equations 4.31 and 4.32 for series A and B samples respectively.

$$SP = \frac{0.41 + 3.16[ABS(PF - 0.205)]}{1.00 + 1.45[ABS(PF - 0.205)]} \text{EXP}[-1.26(PF)^{1.35}], \quad (4.31)$$

$$SP = \frac{0.33 + 3.16[ABS(PF - 0.040)]}{1.00 + 1.45[ABS(PF - 0.040)]} \text{EXP}[-1.30(PF)^{1.13}], \quad (4.32)$$

where: SP = the slope of lines of Figure 4.53;

ABS = absolute value;

PF = percent fine content of the soil (PF = 0.0 to 1.0); and

EXP = exponential function.

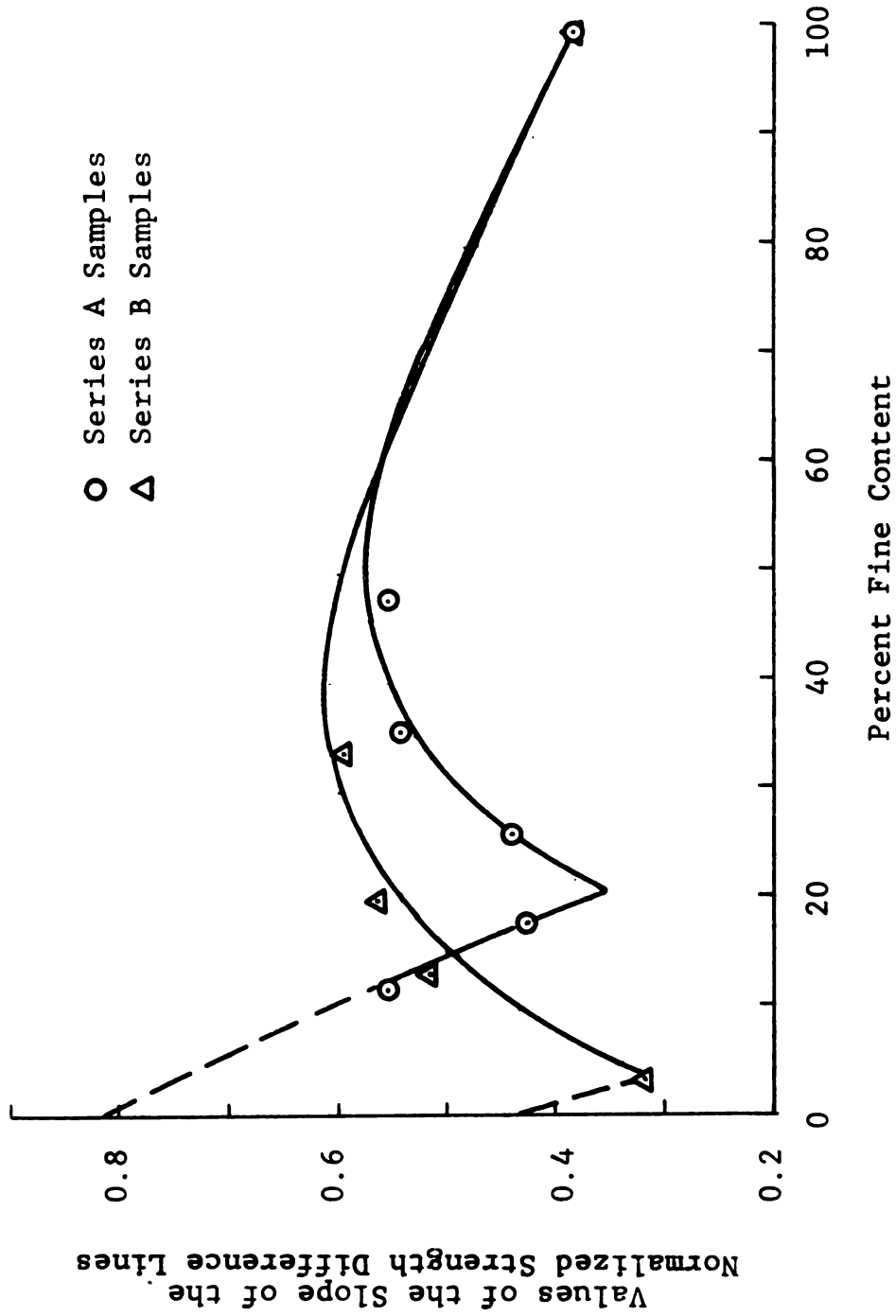


FIGURE 4.53 VALUES OF THE SLOPE OF THE NORMALIZED STRENGTH DIFFERENCE LINES VERSUS PERCENT FINE CONTENT OF SERIES A AND B SAMPLES.

sp

sa

4.

4.

For

CP

For

CP

when

the

int

The

five

the

Thus, the peak angle of internal friction of any soil specimen of the crushed and pulverized material of series A samples could be calculated by combining equations 4.24, 4.30, and 4.31; whereas for series B samples, equations 4.25, 4.30, and 4.32.

For series A samples:

$$\phi_P = 40.0 \{ 1.0 - 45.25(PF) \exp[-5.37(PF)^{0.14}] \} \\ \left\{ \left[\frac{(e_{CR} - e)}{(e_{CR} - e_{MIN})} \right] \left[\frac{0.41 + 3.16[ABS(PF - 0.205)]}{1.00 + 1.45[ABS(PF - 0.205)]} \right] \right\} \\ \exp[-1.26(PF)^{1.35}] + 1.0 \quad (4.33)$$

For series B samples:

$$\phi_P = 40.0 \{ 1.0 - 5.87(PF) \exp[-3.33(PF)^{0.33}] \} \\ \left\{ \left[\frac{(e_{CR} - e)}{(e_{CR} - e_{MIN})} \right] \left[\frac{0.33 + 3.16[ABS(PF - 0.040)]}{1.00 + 1.45[ABS(PF - 0.040)]} \right] \right\} \\ \exp[-1.30(PF)^{1.13}] + 1.0 \quad (4.34)$$

where all terms are as before.

Figures 4.54 and 4.55 shows the correspondence between the calculated and measured values of the peak angle of internal friction for series A and B samples respectively. The locus of the solid line in the figures (drawn at forty five degree from the horizontal) indicate equality between the calculated and measured values, while the dashed lines

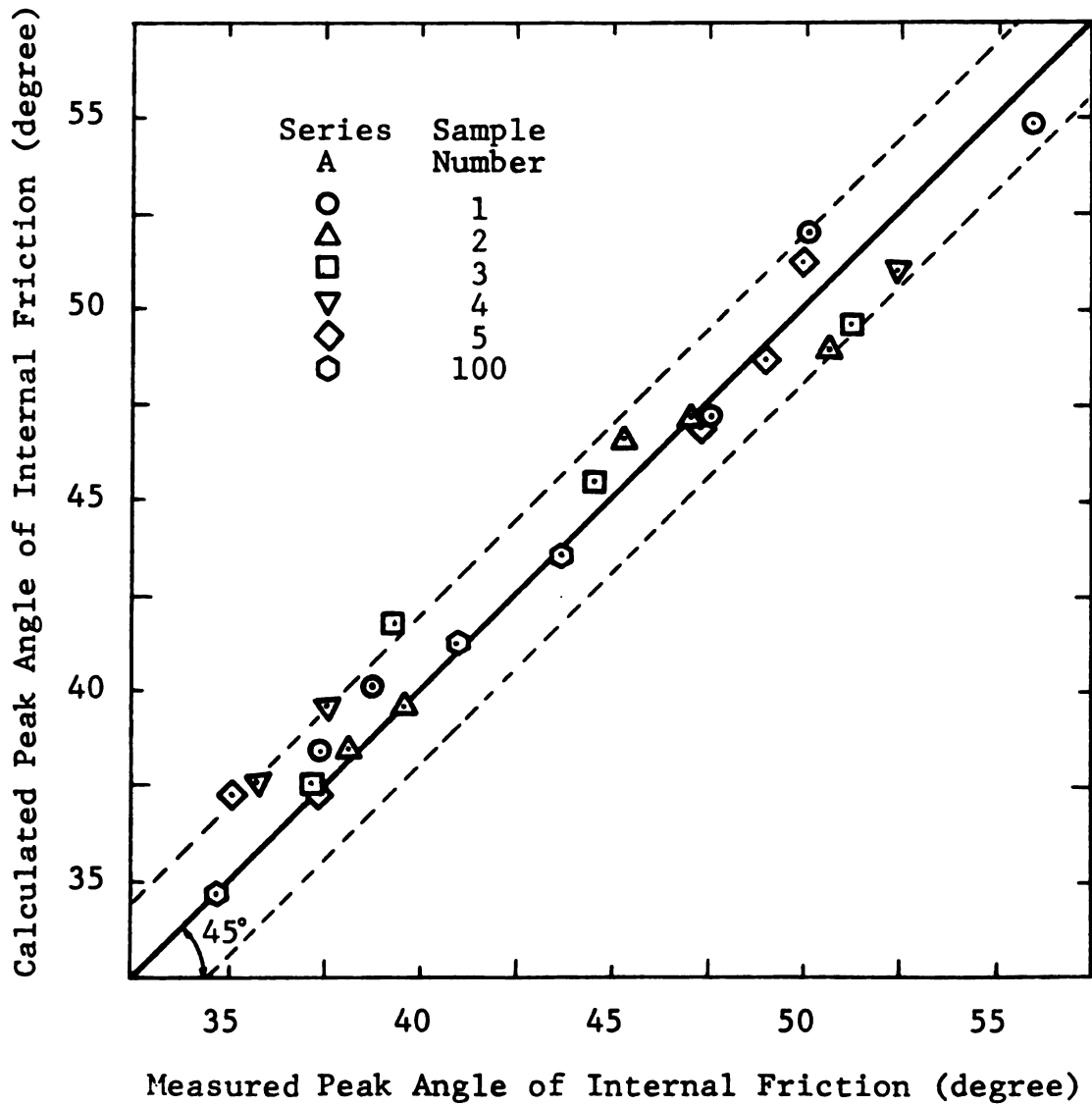


FIGURE 4.54 CALCULATED VERSUS MEASURED PEAK ANGLE OF INTERNAL FRICTION FOR SERIES A SAMPLES.

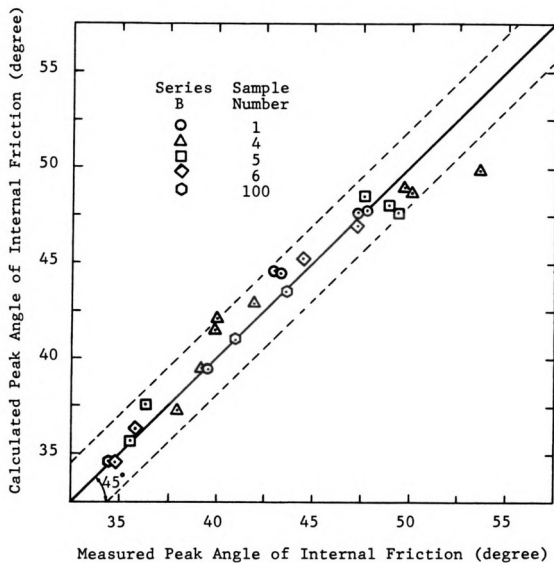


FIGURE 4.55 CALCULATED VERSUS MEASURED PEAK ANGLE OF INTERNAL FRICTION FOR SERIES B SAMPLES.

represent a deviation of two degrees.

The effect of grain size on the peak strength of the soil can then be studied by using equations 4.33 and 4.34 to calculate the peak angle of internal friction at constant levels of percent dilatation. Figures 4.56 and 4.57 depict the calculated peak angle of internal friction plotted against the percent fine content of the soil for percent dilatation of 0.0, 0.25, 0.5, 0.75, and 1.00. Examination of the figures indicates that:

- a) For a constant percent fine content (particle size), the higher the percent dilatation of the soil specimen the higher the value of the peak angle of internal friction. That is the higher the density of the soil the higher the shear resistance.
- b) For a constant value of percent dilatation, the peak angle of internal friction of series A samples decreases as the percent fine content increases from zero to 20.5 percent, then it increases as the percent fine increases from 20.5 to about 40 percent, and finally it decreases once again as the percent fine increases above the 40 percent level. Similar observations were also noted for series B samples except that the corresponding percent fine contents are 4.0 and 30.0.
- c) For the zero PD curve, the value of the peak angle of internal friction decreases with increasing percent

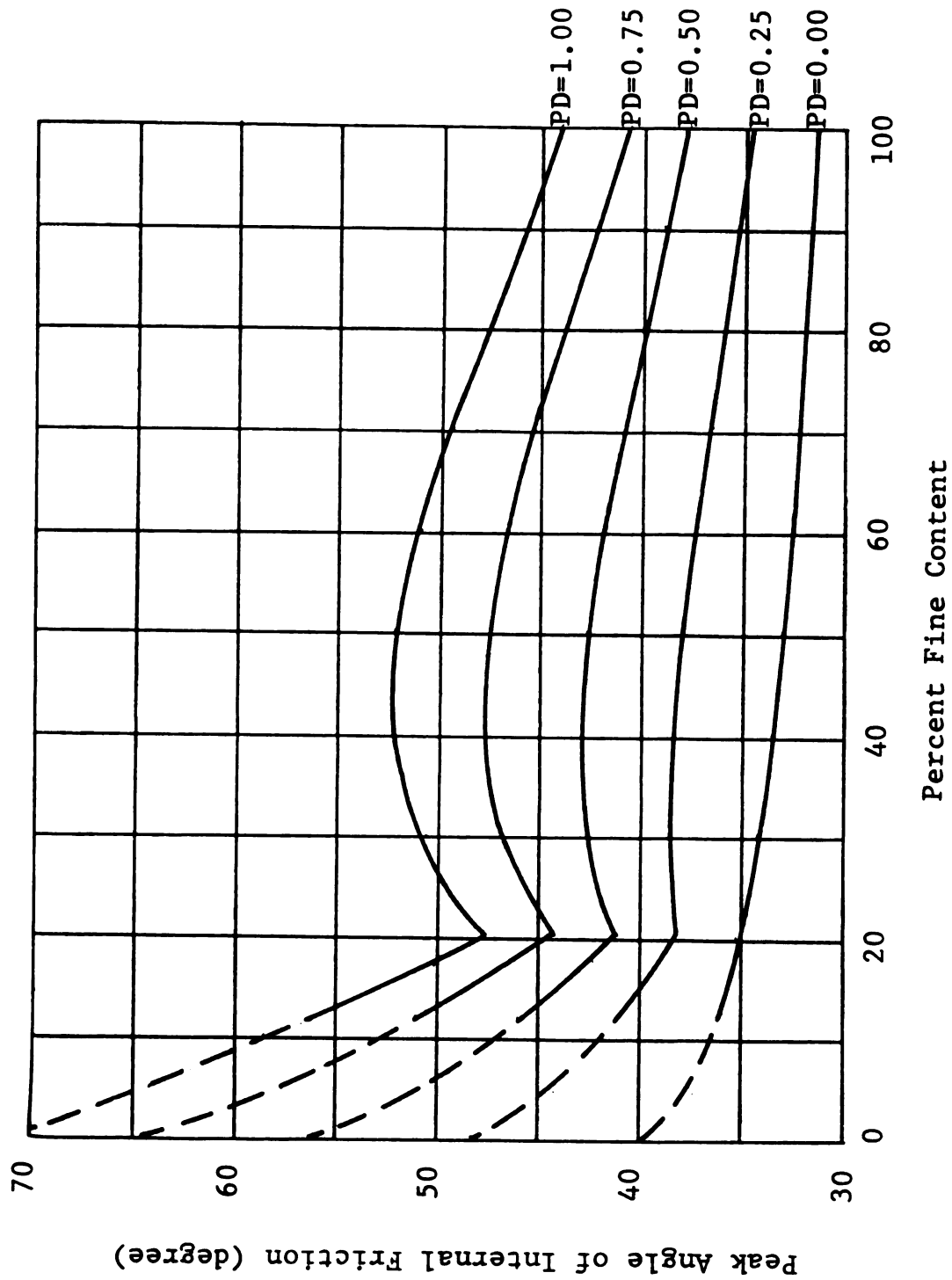


FIGURE 4.56 PEAK ANGLE OF INTERNAL FRICTION VERSUS PERCENT FINE CONTENT OF SERIES A SAMPLES FOR A CONFINING PRESSURE OF 5 PSI, AND FIVE VALUES OF THE PERCENT DILATION.

[illegible]

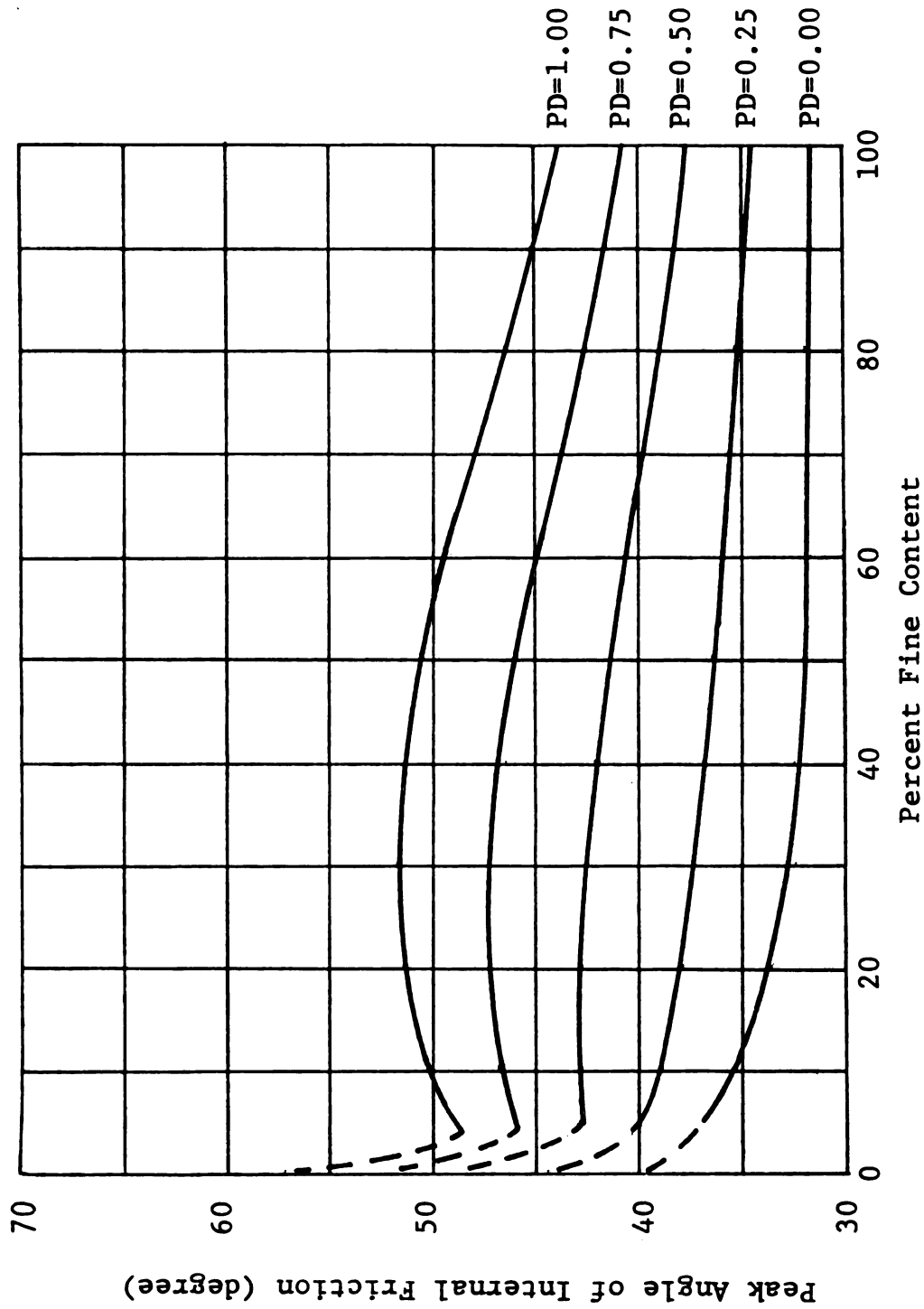


FIGURE 4.57 PEAK ANGLE OF INTERNAL FRICTION VERSUS PERCENT FINE CONTENT OF SERIES B SAMPLES FOR A CONFINING PRESSURE OF 5 PSI, AND FIVE VALUES OF THE PERCENT DILATATION.

fine content and are equal to those of the ultimate angle of internal friction.

The first observation was expected because the higher the percent dilatancy, the lower the void ratio and the higher the density of the soil. The peak angle of internal friction of the soil (also called the total angle of shearing resistance) is a function of the state of compaction of the soil, that is the denser the soil, the higher the shearing resistance. The shearing resistance of cohesionless soils depends on the physical motion between particles which includes particles sliding and rolling relative to each other, and particle plucking and displacement from their interlocking seats. The former is being resisted by the sliding friction (ultimate friction) which is a function of the soil mineral and surface roughness of the grain and is independent of the soil density. The latter consists of physical restraints to relative particle translation affected by adjacent particles. The resistance to this motion is offered by what is called the interlocking friction. Particle interlocking is a function of the soil density, the denser the soil the higher the particle packing and the higher the degree of interlocking. Since the peak angle of internal friction can be taken as the sum of the sliding (ultimate) and interlocking friction, and since the ultimate friction is independent of the soil density, then the higher the degree

of interlocking, the higher the peak angle of internal friction.

The significance of the second observation is that two variables are affecting the peak angle of internal friction. the first is the percent gravel content of the sample, while the second is the percent fine content.

GRAVEL CONTENT

Figures 4.58 and 4.59 show the percent gravel and sand contents of the soil plotted against the percent fine content of series A and B samples respectively. First, the percent fine content of all samples are known. To obtain the percent combination of gravel and sand simply enter the percent fine content of the sample in question on the horizontal axis; draw a vertical line to intercept the gravel and sand lines; then read the percent gravel and sand contents on the vertical axis that correspond to the points of intersection. From the figures, it can be seen that, for series A samples, the percent gravel content decreases as the percent fine increases from zero to 17.9, and it is zero thereafter. For series B samples, the percent gravel content is zero for percent fine contents higher than 5.75. Thus, for percent fine contents lower than 17.9 and 5.75

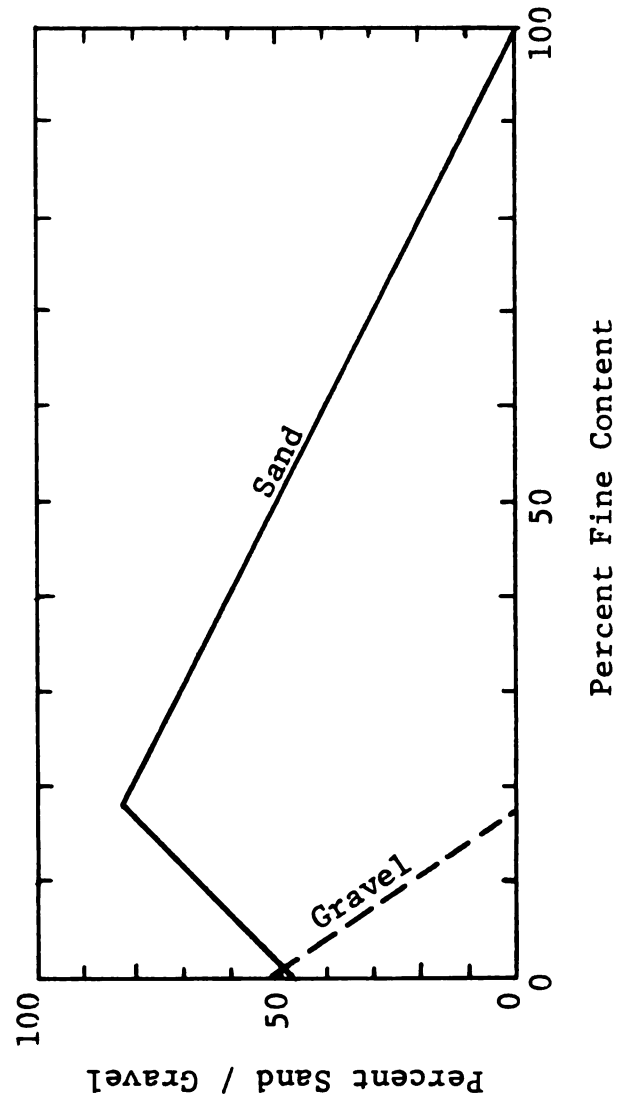


FIGURE 4.58 PERCENT COMBINATION OF GRAVEL AND SAND VERSUS PERCENT FINE CONTENT FOR SERIES A SAMPLES.

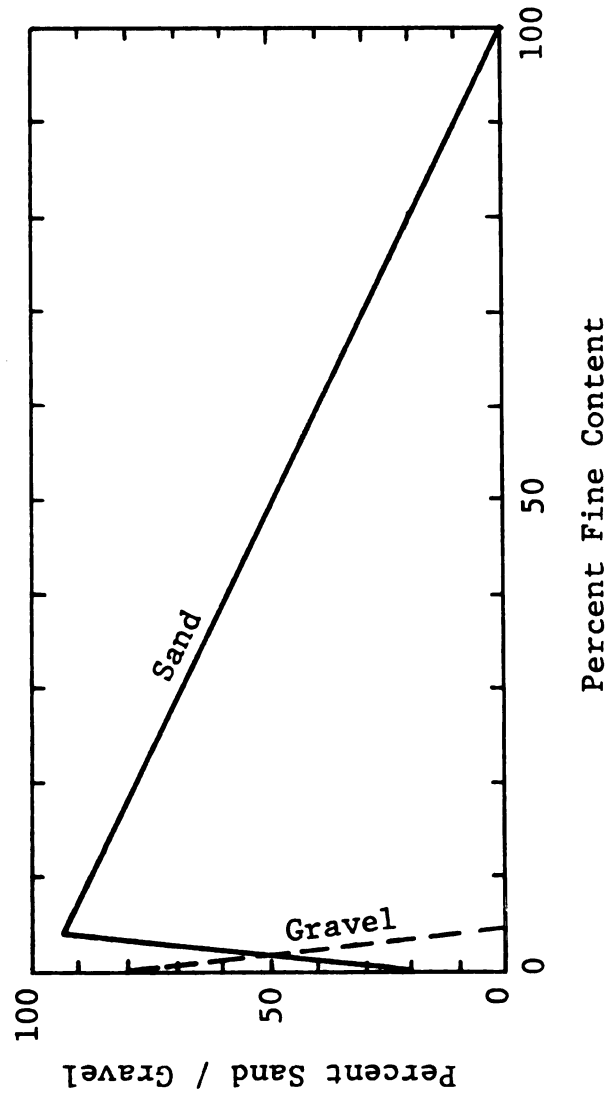


FIGURE 4.59 PERCENT COMBINATION OF GRAVEL AND SAND VERSUS PERCENT FINE CONTENT FOR SERIES B SAMPLES.

percent of series A and B samples respectively, gravel size particles reside in the soil matrix of the specimen. Large particles possess relatively higher degree of interlocking than smaller particles (sand). Consequently, the interlocking friction is expected to increase which causes an increase in the peak angle of internal friction.

FINE CONTENT

Siddiqi (73) concluded that the presence of oversized particles (particles larger than one sixth of the specimen diameter) in a soil matrix decreases its density due to less efficient packing around the oversized materials. The presence of fine material around gravel and sand particles in a soil offers a similar phenomenon, i.e. they form localized loose soil pockets around denser and larger particles. These loose pockets possess lower shearing resistance than the rest of the soil. Consequently, the overall shearing resistance of the soil specimen will suffer. As the percent fine content increases and the gravel content decreases to zero percent, packing efficiency increases and the fine particles are forced closer together. Further increases in the percent fine content will cause fine materials to dominate the

soil behavior which will result in a lower shearing resistance.

The third observation was expected and explained in Section 4.6.

For dense cohesionless soils, the peak angle of internal friction (ϕ_P) can be taken (as stated above) as the sum of the ultimate angle of internal friction (ϕ_U) and the angle of interlocking friction (ϕ_I) as expressed in the following equation:

$$\phi_P = \phi_U + \phi_I \quad (4.35)$$

The effect of grain size upon the former was discussed in Section 4.6. The effect of grain size on the angle of interlocking friction is discussed herein. Figures 4.60 and 4.61 depict the angle of interlocking friction, for three levels of percent dilatation, plotted against the percent fine content of the soil of series A and B samples respectively. Examination of the figures indicates that:

- a) As it was expected, the curves resemble those of the peak angle of internal friction.
- b) For zero percent dilatation, the data points overlap the horizontal axis, i.e., the angle of interlocking friction is zero and the peak angle of internal friction is equal to the ultimate angle of internal friction. At zero percent dilatation, the void ratio

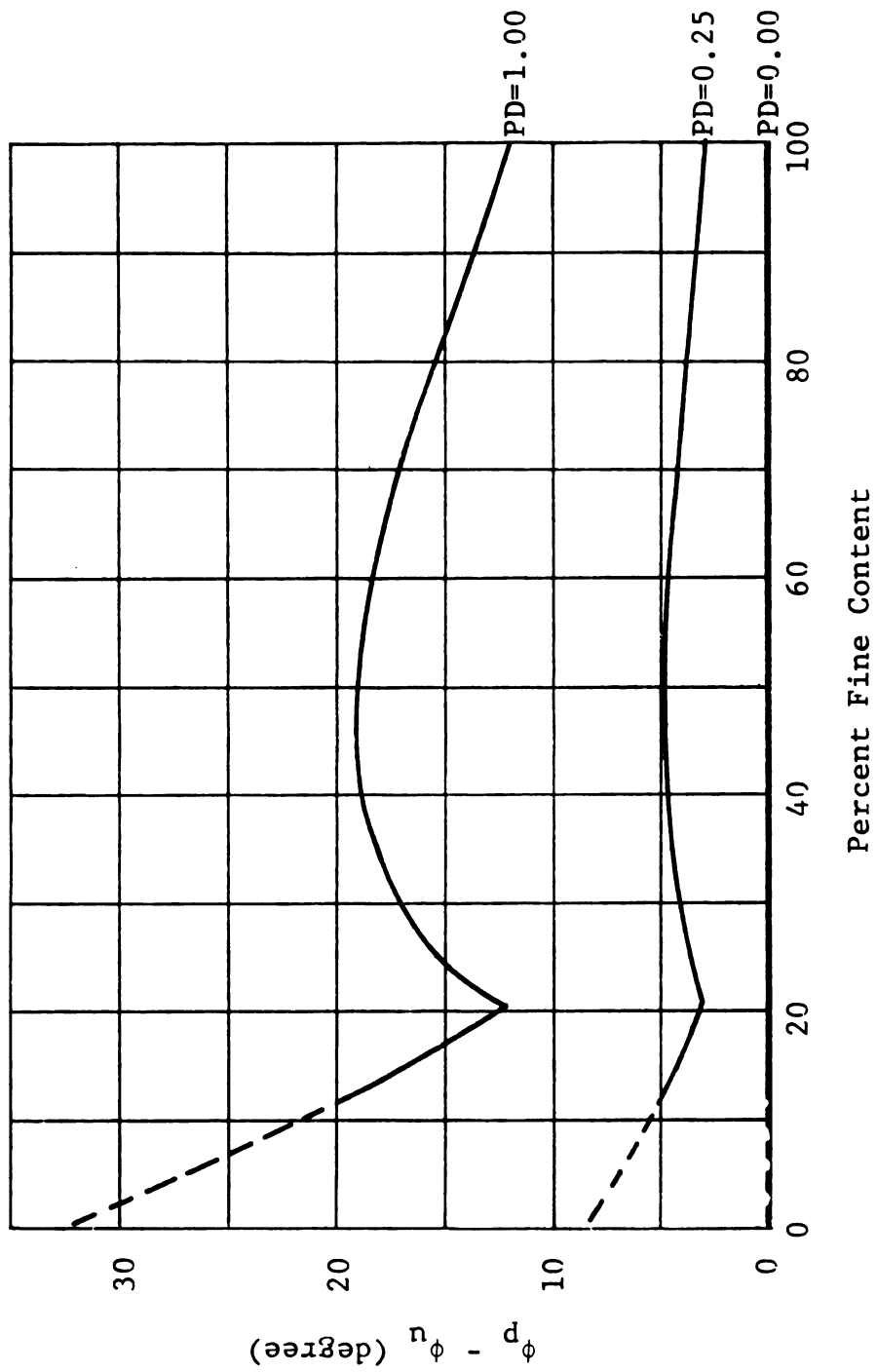


FIGURE 4.60 ANGLE OF INTERLOCKING FRICTION VERSUS PERCENT FINE CONTENT OF SERIES A SAMPLES FOR A CONFINING PRESSURE OF 5 PSI, AND THREE VALUES OF THE PERCENT DILATATION.

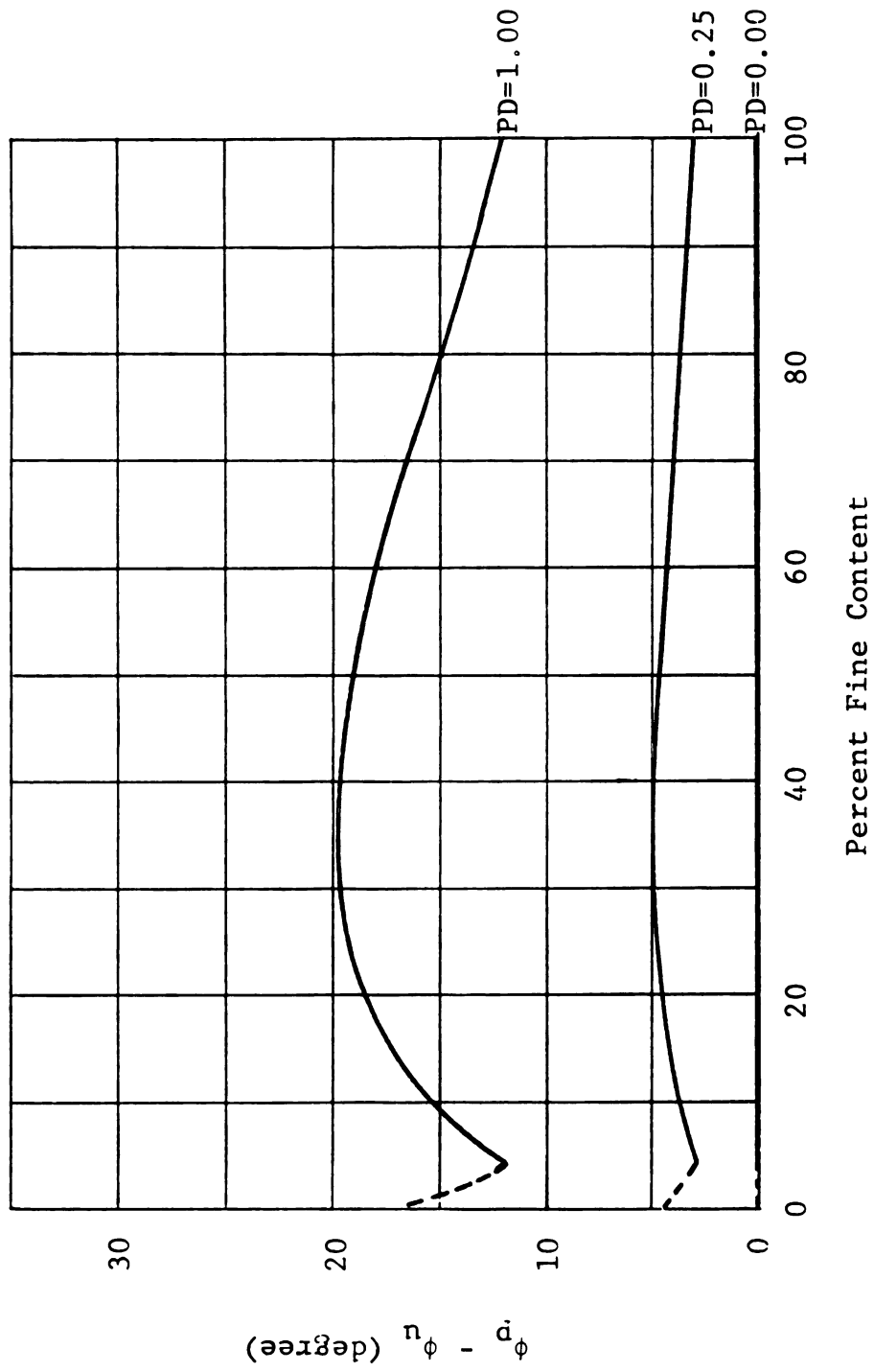


FIGURE 4.61 ANGLE OF INTERLOCKING FRICTION VERSUS PERCENT FINE CONTENT OF SERIES B SAMPLES FOR A CONFINING PRESSURE OF 5 PSI, AND THREE VALUES OF THE PERCENT DILATATION.

of

a,

whi

MAX

the

the

cont

of g

4.8.

A

as th

of i

indep

The e

discus

Fi

fricti

Percent

data pl

of the soil is equal to the critical void ratio (the void ratio at which the volume change of the soil specimen during shear is zero) and the shearing resistance is mainly due to particle sliding and rolling relative to each other.

To summarize, The effect of grain size on the peak angle of internal friction can be separated into two components: a) the effect on the ultimate angle of internal friction which is mainly a function of the percent fine content or maximum particle size of the sample; and b) the effect on the angle of interlocking friction which is a function of the percent dilatation (sample density), percent fine content or maximum grain size, and the percent combination of gravel, sand and fine materials of the sample.

4.8.2 EFFECT OF SAMPLE GRADATION

Again, the peak angle of internal friction can be taken as the sum of the ultimate angle of friction and the angle of interlocking friction. The former was found to be independent of the sample gradation (see Section 4.6.2). The effect of the sample gradation on the latter is discussed herein.

Figures 4.62 shows plots of the angle of interlocking friction for three levels of percent dilatation versus the percent fine content of series A and B samples. The same data plotted against the maximum grain size of the soil is

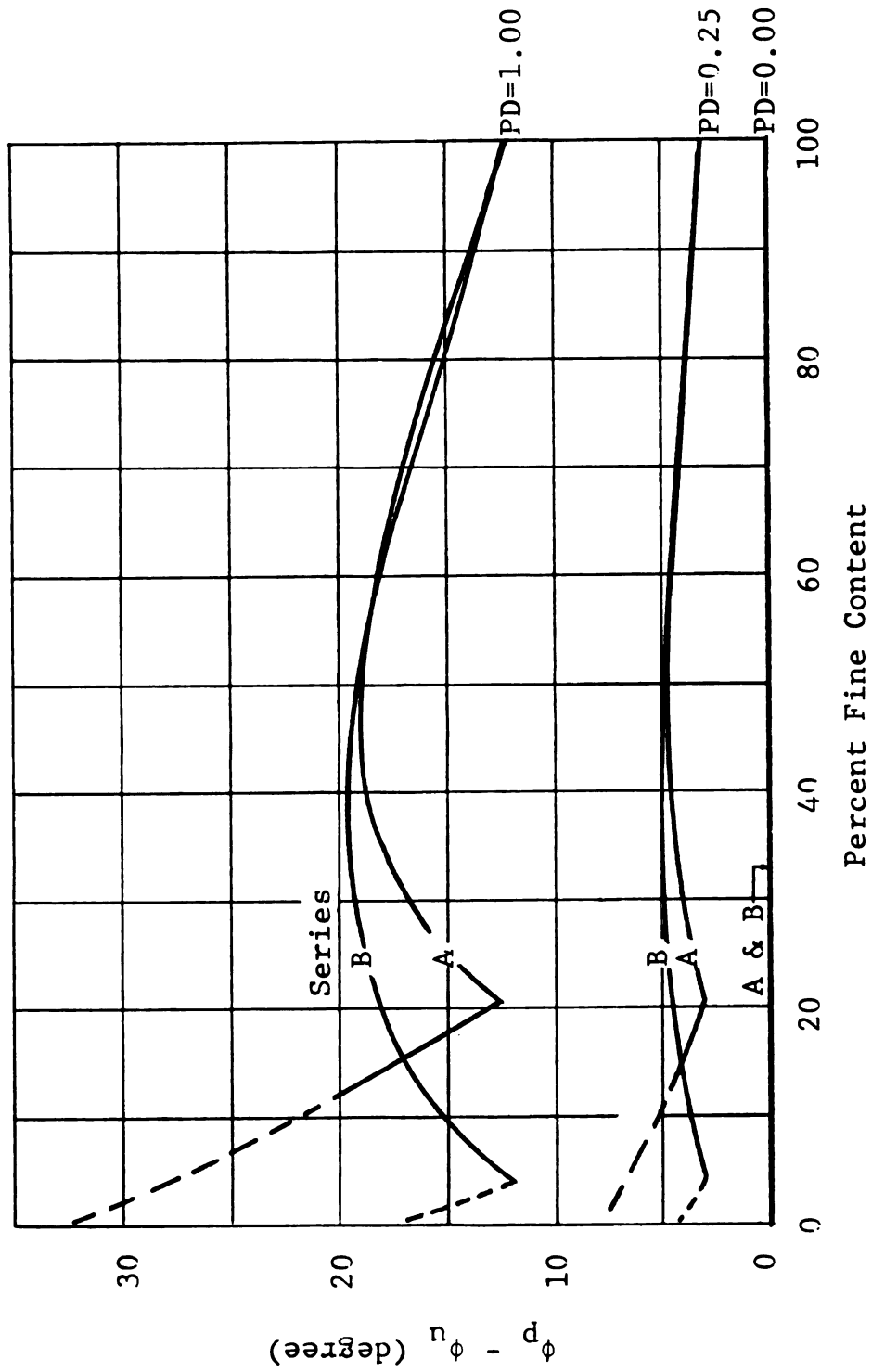


FIGURE 4.62 ANGLE OF INTERLOCKING FRICTION VERSUS PERCENT FINE CONTENT OF SERIES A AND B SAMPLES FOR A CONFINING PRESSURE OF 5 PSI AND THREE VALUES OF THE PERCENT DILATATION.

shown in Figure 4.63. Examination of the figures indicates that:

- a) For a range of the fine content from zero to about sixteen percent (corresponding change of the maximum particle size from 40 to 5 mm), the angle of interlocking friction of series A samples is higher than that of series B. Since the only difference between the two series is the coefficient of uniformity, it follows that the higher the coefficient of uniformity the higher the angle of interlocking friction.
- b) For a range of the percent fine content from sixteen to about fifty percent (corresponding change of the maximum particle size from 5 to 1 mm), the angle of interlocking friction of series A is lower than that of series B. That is the higher the coefficient of uniformity the lower the angle of interlocking friction.
- c) The angle of interlocking friction is independent of the sample gradation for percent fine content higher than fifty.
- d) As the percent dilatation decreases the effect of the sample gradation upon the angle of interlocking friction decreases. At zero percent dilatation, the data points overlap the horizontal axis and consequently the value of the angle of interlocking

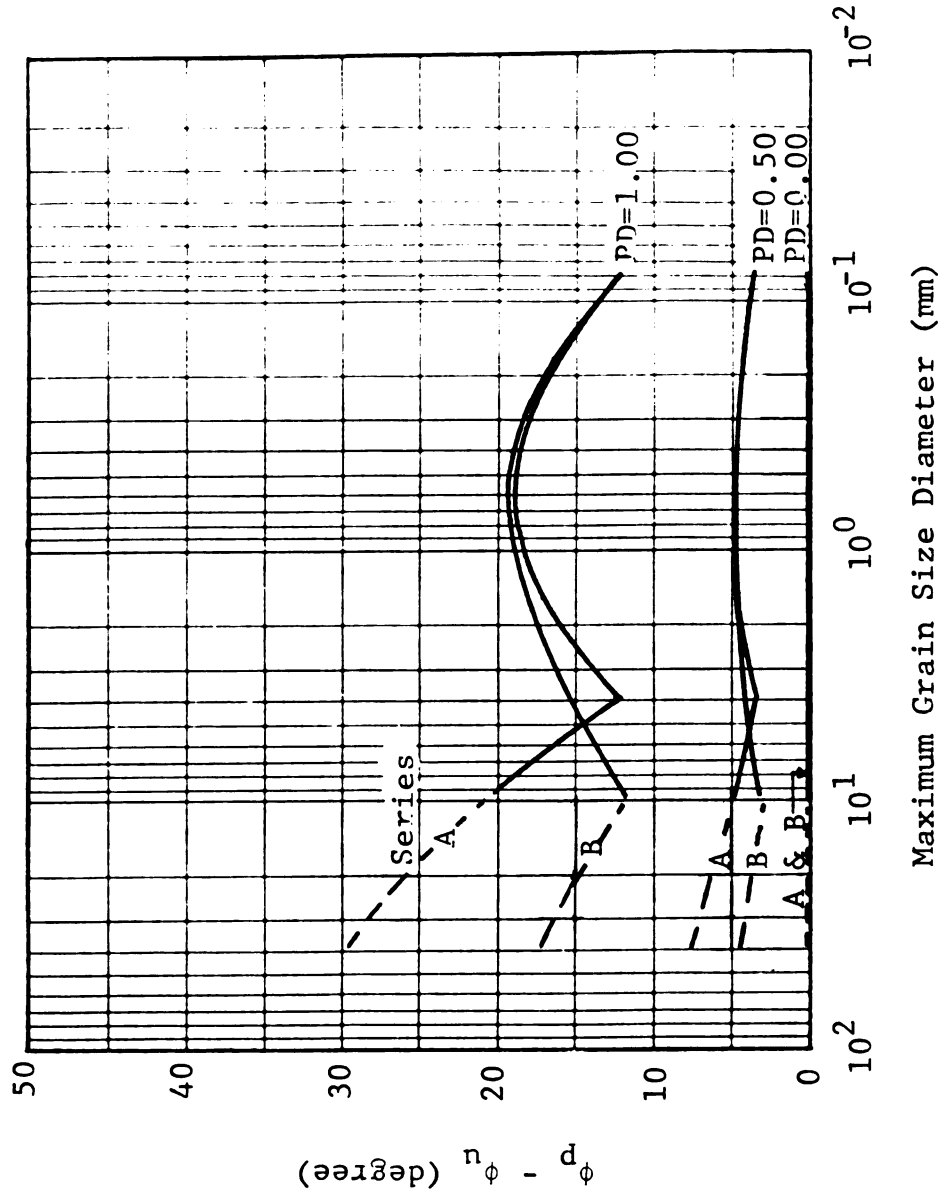


FIGURE 4.63 ANGLE OF INTERLOCKING FRICTION VERSUS MAXIMUM GRAIN SIZE OF SERIES A AND B SAMPLES FOR A CONFINING PRESSURE OF 5 PSI, AND THREE VALUES OF THE PERCENT DILATATION.

friction of series A and B samples is zero.

The first three observations are similar to those of the peak angle of internal friction. Thus, the same discussion concerning the combinations of percent gravel, sand, and fine content of the soil (see Section 4.8.1) could also be used herein to discuss the data. The fourth observation was expected because as the percent dilatation of the soil decreases to zero its void ratio increases to the critical void ratio and consequently there will be no particle interlocking.

The test results were then utilized to modify equations 4.36 and 4.37 to reflect the effect of the sample gradation on the peak angle of internal friction. The modified equations are presented below:

For series A samples:

$$\phi_P = 40.0 \{ 1.0 - 45.25(PF) \exp[-5.37(PF)^{0.14}] \}$$

$$\left\{ \left[\frac{(e_{CR} - e)}{(e_{CR} - e_{MIN})} \right] \left[\frac{0.25(Cu)^{0.13} + 3.16[ABS(PF - 0.00456(Cu))]}{1.00 + 1.45[ABS(PF - 0.00456(Cu))]} \right] \right.$$

$$\left. \exp[-1.26(PF)^{1.35}] + 1.0 \right\} \quad (4.36)$$

For series B samples:

$$\phi_p = 40.0 \{ 1.0 - 5.87(PF) \exp[-3.33(PF)^{0.33}] \}$$

$$\left\{ \left[\frac{(e_{CR} - e)}{(e_{CR} - e_{MIN})} \right] \left[\frac{0.25(Cu)^{0.13} + 3.16[ABS(PF - 0.00456(Cu))]}{1.00 + 1.45[ABS(PF - 0.00456(Cu))]} \right] \right.$$

$$\left. \exp[-1.30(PF)^{1.13}] + 1.0 \right\} \quad (4.37)$$

where all terms are as before.

It should be noted that data calculated using equations 4.36 and 4.37 for series A and B samples were within two degrees of the measured ones.

4.8.3 EFFECT OF GRAIN SHAPE

To study the effect of the grain shape (particle angularity) on the peak angle of internal friction, fourteen triaxial compression tests were conducted on soil specimens of selected samples of series A and B that were blended with the natural and 50/50 materials. These are samples 1 and 3 of series A and sample 4 of series B. The test results are summarized in Table 4.5. Figure 4.64 depicts the normalized stress difference (NSD) data plotted against the percent dilatation of the samples. It can be seen from the figure that the higher the percent dilatation (density) the higher the NSD. This was expected because the higher the density the higher the interlocking friction and consequently the higher the total frictional resistance.

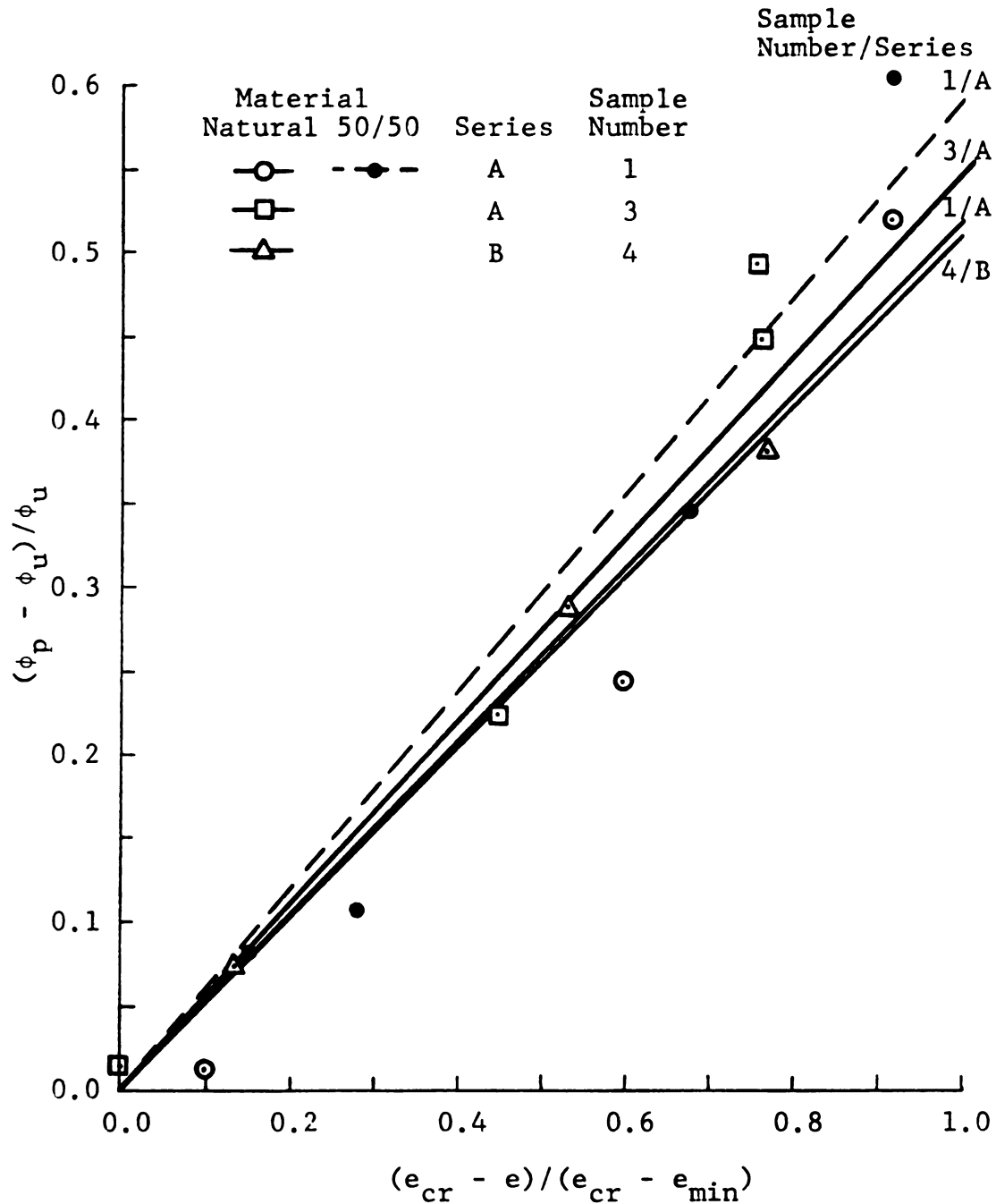


FIGURE 4.64 NORMALIZED STRENGTH DIFFERENCE VERSUS PERCENT DILATATION OF SERIES A AND B SAMPLES THAT CONSISTED OF THE NATURAL AND 50/50 MATERIALS FOR A CONFINING PRESSURE OF 5 PSI.

f
t.
A.
re
th
es
di
phy
inc
eth

The peak angle of internal friction of the soil specimens of the natural and 50/50 materials were then compared to that of the C/P materials by using equations 4.36 and 4.37. Figure 4.65 shows the calculated values of the peak angle of internal friction plotted against the measured ones (test results). The locus of the forty five degree line in the figure indicates the correspondence between the calculated and the measured values. It can be seen that the calculated values are higher than the actual ones. That is the peak angles of internal friction of the crushed and pulverized material (calculated by using the equations) are higher than those of the natural and 50/50 materials. This could also be stated as the higher the degree of angularity of the particles the higher the frictional resistance.

Figure 4.66 shows a plot of the peak angle of internal friction for five values of the percent dilatation versus the coefficient of sample angularity of sample 1 of series A. Examination of the figure indicates that the relationship between the peak angle of internal friction and the coefficient of sample angularity is linear and that the effect of the latter on the former decreases as the percent dilatation decreases. At high percent dilatation, the physical motion between particles (see Section 2.2) includes: a) particle sliding and rolling relative to each other, and b) particle plucking and displacement from their

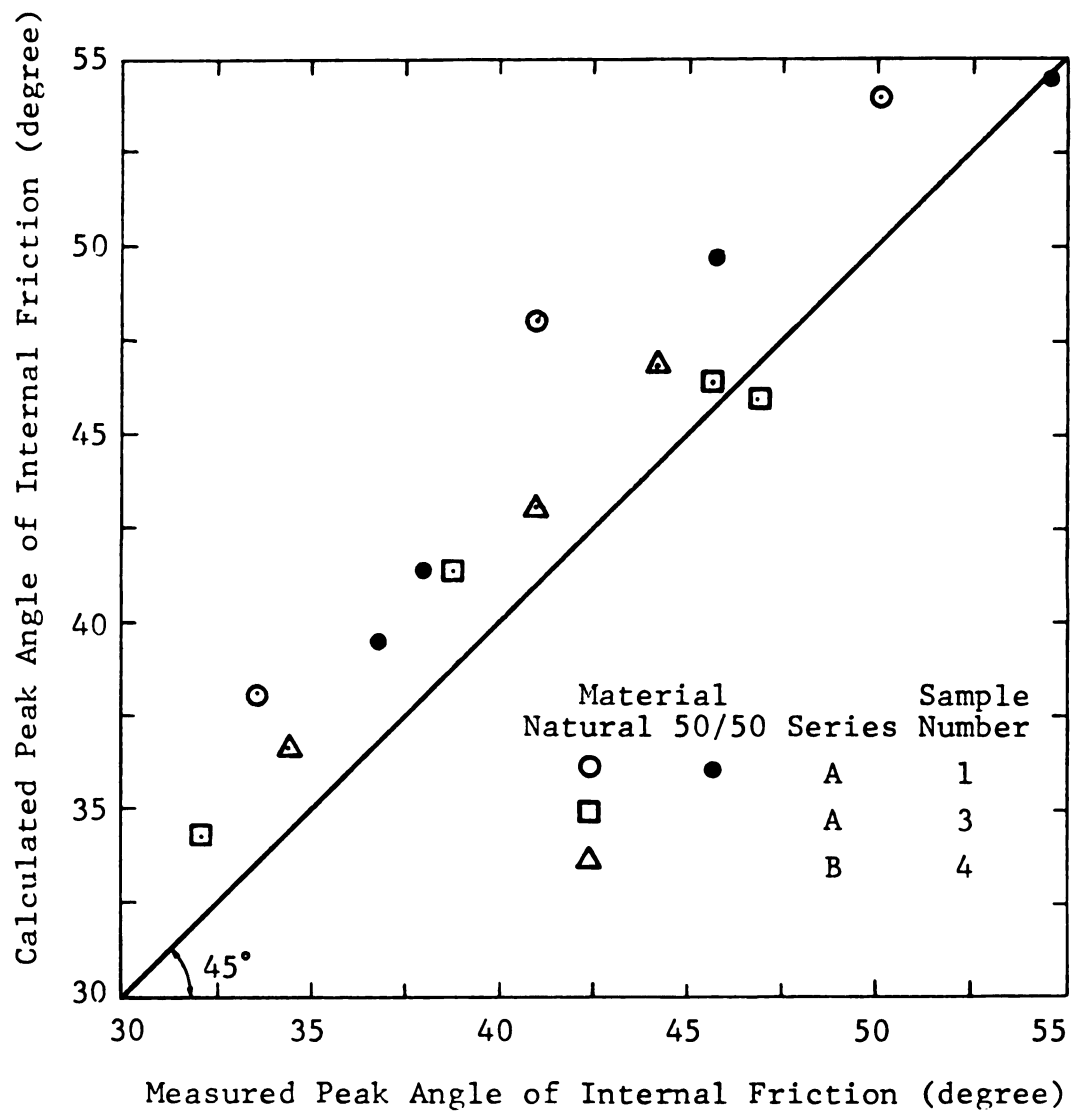


FIGURE 4.65 CALCULATED VERSUS MEASURED PEAK ANGLE OF INTERNAL FRICTION OF SERIES A AND B SAMPLES THAT CONSISTED OF THE NATURAL AND 50/50 MATERIALS.

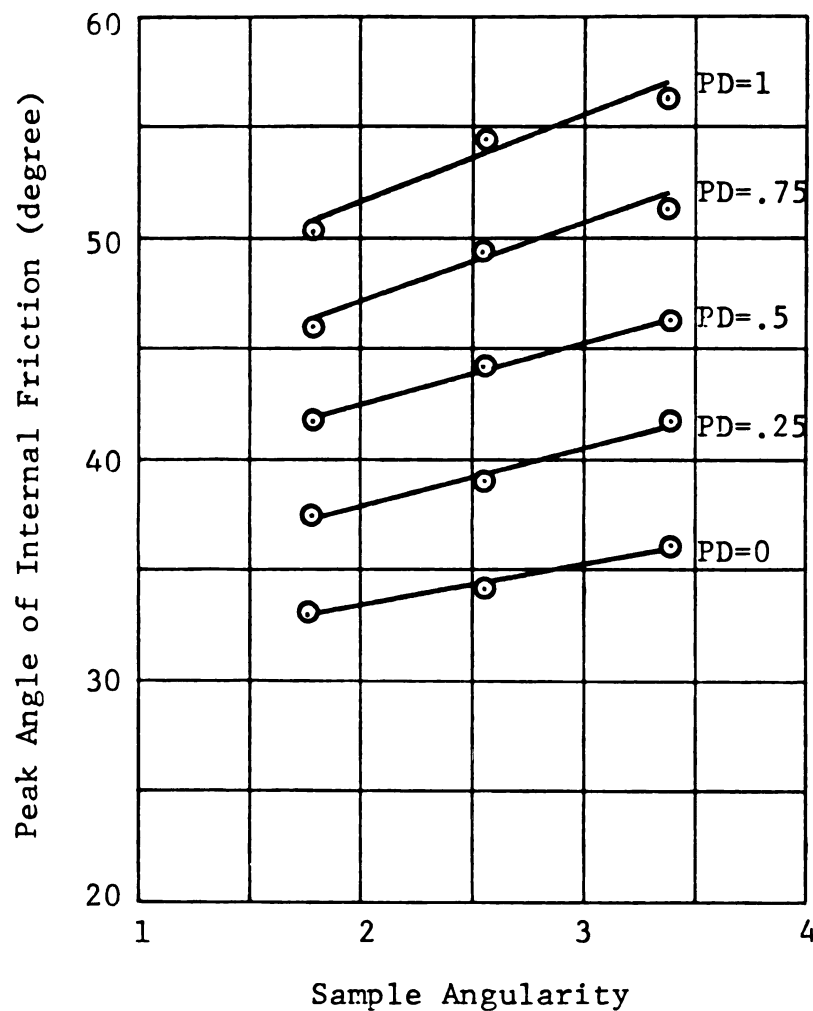


FIGURE 4.66 PEAK ANGLE OF INTERNAL FRICTION VERSUS SAMPLE ANGULARITY OF SAMPLE 1 OF SERIES A FOR A CONFINING PRESSURE OF 5 PSI, AND FIVE VALUES OF THE PERCENT DILATATION.

interlocking seats. At zero percent dilatation on the other hand, only particle sliding and rolling are involved. Thus, the higher the percent dilatation the higher the degree of interlocking. Further, the sample angularity influences both types of motion. That is the more angular the particles the higher the resistance to sliding and rolling and to plucking and displacement. Consequently, the influence of the sample angularity on the peak angle of internal friction is higher at high values of the percent dilatation than that at low values.

Moreover, this last observation (for sample number 1 of series A) should not be generalized and/or extended to include other samples. The reason being is that different samples possess different percent fine content and maximum grain size. The effect of the sample angularity on the peak angle of internal friction is also a function of the maximum grain size or percent fine content (see Section 4.8.1). To illustrate this, consider Figure 4.67 in which the peak angle of internal friction at two levels of the percent dilatation of the samples is plotted against the coefficient of angularity of the test specimens of samples 1 and 3 of series A and 4 of series B. It can be seen that the effect of sample angularity for samples 3 of series A and 4 of series B is more or less constant and independent of the percent dilatation (the slope of the straight lines of these two samples is constant for zero and one hundred percent

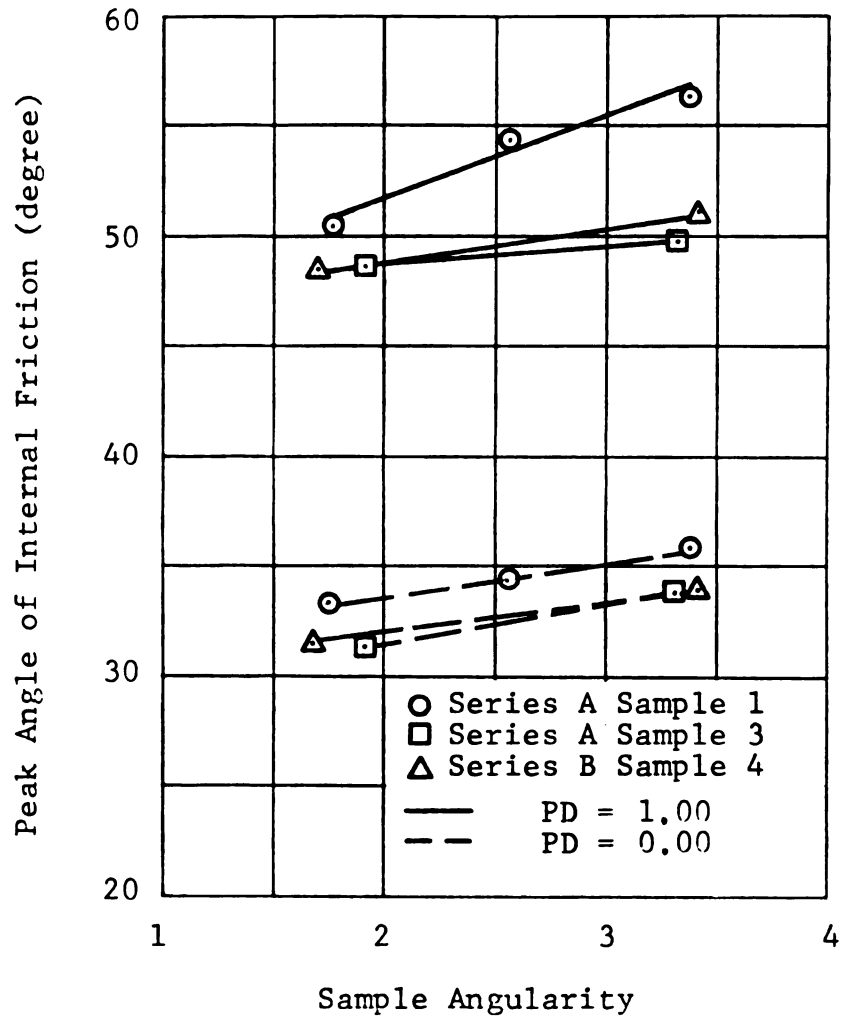


FIGURE 4.67 PEAK ANGLE OF INTERNAL FRICTION VERSUS SAMPLE ANGULARITY OF SERIES A AND B SAMPLES FOR A CONFINING PRESSURE OF 5 PSI, AND TWO VALUES OF THE PERCENT DILATATION.

dilatations). Thus, the effect of sample angularity on the peak angle of internal friction is a function of the percent fine content or the maximum grain size and the percent dilatation of the sample.

4.9 STRENGTH AT THE SIX PERCENT STRAIN LEVEL

Strength at the six percent strain level is defined herein in terms of the angle of internal friction ($\phi_{6\%}$) which is calculated utilizing the applied stresses at the six percent strain level. Thus, the strengths of series A and B samples are being compared and analysed herein utilizing a constant strain value.

Two reasons were identified for choosing the six percent strain level:

- a) The strain required to fully mobilize the peak angle of internal friction of dense cohesionless soils is a function of the confining pressure, moisture content, and soil density. For a dry soil and a constant value of confining pressure, the only factor affecting the strain is the soil density. The higher the density, the lower the vertical strain required to fully mobilize the frictional resistance of the soil. Thus, for the same type of cohesionless soil, different strain levels would have to be utilized when analysing the peak angle of internal friction of the soil at different densities. ($\phi_{6\%}$) on the other

hand is being analysed at a constant strain level.

- b) For a confining pressure of 5 psi (34.5 kN/m²), the peak angle of internal friction of dense specimens of series A and B samples was fully mobilized at relatively low value of vertical strain (generally between 1.0 and 4.0 percent). Thus, the six percent strain represents a data point on the stress-strain curve that is located between the peak and ultimate stresses. Thus, the applicability and validity of the percent dilatation model of Section 4.8 could be examined at different strain levels.

Nevertheless, the strengths of series A and B samples at the six percent strain level were studied utilizing the percent dilatation (PD) model (equation 4.28) of Section 4.8. The development of this model is outlined below.

Figures 4.68 and 4.69 show plots of the normalized strength ratio (the ratio of the angle of internal friction at the six percent strain level to the ultimate angle of internal friction) versus the percent dilatation (PD) of series A and B samples. The best fit lines in the figures were obtained utilizing least square analysis and all data points for PD larger than or equal to zero. The reasons for this restriction are that: a) the model will be consistent with the peak strength model; b) all test specimens of series B samples were dense (PD > 0.0); and c) on the loose side (PD < 0.0) the data points for series A samples showed

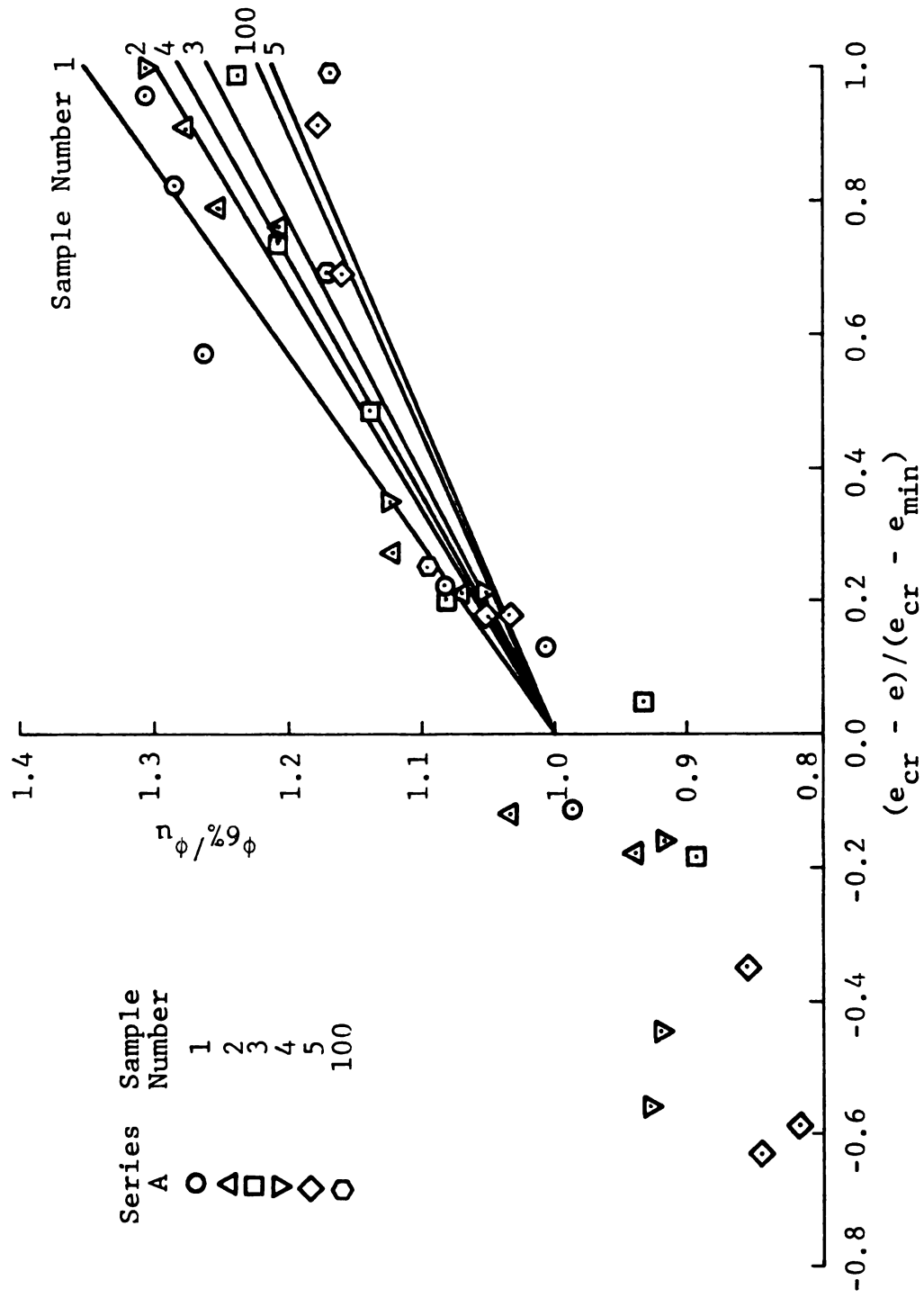


FIGURE 4.68 NORMALIZED STRENGTH AT 6% STRAIN LEVEL VERSUS PERCENT DILATATION OF SERIES A SAMPLES FOR A CONFINING PRESSURE OF 5 PSI.

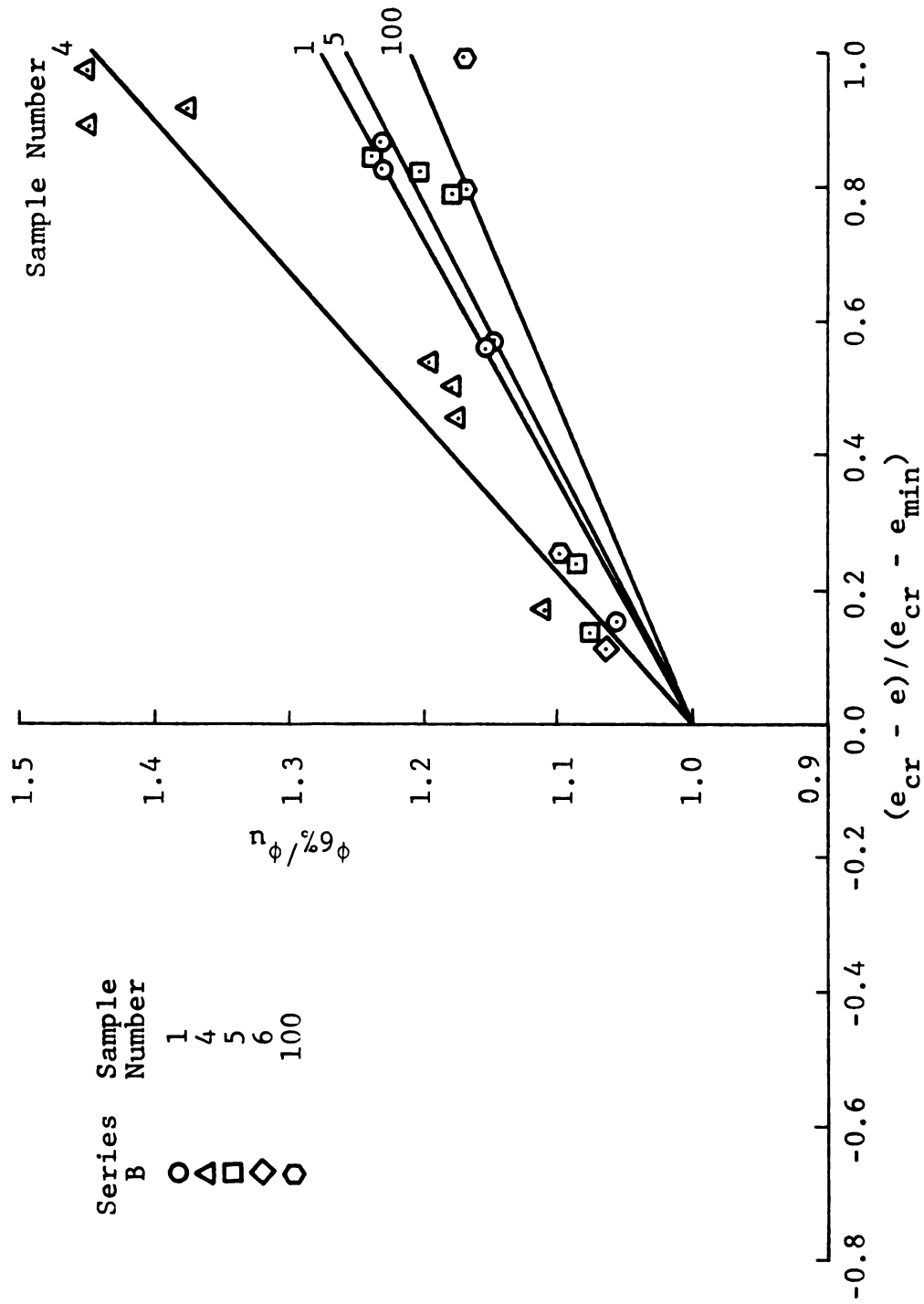


FIGURE 4.69 NORMALIZED STRENGTH AT 6 % STRAIN LEVEL VERSUS PERCENT DILATATION OF SERIES B SAMPLES FOR A CONFINING PRESSURE OF 5 PSI.

no linearity with those on the dense side. Nevertheless, equation 4.38 was used to model the best fit lines.

$$\phi_{6\%}/\phi_U = 1.0 + SP\left(\frac{e_{CR} - e}{e_{CR} - e_{MIN}}\right) \quad (4.38)$$

where: $\phi_{6\%}$ = the angle of internal friction at the six percent strain level

ϕ_U = the ultimate angle of internal friction;

SP = slope of the straight lines of Figures 4.67 and 4.68;

e_{CR} = the critical void ratio;

e_{MIN} = the minimum void ratio; and

e = the void ratio of the soil.

It should be noted herein that the best fit lines were forced to intercept the vertical axis at a normalized strength ratio of 1.0. Because, it was noticed, through examination of the test data, that the strength ratio of the soil specimens with a void ratio near the critical void ratio is almost equal to 1.0.

Examination of Figures 4.68 and 4.69 indicates that, for all samples, the higher the percent dilatation, the higher the strength ratio. Similar observation was also noted in Section 4.8 concerning the peak angle of internal friction.

The equation of the best fit lines (equation 4.38) were then utilized to analyse and discuss the effects of grain size, sample gradation, and grain shape upon the soil

strength at the six percent strain level. These are presented in the following Subsections.

4.9.1 EFFECT OF GRAIN SIZE

The slopes of the best fit lines of Figures 4.68 and 4.69 were then plotted against the percent fine content of the samples as shown in Figure 4.70. Examination of the figure indicates that (with the exception of sample 4 of series B) the higher the percent fine content of the sample, the lower the value of the slope. The curves in the figure were then modeled with respect to the percent fine content of the samples. The resulting equations were then substituted into equation 4.38. This yielded equations 4.39 and 4.40 for series A and B samples respectively.

$$\frac{\phi_{6\%}}{\phi_U} = 1.0 + \left(\frac{0.40 + 1.19(PF)}{1.00 + 6.21(PF)} \right) \left(\frac{e_{CR} - e}{e_{CR} - e_{MIN}} \right) \quad (4.39)$$

$$\frac{\phi_{6\%}}{\phi_U} = 1.0 + \left(\frac{0.35 + 0.40(PF)}{1.00 + 2.43(PF)} \right) \left(\frac{e_{CR} - e}{e_{CR} - e_{MIN}} \right) \quad (4.40)$$

where: all parameters are as before.

Finally equations 4.24 and 4.25 for the ultimate angle of internal friction were substituted into equations 4.39 and 4.40. After simplifying and arranging terms, equations 4.41 and 4.42 were obtained for series A and B samples.

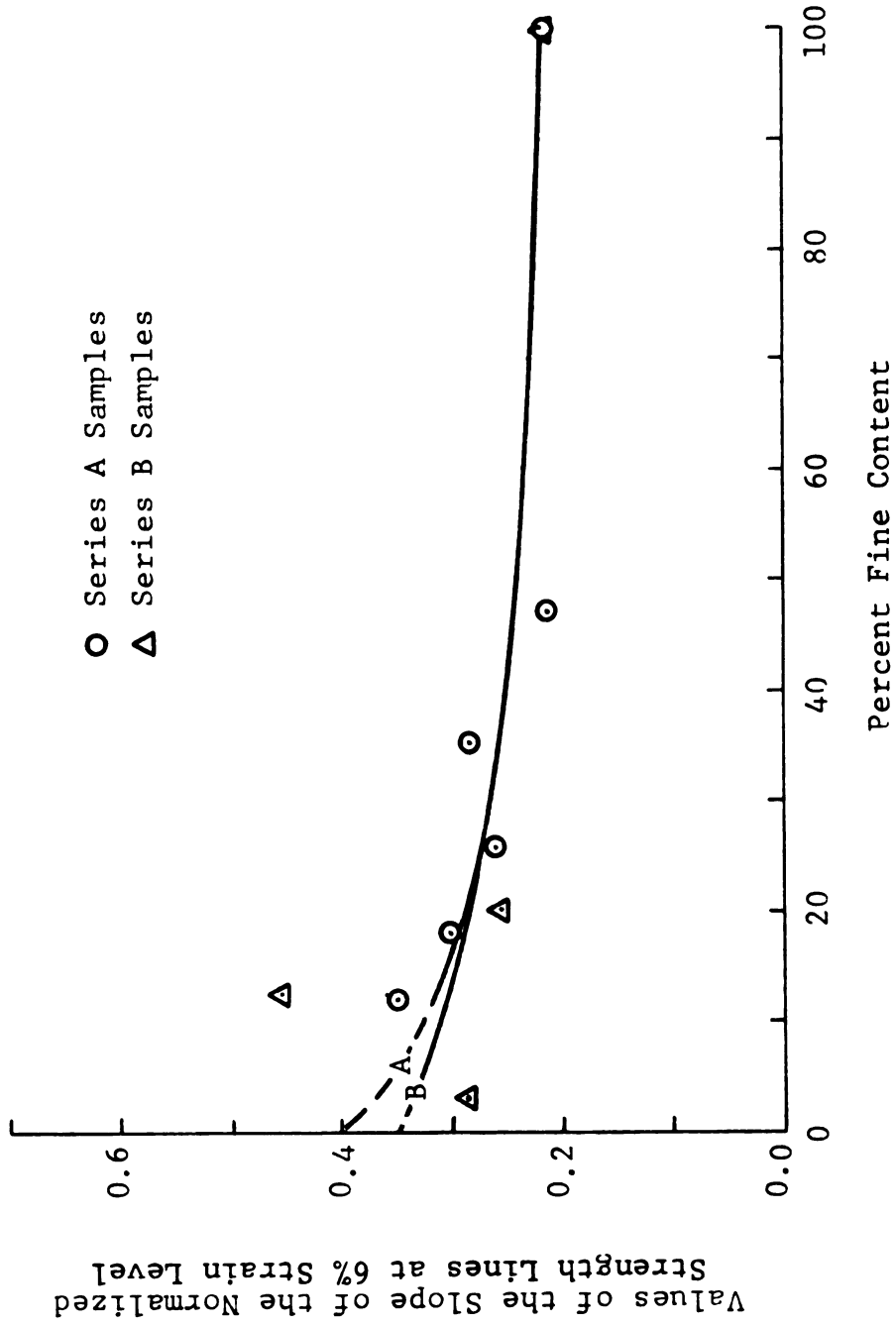


FIGURE 4.70 VALUES OF THE SLOPE OF THE NORMALIZED STRENGTH LINES AT 6% STRAIN LEVEL VERSUS PERCENT FINE CONTENT OF SERIES A AND B SAMPLES.

$$\phi_{6\%} = \left\{ 1.0 + \left(\frac{0.40 + 1.19(PF)}{1.00 + 6.21(PF)} \right) \left(\frac{e_{CR} - e}{e_{CR} - e_{MIN}} \right) \right\} \\ \{ 40.0 [1.0 - 45.25(PF) \text{EXP}(-5.37(PF)^{0.14})] \} \quad (4.41)$$

$$\phi_{6\%} = \left\{ 1.0 + \left(\frac{0.35 + 0.40(PF)}{1.00 + 2.43(PF)} \right) \left(\frac{e_{CR} - e}{e_{CR} - e_{MIN}} \right) \right\} \\ \{ 40.0 [1.0 - 5.87(PF) \text{EXP}(-3.33(PF)^{0.33})] \} \quad (4.42)$$

where: all parameters are as before.

The region between the dashed lines in Figure 4.71 designates the locus of the pairs of calculated and measured $\phi_{6\%}$ of series A and B samples with a maximum discrepancy of two degrees. The solid line (at forty five degree from the horizontal axis) indicates the correspondence between the calculated and measured angle of internal friction at the six percent strain level. It can be seen (except for four data points) that the maximum difference between the calculated and measured values is equal to or less than two degrees. This difference is equal to that between the measured data on duplicate specimens. Thus, equations 4.41 and 4.42 can be considered to predict the measured data quite accurately.

Equations 4.41 and 4.42 were then used to calculate $\phi_{6\%}$ at three levels of percent dilatation of 1.0, 0.5 and 0.0. The calculated values were then plotted against the percent

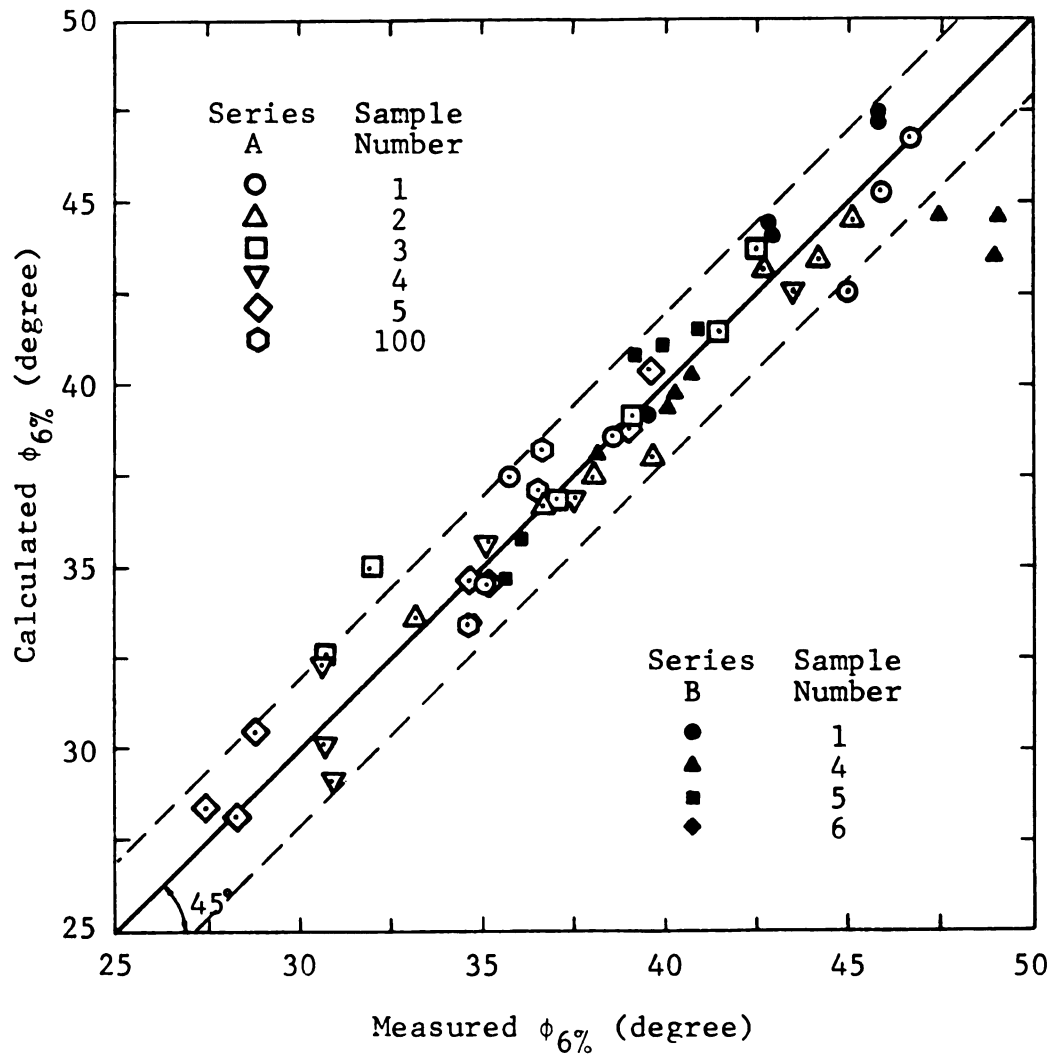


FIGURE 4.71 CALCULATED VERSUS MEASURED ANGLE OF INTERNAL FRICTION AT 6% STRAIN LEVEL FOR SERIES A AND B SAMPLES.

fine content of the soil. These are shown in Figures 4.72 and 4.73 for series A and B samples respectively. Figure 4.74 depicts the same data plotted against the maximum particle size of the soil. Examination of the figures indicates that:

- a) For the same percent dilatation, the higher the percent fine content of the soil, the lower the $\phi_{6\%}$ (Figures 4.72 and 4.73).
- b) For the same percent dilatation, the higher the maximum particle size of the soil, the higher the $\phi_{6\%}$ (Figure 4.74).

These two observations are similar to those reported in Section 4.6 concerning the ultimate angle of internal friction. Indeed, the curves in Figures 4.72, 4.73, and 4.74 resemble those of Figures 4.42 and 4.43. Thus, the effect of grain size on $\phi_{6\%}$ is similar to that on the ultimate angle of internal friction and different than that on the peak angle of internal friction (see Figures 4.56 and 4.57). The reason being is that, for a confining pressure of 5 psi, the physical motion between soil particles at the six percent strain level (after volume dilatation), is mainly due to particle sliding and rolling relative to each other; particle interlocking plays no significant role.

4.9.2 EFFECT OF SAMPLE GRADATION

Figure 4.75 depicts the angle of friction at the six

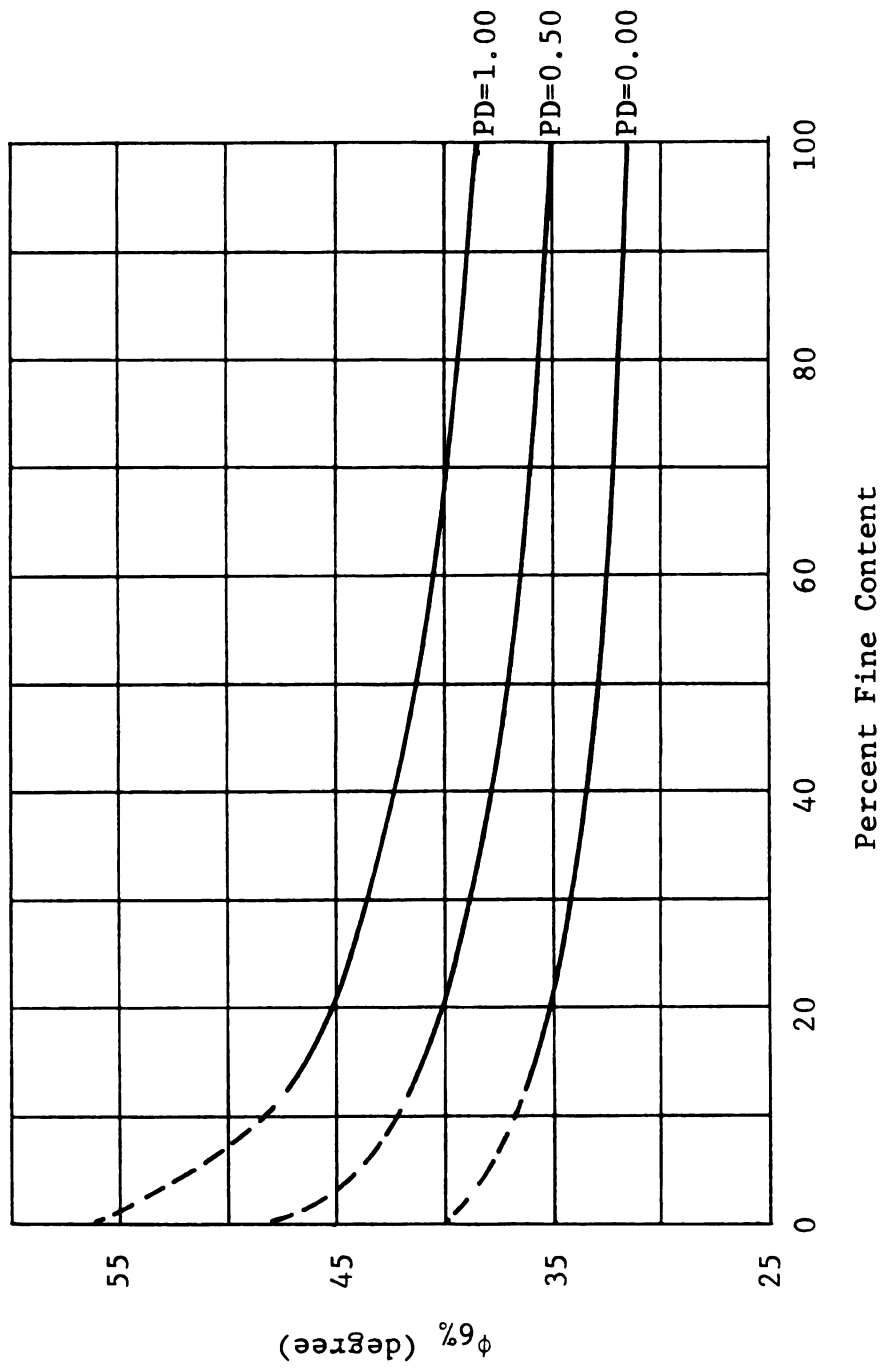


FIGURE 4.72 ANGLE OF INTERNAL FRICTION AT 6% STRAIN LEVEL VERSUS PERCENT FINE CONTENT OF SERIES A SAMPLES FOR A CONFINING PRESSURE OF 5 PSI, AND THREE VALUES OF THE PERCENT DILATATION.

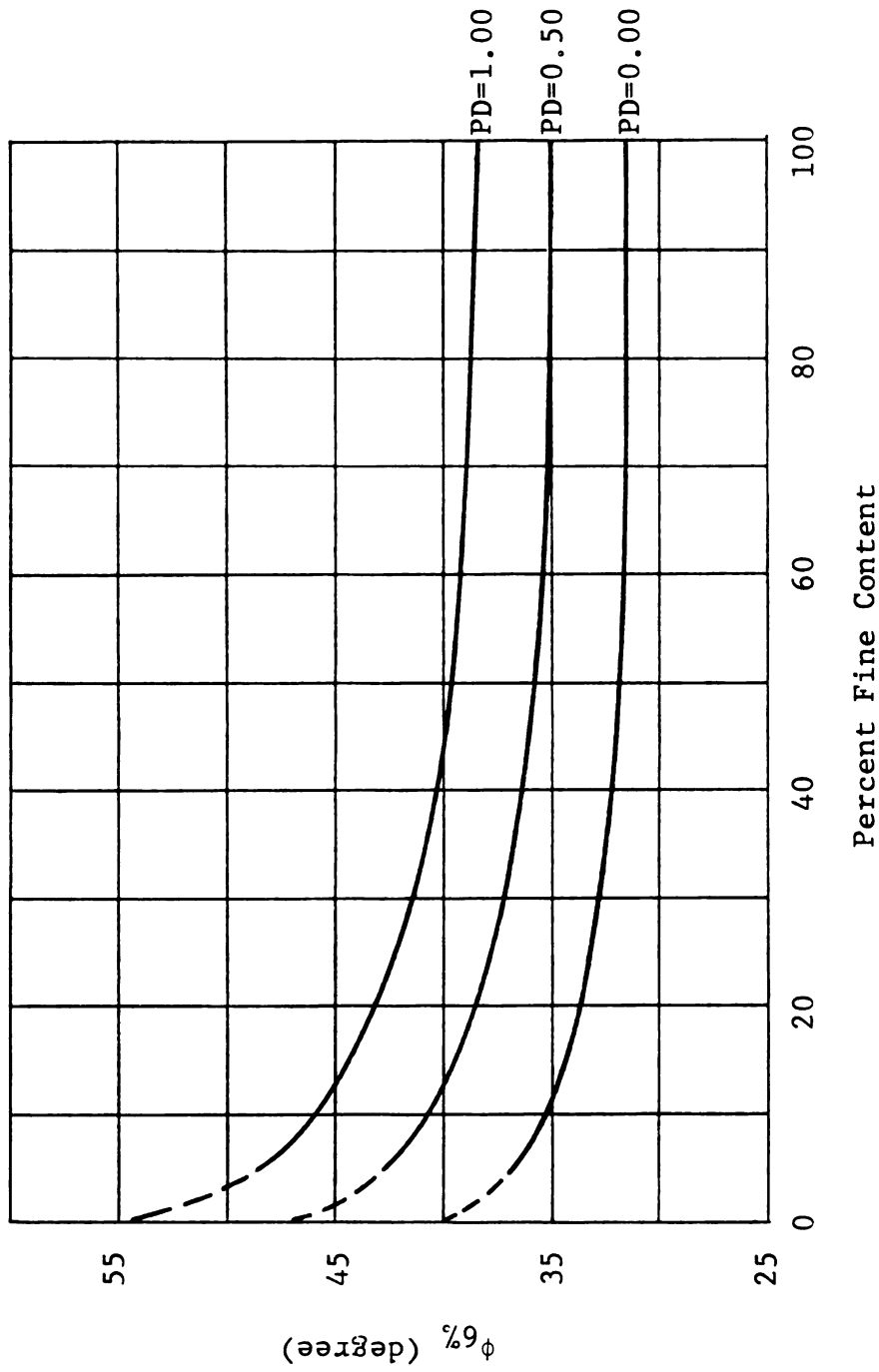


FIGURE 4.73 ANGLE OF INTERNAL FRICTION AT 6% STRAIN LEVEL VERSUS PERCENT FINE CONTENT OF SERIES B SAMPLES FOR A CONFINING PRESSURE OF 5 PSI, AND THREE VALUES OF THE PERCENT DILATATION.

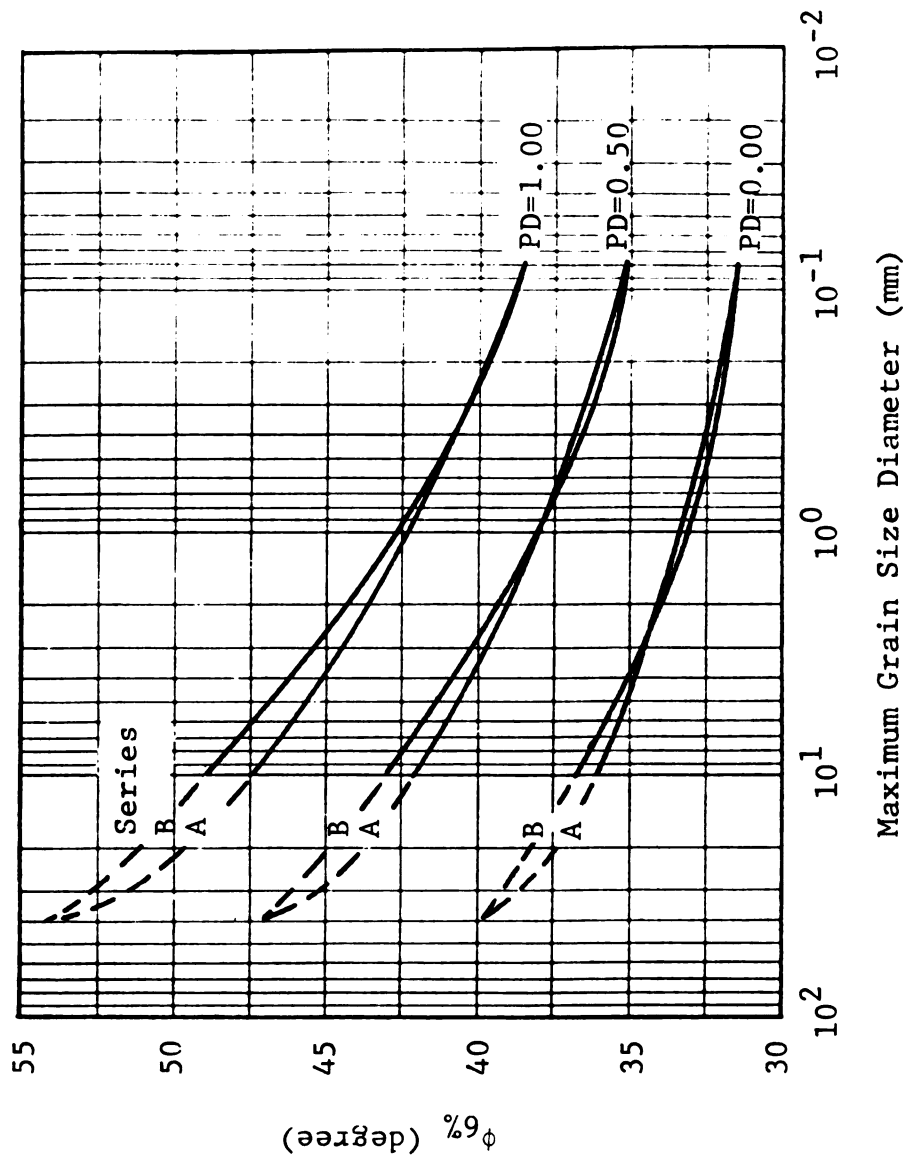


FIGURE 4.74 ANGLE OF INTERNAL FRICTION AT 6% STRAIN LEVEL VERSUS MAXIMUM GRAIN SIZE OF SERIES A AND B SAMPLES FOR A CONFINING PRESSURE OF 5 PSI, AND THREE VALUES OF THE PERCENT DILATATION.

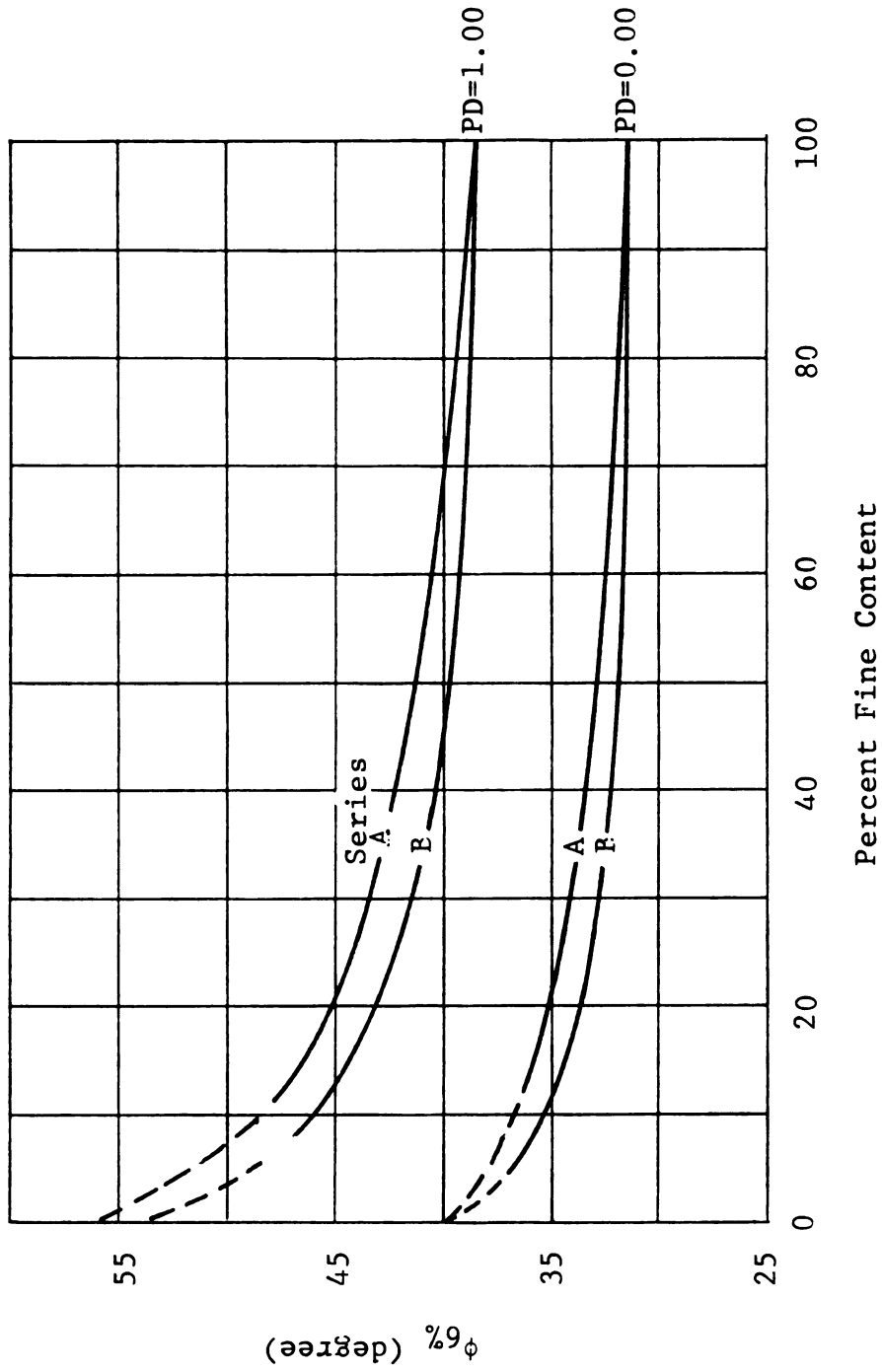


FIGURE 4.75 ANGLE OF INTERNAL FRICTION AT 6% STRAIN LEVEL VERSUS PERCENT FINE CONTENT OF SERIES A AND B SAMPLES FOR A CONFINING PRESSURE OF 5 PSI, AND TWO VALUES OF THE PERCENT DILATATION.

percent strain level plotted against the percent fine content of the soil of series A and B samples. Examination of this figure as well as Figure 4.74 indicates that the sample gradation possesses minor influence on the $\phi_{6\%}$. Again, this observation is similar to that of Section 4.6.2 concerning the effect of sample gradation on the ultimate angle of internal friction. That is at the six percent strain level, particle interlocking plays no significant role concerning the frictional resistance of the soil.

4.9.3 EFFECT OF GRAIN SHAPE

Figure 4.76 shows plots of the angle of friction at the six percent strain level for two values of the percent dilatation versus the coefficient of angularity of samples 1 and 3 of series A and 4 of series B. It can be seen, by inspection of the figure, that the higher the coefficient of angularity, the higher the $\phi_{6\%}$. Once again, this observation is the same as that concerning the effect of sample angularity on the ultimate angle of internal friction.

To summarize, for a confining pressure of 5 psi, the effects of grain size, sample gradation, and grain shape on the angle of friction at the six percent strain level are similar to those on the ultimate angle of internal friction, and dissimilar to those of the peak angle of internal friction. Soil behavior and the physical motion between particles after volume dilatation are mainly due to

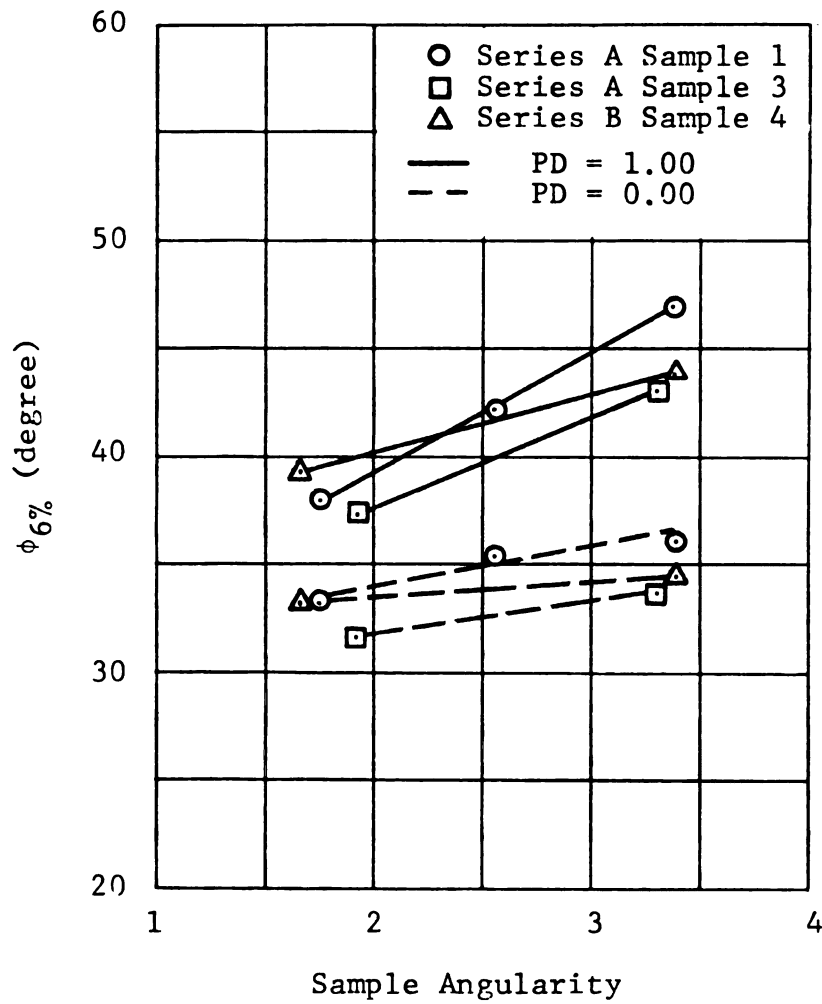


FIGURE 4.76 ANGLE OF INTERNAL FRICTION AT 6% STRAIN LEVEL VERSUS SAMPLE ANGULARITY OF SERIES A AND B SAMPLES FOR A CONFINING PRESSURE OF 5 PSI, AND TWO VALUES OF THE PERCENT DILATATION.

particles sliding and rolling relative to each other; particles interlocking possesses minimum influence on the sample behavior at the six percent strain level and for a confining pressure of 5 psi..

4.10 STRENGTH AT THE ONE PERCENT STRAIN LEVEL

Strength at the one percent strain level is defined herein in terms of the angle of internal friction ($\phi_{1\%}$) which is calculated utilizing the applied stresses at the one percent strain level. Thus, the strengths of series A and B samples are being compared and analysed herein utilizing a constant strain value.

Three reasons were identified while choosing the one percent strain level:

- a) In all tests at 5, 25 and 50 psi, the peak angle of internal friction was not fully mobilized at the one percent strain level. Thus, such a data point on the stress-strain curve is located on the rising part of the curve (increasing stress and strain); the peak strength data point is located at the peak of the curve; the six percent strain on the other hand, is a point on the declining side of the stress-strain curve (decreasing stress while the strain of the soil increases).
- b) The angle of friction at the one percent strain level is equivalent to 50 to 95 percent of the peak angle

of internal friction (the exact percentage point depends on the sample density, the higher the density, the higher the percentage). The angle of friction that is traditionally utilized in the calculation of the allowable bearing capacity of a foundation is well within this range. For example: if the peak angles of internal friction of two cohesionless soil deposits are 33 and 45 degrees, then the effective angles of friction utilized in the design of the allowable bearing capacity for a factor of safety of 3.0 are 28 and 39 degrees respectively. These values represent about 85 percent of the peak angles of internal friction.

- c) To be able to check the applicability and validity of the percent dilatation model of Section 4.8 at the one percent strain level (near design value).

Nevertheless, the angle of internal friction at the one percent strain level is being studied herein utilizing the percent dilatation model of Section 4.8. The procedure employed to develop the model is similar to that presented in Section 4.9. Thus, to avoid unnecessary repetitions, Figures will be introduced and reference will be made to the appropriate Section.

Figures 4.77 and 4.78 show plots of the strength ratio (ratio of the angle of friction at the one percent strain level to the ultimate angle of internal friction) versus the

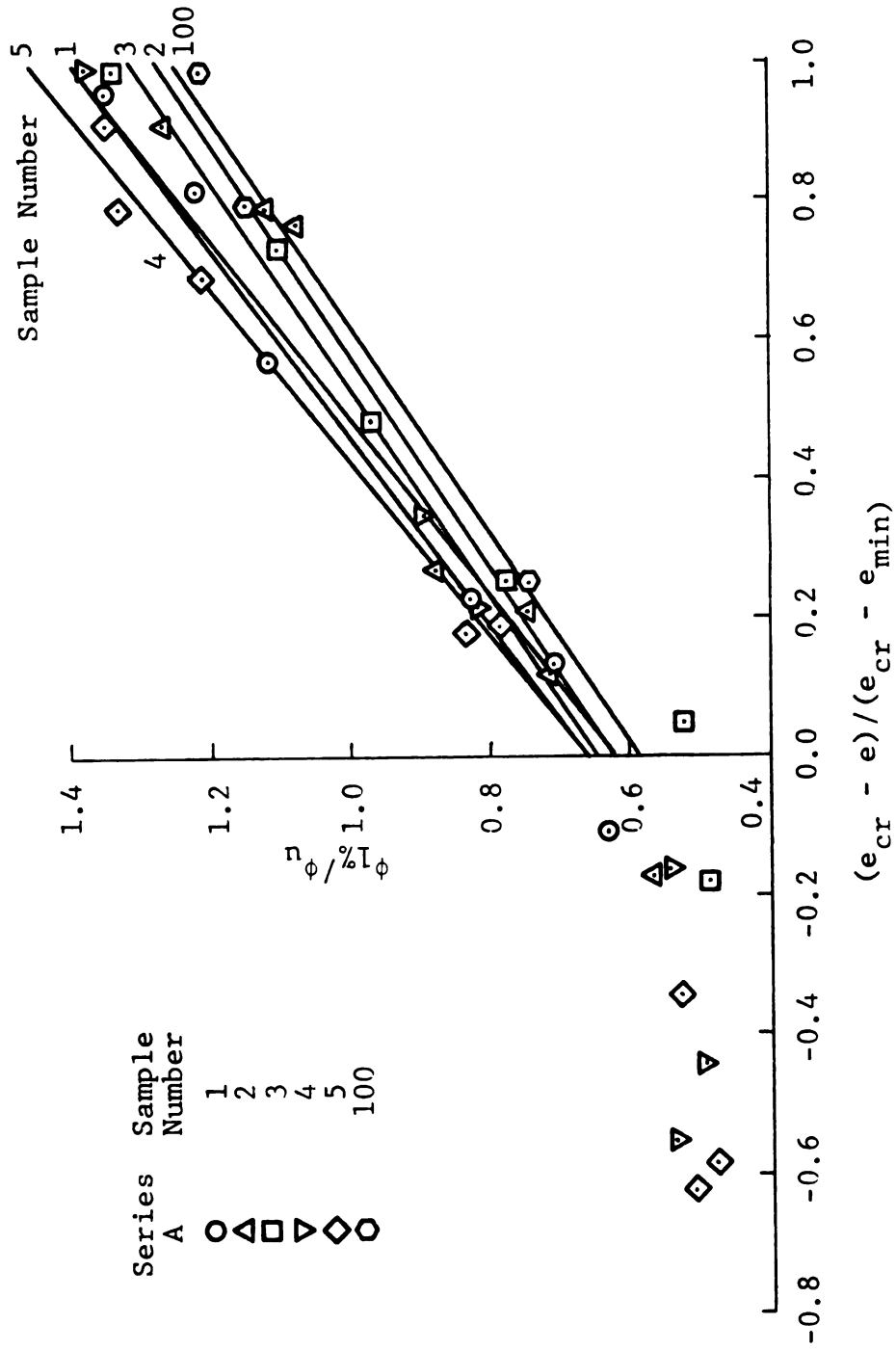


FIGURE 4.77 NORMALIZED STRENGTH AT 1% STRAIN LEVEL VERSUS PERCENT DILATATION OF SERIES A SAMPLES FOR A CONFINING PRESSURE OF 5 PSI.

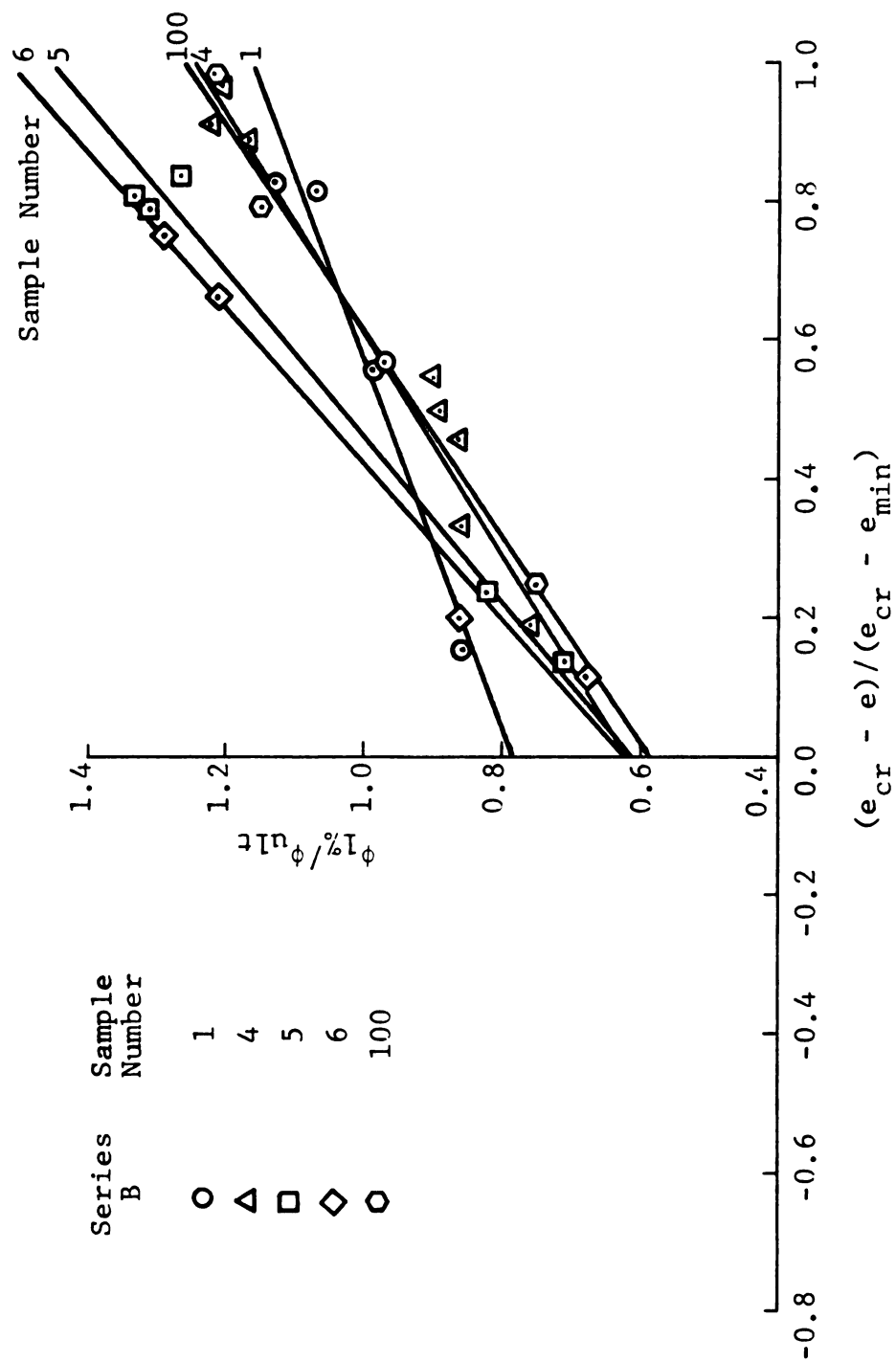


FIGURE 4.78 NORMALIZED STRENGTH AT 1% STRAIN LEVEL VERSUS PERCENT DILATATION OF SERIES B SAMPLES FOR A CONFINING PRESSURE OF 5 PSI.

percent dilatation of series A and B samples. The best fit lines were obtained utilizing least square analysis and equation 4.38 except that the intercept with the vertical axis was not fixed at a strength ratio of 1.0. Again, all the test data on the negative side of the PD axis were not used in the analysis for the same reasons that are given in Section 4.9.

The best fit lines and the corresponding parameters of equation 4.38 were then utilized to analyse and discuss the effects of grain size, sample gradation, and grain shape upon the soil strength at the one percent strain level. These are presented in the following Subsections.

4.10.1 EFFECT OF GRAIN SIZE

The values of the slope and intercept of the best fit lines of Figures 4.77 and 4.78 were then plotted against the percent fine content of the soil as shown in Figures 4.79 and 4.80. It can be seen from the figures that the curves resemble those of Figure 4.53 of the peak angle of internal friction. Consequently, they were modeled using compatible equations. The resulting equations as well as equations 4.24 and 4.25 were then substituted into equation 4.38. After simplifying and arranging terms, the following two equations were then obtained.

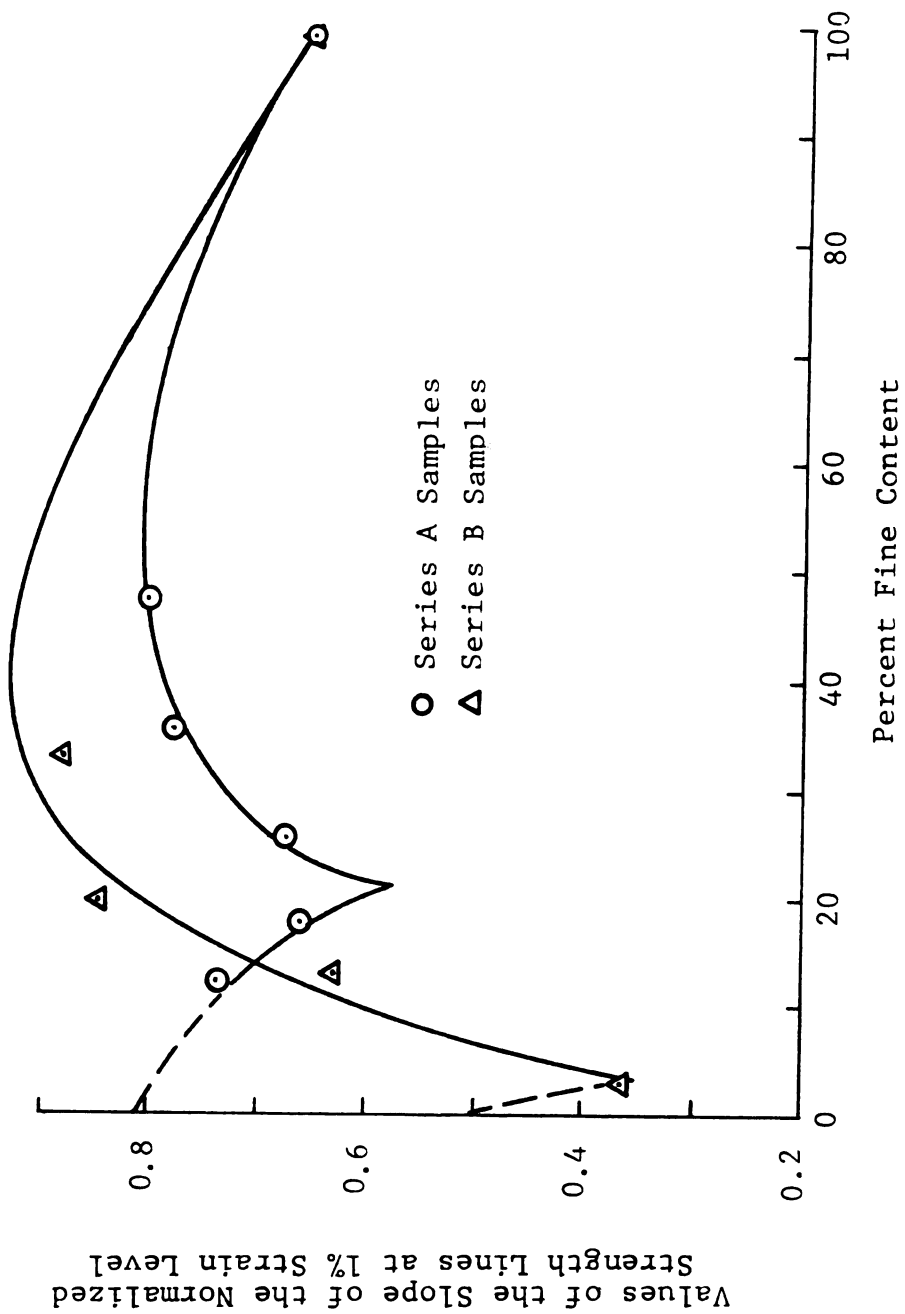


FIGURE 4.79 VALUES OF THE SLOPE OF THE NORMALIZED STRENGTH LINES AT 1% STRAIN LEVEL VERSUS PERCENT FINE CONTENT OF SERIES A AND B SAMPLES.

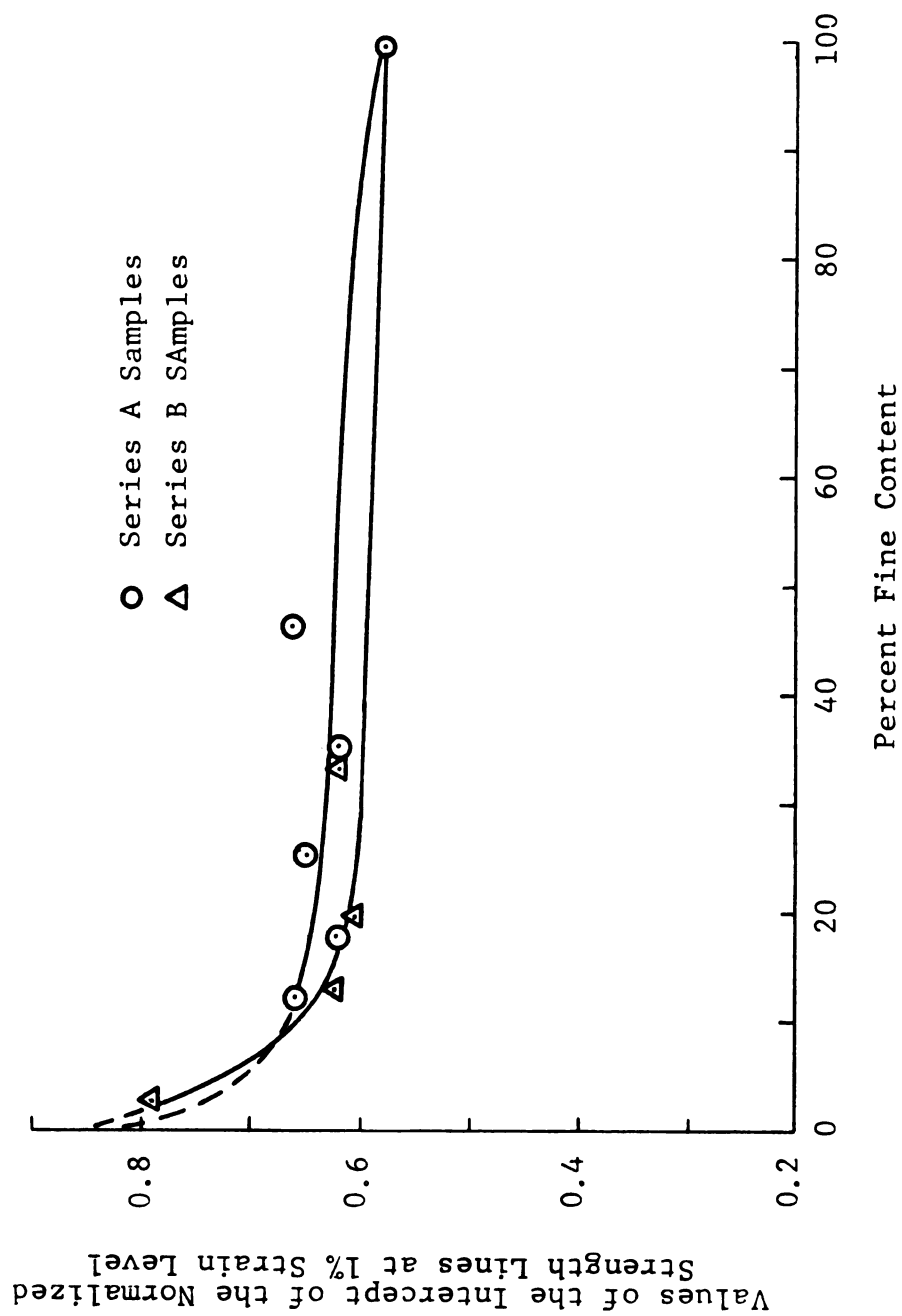


FIGURE 4.80 VALUES OF THE INTERCEPT OF THE NORMALIZED STRENGTH LINES AT 1% STRAIN LEVEL VERSUS PERCENT FINE CONTENT OF SERIES A AND B SAMPLES.

For series A samples;

$$\phi_{1\%} = 40.0 \{ 1.0 - 45.25(PF) \exp[-5.37(PF)^{0.14}] \} \quad (4.43)$$

$$\left\{ \left[\frac{e_{CR} - e}{e_{CR} - e_{MIN}} \right] \left[\frac{0.57 + 8.45[ABS(PF - 0.205)]}{1.00 + 9.00[ABS(PF - 0.205)]} \right] \right.$$

$$\left. [\exp(-0.30(PF)^{3.00})] + \frac{0.85 + 24.11(PF)}{1.00 + 38.94(PF)} \exp[-0.055(PF)^{3.00}] \right\}$$

For series B samples;

$$\phi_{1\%} = 40.0 \{ 1.0 - 5.87(PF) \exp[-3.33(PF)^{0.33}] \} \quad (4.44)$$

$$\left\{ \left[\frac{e_{CR} - e}{e_{CR} - e_{MIN}} \right] \left[\frac{0.35 + 6.48[ABS(PF - 0.040)]}{1.00 + 3.67[ABS(PF - 0.040)]} \right] \right.$$

$$\left. [\exp(-0.80(PF)^{1.40})] + \frac{0.85 + 11.74(PF)}{1.00 + 25.57(PF)} \exp[0.22(PF)^{0.15}] \right\}$$

where: all parameters are as before.

The region between the dashed lines in Figure 4.81 designates the locus of the pairs of calculated and measured $\phi_{1\%}$ of series A and B samples with a maximum discrepancy of two degrees. The solid line (at forty five degree from the horizontal axis) indicates the correspondence between the calculated and measured angle of internal friction at the one percent strain level. It can be seen (except for six data points of loose soil) that the maximum difference between the calculated and measured values is equal to or less than two degrees. This difference is equal to that

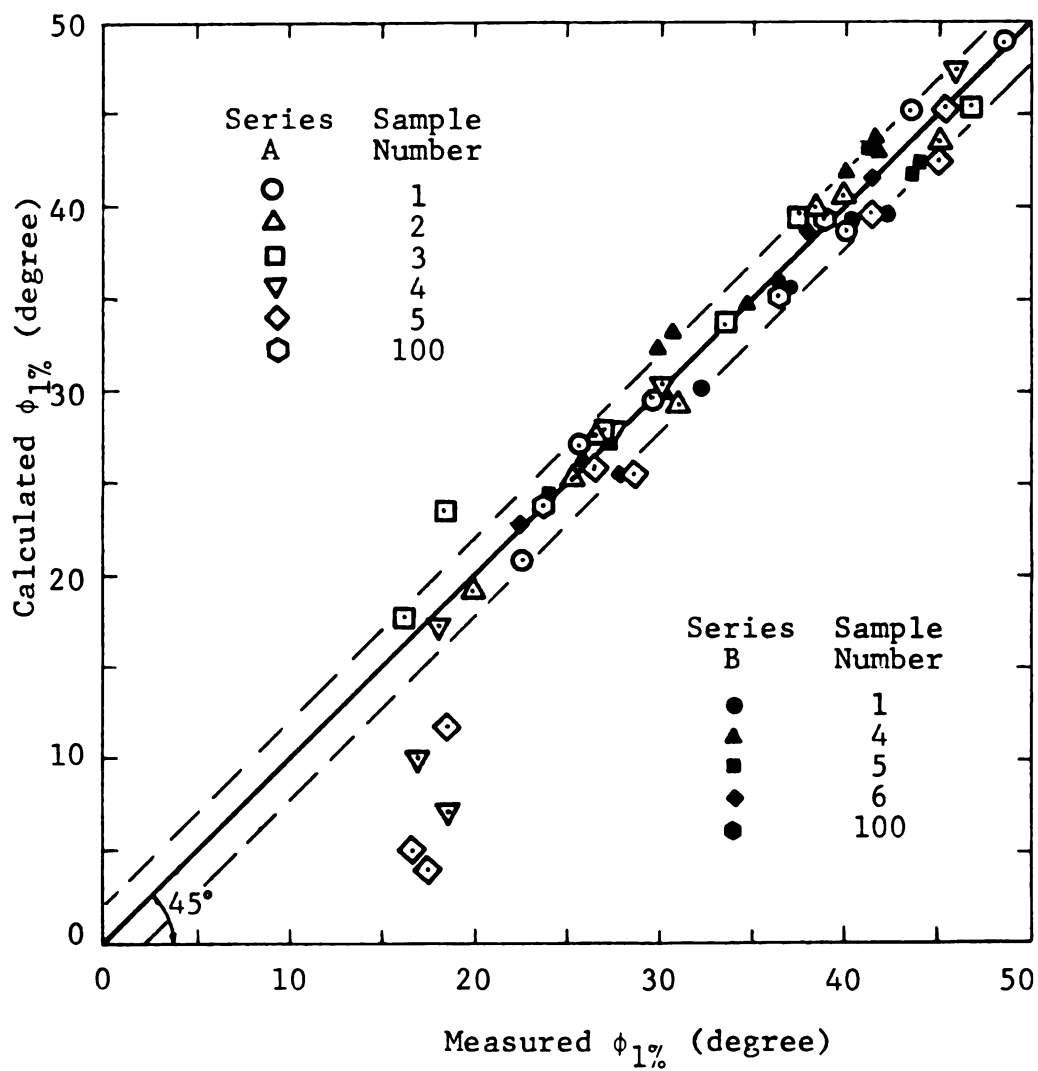


FIGURE 4.81 CALCULATED VERSUS MEASURED ANGLE OF INTERNAL FRICTION AT 1% STRAIN LEVEL FOR SERIES A AND B SAMPLES.

between the measured data on duplicate specimens. Thus, equations 4.43 and 4.44 can be considered to predict the measured data quite accurately.

Equations 4.43 and 4.44 were then used to calculate ϕ_{1s} at three levels of percent dilatation of 1.0, 0.5 and 0.0. The calculated values were then plotted against the percent fine content of the soil. These are shown in Figures 4.82 and 4.83 for series A and B samples respectively. Figure 4.84 depicts the same data plotted against the maximum particle size of the soil. Examination of these figures and Figures 4.56 and 4.57 indicates that the effect of grain size on the angle of friction at the one percent strain level is the same as that on the peak angle of internal friction. Recall that the one percent strain level (for a confining pressure of 5 psi) occurs before the peak stress on the stress-strain curve. Consequently, the frictional resistance of the particles is affected by particles interlocking and particles sliding and rolling relative to each other. These are the same factors affecting the peak angle of internal friction. Thus, the same explanation given in Section 4.8.1 concerning the effect of grain size on the peak angle of internal friction could be repeated herein.

4.10.2 EFFECT OF SAMPLE GRADATION

Figure 4.85 depicts the angle of friction at the one

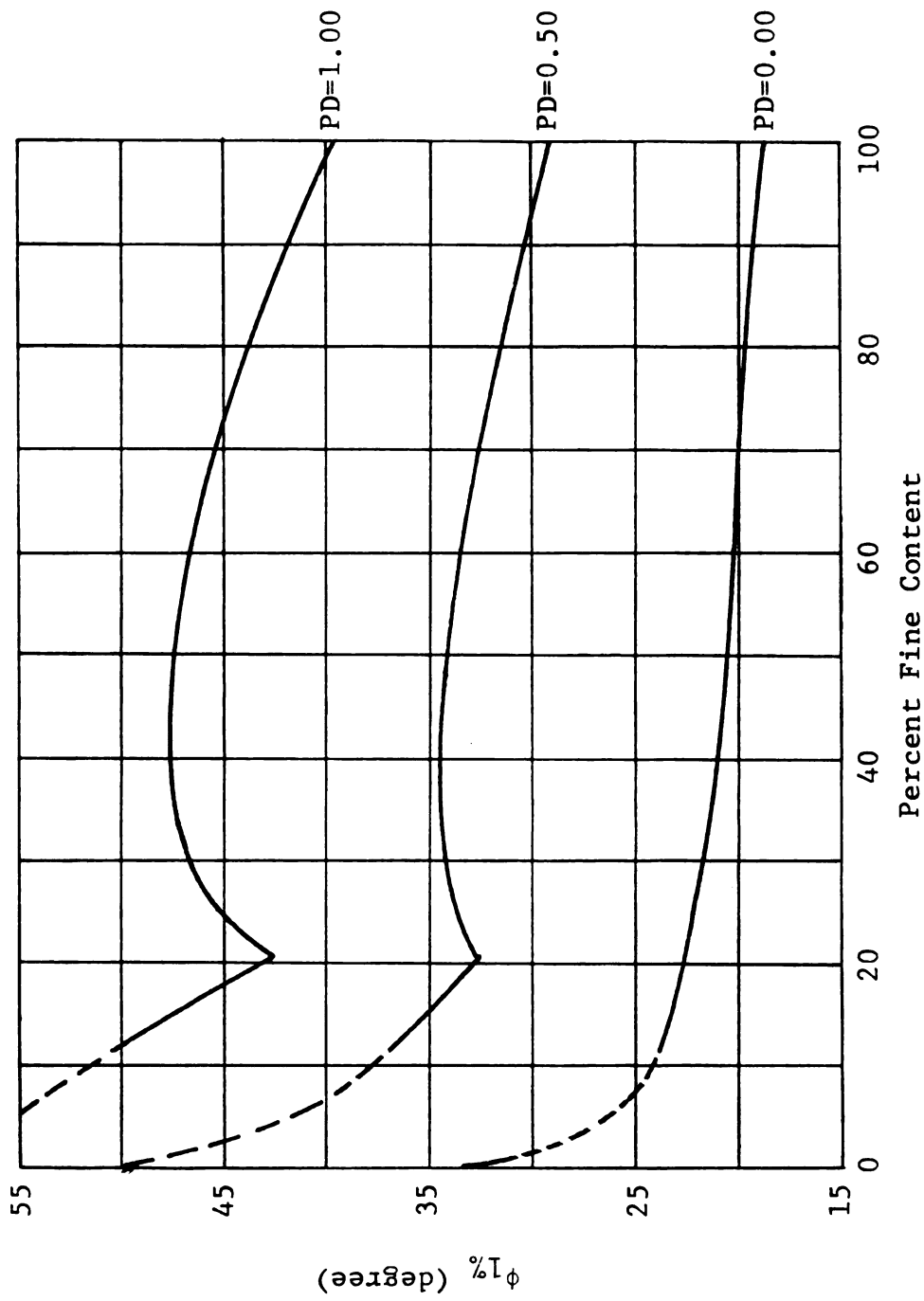


FIGURE 4.82 ANGLE OF INTERNAL FRICTION AT 1% STRAIN LEVEL VERSUS PERCENT FINE CONTENT OF SERIES A SAMPLES FOR A CONFINING PRESSURE OF 5 PSI, AND THREE VALUES OF THE PERCENT DILATATION.

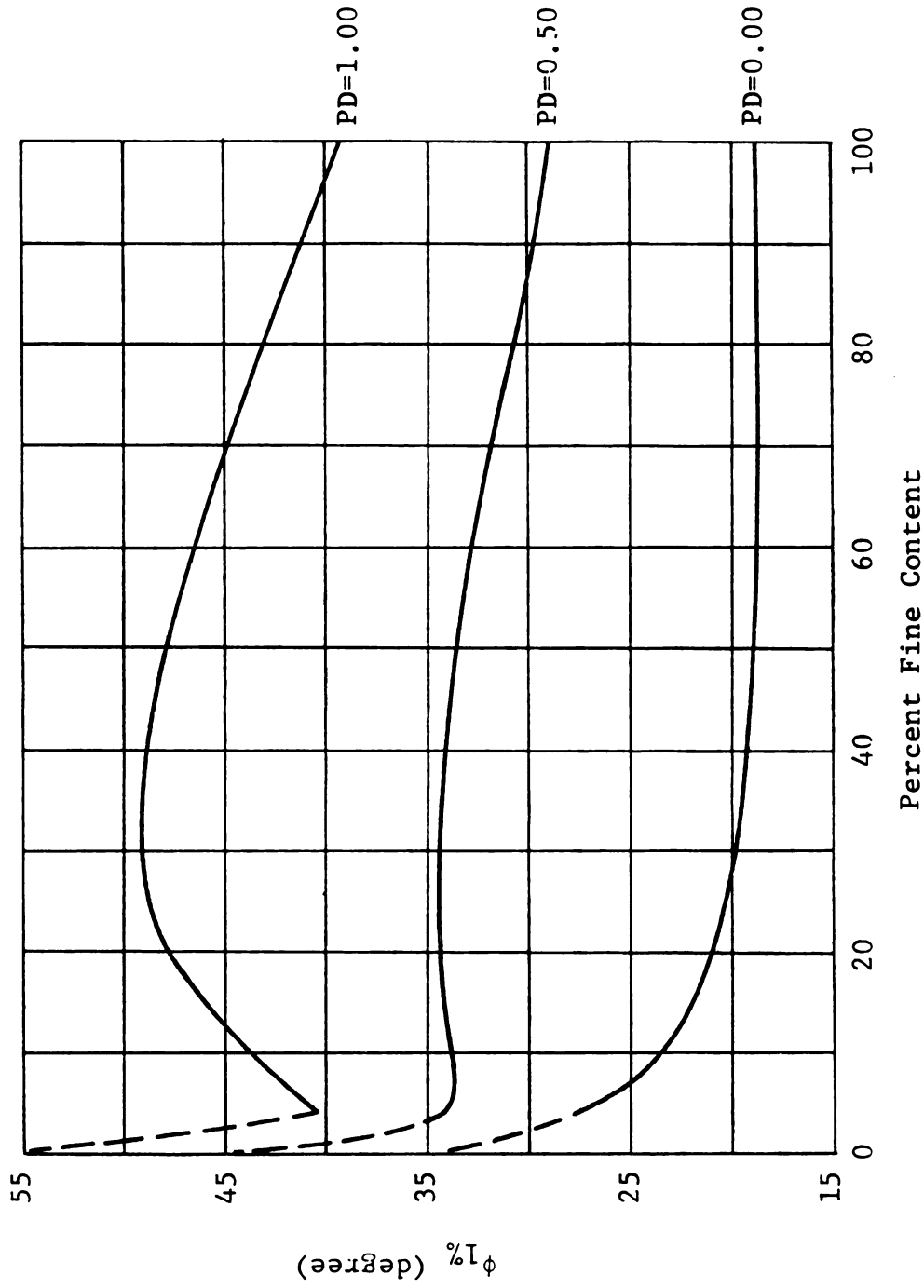


FIGURE 4.83 ANGLE OF INTERNAL FRICTION AT 1% STRAIN LEVEL VERSUS PERCENT FINE CONTENT OF SERIES B SAMPLES FOR A CONFINING PRESSURE OF 5 PSI, AND THREE VALUES OF THE PERCENT DILATATION.

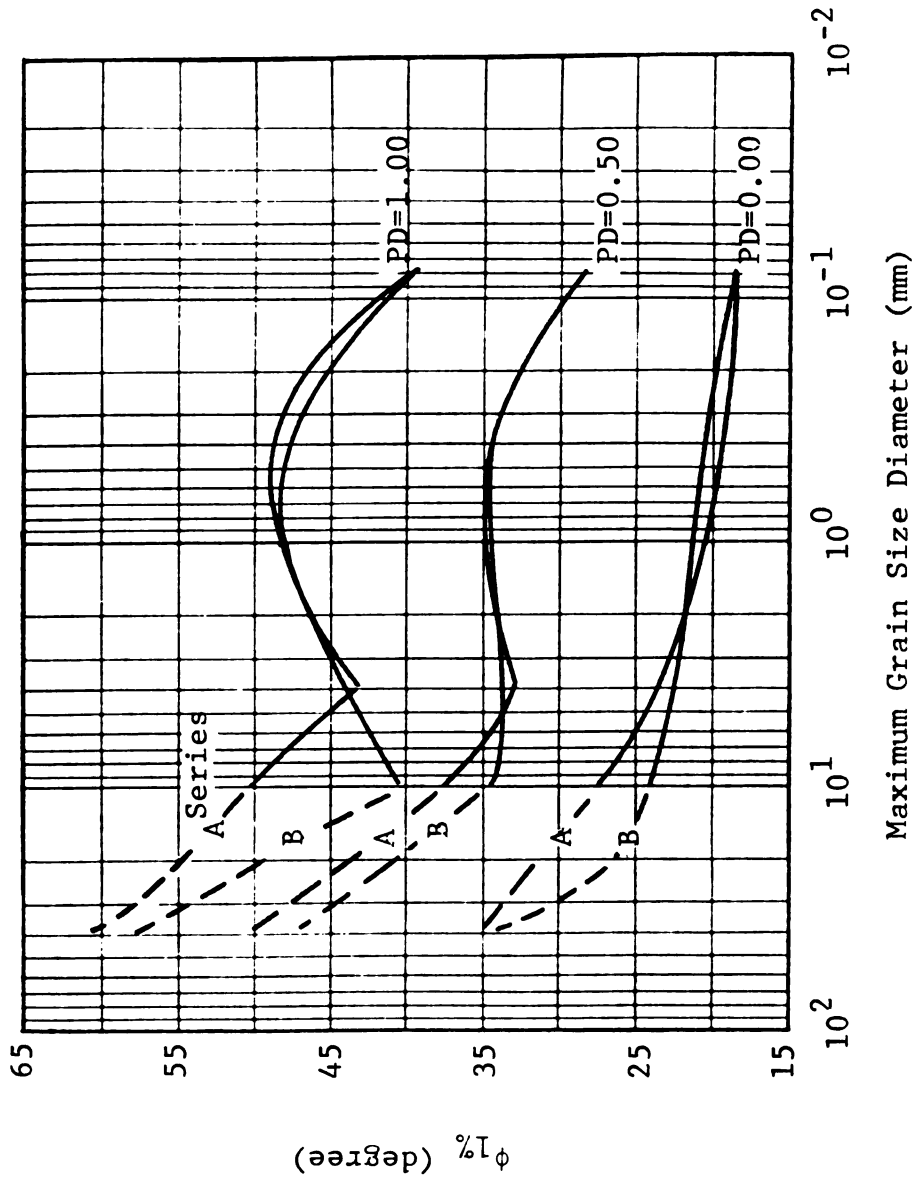


FIGURE 4.84 ANGLE OF INTERNAL FRICTION AT 1% STRAIN LEVEL VERSUS MAXIMUM GRAIN SIZE OF SERIES A AND B SAMPLES FOR A CONFINING PRESSURE OF 5 PSI, AND THREE VALUES OF THE PERCENT DILATATION.

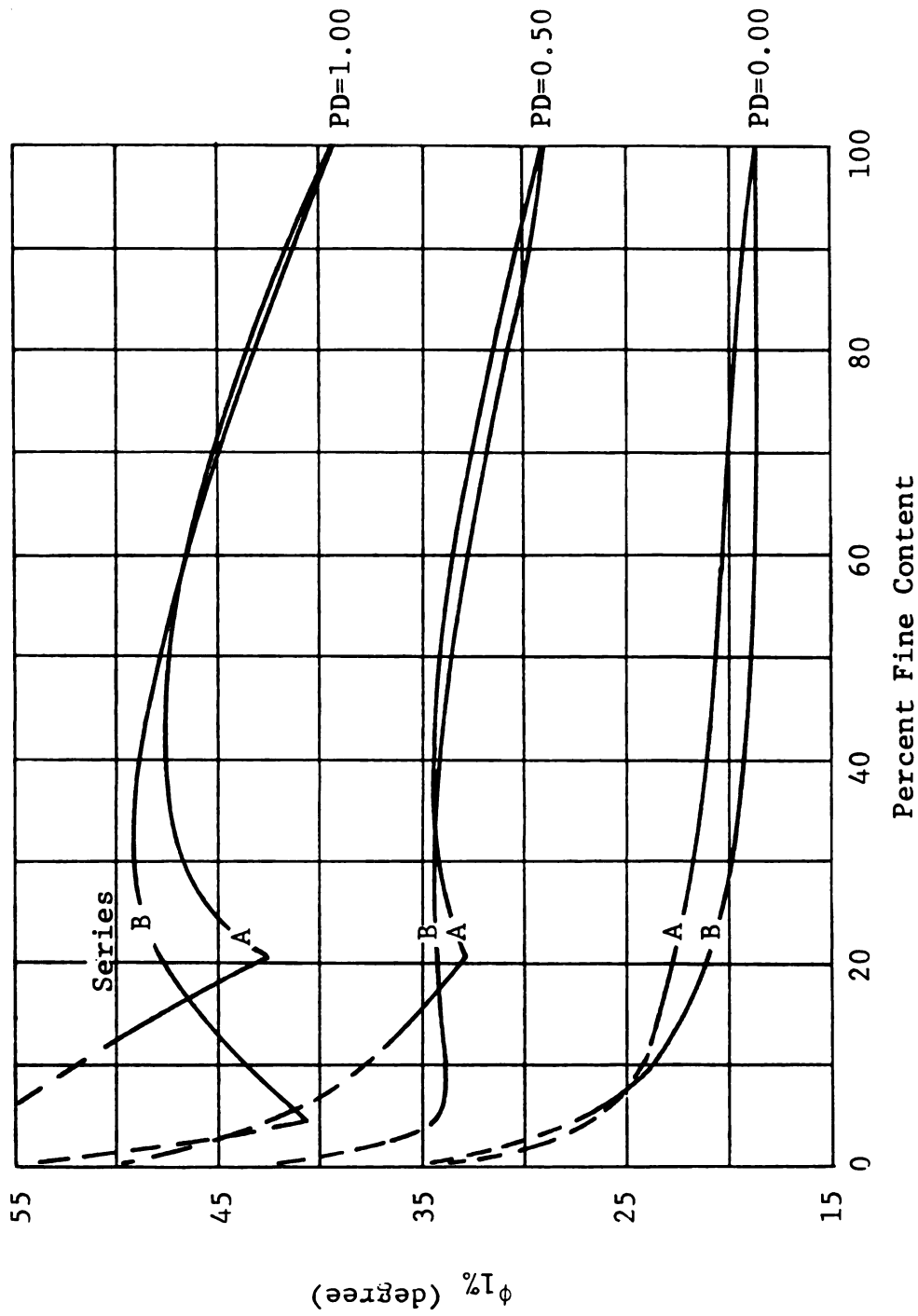


FIGURE 4.85 ANGLE OF INTERNAL FRICTION AT 1% STRAIN LEVEL VERSUS PERCENT FINE CONTENT OF SERIES A AND B SAMPLES FOR A CONFINING PRESSURE OF 5 PSI, AND THREE VALUES OF THE PERCENT DILATATION.

percent strain level and for three values of the percent dilatation plotted against the percent fine content of the soil of series A and B samples. Examination of the figure as well as Figures 4.84, 4.62, and 4.63 indicates that the effect of sample gradation on the ϕ_1 is similar to that on the peak angle of internal friction. Again, the same discussion given in Section 4.8.2 concerning the effect of the sample gradation on the peak angle of internal friction could be repeated herein.

4.10.3 EFFECT OF GRAIN SHAPE

Figure 4.86 shows plots of the angle of friction at the one percent strain level and for three values of the percent dilatation versus the coefficient of angularity of samples 1 and 3 of series A and 4 of series B. Examination of the figure indicates that the angle of friction at the one percent strain level is independent of the sample angularity. This observation is not compatible with that concerning the peak angle of internal friction (the sample angularity influences the peak angle of internal friction, also see Figure 4.66). These two observations however are not hostile. This can be explained with the aid of Figures 4.87 and 4.88. Figure 4.87 shows the actual stress-strain curves of two soil specimens of sample 1 of series A. The first specimen was mixed using the C/P material (angular to subangular particles); the second with the natural material

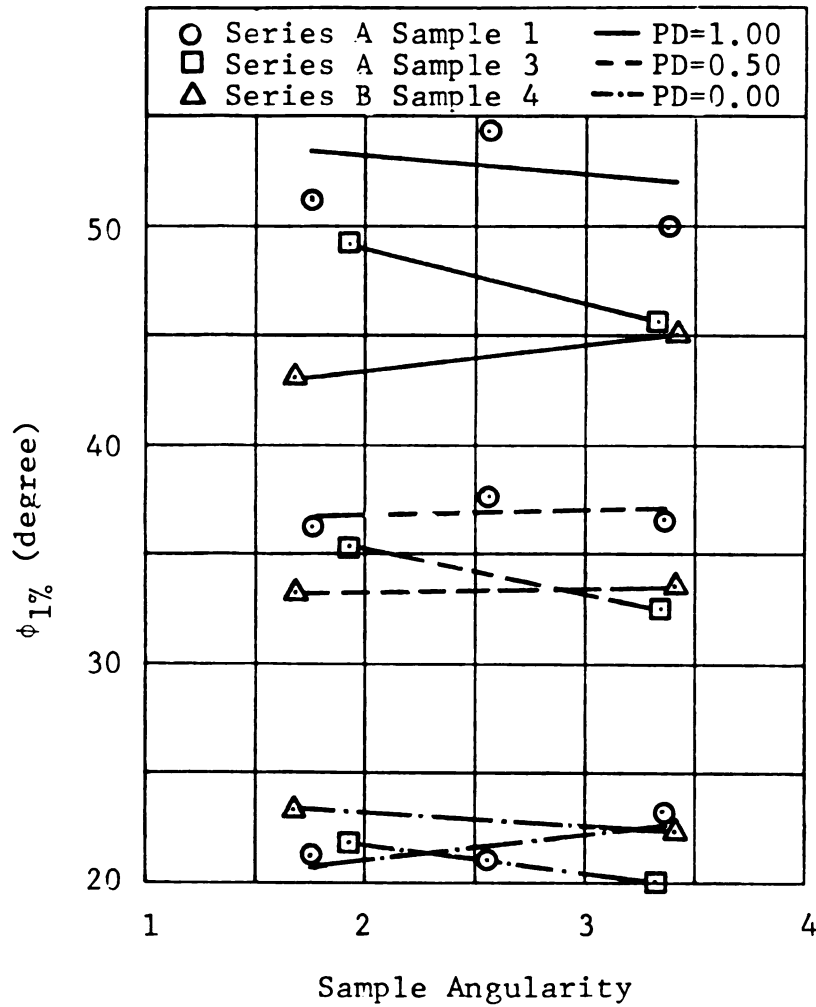


FIGURE 4.86 ANGLE OF INTERNAL FRICTION AT 1% STRAIN LEVEL VERSUS SAMPLE ANGULARITY OF SERIES A AND B SAMPLES FOR A CONFINING PRESSURE OF 5 PSI, AND THREE VALUES OF THE PERCENT DILATATION.

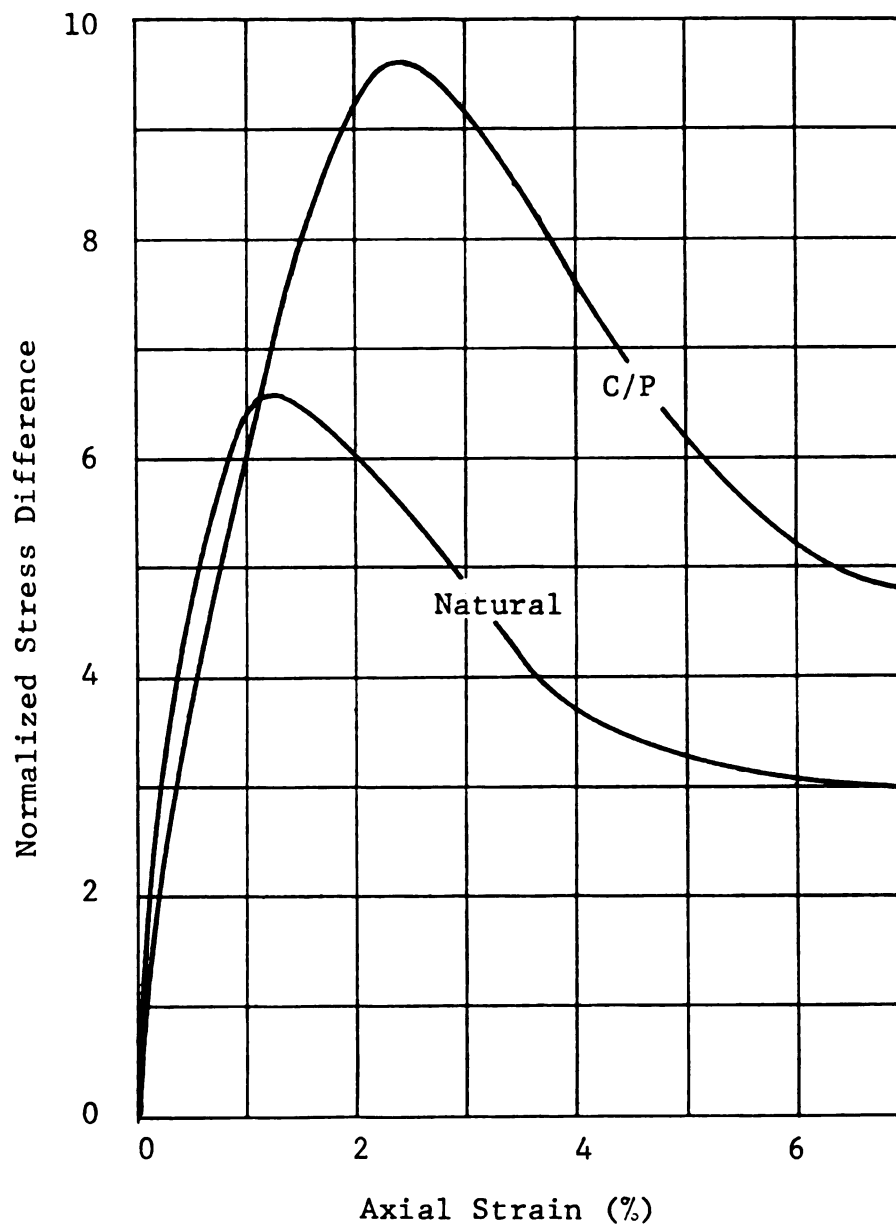


FIGURE 4.87 NORMALIZED STRESS DIFFERENCE VERSUS AXIAL STRAIN OF SAMPLES WITH THE SAME PERCENT DILATATION THAT CONSISTED OF THE C/P AND NATURAL MATERIALS.

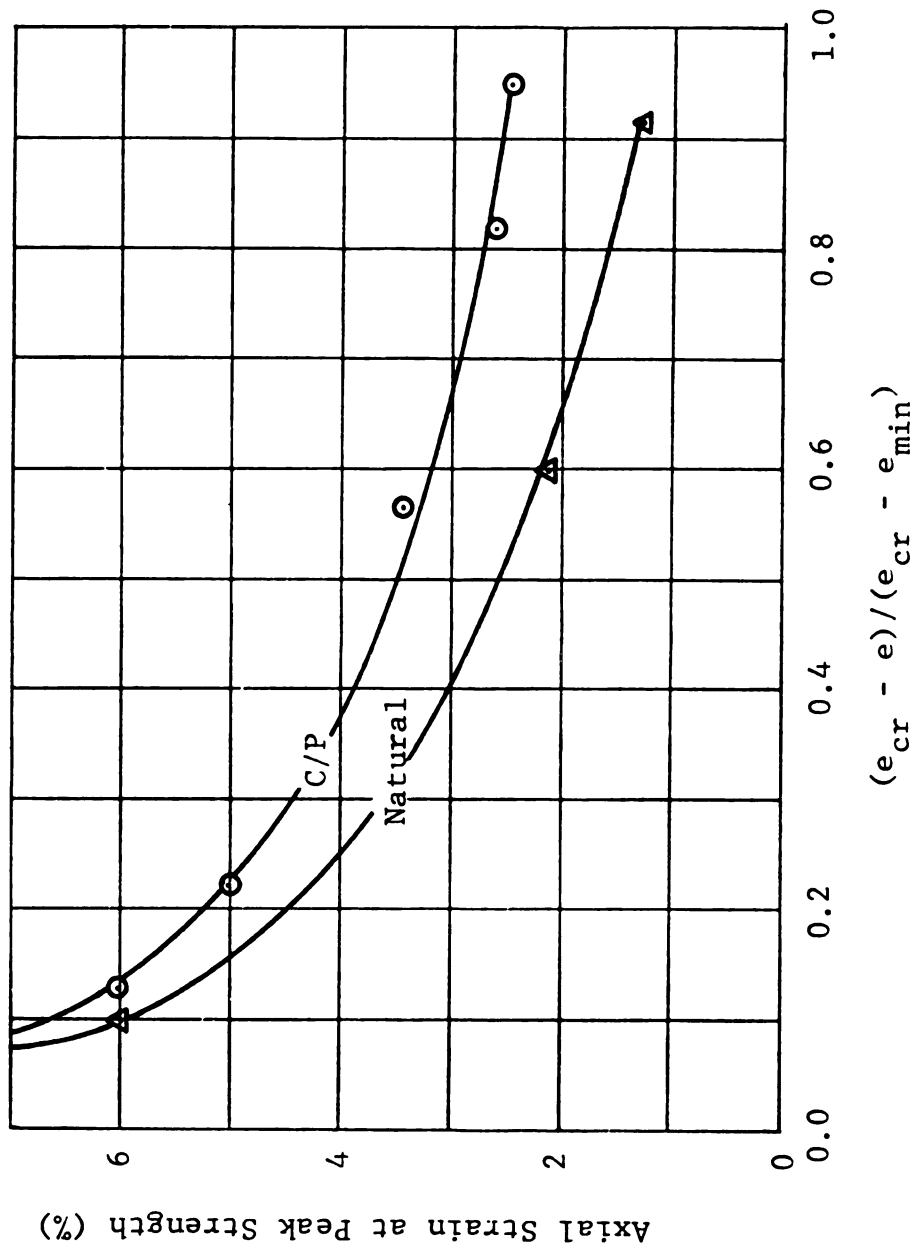


FIGURE 4.88 AXIAL STRAIN AT PEAK STRENGTH VERSUS PERCENT DILATATION OF SAMPLE 1 OF SERIES A THAT CONSISTED OF THE C/P AND NATURAL MATERIALS FOR A CONFINING PRESSURE OF 5 PSI.

(rounded to subrounded particles). Figure 4.88 shows plots of the axial strain at peak stress versus the percent dilatation of the test specimens. Examination of the figures indicates that the strain at the peak stress for the C/P material is higher than that of the natural. That is the strain required to mobilize the peak angle of internal friction increases as the sample angularity increases. In addition, the stresses at the one percent strain level (Figure 4.87) for the rounded particles are much closer to the peak than those of the C/P particles. The higher the stresses, the higher the angle of friction. Thus, the particle angularity influences the stress-strain behavior of the soil. This influence however was not detected in the observation of Figure 4.86 mainly due to the analysis method. If the angles of friction of the C/P and natural materials are to be compared at some other strain level (say 2.0 percent) then the effect of particle angularity would be magnified. Because, at this strain level, the peak angle of internal friction of the natural material is fully mobilized while that of the C/P material has not. In short, sample angularity possesses a significant influence on the shear strength of cohesionless soil. The method of analysis employed however, may lead to an erroneous conclusion.

4.11 CONFINING PRESSURE

To study the effect of confining pressure on the shear

strength of the test material, triaxial compression tests were conducted on series A samples utilizing confining pressures of 5, 25, and 50 psi (34.5, 172.4, and 344.8 kN/m²). The stress-strain curves are shown in Figures E.16 through E.27 of Appendix E. The test results are summarized in Tables 4.2 and 4.3. It should be noted that, for samples 1, 3 and 5 of series A, tests on some specimens were continued until the ultimate strength was reached; others were terminated at the six percent strain level or when the peak angle of internal friction was fully mobilized.

The effect of the confining pressure on the peak angle of internal friction which is the sum of the ultimate and interlocking angles of friction can be divided into two:

- a) The effect on the ultimate angle of internal friction.
- b) The effect on the angle of interlocking friction.

Figure 4.89 depicts the ultimate angle of internal friction plotted as a function of the percent fine content of series A samples for three values of the confining pressure. Examination of the figure indicates that, for all values of the confining pressure, the ultimate angle of internal friction decreases with increasing percent fine content. Figure 4.90 shows plots of the ultimate angle of internal friction versus the confining pressure for samples 1, 3 and 5 of series A. Examination of the figure indicates that (for all three samples) the ultimate angle of internal

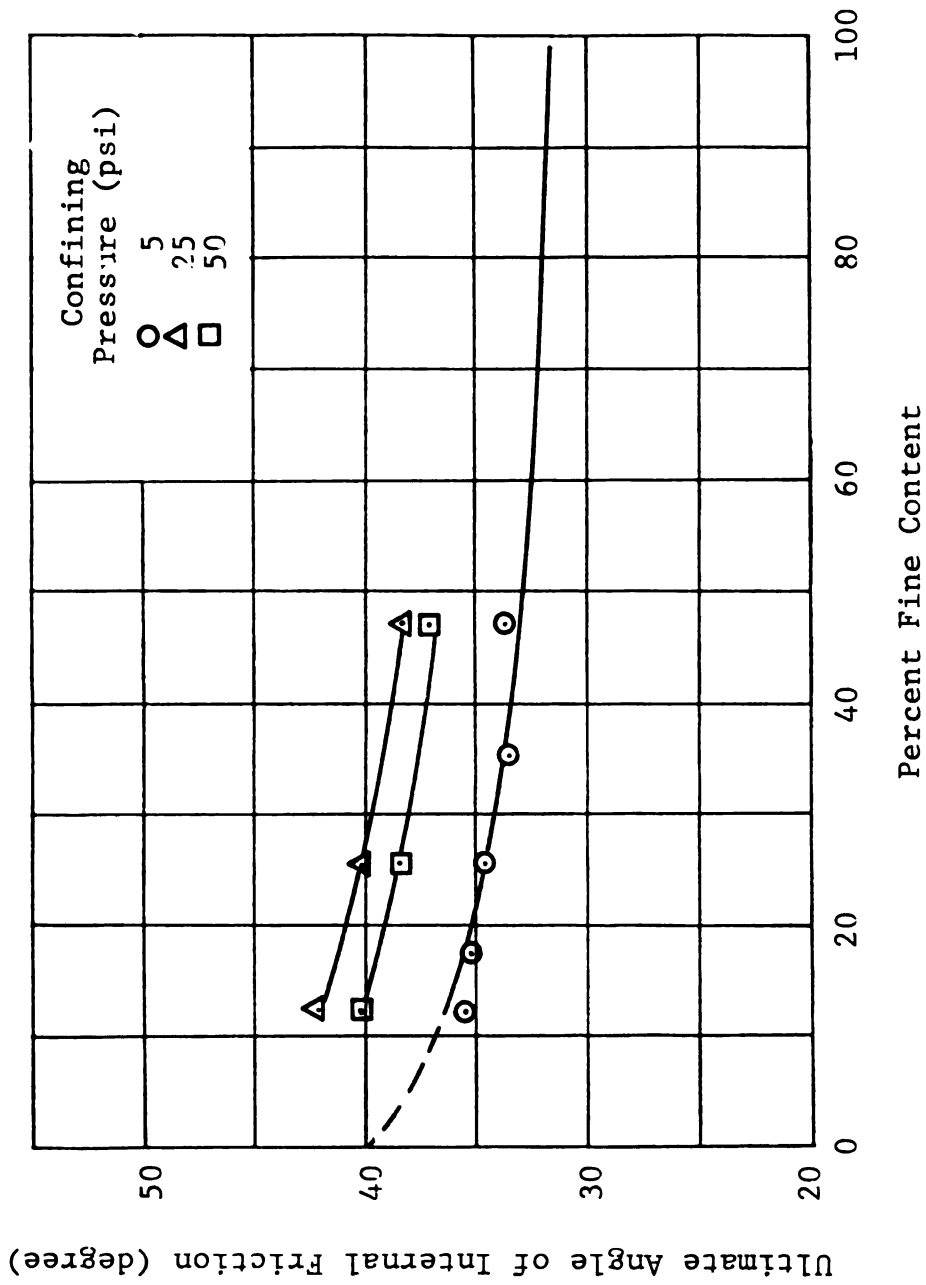


FIGURE 4.89 ULTIMATE ANGLE OF INTERNAL FRICTION VERSUS PERCENT FINE CONTENT OF SERIES A SAMPLES FOR THREE VALUES OF THE CONFINING PRESSURE.

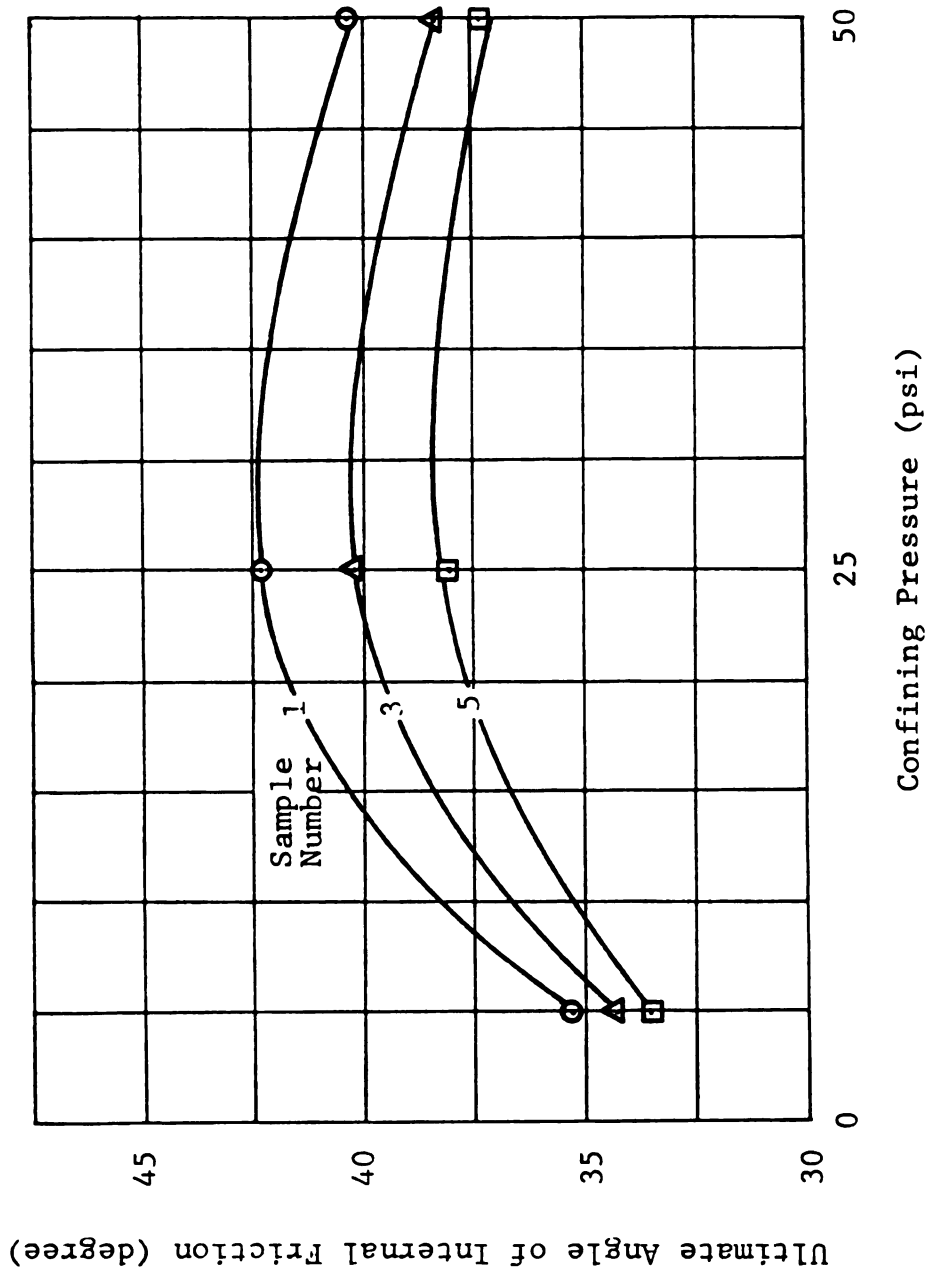


FIGURE 4.90 ULTIMATE ANGLE OF INTERNAL FRICTION OF SERIES A SAMPLES VERSUS CONFINING PRESSURE.

friction increases as the confining pressure increases from 5 to 25 psi and it decreases thereafter. The resistance of the soil particles to sliding is proportional to the normal stress at contact points. For low stress values, the higher the stress, the higher the resistance to sliding. At a relatively high stress values however, the soil particles are forced to become flatter and the microscopic interlocking due to surface roughness decreases. Consequently, the resistance to sliding decreases.

Figures 4.91, 4.92, and 4.93 show the angle of interlocking friction of samples 1, 3, and 5 of series A plotted against the confining pressure. It can be seen that, for all three samples, the higher the confining pressure, the lower the angle of interlocking friction. This observation is explained below.

The effect of the confining pressure on the angle of interlocking friction depends upon the initial density of the test specimen or the percent dilatation. For a zero percent dilatation (loose soil), the confining pressure tends to compress the specimen resulting in a higher density and hence higher degree of interlocking. Further increases in the confining pressure may result in a breakdown of sharp corners and consequently a decrease in the degree of interlocking. For the one hundred percent dilatation (dense specimen), the breakdown of the particles takes place at lower confining pressure than that for loose specimens.

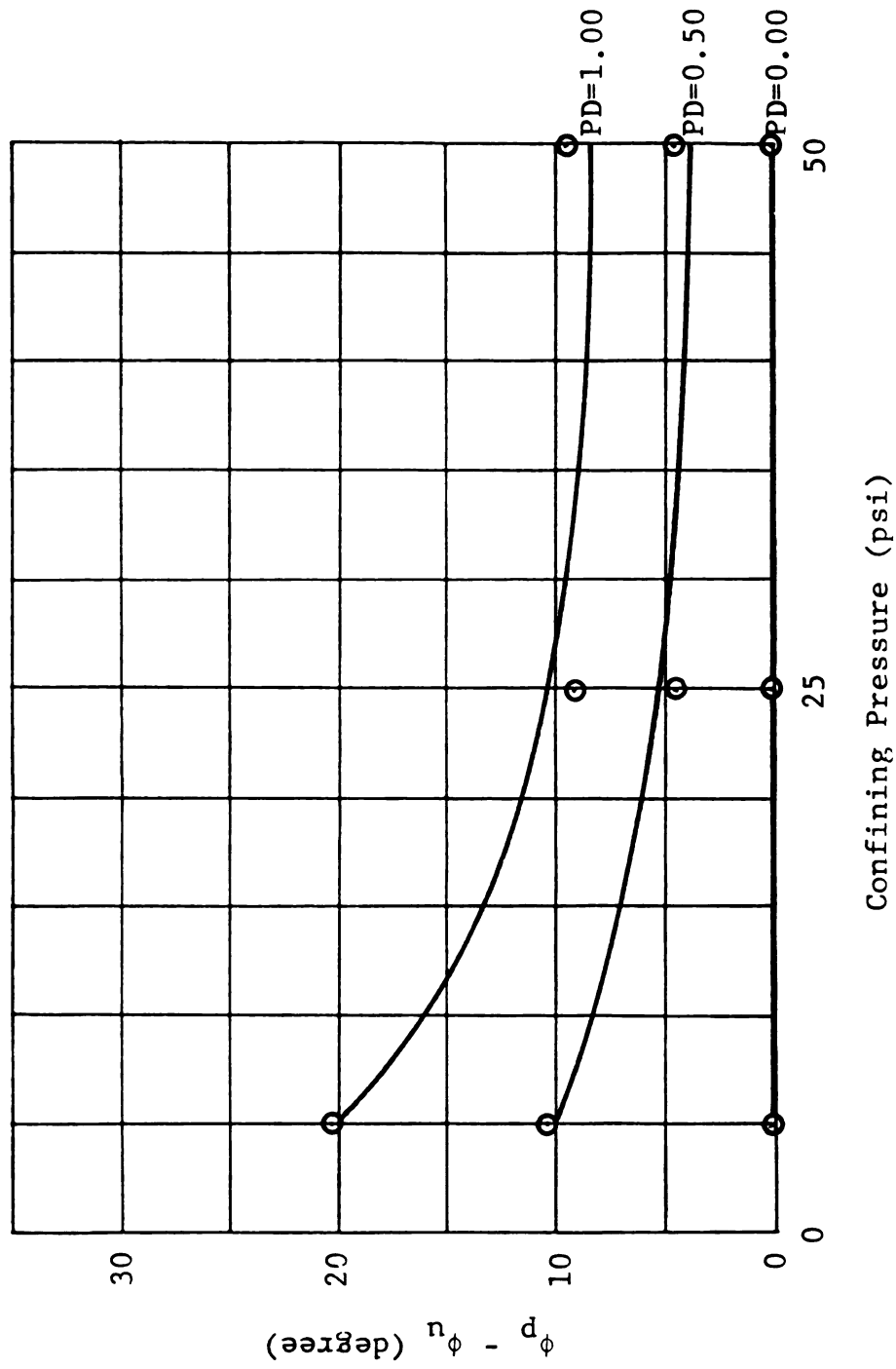


FIGURE 4.91 ANGLE OF INTERLOCKING FRICTION VERSUS CONFINING PRESSURE FOR SAMPLE 1 OF SERIES A, AND THREE VALUES OF THE PERCENT DILATATION.

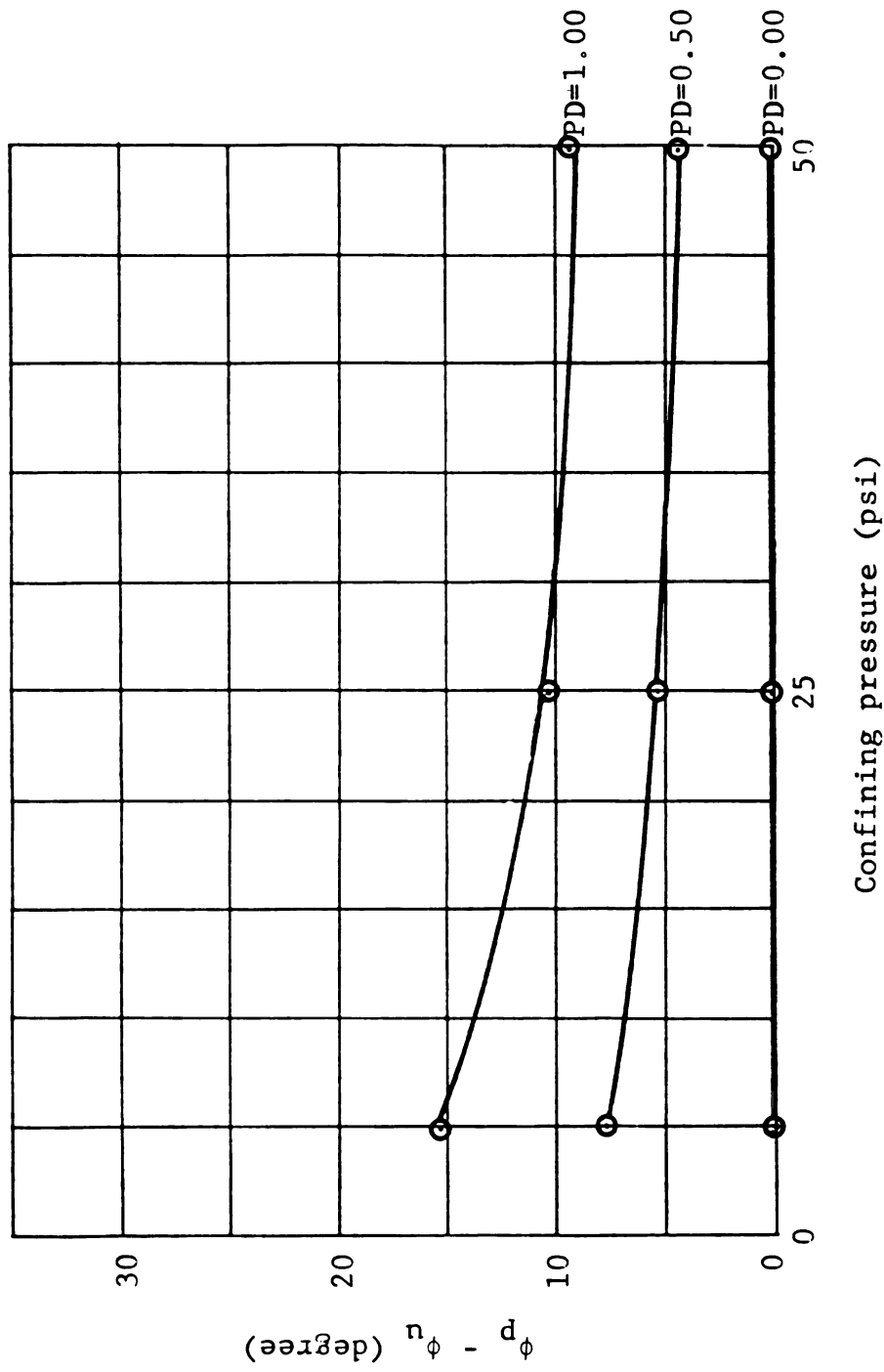


FIGURE 4.92 ANGLE OF INTERLOCKING FRICTION VERSUS CONFINING PRESSURE FOR SAMPLE 3 OF SERIES A, AND THREE VALUES OF THE PERCENT DILATATION.

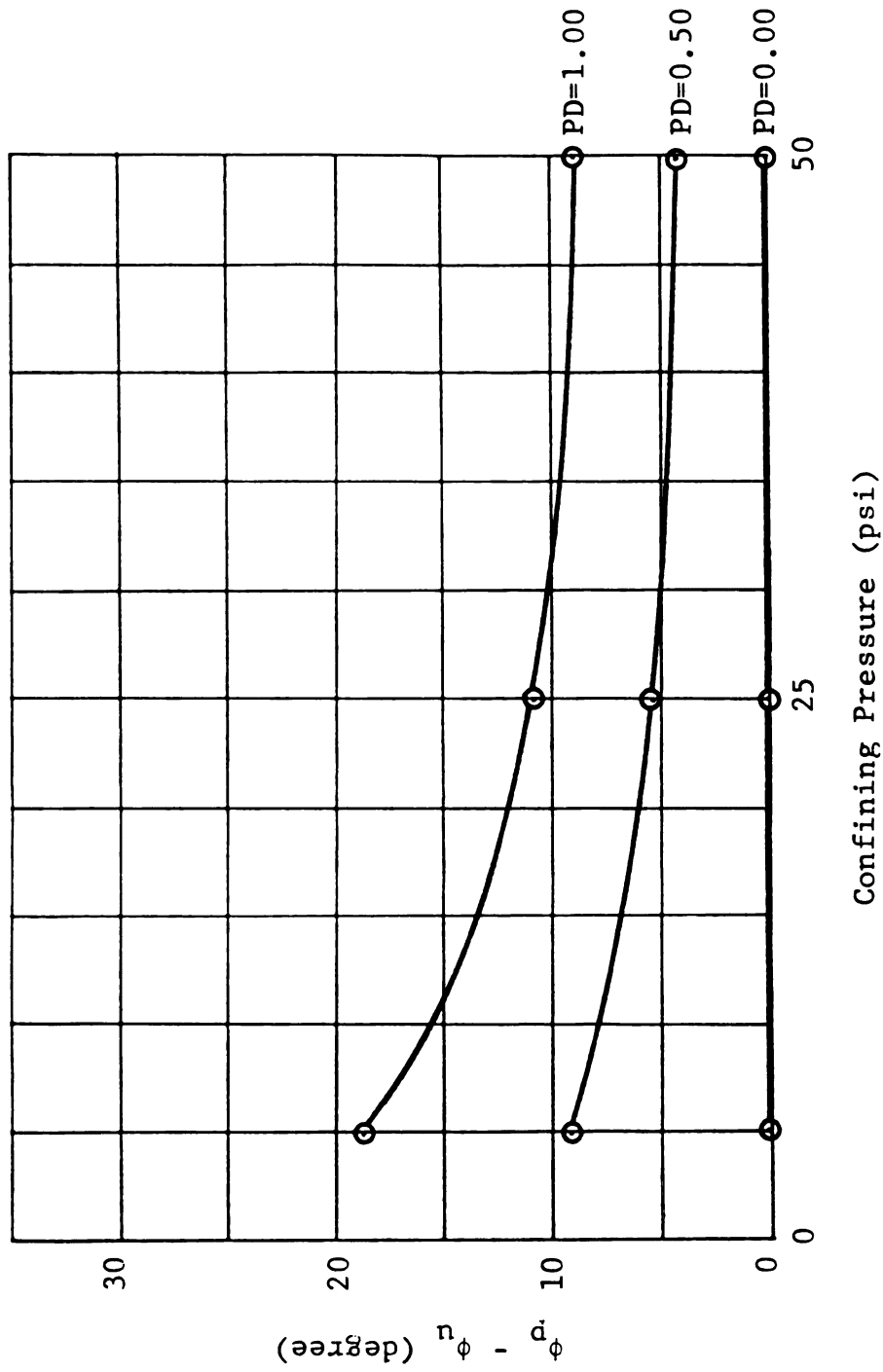


FIGURE 4.93 ANGLE OF INTERLOCKING FRICTION VERSUS CONFINING PRESSURE FOR SAMPLE 5 OF SERIES A, AND THREE VALUES OF THE PERCENT DILATATION.

Thus, for dense specimens, the angle of interlocking friction decreases as the confining pressure increases.

Figures 4.94, 4.95, and 4.96 depict the peak angle of internal friction at three levels of percent dilatation plotted against the confining pressure for samples 1, 3, and 5 of series A respectively. Examination of the Figures indicates that, for all three samples, the peak angle of internal friction at the one hundred percent dilatation level decreases as the confining pressure increases; it remains almost constant at the fifty percent dilatation; and for zero percent dilatation, it increases as the confining pressure increases from 5 to 25 psi then it decreases thereafter. The rate of increase or decrease of the peak angle of internal friction however varies from sample 1 to that of sample 5. This observation suggests that the effect of the confining pressure upon the peak angle of internal friction is also a function of the percent fine content of the soil. The functional relationship however, can not be determined in this study because only three samples of series A were tested to determine the peak and ultimate strengths. Further, this type of relationship is beyond the objective of this study.

Figure 4.97 depicts the axial strain at peak strength (peak angle of internal friction) for three confining pressures plotted against the percent dilatation of the soil of samples 1 and 3 of series A. It can be seen that:

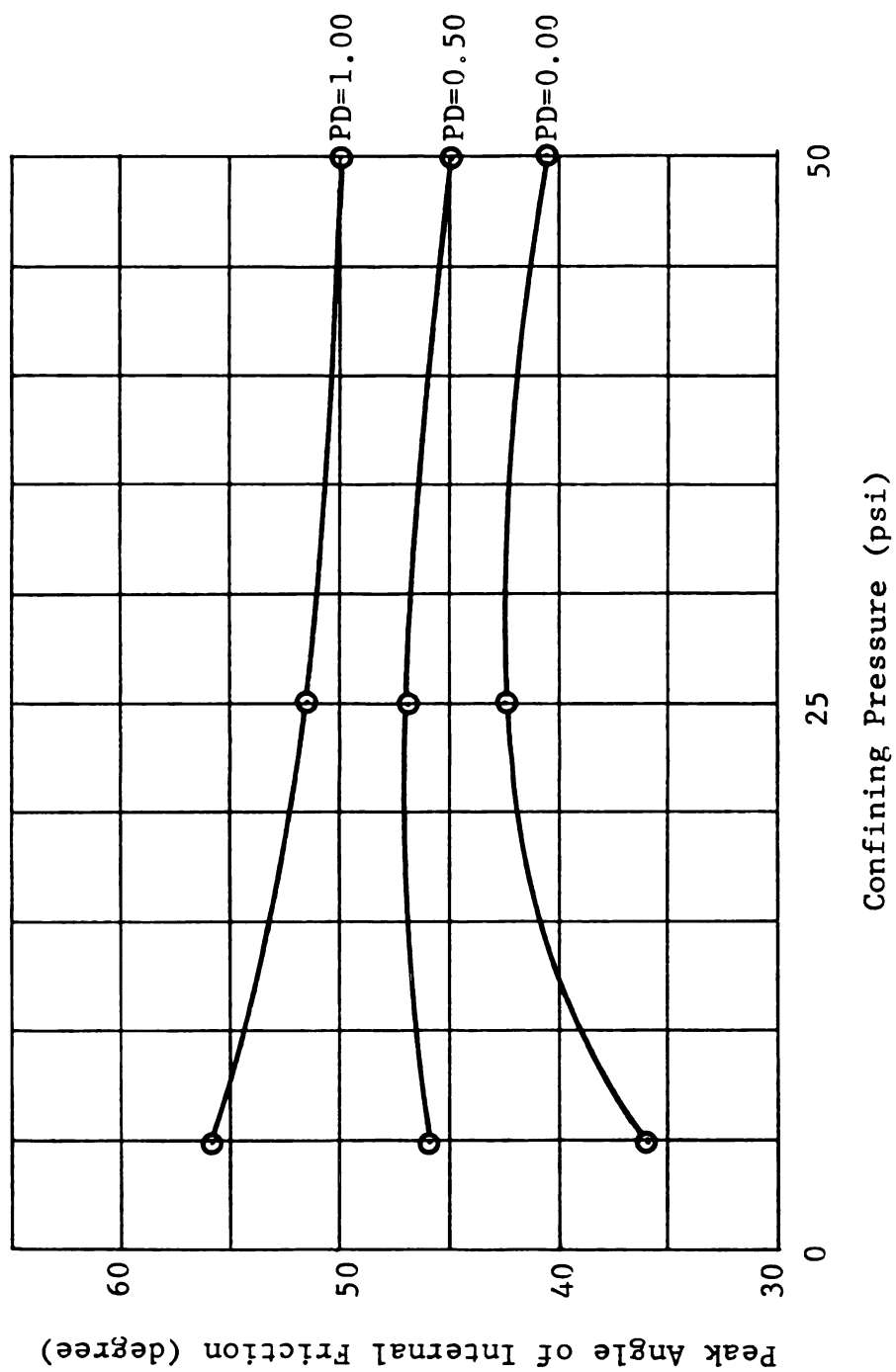


FIGURE 4.94 PEAK ANGLE OF INTERNAL FRICTION VERSUS CONFINING PRESSURE FOR SAMPLE 1 OF SERIES A, AND THREE VALUES OF THE PERCENT DILATATION.

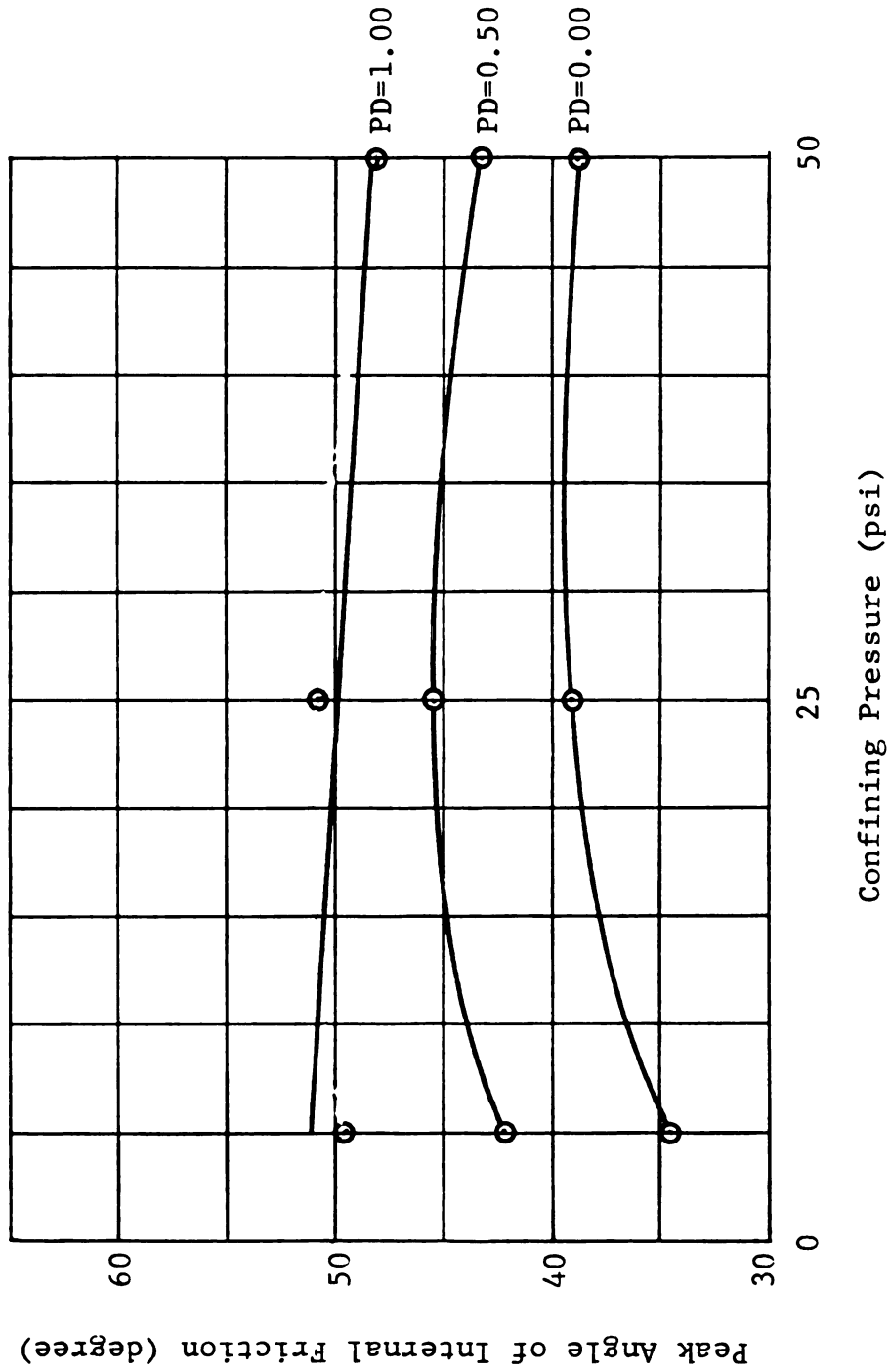


FIGURE 4.95 PEAK ANGLE OF INTERNAL FRICTION VERSUS CONFINING PRESSURE FOR SAMPLE 3 OF SERIES A, AND THREE VALUES OF THE PERCENT DILATATION.

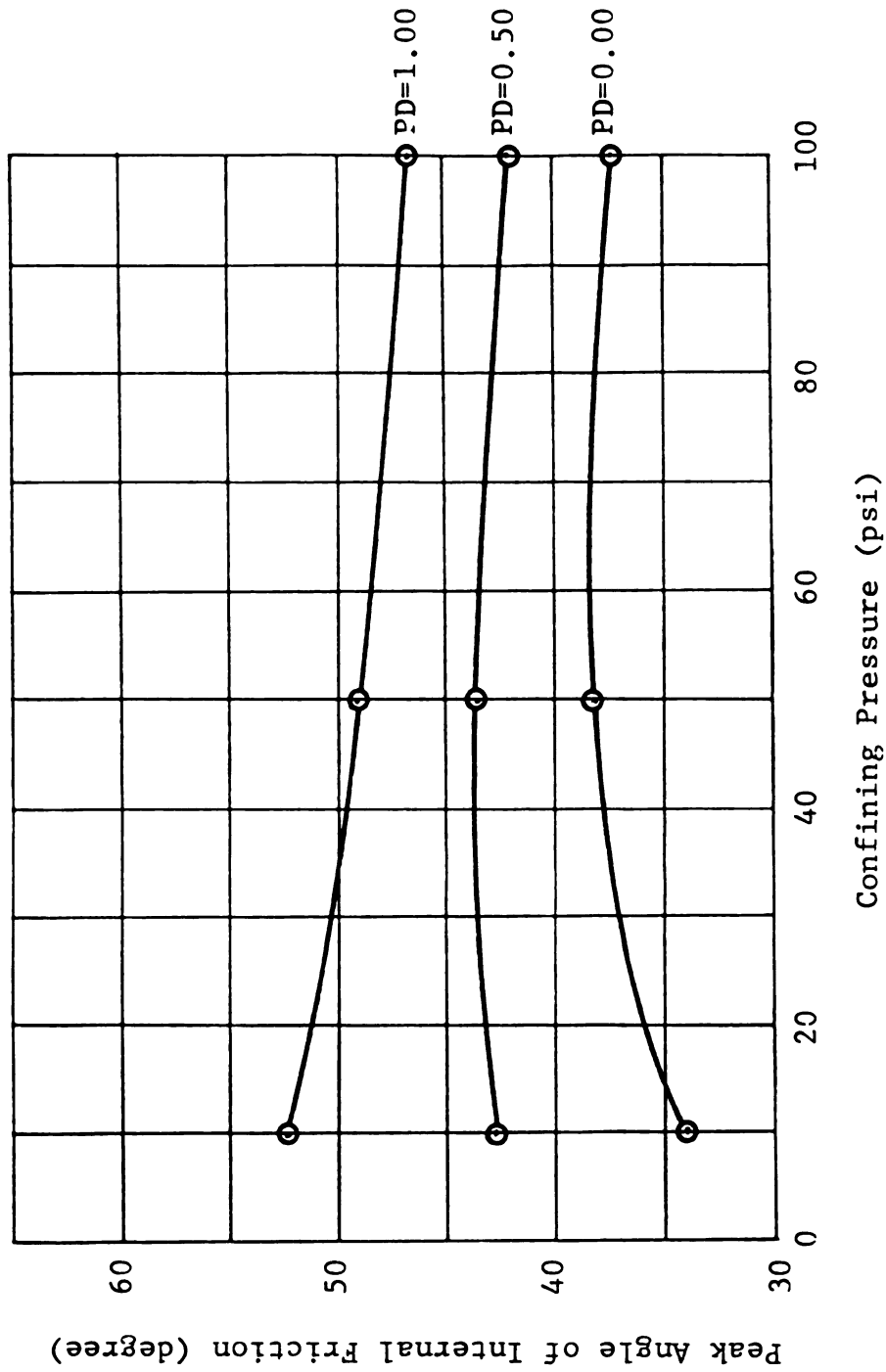


FIGURE 4.96 PEAK ANGLE OF INTERNAL FRICTION VERSUS CONFINING PRESSURE FOR SAMPLE 5 OF SERIES A, AND THREE VALUES OF THE PERCENT DILATATION.

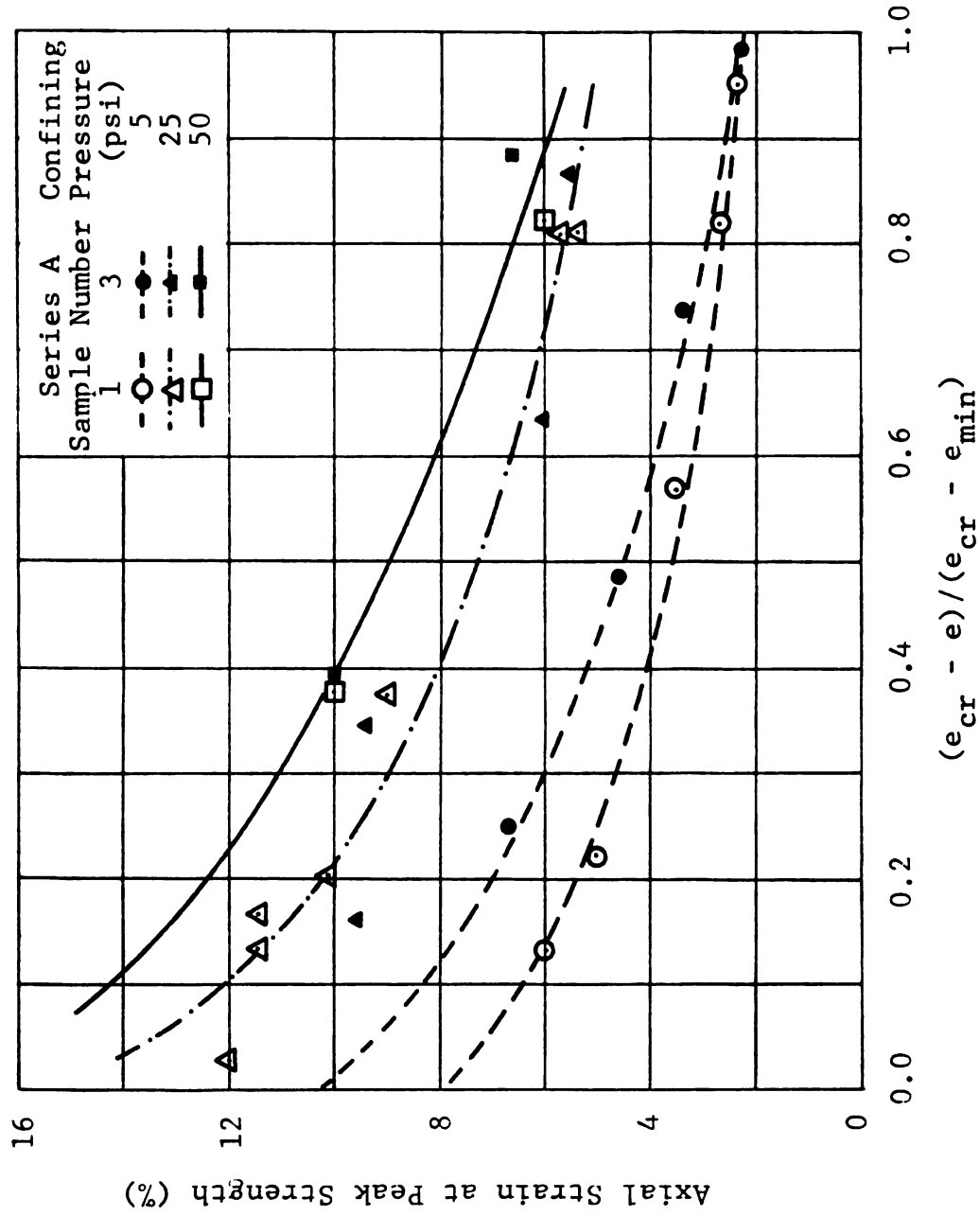


FIGURE 4.97 AXIAL STRAIN AT PEAK STRENGTH VERSUS PERCENT DILATATION OF SERIES A SAMPLES FOR THREE VALUES OF THE CONFINING PRESSURE.

- a) For each sample, the higher the confining pressure, the higher the required axial strain to fully mobilize the peak angle of internal friction.
- b) The axial strains at peak strength for samples 1 and 3 are almost the same for confining pressures of 25 and 50 psi. For a confining pressure of 5 psi however, the axial strain at peak strength of sample 1 is much lower than that of sample 3 at low percent dilatation, and they are almost the same at high percent dilatation.

These two observations indicate that irrespective of the soil density (percent dilatation), the confining pressure influences the stress-strain behavior of the soil. The higher the confining pressure, the higher the axial strain required to fully mobilize the peak angle of internal friction. Also, in the limited range of the available data, the influence of the percent fine content of the soil decreases as the confining pressure and percent dilatation increase.

4.12 MOISTURE CONTENT

One of the objectives of this investigation is to analyze the effect of the moisture content upon the total shearing resistance of the test materials. A total of forty triaxial compression drained tests were conducted utilizing two targets of water content of 5 and 9.6 percent,

one confining pressure of 5 psi (34.5 kN/m²), and series A samples. It should be noted herein that the actual water content of the soil specimen varied slightly from the target water content. Further, all tests were conducted up to six percent strain level. The stress-strain curves are presented in Figures E.28 through E.37 of Appendix E. Table 4.6. summarizes the water content, relative density, void ratio, the percent dilatation of the test specimens, the axial strain at peak stress, and the angles of shearing resistance at peak stress, and at the one and six percent strain levels that were calculated in terms of the total stresses. The percent dilatation of the soil specimens were calculated by using their void ratios and the critical and minimum void ratios of the dry soil of the appropriate samples of series A. Further, it should be noted herein that no volume change during the application of the confining pressure was noted for the wet tests.

The presence of moisture films around the individual grains of the soil results in "apparent cohesion" which is not a true cohesion in a physical sense. Thus, the soil grains are being held together by means of the water-grain surface tension (capillary tension) which is a function of the size of the void space between the grains. The smaller the pore space diameter, the greater the capillary tension, and the greater the intergrain contact stresses. Therefore, a higher frictional resistance develops between the grains.

It was noticed during the preparation of the test specimen that reconstituting wet soil specimens at a relatively high density (low void ratio) requires substantial compaction efforts which resulted in particles breakdown and thus a change in the sample gradation. In addition, the required compaction efforts increased as the percent fine content of the soil increased. Consequently, wet specimens were compacted utilizing the same compaction efforts as that of the dry specimens. This procedure resulted in higher void ratio (low percent dilatation) of the wet soil of series A samples than those of the dry soil.

Figures 4.98 through 4.102 show plots of the peak angle of internal friction for two levels of water content versus the percent dilatation of samples 1 through 5 of series A. The solid best fit lines in the figures were obtained using least square analysis utilizing the wet test data. The dashed lines represent the dry test data. It can be seen from the figures that:

- a) The peak angle of internal friction (calculated in terms of total stresses) increases as the water content increases from zero to about five percent and it decreases thereafter.
- b) The differences between the dry and wet test data are almost constant and independent of the percent dilatation of the soil.

The first observation was expected and it is consistent

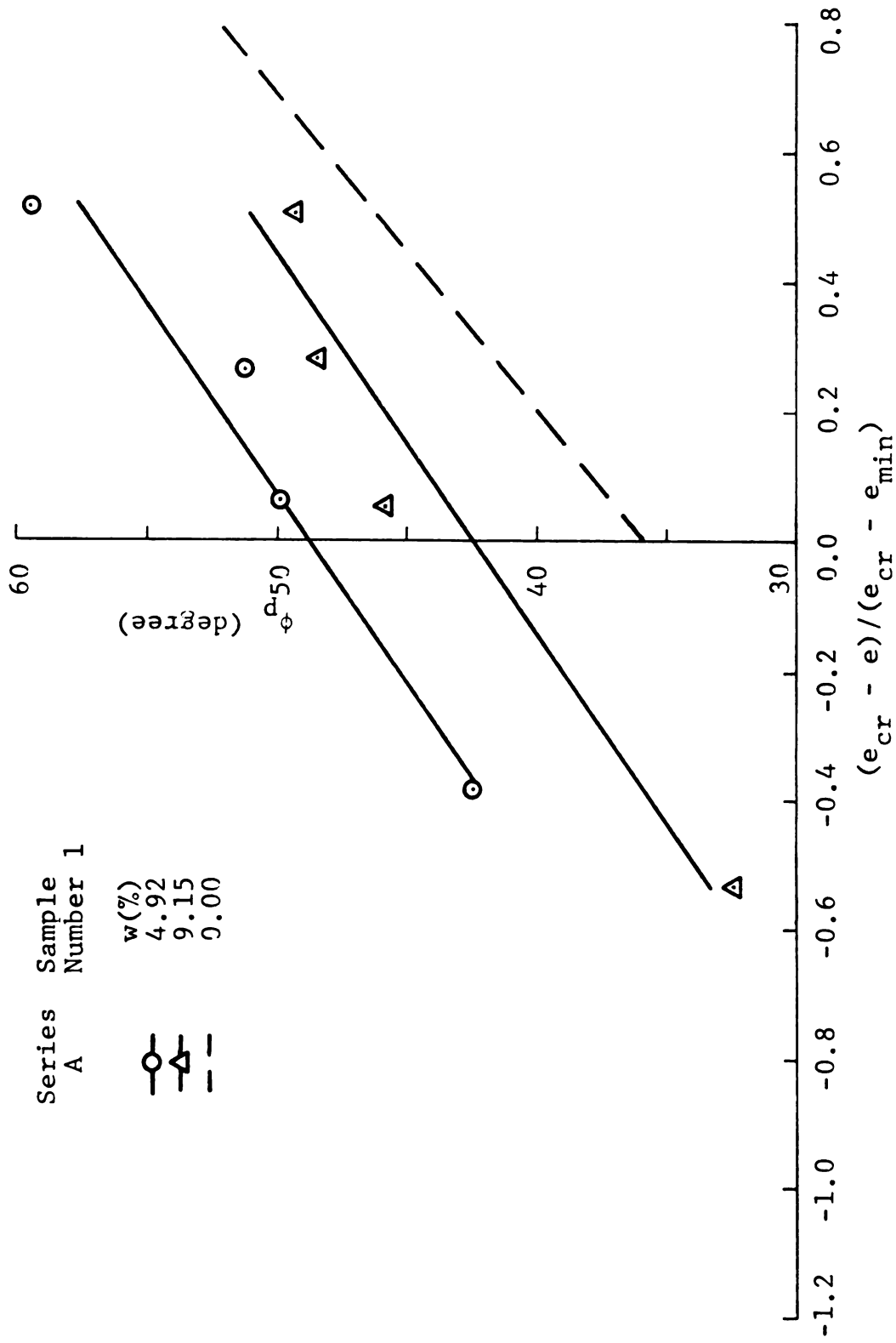


FIGURE 4.98 PEAK ANGLE OF INTERNAL FRICTION VERSUS PERCENT DILATATION OF SAMPLE 1 OF SERIES A THAT CONSISTED OF DRY AND WET MATERIALS FOR A CONFINING PRESSURE OF 5 PSI.

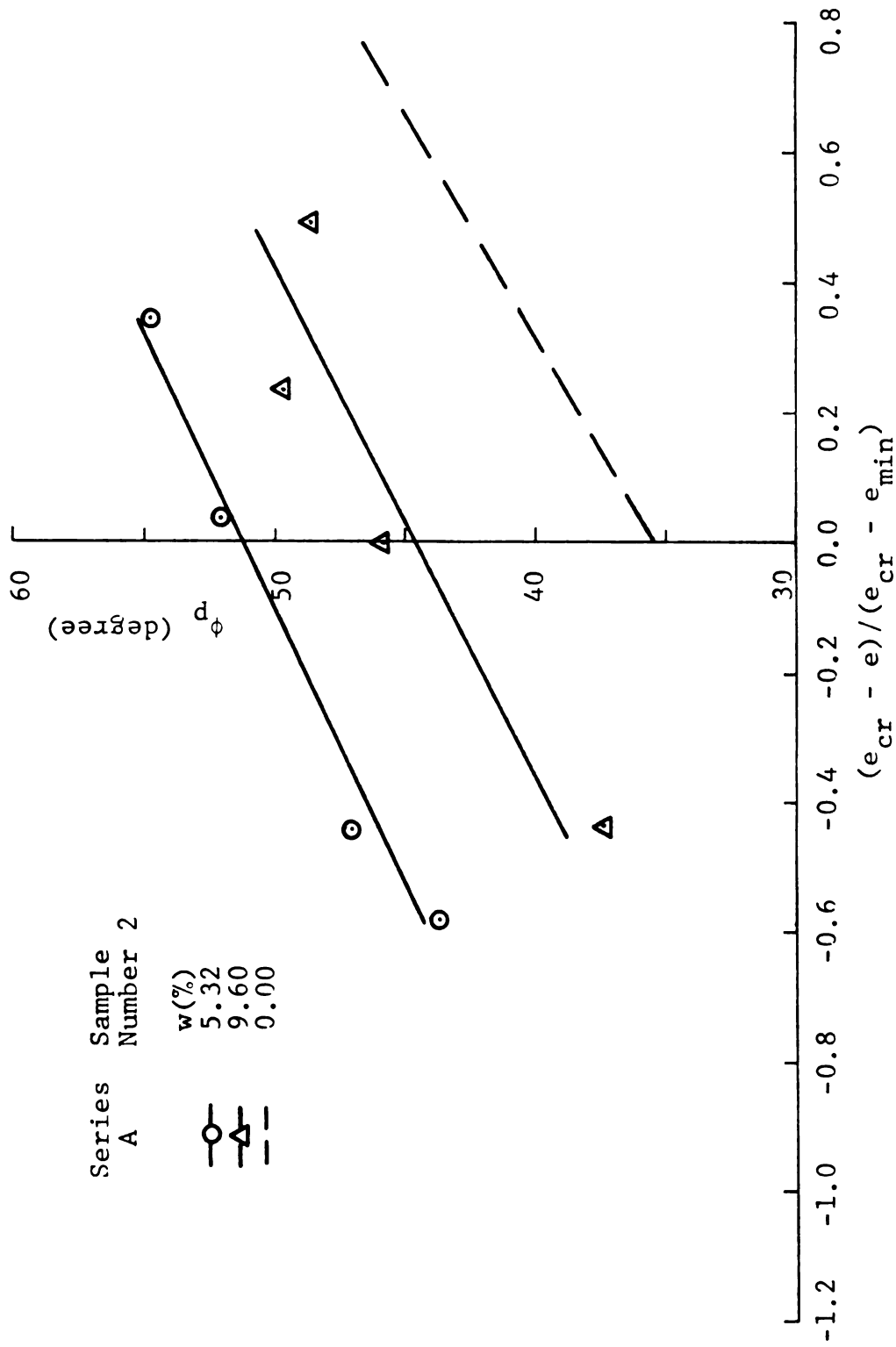


FIGURE 4.99 PEAK ANGLE OF INTERNAL FRICTION VERSUS PERCENT DILATATION OF SAMPLE 2 OF SERIES A THAT CONSISTED OF DRY AND WET MATERIALS FOR A CONFINING PRESSURE OF 5 PSI.

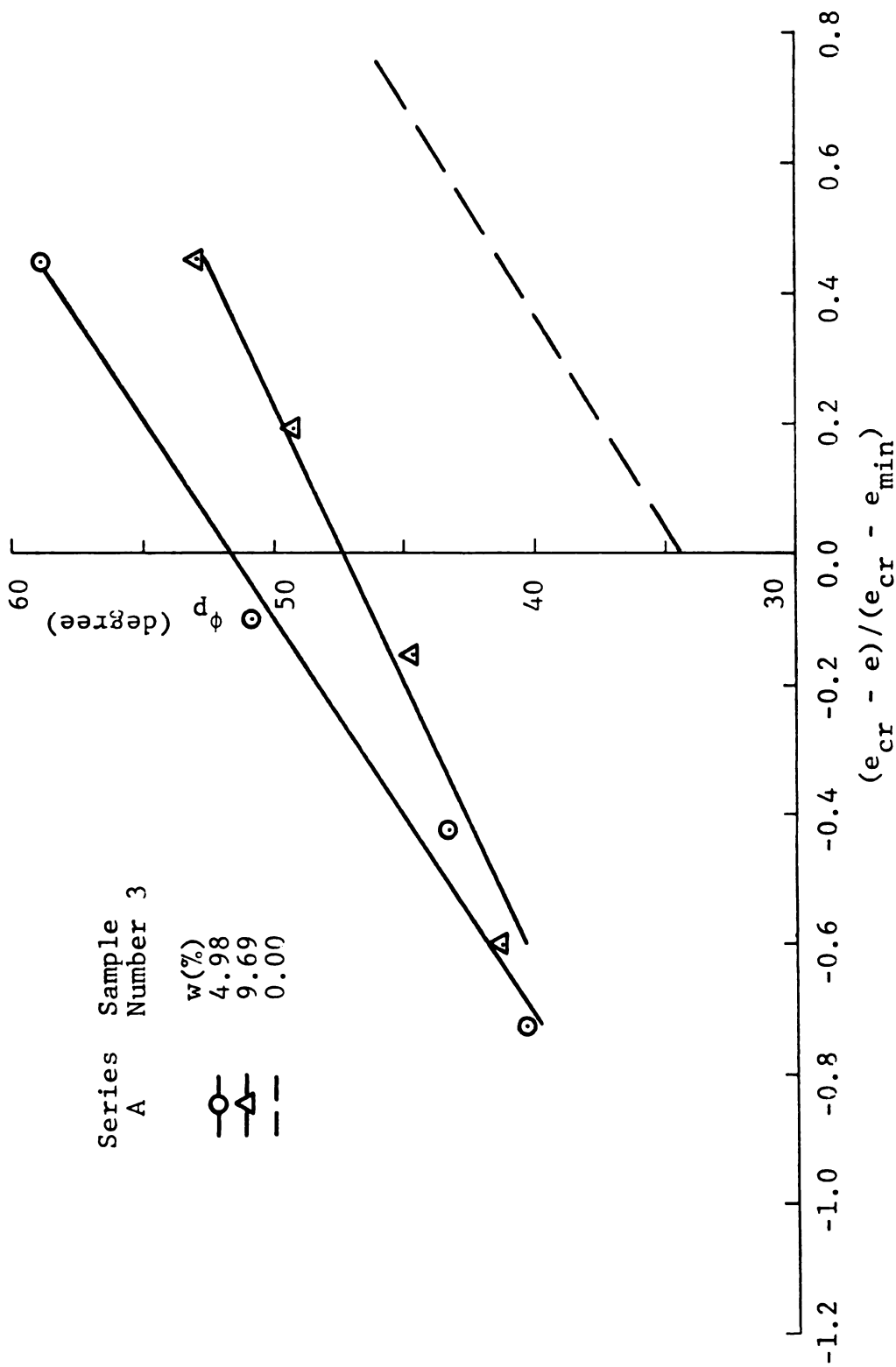


FIGURE 4.100 PEAK ANGLE OF INTERNAL FRICTION VERSUS PERCENT DILATATION OF SAMPLE 3 OF SERIES A THAT CONSISTED OF DRY AND WET MATERIALS FOR A CONFINING PRESSURE OF 5 PSI.

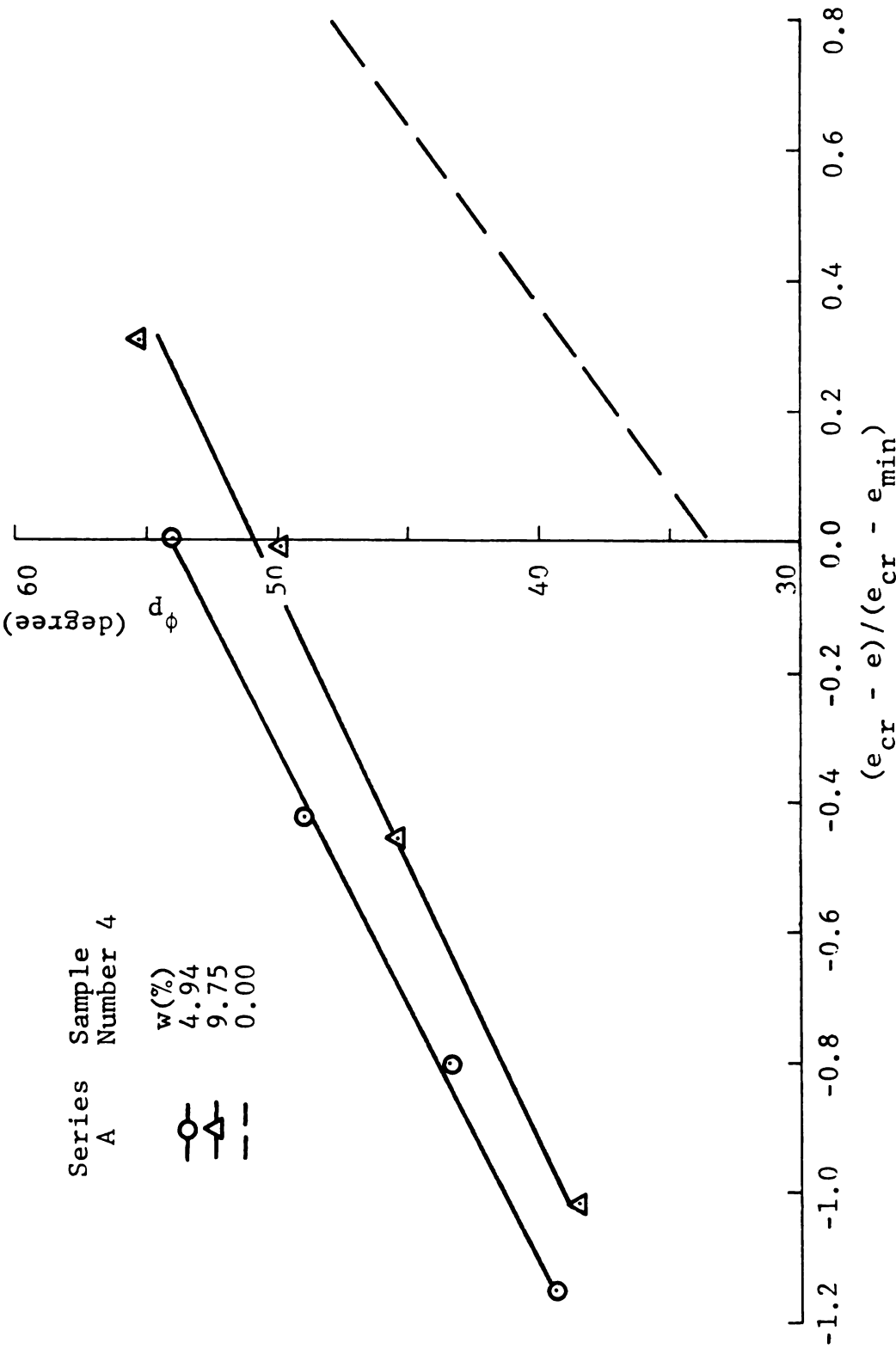


FIGURE 4.101 PEAK ANGLE OF INTERNAL FRICTION VERSUS PERCENT DILATATION OF SAMPLE 4 OF SERIES A THAT CONSISTED OF DRY AND WET MATERIALS FOR A CONFINING PRESSURE OF 5 PSI.

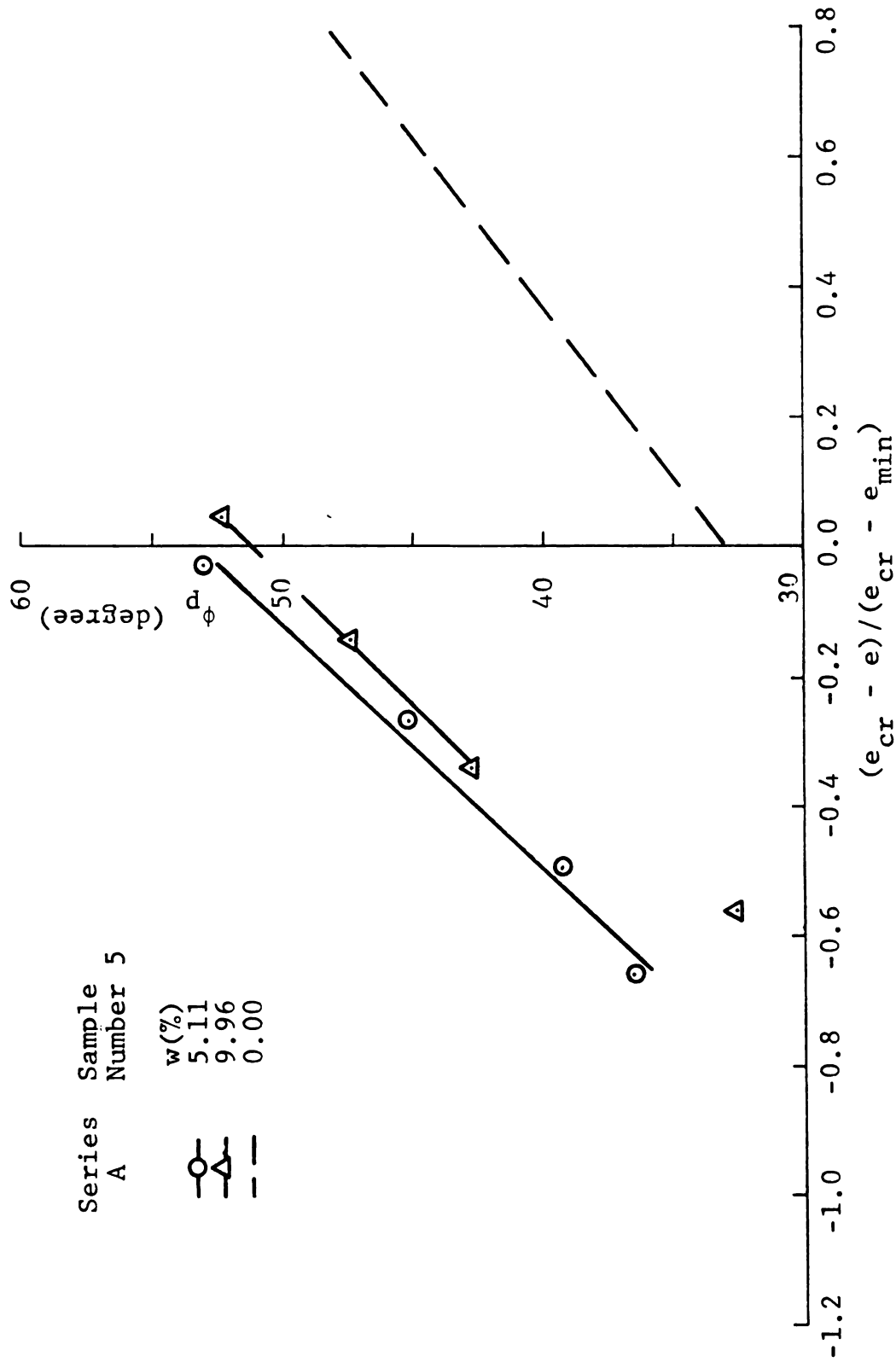


FIGURE 4.102 PEAK ANGLE OF INTERNAL FRICTION VERSUS PERCENT DILATATION OF SAMPLE 5 OF SERIES A THAT CONSISTED OF DRY AND WET MATERIALS FOR A CONFINING PRESSURE OF 5 PSI.

with that of reference 33. As the water content increases, the degree of saturation of the soil increases which decreases the capillary tension. Fully saturated cohesionless soils possess no apparent cohesion.

The second observation on the other hand, may be seen unreasonable. Because, the higher the percent dilatation of the soil, the denser the soil, and the smaller the pore space. Further, the smaller the void space, the higher the capillary tension, and the higher the intergrain stresses which contradicts the observation. One may expect that the higher the percent dilatation, the higher the difference between the dry and wet test data. However, for one type soil and a constant water content, the higher the density the higher the degree of saturation. Consequently, the gain made by decreasing the void spaces by densifying the sample (higher percent dilatation) is being lost due to increasing degree of saturation.

Figure 4.103 depicts the difference between the dry and wet test data plotted against the water content of the soil of samples 1 through 5 of series A. Figure 4.104, shows the peak angle of internal friction plotted against the percent fine content for two levels of water content. Examination of the figures indicates that:

- a) The total angle of internal friction reaches its maximum value at an optimum water content of about five percent (Figure 4.103).

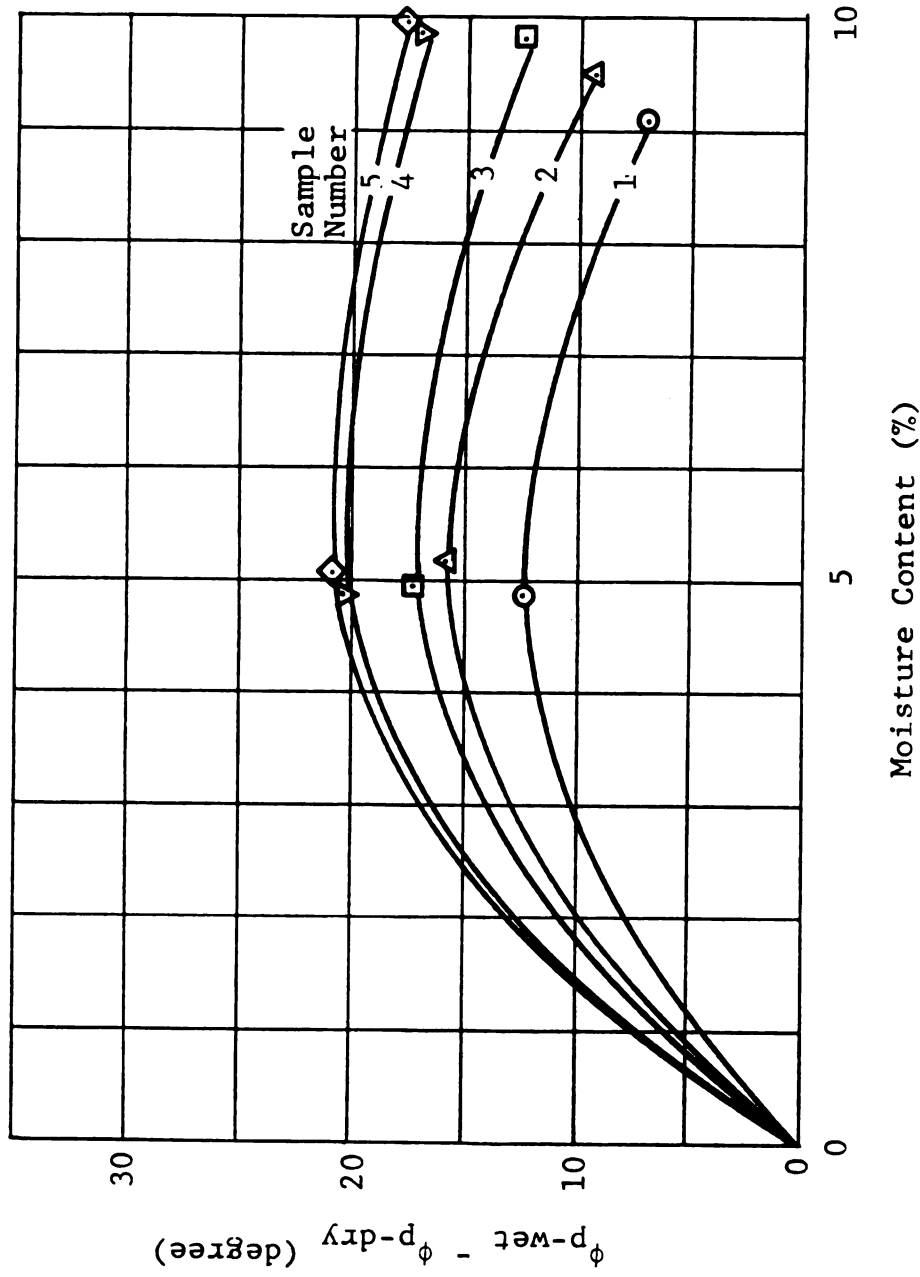


FIGURE 4.103 DIFFERENCE IN THE ANGLE OF INTERNAL FRICTION BETWEEN THE WET AND DRY MATERIALS OF SERIES A SAMPLES FOR A CONFINING PRESSURE OF 5 PSI AND ZERO PERCENT DILATATION.

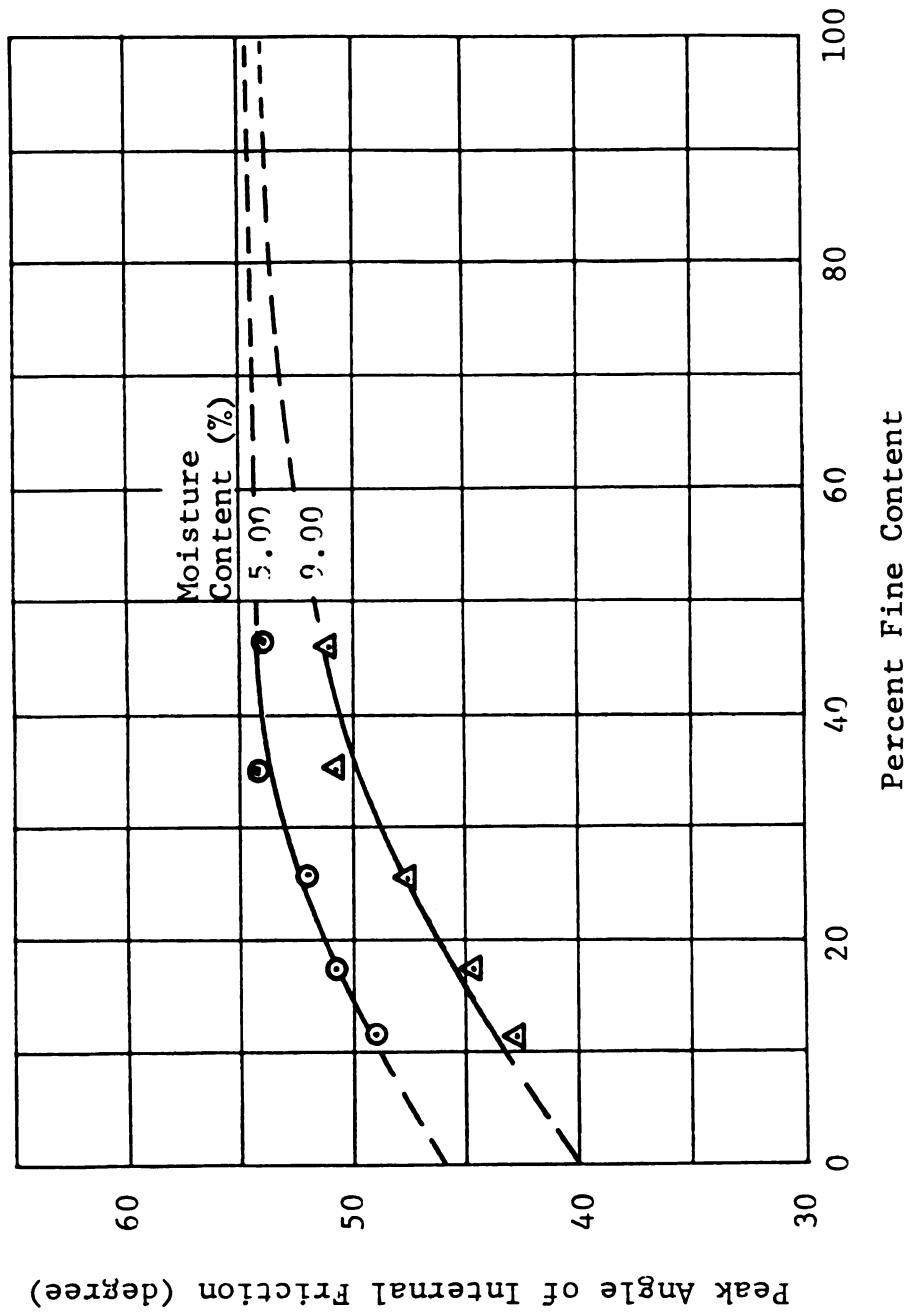


FIGURE 4.104 PEAK ANGLE OF INTERNAL FRICTION VERSUS PERCENT FINE CONTENT OF SERIES A SAMPLES FOR TWO VALUES OF THE MOISTURE CONTENT, A CONFINING PRESSURE OF 5 PSI, AND ZERO PERCENT DILATATION.

- b) As the percent fine content of the soil increases, the total peak angle of internal friction for a constant water content increases.

The reason for the first observation was stated above. The second observation is explained herein. As the percent fine content increases, the maximum particle size of the soil decreases, and the effective pore diameter decreases. The smaller the pore diameter, the smaller the radii of the menisci, and the higher the height of capillary rise and the corresponding capillary pressure. To illustrate this point, one can use the analogy of two small diameter open ended glass tubes to represent the voids between the soil grains. The height of capillary rise in the tubes is inversely proportional to the diameter of the tube; the smaller the inside diameter of the tube, the greater the height of capillary rise and the smaller the radii of the menisci. In equation form, the height of capillary rise can be given as (36):

$$H_c = 4(T)/(\gamma_w)(D) \quad (4.45)$$

where: H_c = height of capillary rise;

T = water surface tension;

γ_w = unit weight of water; and

D = tube diameter.

It should be noted herein that the height of capillary rise in soil media is a function of the effective pore

diameter and pore size distribution in the soil. The former is commonly assumed about 20 percent of the effective grain size (D_{10}) of the soil; the grain size at the ten percent passing by weight on the grain size distribution curve. The latter is a function of the compaction effort and molding water content (36).

Finally, the test data (angle of friction) at the one and six percent strain levels showed similar trends to those of Figures 4.98 through 4.102.

5.

sh

st

ha

in

de

co

cr

wi

pa

re

pr

re

Ch

ea

gi

st

co

CHAPTER 5

SUMMARY, CONCLUSIONS AND RECOMMENDATIONS

5.1 GENERAL

The effects of grain size, sample gradation, grain shape, confining pressure, and moisture content on the strength and engineering behavior of cohesionless materials have been studied using several types of tests. These included standard triaxial compression, maximum and minimum densities, and angle of repose tests. The test materials consisted of natural deposit of gravel mix that were crushed, pulverized, sieved, and recombined in accordance with two series of parallel gradation curves. The maximum particle size of all the triaxial test specimens was restricted to one sixth of its diameter. The employed test procedures were described in Chapter 3, and The test results, data analysis and discussion were presented in Chapter 4.

A brief summary followed by conclusions pertinent to each area is presented herein under five headings: effect of grain size; effect of sample gradation; effect of grain shape; effect of confining pressure; effect of moisture content; and future research needs.

5.

a.

g

c

g

w

t

r

c

5.2 EFFECT OF GRAIN SIZE

The effect of grain size on the soil behavior was analysed utilizing the percent fine content and the maximum grain size of the soil specimen. The contradictory conclusions made in the literature concerning the effect of grain size on the shear strength of cohesionless material were resolved by introducing a new analytical model based on the dilatant behavior of the soil. Based upon the test results and decreasing grain size of the soil, the following conclusions are drawn.

- 1) The maximum and minimum dry densities of the soil decrease.
- 2) The angle of repose of the soil decreases.
- 3) The specimen volume change during the application of the confining pressure (prior to shear) increases, especially for the loose or medium dense specimens.
- 4) The critical void ratio of the soil increases.
- 5) The ultimate angle of internal friction decreases.
- 6) the degree of particle interlocking decreases.
- 7) the peak angle of internal friction decreases.
- 8) The percent dilatancy model introduced in Chapter 4 has several advantages over the traditional analysis methods.

5.3 EFFECT OF SAMPLE GRADATION

The effect of sample gradation on the soil behavior was analysed utilizing the coefficient of uniformity of the soil samples. Based upon the test results and decreasing value of the coefficient of uniformity, the following conclusions are drawn.

- 1) The maximum and minimum dry densities decreases for large particled soils and they are independent of the sample gradation for small particled soils.
- 2) The angle of repose is independent of the sample gradation.
- 3) The volume change during the application of the confining pressure increases.
- 4) The critical void ratio of the soil increases.
- 5) The ultimate angle of internal friction is not affected by the sample gradation.
- 6) The degree of particle interlocking decreases.
- 7) The peak angle of internal friction decreases.

5.4 EFFECT OF GRAIN SHAPE

The effect of grain shape on the soil behavior was analysed using the coefficient of sample angularity. Based upon the test results and decreasing value of the coefficient of angularity, the following conclusions are drawn.

- 1) The maximum and minimum dry densities increases.
- 2) The angle of repose decreases.
- 3) The volume change during the application of the confining pressure decreases.
- 4) The critical void ratio of the soil decreases.
- 5) The ultimate angle of internal friction decreases.
- 6) The degree of particle interlocking decreases.
- 7) The peak angle of internal friction decreases.

5.5 EFFECT OF CONFINING PRESSURE

The effects of confining pressure on the stress-strain behavior of the soil were analysed using triaxial compression tests conducted on dry soils. Based upon the test results and decreasing confining pressure, the following conclusions are drawn.

- 1) The strain at peak strength decreases.
- 2) The ultimate angle of internal friction is slightly affected.
- 3) The degree of particle interlocking increases.
- 4) The peak angle of internal friction decreases.

5.6 EFFECT OF MOISTURE CONTENT

The effect of moisture content on the shear strength of cohesionless soils were analysed using drained triaxial compression tests. The strength was analysed and discussed in terms of the total stress. Based upon the test results,

the

5.7

abi

the

dil

dev

app

tra

or

cor

pro

cor

ve

pa

adv

ba

anc

the following conclusions are drawn.

- 1) The total angle of internal friction reaches a maximum value at an optimum moisture content of about five percent.
- 2) For a constant moisture content, the increase in the value of the total angle of internal friction between the dry and wet specimens is constant and independent of the specimen initial density.

5.7 FUTURE RESEARCH NEEDS

The results of this investigation have demonstrated the ability to evaluate the effects of grain characteristics on the shear strength of cohesionless soils utilizing the dilatant behavior of the soil. The percent dilatancy model developed in this study was proven to be accurate and applicable at several stress and strain levels. The traditional analysis methods that utilize relative density or void ratio of the soil may lead to inconsistent conclusions. On the contrary, the percent dilatancy model produced accurate results and has led to consistent conclusions throughout this study. The model however was verified utilizing parallel gradation curves and maximum particle size of half of an inch. Consequently, it is advisable that a study be undertaken to expand on the data bank and to verify the model utilizing larger size particles and scalped and replaced types of gradation curves. The

former can be accomplished using large size triaxial apparatus. The latter could be accomplished using any natural or crushed gravel materials.

REFERENCES

REFERENCES

1. The American Association of State Highway and Transportation Officials, "Method of Sampling and Testing," Part 2, 13th edition, 1982.
2. Arpad Kezdi, "Soil Physics," Handbook of Soil Mechanics, vol. 1, Elsevier Scientific Publishing Co., 1974.
3. The American Society for Testing and Materials, "Annual Book of ASTM Standards," section 4, vol. 04.08, March 1984.
4. Adams, F.D., and Nicholson, J.J., "An Experimental Investigation into the Flow of Marble," Philosophical Transactions, Royal Society of London, 1901.
5. Atakal, K., and Larew, H.G., "Dynamic Shearing Resistance of Dry Ottawa Sand," Journal of the Soil Mechanics and Foundations Division, ASCE, vol. 96, SM2, March 1970.
6. Balla, A., "Stress Conditions in Triaxial Compression," Journal of the Soil Mechanics and Foundations Division, ASCE, Vol. 86, SM6, Dec. 1960.
7. Barden L., and McDermott, J.W., "The Use of Free Ends in Triaxial Testing of Clays," Journal of the Soil Mechanics and Foundations Division, ASCE, Vol. 91, SM6, Nov. 1965.
8. Belidor, B.F., "La Science des Ingenieurs dans la Conduite des Travaux de Fortification et D'Architecture," Paris 1929.
9. Bishop, A.W., "A Large Shear Box for Testing Sands and Gravels," Proceedings, the Second International Conference on Soil Mechanics and Foundation Engineering, Rotterdam, Vol. 1, 1948.
10. Bishop, A.W., and Henkel, D.J., "The Measurement of Soil Properties in the Triaxial Test," 2nd edition, Arnold, London, 1962.
11. Boughton, N.O., "Elastic Analysis for Behavior of Rockfill Materials," Journal of Soil Mechanics and Foundations Division, ASCE, Vol. 96, SM9, Sept. 1970.

12. Buisman, A.S.K., "Proefanderuinelyke bepaling Van de Greas Van inwending ev enwient van een Grandmassa," De Ingenieur, Vol. 49, Part B, June 1934.
13. Chen, L.S., "An Investigation of Stress-Strain and Strength Characteristics of Cohesionless Soils by Triaxial Compressive Tests," Proceedings, the Second International Conference on Soil Mechanics and Foundation Engineering, Rotterdam, Vol. 5, 1948.
14. Collin, A., "Experimental Investigation on Sliding of Clay Slopes," Paris 1846.
15. Cornforth, D.H., "Predicting of Drained Strength of Sands from Relative Density Measurements," American Society of Testing and Materials, STP 523, 1973.
16. Coulomb, C.A., "Sur une Application des regales de Maximis et Minimis a Que lques Problems es Statique, Relatufs a L'Architecture," Memous Academic Royale des Sciences, Vol. 7, 1776.
17. D'Appolonia, D.J., and D'Appolonia, E.D., "Determination of the Maximum Density of Cohesionless Soils," Proceedings, the Third Asian Conference on Soil Mechanics and Foundation Engineering, Haifa, Vol. 1, Sept 1967.
18. D'Appolonia, E.D., and Newmark, N.M., "A Method for Solution of the Restrained Cylinder Under Axial Compression," Proceedings, the First U.S. Nat. Conference of Applied Mechanics, ASME, 1951.
19. Dickin, E.A., "Influence of Grain Shape and Size Upon Limiting Porosities o f Sands," American Society of Testing and Materials, STP 523, 1973.
20. Donaghe, R.T., and Cohen, M.W., "Strength and Deformation Properties of Rock fill," Technical Report 5-78-1, U.S. Army Engineer Waterways Experiment Station, Vicksburg, Mississippi, January 1978.
21. Donaghe, R.T., and Torrey, V.H., "Scalping and Replacement Effects on Strength Parameters of Earth Rockfill Mixtures," British Geotechnical Society, London , 1979.
22. Donaghe, R.T., and Torrey, V.H., "Strength and Deformation Properties of Earth-Rock Mixtures," U.S. Army Engineer Waterways Experiment Station, Vicksburg, Mississippi, Final Report on project CWIS 31209, Sept. 1982.

23. Donaghe, R.T., and Townsend, F.C., "Scalping and Replacement Effects on the Compaction Characteristics of Earth-Rock Mixtures," American Society of Testing and Materials, STP 599, 1976.
24. Drnevich, V.P., Ebelhar, R.J., and Williams, G.P., "Geotechnical Properties of Surface Mine Soils," Proceedings, the Seventh Ohio River Valley Soils Seminar on Shales and Mine Waste: Geotechnical Properties, Design and Construction, Oct. 1976.
25. Duncan, J.M., and Chang, E.Y., "Nonlinear Analysis of Stress and Strain in Soils," Journal of the Soil Mechanics and Foundations Division, ASCE, vol. 96, SM5, Sept. 1970.
26. Duncan, J.M., and Dunlop, P., "The Significance of Cap and Base Restraint," Journal of the Soil Mechanics and Foundations Division, ASCE, Vol. 94, SM1, Jan. 1968.
27. Edil, T.B., Krizek, R.J., and Zelasko, J.S., "Effect of Grain Characteristics on Packing of Sands," Proceedings, the Istanbul Conference on Soil Mechanics and Foundation Engineering, Istanbul, 1975.
28. Filon, L.N.G., "The Elastic Equilibrium of Circular Cylinders Under Certain Practical Systems of Load," Phil. Trans. Royal Society, London, Series A, Vol. 198, 1902.
29. Frost, R.J., Discussion of "Evaluation of Properties of Rockfill Materials" by Marachi, Chan and Seed, Journal of Soil Mechanics and Foundations Division, ASCE, Vol. 98, SM12, Dec. 1969.
30. Fumagalli, E., "Tests on Cohesionless Materials for Rockfill Dams," Journal of Soil Mechanics and Foundations Division, ASCE, Vol. 95, SM1, Jan. 1969.
31. Gray, J.E., "Characteristics of Graded Base Course Aggregates Determined by Triaxial Tests," Engineering Bulletin No. 12, National Crushed Stone Association, July 1962.
32. Haruyama, M., "Effect of Surface Roughness on the Shear Characteristics of Granular Materials," Soil and Foundation, Vol. 9, No. 4, 1969.
33. Haruyama, M., "Effect of Water Content on the Shear Characteristics of Granular Soils such as Shirasu," Soil and Foundation, Vol. 9, No. 3, 1969.

34. Holtz, W.G., "The Relative Density Approach - Uses, Testing Requirements, Reliability and Shortcomings," American Society of Testing and Materials, STP 523, 1973.
35. Holtz, W.G., and Gibbs, H.J., "Triaxial Shear Tests on Pervious Gravelly Soils," Journal of Soil Mechanics and Foundations Division, ASCE, vol. 82, SM1, Jan. 1956.
36. Holtz, R.D., and Kovacs, W.D., "An Introduction to Geotechnical Engineering," Prentice Hall Inc., Englewood Cliffs, New Jersey, 1981.
37. Holubec, I., and D'Appolonia, E.P., "Effects of Particle Shape on the Engineering Properties of Granular Soils," American Society of Testing and Materials, STP 523, 1973.
38. Hough, B.K., "Basic Soils Engineering," The Ronald Press Company, New York, 1957.
39. Hutchinson, B., and Townsend D., "Some Grading-Density Relationships for Sands," Proceedings, the Fifth International Conference on Soil Mechanics and Foundation Engineering, Paris, Vol. 1, 1961.
40. Hveen, F.N., "The Role of the Laboratory in the Preliminary Investigation and Control of Materials for Low Cost Bituminous Pavements," Proceedings, the Highway Research Board, Vol. 14, Part 2, 1934.
41. Jain, S.P., and Gupta, R.C., "Insitu Shear Test for Rockfills," Journal of Soil Mechanics and Foundations Division, ASCE, Vol. 100, SM9, Sept. 1974.
42. Janardhanam, R., and Desai, C.S., "Three Dimensional Testing and Modeling of a Ballast," Geotechnical Engineering Journal, Vol. 109n, June 1983.
43. Johnston, M.M., "Laboratory Studies of Maximum and Minimum Dry Density of Cohesionless Soils," American Society of Testing and Materials, STP 523, 1973.
44. King, G.J.W., and Dickin, E.A., "Comparison of Stress Dilatancy Theory," Journal of the Soil Mechanics and Foundations Division, ASCE, vol. 96, SM5, Sept. 1970.
45. Kirkpatrick, W.M., "Effects of Grain Size and Grading of the Shearing Behavior of Granular Materials," Proceedings, the Sixth International Conference on Soil Mechanics and Foundation Engineering, Montreal, vol. 1, 1965.

46. Koerner, R.M., "Effect of Particle Characteristics on Soil Strength," Journal of the Soil Mechanics and Foundations Division, ASCE, vol. 96, SM4, July 1970.
47. Kolbuszewski, J.J., "An Experimental Study of Maximum and Minimum Porosities of Sands," Proceedings, the Second International Conference on Soil Mechanics and Foundation Engineering, Rotterdam, vol. 1, 1948.
48. Kolbuszewski, J.J., "Fundamental Factors Affecting Experimental Procedures Dealing with Pressure Distribution in Sands," Proceedings, the Brussels Conference on Earth Pressure Problems, Brussels, 1958.
49. Korfiatis, G.P., and Manikopoulos, C.N., "Correlation of Maximum Dry Density and Grain Size," Journal of Geotechnical Engineering, ASCE, Vol. 108, No. GT9, Sept. 1982.
50. Lambe, T.W., and Whitman, R.V., "Soil Mechanics," John Wiley and Sons, Inc., N.Y., 1969.
51. Leary, D.J., and Woodward, R.J. III, "Experience with Relative Density as a Construction Control Criterion," American Society of Testing and Materials, STP 523, 1973.
52. Lee, K.L., "Comparison of Plane Strain and Triaxial Tests on Sand," Journal of the Soil Mechanics and Foundations Division, ASCE, vol. 96, SM3, May 1970.
53. Lee, K.L., and Farhoomand, I., "Compressibility and Crushing of Granular Soils in Anisotropic Compression," Canadian Geotechnical Journal, vol. 4, no. 1, 1967.
54. Lee, K.L., and Seed, H.B., "Undrained Strength of Anisotropically Consolidated Sand," Journal of the Soil Mechanics and Foundations Division, ASCE, vol. 96, SM2, March 1970.
55. Lee, K.L., Seed, H.B., and Dunlop, P., "Effect of Moisture on the Strength of a Clean Sand," Journal of Soil Mechanics and Foundations Division, ASCE, vol. 93, SM6, Nov. 1967.
56. Leps, T.M., "Review of Shearing Strength of Rockfill," Journal of Soil Mechanics and Foundations Division, ASCE, vol. 96, SM4, July 1970.

57. Leslie, D.D., "Large Scale Triaxial Tests on Gravelly Soils," Proceedings, the Second Pan. Am. Conference on Soil Mechanics and Foundation Engineering, STMao Paulo, 1963.
58. Leussink, H., and Wittke, W., "Difference in Triaxial and Plain Strain Shear Strength," American Society of Testing and Materials, STP 361, Sept. 1963.
59. Lewis, J.G., "Shear Strength of Rockfill," Proceedings, the Second Australia-New Zealand Conference on Soil Mechanics and Foundation Engineering, 1965.
60. Low, W.I., and Sener, C., "Field and Laboratory Determination of Maximum and Minimum Density in Coarse Sands and Gravels for Mica Dam," American Society of Testing and Materials, STP 523, 1973.
61. Marachi, N.D., "Evaluation of Properties of Rockfill Materials," Journal of Soil Mechanics and Foundations Division, ASCE, vol. 98, SM1, Jan. 1972.
62. Marsal, R.J., "Large Scale Testing of Rockfill Materials," Journal of Soil Mechanics and Foundations Division, ASCE, vol. 93, SM2, March 1967.
63. Marsal, R.J., "Plain Strain Testing of Rockfill Materials," Proceedings, the 3rd Pan American Conference, Caracas, vol. 1, 1967.
64. Meyerhof, G.G., "Theories," General Report on Theories, American Society of Testing and Materials, STP 361, Sept. 1963.
65. Mitterilung der Preussischen Versuchsanstalt Fur Wasserbau and Schiffsbau, Vol. 14, No. 45, Berlin 1933.
66. Moore, W.M., "Effect of Variations in Poisson's Ratio on Soil Triaxial Testing," Highway Research Record, No. 108, 1965.
67. Perloff, W.H., and Baron, W., "Soil Mechanics Principles and Applications," John Wiley & Sons, Inc., N.Y. 1976.
68. Perloff, W.H., and Pombo, L.E., "End Restraint Effect in the Triaxial Test," Proceedings, the Seventh International Conference on Soil Mechanics and Foundation Engineering, Mexico, vol. 1, 1969.

69. Pickett, G., "Application of the Fourier Method to the Solution of Certain Boundary Problems in the Theory of Elasticity," *Journal Applied Mechanics*, vol. 2, 1944.
70. Rowe, P.W., "The Stress-Dilatency Relation for Static Equilibrium of an Assembly of Particles in Concrete," *Proceedings, the Royal Society, London, Series A*, vol. 269, 1962.
71. Rutledge, P.C., "Cooperative Triaxial Shear Research Program," *Progress Report on Soil Mechanics Fact Finding Survey*, U.S. Army Engineer Waterways Experiment Station, Vicksburg, Mississippi, 1947.
72. Saada, S.A., and Townsend, F.C., "State of the Art: Laboratory Strength Testing of Soils," *American Society of Testing and Materials*, STP 740, 1981.
73. Siddiqi, F.H., "Strength Evaluation of Cohesionless Soils with Oversize Particles," *Ph.D. Thesis*, University of California, Davis, 1984.
74. Silver, M.L., "Laboratory Triaxial Testing Procedures to Determine the Cyclic Strength of Soils," *Nuclear Regulatory Commission Report No. NURZG-0031*, June 1977.
75. Sower, F.G., "Strength Testing of Soils," *American Society of Testing and Materials*, STP 361, Sept. 1963.
76. Taylor, D.W., "Seventh Progress Report on Shear Research to U.S. Engineers," *MIT Publication*, Cambridge, Mass. 1941.
77. Tavenas, F.A., and Ladd, R.S., and Rochelle, P. L., "Accuracy of Relative Density Measurements: Results of a Comparative Test Program," *American Society of Testing and Materials*, STP 523, 1973.
78. Terzaghi, K., and Peck, R.B., "Soil Mechanics in Engineering Practice," *John Wiley and Sons, Inc.*, 2nd Edition.
79. Tiedemann, D.A., "Variability of Laboratory Relative Density Test Results," *American Society of Testing and Materials*, STP 523, 1973.
80. Vallergera, B.A., et al., "Effect of Shape, Size and Surface Roughness of Aggregate Particles on the Strength of Granular Materials," *American Society of Testing and Materials*, STP 212, 1957.

8

8

8

8

8

86

87

88

81. Wu, T.H., "Relative Density and Shear Strength of Sand," Journal of Soil Mechanics and Foundations Division, ASCE, vol. 83, SM1, Jan. 1957.
82. Wu, W.K., "Effect of Rock Content on Cyclic Strength of Soil," City of Los Angeles, Department of Water and Power, Report No. AX279-40, July 1980.
83. Yong, N.R., and Warkentin, P.B., "Soil Properties and Behaviors," Elsevier Scientific Publishing Co., N.Y., 1975.
84. Yoshimi, Y, and Tohno, Ikuo, "Statistical Significance of the Relative Density," American Society of Testing and Materials, STP 523, 1973.
85. Youd, T.C., "Factors Controlling Maximum and Minimum Density of Sands," American Society of Testing and Materials, STP 523, 1973.
86. Youd, T.C., "Densification and Shear of Sand During Vibration," Journal of the Soil Mechanics and Foundations Division, ASCE, vol. 96, SM3, May 1970.
87. Zelasko, J.S., Kirzek, R.J., and Edil, T.B., "Shear Behavior of Sands as a Function of Grain Characteristics," Proceedings, the Istanbul Conference on Soil Mechanics and Foundation Engineering, Instabul, 1975.
88. Zeller, J., and Wulliman, R., "The Shear Strength of Shell Materials For The Goschenenalp Dam, Switzerland," Proceedings, the Fourth International Conference on Soil Mechanics and Foundation Engineering, London, Vol. 2, 1957.

APPENDIX A

TAB

S
N
(

TABLE A.1 MEASURED X, Y, AND Z DIMENSIONS OF PARTICLE NUMBER (I) RETAINED ON SIEVE NUMBER (J) OF THE CRUSHED AND PULVERIZED MATERIAL.

Sieve Number (J)	Sieve Size	Sieve Opening (mm)	Particle Number (I)	Dimension (mm)		
				X	Y	Z
1	4	4.750	1	8.00	6.10	2.20
			2	6.70	5.70	4.60
			3	7.00	6.00	2.70
			4	12.20	10.20	5.30
			5	13.10	9.90	5.30
			6	7.40	6.90	2.90
			7	6.70	5.60	2.00
			8	8.60	7.10	4.50
			9	7.90	6.80	3.50
			10	8.70	8.00	2.90
			11	8.60	6.20	3.40
			12	10.50	7.30	5.10
			13	7.00	5.00	4.50
			14	8.20	7.40	4.10
			15	7.50	6.20	2.20
			16	9.20	7.70	2.00
			17	8.30	6.50	4.60
			18	7.20	7.00	2.70
			19	6.60	5.60	4.70
			20	6.70	5.70	4.50
			21	8.70	5.30	5.20
			22	6.20	5.20	5.20
			23	5.50	5.00	3.50
			24	9.20	5.10	4.50
			25	7.80	5.00	4.20

TABLE A.1 CONTINUED.

Sieve Number (J)	Sieve Size	Sieve Opening (mm)	Particle Number (I)	Dimension (mm)		
				X	Y	Z
2	8	2.360	1	5.00	4.60	3.00
			2	4.80	2.80	1.60
			3	6.20	3.70	3.00
			4	7.00	3.80	1.70
			5	4.50	3.20	1.00
			6	7.10	3.90	1.60
			7	5.20	3.10	2.60
			8	5.10	3.40	2.80
			9	3.60	2.00	1.80
			10	4.80	4.00	1.20
			11	3.30	2.70	1.80
			12	4.30	3.40	0.70
			13	4.30	3.30	1.20
			14	5.60	3.20	1.70
			15	5.65	4.15	3.20
			16	6.95	3.60	2.10
			17	3.75	3.65	1.50
			18	5.60	5.10	1.60
			19	6.45	4.50	1.00
			20	3.80	3.70	3.35
			21	4.00	2.20	1.60
			22	5.75	5.30	1.90
			23	6.20	4.10	2.60
			24	4.80	3.15	2.75
			25	5.00	3.60	1.50

TABLE A.1 CONTINUED.

Sieve Number (J)	Sieve Size	Sieve Opening (mm)	Particle Number (I)	Dimension (mm)		
				X	Y	Z
3	16	1.180	1	3.35	1.45	1.50
			2	3.35	1.60	1.50
			3	3.65	2.80	1.70
			4	2.10	1.75	0.65
			5	2.95	2.25	1.65
			6	2.65	2.25	1.65
			7	2.75	1.60	0.50
			8	3.60	2.65	1.00
			9	2.25	1.80	0.70
			10	2.80	1.15	1.00
			11	4.00	1.85	1.40
			12	2.45	2.40	0.80
			13	2.30	1.85	1.00
			14	3.10	2.75	1.40
			15	1.75	1.55	0.85
			16	4.75	3.10	1.15
			17	3.70	2.30	1.40
			18	3.85	2.85	1.60
			19	2.40	1.70	0.70
			20	4.10	1.60	1.55
			21	2.65	2.60	1.30
			22	2.20	1.30	1.10
			23	1.90	1.70	1.10
			24	2.50	2.40	1.30
			25	3.00	2.15	0.50

TABLE A.1 CONTINUED.

Sieve Number (J)	Sieve Size	Sieve Opening (mm)	Particle Number (I)	Dimension (mm)		
				X	Y	Z
4	30	0.600	1	1.60	1.20	0.75
			2	2.60	1.60	0.40
			3	1.20	0.85	0.60
			4	1.15	0.70	0.45
			5	1.95	1.25	0.40
			6	1.70	1.20	0.85
			7	1.70	0.85	0.70
			8	2.15	1.10	0.25
			9	2.00	1.10	0.60
			10	1.15	0.85	0.60
			11	2.10	1.45	0.50
			12	2.50	1.80	0.50
			13	1.20	1.05	0.60
			14	1.65	0.80	0.80
			15	2.15	1.60	0.70
			16	2.00	1.40	0.70
			17	1.80	1.10	0.70
			18	2.15	1.10	0.45
			19	2.50	1.10	0.50
			20	1.25	1.10	0.65
			21	1.50	0.90	0.65
			22	2.00	1.15	0.65
			23	1.60	0.60	0.60
			24	3.80	1.20	0.60
			25	1.40	0.80	0.65

TABLE A.2 MEASURED X, Y, AND CALCUATED Z DIMENSIONS OF PARTICLE NUMBER (I) RETAINED ON SIEVE NUMBER (J) OF THE CRUSHED AND PULVERIZED MATERIAL.

Sieve Number (J)	Sieve Size	Sieve Opening (mm)	Particle Number (I)	Dimension (mm)		
				X	Y	Z
5	50	0.300	1	0.96	0.66	0.64
			2	1.04	0.40	0.38
			3	0.68	0.66	0.58
			4	1.12	0.62	0.52
			5	0.80	0.50	0.40
			6	1.04	0.48	0.37
			7	1.00	0.56	0.42
			8	0.68	0.38	0.28
			9	1.16	0.78	0.52
			10	0.54	0.30	0.20
			11	0.76	0.36	0.23
			12	0.51	0.34	0.20
			13	0.66	0.55	0.31
			14	0.66	0.44	0.24
			15	0.72	0.64	0.33
			16	0.66	0.42	0.20
			17	0.58	0.53	0.25
			18	0.48	0.36	0.16
			19	0.75	0.36	0.14
			20	0.80	0.36	0.14
			21	0.80	0.48	0.17
			22	1.28	0.68	0.23
			23	0.80	0.60	0.19
			24	0.60	0.34	0.09
			25	0.68	0.38	0.09

TABLE A.2 CONTINUED.

Sieve Number (J)	Sieve Size	Sieve Opening (mm)	Particle Number (I)	Dimension (mm)		
				X	Y	Z
6	100	0.150	1	0.38	0.18	0.14
			2	0.34	0.34	0.15
			3	0.30	0.21	0.10
			4	0.28	0.27	0.11
			5	0.34	0.16	0.06
			6	0.44	0.20	0.19
			7	0.34	0.24	0.08
			8	0.31	0.17	0.16
			9	0.28	0.20	0.07
			10	0.20	0.18	0.12
			11	0.20	0.18	0.12
			12	0.20	0.14	0.04
			13	0.32	0.16	0.14
			14	0.28	0.16	0.10
			15	0.26	0.20	0.17
			16	0.27	0.16	0.08
			17	0.28	0.20	0.11
			18	0.40	0.20	0.15
			19	0.28	0.27	0.15
			20	0.44	0.25	0.13
			21	0.24	0.18	0.13
			22	0.20	0.19	0.05
			23	0.34	0.17	0.35
			24	0.34	0.20	0.50
			25	0.30	0.19	0.13

TABLE A.2 CONTINUED.

Sieve Number (J)	Sieve Size	Sieve Opening (mm)	Particle Number (I)	Dimension (mm)		
				X	Y	Z
7	200	0.075	1	0.11	0.08	0.07
			2	0.07	0.05	0.03
			3	0.09	0.07	0.08
			4	0.07	0.05	0.05
			5	0.03	0.02	0.01
			6	0.14	0.14	0.08
			7	0.10	0.04	0.04
			8	0.17	0.11	0.06
			9	0.07	0.04	0.02
			10	0.05	0.04	0.03
			11	0.20	0.12	0.06
			12	0.12	0.06	0.03
			13	0.18	0.12	0.10
			14	0.20	0.15	0.06
			15	0.12	0.12	0.05
			16	0.09	0.05	0.02
			17	0.09	0.04	0.01
			18	0.23	0.14	0.10
			19	0.14	0.13	0.08
			20	0.16	0.10	0.07
			21	0.20	0.15	0.05
			22	0.20	0.12	0.09
			23	0.24	0.12	0.03
			24	0.17	0.08	0.02
			25	0.22	0.14	0.11

TAB

S
N
(

TABLE A.3 MEASURED X, Y, AND Z DIMENSIONS OF PARTICLE NUMBER (I) RETAINED ON SIEVE NUMBER (J) OF THE NATURAL MATERIAL.

Sieve Number (J)	Sieve Size	Sieve Opening (mm)	Particle Number (I)	Dimension (mm)		
				X	Y	Z
1	4	4.750	1	13.10	10.00	7.40
			2	7.90	6.60	4.15
			3	12.80	8.85	6.90
			4	14.40	10.30	4.30
			5	8.80	7.60	6.60
			6	8.85	6.80	3.00
			7	14.10	9.90	7.20
			8	7.65	6.00	5.00
			9	12.35	10.50	7.60
			10	12.00	9.70	8.35
			11	10.70	7.90	4.20
			12	11.20	8.20	7.00
			13	11.00	9.40	5.25
			14	12.70	8.40	6.85
			15	8.50	5.15	5.00
			16	14.30	8.90	7.05
			17	12.30	9.10	6.80
			18	10.65	8.25	5.15
			19	13.65	11.55	4.55
			20	8.00	6.20	5.85
			21	11.10	9.05	4.80
			22	14.50	10.35	7.20
			23	15.65	10.50	6.80
			24	11.65	7.80	6.45
			25	11.80	11.60	4.65

TABLE A.3 CONTINUED.

Sieve Number (J)	Sieve Size	Sieve Opening (mm)	Particle Number (I)	Dimension (mm)		
				X	Y	Z
2	8	2.360	1	5.00	3.60	2.60
			2	6.10	4.20	3.65
			3	6.70	4.20	2.15
			4	4.20	3.40	1.70
			5	4.30	3.10	1.60
			6	6.70	4.20	1.60
			7	4.10	3.80	3.70
			8	5.60	3.70	2.75
			9	4.55	3.15	2.40
			10	5.00	3.40	1.60
			11	4.60	4.50	2.52
			12	6.20	4.30	2.65
			13	4.60	3.50	1.65
			14	4.80	3.50	2.15
			15	4.00	2.70	2.40
			16	4.00	3.60	2.15
			17	3.70	3.30	1.60
			18	4.65	3.25	2.10
			19	3.65	3.05	1.60
			20	4.65	3.00	1.75
			21	3.00	2.80	1.80
			22	5.40	4.15	2.65
			23	6.10	4.40	2.50
			24	5.35	5.20	3.00
			25	3.50	2.60	2.30

TABLE A.3 CONTINUED.

Sieve Number (J)	Sieve Size	Sieve Opening (mm)	Particle Number (I)	Dimension (mm)		
				X	Y	Z
3	16	1.180	1	2.60	1.80	1.20
			2	3.00	2.00	1.00
			3	2.20	1.65	1.20
			4	3.20	2.55	1.15
			5	2.60	2.10	1.20
			6	2.50	1.50	1.15
			7	2.55	1.60	1.60
			8	2.40	2.00	1.20
			9	1.90	1.60	1.45
			10	2.20	1.90	0.35
			11	2.50	1.70	0.65
			12	2.10	1.65	1.45
			13	2.25	1.60	1.20
			14	3.00	2.40	1.60
			15	2.20	1.65	0.90
			16	1.90	1.30	1.00
			17	2.55	1.50	1.00
			18	3.35	1.90	1.20
			19	2.00	1.70	1.45
			20	2.15	1.45	1.00
			21	1.65	1.30	1.25
			22	2.55	1.65	1.20
			23	2.20	1.60	1.40
			24	2.75	2.00	1.20
			25	3.15	2.60	1.65

TABLE A.3 CONTINUED.

Sieve Number (J)	Sieve Size	Sieve Opening (mm)	Particle Number (I)	Dimension (mm)		
				X	Y	Z
4	30	0.600	1	1.60	1.10	0.60
			2	2.15	1.60	0.60
			3	1.40	1.10	0.65
			4	1.50	1.15	1.10
			5	1.30	1.00	0.60
			6	1.80	1.20	0.75
			7	1.35	1.15	0.65
			8	1.30	0.80	0.65
			9	1.25	0.70	0.50
			10	1.65	1.00	1.00
			11	1.40	1.00	0.70
			12	1.20	0.70	0.65
			13	1.15	0.90	0.70
			14	1.70	1.45	0.75
			15	1.25	1.00	0.75
			16	1.65	1.00	1.00
			17	1.00	1.00	0.65
			18	1.45	0.90	0.60
			19	1.70	0.80	0.65
			20	1.60	1.40	0.65
			21	1.50	1.25	1.10
			22	1.60	1.20	1.00
			23	1.00	1.00	1.00
			24	1.60	1.10	0.90
			25	1.20	0.75	0.70

TABLE A.4 MEASURED X, Y, AND CALCULATED Z DIMENSIONS OF PARTICLE NUMBER (I) RETAINED ON SIEVE NUMBER (J) OF THE NATURAL MATERIAL.

Sieve Number (J)	Sieve Size	Sieve Opening (mm)	Particle Number (I)	Dimension (mm)		
				X	Y	Z
5	50	0.300	1	0.66	0.44	0.43
			2	0.50	0.42	0.40
			3	0.48	0.32	0.29
			4	0.40	0.37	0.33
			5	0.74	0.44	0.38
			6	0.66	0.56	0.47
			7	0.56	0.54	0.43
			8	0.62	0.49	0.37
			9	0.66	0.50	0.37
			10	0.60	0.50	0.37
			11	0.60	0.60	0.43
			12	0.58	0.48	0.34
			13	0.47	0.41	0.28
			14	0.60	0.36	0.24
			15	0.42	0.41	0.27
			16	0.53	0.41	0.25
			17	0.50	0.49	0.30
			18	0.50	0.48	0.28
			19	0.40	0.36	0.20
			20	0.75	0.75	0.41
			21	0.76	0.71	0.38
			22	0.58	0.56	0.27
			23	0.80	0.64	0.29
			24	0.66	0.52	0.22
			25	0.46	0.46	0.14

TABLE A.4 CONTINUED.

Sieve Number (J)	Sieve Size	Sieve Opening (mm)	Particle Number (I)	Dimension (mm)		
				X	Y	Z
6	100	0.150	1	0.31	0.21	0.21
			2	0.23	0.21	0.20
			3	0.25	0.20	0.19
			4	0.42	0.20	0.18
			5	0.22	0.17	0.14
			6	0.36	0.32	0.27
			7	0.18	0.17	0.13
			8	0.44	0.28	0.21
			9	0.28	0.18	0.13
			10	0.24	0.22	0.16
			11	0.28	0.26	0.19
			12	0.40	0.35	0.25
			13	0.34	0.24	0.16
			14	0.30	0.28	0.19
			15	0.36	0.35	0.23
			16	0.30	0.23	0.15
			17	0.23	0.20	0.12
			18	0.40	0.18	0.11
			19	0.35	0.27	0.15
			20	0.26	0.21	0.11
			21	0.38	0.32	0.17
			22	0.27	0.26	0.13
			23	0.32	0.30	0.14
			24	0.44	0.28	0.12
			25	0.44	0.39	0.12

TABLE A.4 CONTINUED.

Sieve Number (J)	Sieve Size	Sieve Opening (mm)	Particle Number (I)	Dimension (mm)		
				X	Y	Z
7	200	0.075	1	0.15	0.12	0.11
			2	0.17	0.13	0.12
			3	0.15	0.10	0.09
			4	0.14	0.12	0.11
			5	0.11	0.10	0.09
			6	0.19	0.14	0.12
			7	0.17	0.12	0.09
			8	0.13	0.09	0.07
			9	0.20	0.16	0.12
			10	0.11	0.10	0.07
			11	0.20	0.11	0.08
			12	0.10	0.09	0.06
			13	0.19	0.14	0.10
			14	0.09	0.05	0.04
			15	0.18	0.16	0.11
			16	0.15	0.08	0.05
			17	0.19	0.14	0.09
			18	0.11	0.11	0.07
			19	0.12	0.10	0.06
			20	0.16	0.15	0.08
			21	0.19	0.14	0.07
			22	0.10	0.05	0.03
			23	0.13	0.11	0.05
			24	0.16	0.13	0.06
			25	0.19	0.12	0.04

APPENDIX B

TABLE B.1 REQUIRED SOIL DENSITY AND WEIGHT OF THE TRIAXIAL TEST SPECIMENS OF SERIES A SAMPLES FOR A RANGE OF RELATIVE DENSITY.

Sample Number		Relative Density (Dr)						
		1.00	0.90	0.80	0.70	0.60	0.50	0.40
1	Density (pcf)	131.00	127.61	124.39	121.33	118.41	115.64	112.99
	Weight (gm)	1400.2	1364.0	1329.6	1296.9	1265.7	1236.0	1207.7
2	Density (pcf)	129.50	125.71	122.14	118.76	115.56	112.53	109.66
	Weight (gm)	1384.2	1343.7	1305.5	1269.4	1235.2	1202.9	1172.1
3	Density (pcf)	126.50	122.27	118.32	114.61	111.13	107.85	104.77
	Weight (gm)	1352.1	1306.9	1264.7	1225.1	1187.9	1152.8	1119.8
4	Density (pcf)	123.00	118.39	114.10	110.12	106.41	102.94	99.68
	Weight (gm)	1314.7	1265.4	1219.6	1177.1	1137.4	1100.3	1065.5
5	Density (pcf)	118.00	112.65	107.76	103.28	99.16	95.35	91.83
	Weight (gm)	1261.3	1204.1	1151.8	1104.0	1059.9	1019.2	981.5

TABLE B.2 REQUIRED SOIL DENSITY AND WEIGHT OF THE TRIAXIAL TEST SPECIMENS OF SERIES B SAMPLES FOR A RANGE OF RELATIVE DENSITY.

Sample Number		Relative Density (Dr)						
		1.00	0.90	0.80	0.70	0.60	0.50	0.40
1	Density (pcf)	117.78	115.15	112.63	110.23	107.92	105.71	103.58
	Weight (gm)	1258.9	1230.8	1203.9	1178.2	1153.5	1129.9	1107.2
2	Density (pcf)	115.99	113.40	110.92	108.55	106.28	104.10	102.01
	Weight (gm)	1239.8	1212.1	1185.6	1160.3	1136.0	1112.7	1090.3
3	Density (pcf)	116.19	113.19	110.34	107.63	105.05	102.59	100.24
	Weight (gm)	1241.9	1209.9	1179.4	1150.4	1122.9	1096.6	1071.5
4	Density (pcf)	117.52	113.79	110.30	107.01	103.91	100.99	98.22
	Weight (gm)	1256.1	1216.3	1178.9	1143.8	1110.7	1079.4	1049.9
5	Density (pcf)	116.39	112.05	108.02	104.28	100.78	97.51	94.45
	Weight (gm)	1244.1	1197.7	1154.6	1114.6	1077.2	1042.3	1009.5
6	Density (pcf)	113.61	108.85	104.48	100.45	96.71	93.24	90.02
	Weight (gm)	1214.4	1163.5	1116.8	1073.7	1033.7	996.7	962.2

TABLE B.3 THE REQUIRED WEIGHT OF THE SOIL RETAINED ON EACH SIEVE FRACTION FOR A RANGE OF RELATIVE DENSITY, SERIES A SAMPLES.

Sample Number 1		Weights of Soil Retained on each Sieve Fraction in (gm) for a Relative Density (Dr) of						
Sieve Size	Percent Retained	1.0	0.9	0.8	0.7	0.6	0.5	0.4
4	19.20	268.8	261.9	255.3	249.0	243.0	237.3	231.9
8	19.03	266.5	259.6	253.0	246.8	240.9	235.2	229.8
16	14.08	197.1	192.1	187.2	182.6	178.2	174.0	170.0
30	12.18	170.5	166.1	161.9	158.0	154.2	150.5	147.1
50	9.42	131.9	128.5	125.2	122.2	119.2	116.4	113.8
100	8.15	114.1	111.2	108.4	105.7	103.2	100.7	98.4
200	5.93	83.0	80.9	78.8	76.9	75.1	73.3	71.6
Pan	12.00	168.0	163.7	159.6	155.6	151.9	148.3	144.9

Sample Number 2		Weights of Soil Retained on each Sieve Fraction in (gm) for a Relative Density (Dr) of						
Sieve Size	Percent Retained	1.0	0.9	0.8	0.7	0.6	0.5	0.4
8	19.20	265.8	258.0	250.7	243.7	237.2	231.0	225.0
16	19.03	263.4	255.7	248.4	241.6	235.1	228.9	223.1
30	14.08	194.9	189.2	183.8	178.7	173.9	169.4	165.0
50	12.18	168.6	163.7	159.0	154.6	150.4	146.5	142.8
100	9.42	130.4	126.6	123.0	119.6	116.4	113.3	110.4
200	8.15	112.8	109.5	106.4	103.5	100.7	98.0	95.5
Pan	17.93	248.0	240.9	234.1	227.6	221.5	215.7	210.2

TABLE B.3 CONTINUED.

Sample Number 3		Weights of Soil Retained on each Sieve Fraction in (gm) for a Relative Density (Dr) of						
Sieve Size	Percent Retained	1.0	0.9	0.8	0.7	0.6	0.5	0.4
16	19.20	259.6	250.9	242.8	235.2	228.1	221.3	215.0
30	19.03	257.3	248.7	240.7	233.1	226.1	219.4	213.1
50	14.08	190.4	184.0	178.1	172.5	167.3	162.3	157.7
100	12.18	164.7	159.2	154.0	149.2	144.7	140.4	136.4
200	9.42	127.4	123.1	119.1	115.4	111.9	108.6	105.5
Pan	26.08	352.6	340.8	329.8	319.5	309.8	300.7	292.0

Sample Number 4		Weights of Soil Retained on each Sieve Fraction in (gm) for a Relative Density (Dr) of						
Sieve Size	Percent Retained	1.0	0.9	0.8	0.7	0.6	0.5	0.4
30	19.20	252.4	243.0	234.2	226.0	218.4	211.3	204.6
50	19.03	250.2	240.8	232.1	224.0	216.4	209.4	202.8
100	14.08	185.1	178.2	171.7	165.7	160.1	154.9	150.0
200	12.18	160.1	154.1	148.5	143.4	138.5	134.0	129.8
Pan	35.50	466.7	449.2	433.0	417.9	403.8	390.6	378.3

Sample Number 5		Weights of Soil Retained on each Sieve Fraction in (gm) for a Relative Density (Dr) of						
Sieve Size	Percent Retained	1.0	0.9	0.8	0.7	0.6	0.5	0.4
50	19.20	242.2	231.2	221.1	212.0	203.5	195.7	188.4
100	19.03	240.0	229.1	219.2	210.1	201.7	194.0	186.8
200	14.08	177.6	196.5	162.2	155.4	149.2	143.5	138.2
Pan	47.68	601.4	574.1	549.2	526.4	505.4	486.0	468.8

TABLE B.4 THE REQUIRED WEIGHT OF THE SOIL RETAINED ON EACH SIEVE FRACTION FOR A RANGE OF RELATIVE DENSITY, SERIES B SAMPLES.

Sample Number 1		Weights of Soil Retained on each Sieve Fraction in (gm) for a Relative Density (Dr) of						
Sieve Size	Percent Retained	1.0	0.9	0.8	0.7	0.6	0.5	0.4
3/8"	0.61	7.7	7.5	7.3	7.2	7.0	6.9	6.8
4	28.98	364.8	356.7	348.9	341.4	334.3	327.4	320.9
8	36.81	463.4	453.1	443.2	433.7	424.6	415.9	407.6
16	13.81	173.9	170.0	166.3	162.7	159.3	156.0	152.9
30	6.81	85.7	83.8	82.0	80.2	78.6	76.9	75.4
50	4.15	52.2	51.1	50.0	48.9	47.9	46.9	45.9
100	3.08	38.8	37.9	37.1	36.3	35.5	34.8	34.1
200	2.07	26.1	25.5	24.9	24.4	23.9	23.4	22.9
Pan	3.68	46.3	45.3	44.3	43.4	42.4	41.6	40.7

Sample Number 2		Weights of Soil Retained on each Sieve Fraction in (gm) for a Relative Density (Dr) of						
Sieve Size	Percent Retained	1.0	0.9	0.8	0.7	0.6	0.5	0.4
4	0.61	7.6	7.4	7.2	7.1	6.9	6.8	6.7
8	28.98	359.3	351.3	343.6	336.3	329.2	322.5	316.0
16	36.81	456.4	446.2	436.4	427.1	418.2	409.6	401.3
30	13.81	171.2	167.4	163.7	160.2	156.9	153.7	150.6
50	6.81	84.4	82.5	80.7	79.0	77.4	75.8	74.2
100	4.15	51.5	50.3	49.2	48.2	47.1	46.2	45.2
200	3.08	38.2	37.3	36.5	35.7	35.0	34.3	33.6
Pan	5.75	71.3	69.7	68.2	66.7	65.3	64.0	62.7

TABLE B.4 CONTINUED.

Sample Number 3		Weights of Soil Retained on each Sieve Fraction in (gm) for a Relative Density (Dr) of						
Sieve Size	Percent Retained	1.0	0.9	0.8	0.7	0.6	0.5	0.4
8	0.61	7.6	7.4	7.2	7.0	6.8	6.7	6.5
16	28.98	359.9	350.6	341.8	333.4	325.4	317.8	310.5
30	36.81	457.1	445.4	434.1	423.5	413.3	403.7	394.4
50	13.81	171.5	167.1	162.9	158.9	155.1	151.4	148.0
100	6.81	84.6	82.4	80.3	78.3	76.5	74.7	73.0
200	4.15	51.5	50.2	48.9	47.7	46.6	45.5	44.5
Pan	8.83	109.7	106.8	104.1	101.6	99.2	96.8	94.6

Sample Number 4		Weights of Soil Retained on each Sieve Fraction in (gm) for a Relative Density (Dr) of						
Sieve Size	Percent Retained	1.0	0.9	0.8	0.7	0.6	0.5	0.4
16	0.61	7.7	7.4	7.2	7.0	6.8	6.6	6.4
30	28.98	364.0	352.5	341.6	331.5	321.9	312.8	304.3
50	36.81	462.4	447.7	434.0	421.0	408.8	397.3	386.5
100	13.81	173.5	168.0	162.8	158.0	153.4	149.1	145.0
200	6.81	85.5	82.8	80.3	77.9	75.6	73.5	71.5
Pan	12.98	163.0	157.9	153.0	148.5	144.2	140.1	136.3

TABLE B.4 CONTINUED.

Sample Number 5		Weights of Soil Retained on each Sieve Fraction in (gm) for a Relative Density (Dr) of						
Sieve Size	Percent Retained	1.0	0.9	0.8	0.7	0.6	0.5	0.4
30	0.61	7.6	7.3	7.0	6.8	6.6	6.4	6.2
50	28.98	360.5	347.2	334.6	323.0	312.2	302.1	292.6
100	36.81	458.0	440.9	425.0	410.3	396.5	383.7	371.6
200	13.81	171.8	165.4	159.5	153.9	148.8	143.9	139.4
Pan	19.79	246.2	237.1	228.5	220.6	213.2	206.3	199.8

Sample Number 6		Weights of Soil Retained on each Sieve Fraction in (gm) for a Relative Density (Dr) of						
Sieve Size	Percent Retained	1.0	0.9	0.8	0.7	0.6	0.5	0.4
50	0.61	7.4	7.1	6.8	6.5	6.3	6.1	5.9
100	28.98	351.9	337.2	323.6	311.2	299.6	288.8	278.8
200	36.81	447.0	428.3	411.1	395.2	380.5	366.9	354.2
Pan	33.60	408.0	390.9	375.2	360.8	347.3	334.9	323.3

APPENDIX C

**TABLE C.1 MAXIMUM AND MINIMUM DENSITIES AND VOID RATIOS OF
SERIES A SAMPLES, C/P MATERIAL.**

Sample Number	0	1	2	3	4	5	100
Percent Fine	0.0	12.00	17.90	26.10	35.50	47.70	100
Maximum Grain Size (mm)	40.00	9.50	4.75	2.36	1.18	0.60	0.075
Maximum Density (pcf)	134.4	131.0	129.5	126.5	123.0	118.0	102.6
Minimum Density (pcf)	111.0	103.5	99.5	94.0	88.5	80.0	68.3
Maximum void Ratio	0.539	0.650	0.716	0.817	0.930	1.135	1.501
Minimum Void Ratio	0.271	0.304	0.319	0.350	0.388	0.447	0.665

1 pcf = $1.602(10^{-2})$ g/cm³

1 inch = 25.4 mm

**TABLE C.2 MAXIMUM AND MINIMUM DENSITIES AND VOID RATIOS OF
SERIES B SAMPLES, C/P MATERIAL.**

Sample Number	0	1	2	3	4	5	6	100
Percent Fine	0.0	3.68	5.75	8.75	12.93	19.79	33.60	100
Maximum Grain Size (mm)	40.0	12.70	9.50	4.75	2.36	1.18	0.60	0.075
Maximum Density (pcf)	119.0	118.7	118.2	118.9	117.5	116.4	113.6	102.6
Minimum Density (pcf)	98.0	95.9	94.4	91.8	88.5	83.9	79.1	68.3
Maximum void Ratio	0.743	0.781	0.809	0.860	0.929	1.036	1.160	1.501
Minimum Void Ratio	0.435	0.439	0.445	0.436	0.453	0.467	0.503	0.665

1 pcf = $1.602(10^{-2})$ g/cm³

1 inch = 25.4 mm

**TABLE C.3 MAXIMUM AND MINIMUM DENSITIES AND VOID RATIOS OF
SERIES A AND B SAMPLES, NATURAL AND 50/50
MATERIALS.**

Material	Natural				50/50	
Series	A		B		A	B
Sample Number	1	2	3	4	1	4
Percent Fine	12.00	17.90	26.10	12.93	12.00	12.93
Maximum Grain Size (mm)	9.50	4.75	2.36	2.36	9.50	2.36
Maximum Density (pcf)	139.6	133.6	128.2	124.1	139.0	121.8
Minimum Density (pcf)	111.9	102.8	94.7	94.6	109.1	92.2
Maximum void Ratio	0.526	0.662	0.804	0.806	0.565	0.851
Minimum Void Ratio	0.223	0.278	0.332	0.376	0.230	0.403

1 pcf = $1.602(10^{-2})$ g/cm³

1 inch = 25.4 mm

APPENDIX D

TABLE D.1 ANGLE OF REPOSE OF SERIES A SAMPLES, C/P MATERIAL.

Sample Number	0	1	2	3	4	5	100
Percent Fine	0.0	12.00	17.90	26.10	35.50	47.70	100.0
Maximum Grain Size (mm)	40.00	9.50	4.75	2.36	1.18	0.60	0.075
Angle of Repose (ϕ_r)	37.00	35.00	32.00	28.00	28.00	23.00	26.00
	40.00	34.00	30.00	29.00	27.00	28.00	24.00
	37.00	32.00	33.00	27.00	26.00	26.00	21.00
	35.00	-	-	30.00	30.00	30.00	-
	40.00	-	-	-	-	-	-
Average Value of The Angle of Repose (ϕ_r)	37.80	33.67	31.61	28.50	27.75	26.75	23.67

1 inch = 24.5 mm

TABLE D.2 ANGLE OF REPOSE OF SERIES B SAMPLES, C/P MATERIAL.

Sample Number	0	1	4	5	6	100
Percent Fine	0.0	3.68	12.93	19.79	33.60	100.0
Maximum Grain Size (mm)	40.00	12.70	2.36	1.18	0.60	0.075
Angle of Repose (ϕ_r)	37.00	34.00	30.00	25.00	23.00	26.00
	40.00	36.00	31.00	26.00	23.00	24.00
	37.00	37.00	31.00	27.00	24.00	21.00
	35.00	32.00	28.00	27.00	24.00	-
	40.00	34.00	26.00	28.00	26.00	-
	-	34.00	30.00	-	-	-
	-	-	30.00	-	-	-
	-	-	31.00	-	-	-
Average Value of The Angle of Repose (ϕ_r)	37.80	34.50	29.63	26.60	24.00	23.67

1 inch = 24.5 mm

**TABLE D.3 ANGLE OF REPOSE OF SERIES A AND B SAMPLES,
NATURAL AND 50/50 MATERIALS.**

Material	Natural				50/50	
Series	A		B		A	B
Sample Number	1	2	3	4	1	4
Percent Fine	12.00	17.90	26.10	12.93	12.00	12.93
Maximum Grain Size (mm)	9.50	4.75	2.36	2.36	9.50	2.36
Angle of Repose (ϕ_r)	26.00	27.00	25.00	24.00	29.00	28.00
	28.00	28.00	26.00	25.00	27.00	29.00
	29.00	28.00	26.00	29.00	28.00	28.00
	32.00	28.50	27.00	30.00	30.00	27.00
	-	-	29.00	-	30.00	-
	-	-	29.00	-	30.00	-
	-	-	-	-	30.00	-
Average Value of The Angle of Repose (ϕ_r)	28.75	27.88	27.00	27.00	29.25	28.00

1 inch = 24.5 mm

APPENDIX E

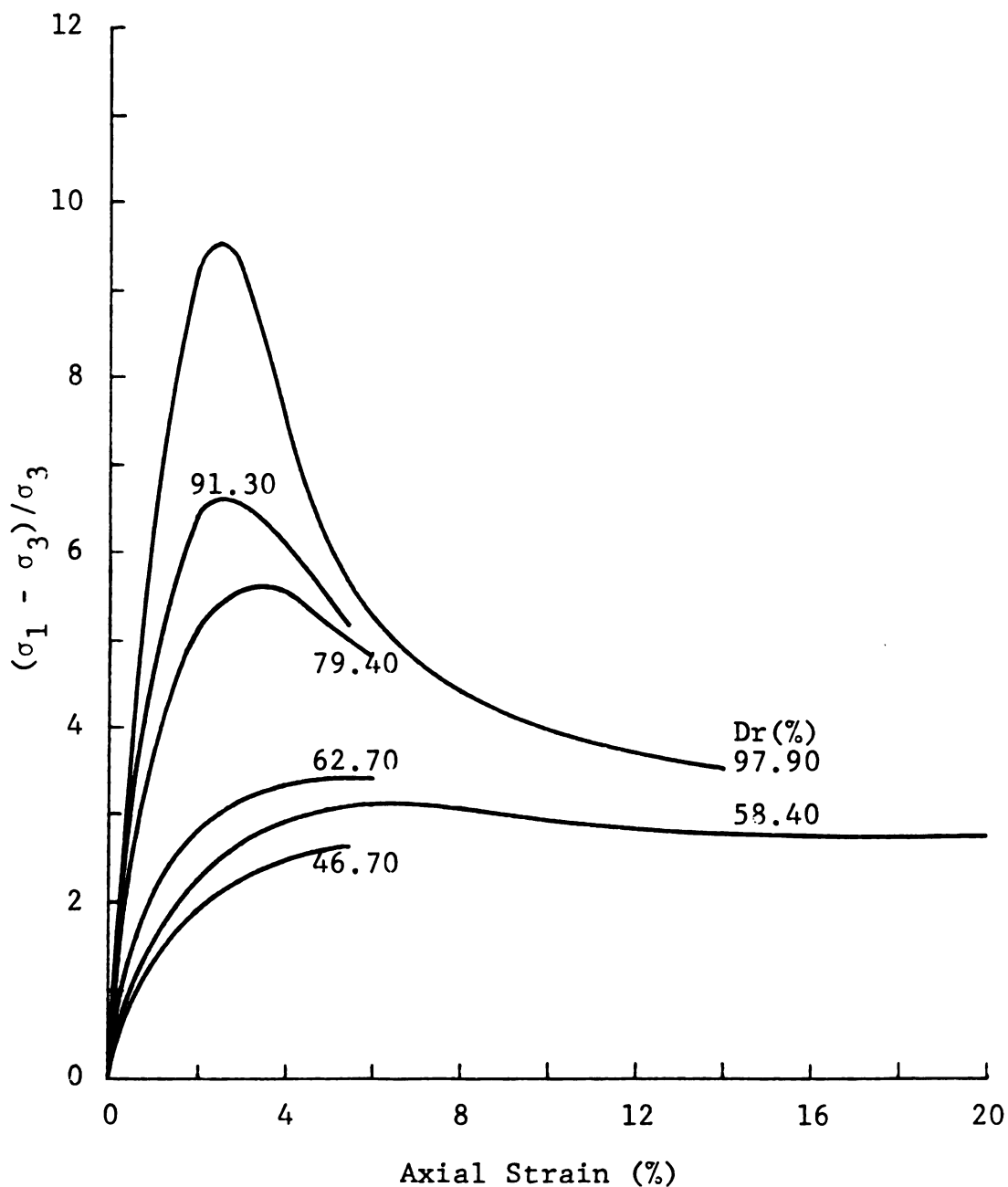


FIGURE E.1 NORMALIZED PRINCIPAL STRESS DIFFERENCE VERSUS AXIAL STRAIN FOR A CONFINING PRESSURE OF 5 PSI, AND DIFFERENT RELATIVE DENSITY (D_r) OF SAMPLE 1 OF SERIES A OF THE C/P MATERIAL.

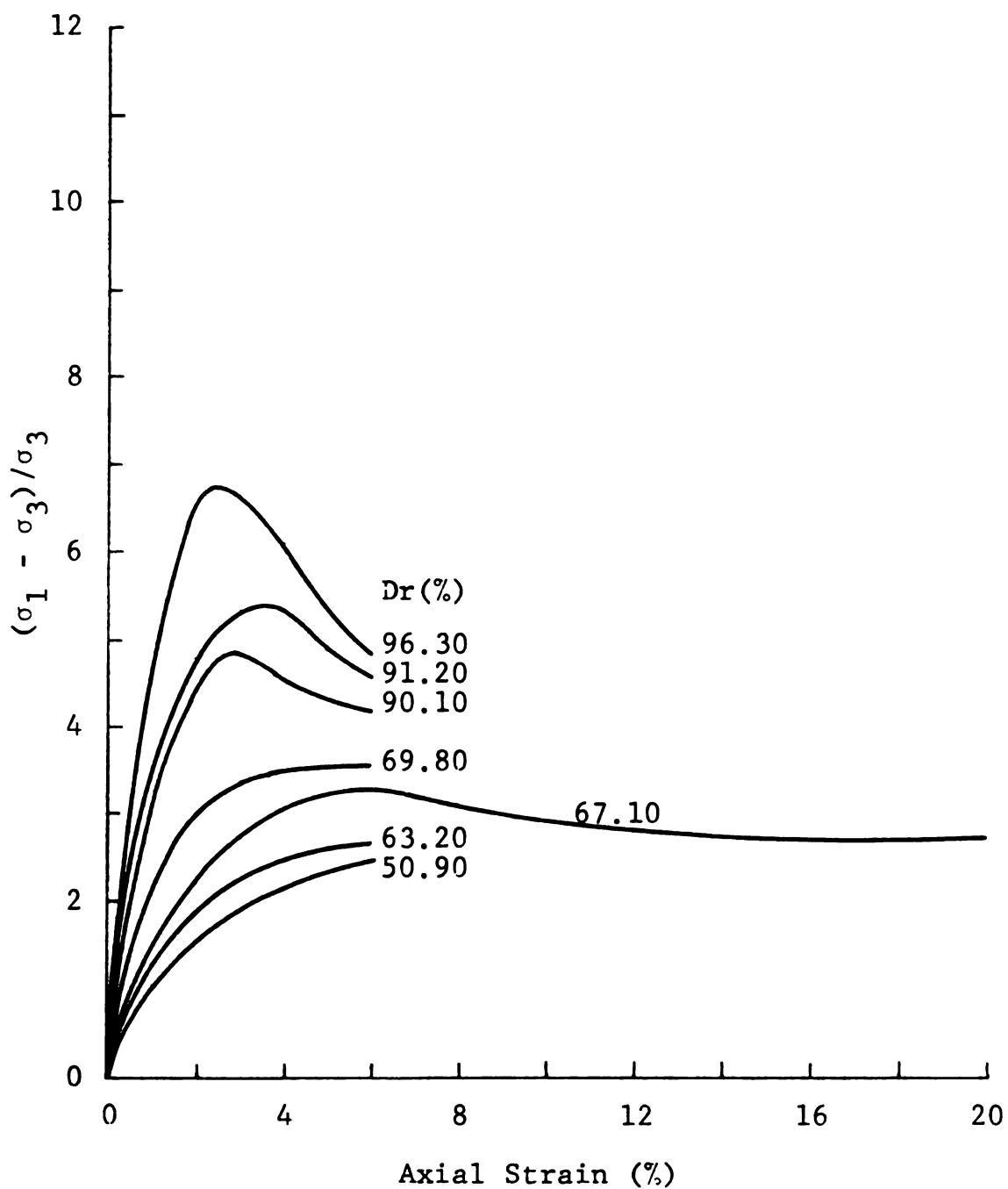


FIGURE E.2 NORMALIZED PRINCIPAL STRESS DIFFERENCE VERSUS AXIAL STRAIN FOR A CONFINING PRESSURE OF 5 PSI, AND DIFFERENT RELATIVE DENSITY (D_r) OF SAMPLE 2 OF SERIES A OF THE C/P MATERIAL.

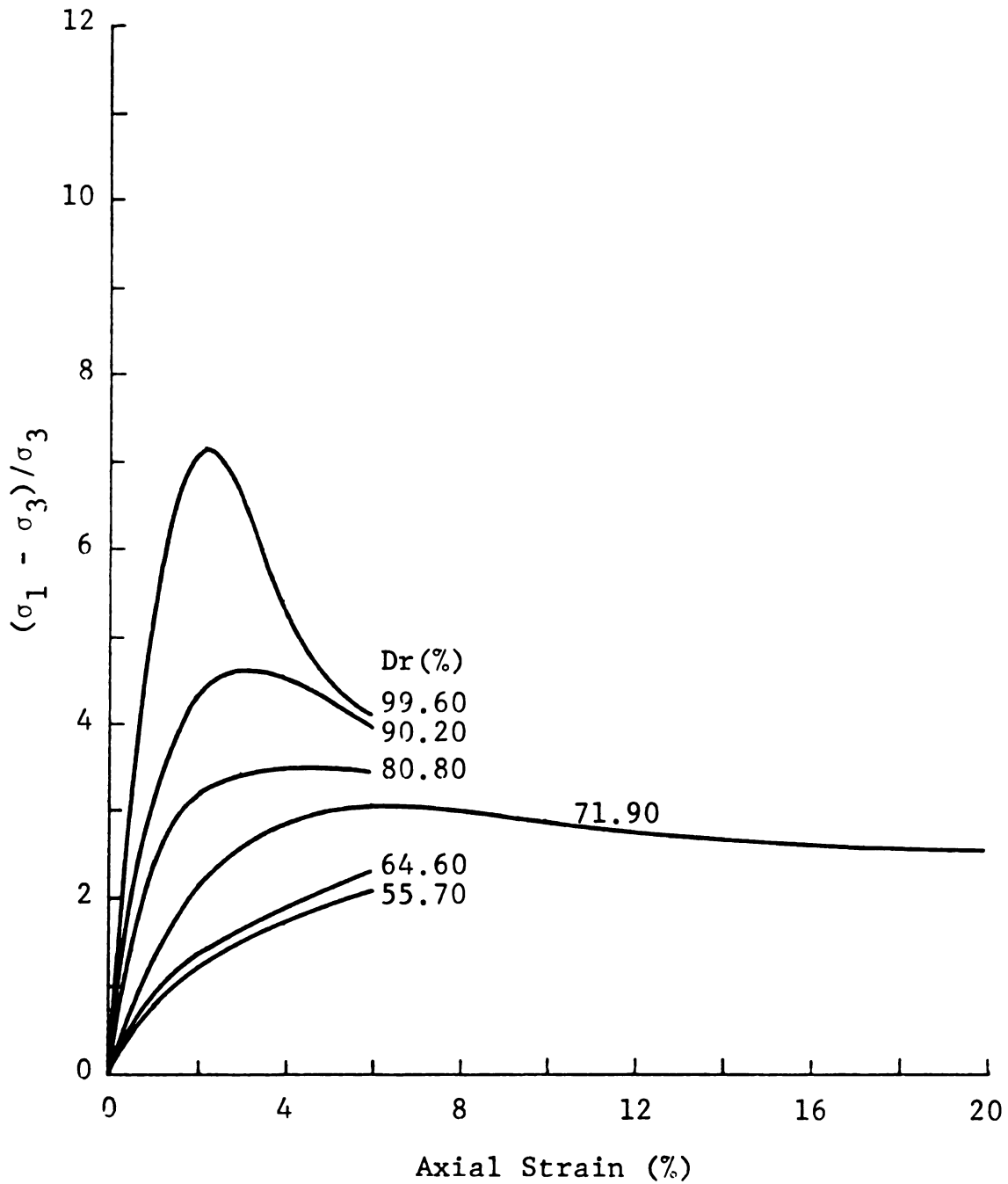


FIGURE E.3 NORMALIZED PRINCIPAL STRESS DIFFERENCE VERSUS AXIAL STRAIN FOR A CONFINING PRESSURE OF 5 PSI, AND DIFFERENT RELATIVE DENSITY (D_r) OF SAMPLE 3 OF SERIES A OF THE C/P MATERIAL.

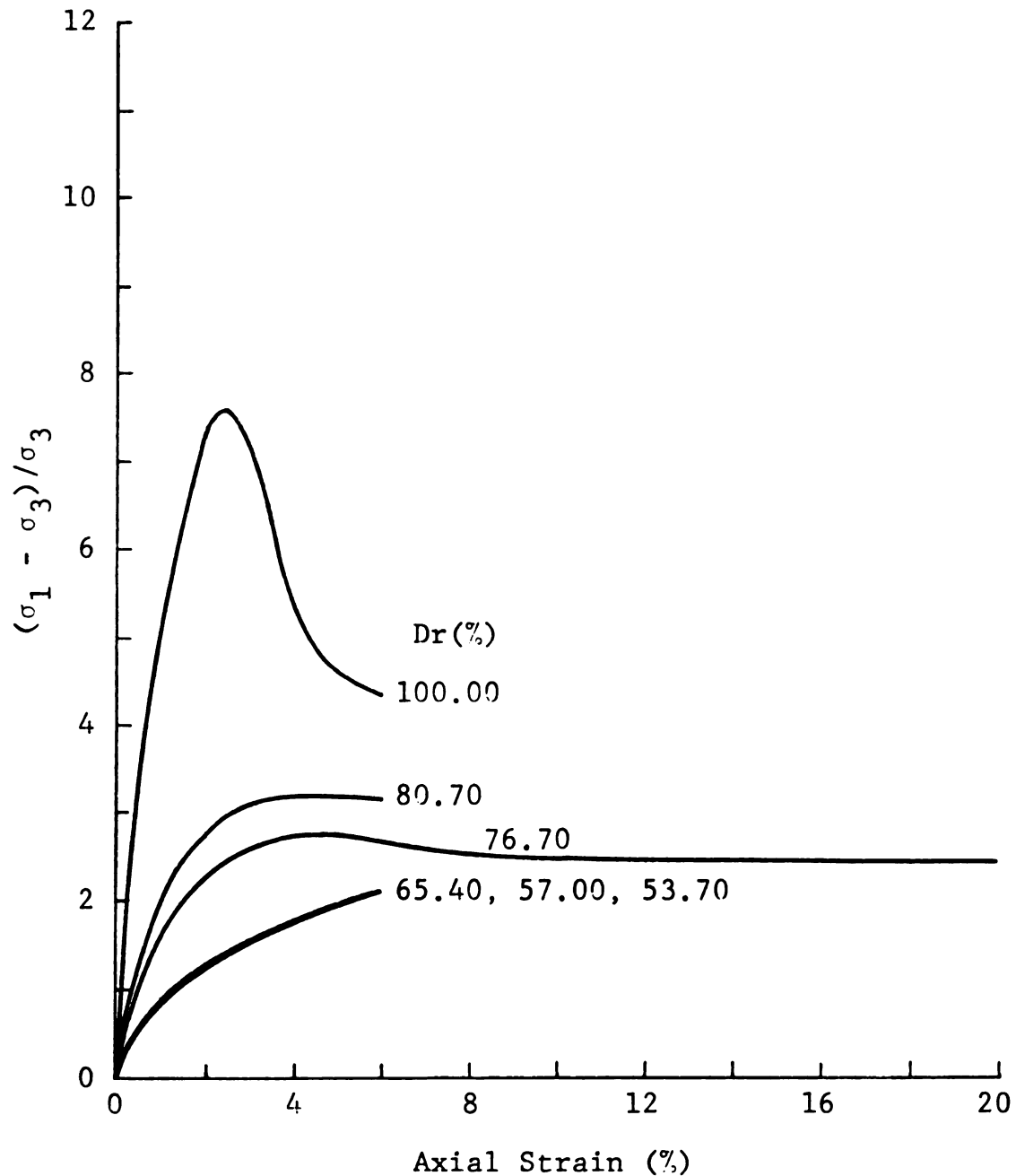


FIGURE E.4 NORMALIZED PRINCIPAL STRESS DIFFERENCE VERSUS AXIAL STRAIN FOR A CONFINING PRESSURE OF 5 PSI, AND DIFFERENT RELATIVE DENSITY (D_r) OF SAMPLE 4 OF SERIES A OF THE C/P MATERIAL.

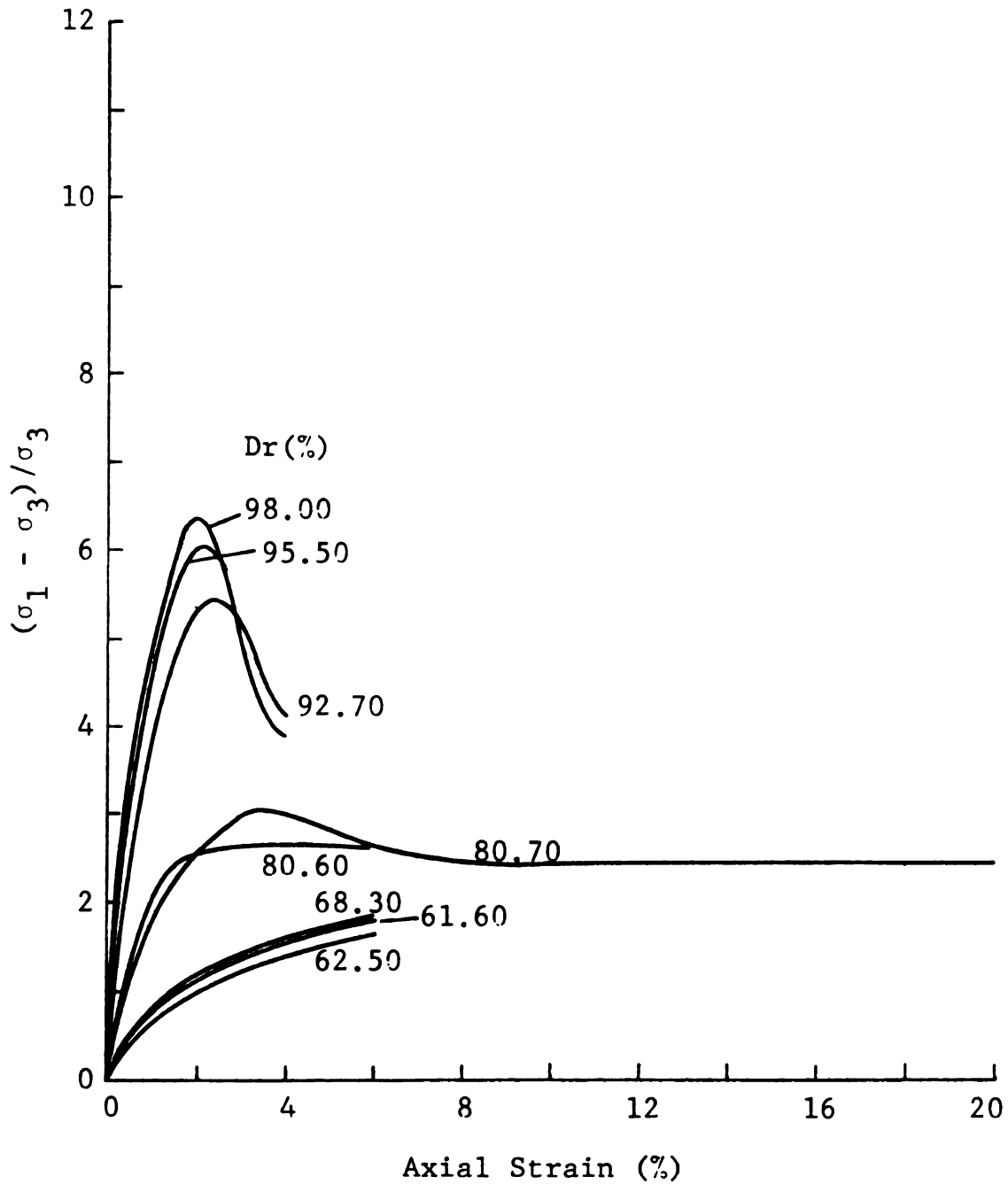


FIGURE E.5 NORMALIZED PRINCIPAL STRESS DIFFERENT VERSUS AXIAL STRAIN FOR A CONFINING PRESSURE OF 5 PSI, AND DIFFERENT RELATIVE DENSITY (D_r) OF SAMPLE 5 OF SERIES A OF THE C/P MATERIAL.

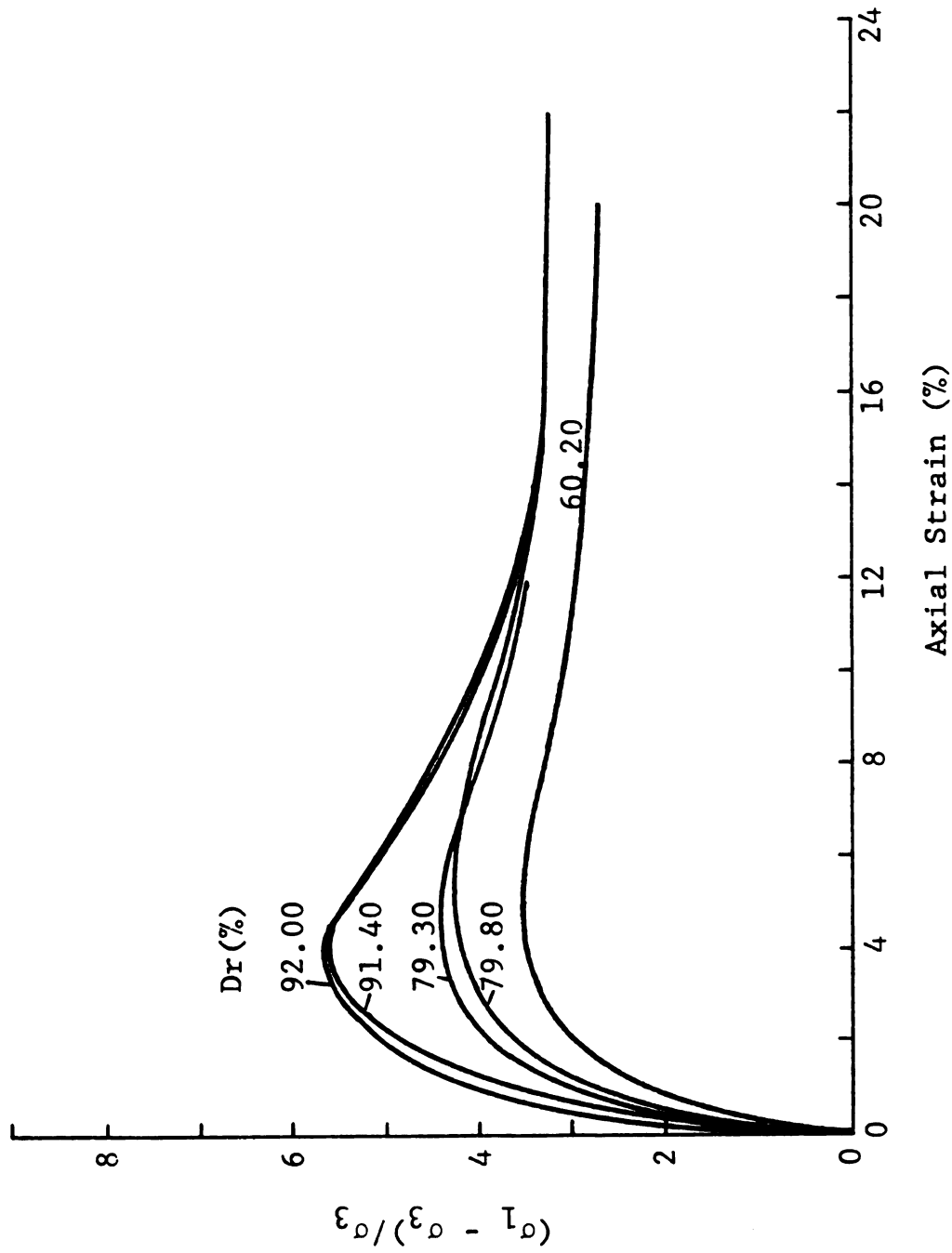


FIGURE E.6 NORMALIZED PRINCIPAL STRESS DIFFERENCE VERSUS AXIAL STRAIN FOR A CONFINING PRESSURE OF 5 PSI, AND DIFFERENT RELATIVE DENSITY (D_r) OF SAMPLE 1 OF SERIES B OF THE C/PMATERIAL.

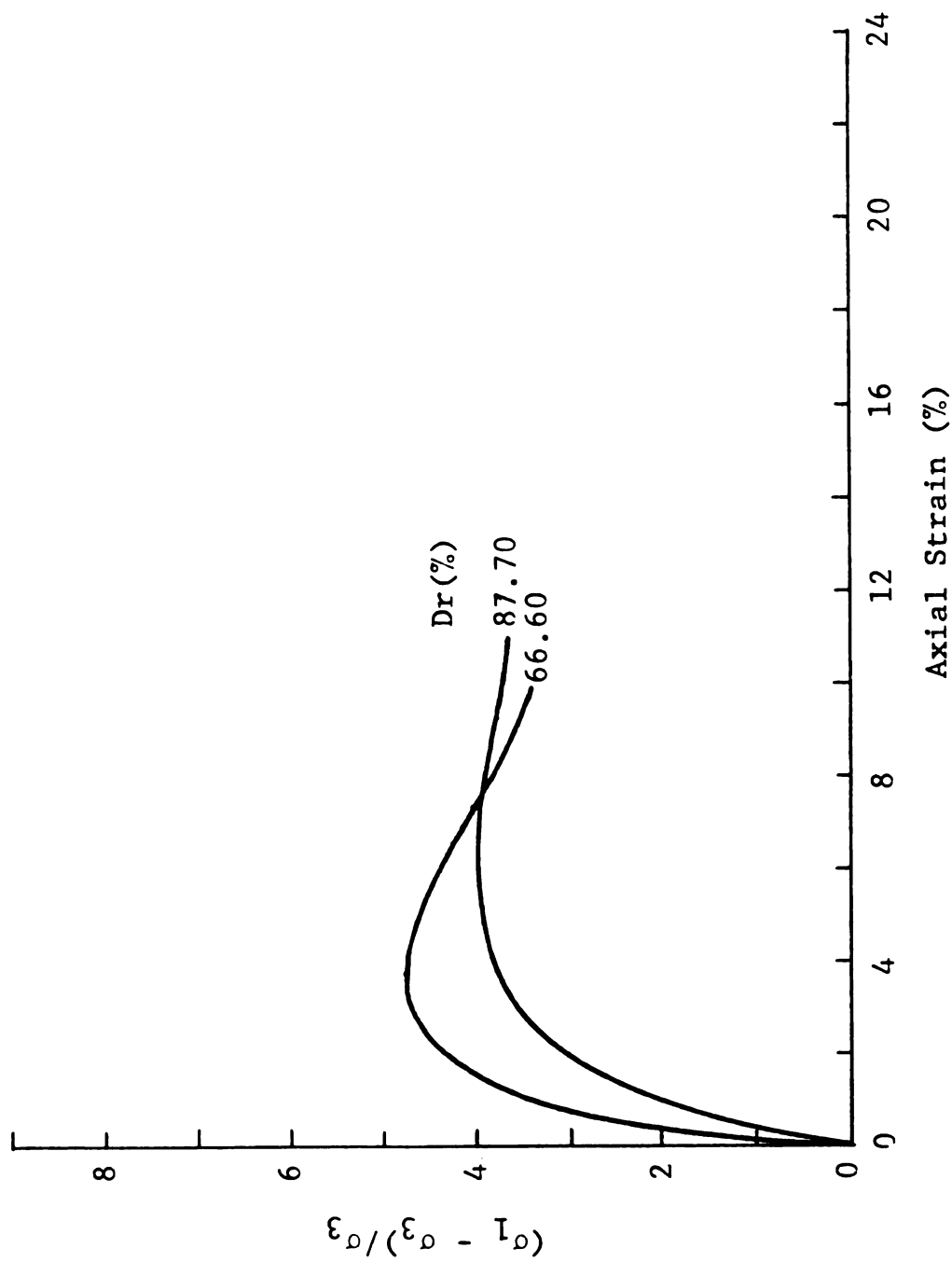


FIGURE E.7 NORMALIZED PRINCIPAL STRESS DIFFERENCE VERSUS AXIAL STRAIN FOR A CONFINING PRESSURE OF 5 PSI, AND DIFFERENT RELATIVE DENSITY (Dr) OF SAMPLE 3 OF SERIES B OF THE C/P MATERIAL.

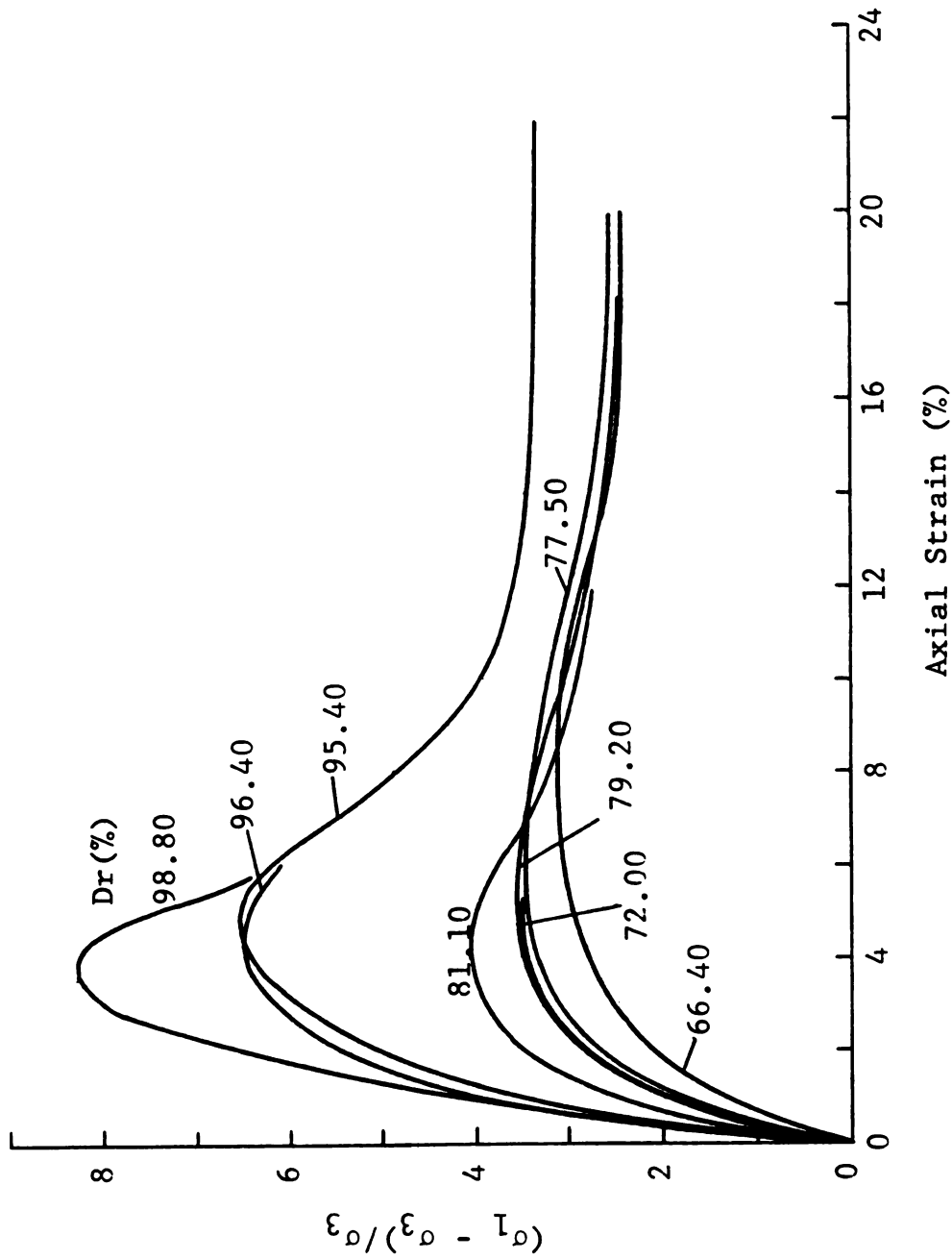


FIGURE E.8 NORMALIZED PRINCIPAL STRESS DIFFERENCE VERSUS AXIAL STRAIN FOR A CONFINING PRESSURE OF 5 PSI, AND DIFFERENT RELATIVE DENSITY (D_r) OF SAMPLE 4 OF SERIES B OF THE C/P MATERIAL.

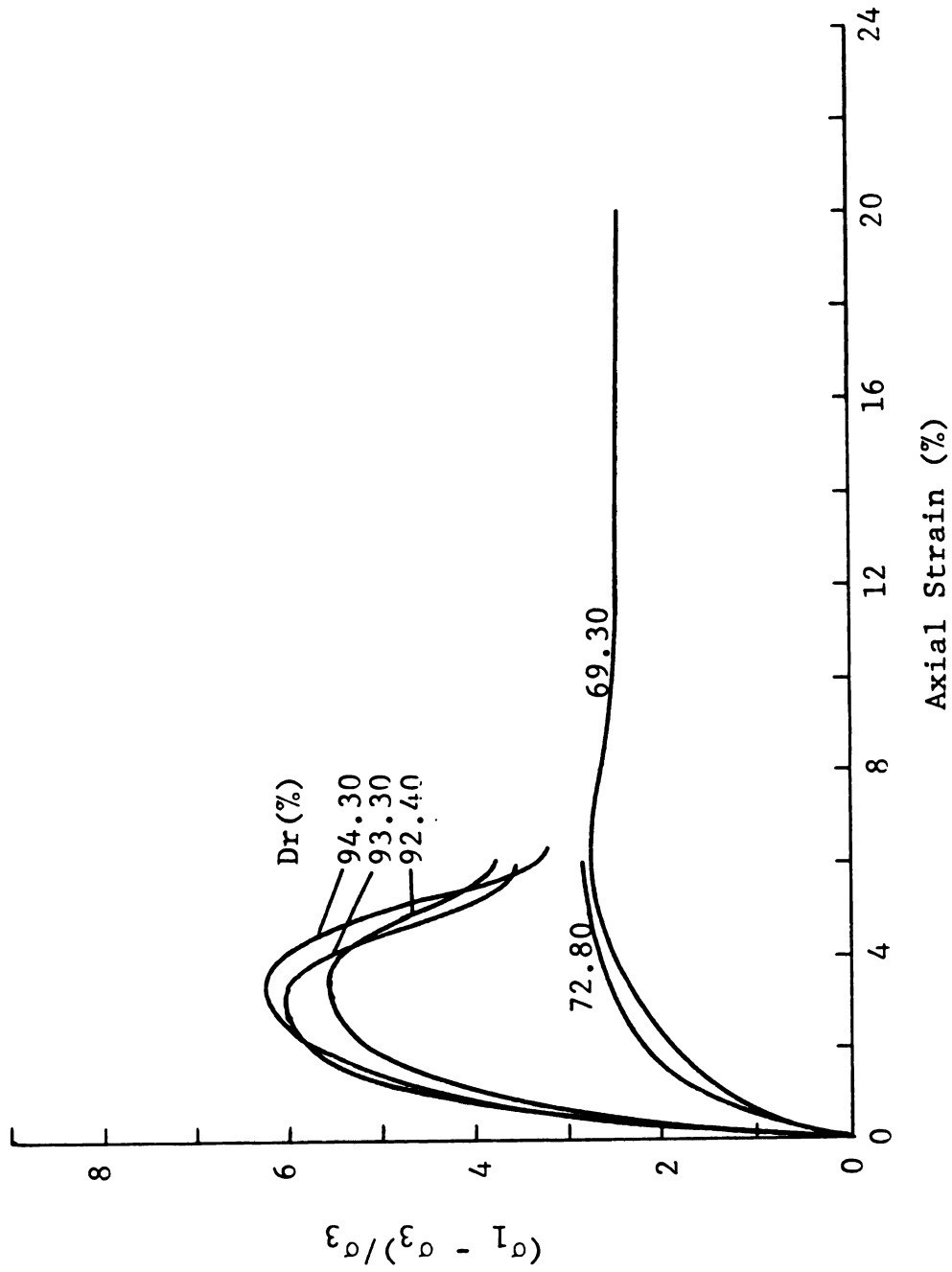


FIGURE E.9 NORMALIZED PRINCIPAL STRESS DIFFERENCE VERSUS AXIAL STRAIN FOR A CONFINING PRESSURE OF 5 PSI, AND DIFFERENT RELATIVE DENSITY (Dr) OF SAMPLE 5 OF SERIES B OF THE C/P MATERIAL.

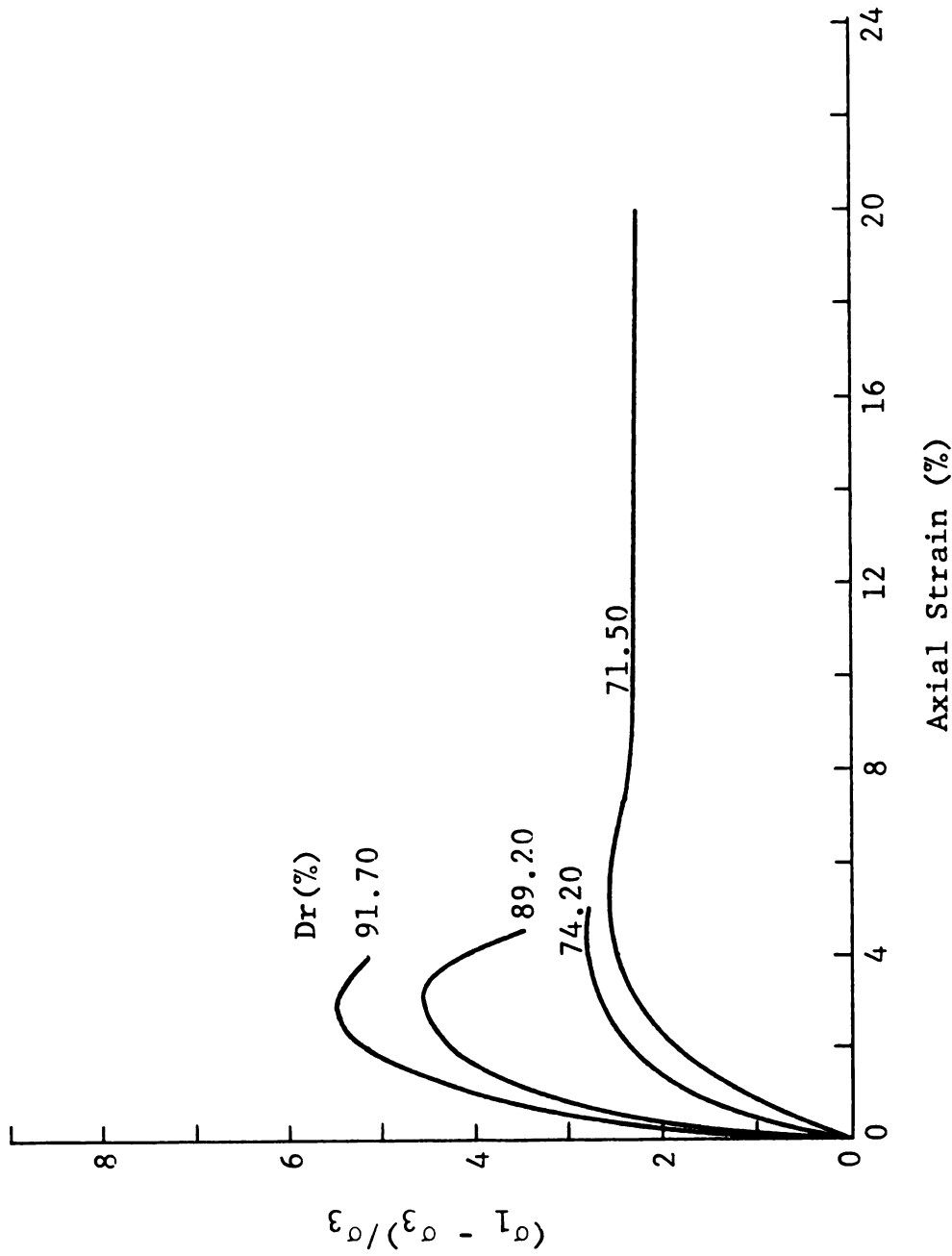


FIGURE E.10 NORMALIZED PRINCIPAL STRESS DIFFERENCE VERSUS AXIAL STRAIN FOR A CONFINING PRESSURE OF 5 PSI, AND DIFFERENT RELATIVE DENSITY (Dr) OF SAMPLE 6 OF SERIES B OF THE C/P MATERIAL.

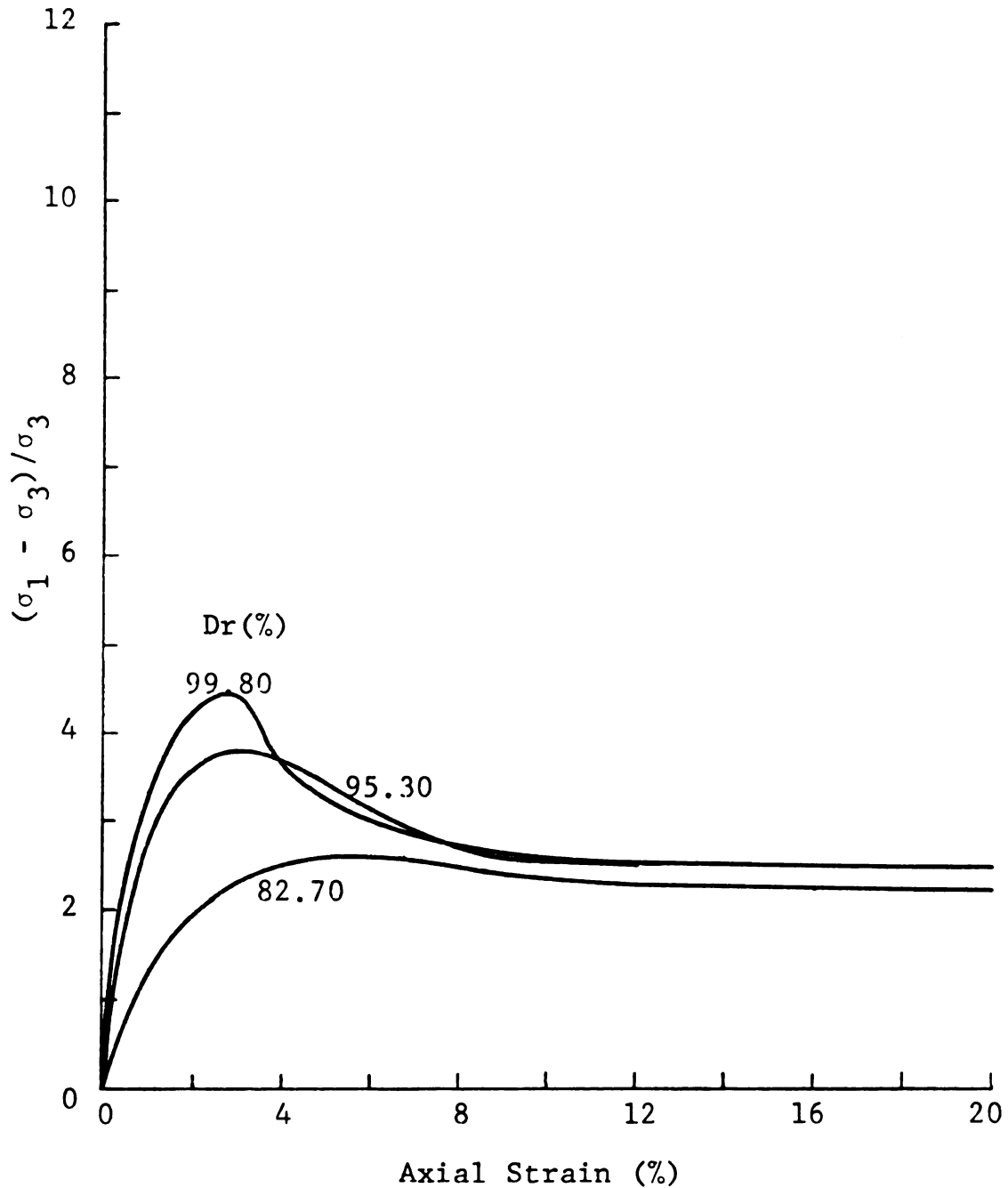


FIGURE E.11 NORMALIZED PRINCIPAL STRESS DIFFERENCE VERSUS AXIAL STRAIN FOR A CONFINING PRESSURE OF 5 PSI, AND DIFFERENT RELATIVE DENSITY (D_r) OF SAMPLE 100 (ONE HUNDRED PERCENT FINE CONTENT) OF SERIES A OR B OF THE C/P MATERIAL.

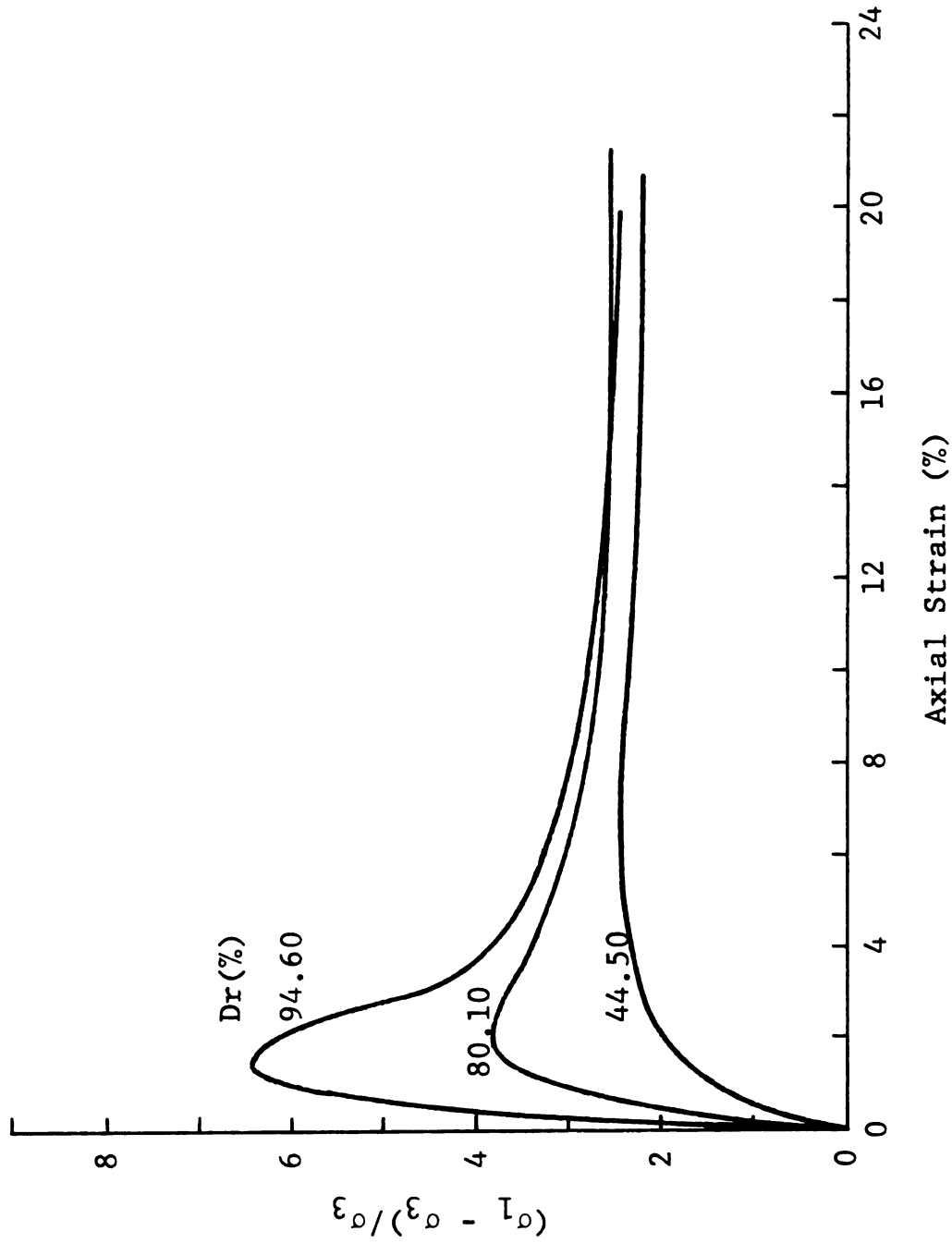


FIGURE E.12 NORMALIZED PRINCIPAL STRESS DIFFERENCE VERSUS AXIAL STRAIN FOR A CONFINING PRESSURE OF 5 PSI, AND DIFFERENT RELATIVE DENSITY (Dr) OF SAMPLE 1 OF SERIES A OF THE NATURAL MATERIAL.

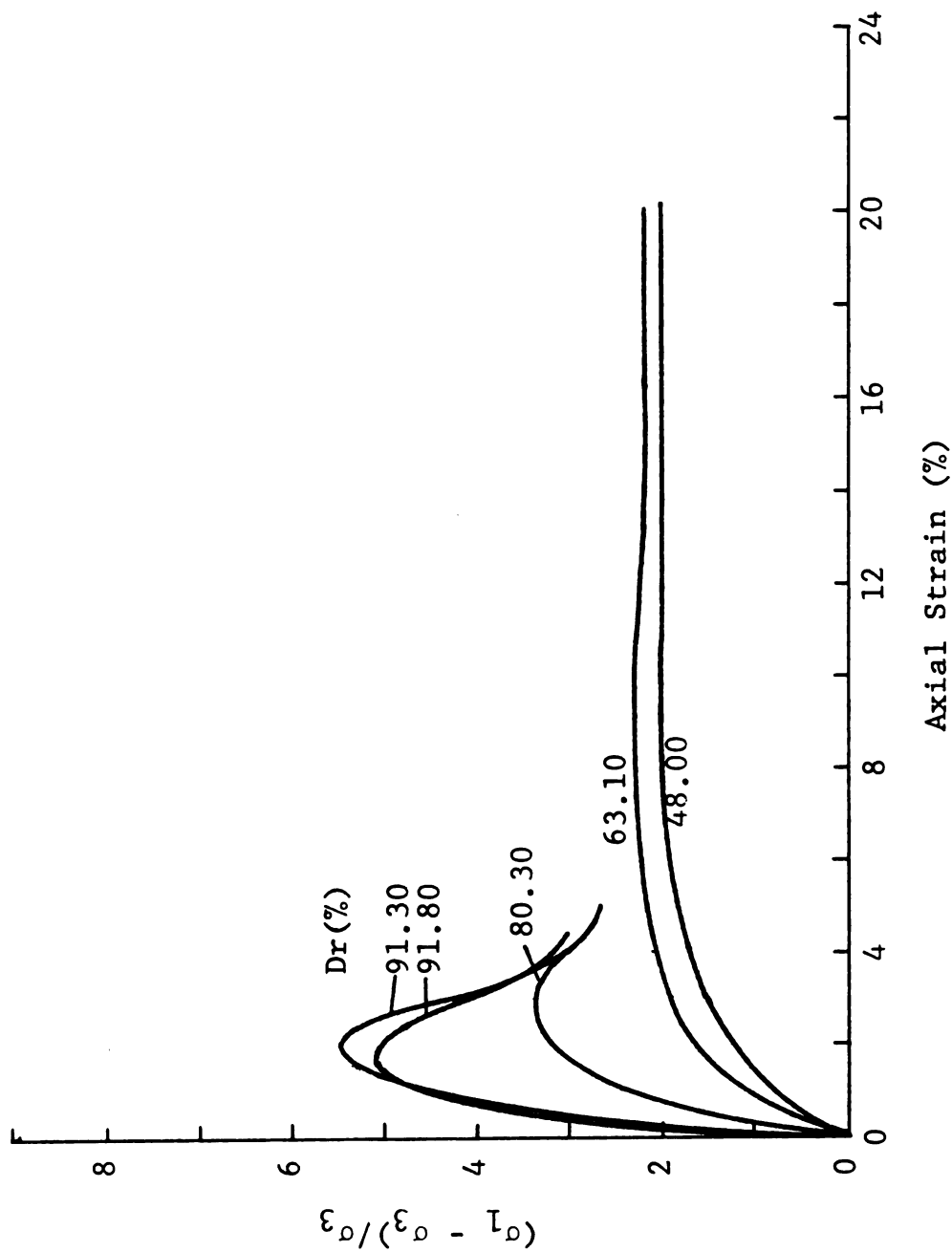


FIGURE E.13 NORMALIZED PRINCIPAL STRESS DIFFERENCE VERSUS AXIAL STRAIN FOR A CONFINING PRESSURE OF 5 PSI, AND DIFFERENT RELATIVE DENSITY (D_r) OF SAMPLE 3 OF SERIES A OF THE NATURAL MATERIAL.

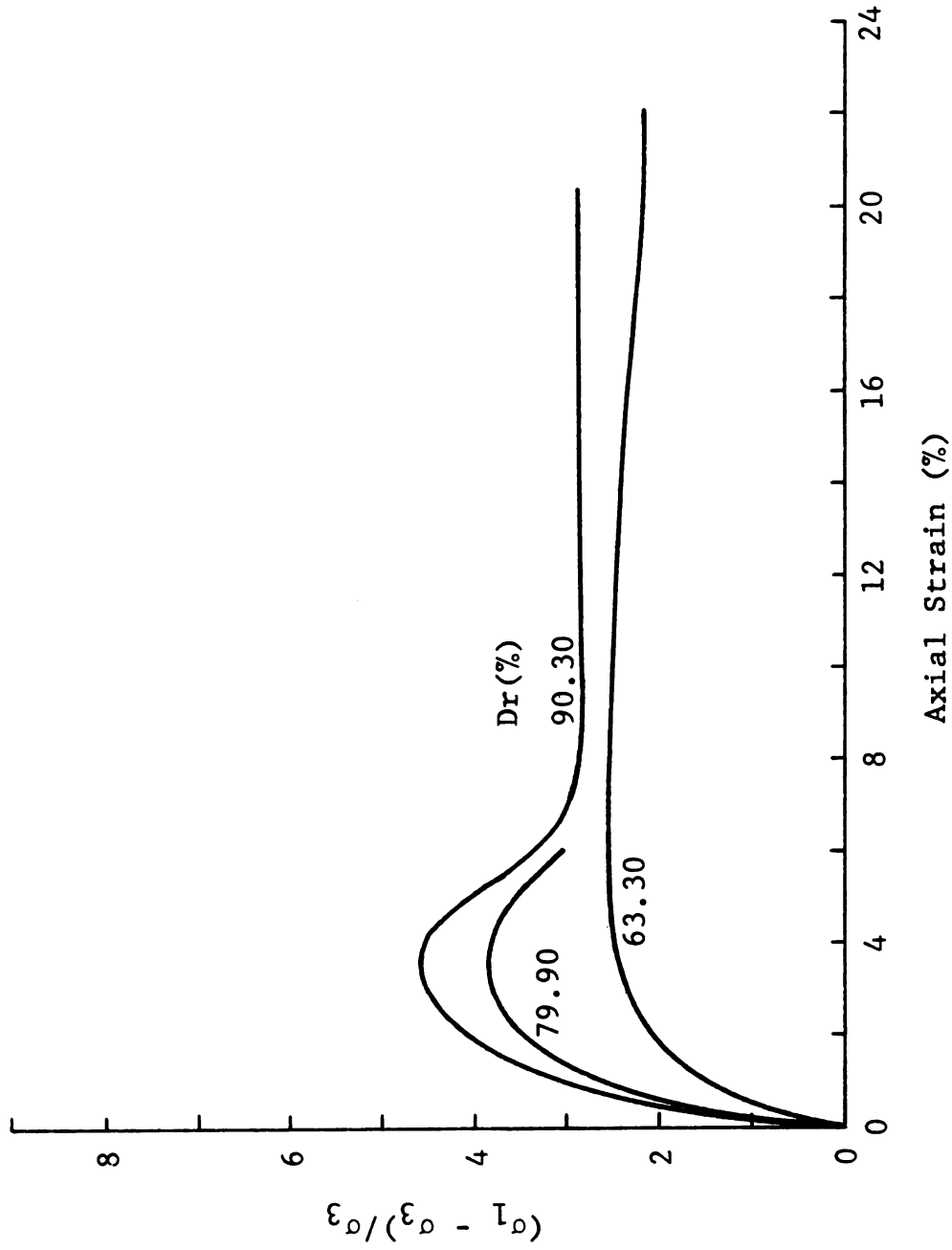


FIGURE E.14 NORMALIZED PRINCIPAL STRESS DIFFERENCE VERSUS AXIAL STRAIN FOR A CONFINING PRESSURE OF 5 PSI, AND DIFFERENT RELATIVE DENSITY (Dr) OF SAMPLE 4 OF SERIES B OF THE NATURAL MATERIAL.

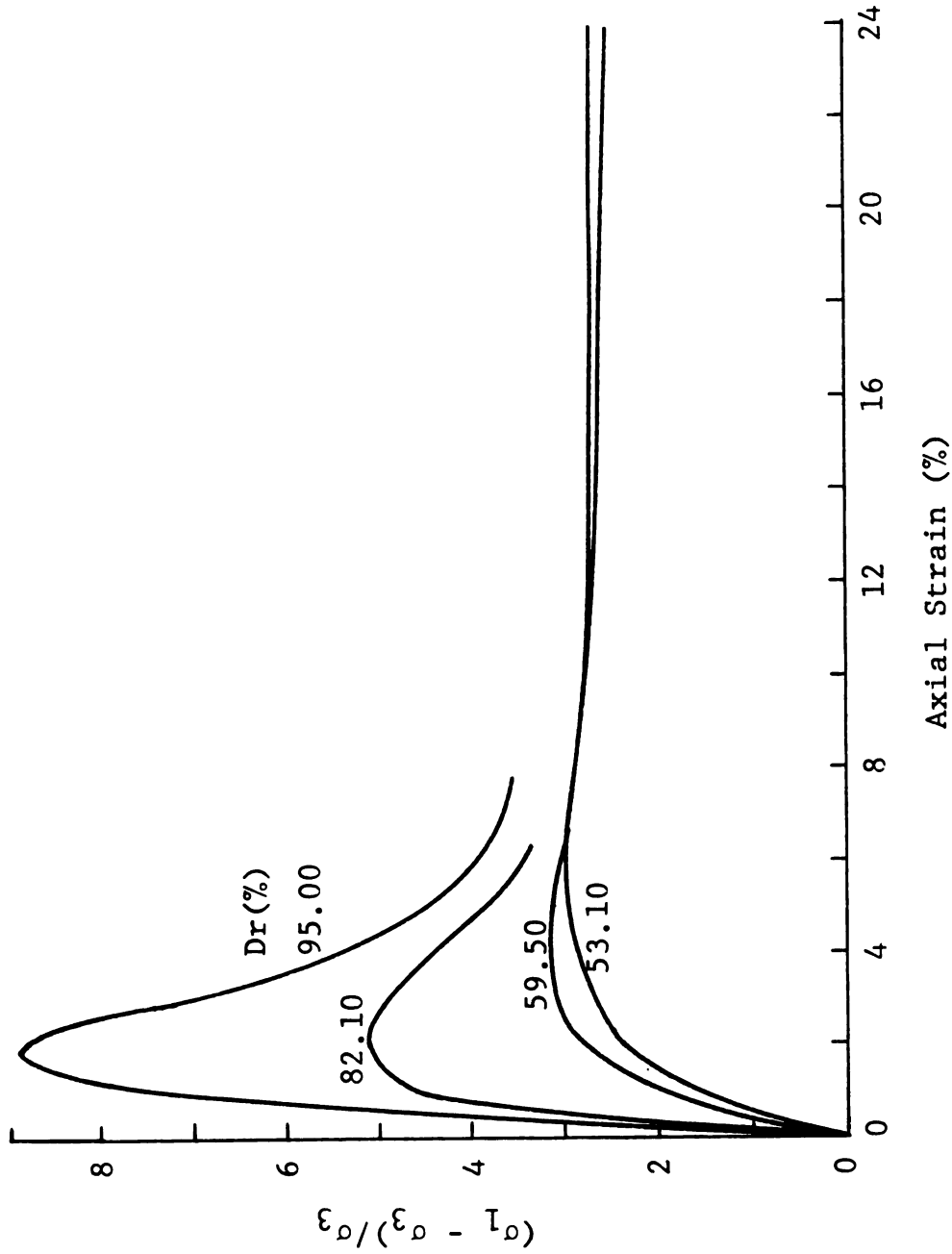


FIGURE E.15 NORMALIZED PRINCIPAL STRESS DIFFERENCE VERSUS AXIAL STRAIN FOR A CONFINING PRESSURE OF 5 PSI, AND DIFFERENT RELATIVE DENSITY (Dr) OF SAMPLE 1 OF SERIES A OF THE 50/50 MATERIAL.

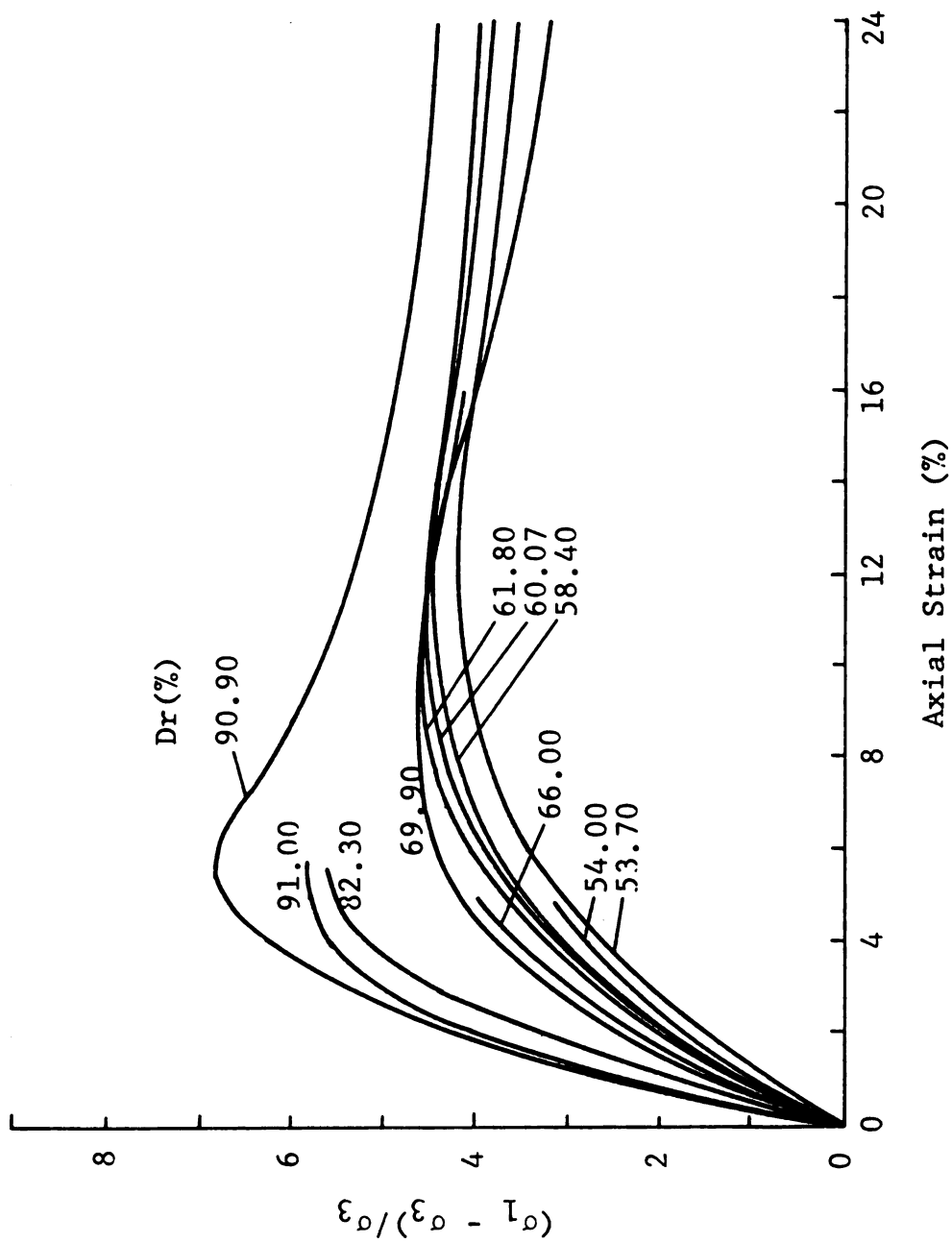


FIGURE E.16 NORMALIZED PRINCIPAL STRESS DIFFERENCE VERSUS AXIAL STRAIN FOR A CONFINING PRESSURE OF 25 PSI, AND DIFFERENT RELATIVE DENSITY (D_r) OF SAMPLE 1 OF SERIES A OF THE C/P MATERIAL.

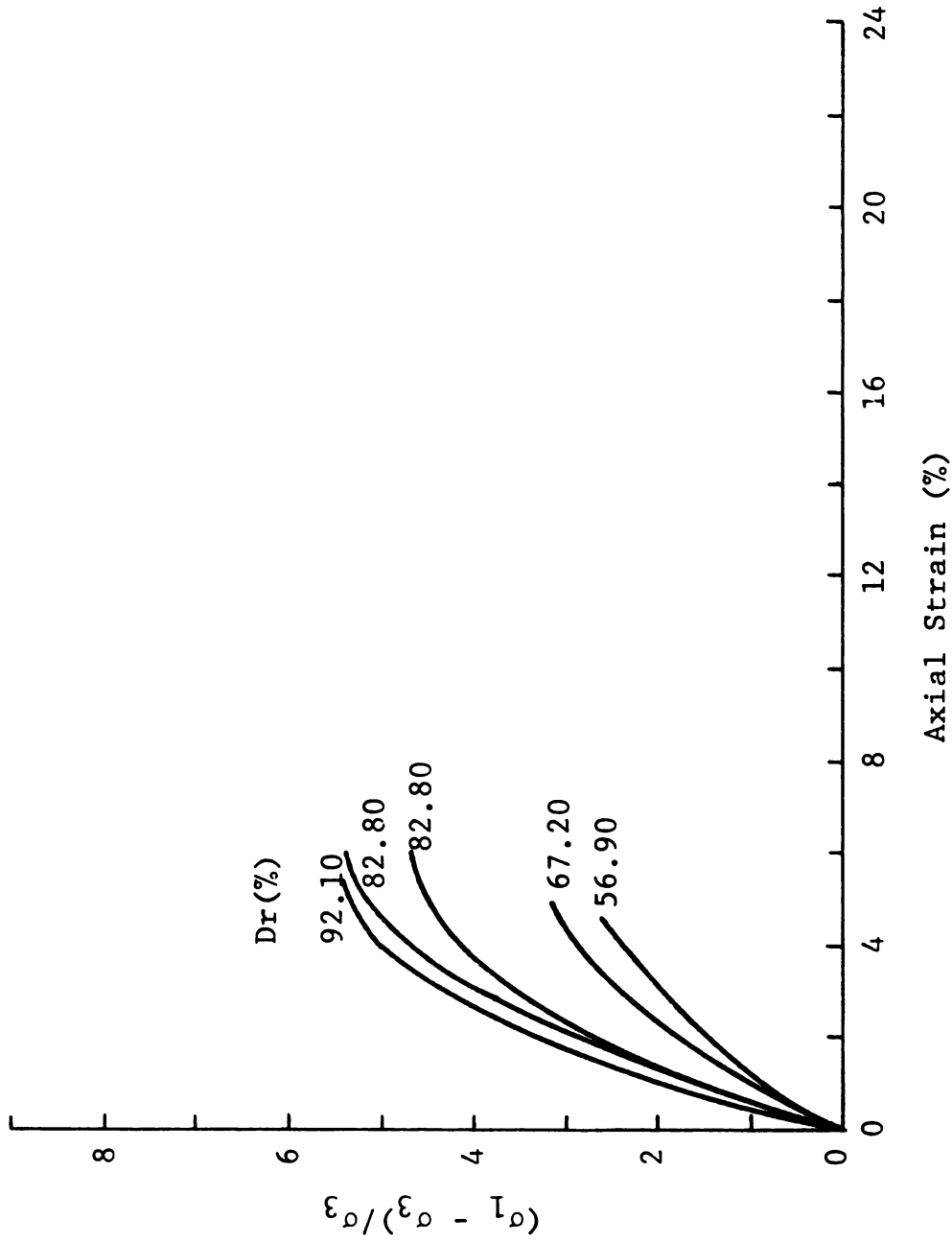


FIGURE F.17 NORMALIZED PRINCIPAL STRESS DIFFERENCE VERSUS AXIAL STRAIN FOR A CONFINING PRESSURE OF 25 PSI, AND DIFFERENT RELATIVE DENSITY (Dr) OF SAMPLE 2 OF SERIES A OF THE C/P MATERIAL.

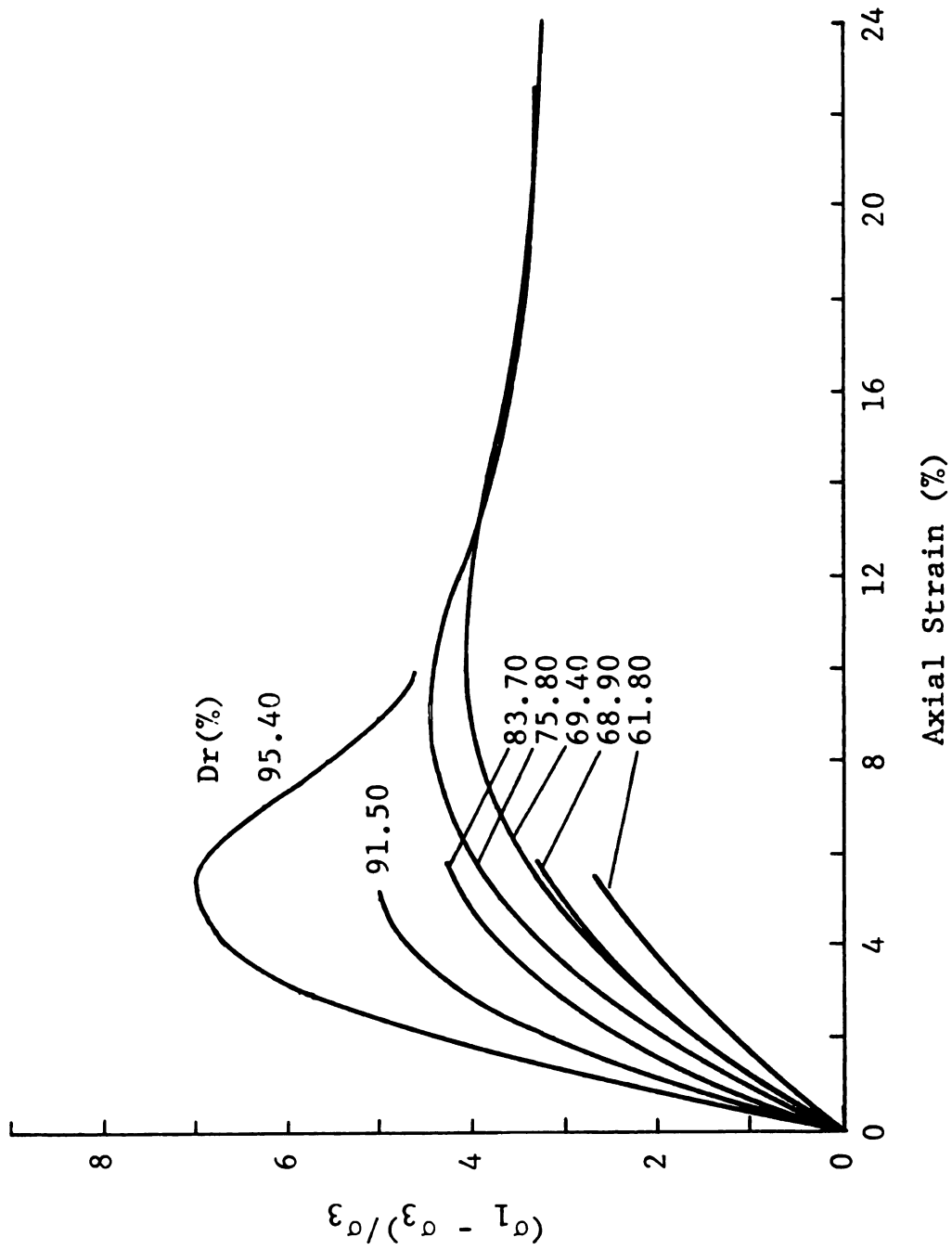


FIGURE E.18 NORMALIZED PRINCIPAL STRESS DIFFERENCE VERSUS AXIAL STRAIN FOR A CONFINING PRESSURE OF 25 PSI, AND DIFFERENT RELATIVE DENSITY (Dr) OF SAMPLE 3 OF SERIES A OF THE C/P MATERIAL.

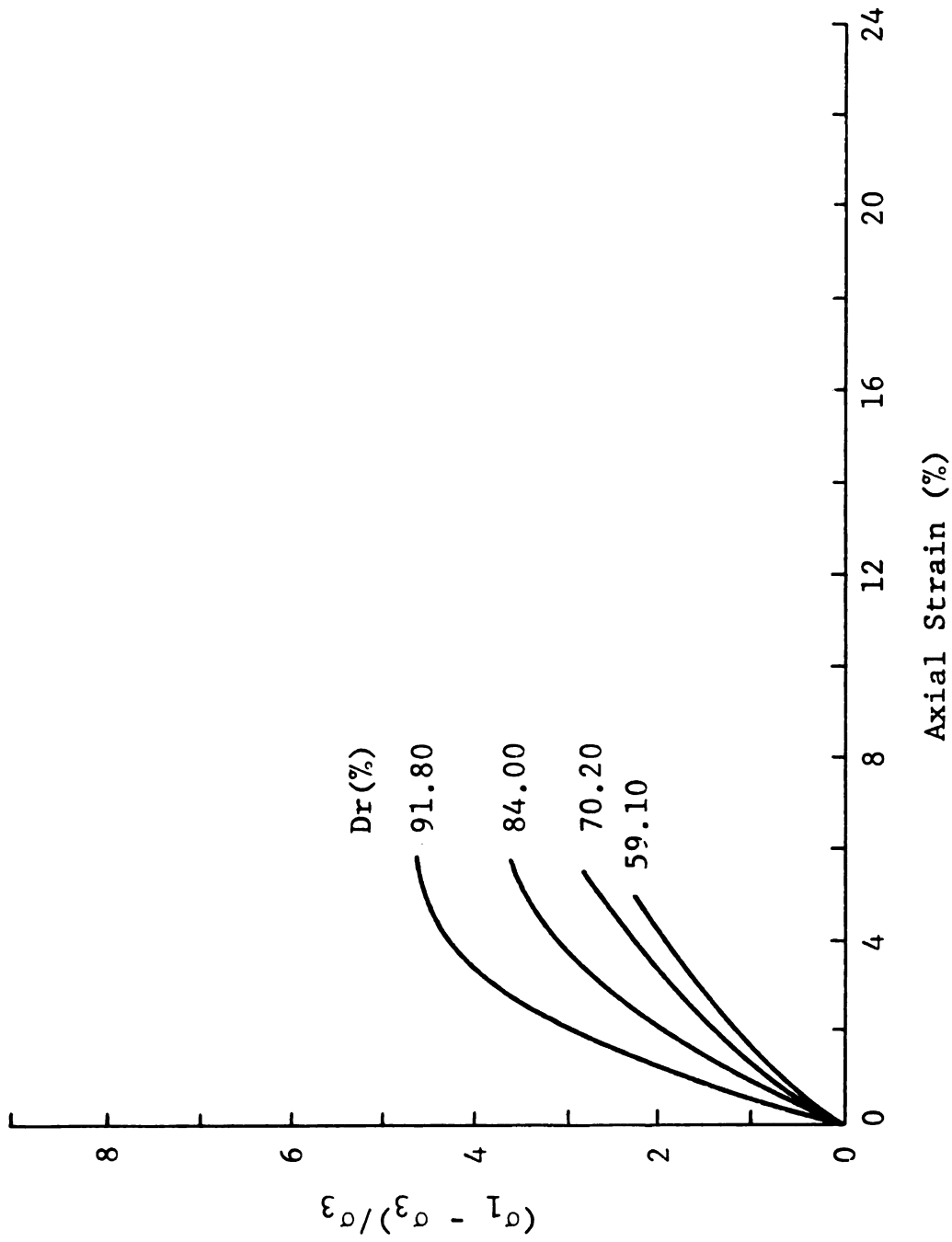


FIGURE E.19 NORMALIZED PRINCIPAL STRESS DIFFERENCE VERSUS AXIAL STRAIN FOR A CONFINING PRESSURE OF 25 PSI, AND DIFFERENT RELATIVE DENSITY (Dr) OF SAMPLE 4 OF SERIES A OF THE C/P MATERIAL.

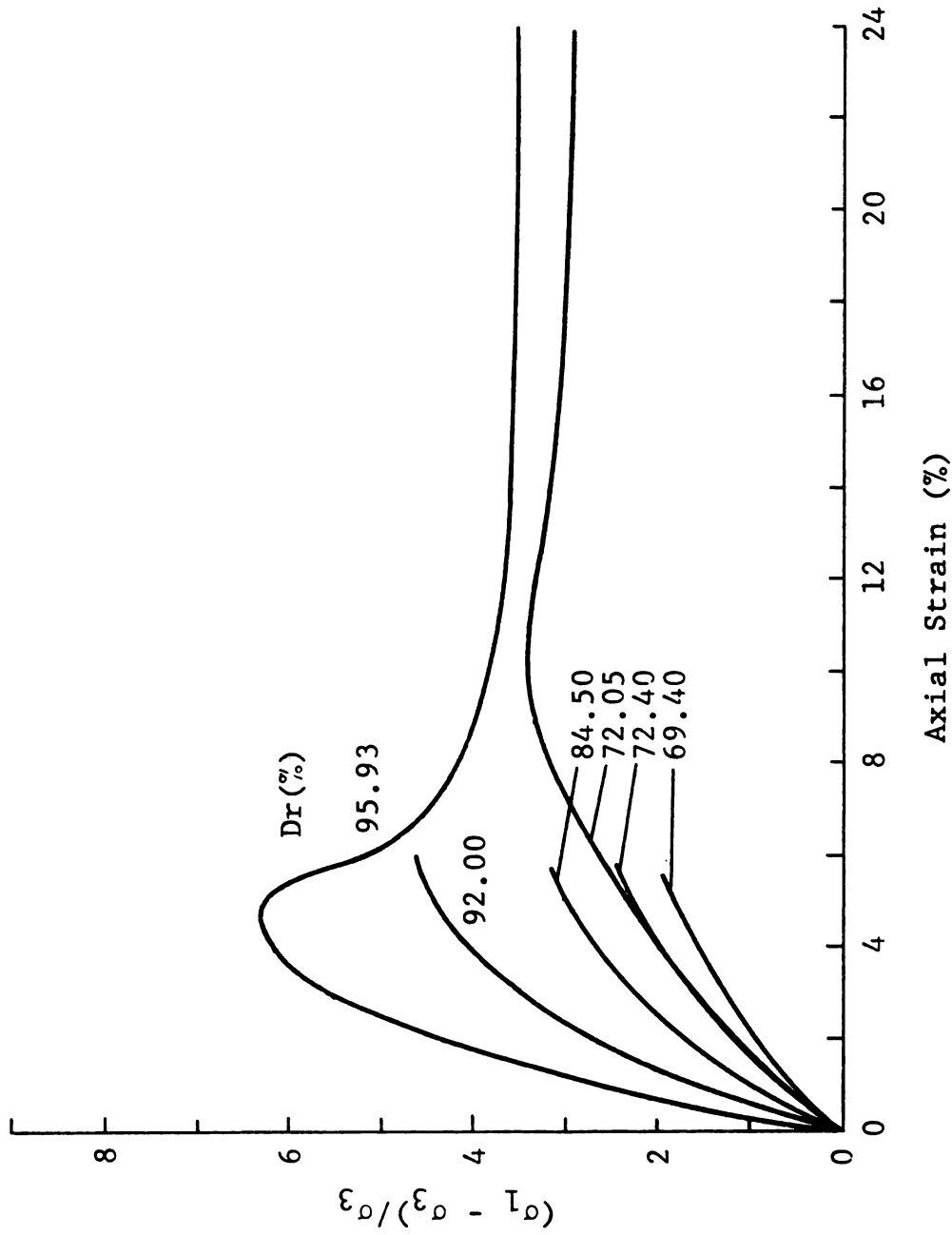


FIGURE E.20 NORMALIZED PRINCIPAL STRESS DIFFERENCE VERSUS AXIAL STRAIN FOR A CONFINING PRESSURE OF 25 PSI, AND DIFFERENT RELATIVE DENSITY (Dr) OF SAMPLE 5 OF SERIES A OF THE C/P MATERIAL.

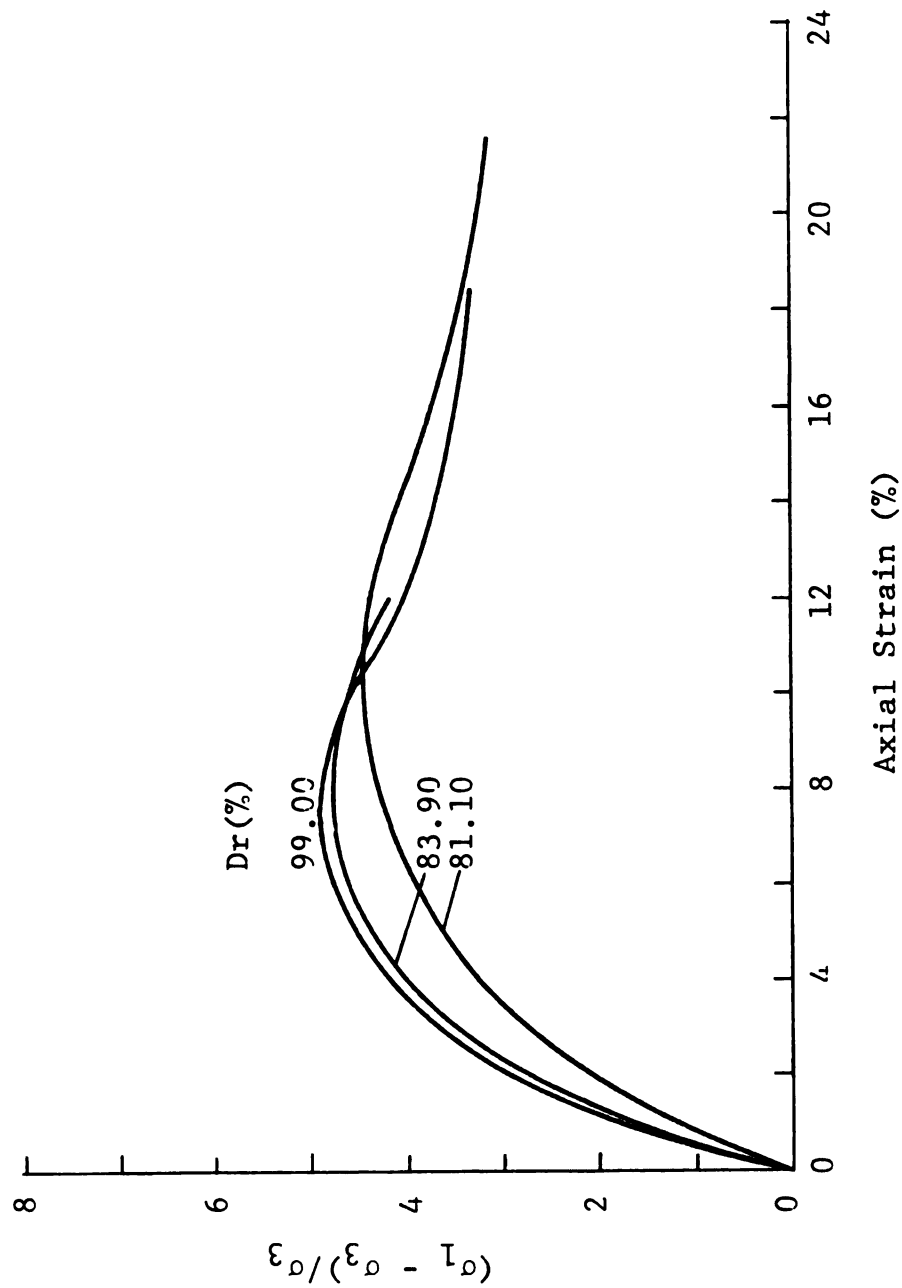


FIGURE E.21 NORMALIZED PRINCIPAL STRESS DIFFERENCE VERSUS AXIAL STRAIN FOR A CONFINING PRESSURE OF 25 PSI, AND DIFFERENT RELATIVE DENSITY (Dr) OF SAMPLE 4 OF SERIES B OF THE C/P MATERIAL.

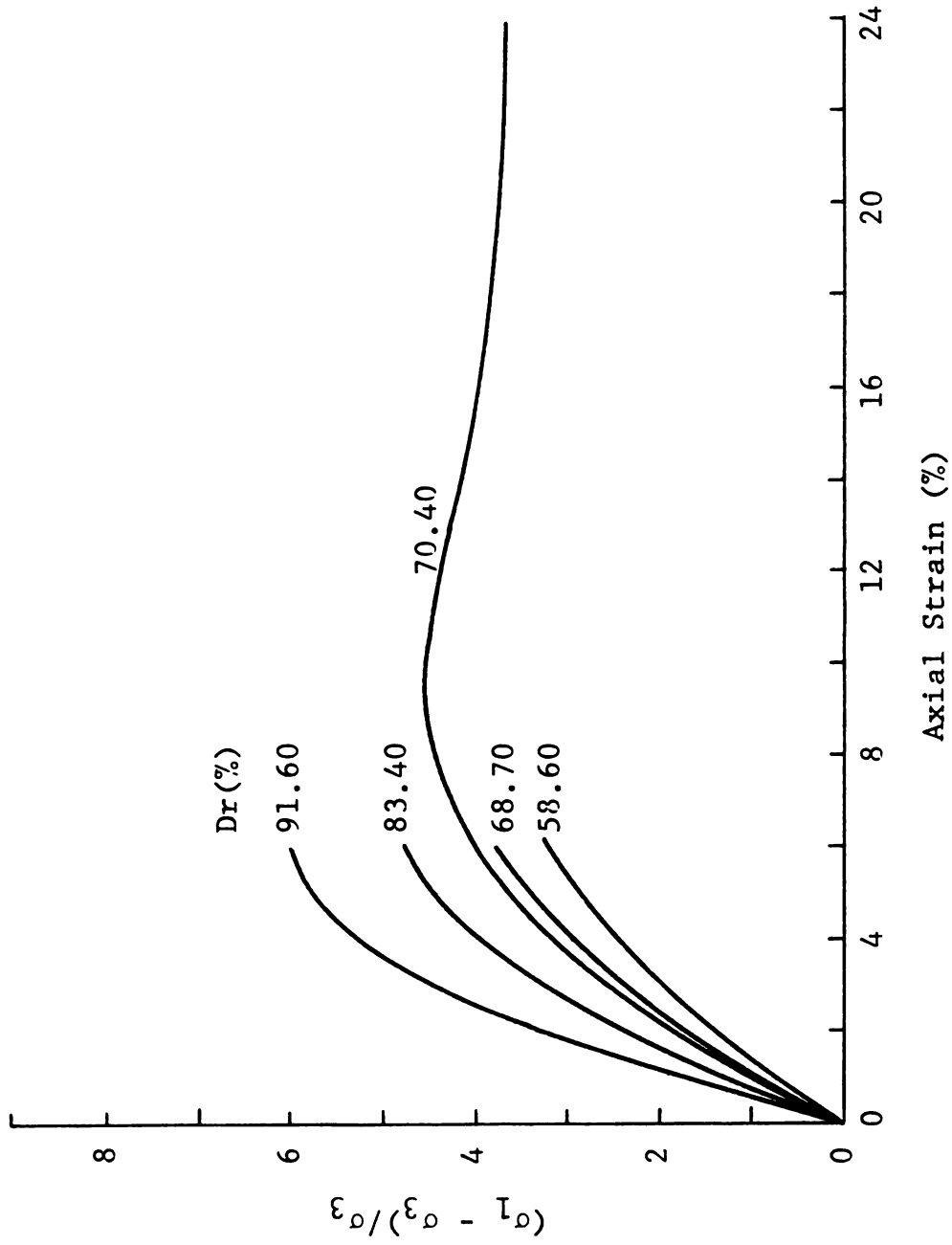


FIGURE E.22 NORMALIZED PRINCIPAL STRESS DIFFERENCE VERSUS AXIAL STRAIN FOR A CONFINING PRESSURE OF 50 PSI, AND DIFFERENT RELATIVE DENSITY (Dr) OF SAMPLE 1 OF SERIES A OF THE C/P MATERIAL.

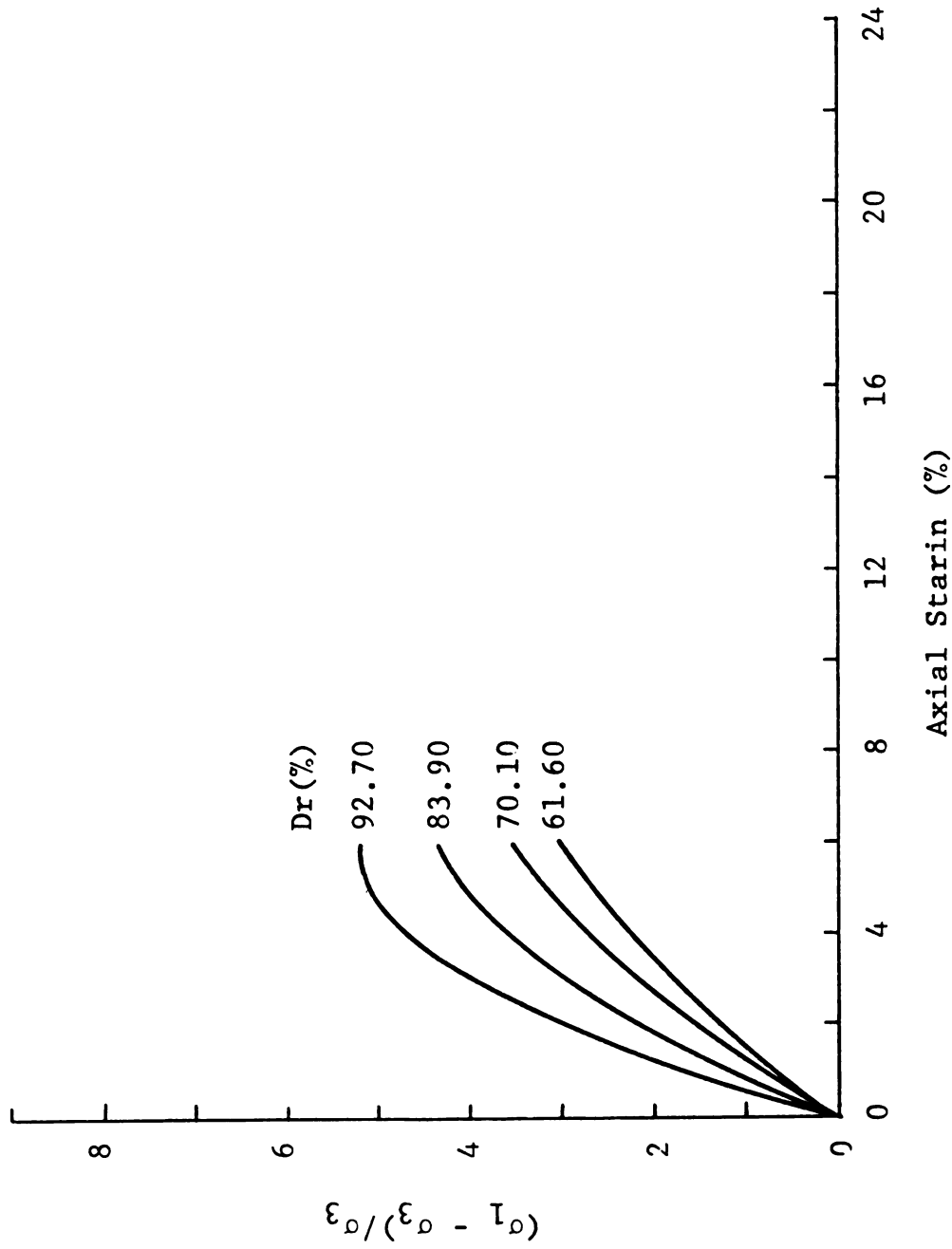


FIGURE E.23 NORMALIZED PRINCIPAL STRESS DIFFERENCE VERSUS AXIAL STRAIN FOR A CONFINING PRESSURE OF 50 PSI, AND DIFFERENT RELATIVE DENSITY (Dr) OF SAMPLE 2 OF SERIES A OF THE C/P MATERIAL.

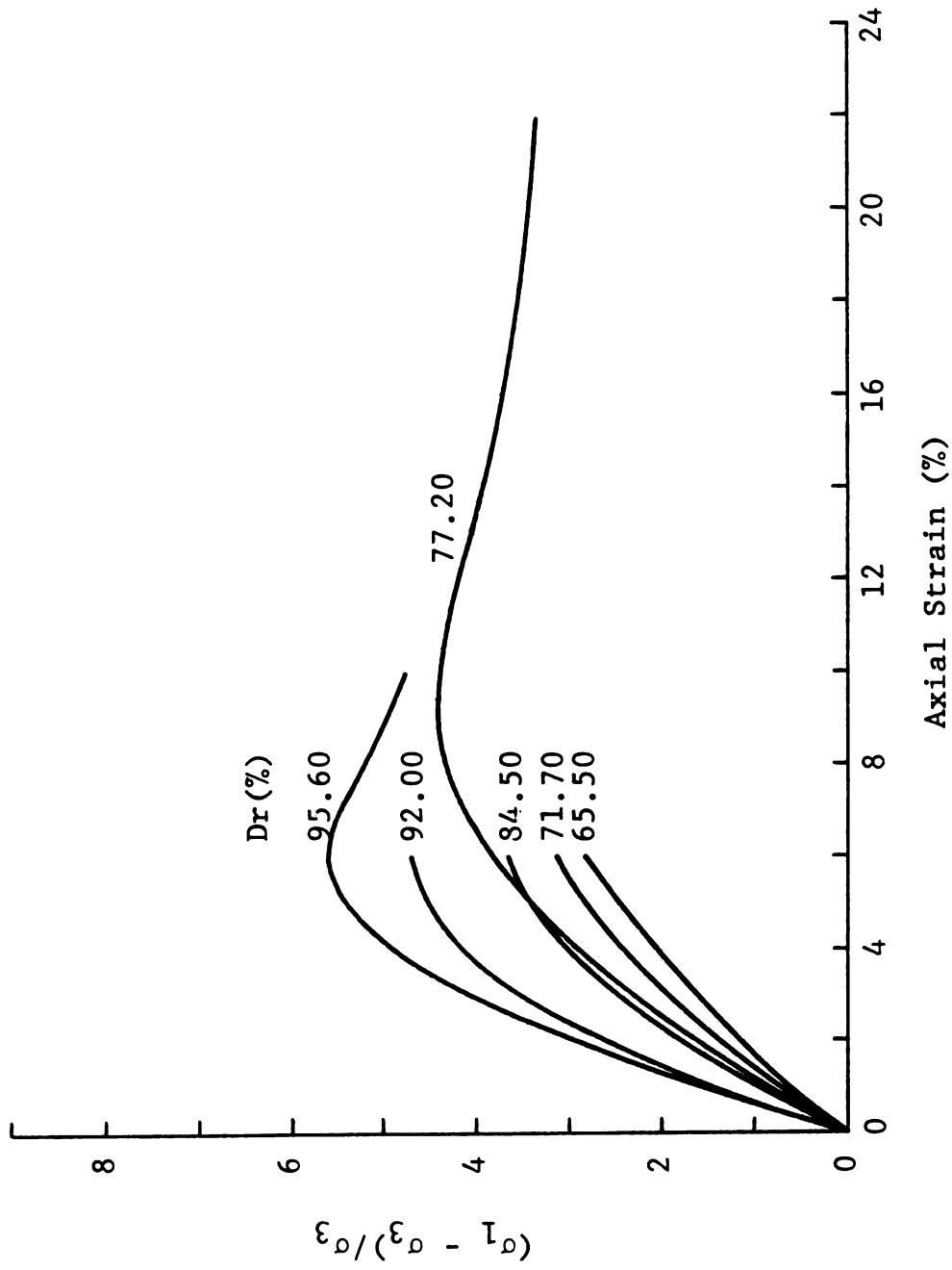


FIGURE E.24 NORMALIZED PRINCIPAL STRESS DIFFERENCE VERSUS AXIAL STRAIN FOR A CONFINING PRESSURE OF 50 PSI, AND DIFFERENT RELATIVE DENSITY (Dr) OF SAMPLE 3 OF SERIES A OF THE C/P MATERIAL.

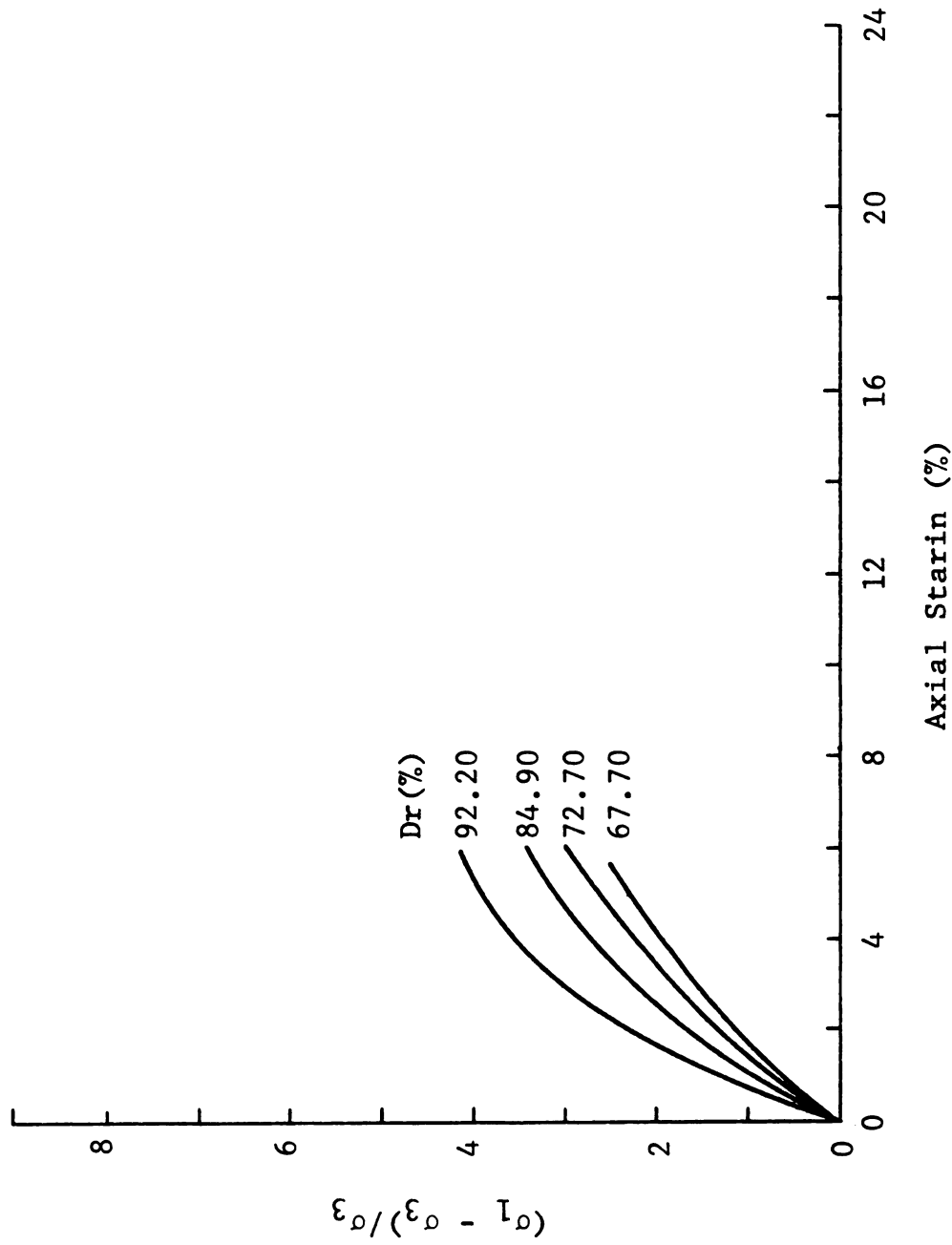


FIGURE E.25 NORMALIZED PRINCIPAL STRESS DIFFERENCE VERSUS AXIAL STRAIN FOR A CONFINING PRESSURE OF 50 PSI, AND DIFFERENT RELATIVE DENSITY (D_r) OF SAMPLE 4 OF SERIES A OF THE C/P MATERIAL.

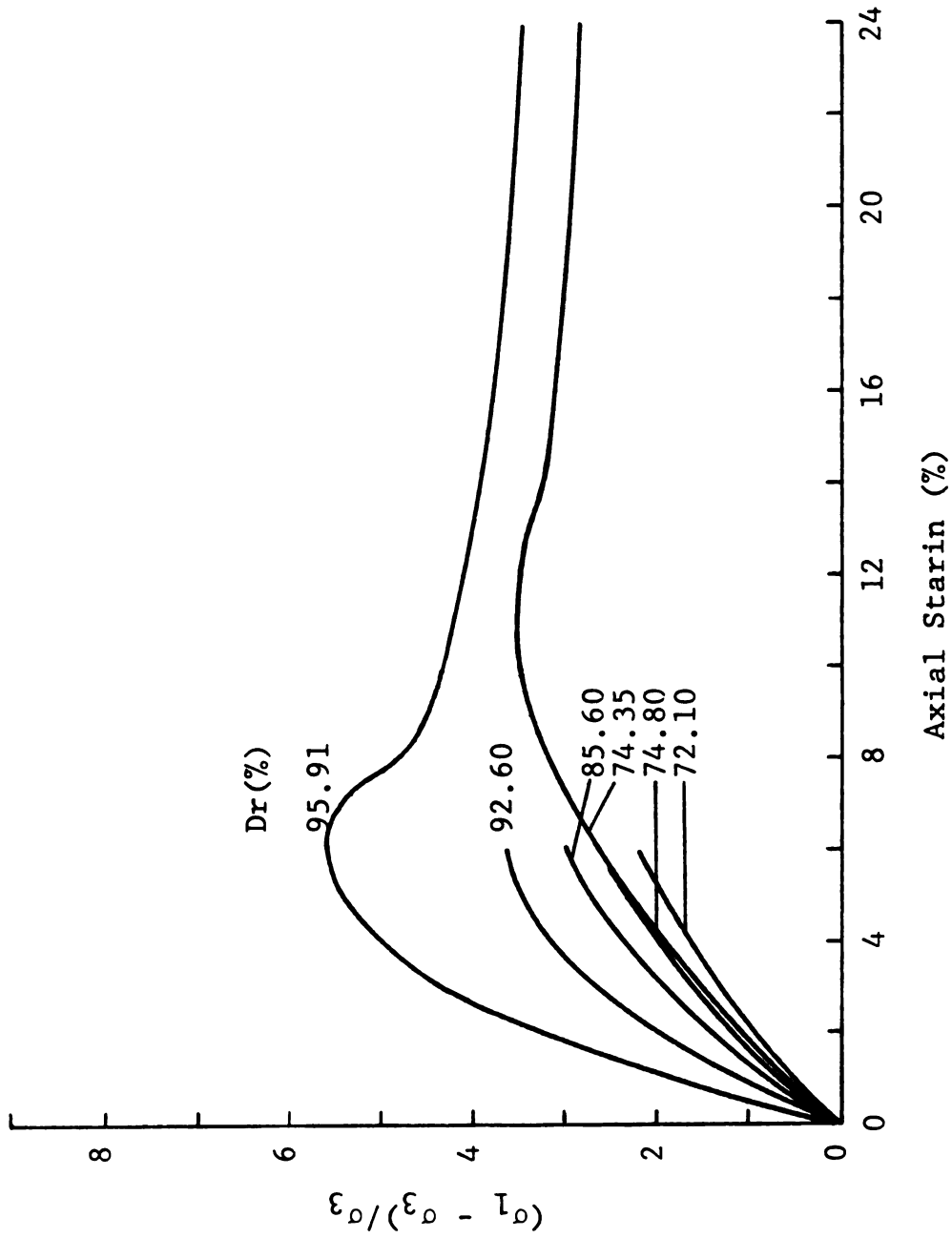


FIGURE E.26 NORMALIZED PRINCIPAL STRESS DIFFERENCE VERSUS AXIAL STRAIN FOR A CONFINING PRESSURE OF 50 PSI, AND DIFFERENT RELATIVE DENSITY (Dr) OF SAMPLE 5 OF SERIES A OF THE C/P MATERIAL.

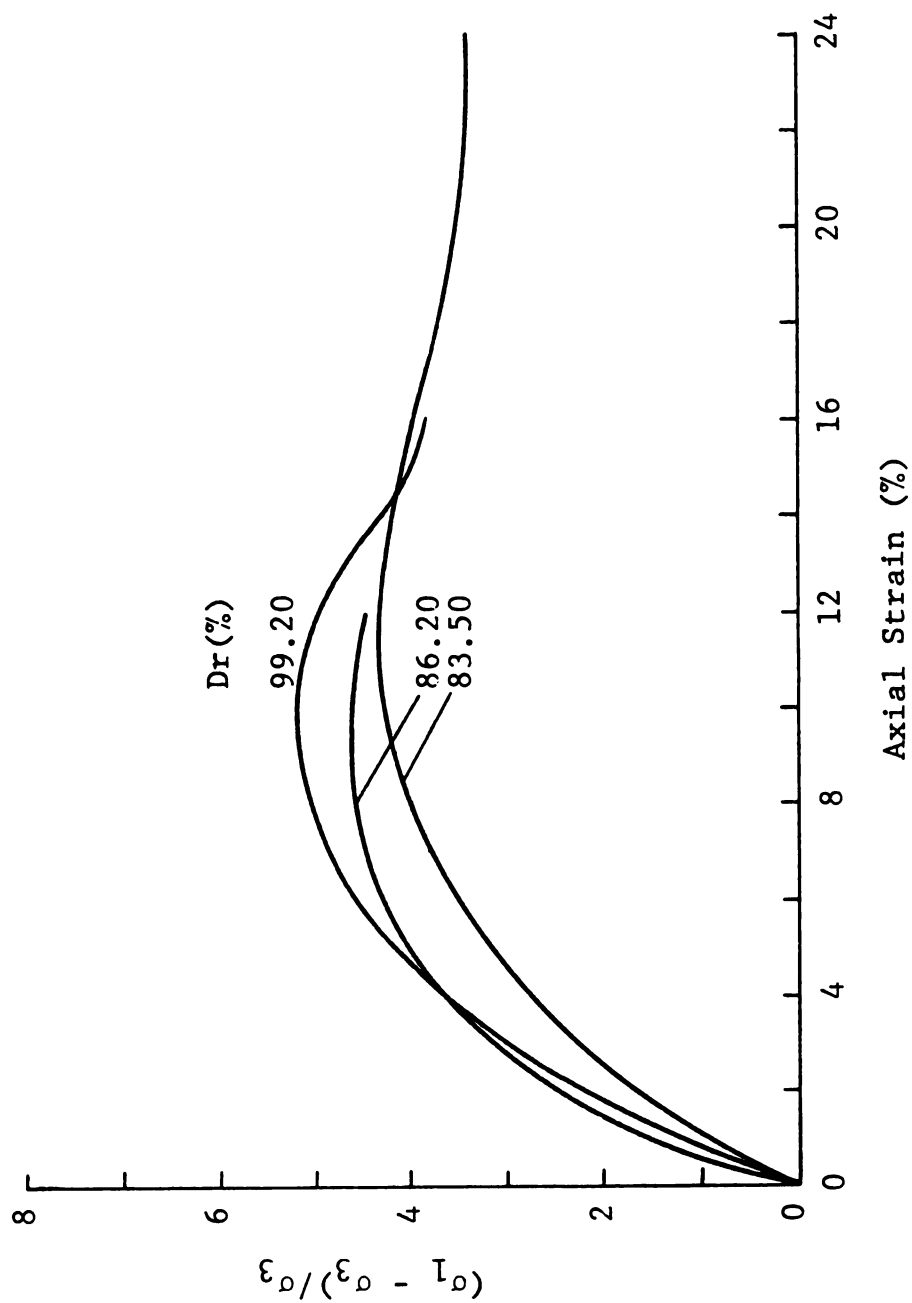


FIGURE E.27 NORMALIZED PRINCIPAL STRESS DIFFERENCE VERSUS AXIAL STRAIN FOR A CONFINING PRESSURE OF 50 PSI, AND DIFFERENT RELATIVE DENSITY (Dr) OF SAMPLE 4 OF SERIES B OF THE C/P MATERIAL.

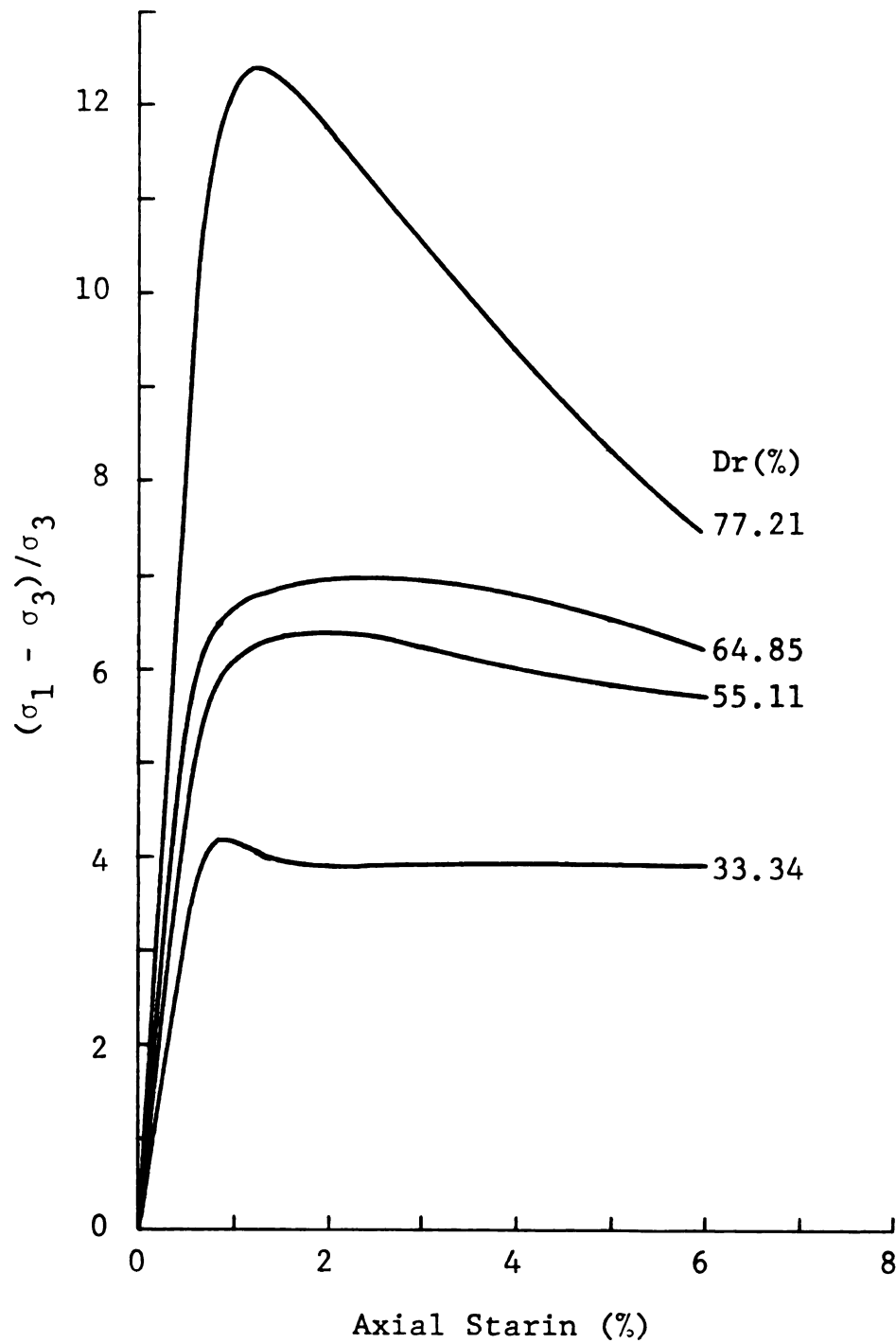


FIGURE E.28 NORMALIZED PRINCIPAL STRESS DIFFERENCE VERSUS AXIAL STRAIN FOR A CONFINING PRESSURE OF 5 PSI, AN AVERAGE WATER CONTENT OF 4.92%, AND DIFFERENT RELATIVE DENSITY (D_r) OF SAMPLE 1 OF SERIES A OF THE C/P MATERIAL.

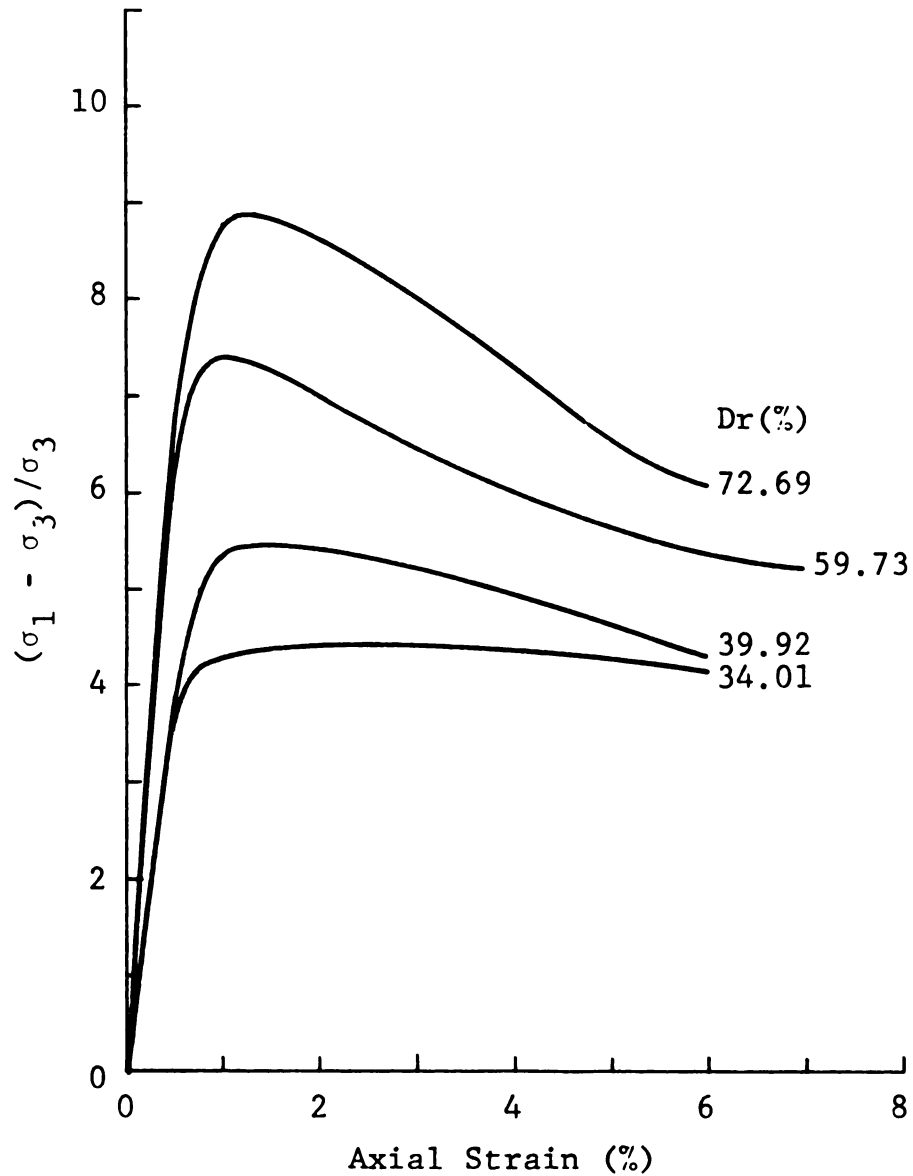


FIGURE E.29 NORMALIZED PRINCIPAL STRESS DIFFERENCE VERSUS AXIAL STRAIN FOR A CONFINING PRESSURE OF 5 PSI, AN AVERAGE WATER CONTENT OF 5.32%, AND DIFFERENT RELATIVE DENSITY (D_r) OF SAMPLE 2 OF SERIES A OF THE C/P MATERIAL.

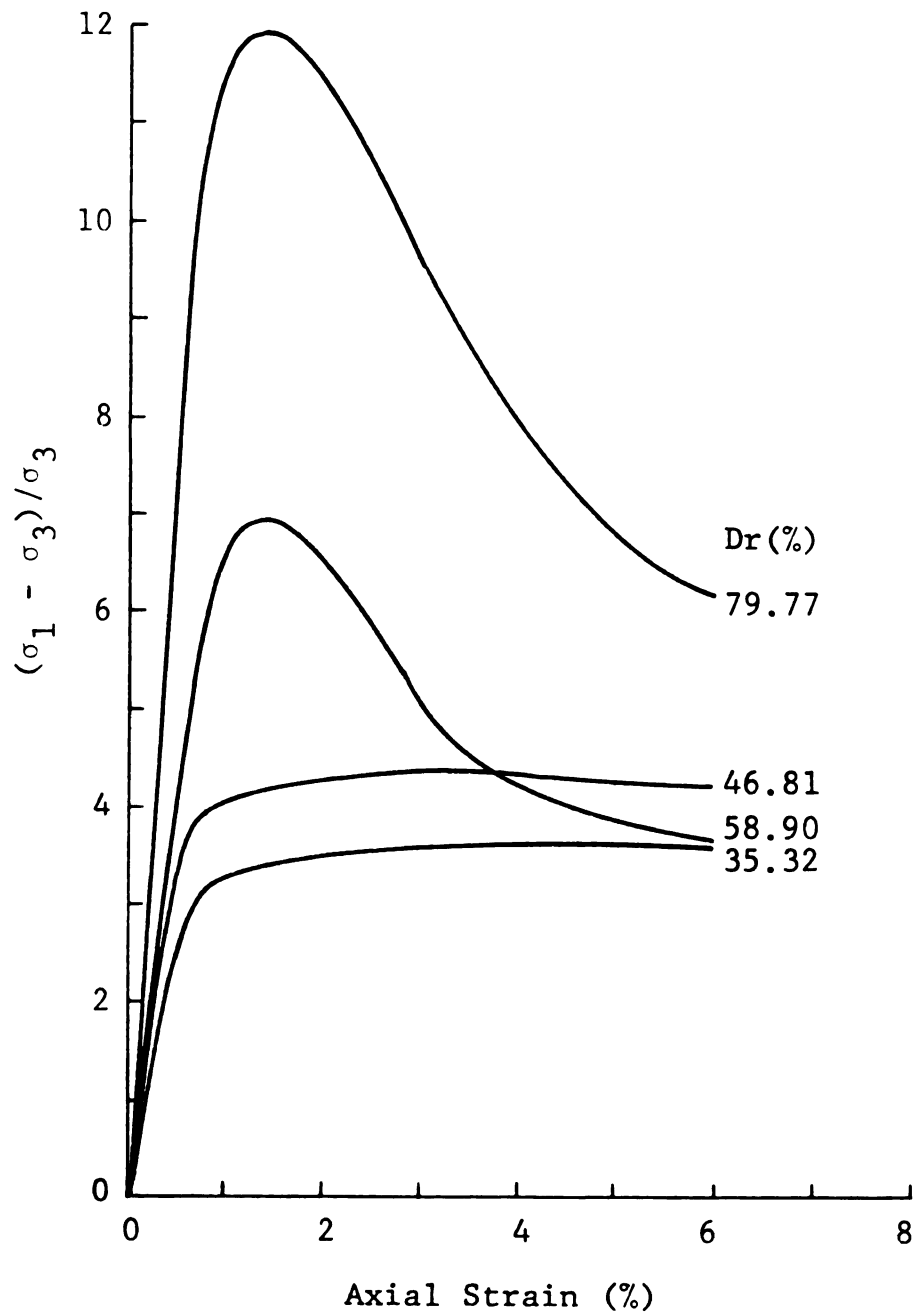


FIGURE E.30 NORMALIZED PRINCIPAL STRESS DIFFERENCE VERSUS AXIAL STRAIN FOR A CONFINING PRESSURE OF 5 PSI, AN AVERAGE WATER CONTENT OF 4.98%, AND DIFFERENT RELATIVE DENSITY (D_r) OF SAMPLE 3 OF SERIES A OF THE C/P MATERIAL.

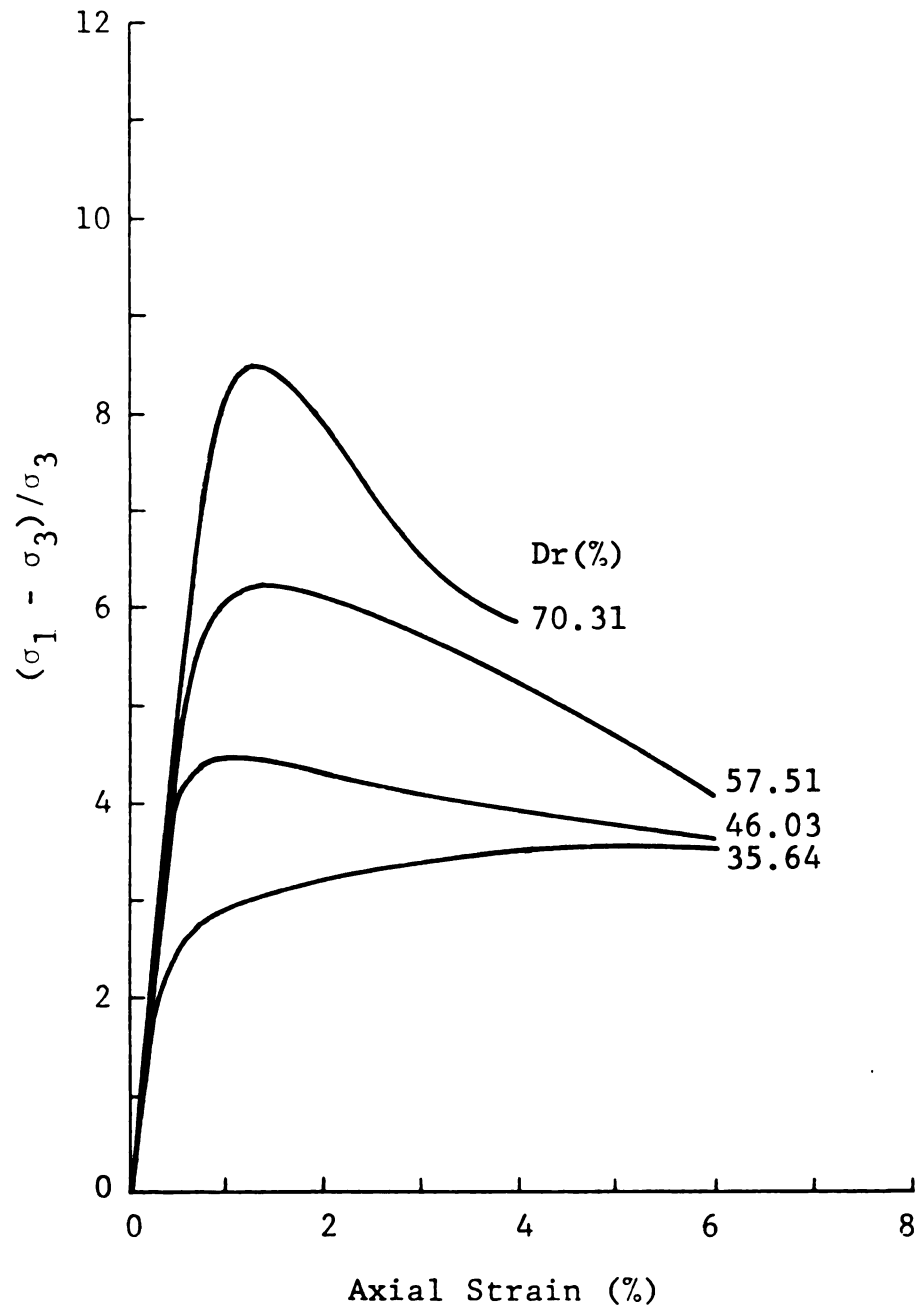


FIGURE E.31 NORMALIZED PRINCIPAL STRESS DIFFERENCE VERSUS AXIAL STRAIN FOR A CONFINING PRESSURE OF 5 PSI, AN AVERAGE WATER CONTENT OF 4.94%, AND DIFFERENT RELATIVE DENSITY (D_r) OF SAMPLE 4 OF SERIES A OF THE C/P MATERIAL.

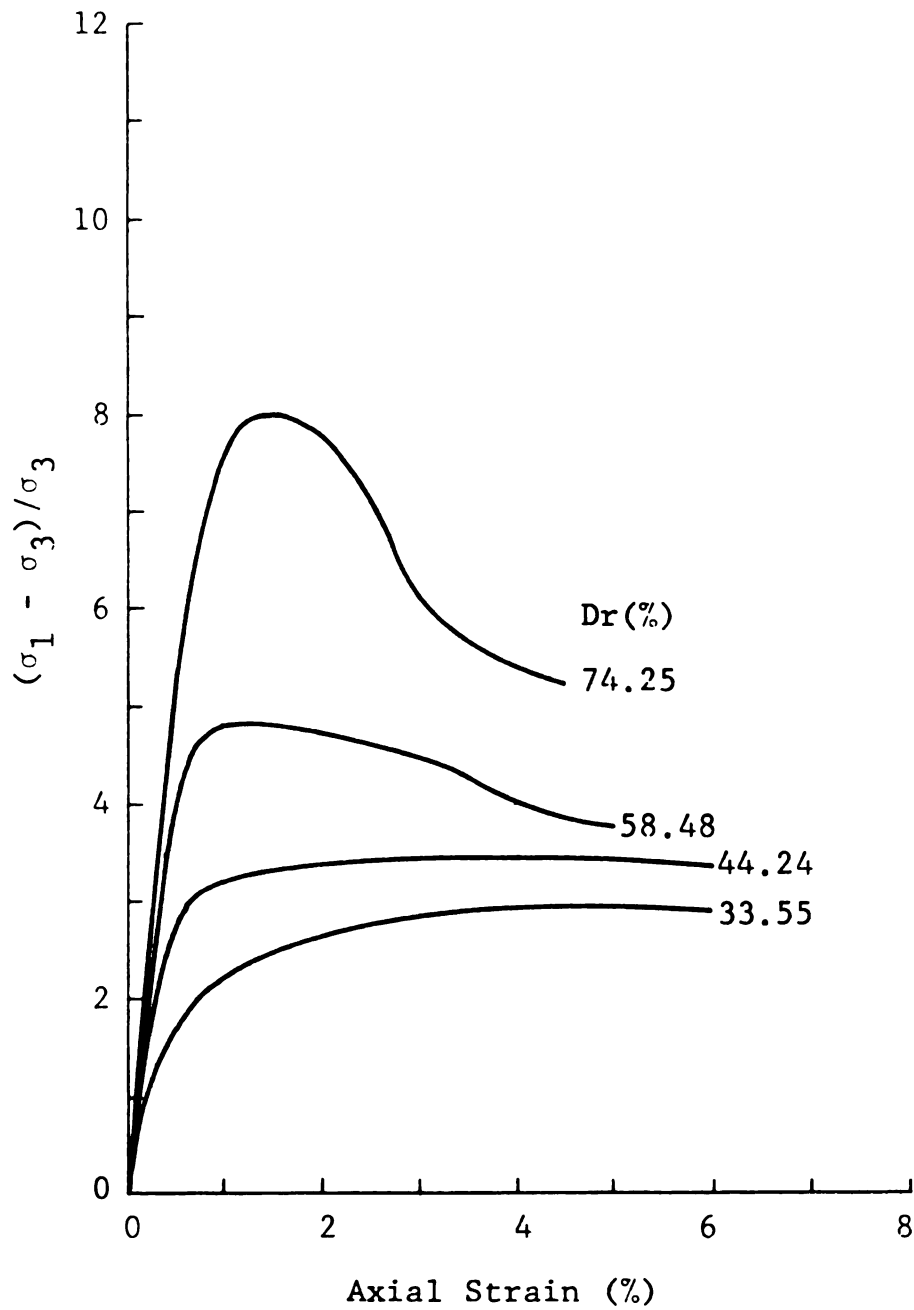


FIGURE E.32 NORMALIZED PRINCIPAL STRESS DIFFERENCE VERSUS AXIAL STRAIN FOR A CONFINING PRESSURE OF 5 PSI, AN AVERAGE WATER CONTENT OF 5.11%, AND DIFFERENT RELATIVE DENSITY (D_r) OF SAMPLE 5 OF SERIES A OF THE C/P MATERIAL.

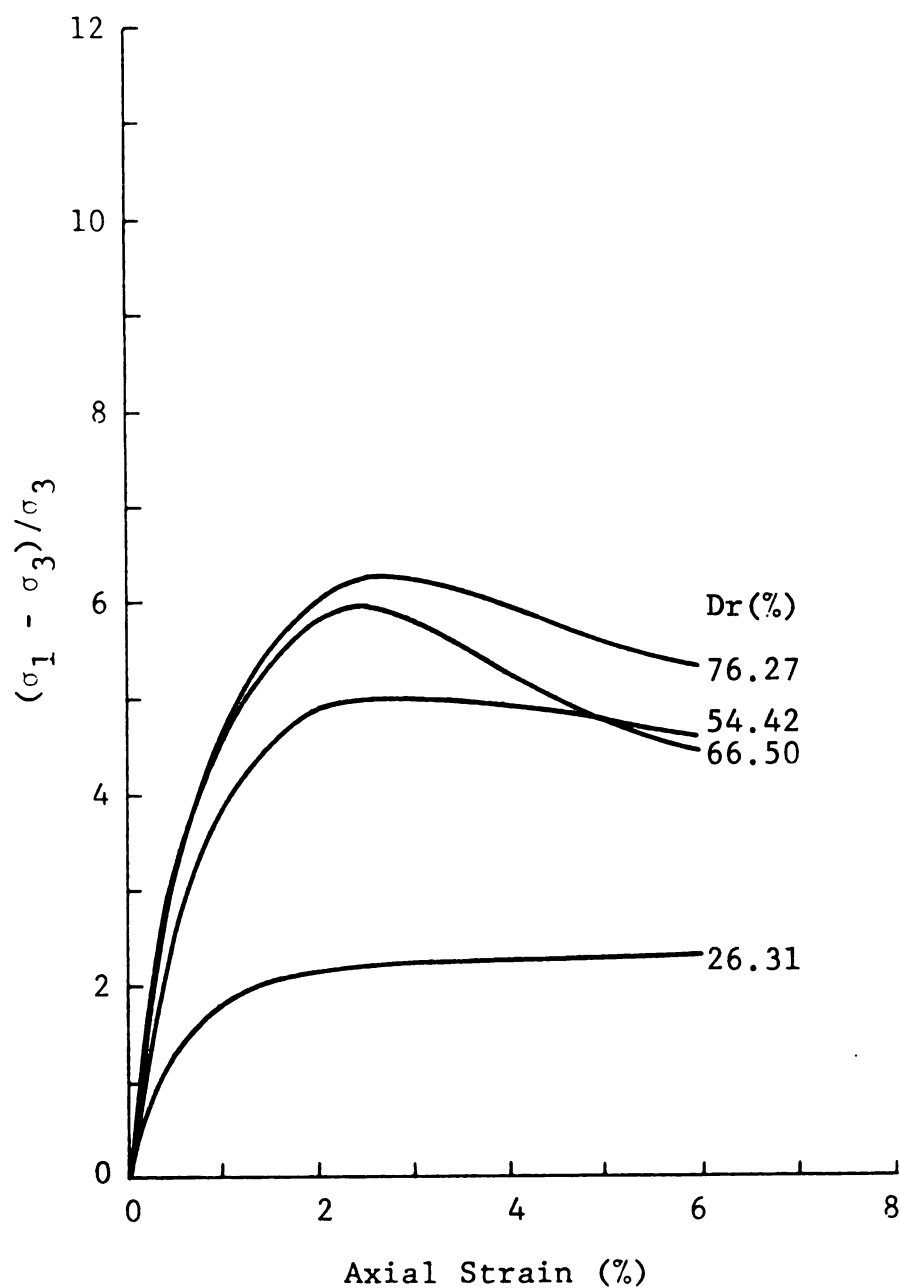


FIGURE E.33 NORMALIZED PRINCIPAL STRESS DIFFERENCE VERSUS AXIAL STRAIN FOR A CONFINING PRESSURE OF 5 PSI, AN AVERAGE WATER CONTENT OF 9.15%, AND DIFFERENT RELATIVE DENSITY (D_r) OF SAMPLE 1 OF SERIES A OF THE C/P MATERIAL.

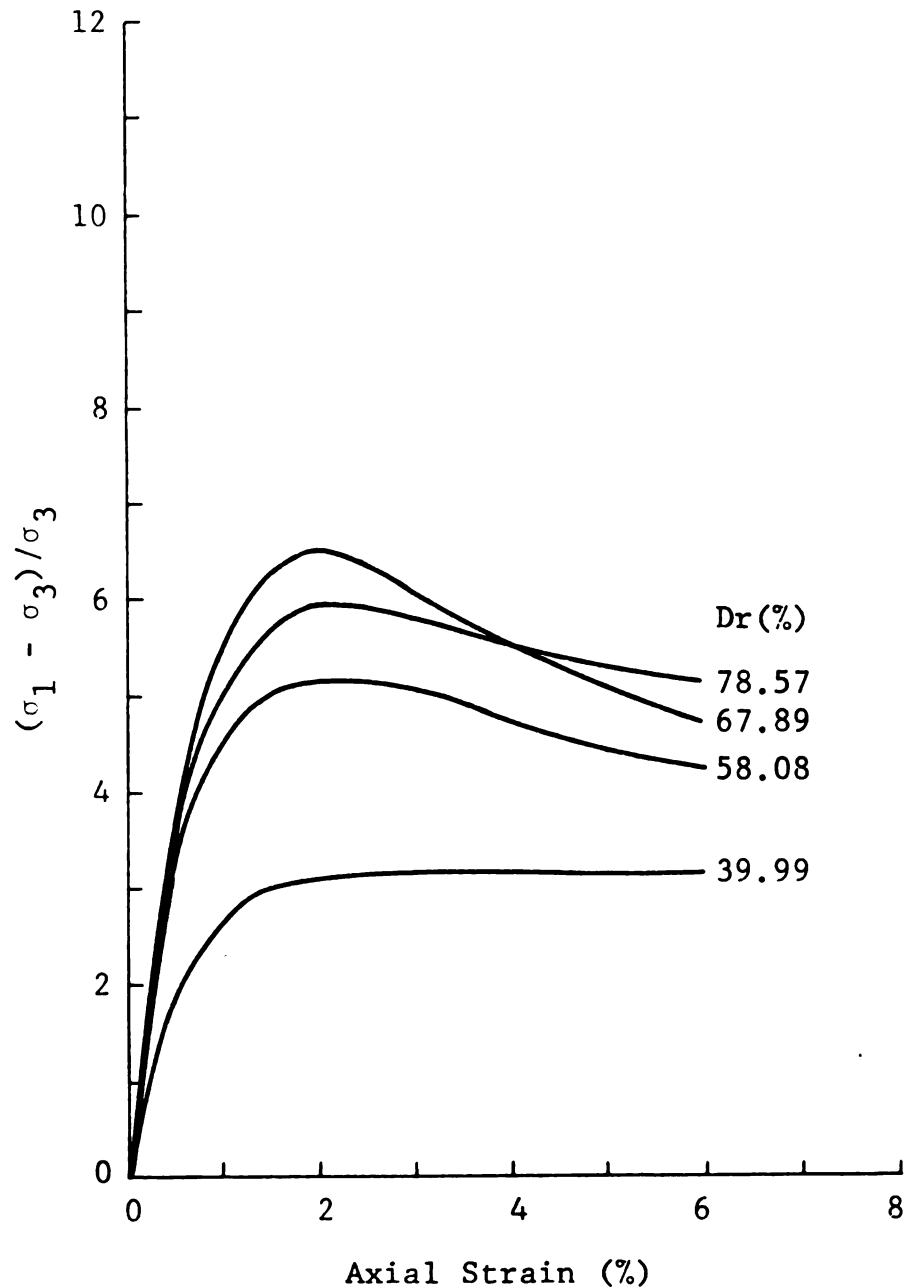


FIGURE E.34 NORMALIZED PRINCIPAL STRESS DIFFERENCE VERSUS AXIAL STRAIN FOR A CONFINING PRESSURE OF 5 PSI, AN AVERAGE WATER CONTENT OF 9.60%, AND DIFFERENT RELATIVE DENSITY (D_r) OF SAMPLE 2 OF SERIES A OF THE C/P MATERIAL.

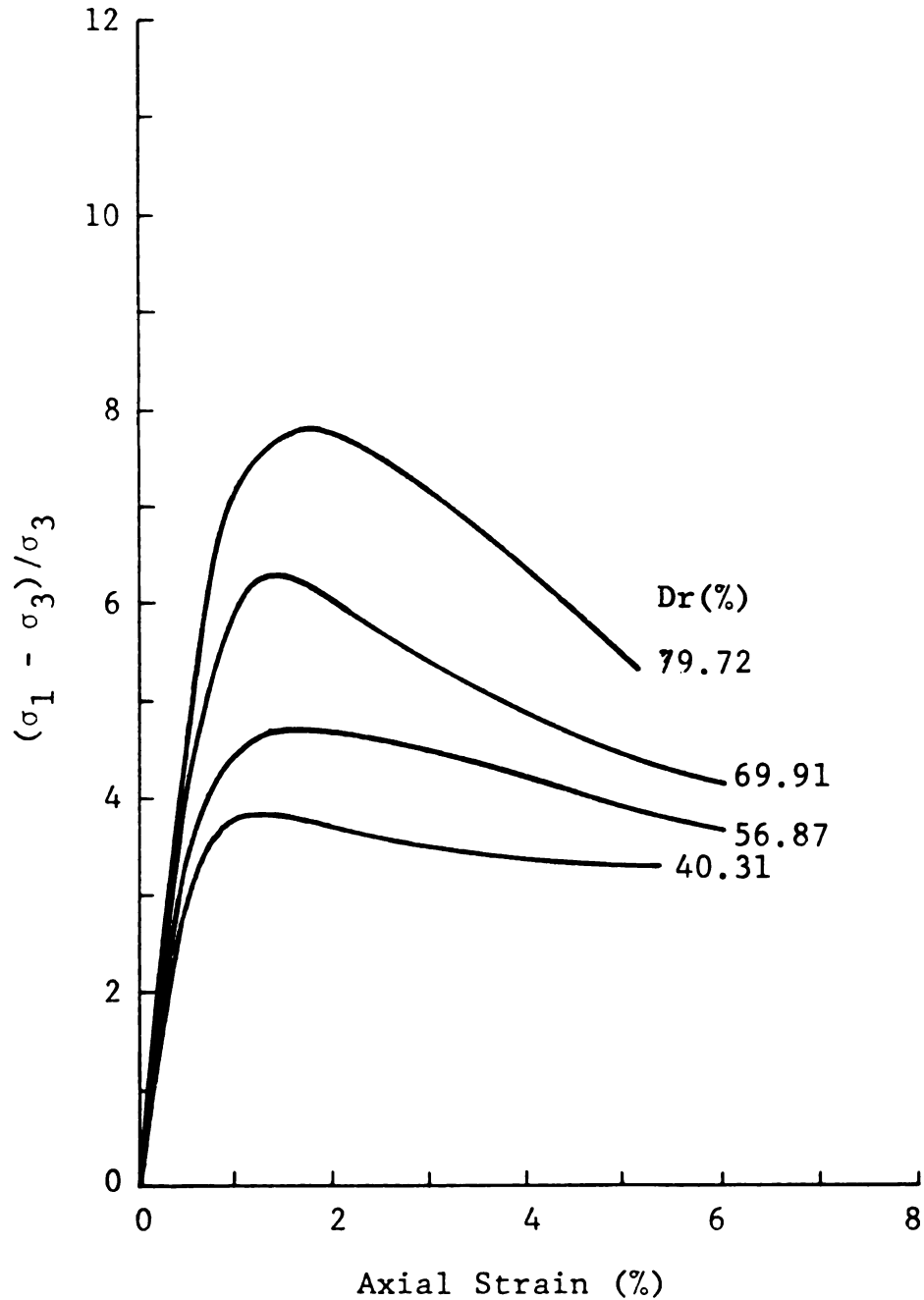


FIGURE E.35 NORMALIZED PRINCIPAL STRESS DIFFERENCE VERSUS AXIAL STRAIN FOR A CONFINING PRESSURE OF 5 PSI, AN AVERAGE WATER CONTENT OF 9.69%, AND DIFFERENT RELATIVE DENSITY (D_r) OF SAMPLE 3 OF SERIES A OF THE C/P MATERIAL.

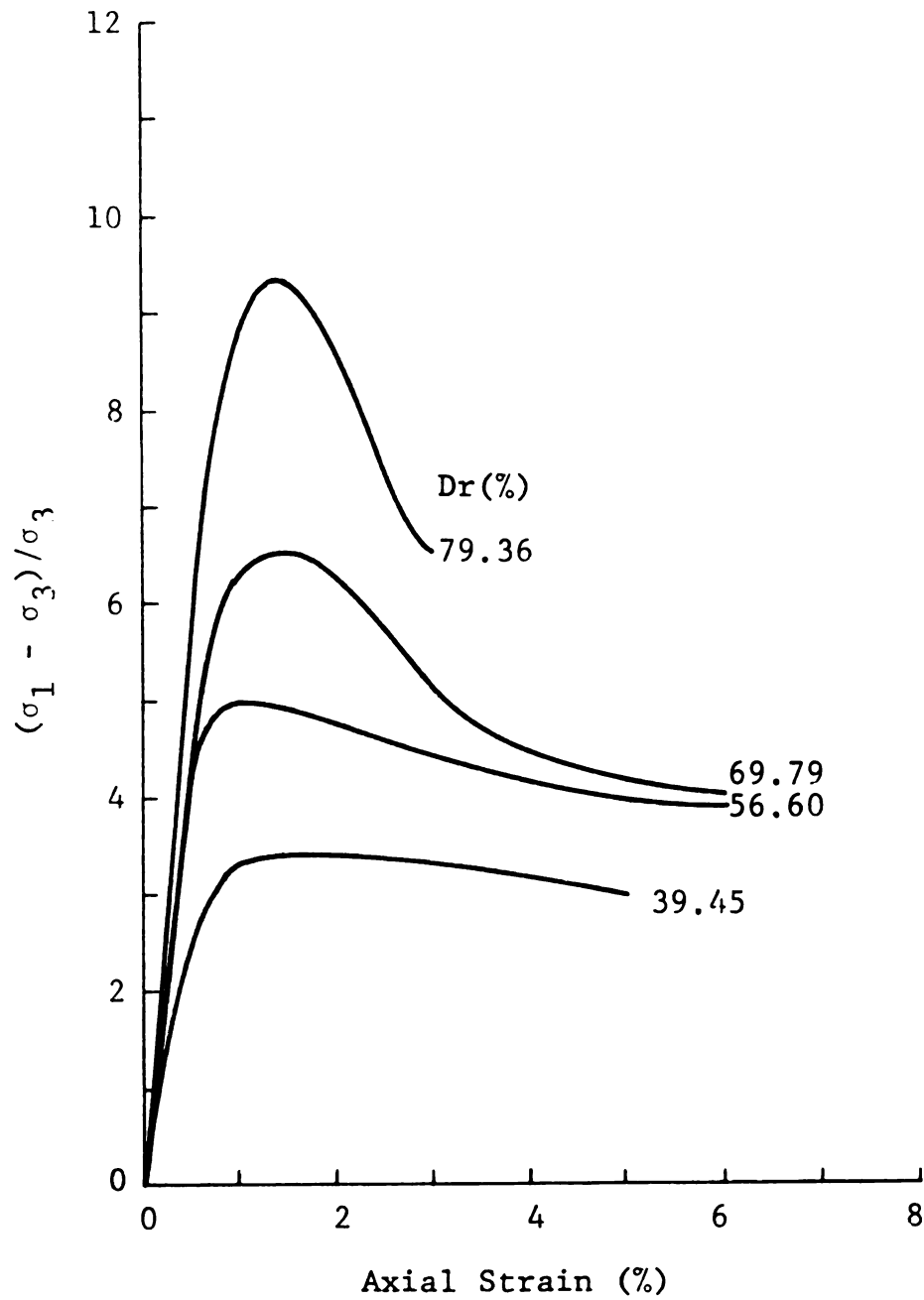


FIGURE E.36 NORMALIZED PRINCIPAL STRESS DIFFERENCE VERSUS AXIAL STRAIN FOR A CONFINING PRESSURE OF 5 PSI, AN AVERAGE WATER CONTENT OF 9.75%, AND DIFFERENT RELATIVE DENSITY (D_r) OF SAMPLE 4 OF SERIES A OF THE C/P MATERIAL.

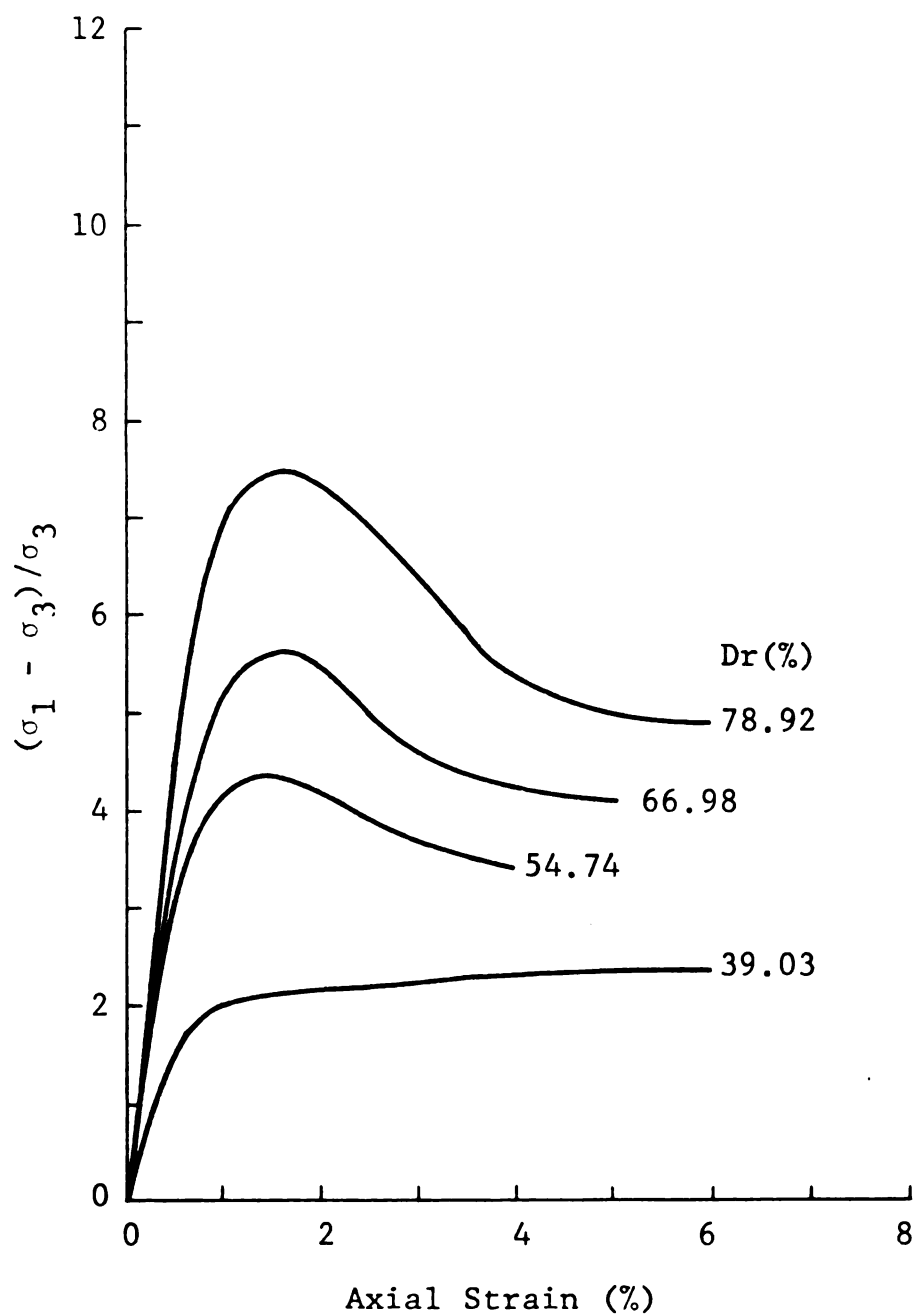


FIGURE E.37 NORMALIZED PRINCIPAL STRESS DIFFERENCE VERSUS AXIAL STRAIN FOR A CONFINING PRESSURE OF 5 PSI, AN AVERAGE WATER CONTENT OF 9.96%, AND DIFFERENT RELATIVE DENSITY (D_r) OF SAMPLE 5 OF SERIES A OF THE C/P MATERIAL.

MICHIGAN STATE UNIVERSITY LIBRARIES



3 1293 03169 5830